



University
of Glasgow

McCarroll, Douglas (2014) *The effects of Trypanosoma brucei and mammalian-derived extracellular cathepsin-L on myocardial function.* PhD thesis.

<http://theses.gla.ac.uk/5170/>

Copyright and moral rights for this work are retained by the author

A copy can be downloaded for personal non-commercial research or study, without prior permission or charge

This work cannot be reproduced or quoted extensively from without first obtaining permission in writing from the author

The content must not be changed in any way or sold commercially in any format or medium without the formal permission of the author

When referring to this work, full bibliographic details including the author, title, awarding institution and date of the thesis must be given

Enlighten:Theses
<http://theses.gla.ac.uk/>
theses@gla.ac.uk

**The Effects of *Trypanosoma brucei* and
Mammalian-Derived Extracellular Cathepsin-L on
Myocardial Function**

Mr. Douglas McCarroll BVMS (Hons) MSc (VetSci) MRCVS

Submitted in fulfilment of the requirements for the Degree of Doctor of
Philosophy to the Institute of Cardiovascular and Medical Sciences, College of
Medical, Veterinary and Life Sciences, University of Glasgow, U.K.

Research conducted at the British Heart Foundation Glasgow Cardiovascular
Research Centre, Institute of Cardiovascular and Medical Sciences, University
of Glasgow, U.K.

January 2014

Abstract

African trypanosomiasis is a neglected tropical disease affecting both animals and humans in sub-Saharan Africa. The disease is caused by the protozoan parasite *Trypanosoma brucei*, which is transmitted by the tsetse fly (*Glossina* sp.) vector. In animals, infection leads to severe muscle atrophy and anaemia resulting in significant production and economic losses. In humans, infection leads to both neurological and cardiac dysfunction and can be fatal if untreated. While the neurological-related pathogenesis is well studied, and indeed is responsible for the colloquial name “Sleeping Sickness”, the cardiac pathogenesis remains unknown. Previous studies interpreted cardiac dysfunction as being due to immune/inflammatory responses. However, recent work examining the parasite’s interaction with the blood brain barrier, the traversal of which is important for development of neurological signs, has identified direct immune/inflammatory independent mechanisms involving calcium (Ca^{2+}) signalling. The current study exposed isolated ventricular cardiomyocytes and adult rat hearts to *T. brucei* to test whether trypanosomes can alter Ca^{2+} signalling and cardiac function independent of a systemic immune/inflammatory response.

Using a high-throughput method of observing spontaneous contractile activity in isolated cardiomyocytes, we were able to determine that the presence of *T. b. brucei* parasites resulted in more cardiomyocytes exhibiting spontaneous contractile events. Moreover, when the parasites were removed by careful centrifugation, the culture supernatant had the same effect. Confocal Ca^{2+} imaging identified an increase in the frequency of arrhythmogenic spontaneous diastolic sarcoplasmic reticulum (SR)-mediated Ca^{2+} release (Ca^{2+} waves). Studies utilising specific inhibitors, recombinant protein and RNA interference all demonstrated that this altered SR function was due to cathepsin-L; a cysteine protease produced by *T. brucei* (TbCatL). Experiments utilising a Langendorff perfusion method revealed that trypanosome culture supernatant could induce ventricular premature contractions in 50% of a cohort of *ex vivo* whole rat hearts.

Mechanistic experiments were performed on single isolated cardiomyocytes stimulated at 1.0 Hz and perfused first with control media followed by

trypanosome culture supernatant. The protocol utilised triple caffeine applications: (i) prior to stimulation to empty the SR of Ca^{2+} , (ii) after perfusion with control media and after supernatant to determine the SR Ca^{2+} content and sarcolemmal extrusion of Ca^{2+} following each solution. Results were normalised to a parallel set of cardiomyocytes perfused with control media only as time controls. These experiments revealed a 10-15% increase in SR Ca^{2+} reuptake by the SR Ca^{2+} ATPase (SERCA) but a reduced SR Ca^{2+} content suggesting a concomitant increase in SR-mediated Ca^{2+} leak. This conclusion was supported by the data demonstrating that TbCatL increased Ca^{2+} wave frequency. These effects were abolished by autocamtide-2-related inhibitory peptide (AIP), highlighting a role for Ca^{2+} /calmodulin kinase II (CaMKII) in the TbCatL action on SR function. When cytosolic diastolic Ca^{2+} was measured in cardiomyocytes with SR function inhibited by ryanodine and thapsigargin, trypanosome supernatant prevented a decline in cytosolic diastolic Ca^{2+} that was observed in control media. AIP did not abolish this effect suggesting that TbCatL may raise diastolic Ca^{2+} that could activate CaMKII leading to the observed effects.

These data demonstrated for the first time that African trypanosomes alter cardiac function independent of a systemic immune response *via* a mechanism involving extracellular cathepsin-L-mediated changes in SR function.

Utilising the same (culture adapted and monomorphic) strain of *T. brucei* as the *in vitro* experiments, Lister 427, in a rat model of infection we found no significant increase in the arrhythmia frequency as measured by a 15 min electrocardiogram (ECG). However, when hearts were removed and Langendorff perfused with the addition of isoproterenol the arrhythmia frequency was increased. When the pleomorphic strain *T. b. brucei* TREU 927 was used in rats with continuous ECG recording from biopotential telemetry there was a significant increase in arrhythmia frequency in the infected rats. When hearts were removed and Langendorff perfused with isoproterenol there was a similar increase in arrhythmia frequency as observed with the 427 infected hearts. This suggests that a cardiac dysfunction phenotype is present during trypanosome infections in an animal model providing the basis for future therapeutic work.

The relationship between arrhythmogenic SR-mediated Ca^{2+} release and TbCatL has parallels with endogenous extracellular cathepsin-L (CatL). It has been

demonstrated that a basal level of CatL is necessary for normal cardiac function. However, in coronary heart disease (CHD) CatL levels are increased in the serum of patients correlating with the severity of disease. The effects of raised CatL on cardiac function remain unknown. Work in our lab has identified that *ex vivo* Langendorff perfused hearts that have undergone a 30 min period of ischaemia followed by 90 min reperfusion show greater CatL activity in coronary effluent than hearts perfused without ischaemia. In addition, preliminary data collected in this thesis suggest that human patients that have suffered a myocardial infarction and have undergone reperfusion *via* percutaneous coronary intervention (PCI) showed higher CatL levels in post-reperfusion serum samples compared to pre-reperfusion serum. When severity of heart function in patients (measured as left ventricular volume at systole and diastole, ejection fraction, infarct size and area at risk) was assessed by magnetic resonance imaging (MRI) in a preliminary study, there was a positive correlation with serum CatL levels. Using recombinant CatL on isolated rat ventricular cardiomyocytes it was found that the SR Ca^{2+} content and the stimulated Ca^{2+} transient were significantly reduced in a concentration dependent manner. This suggests a CatL dependent SR dysfunction. This conclusion was supported by an increase in Ca^{2+} wave frequency measured by confocal Ca^{2+} imaging in isolated cardiomyocytes.

The work in this thesis demonstrates a role for both mammalian-derived and exogenous extracellular cathepsin-L proteases in arrhythmogenic SR-mediated Ca^{2+} release.

Table of Contents

The Effects of <i>Trypanosoma brucei</i> and Mammalian-Derived Extracellular Cathepsin-L on Myocardial Function	1
Abstract	2
List of Figures	12
List of Tables	15
Acknowledgements	17
Author's Declaration	19
Definitions/Abbreviations	20
1 CHAPTER 1 - General Introduction	26
1.1 Introduction	27
1.2 What is Trypanosomiasis?.....	28
1.2.1 Lifecycle of <i>Trypanosoma spp.</i>	29
1.2.2 What are Trypanosomes and How do they Function?	30
1.2.3 How do Trypanosomes Survive in the Host?	31
1.2.4 What are the Clinical Features of Trypanosomiasis?	32
1.2.5 How is HAT Diagnosed?.....	38
1.2.6 What are the Current Treatment Strategies?	40
1.2.7 How do Trypanosomes Cross the Blood Brain Barrier	43
1.2.8 Trypanosome Cysteine Proteases	49
1.3 Ca ²⁺ and the Heart.....	50
1.3.1 The Heart	50
1.3.2 The Cardiomyocyte	51
1.3.3 The Cardiac Action Potential	52
1.3.4 The Electrocardiogram.....	54
1.4 Excitation-Contraction Coupling	57
1.4.1 Systole	58
1.4.2 Diastole.....	69
1.5 β -Adrenergic Stimulation	75
1.6 Abnormal Ca ²⁺ Dynamics and Arrhythmias.....	77
1.6.1 Ca ²⁺ Waves	77
1.6.2 Progression to Arrhythmias.....	78
1.6.3 Ca ²⁺ Handling in Heart Failure	80
1.6.4 Ischaemia/Reperfusion Injury	81
1.6.5 Endogenous Cathepsins	85
1.7 Overall Aims	91
2 CHAPTER 2 - General Methods	93
2.1 Trypanosome Culture and Supernatant Preparation	94

2.1.1	Axenic Culture of <i>Trypanosoma brucei brucei</i>	94
2.1.2	Stabilate Preparation	95
2.1.3	Stabilate Thawing.....	96
2.1.4	Preparation of Live Trypanosomes for Experimentation	96
2.1.5	Preparation of Supernatant	96
2.2	Trypanosome Infections - <i>In Vivo</i> ECG Acquisition	97
2.2.1	<i>T. b. brucei</i> Lister 427 Infection Model	97
2.2.2	<i>T. b. brucei</i> TREU 927 Infection Model	101
2.3	Ventricular Cardiomyocyte Isolation	109
2.3.1	Isolation of Adult Rat Left Ventricular Cardiomyocytes	109
2.3.2	Isolation of Adult Rabbit Left Ventricular Cardiomyocytes	113
2.4	Cardiomyocyte Spontaneous Contractile Activity Measurements	113
2.5	Langendorff Perfusion of <i>ex vivo</i> Whole Rat Hearts.....	114
2.5.1	Principles of Langendorff Perfusion	114
2.5.2	System Design and Implementation.....	117
2.5.3	Exclusion Criteria	119
2.5.4	Data Analysis	119
2.6	Measuring Intracellular Calcium.....	121
2.6.1	Ca ²⁺ Fluorophores for LASER-Scanning Confocal Microscopy.....	121
2.6.2	Loading Cardiomyocytes with Fluorophore	123
2.6.3	Disadvantages of Ca ²⁺ Sensitive Fluorophores.....	124
2.6.4	Ratiometric Ca ²⁺ Fluorophores for Epifluorescence Microscopy....	126
2.7	Imaging Ca ²⁺ with LASER-Scanning Confocal Microscopy	128
2.7.1	Principles of Image Collection	128
2.7.2	Spatial and Temporal Resolution.....	129
2.7.3	Image Acquisition	130
2.7.4	Image Analysis.....	131
2.8	Imaging Ca ²⁺ with Ratiometric Epifluorescence Imaging	132
2.8.1	Principles of Epifluorescence Microscopy.....	132
2.8.2	Data Acquisition and Analysis.....	134
2.9	Dissection of <i>T. brucei</i> Mechanism.....	135
2.9.1	Specific Protease Inhibitors	135
2.9.2	Recombinant <i>T. brucei</i> Cathepsin-L	137
2.9.3	RNA Interference of <i>T. brucei</i> Cathepsin-L.....	142
2.10	Statistical Analysis	155
2.10.1	Student's Two-Sample T-Test	155
2.10.2	Student's Paired T-Test	157
2.10.3	ANOVA and Multiple Linear Regression	158

3	CHAPTER 3 - The Effects of <i>Trypanosoma brucei</i> on Isolated Cardiomyocytes and Whole Hearts	161
3.1	Introduction	162
3.1.1	African Trypanosomiasis	162
3.1.2	Cardiac Involvement in HAT	162
3.1.3	Trypanosome Secreted Factor Affects Ca ²⁺ Signalling in a Blood Brain Barrier Model.....	163
3.1.4	Ca ²⁺ in the Cardiomyocyte	163
3.1.5	Aims.....	164
3.2	Methods	165
3.2.1	Adult Cardiomyocyte Isolation.....	165
3.2.2	Preparation of Trypanosomes, Media and Supernatant.....	165
3.2.3	Light Microscopy-Based Spontaneous Contractile Activity Measurements.....	165
3.2.4	Confocal Fluorescence-Based [Ca ²⁺] _i Measurements	166
3.2.5	Field Stimulation and Fluorescence-Based [Ca ²⁺] _i Measurements ..	167
3.2.6	RNA Interference of <i>Trypanosoma brucei</i> cathepsin L.....	167
3.2.7	Langendorff Perfusion of <i>Ex Vivo</i> Adult Rat Hearts	169
3.2.8	Statistical Analysis.....	170
3.3	Results.....	171
3.3.1	Trypanosomes Increase Ca ²⁺ Wave Frequency in Cardiomyocytes .	171
3.3.2	Contractile Event Frequency Increase Abolished by Heating	172
3.3.3	Ca ²⁺ Wave Velocity and Frequency are Increased by Trypanosome Culture Supernatant	173
3.3.4	Supernatant Increases the Rate of Stimulated Ca ²⁺ Transient Decline 175	
3.3.5	The Effects of Supernatant on the stimulated Ca ²⁺ Transient During B-adrenergic Stimulation.....	176
3.3.6	Ca ²⁺ Waves are Reduced by Cathepsin-L Inhibition but not Cathepsin-B Inhibition	179
3.3.7	Recombinant TbCatL Increases Ca ²⁺ Wave Frequency	180
3.3.8	Ca ²⁺ Waves are Reduced by RNA Interference of TbCatL	181
3.3.9	Supernatant Can Cause Arrhythmic Events in Whole Hearts.....	182
3.3.10	Arrhythmic Events Occurred in a Proportion of Hearts	184
3.3.11	QT Interval Was Not Affected	185
3.4	Discussion	187
3.4.1	Trypanosomes Increase Ca ²⁺ Wave Frequency in Cardiomyocytes .	187
3.4.2	Ca ²⁺ Wave Velocity and Frequency are Increased by Trypanosome Culture Supernatant	188
3.4.3	Supernatant Increases the Rate of Stimulated Ca ²⁺ Transient Decline 188	

3.4.4	The Effects of Supernatant on the Stimulated Ca ²⁺ Transient During B-adrenergic Stimulation.....	190
3.4.5	Ca ²⁺ Waves are Reduced by Cathepsin-L Inhibition but not Cathepsin-B Inhibition	190
3.4.6	Recombinant Cathepsin-L Increases Ca ²⁺ Wave Frequency	191
3.4.7	Ca ²⁺ Waves are Reduced by RNA Interference of TbCatL	191
3.4.8	Supernatant Can Cause Arrhythmic Events in Whole Hearts.....	192
3.4.9	Arrhythmic Events Occurred in a Proportion of Hearts	194
3.5	Conclusions	194
4	CHAPTER 4 - Investigating the Mechanisms of Arrhythmogenic Sarcoplasmic Reticulum-Mediated Ca ²⁺ Release Caused by <i>Trypanosoma brucei</i>	195
4.1	Introduction	196
4.1.1	Trypanosomes and Intracellular Ca ²⁺	196
4.1.2	African Trypanosomes and [Ca ²⁺] _i in the Heart	196
4.1.3	Mechanisms to Explore.....	197
4.1.4	Aims of the Chapter	197
4.2	Methods	199
4.2.1	Adult Rat Cardiomyocyte Isolation.....	199
4.2.2	Preparation of Control Media and Supernatant.....	199
4.2.3	Normal Extracellular Ca ²⁺ Epifluorescence Measurements.....	199
4.2.4	Low Extracellular Ca ²⁺ Epifluorescence Measurements.....	200
4.2.5	First Post-Caffeine Ca ²⁺ Transient Analysis	201
4.2.6	Fractional Shortening Measurements	201
4.2.7	Epifluorescence Measurements of Diastolic [Ca ²⁺] _i During SR Inhibition	202
4.2.8	Spontaneous Contractile Event Measurement in Isolated Cardiomyocytes With H-89 and AIP.....	202
4.2.9	Epifluorescence Measurements with CaMKII Inhibition	202
4.2.10	Statistical Analysis	203
4.3	Results.....	204
4.3.1	Supernatant Increased the Decay Rate Constant of the Stimulated Ca ²⁺ Transient.....	204
4.3.2	Supernatant Reduces the SR Ca ²⁺ Content.....	206
4.3.3	Myofilament Ca ²⁺ Sensitivity	208
4.3.4	Supernatant Increases Diastolic [Ca ²⁺] _i via a Non-SR Dependent Route	210
4.3.5	Supernatant Does Not Likely Alter the L-Type Ca ²⁺ Channel	210
4.3.6	Supernatant Alteration of SR Function is CaMKII Dependent	211
4.3.7	Supernatant Effects on Ca ²⁺ Handling with CaMKII Inhibition	212
4.4	Discussion	215
4.4.1	Supernatant Effects on SR Function	215

4.4.2	Supernatant Does Not Alter Myofilament Ca^{2+} Sensitivity.....	217
4.4.3	Effects of Supernatant on Diastolic $[\text{Ca}^{2+}]_i$	218
4.4.4	Increase in Spontaneous Ca^{2+} Release Caused by Supernatant is Prevented by CaMKII Inhibition	220
4.4.5	CaMKII Inhibition Prevents Supernatant Effects on SR Function ...	221
4.4.6	CaMKII Inhibition Does Not Reduce Diastolic $[\text{Ca}^{2+}]_i$	221
4.4.7	Proposed Mechanism	222
5	CHAPTER 5 - Investigating the Cardiovascular Effects of <i>Trypanosoma brucei</i> Using an <i>In Vivo</i> Infection Model in Rats	224
5.1	Introduction	225
5.1.1	Trypanosomiasis and the Heart.....	225
5.1.2	Electrocardiographic Findings	225
5.1.3	Aims of the Chapter	226
5.2	Methods	228
5.2.1	<i>T. b. brucei</i> Lister 427 Infections	228
5.2.2	<i>T. b. brucei</i> TREU 927 Infections.....	231
5.3	Results.....	234
5.3.1	<i>In Vivo</i> ECG Parameters for <i>T. b. brucei</i> Lister 427 Infection	234
5.3.2	<i>Ex Vivo</i> Langendorff Perfused Heart Pseudo-ECG Parameters for <i>T. b. brucei</i> Lister 427 Infection.....	237
5.3.3	<i>In Vivo</i> ECG Parameters for <i>T. b. brucei</i> TREU 927 Infection.....	240
5.3.4	<i>Ex Vivo</i> Langendorff Perfused Heart Pseudo-ECG Parameters for <i>T. b. brucei</i> TREU 927 Infection	244
5.3.5	<i>T. b. brucei</i> TREU 927 Infected <i>Ex Vivo</i> Hearts Show Increased Frequency of Arrhythmias in the Presence of Isoproterenol	247
5.3.6	Organ Mass Data	249
5.4	Discussion	252
5.4.1	<i>In Vivo</i> ECGs for <i>T. b. brucei</i> Lister 427 Infection	252
5.4.2	<i>Ex Vivo</i> Langendorff Perfused Heart Pseudo-ECGs for <i>T. b. brucei</i> Lister 427 Infection	254
5.4.3	<i>In Vivo</i> ECGs for <i>T. b. brucei</i> TREU 927 Infection	256
5.4.4	<i>T. b. brucei</i> TREU 927 Infections Exhibit Greater Arrhythmia Frequency than Lister 427 Infections	257
5.4.5	<i>Ex Vivo</i> Langendorff Perfused Heart Pseudo-ECGs for <i>T. b. brucei</i> TREU 927 Infection.....	258
5.4.6	<i>T. b. brucei</i> TREU 927 Infected <i>Ex Vivo</i> Hearts Show Increased Frequency of Arrhythmias	259
5.4.7	Organ Mass.....	260
5.4.8	A Role For Cathepsin-L In HAT.....	261
6	CHAPTER 6 - The Cardiac Effects of Endogenous Extracellular Cathepsin-L	263

6.1	Introduction	264
6.1.1	Cathepsins	264
6.1.2	Cathepsins in the Heart.....	264
6.1.3	Ischaemia/Reperfusion Injury and Heart Failure	266
6.1.4	Aims of the Chapter	268
6.2	Methods	269
6.2.1	Fluorometric Enzyme Activity Assays.....	269
6.2.2	Cardiomyocyte Isolations.....	270
6.2.3	Epifluorescence Measurements of the Field Stimulated Ca ²⁺ Transient 271	
6.2.4	Confocal Imaging of Spontaneous SR-mediated Ca ²⁺ Release.....	272
6.2.5	Langendorff Perfusion Global Ischaemia/Reperfusion.....	273
6.2.6	Enzyme-Linked Immunosorbent Assay of Human Serum.....	273
6.2.7	Cardiac Magnetic Resonance Imaging	274
6.2.8	Statistical Analysis.....	274
6.3	Results.....	275
6.3.1	Mammalian Cathepsin-L is Active at Physiological pH	275
6.3.2	Cathepsin-L Can be Detected in Coronary Effluent from Ischaemic Hearts 276	
6.3.3	Cathepsin-L is Increased in Serum of Human Patients That Have Undergone Reperfusion Following Myocardial Infarction	277
6.3.4	Serum Cathepsin-L Levels Correlate With Severity of Cardiac Dysfunction Measured by MRI.....	278
6.3.5	Cathepsin-L Reduces Stimulated Ca ²⁺ Transient Amplitude in Rat Left Ventricular Cardiomyocytes	280
6.3.6	Cathepsin-L Reduces SR Ca ²⁺ Content in Rat Left Ventricular Cardiomyocytes.....	281
6.3.7	Cathepsin-L Reduces Stimulated Ca ²⁺ Transient Amplitude in Rabbit Left Ventricular Cardiomyocytes	282
6.3.8	Cathepsin-L Reduces SR Ca ²⁺ Content in Rabbit Left Ventricular Cardiomyocytes.....	284
6.3.9	Cathepsin-L Increases Ca ²⁺ Wave Frequency in Resting Cardiomyocytes.....	285
6.4	Discussion	287
6.4.1	Mammalian Cathepsin-L is Active at Physiological pH	287
6.4.2	Cathepsin-L is Detected in Coronary Effluent from Ischaemia/Reperfusion Hearts	288
6.4.3	Cathepsin-L is Increased in Serum of Human Patients That Have Undergone Reperfusion Following Myocardial Infarction	289
6.4.4	Cathepsin-L Effects on Ca ²⁺ Handling in Rat Left Ventricular Cardiomyocytes.....	290

6.4.5	Cathepsin-L Effects on Ca ²⁺ Handling in Rabbit Left Ventricular Cardiomyocytes.....	293
6.4.6	Cathepsin-L Increases Ca ²⁺ Wave Frequency in Resting Cardiomyocytes.....	294
6.4.7	Conclusions	296
7	CHAPTER 7 - Conclusions.....	297
7.1	Study Rationale	298
7.2	The Effects of <i>T. b. brucei</i> on the Heart at the Cardiomyocyte and Whole Organ Level	299
7.3	The Mechanisms of SR-Mediated Ca ²⁺ Release Caused by <i>T. b. brucei</i> .	301
7.4	<i>In Vivo</i> Model of Infection and the Cardiac Effects of <i>T. b. brucei</i>	303
7.5	The Cardiac Effects of Endogenous Extracellular Cathepsin-L	304
7.6	Final Conclusions.....	305
8	References.....	308

List of Figures

Figure 1.1: Lifecycle of African trypanosomes.....	30
Figure 1.2: Schematic representation of bloodstream form <i>T. brucei</i> from International Laboratory for Research on Animal Diseases with permission ⁽¹⁴⁾ ...	31
Figure 1.3: Tsetse Belt in Africa.....	33
Figure 1.4: WHO reported cases of HAT.	35
Figure 1.5: Photomicrograph of Giemsa stained <i>T. b. gambiense</i>	39
Figure 1.6: Schematic drawing of the layers of the blood brain barrier.....	44
Figure 1.7: Cysteine protease activity from <i>T. brucei spp.</i>	46
Figure 1.8: Ca ²⁺ oscillations of HBMECs.	47
Figure 1.9: Proposed model for African trypanosome-induced BBB dysfunction .	48
Figure 1.10: Ultrastructure of the cardiomyocyte.	51
Figure 1.11: Ventricular cardiomyocyte action potential.	53
Figure 1.12: Sino-atrial node pacemaker action potential.....	54
Figure 1.13: Schematic of the conduction system of the heart.	55
Figure 1.14: The ECG in relation to cardiac polarity (taken from rat).....	56
Figure 1.15: Ca ²⁺ dynamics during systole.	58
Figure 1.16: Ca ²⁺ requirements for contractile activation.	60
Figure 1.17: Voltage dependence of I _{Ca} , Ca ²⁺ transient amplitude, contraction and charge movement in isolated guinea-pig ventricular cardiomyocytes.	62
Figure 1.18: Ca ²⁺ activation of the myofilaments.	68
Figure 1.19: Ca ²⁺ dynamics during diastole.....	70
Figure 1.20: SERCA Ca ²⁺ transport.	72
Figure 1.21: Schematic of PLB-SERCA Interaction.....	73
Figure 1.22: NCX Ca ²⁺ transport in forward mode.	74
Figure 1.23: β-adrenergic signalling in the cardiomyocyte.	76
Figure 1.24: Mediators of Reperfusion Injury	83
Figure 1.25: The cathepsin cysteine proteases expressed in cardiovascular cells.	89
Figure 2.1: Counting trypanosomes with a Neubauer Improved Haemocytometer.	95
Figure 2.2: Photographs of the infected rat ECG acquisition.....	99
Figure 2.3: Chart and tables for estimating trypanosome parasitaemia.....	100
Figure 2.4: Photographs of the steps of the telemetry probe implantation procedure.	108
Figure 2.5: Photographs of rat heart removal and cannulation.	110
Figure 2.6: Langendorff perfusion of the heart.....	111
Figure 2.7: Photomicrographs of isolated cardiomyocytes.....	112
Figure 2.8: Langendorff system.	118
Figure 2.9: Measurable ECG parameters.	120
Figure 2.10: ECG recording of a rat heart with VPC.	121
Figure 2.11: Schematic of fluorescence.....	122
Figure 2.12: Emission spectrum for fluo-3.....	123
Figure 2.13: Diagram of differences in resting fluorescence signals due to different path lengths.....	126
Figure 2.14: Emission spectrum for Fura-2.	127
Figure 2.15: Emission spectrum for Fura-4F.....	127
Figure 2.16: Principles of LASER-scanning confocal microscopy	129
Figure 2.17: Line-scan confocal imaging.....	131
Figure 2.18: Epifluorescence imaging.	133
Figure 2.19: Structure and binding of K11777.....	136

Figure 2.20: Structure and binding of CA074.....	137
Figure 2.21: Schematic of a fluorogenic activity assay.....	138
Figure 2.22: Activity assays and cardiomyocyte population assay to test activating quantity of DTT for TbCatL.	140
Figure 2.23: The RNAi pathway in Trypanosomatids.....	143
Figure 2.24: Synthesis of cDNA by reverse transcription.	146
Figure 2.25: Amplification of template DNA by PCR:	150
Figure 2.26: Amplification plot and melting curve examples.	154
Figure 2.27: Sample calculations using $2^{-\Delta\Delta Ct}$ method.	155
Figure 2.28: Normality distribution plots for media and supernatant.....	157
Figure 2.29: Residual plot for RNAi example data.....	159
Figure 2.30: Output tables for RNAi example data from SPSS software.	160
Figure 3.1: Mean percentage of cells waving.	172
Figure 3.2: Percentage change in cells exhibiting spontaneous contractile events in heated supernatant.	173
Figure 3.3: Confocal imaging of spontaneous contractile events using Fluo-3AM loaded cardiomyocytes.	174
Figure 3.4: Stimulated (1.0 Hz) epifluorescent imaging of Ca^{2+} transients with Fura-4F AM.....	176
Figure 3.5: Stimulated (1.0 Hz) epifluorescent imaging of Ca^{2+} transients with 100 nM isoproterenol (ISO).	178
Figure 3.6: Percentage change in spontaneous contractile events with inhibitors and recombinant protein.	180
Figure 3.7: RNA interference (RNAi) of <i>T. brucei</i> cathepsin L (TbCatL).	182
Figure 3.8 ECG data from <i>ex vivo</i> perfused rat hearts.....	184
Figure 3.9: QT intervals from <i>ex vivo</i> whole rat hearts perfused with media and supernatant.	186
Figure 4.1: Spontaneous contractile events in low and normal $[Ca^{2+}]_o$	201
Figure 4.2: Stimulated Ca^{2+} transients at low and physiological extracellular Ca^{2+}	206
Figure 4.3: Caffeine-induced Ca^{2+} transient parameters at low and normal extracellular Ca^{2+}	208
Figure 4.4: Fractional shortening of cardiomyocytes.	209
Figure 4.5: Diastolic $[Ca^{2+}]_i$ measurements with an inhibited SR.	210
Figure 4.6: First post-caffeine Ca^{2+} amplitude at low and normal extracellular Ca^{2+}	211
Figure 4.7: Percentage change in spontaneous contractile events with AIP or H89.	212
Figure 4.8: Supernatant effects on Ca^{2+} parameters with AIP.....	214
Figure 4.9: Proposed mechanism for TbCatL on Ca^{2+} handling in the ventricular cardiomyocyte.....	223
Figure 5.1: <i>In vivo</i> ECG parameters for <i>T. b. brucei</i> Lister 427 infection.	236
Figure 5.2: <i>Ex vivo</i> Langendorff ECG parameters for <i>T. b. brucei</i> Lister 427 infection.....	239
Figure 5.3: Parasitaemia levels for infection models.	241
Figure 5.4: <i>In vivo</i> ECG parameters for <i>T. b. brucei</i> TREU 927 infection.	243
Figure 5.5: <i>Ex vivo</i> Langendorff ECG parameters for <i>T. b. brucei</i> TREU 927 infection.....	246
Figure 5.6: Arrhythmic events in Langendorff perfused infected and control hearts.	248
Figure 5.7: Organ mass data for <i>T. b. brucei</i> Lister 427 infection model.	250
Figure 5.8: Organ mass data for <i>T. b. brucei</i> TREU 927 infection model.....	251

Figure 6.1: Fluorometric activity assay of recombinant mouse CatL at different pH.	275
Figure 6.2: CatL activity in coronary effluent samples from ischaemia/reperfusion hearts	277
Figure 6.3: Serum concentration of CatL in human patients following myocardial infarction.....	278
Figure 6.4: Serum CatL vs. MRI parameters.	279
Figure 6.5: Stimulated Ca ²⁺ transients at different CatL concentrations.	281
Figure 6.6: Caffeine-induced Ca ²⁺ transients at different CatL concentrations.	282
Figure 6.7: Stimulated Ca ²⁺ transients with CatL in rabbit left ventricular cardiomyocytes.	284
Figure 6.8: Caffeine-induced Ca ²⁺ transients in rabbit cardiomyocytes with CatL.	285
Figure 6.9: Confocal images of unstimulated cardiomyocytes.	286
Figure 7.1: Proposed mechanism for TbCatL action on cardiomyocyte Ca ²⁺ handling.	306

List of Tables

Table 1.1: Standard treatment options for HAT and main adverse reactions. ...	43
Table 1.2: Clan C1A cysteine proteases.....	86
Table 2.1: Exclusion criteria for Langendorff perfusion of mice, rats and rabbits	119
Table 2.2: Reverse Transcription Reaction Components	147
Table 2.3: Components and functions of a PCR reaction.....	148
Table 2.4: Formulae for ANOVA statistical analysis	158
Table 2.5: Formulae for dummy indicators for each incubation solution	158
Table 5.1: ECG findings in patients with HAT	226
Table 5.2: <i>T. b. brucei</i> Lister 427 <i>ex vivo</i> Langendorff raw parameters.....	237
Table 5.3: <i>T. b. brucei</i> TREU 927 <i>ex vivo</i> Langendorff raw parameters	244

In Loving Memory of My Grandfather, Dr. John R. Anderson

He was there for the beginning of this journey, but sadly missed the end. I am certain he is proud of the achievement.

Acknowledgements

I would like to thank both my supervisors. Firstly, thanks go to Dr. Chris Loughrey for all the advice and support in the field of cardiovascular physiology. He has helped me develop the analytical abilities, critical thinking and healthy scepticism of a scientist after my clinical training as a veterinary surgeon. Secondly, thanks go to Dr. Liam Morrison for a calming relaxed influence and alternative viewpoint enabling me to keep an open mind. Also great thanks for invaluable advice in the field of parasitology. It is a unique challenge combining two disparate fields, but Liam has been of great help in this.

Throughout the course of the project there have been several people who have contributed either in support and advice or as physical contributions to the work. Dr. Elspeth Elliott performed some of the preliminary work that helped give me a running start in the trypanosome work and shared joint first authorship with me on the paper arising from these chapters. She was also very helpful in getting me settled into the lab at the beginning before I took over running the lab when she left. Thanks especially to Caron Hawksby, our technician, for some technical assistance but primarily for support in my more frustrated moments! Thanks go to the parasitologists for contributions in time and advice as well as including me in social activities; Nath Jones, Jane Munday and Anne Donachie as well as the rest of the Wellcome Trust Centre for Molecular Parasitology people. Finally, thanks should go to the students whom I have had the fortune to supervise throughout the course of my PhD and have contributed some of the data; Katrin Nather, Karen Dunbar, Amanda Panissidi, Helen Heathcoate and Charlotte Rossor.

A PhD is not only about the research but also about forming friendships and contacts so some special thanks to the old friends from whom I have had support and encouragement; Mark Naguib and Liam Reid from my vet school days as well as Emily Cope, Liam's partner who has become a good friend. Also Christina and Richard Gill my good friends from my Liverpool internship, without whom I would not have had a weekend retreat during the times of failure and frustration. Particular acknowledgement should go to the new friends that will hopefully become old friends that I carry throughout my life; Allen Kelly my flatmate for some of the time as well as previous student in our lab so had some

vital advice supervisors may not always provide! Thanks to Caroline who joined our lab in my second year and has been good fun along with her partner Allan for plenty of evenings of board games and wine! In addition thanks to Annabel and Omar for the hosting of many an event as well as the rest of the Godfrey Smith group for being inclusive in many social (and scientific) functions.

Finally, I would like to thank my parents for their support throughout these last three years.

Financial support gratefully received from the BBSRC.



Author's Declaration

The work presented in this thesis is my own work except where acknowledged in the text and has not been presented as part of any other degree. Some of the data in this thesis has been published in paper or abstract form as detailed below:

*Joint First Author

E.B. Elliott^{†*}, D. McCarroll^{†*}, H. Hasumi, C.E. Welsh, A.A. Panissidi, N.G. Jones, C.L. Rossor, A. Tait, G.L. Smith, J.C. Mottram, L.J. Morrison[†] and C.M. Loughrey[†]. *Trypanosoma brucei* cathepsin-L increases arrhythmogenic sarcoplasmic reticulum-mediated calcium release in rat cardiomyocytes. *Cardiovascular Research* (2013) 100: 325-335

D. McCarroll, E.B. Elliott, N.G. Jones, C.E. Walls, J.C. Mottram, L.J. Morrison and C.M. Loughrey. Trypanosome cathepsin-L increases calcium waves in cardiomyocytes. Abstract - British Society of Parasitology Spring Meeting, Strathclyde (2011) P158: 190

D. McCarroll, E.B. Elliott and C.M. Loughrey. Extracellular cathepsin-L alters spontaneous and triggered sarcoplasmic reticulum-mediated calcium release in adult rat cardiomyocytes. Abstract - Physiological Society Meeting, Edinburgh (2012) *Proceedings of the Physiological Society* 27 PC192

D. McCarroll, E.B. Elliott, K. Nather, L.J. Morrison and C.M. Loughrey. Extracellular cathepsin-L alters spontaneous and triggered sarcoplasmic reticulum-mediated calcium release in adult rat and rabbit cardiomyocytes. Abstract - Biophysical Society 57th Annual Meeting, Philadelphia (2013) *Biophysical Journal* 104(2) pp. 436a

Definitions/Abbreviations

$[Ca^{2+}]_i$	Intracellular calcium ion concentration
$[Ca^{2+}]_o$	Extracellular calcium ion concentration
$[Ca^{2+}]_{SR}$	Sarcoplasmic reticulum calcium ion concentration
AAT	Animal African trypanosomiasis
AC	Adenylyl cyclase (forms cAMP from AMP)
AGO1	Argonaute 1 (RNAi pathway enzyme)
AIP	Autocamtide-2-related inhibitory peptide (inhibits CaMKII)
AJ	Adherens junction
AM	Acetoxymethyl ester (fluorophore loading)
AMC	7-amido-4-methyl-coumarin (fluorescent moiety of enzyme substrate)
ANOVA	Analysis of variance (statistical test)
AP	Action potential
Ar	Argon
Arg	Arginine (amino acid)
ATP	Adenosine triphosphate
AV	Atrio-ventricular
B	Change in fluorescence between zero and saturating $[Ca^{2+}]$ at 380 nm
BBB	Blood brain barrier
BCA	Bicinchoninic acid
BSA	Bovine serum albumin
CA074	L-3-trans-(propylcarbonyl)oxirane-2-carbonyl-L-isoleucyl-L-proline (Cathepsin B inhibitor)
Ca^{2+}	Calcium ion
CAA0225	(2S,3S)-oxirane-2,3-dicarboxylic acid 2-(((S)-1-benzylcarbonyl-2-phenyl-ethyl)-amide) 3-{[2-(4-hydroxy-phenyl)-ethyl]-amide} (Cathepsin L inhibitor)
$CaCl_2$	Calcium chloride
CaM	Calmodulin
CaMKII	Calcium calmodulin kinase II
cAMP	3'-5'-cyclic adenosine monophosphate
CatL	Cathepsin-L
CATT	Card agglutination test for trypanosomiasis
CBSS	Carter's balanced salt solution
CCD	Charge coupled device
cDNA	Complementary DNA
CHD	Coronary heart disease
CICR	Calcium induced calcium release
CNS	Central nervous system

CO ₂	Carbon dioxide
CPVT	Catecholaminergic polymorphic ventricular tachycardia
CSF	Cerebrospinal fluid
C _t	Cycle threshold
CysC	Cystatin C
Δ	Change in ...
d[Ca ²⁺] _i /dt _{max}	Maximum rate of [Ca ²⁺] _i rise
d[Ca ²⁺] _i /dt _{min}	Maximum rate of [Ca ²⁺] _i decline
DAD	Delayed after depolarisation
DNA	Deoxyribonucleic acid
dNTP	DNA bases (A, adenine; C, cytosine; G, guanine; T, thymine)
dsRNA	Double stranded ribonucleic acid
DTT	Dithiothreitol
E-64	(1S,2S)-2-(((S)-1-((4-Guanidinobutyl)amino)-4-methyl-1-oxopentan-2-yl)carbonyl)cyclopropanecarboxylic acid (Protease inhibitor)
EAD	Early after depolarisation
E _{Ca}	Equilibrium potential of calcium ion
ECC	Excitation contraction coupling
ECG	Electrocardiogram
ECM	Extracellular matrix
EDTA	Ethylene diamine tetraacetic acid
EGTA	Ethylene glycol tetraacetic acid
ELISA	Enzyme-linked immunosorbent assay
E _m	Membrane potential
E _{Na}	Equilibrium potential of sodium ion
F/F ₀	Fluorescence over minimum fluorescence
FKBP	FK-506 binding protein
Fluo-3	Calcium ion binding fluorophore
Fura-2	Ratiometric calcium ion binding fluorophore
Fura-4F	Ratiometric calcium binding fluorophore
g	Gravity, force unit
g	Grams, mass unit
GJNH	Golden Jubilee National Hospital
GPCR	G-protein coupled receptor
GPI	Glycophosphatidylinositol
GTP	Guanosine triphosphate
H ⁺	Hydrogen ion (proton)
H ₀	Null hypothesis
H ₁	Test hypothesis
H-89	N-[2-(p-bromocinnamylamino)ethyl]-5-iso-quinolinesulphonamide (PKA inhibitor)

HAT	Human African trypanosomiasis
HBMEC	Human brain microvascular endothelial cell
HCl	Hydrochloric acid
HCO ₃ ⁻	Bicarbonate
HEPES	2-[4-(2-hydroxyethyl)piperazin-1-yl]ethanesulfonic acid
HF	Heart failure
HMI-9	Trypanosome growth media
hr	Hour, time unit
Hz	Hertz, frequency unit
I/R	Ischaemia/reperfusion
IC ₅₀	Concentration of compound at which there is 50% inhibition of target
I _{Ca}	Calcium ion current
I _{Ca L}	L-type calcium ion current
I _{Ca T}	T-type calcium ion current
I _f	Funny current
IFN γ	Interferon gamma
IgG	Immunoglobulin G
I _{K1}	Inwardly rectifying potassium ion current
I _{Kr}	Rapid outwardly rectifying potassium ion current
I _{Ks}	Slow outwardly rectifying potassium ion current
I _{Kto}	Transient outward potassium ion current
I _{Kur}	Ultra-rapid outwardly rectifying potassium ion current
IL-1	Interleukin 1
IL-10	Interleukin 10
IMDM	Iscove's modified Dulbecco's medium
I _{Na}	Sodium ion current
I _{Na/Ca}	Sodium/calcium ion exchanger current
IP ₃	Inositol triphosphate
IP ₃ R	Inositol triphosphate receptor
ISO	Isoproterenol
JTV519	1,4-benzothiazepine based calcium ion channel blocking drug
K ⁺	Potassium ion
K11777	N-methyl-piperazine-Phe-homoPhe-vinylsulfone-phenyl (Cathepsin L inhibitor)
KCl	Potassium chloride
K _d	Dissociation constant
kDa	Kilo Dalton, protein mass
K _m	Affinity constant
K _{SERCA}	SERCA activity
L	Litre, volume unit
L/L ₀	Length over minimum length

λ	Wavelength
LAMP	Loop-mediated isothermal amplification of DNA
LASER	Light amplification by stimulated emission radiation
Leu	Leucine (amino acid)
LSCM	LASER scanning confocal microscopy
LTCC	L-type calcium channel
M	Molar, concentration unit
MES	2-(<i>N</i> -morpholino)ethanesulfonic acid
$MgCl_2 \cdot 6H_2O$	Magnesium chloride hexahydrate
$MgSO_4 \cdot 7H_2O$	Magnesium sulphate heptahydrate
MI	Myocardial infarction
MIKH	Modified isolation Krebs-Henseleit solution
min	Minute, time unit
ml	Millilitre, volume unit
MLCK	Myosin light chain kinase
MLP	Muscle LIM protein
MPTP	Mitochondrial permeability transition pore
MRI	Magnetic resonance imaging
mRNA	Messenger ribonucleic acid
ms	Millisecond, time unit
mV	Millivolt, potential difference unit
NA	Numerical aperture, lens curvature unit
Na^+	Sodium ion
NaCl	Sodium chloride
NaH_2PO_4	Sodium dihydrogen orthophosphate
$NaHCO_3$	Sodium bicarbonate
NaOAc	Sodium acetate
NaOH	Sodium hydroxide
NCX	Sodium/calcium ion exchanger
NECT	Nifurtimox-eflornithine combination therapy
nM	Nanomolar, concentration unit
NO	Nitric oxide
NTC	No template control
NT-proBNP	N-terminal prohormone of brain natriuretic peptide
O_2	Oxygen gas
$^{\circ}C$	Degrees Celsius, temperature unit
<i>P</i>	Probability
pA	Picoampere, current unit
PAR-2	Protease activate receptor 2
PCI	Percutaneous coronary intervention
PCR	Polymerase chain reaction
Phe	Phenylalanine (amino acid)

PKA	Protein kinase A
PKC	Protein kinase C
PLB	Phospholamban
PLC	Phospholipase C
PMCA	Plasma membrane calcium ion ATPase pump
PMT	Photo multiplier tube
P_o	Open probability
P-R	Time interval from beginning of ECG P wave to beginning of Q
PTx	Pertussis sensitive toxin
QRS	Time interval from beginning of Q to end of S wave of ECG
qRT-PCR	Quantitative real-time polymerase chain reaction
QT	Time interval from beginning of Q to end of T wave on ECG
QT ₅₀	Time interval from beginning of Q to 50% return to baseline of T wave on ECG
QT ₉₀	Time interval from beginning of Q to 90% return to baseline of T wave on ECG
QTc	Time interval from beginning of Q to end of T wave on ECG corrected for heart rate
RCF	Relative centrifugal force
RISK	Reperfusion injury salvage kinase
R_{max}	Fluorescence ratio at saturatingly high $[Ca^{2+}]_i$
rmCatL	Recombinant mouse cathepsin-L
R_{min}	Fluorescence ratio at minimal $[Ca^{2+}]_i$
R_n	Normalised fluorescence of reporter dye (quantitative real-time polymerase chain reaction)
RNA	Ribonucleic acid
RNAi	Ribonucleic acid interference
RNS	Reactive nitrogen species
ROS	Reactive oxygen species
RQ	Relative quantity
RT	Reverse transcriptase
RyR	Ryanodine receptor
s	Second, time unit
SA	Sino-atrial
SAPO	Specified Animal Pathogens (Scotland) Order
SEM	Standard error of the mean
Ser	Serine (amino acid)
SERCA	Sarco (endo)plasmic reticulum calcium ion ATPase channel
siRNA	Small interfering ribonucleic acid
SN	Supernatant
SR	Sarcoplasmic reticulum
ssRNA	Single stranded ribonucleic acid

Stage I	Haemolympathic stage of trypanosomiasis
Stage II	Meningoencephalitic stage of trypanosomiasis
STEMI	ST elevated myocardial infarction
τ	Constant of decay (time taken to decay to 1/e)
<i>T. b. brucei</i>	Strain of <i>Trypanosoma brucei brucei</i>
GVR35	
<i>T. b. brucei</i>	Strain of <i>Trypanosoma brucei brucei</i>
Lister 427	
<i>T. b. brucei</i>	Strain of <i>Trypanosoma brucei brucei</i>
TREU 927	
<i>T. b.</i>	Strain of <i>Trypanosoma brucei rhodesiense</i>
<i>rhodesiense</i>	
IL1825	
TbCatB	<i>Trypanosoma brucei</i> derived cathepsin B
TbCatL	<i>Trypanosoma brucei</i> derived cathepsin L
<i>TbCatL</i>	<i>Trypanosoma brucei</i> derived cathepsin L gene
TcoCatB	<i>Trypanosoma congolense</i> derived cathepsin B
TcoCatL	<i>Trypanosoma congolense</i> derived cathepsin L
TcrCatB	<i>Trypanosoma cruzi</i> derived cathepsin B
TcrCatL	<i>Trypanosoma cruzi</i> derived cathepsin L
Θ	Half the angle of the collection cone of a lens
Thr	Threonine (amino acid)
TJ	Tight junction
TLF	Trypanosome lytic factor
T_m	Melting point - temperature at which dsDNA denatures into two separate strands of DNA
TnC	Troponin C
TNF α	Tumour necrosis factor α
TnI	Troponin I
TRIS	tris(hydroxymethyl)aminomethane
TSF	Trypomastigote soluble fraction
T-tubule	Transverse tubule
μL	Microlitre, volume unit
μM	Micromolar, concentration unit
μm	Micrometre, length unit
VF	Ventricular fibrillation
VPC	Ventricular premature complex
VSG	Variable surface glycoprotein
VT	Ventricular tachycardia
WHO	World health organisation
WO	Washout

1 CHAPTER 1 – General Introduction

1.1 Introduction

In a multicellular organism it is important to deliver oxygen and nutrients to all the cells of all the tissues and organs of the organism that cannot be achieved by diffusion alone. The nutrient rich media or blood must be delivered somehow to an organism's tissues. The solution of millions of years of evolution is a muscular pump pushing blood through a circulatory system. In mammals this is achieved by the four-chambered muscular heart. The heart is a syncytium of contractile cells that under normal circumstances work together to contract synchronously to deliver the vital nutrient and oxygen rich blood to the tissues. In order for this to happen a series of events occur from electrical depolarisation of pacing cells spreading to the contractile cells resulting in mechanical work and the heart beat. This is achieved by a secondary messenger of calcium ions (Ca^{2+}). A series of channels and pumps within the contractile cells or cardiomyocytes enables the continual cycling of Ca^{2+} from the extracellular space into the cardiomyocyte, induction of Ca^{2+} release from intracellular stores, activation of the contractile myofilaments within the cardiomyocyte that constitutes the shortening of the cell or systole. The Ca^{2+} is then recycled in the same quantities in an elegant balance of fluxes back into the intracellular store and the extracellular space by channels and pumps constituting the relaxation of the cell or diastole. This cycle must continue without fatigue for the duration of the organism's life with the ability to adapt to the ever changing environment an animal encounters from rest and relaxation to emergency activity when chasing prey or escaping predators.

When this delicate balance of Ca^{2+} fluxes goes astray, the result can be disastrous with dysynchrony of the heart beat as arrhythmias and failure of contraction. This leads to failure of the pump and insufficient delivery of blood to the tissues. There are many known causes of disruption to the Ca^{2+} flux balance of the cardiomyocyte and heart as a whole but equally many unknown and in hitherto unexplored potential sources of Ca^{2+} signalling dysfunction. One such unexplored source is African trypanosomiasis which will be investigated in this thesis. This work has also led to interesting parallels in known causes of Ca^{2+} signalling dysfunction such as ischaemia/reperfusion (I/R) injury, which will also be explored. This chapter will discuss the literature in the context of African trypanosomiasis, and also with respect to Ca^{2+} handling dynamics in I/R

injury and heart failure. The following chapters will investigate the role of a potential common factor - the cysteine protease cathepsin-L.

1.2 What is Trypanosomiasis?

Trypanosomiasis is a vector-borne parasitic disease caused by kinetoplastid protozoa of the genus *Trypanosoma spp.* There are multiple trypanosome species causing different diseases in different hosts transmitted by insect vectors throughout the tropical world. In sub-Saharan Africa, multiple species of trypanosome cause disease in animals, (Animal African trypanosomiasis (AAT); ‘Nagana’) and humans (Human African trypanosomiasis (HAT); ‘Sleeping Sickness’). HAT is caused by two subspecies of *T. brucei* transmitted by tsetse flies of the genus *Glossina*. Specifically, they are *T. b. rhodesiense* causing East African HAT and *T. b. gambiense* type I and II causing West African HAT. The main species causing AAT in cattle and other ruminants are *T. vivax*, *T. congolense* and *T. brucei* causing severe muscle wastage, anaemia and loss of productivity⁽¹⁾. *T. b. brucei* also causes severe disease in equines and canines with *T. simiae* causing high mortality in pigs⁽¹⁾. In Latin America *T. cruzi*, transmitted by triatomine insects, is maintained in >100 species of mammalian hosts as a reservoir⁽²⁾. *T. cruzi* is transmitted to humans by the triatomine vectors⁽³⁾ causing Chagas disease characterised by dilated cardiomyopathy and arrhythmias discovered by Carlos Chagas in 1909⁽⁴⁾. In Asia *T. evansi* causes ‘Surra’ a wasting disease in camels, water buffalo and horses. *T. evansi* and the equine infective relative *T. equiperdum* are *T. brucei* derivatives that are mechanically or sexually transmitted no longer requiring the tsetse vector due to partial or complete loss of the kinetoplast⁽⁵⁾. Much of the focus of this thesis will be on *T. b. brucei* as a model for HAT. However, animal infections should not be ignored as they have significant economic impact in sub-Saharan Africa with an estimated 48 million cattle infected with losses of \$1-1.2 billion annually^(6;7). Cattle are not only important for meat and milk, but also have impact on livelihoods in poor areas of Africa as a means of traction where mechanical farm equipment is too expensive or cannot be maintained⁽⁶⁾.

1.2.1 Lifecycle of *Trypanosoma spp.*

Trypanosomes are transmitted by blood-feeding tsetse flies of the genus *Glossina*. There are about 30 different species and subspecies of tsetse broadly categorised into three groups with different habitat predilections with different abilities to transmit different species and strains of trypanosome⁽⁸⁾. Tsetse flies are viviparous, i.e. produce a fully developed live larva, which burrows into the soil, pupates and emerges as an adult fly one month later. The fly becomes infected when it takes a blood meal from an infected mammalian host (Figure 1.1). Short-stumpy bloodstream form trypomastigote parasites taken into the fly's digestive tract undergo several differentiation steps involving metabolic and anatomical changes⁽⁹⁾ to become procyclic trypomastigotes during the following 3-5 weeks⁽¹⁰⁾. The procyclics then leave the fly's midgut, transform into epimastigotes and migrate to the salivary gland. In the salivary gland the epimastigotes transform into infectious metacyclic trypomastigotes. When the infected tsetse fly bites a susceptible individual the metacyclics are injected into the host. There they transform into long-slender bloodstream form trypomastigotes and are carried in the mammalian host's bloodstream to other sites such as lymph nodes, spleen, liver, heart, eyes and endocrine organs in what is known as the haemolymphatic or stage I disease⁽¹⁰⁾. The long-slender bloodstream forms multiply by binary fission. In density-dependent manner a proportion of the long-slender trypomastigotes terminally differentiate into short-stumpy trypomastigotes⁽¹¹⁾ and can be transmitted to more tsetse flies when they take a blood meal and ingest the short-stumpy bloodstream form trypomastigotes⁽¹²⁾ perpetuating the cycle.

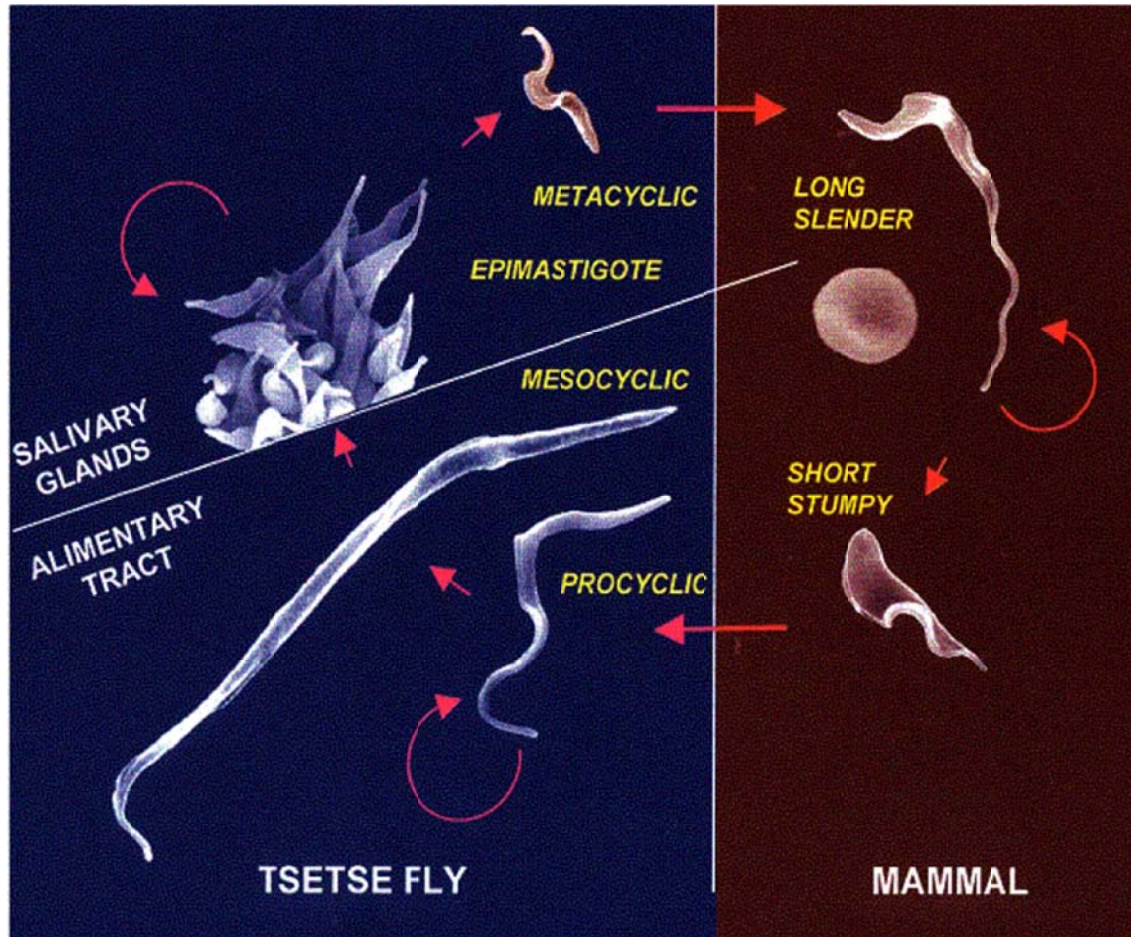


Figure 1.1: Lifecycle of African trypanosomes.

Mammalian hosts are infected when infected flies inject metacyclic trypomastigotes during feeding. The long slender form parasites divide in the host leading to clinical signs of infection. The parasites differentiate under a parasite driven trigger into the insect infective short stumpy form. Tsetse flies are infected from feeding on infected hosts. The parasites undergo development stages in the tsetse fly before migrating to the salivary glands in preparation of infecting the next host. Figure adapted from Barry and McCulloch (2001) with permission⁽¹³⁾.

1.2.2 What are Trypanosomes and How do they Function?

Trypanosomes are single cellular organisms approximately 15-30 μm in length belonging to the family Trypanosomatidae. They are distinguished by the presence of a single flagellum by which they gain their motility, the presence of a condensation of DNA in the proximal end of a single long tubular mitochondrion called the kinetoplast and a unique metabolic organelle called the glycosome (Figure 1.2). Other features are classical of eukaryotic organisms such as the nucleus, endoplasmic reticulum, Golgi apparatus, endosomes and lysosomes (Figure 1.2).

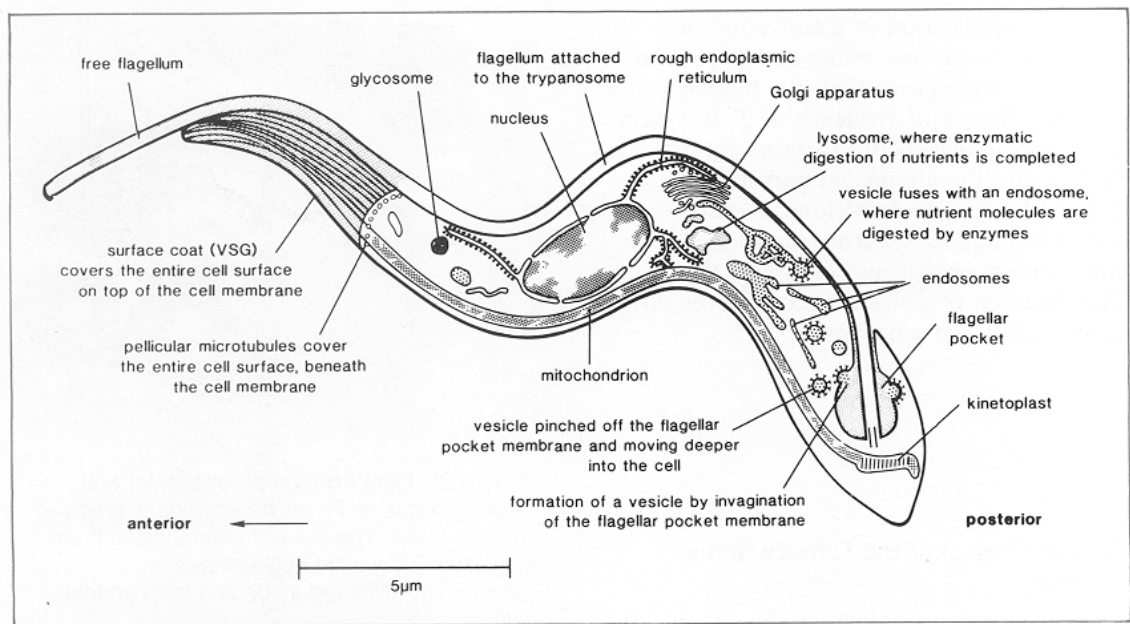


Figure 1.2: Schematic representation of bloodstream form *T. brucei* from International Laboratory for Research on Animal Diseases with permission⁽¹⁴⁾.

1.2.3 How do Trypanosomes Survive in the Host?

1.2.3.1 Variable Surface Glycoprotein

Trypanosomes are surrounded by a variable surface glycoprotein (VSG) coat that protects against complement-mediated lysis. *T. brucei* has >1000 VSG genes of which only one at a time are expressed from one of multiple telomeric VSG expression sites. The mammalian host's immune system eventually recognises and mounts an effective immune response against the predominant VSG variants leading to antibody-mediated lysis of the trypanosomes. However, trypanosomes will continually switch VSG expression to produce unique VSG proteins that the host's antibody response will not recognise. In this way an infection can last many years⁽¹⁵⁻¹⁷⁾. The continual switching of VSG coats makes development of an effective vaccine for HAT and AAT almost impossible⁽¹⁸⁾.

1.2.3.2 Resistance

Wild animals have developed tolerance of trypanosome infections as have the indigenous *Bos taurus* derived breeds of cattle (N'dama). *Bos indicus* (Zebu) derived breeds of cattle remain susceptible⁽¹⁹⁾. In the case of HAT there is a continual evolutionary battle between host and parasite. While *T. brucei* and

other trypanosome species are infective to many mammalian species, usually only *T. b. gambiense* and *T. b. rhodesiense* are infective to humans. This is due to trypanosome lytic factors (TLFs), which are present in normal human serum and destroy trypanosomes infective to animals⁽²⁰⁻²²⁾.

1.2.4 What are the Clinical Features of Trypanosomiasis?

1.2.4.1 Animal African Trypanosomiasis

AAT occurs in livestock throughout the tsetse belt of Africa (Figure 1.3). The host-parasite interaction produces extensive immune-mediated pathology and severe anaemia⁽²³⁾, including cardiac involvement with perimyocarditis observed in both field^(24;25) and experimental infections⁽²⁶⁻²⁸⁾. Clinically infected animals lose condition, become weak and unproductive often resulting in death. All aspects of production are affected including fertility, milk yields, growth and work output. Therefore treatment and control strategies need to incorporate AAT in addition to HAT to improve the socio-economic situation as well as physical health of at risk communities.

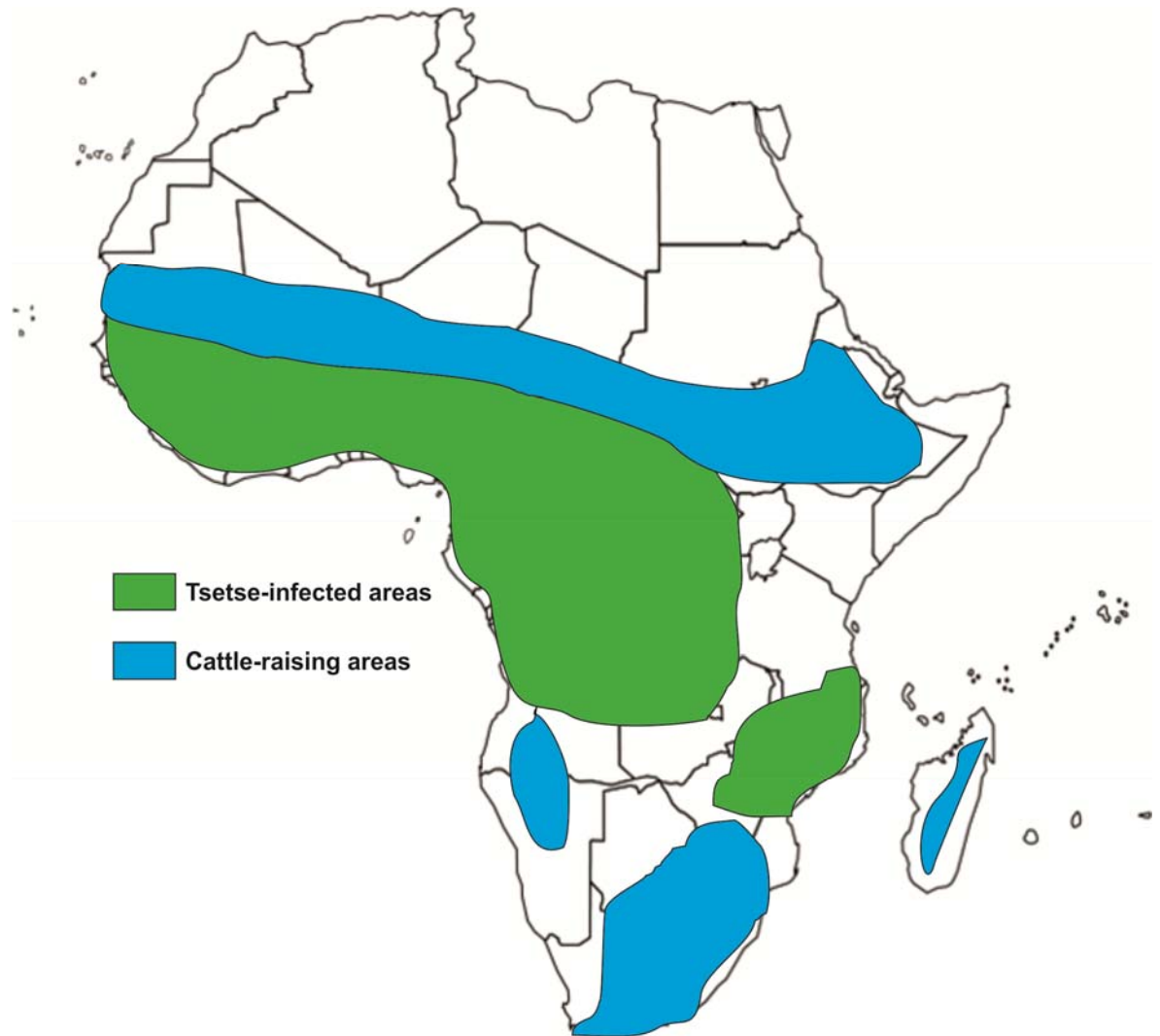


Figure 1.3: Tsetse Belt in Africa.

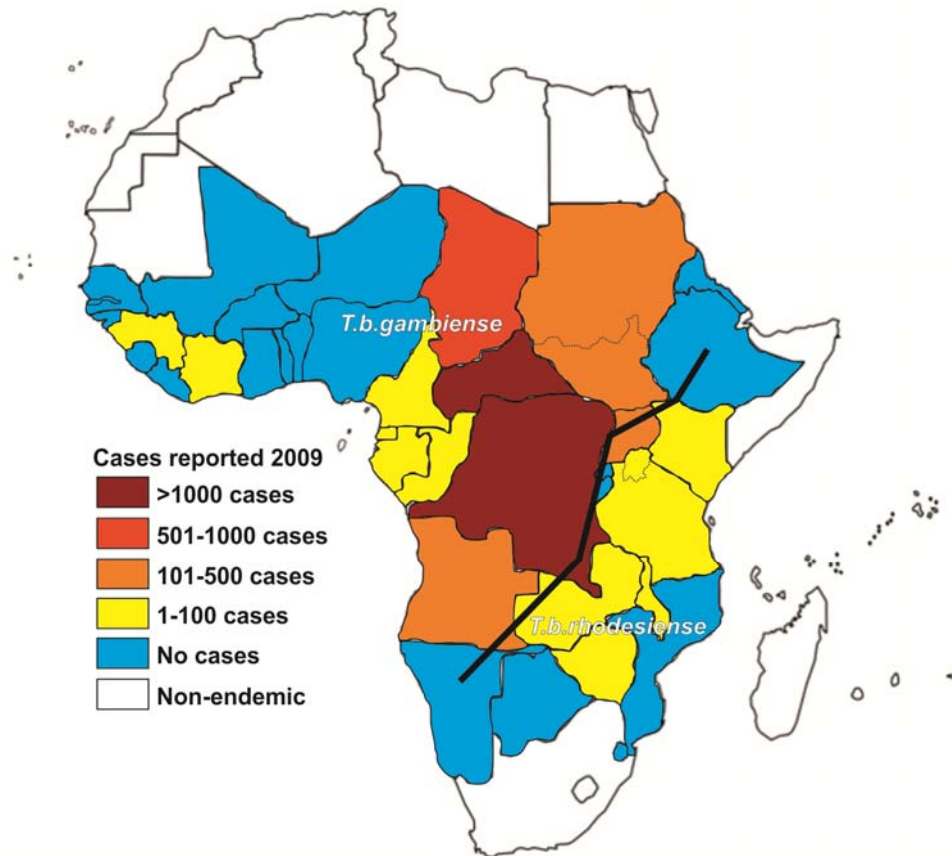
Natural habitat regions of the trypanosome vector tsetse flies (*Glossina spp.*) are shown in green. The areas left for cattle rearing are shown in blue.

1.2.4.2 Human African Trypanosomiasis

Historically HAT has had epidemics and resurgences over the last century. At the turn of the 20th century it was estimated that many hundreds of thousands of people were killed⁽⁸⁾. However, in the first half of the 20th century strong measures were taken including cull of the animal reservoir and destruction of the tsetse habitat combined with advances in insect vector control which led to a reduction in the reported cases by the 1960s⁽⁸⁾. Unfortunately factors such as war, famine and socio-economic instability led to reduced surveillance and vector control resulting in a resurgence of the disease by the late 1990s. The World Health Organisation (WHO) estimated there were over 300,000 cases in 1998⁽²⁹⁾. This resurgence led to a concerted effort by WHO and local governments to improve human case detection and treatment and better vector

control⁽¹⁰⁾. As a result WHO now reports that the reported number of human cases in Africa were 9875 in 2009, 7139 in 2010 and 6743 in 2011⁽³⁰⁾. The changing pattern of reported HAT cases from 2009 to 2011 shows a favourable picture of the epidemiological situation in Africa (Figure 1.4); however these figures should be taken with caution. It is estimated that there may be as many as 10 times more cases that go unreported. One study in particular noted that in Uganda, 2005 that *T. b. rhodesiense* cases were underestimated by a factor of 12⁽³¹⁾. Therefore, despite encouraging statistics, it is increasingly important to maintain a high level of surveillance, treatment and control in endemic countries to prevent a possible resurgence of the disease. Approximately 70 million people are still at risk of infection⁽³²⁾. Finding new drug targets will aid in the WHO's goal of eradication by 2020 by improving treatment administration and response, reducing drug resistance and reducing cost.

A



B

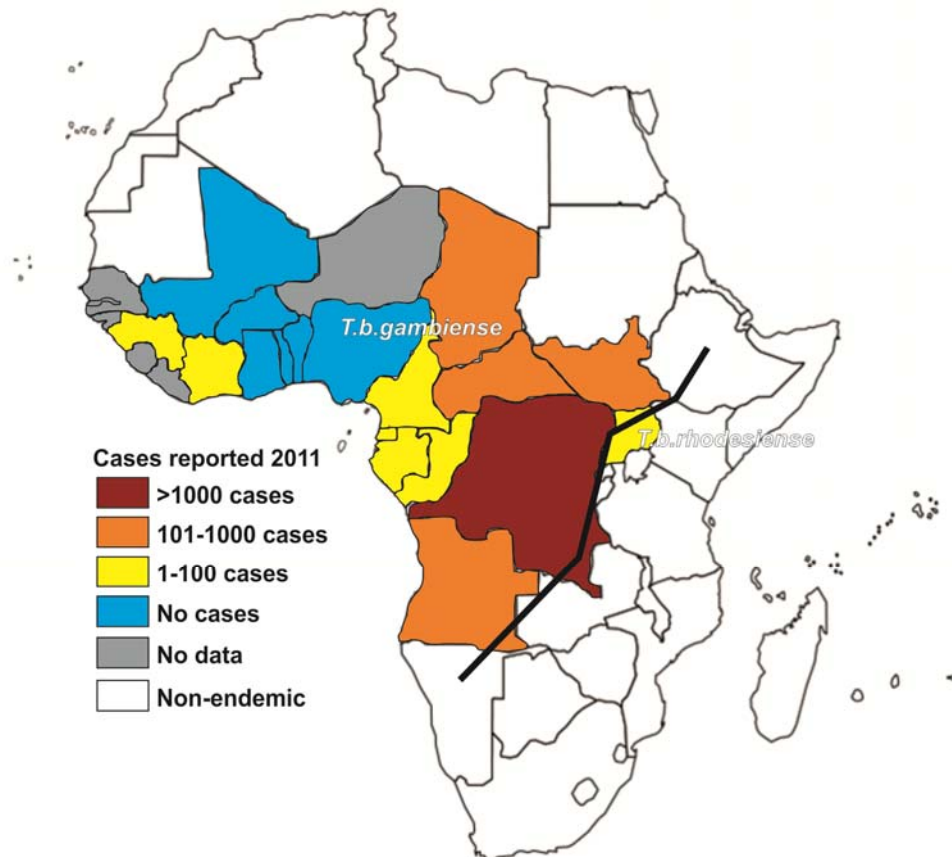


Figure 1.4: WHO reported cases of HAT.

The black 'border' indicates the division between *T. b. gambiense* and *T. b. rhodesiense*. Uganda can have infections of both species of trypanosome⁽³³⁾.

Traditionally HAT disease is described in two stages, the early haemolympathic stage (Stage I) and the late meningoencephalitic stage (Stage II), the latter being characterised by central nervous system (CNS) invasion^{Bucheton, 2011 385 /id}. Without treatment HAT is often fatal^(35;36), however there are reports of untreated cases of *T. b. gambiense* being cleared from hosts or developing a long-lasting serological response without symptoms⁽³⁷⁻⁴⁰⁾. *T. b. gambiense* accounts for at least 96% of HAT cases⁽⁴¹⁾ and has a chronic progressive course typically lasting around 3 years⁽³⁸⁾, although there have been reports of recrudescence after decades⁽⁴²⁾ and more acute progressions of disease as well^(43;44). *T. b. rhodesiense* typically has a much more acute course with death occurring within weeks or months⁽³⁶⁾.

Stage I clinical signs are usually non-specific with an onset typically 1-3 weeks following the tsetse bite. The signs include headache, malaise, arthralgia, weight loss, fatigue and intermittent fever^(10;45). Often patients presenting with these signs are mis-diagnosed with malaria⁽¹⁰⁾. Progression begins to manifest as lymphadenopathy, splenomegaly, hepatomegaly; cardiac signs including myocarditis, perimyocarditis and congestive heart failure; ophthalmological signs such as iritis, keratitis and conjunctivitis; endocrine dysfunction and fertility problems^(8;10).

The intermittent periods of fever can last up to a week separated by intervals of several days to months⁽⁴⁶⁾. These episodes correspond to a type I inflammatory reaction associated with macrophage activation, interferon γ , tumour necrosis factor α (TNF α), reactive oxygen species (ROS) and nitric oxide (NO)⁽⁸⁾. The immune/inflammatory reaction controls parasitaemia levels and tissue invasion but itself can have damaging consequences⁽⁴⁷⁾. The host can also mount type II immune reactions which consists of interleukin-10 (IL-10) production than can have anti-inflammatory properties⁽⁴⁷⁾.

Stage II disease is characterised by sleep disturbances giving HAT its colloquial name 'Sleeping Sickness'⁽⁴⁸⁾. The disease disrupts the circadian rhythm of the sleep/wake cycle resulting in a fragmented sleep pattern rather than a true inversion of sleep⁽⁴⁹⁾. Other neurological signs include; tremors, fasciculations, motor weakness, limb paralysis and abnormal movement. These disorders are rarely seen during Stage I and increase in frequency with the duration of the

disease^(45;50). Psychiatric symptoms such as irritability, psychotic reactions, aggressive behaviour, or inactivity with apathy can dominate the clinical picture⁽⁵⁰⁾. Death occurs from the progression of neurological signs, inflammation and multiple organ failure⁽¹⁰⁾.

1.2.4.3 Cardiac Abnormalities in HAT

Cardiac involvement is frequently seen in patients with *T. b. gambiense* infection. Signs are evident on the electrocardiogram (ECG) as corrected QT (QTc) prolongation (an indicator of the time taken for ventricular depolarisation and repolarisation), repolarisation changes and low voltage⁽⁵¹⁻⁵⁴⁾. Blum *et al.* (2007) reported prolongation of QTc, repolarisation changes and low voltage were observed in 50% of stage I patients and up to 71% of stage II HAT patients⁽⁵¹⁾. Palpitations (arrhythmic heart beats) were reported in 18% of *T. b. gambiense* infected individuals compared with non-infected controls reporting 5% of individuals with palpitations⁽⁵¹⁾. QTc prolongation carries an increased risk for ventricular arrhythmia and sudden cardiac death⁽⁵⁵⁾. These ECG changes have been attributed to perimyocarditis without myocardial necrosis as demonstrated by negative troponin measurements^(51;55-58). In *T. b. rhodesiense* infections perimyocarditis can be more severe^(59;60). Post mortem examination of animals⁽²⁶⁻²⁸⁾ and humans^(56;57) revealed that trypanosomes infiltrate the myocardium leading to a mononuclear inflammatory response and fibrosis, which may progress to heart failure. Adams *et al.* (1986) found in a study of 16 HAT deaths from *T. b. gambiense* that two were a result of pulmonary oedema from cardiac failure⁽⁵⁶⁾. Bertrand *et al.* (1973) identified inflammation of the conduction system of the heart in 70% of 100 patients examined⁽⁵⁷⁾, however conduction problems were uncommon despite this finding. Two studies assessing atrio-ventricular (AV) block identified type I AV block in 3.7% and 14% of patients examined^(61;62), type II AV block in 1% and 2.5% respectively^(61;62), and type III AV block was found in one patient described in a case report⁽⁶³⁾. Enlargement of the cardiac silhouette of >50% of the thoracic diameter on radiographic examination has been reported in 40 (34%) of 118 patients⁽⁶¹⁾ and 14 (24%) of 59 HAT patients⁽⁶⁴⁾. Whether the enlargement was due to true cardiomegaly or if it was pericardial effusion was not examined in these studies^(61;64). Echocardiography findings are not commonly looked for, however one study identified right-ventricular dilatation in 16 (64%) of 25 HAT patients and

pericardial effusion in three (12%) individuals⁽⁶⁴⁾. Blum *et al.* (2007) assessed troponin and NT-proBNP (N-terminal prohormone of brain natriuretic peptide) as indicators of systolic cardiac function in HAT patients⁽⁵¹⁾. The troponin levels, an indicator of myocardial damage and necrosis, were within the normal range. NT-proBNP, an indicator of excessive myocardial stretching, was significantly higher in patients than in non-infected controls ($p < 0.001$)⁽⁵¹⁾. The ejection fraction was predicted by using suggested gender and age specific criteria for NT-proBNP⁽⁶⁵⁾. An ejection fraction of $< 40\%$ was predicted in 14 (24%) of 59 patients suggesting consistent with left-ventricular systolic dysfunction⁽⁵¹⁾. While the cardiac abnormalities reported in the literature can be attributed to inflammation and fibrosis, recent evidence has shown direct effects of trypanosomes and their secreted factors within *in vitro* blood brain barrier (BBB) models⁽⁶⁶⁻⁶⁹⁾. Whether African trypanosomes and their secreted products can have a direct effect on the myocardium has not been explored and will therefore be investigated in this thesis.

1.2.5 How is HAT Diagnosed?

Due to the non-specific clinical signs of HAT the mainstay of diagnosis is by laboratory examination of blood and/or cerebrospinal fluid (CSF)^(70;71). A three-stage programme is used in current control strategies for HAT surveillance; screening, diagnostic confirmation and staging⁽⁸⁾.

1.2.5.1 Screening

The most efficient and low cost method available is the card agglutination test for trypanosomiasis (CATT), however this is only available for HAT caused by *T. b. gambiense*⁽¹⁰⁾. The test was developed in the 1970s and can be performed on serum, capillary blood from a finger prick or blood from impregnated filter papers⁽⁷²⁻⁷⁴⁾. CATT is reported to have a sensitivity of 87-98% and specificity of 93-95%⁽⁷⁵⁻⁷⁸⁾ making it an effective tool for screening large numbers of individuals. However, due to the test not being 100% sensitive, individuals with suggestive clinical features such as a tsetse bit 'chancre' further examination is warranted even in the case of a negative CATT⁽⁸⁾.

1.2.5.2 Diagnostic Confirmation

Microscopic examination of the blood and/or lymph node aspirates is required for confirmation (Figure 1.5). Lymph node aspiration is commonly from the cervical lymph nodes and has a sensitivity of 40-80% depending on the parasite strain and stage of disease⁽⁷⁹⁾. The test is more sensitive during Stage I disease⁽⁷⁹⁾. Examination of blood films has a low sensitivity so concentration techniques such as centrifugation are routinely performed⁽⁸⁰⁾. Diagnosis using the DNA Polymerase Chain Reaction (PCR) is becomingly an increasingly accurate tool with reported sensitivity of 99% and specificity of 97.7% in a systematic review of 16 studies⁽⁸¹⁾. Unfortunately PCR is not generally an available option in the field. An attractive alternative is loop-mediated isothermal amplification of DNA (LAMP) which has been developed for both *T. b. rhodesiense* and *T. b. gambiense*⁽⁸²⁻⁸⁴⁾. LAMP has the benefit that DNA can be amplified with high specificity rapidly under isothermal conditions with simple incubators. The DNA amplification can be monitored either spectrophotometrically or with the naked eye without the use of expensive dyes.

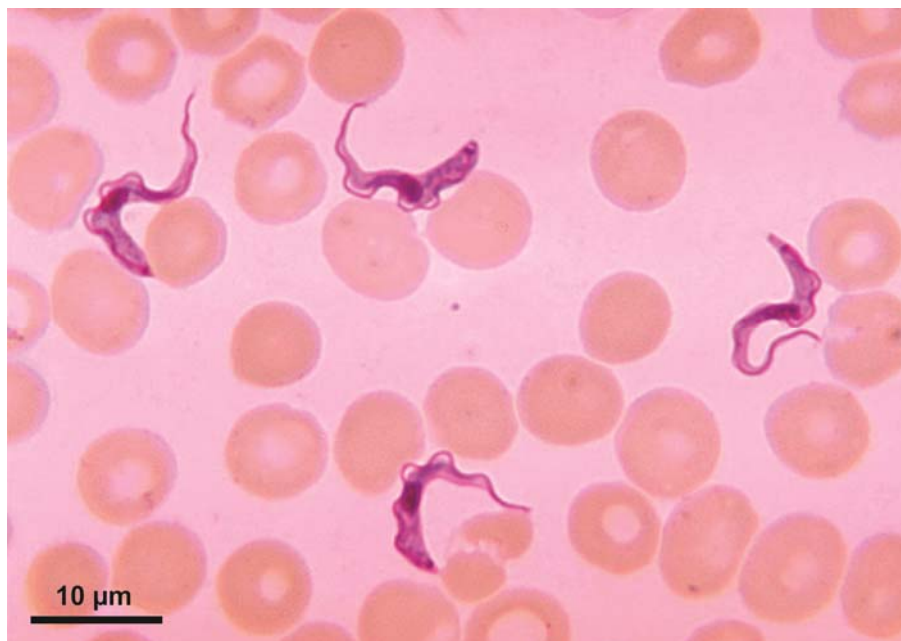


Figure 1.5: Photomicrograph of Giemsa stained *T. b. gambiense*. Blood smear from patient with African trypanosomiasis. Image approved for reproduction by Centers for Disease Control and Prevention.

1.2.5.3 Staging

Treatment of HAT depends heavily on the stage of disease as the drugs for Stage II disease are required to enter the CNS and are often highly toxic (see below). Therefore, diagnostic staging by examination of CSF *via* lumbar puncture is considered essential before Stage II drugs are administered⁽⁸⁵⁾. The current WHO definition of Stage II disease is when there are >5 leukocytes. μL^{-1} CSF, trypanosomes or protein content of >370 mg.L⁻¹⁽²⁹⁾. Many use the >5 leukocytes. μL^{-1} CSF guideline, however uncertainty surrounds the cohort of patients that have 6-20 leukocytes. μL^{-1} CSF as they may have variable signs of neuroinflammation and variable responses to first-line treatments^(8;85;86). Microscopic finding of trypanosomes is unequivocal for diagnosis but a PCR positive on CSF is controversial as patients that have achieved a successful resolution of Stage I disease may still have a positive PCR result^(87;88). CNS staging is still a controversial area with a lack of a gold standard with which to compare new methodologies⁽¹⁰⁾. However new markers are being tested such as chemokines and acute phase proteins⁽¹⁰⁾.

1.2.5.4 *T. b. rhodesiense*

Unfortunately there is no serological screening test for *T. b. rhodesiense* yet. Current strategies consist of clinical signs and history of exposure. However, parasitological examination is often more straightforward as parasitaemias are higher than for *T. b. gambiense*⁽⁸⁾. As a result WHO launched an initiative in 2006 in collaboration with the Foundation for Innovative Diagnostics (FIND) to improve diagnosis and staging of HAT cause by both *T. b. rhodesiense* and *T. b. gambiense*⁽⁸⁹⁾.

1.2.6 What are the Current Treatment Strategies?

As HAT has two stages, the haemolymphatic stage and the meningoencephalitic stage, the treatment strategies must be adapted accordingly. Stage II is characterised by individual parasites crossing the blood brain barrier (BBB) therefore drugs to treat Stage II must be able to cross the BBB.

1.2.6.1 Pentamidine

Pentamidine is the drug of choice for Stage I West African HAT. It can be given intramuscularly for one week or as an intravenous infusion⁽⁸⁾. The drug is usually effective for early stage disease, but has the potential complications of hyperglycaemia or hypoglycaemia, prolongation of the QT interval on the ECG, hypotension, and gastrointestinal features^(8;10) (Table 1.1). Pentamidine is less effective for intermediate stage disease (10-20 leukocytes. μL^{-1} CSF) (section 1.2.5.3)⁽⁹⁰⁻⁹²⁾ with up to 48% treatment failure in one study⁽⁹²⁾.

1.2.6.2 Suramin

Suramin is used for Stage I East African HAT but avoided for West African HAT due to increased prevalence of *Onchocerca spp.* which are very effectively killed by Suramin increasing the risk of severe allergic responses in patients⁽⁸⁾. Recommended dosing regimens are complex lasting up to 30 days. Potential adverse reactions are frequent but often mild and reversible such as nephrotoxicity and peripheral neuropathy. Acute and late hypersensitivity reactions can occur, so a lower test dose is trialled before treatment⁽⁸⁾ (Table 1.1).

1.2.6.3 Melarsoprol

Melarsoprol, an organoarsenic compound, is the most widely used treatment for Stage II East African HAT and West African where eflornithine is unavailable. Treatment regimens differ depending on the parasite subspecies (Table 1.1). Adverse reactions are frequent and can be life-threatening. The most important is an encephalopathic syndrome which occurs in an average of 4.7% of patients with *T. b. gambiense* infections and 8.0% of patients with *T. b. rhodesiense* infections, with fatality rates of 44% and 57% respectively^(93;94). Other adverse reactions are skin reactions such as pruritus and maculopapular eruptions, peripheral neuropathies, cardiac arrhythmias⁽⁹³⁾ and thrombophlebitis if injection technique is poor⁽⁸⁾. In several areas up to 30% treatment failures have been reported suggesting emerging resistance in which a P2 adenosine transporter is implicated⁽⁹⁵⁾.

1.2.6.4 Eflornithine

Eflornithine, an ornithine decarboxylase inhibitor, has been made widely available to patients thanks to efforts from WHO and pharmaceutical companies⁽¹⁰⁾. It is used in combination with the drug nifurtimox, nifurtimox-eflornithine combination therapy (NECT)⁽¹⁰⁾. Mortality from eflornithine is significantly less than from melarsoprol with 1 (0.7%) out of 143 vs. 3 (2.1%) out of 144 patients dying from treatment⁽⁹⁶⁾. Eflornithine is now recommended as the first-line treatment for Stage II West African HAT⁽⁹⁷⁻⁹⁹⁾, but not for East African HAT as *T. b. rhodesiense* is innately less susceptible to the drug than *T. b. gambiense*⁽¹⁰⁰⁾. Unfortunately eflornithine has a short half-life meaning that 4 intravenous infusions must be given daily making it awkward to administer in rural public treatment facilities (Table 1.1). Adverse reactions included cytotoxicity leading to anaemia, leukopaenia and thrombocytopenia (25-50%), gastrointestinal signs (10-39%) and convulsions (7%)⁽¹⁰¹⁾.

Table 1.1: Standard treatment options for HAT and main adverse reactions.

Drug	Stage	Route of Application	Dosing	Adverse Reactions
<i>Trypanosoma brucei gambiense</i>				
Pentamidine*	First	Intramuscular	4 mg.kg ⁻¹ q 24 h for 7 days	Hypoglycaemia, injection site pain, diarrhoea, nausea, vomiting, prolongation of QT
Eflornithine	Second	Intravenous (30 min infusion)	100 mg.kg ⁻¹ q 6 h for 14 days	Diarrhoea, nausea, vomiting, convulsions, anaemia, leukopaenia, thrombocytopenia
Melarsoprol†	Second	Intravenous	2.2 mg.kg ⁻¹ q 24 h for 10 days	Encephalopathic syndromes, pruritus, peripheral neuropathies, thrombophlebitis
<i>Trypanosoma brucei rhodesiense</i>				
Suramin*	First	Intravenous	Test dose 4-5 mg.kg ⁻¹ day 1, then 20 mg.kg ⁻¹ q 7 days for 5 weeks (max dose 1g per injection)	Hypersensitivity reactions (acute and late), albuminuria, cylinduria, haematuria, peripheral neuropathy
Melarsoprol*	Second	Intravenous	3.6 mg.kg ⁻¹ q 7 days for 3 weeks (max dose 180 mg per injection)	Encephalopathic syndromes, pruritus, peripheral neuropathies, thrombophlebitis

* Endemic countries: according to national legislature or guidelines

† Only where eflornithine is not available or where melarsoprol is first-line treatment.

Reproduced with permission from Brun *et al.* 2010⁽⁸⁾

1.2.7 How do Trypanosomes Cross the Blood Brain Barrier

1.2.7.1 Blood Brain Barrier

Much of the severity of HAT and the eventual death of a sufferer stems from the parasite crossing the BBB. The BBB serves to maintain a constant internal environment vital for CNS function by strictly regulating the passage of molecules across blood vessels^(102;103). The BBB consists of multiple layers; the endothelial cells of the vasculature, endothelial basement membrane, parenchymal basement membrane and foot processes of the astrocytes of the brain parenchyma⁽¹⁰⁴⁾ (Figure 1.6).

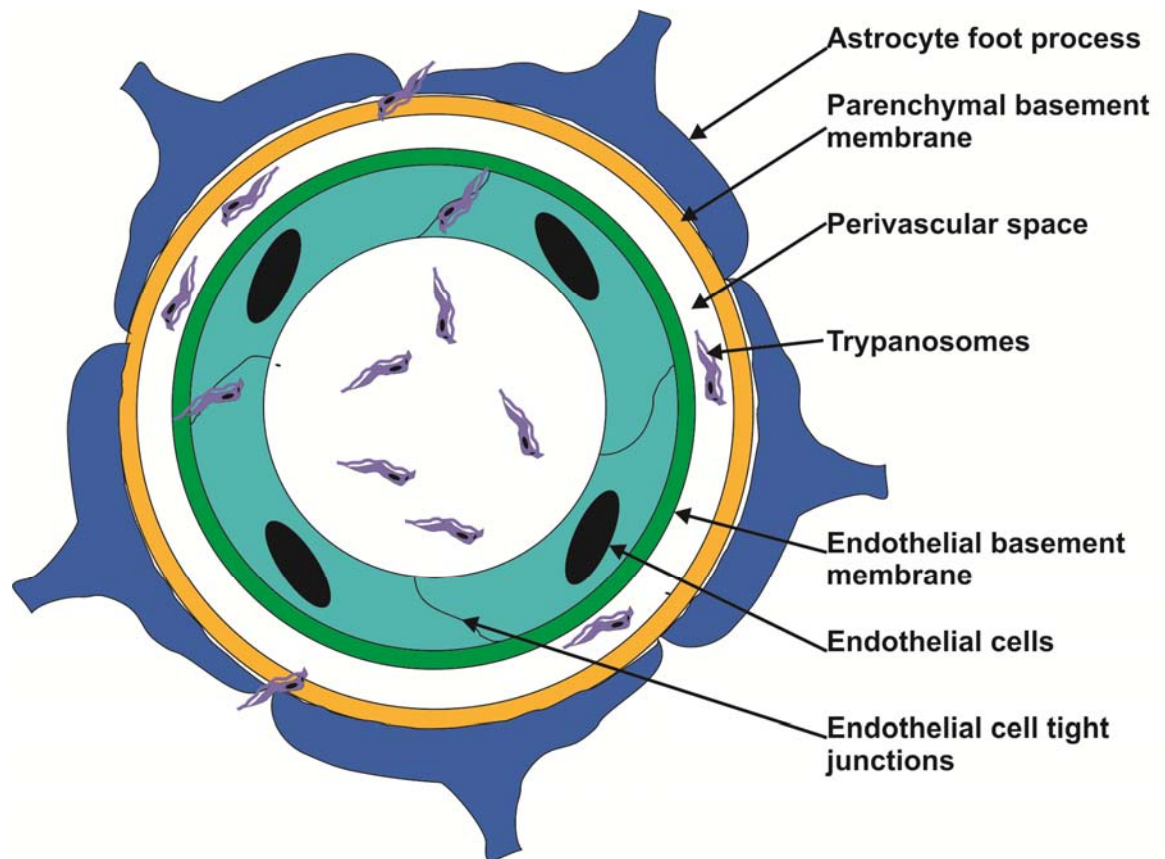


Figure 1.6: Schematic drawing of the layers of the blood brain barrier.

Trypanosomes cross from the lumen of the vessel between the tight junctions of the endothelial cells and across the endothelial basement membrane into the perivascular space. They can then cross the parenchymal basement membrane and between the foot processes of the astrocytes that make up the astrocyte glia limitans and enter the brain parenchyma.

1.2.7.2 Parasite Proteases and the BBB

In order to enter tissues or individual cells many parasites produce and secrete proteases to facilitate their passage across the skin, epithelial cell layers or plasma membranes⁽¹⁰⁵⁻¹⁰⁸⁾. Therefore it is possible that *T. brucei* spp. could produce and secrete proteases to facilitate traversal of the BBB. Indeed, this appears to be the case, as studies have identified that trypanosomes express phosphatases on their external surface and can release cysteine proteases and metallo-proteases^(67;109-111). Further work by Grab and colleagues have identified using *in vitro* BBB models that cysteine proteases, specifically the cathepsin-L like cysteine protease (TbCatL) is necessary for traversal of their BBB models^(66;112-114). RNA interference of TbCatL in *T. b. brucei* led to infected mice surviving 60 days longer with a 50% reduced ability of the parasites to cross the BBB⁽¹¹²⁾. Human infective trypanosomes such as *T. b. rhodesiense* have a much greater efficiency of traversal of the BBB model consisting of a monolayer of human brain microvascular endothelial cells (HBMECs) crossing paracellularly

without disruption of the barrier measured by transendothelial resistance⁽⁶⁷⁾. It was found that *T. b. rhodesiense* had higher levels and activity of TbCatL and therefore may be the critical factor in BBB traversal⁽⁶⁹⁾. Nikolskaia *et al.* (2006) were able to inhibit traversal of the HBMEC model with a cathepsin-L specific inhibitor, K11777 (N-methyl-piperazine-Phe-homoPhe-vinylsulfone-benzene) but not a cathepsin-B specific inhibitor, CA074 (L-3-trans-(propylcarbonyl)oxirane-2-carbonyl)-L-isoleucyl-L-proline)⁽⁶⁹⁾. Interestingly, incubation of *T. b. brucei* in media from *T. b. rhodesiense* with the HBMEC model enhanced traversal⁽⁶⁹⁾. They also showed the comparative contributions of protease activity in the different subspecies of *T. brucei* (Figure 1.7) as measured by a fluorometric activity assay with the fluorescent substrate Z-Phe-Arg-AMC (this technique was also used in this thesis and is described in detail in General Methods). They showed that *T. b. rhodesiense* possessed approximately 8-fold more active cysteine proteases than *T. b. brucei* (Figure 1.7A). The cysteine protease inhibitors E-64 and K11777 decreased peptidase activity by 94%, showing that they were detecting mainly the activity of papain-like cysteine proteases. In contrast, CA074 led only to a 25% decrease in the overall activity of bloodstream-form lysates, suggesting that TbCatB is a minor component in these lysates. Analysis of bloodstream-form secretion products (supernatants) showed that *T. b. rhodesiense* secreted 10-fold more active cysteine proteases (85% inhibition with E-64) than did *T. b. brucei* (30% inhibition with E-64; Figure 1.7B). No inhibition was observed using CA074, suggesting that the bloodstream-form trypanosomes secrete TbCatL but not TbCatB. To further characterise TbCatL expression by *T. b. gambiense*, *T. b. rhodesiense*, and *T. b. brucei*, they conducted Western blots on lysed parasites to confirm that *T. b. gambiense* and *T. b. rhodesiense* expressed higher levels of TbCatL than *T. b. brucei* (Figure 1.7C)⁽⁶⁹⁾. However, a band is still clearly visible for *T. b. brucei* indicating it can produce TbCatL albeit in lower quantities. It has also been shown in another study that *T. b. brucei* is capable of crossing HBMECs⁽⁶⁷⁾.

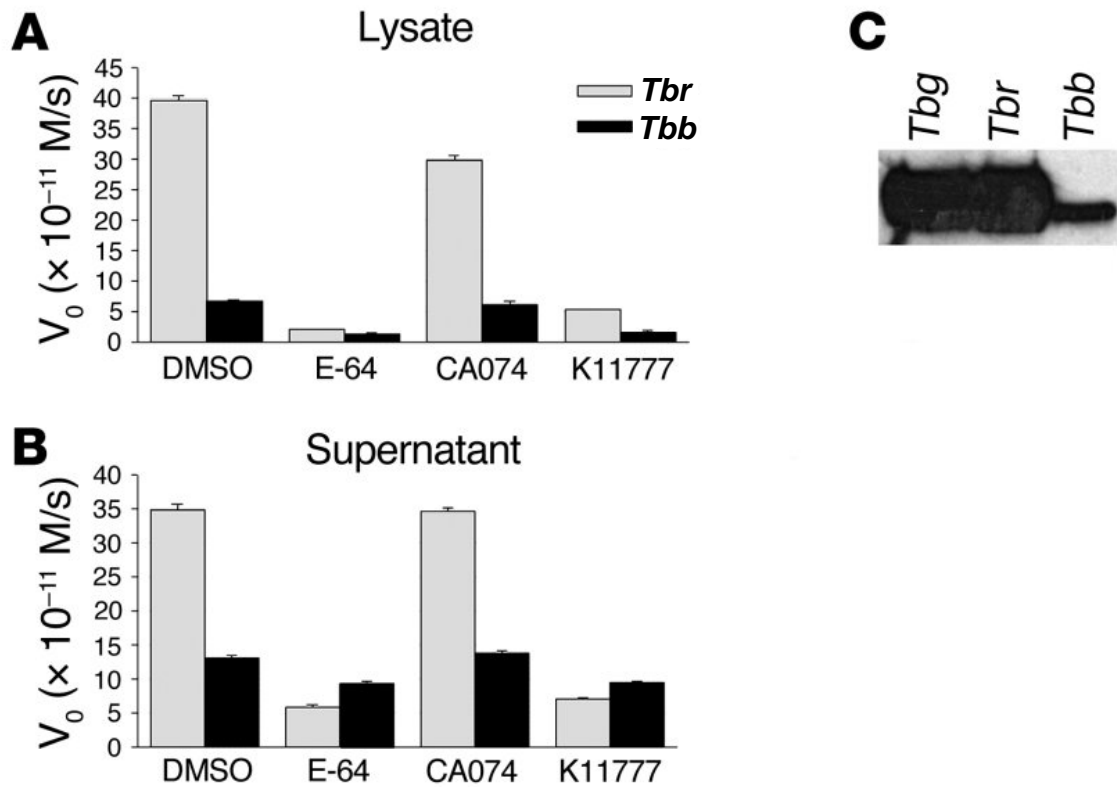


Figure 1.7: Cysteine protease activity from *T. brucei* spp.

(A) Protease maximal rate of activity from lysates of *T. b. rhodesiense* (*Tbr*) and *T. b. brucei* (*Tbb*). Incubated with DMSO vehicle, E-64 to differentiate serine protease activity, CA074 to discriminate between TbCatB activity and K11777 to discriminate between TbCatL activity. (B) As in (A) but with culture media supernatants. (C) Western blot of *T. b. gambiense* (*Tbg*), *T. b. rhodesiense* (*Tbr*) and *T. b. brucei* (*Tbb*) lysates equivalent to 2×10^6 parasites incubated for 30 min with 5 mM DTT and 20 μ M APC336 label with anti-biotin antibody. Figure from Nikolskaia *et al.* (2006) with permission.

1.2.7.3 Trypanosomes Induce Ca^{2+} Oscillations in HBMECs

How does TbCatL enable trypanosomes to cross the BBB? Nikolskaia *et al.* (2006) demonstrated effectively that trypanosomes induce intracellular Ca^{2+} fluxes within the endothelial cells of their BBB model⁽⁶⁹⁾ (Figure 1.8). HBMECs were loaded with Fura-2AM (section 2.6.4 for details on Ca^{2+} sensitive fluorophores) and the 340/380 nm excitation wavelength ratio measured. Their initial interpretation was that the trypanosomes induced the intracellular Ca^{2+} concentration ($[\text{Ca}^{2+}]_i$) via mechanical stimulation⁽⁶⁷⁾ based on the findings of Paemeleire *et al.* 1999 who found that mechanical stimulation of rat cortical capillary endothelial cells induced Ca^{2+} waves⁽¹¹⁵⁾. However when the experiments were repeated but with the culture supernatants the $[\text{Ca}^{2+}]_i$ oscillations were also induced⁽⁶⁹⁾. Use of the cathepsin-L inhibitor K11777 abolished the $[\text{Ca}^{2+}]_i$ oscillations which was interpreted as TbCatL inducing the Ca^{2+} changes⁽⁶⁹⁾. In conjunction with the Grab group's previous work⁽⁶⁷⁾ it appears that the parasites secrete the cysteine protease TbCatL, which induces

$[Ca^{2+}]_i$ oscillations in HBMECs and allows the parasites to traverse the monolayer paracellularly.

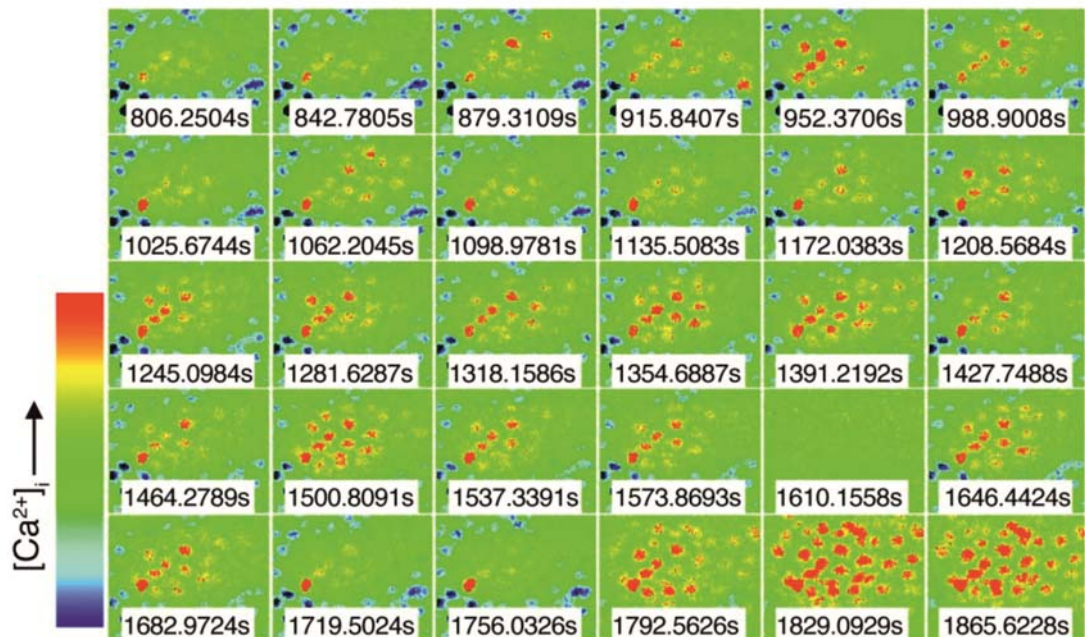


Figure 1.8: Ca^{2+} oscillations of HBMECs.

Time-lapse images of $[Ca^{2+}]_i$ changes in HBMECs measured as the 340/380 nm ratio in Fura 2-AM loaded cells. Figure panel from Nikolskaia *et al.* (2006) with permission.

Interestingly, induction of changes in $[Ca^{2+}]_i$ by *T. cruzi* by its cathepsin-L like cysteine protease, historically referred to as cruzipain in the literature but more recently referred to as TcrCatL, is required for intracellular invasion^(116;117). In the case of *T. cruzi* the TcrCatL activates G-protein coupled receptors (GPCRs) which in turn raise $[Ca^{2+}]_i$ leading to synaptotagmin VII-dependent lysosome migration. The lysosomes fuse to the parasite attachment site which precedes the formation of the parasitophorous vacuole required for cell entry^(118;119). In the case of *T. brucei* spp., which is extracellular, secreted/excreted TbCatL appears to activate the GPCR protease-activated receptor 2 (PAR-2) in endothelial cells⁽⁶⁶⁾. This in turn raises $[Ca^{2+}]_i$ which is thought to increase the permeability of the BBB through the effects of phospholipase C (PLC) and protein kinase C (PKC)⁽⁶⁶⁾. These effects are hypothesised to act on cytoskeletal components resulting in cell retraction and loosening of the tight junctions from calmodulin (CaM) activation of myosin light chain kinase (MLCK)⁽⁶⁶⁾ (Figure 1.9).

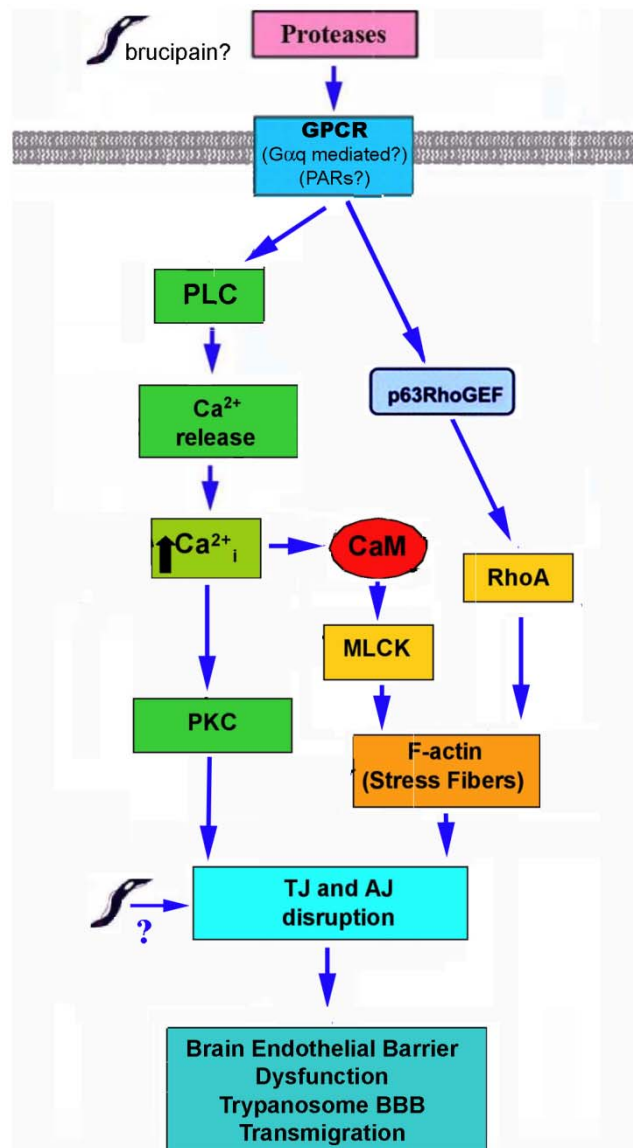


Figure 1.9: Proposed model for African trypanosome-induced BBB dysfunction

It is proposed that TbCatL (aka brucipain) triggers GPCRs such as PAR-2 *via* Gαq activation leading to PLC-mediated Ca²⁺ release from intracellular stores. The increase in [Ca²⁺]_i leads to calmodulin (CaM) activation of myosin light chain kinase (MLCK) potentially leading to cytoskeletal changes and barrier dysfunction. Ca²⁺ independent activation of cytoskeleton mediated by Ras-superfamily GTPases (i.e. RhoA) is also possible *via* p63RhoGEF. Parasite and/or host-derived proteases may also contribute by degrading or altering adherens junction (AJ) and tight junction (TJ) proteins. Figure from Grab *et al.* (2009) with permission⁽⁶⁶⁾.

Independent of the parasite effects, the host response may also contribute to BBB traversal through processes such as the neuroinflammatory response^(120;121).

There is a fine balance between pro-inflammatory cytokines such as IFN-γ, IL-1 and TNFα, and counter-inflammatory cytokines such as IL-10⁽¹²²⁾. A role for cytokines in determining entry of trypanosomes into the CNS was provided by a study in knockout mice where the gene for IFN-γ had been disrupted⁽¹²³⁾.

Following systemic infection, it was found that trypanosomes accumulated in the perivascular regions (Figure 1.6), unable to traverse between the endothelial

and the parenchymal basement membranes⁽¹²³⁾. These findings suggested that lymphocyte-derived IFN- γ is required for trypanosome traversal across cerebral blood vessels although it is unclear how at present.

1.2.8 Trypanosome Cysteine Proteases

Trypanosomes exhibit protease activity to enable them to carry out regulatory functions and to infect hosts⁽¹²⁴⁾. There are several families of cysteine protease activity; Clan CA family C2 (calpains) and Clan CD families C13 (GPI:protein transamidase), C14 (metacaspase) and C50 (separase) involved in regulatory processes within the trypanosome cells⁽¹²⁵⁾. The primary focus in this thesis is the Clan CA family C1, papain-like cysteine proteases or the cathepsins.

Cysteine protease activity very similar to that of the mammalian cathepsin-L was identified and localised to the endo-lysosomal system of trypanosomes⁽¹²⁶⁻¹²⁸⁾.

The expression of the cathepsin-L-like proteases is developmentally regulated among the different life-cycle stages of trypanosome species. For example, in *T. brucei* spp. greater expression of a cathepsin-L-like cysteine protease is found in the bloodstream short-stumpy insect infective stage than the bloodstream long slender form or the insect procyclic stage^(129;130). Genes for cathepsin-L-like proteases have been described in *T. brucei* spp.^(131;132) and *T. cruzi*⁽¹³³⁾, as well as *T. congolense*⁽¹³⁴⁾ (a causative agent of AAT). In addition cathepsin-B-like proteases have been described in *T. brucei* spp.⁽¹³⁵⁾, *T. cruzi*^(136;137) and *T. congolense*⁽¹³⁸⁾. From the Tritryp genome resource database

(www.tritrypdb.org) there are 11 annotated copies of the *TbCatL* gene in the genomes of all species and strains of *T. brucei*, with no amino acid sequence differences; although trypanosomes are diploid and the consensus genome sequences are haploid so allelic differences cannot be formally ruled out⁽¹³⁹⁾.

1.2.8.1 Cysteine Protease Activities of Trypanosomes.

1.2.8.1.1 *Trypanosoma brucei* spp.

Cathepsin-L-like protease activity for *T. b. brucei* and *T. b. rhodesiense* is used for degradation of anti-VSG IgG⁽¹²⁴⁾, lysosomal protein trafficking⁽¹⁴⁰⁾, trypanosome replication⁽¹⁴¹⁾ and BBB traversal^(66;69). The cathepsin-B-like activity is involved in protein turnover in lysosomes⁽¹³⁵⁾, transferring degradation⁽¹⁴²⁾ and cytokinesis⁽¹¹²⁾. The involvement of Clan CA cysteine

proteases in so many cellular processes of parasites makes them attractive targets for drug and vaccine development.

1.2.8.1.2 *T. congolense*

T. congolense cathepsin-L activity (TcoCatL) is involved in trypanotolerance in cattle⁽¹⁴³⁻¹⁴⁶⁾. Indeed TcoCatL (aka congopain) is being investigated as a vaccine target for AAT due to its conserved nature in comparison with VSGs⁽¹⁴⁷⁾. Cathepsin-B-like activity (TcoCatB) is involved in degradation of endocytosed proteins⁽¹³⁸⁾.

1.2.8.1.3 *T. cruzi*

The activities of the *T. cruzi* cathepsin-L-like cysteine protease (TcrCatL) is grouped into two categories; TcrCatL1 and TcrCatL2. TcrCatL is involved in metacyclogenesis, host cell invasion, host cell signalling, amastigote survival/nutrition, generation of kinins, inflammation and antigen presentation summarised in a review by Caffrey *et al.* (2011)⁽¹²⁴⁾. The function of cathepsin-B-like activity (TcrCatB) has yet to be determined.

In the fight against African trypanosomiasis many of the unique features of trypanosomes make attractive targets for new drug development. This thesis will focus on the cathepsin-L like cysteine protease TbCatL secreted/excreted by African trypanosomes and its role in altering intra-cardiomyocyte Ca^{2+} dynamics and cardiac function. Understanding how TbCatL affects Ca^{2+} signalling may yield a potential avenue of treatment that could prevent not only cardiac abnormalities but also BBB traversal and limit the disease to Stage I where current drug regimens carry less risk.

1.3 Ca^{2+} and the Heart

1.3.1 The Heart

The synchronous beat of the heart is achieved by the process of excitation-contraction coupling (ECC), which is the process by which electrical stimulation is transformed to mechanical work performed by the muscle.

1.3.2 The Cardiomyocyte

The heart is made up of many different cell types including fibroblasts/fibrocytes, endothelial cells, immune cells etc. but the cells that give the heart its contractile ability are the cardiomyocytes. Cardiomyocytes are discrete striated cells. The striations correspond with the light and dark I and A bands of the myofilaments made up from the contractile proteins actin and myosin. The darker A band is the overlapping region of the two proteins where cross-bridges are formed during the contractile cycle of the muscle. The I band consists of the thinner actin filaments anchored at the Z-line. The plasma membrane (sarcolemma) of cardiomyocytes has invaginations called transverse tubules (T-tubules) that are electrically continuous with the sarcolemma. A complex web-like organelle called the sarcoplasmic reticulum (SR) extends throughout the cytoplasm. In close approximation (15-20 nm)⁽¹⁴⁸⁾ with the T-tubules terminal cisternae form the junctional SR. There can be unattached expansions of SR termed corbular SR. The remainder of the SR is network SR. A high density of mitochondria provides the energy for cross-bridge cycling (Figure 1.10). An understanding of the structure of the cardiomyocyte is important when understanding the events that must transpire from the electrical depolarisation or action potential to the contraction of the cardiomyocyte and the whole heart.

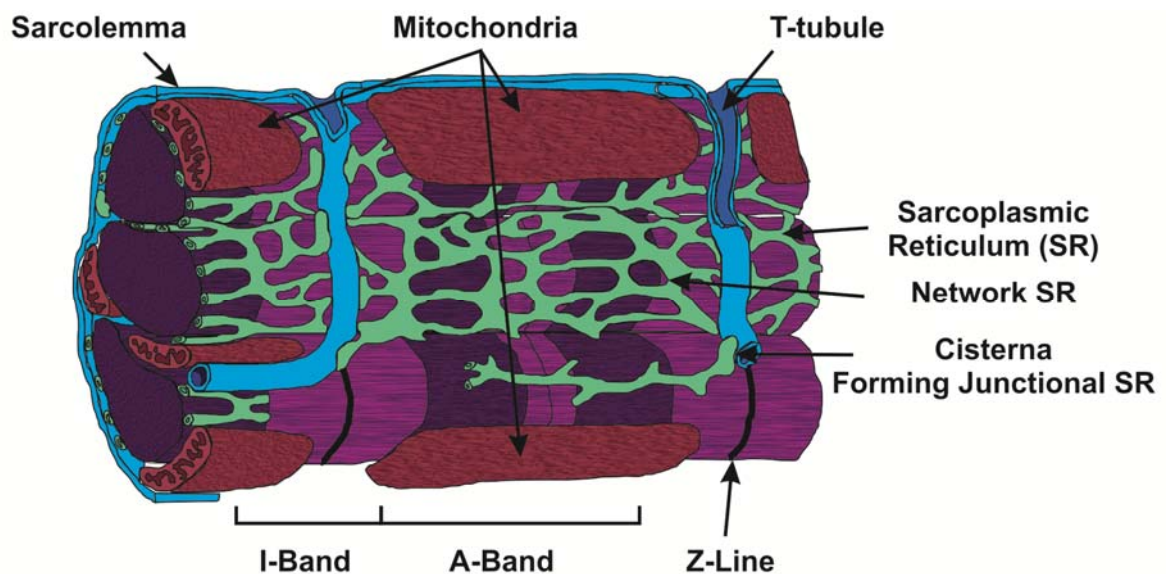


Figure 1.10: Ultrastructure of the cardiomyocyte. Figure redrawn and adapted from Katz (2001)⁽¹⁴⁹⁾ with permission.

1.3.3 The Cardiac Action Potential

The cardiac action potential (AP) varies in form depending on the cell type. However it broadly fits five phases:

- Phase 0 - Rapid upstroke
- Phase 1 - Repolarisation
- Phase 2 - Plateau
- Phase 3 - Late repolarisation
- Phase 4 - Resting membrane potential/Depolarisation (pacemaker cells)

In the ventricular cardiomyocyte these phases can be easily identified (Figure 1.11). When stimulated by the passive current spread from an adjacent electrically coupled cardiomyocyte Na^+ channels are activated such that the Na^+ current I_{Na} exceeds the transient outward K^+ current (I_{Kto}). The activation of Na^+ channels brings about further activation in a positive feedback loop such that there is a rapid upstroke of depolarisation or Phase 0 ($200 \text{ V}\cdot\text{s}^{-1}$) to approximately $35\text{-}50 \text{ mV}^{(148)}$. The end of Phase 0 occurs when Na^+ channels inactivate. Inward and outward currents are balanced. Phase 1 is mostly due to I_{Kto} due to its fast nature leading to the notch which is much more prominent in rodents compared to rabbits and humans⁽¹⁴⁸⁾. Phase 2 or the plateau phase is a state of balance brought about by inward Ca^{2+} current (I_{Ca}) through the L-type Ca^{2+} channel (LTCC) and outward current by delayed K^+ rectifier currents (I_{Ks} , I_{Kr} , I_{Kur}) (slow, rapid and ultra-rapid)⁽¹⁴⁸⁾. Phase 3 is when repolarisation accelerates due to increased I_{Ks} , I_{Kr} , I_{Kur} and inactivation of LTCCs. The LTCC is inactivated both by voltage and Ca^{2+} -dependent means, though the Ca^{2+} -dependent means is predominant *via* CaM binding⁽¹⁵⁰⁻¹⁵²⁾. Phase 4 for ventricular cardiomyocytes is maintenance of the resting membrane potential at $-80\text{-}90 \text{ mV}$ predominantly due to inward rectifier K^+ currents such as I_{K1} ⁽¹⁴⁸⁾.

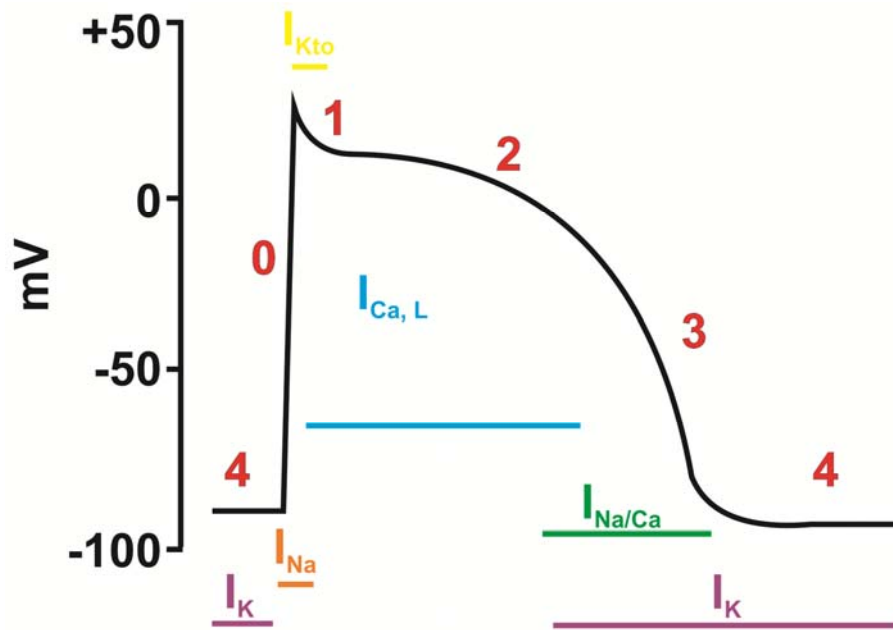


Figure 1.11: Ventricular cardiomyocyte action potential.

The heart unlike other tissues requires no central nervous system input. If the heart were to be removed and be provided with oxygen and nutrients it would continue to beat. This is achieved by pacemaker cells within the sino-atrial node located in the right atrium. Pacemaker cells have a naturally drifting membrane potential (E_m) that slowly returns toward zero due to declining outward K^+ currents and increased inward I_f , $I_{Na/Ca}$, I_{CaT} , I_{CaL} and I_{Na} ⁽¹⁴⁸⁾ (Figure 1.12). Once threshold is reached (≈ -40 mV) the L-type Ca^{2+} channels activate and depolarise the cell. All cardiac cells have some degree of pacemaker ability but in the normal situation there is a hierarchy of pacemakers defined by the rate at which the cells depolarise. Cells of the SA node are usually fastest followed by the AV node, Purkinje cells and finally the cardiomyocytes themselves. The funny current (I_f) (so-called because it is activated by hyperpolarisation as opposed to depolarisation) seems to play a more significant role in the pacemaker ability of other cell types such as the Purkinje fibres rather than the SA node, although this is controversial⁽¹⁴⁸⁾.

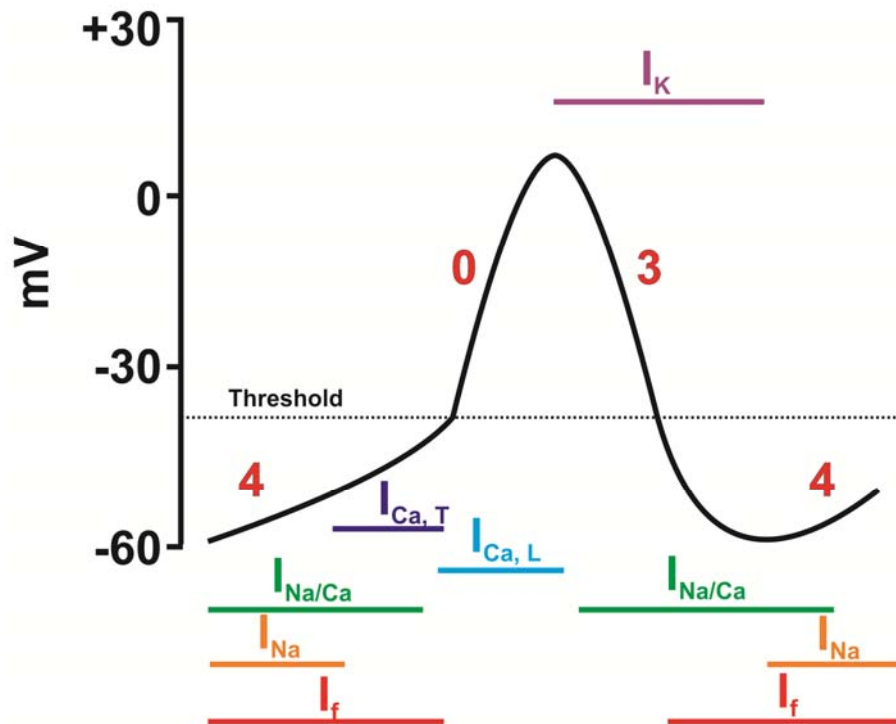


Figure 1.12: Sino-atrial node pacemaker action potential.

Although the heart does not require nervous input to beat it is innervated by the sympathetic and parasympathetic nervous systems to modulate the heart rate. Sympathetic stimulation results in release of noradrenaline that binds to β -adrenergic receptors triggering a cascade of cyclic adenosine monophosphate (cAMP) mediated affects that serve to increase the rate and force of contraction. One of the main effects is modulation of LTCC activity increasing the Ca^{2+} influx⁽¹⁵³⁾ the main component of the pacemaker Phase 0. Conversely parasympathetic stimulation *via* the vagus nerve releases acetylcholine which binds to muscarinic receptors which act to decrease cAMP and the slope of the pacemaker Phase 0 thereby slowing the heart rate.

1.3.4 The Electrocardiogram

The wave of depolarisation initiated at the SA node spreads across the atria to the atrio-ventricular (AV) node and then through the conduction system to the ventricles. The ventricles and atria are electrically isolated from one another apart from *via* the AV node. The depolarisation spreads through the bundle branches and through the myocardium (Figure 1.13). This wave of

depolarisation can be recorded as an average electrical potential or the electrocardiogram (ECG).

Electrical System of the Heart

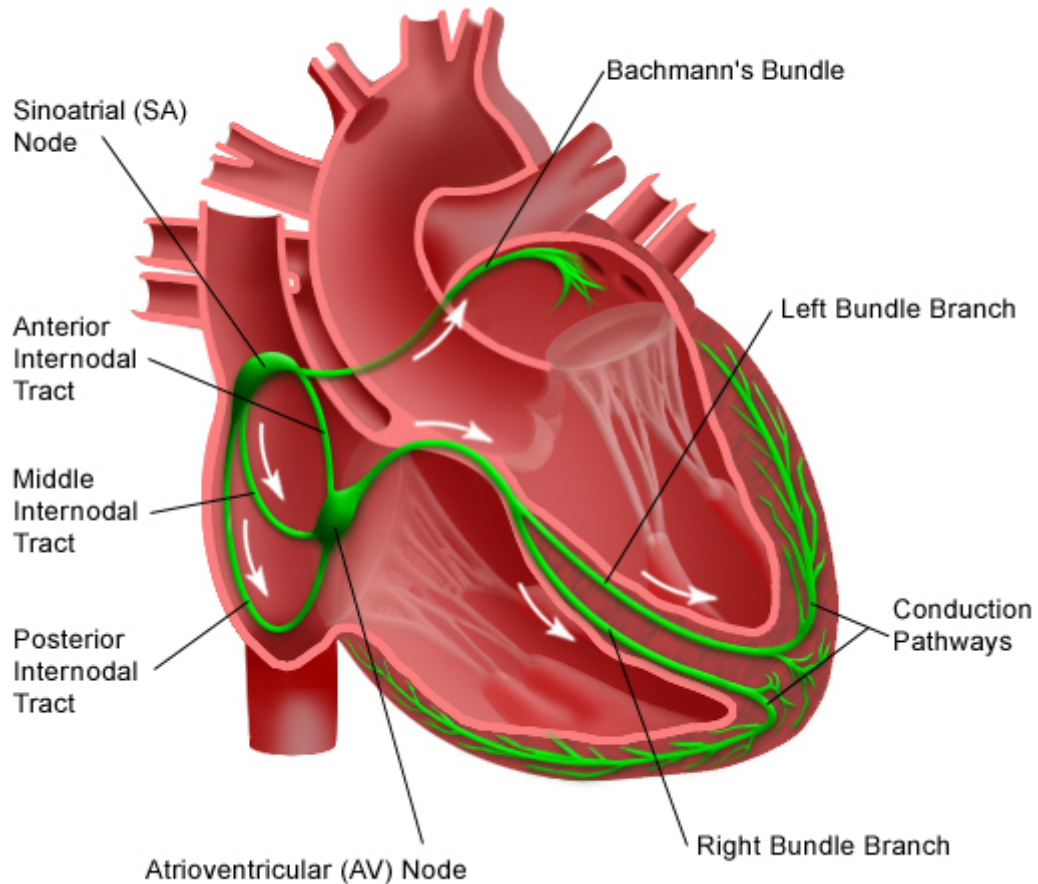


Figure 1.13: Schematic of the conduction system of the heart.

Essentially the heart can be thought of as an electrical dipole much like a battery with a positive and negative terminal due to the electrical connectivity of the heart through gap-junctions⁽¹⁵⁴⁾. The ECG leads placed on an individual act as a voltmeter. Beginning with rest there is no net charge as all cardiomyocytes will be at their resting membrane potential. As the AP begins usually starting with the pacemaker cells of the SA node a wave of depolarisation spreads through the atria⁽¹⁴⁸⁾. This is a spread from the right atrium where the negative electrode is toward the left where the positive electrode is so manifests as a positive deflection called the P-wave. Once the atria are depolarised the net change is zero so the ECG trace returns to zero.

The next phase is early depolarisation of the ventricles representing the change in voltage as the depolarisation spreads across the septum from the left to the right so manifests as a negative deflection called the Q-wave. Then the ventricular myocardium depolarises from endocardium to epicardium. The net depolarisation from all dipoles across the myocardium is leftward thus positive called the R-wave. The wave of depolarisation ceases so the trace returns to baseline, sometimes with a negative deflection called the S-wave. Repolarisation then progresses across the myocardium from epicardium to endocardium producing the T-wave (Figure 1.14).

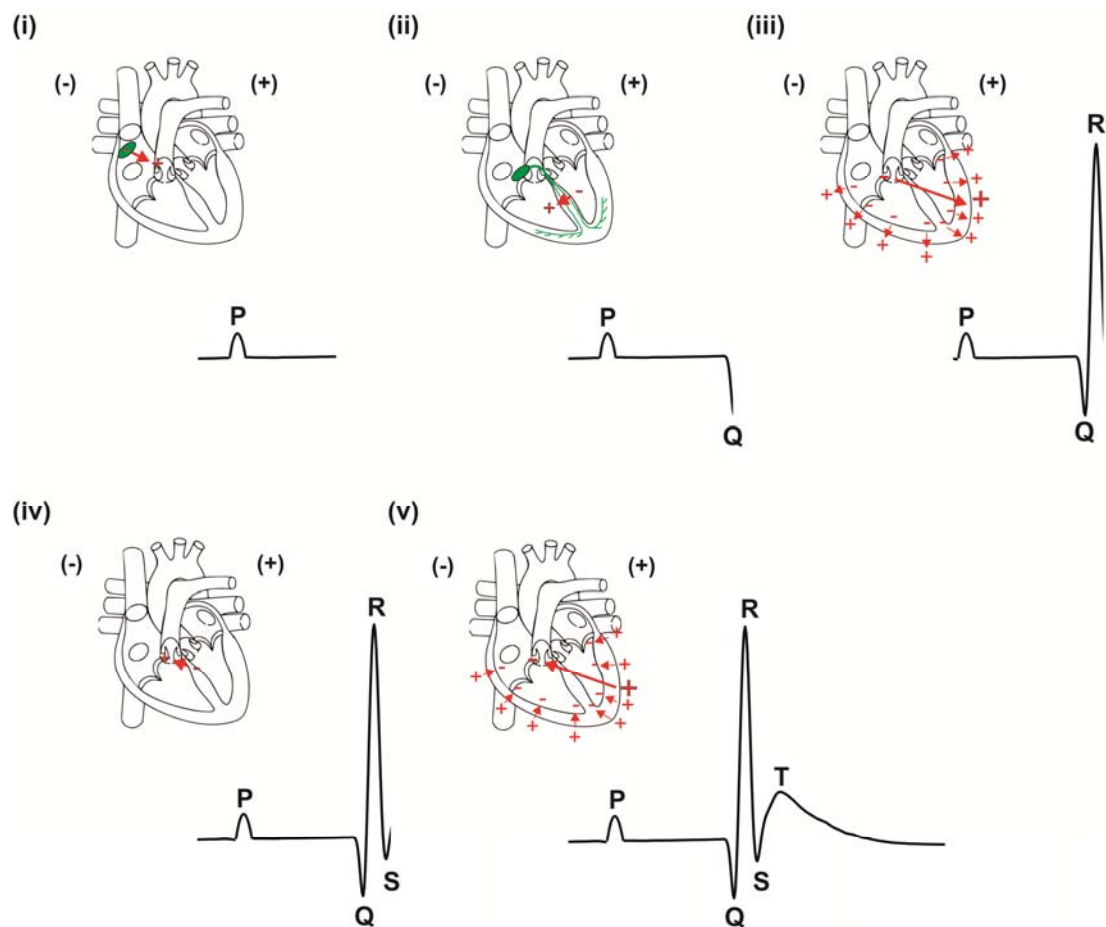


Figure 1.14: The ECG in relation to cardiac polarity (taken from rat).

Starting top left, depolarisation of the atria is from (-) to (+) therefore positive deflection and manifests as the P-wave. Depolarisation spreads through the conduction system with a net change away from (+) manifesting as a negative Q-wave. Ventricular depolarisation spreads from the endocardium to the epicardium with a net voltage change toward (+) as the R-wave. The S-wave occurs when there is some voltage change toward (-). Finally ventricular repolarisation occurs as the T-wave. This can be in either direction depending on the positioning of the leads and the position of the heart in the thorax.

1.4 Excitation-Contraction Coupling

At the single cell level the depolarisation of the plasma membrane (sarcolemma) spreads through the cardiomyocyte *via* invaginations called transverse tubules (T-tubules). The distribution of ion channels in the surface sarcolemma differ from that of the T-tubules such that the density of Na⁺ and K⁺ channels responsible for the polarity shifts of the AP are increased^(155;156). The depolarisation of the sarcolemma activates the L-type Ca²⁺ channels which are present at a >4 times density in the T-tubules than at the surface⁽¹⁵⁷⁾, this allows Ca²⁺ to enter the cardiomyocyte from the extracellular space⁽¹⁵⁸⁾. T-type Ca²⁺ channels are not thought to play a significant role in ventricular cardiomyocytes in contrast with pacemaker cells⁽¹⁵⁹⁾. The difference in channel distribution reflects the importance of Ca²⁺ in the generation of cardiomyocyte contractile function from the AP. Indeed, it has been known since the late 19th Century that Ca²⁺ was vital for the heart beat. Sydney Ringer identified that a frog heart ceased to beat when Ca²⁺ was accidentally removed from perfusion solution⁽¹⁶⁰⁻¹⁶³⁾. For clarity, the Ca²⁺ dynamics will be considered for contraction (systole) and relaxation (diastole) separately. The Ca²⁺ dynamics during systole are discussed first (Figure 1.15).

1.4.1 Systole

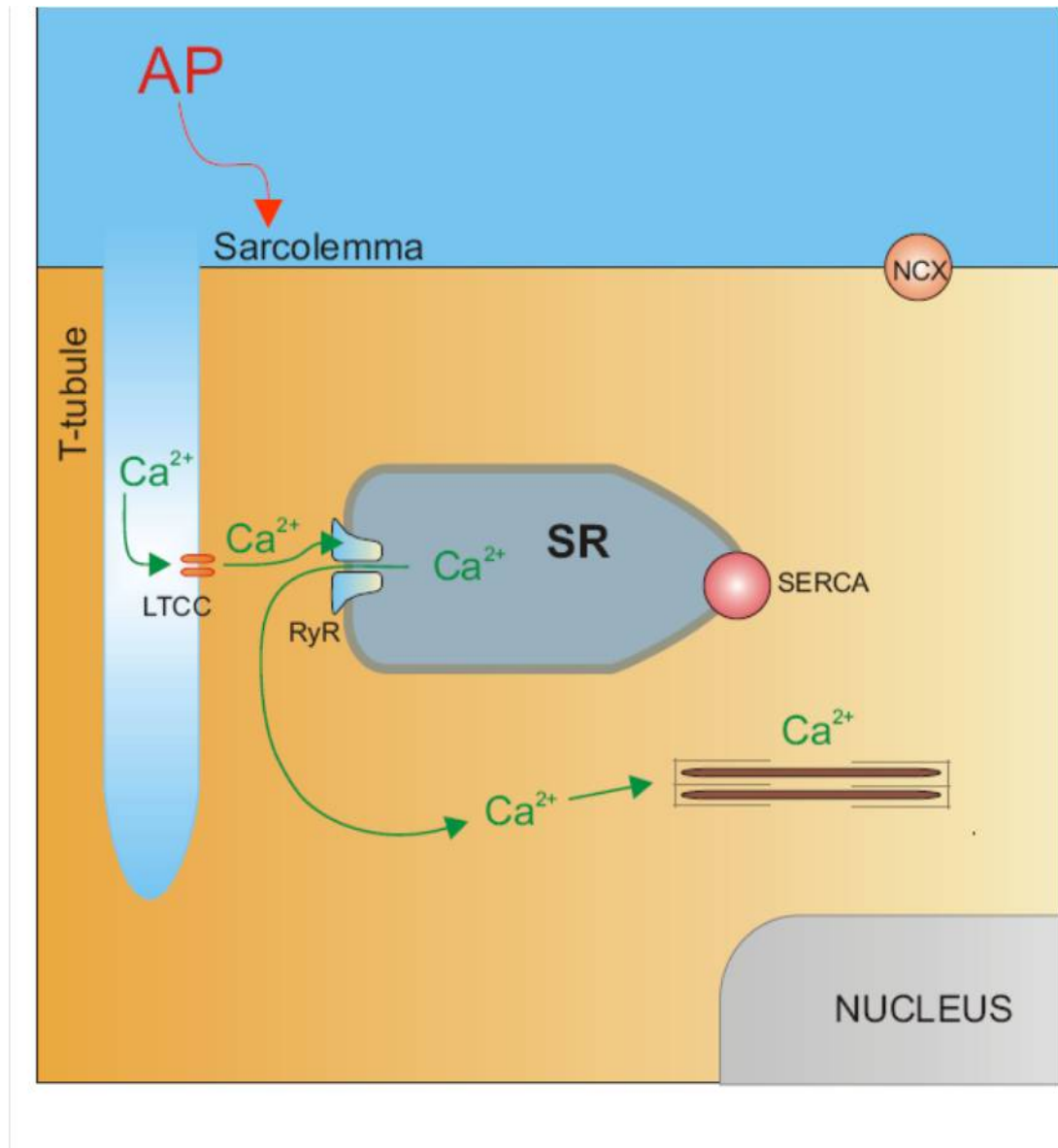


Figure 1.15: Ca²⁺ dynamics during systole.

An AP depolarises the sarcolemma and T-tubule activating the voltage-gated LTCC. Extracellular Ca²⁺ enters through the LTCC before the channel is inactivated by Ca²⁺ preventing overload. The relatively small amount of Ca²⁺ that enters activates the RyR triggering release of Ca²⁺ from the SR into the cytosol and binding to the myofilaments causing contraction.

1.4.1.1 Ca²⁺ Influx Through the L-Type Ca²⁺ Channel

Spatially the T-tubule and terminal cisternae of the intracellular Ca²⁺ store the sarcoplasmic reticulum (SR) are in close apposition in a space termed the dyadic cleft which can be $<1.5 \times 10^5 \text{ nm}^3$ in volume⁽¹⁶⁴⁾. Within these junctional spaces are LTCCs on the T-tubule surface and Ca²⁺ release channels also called ryanodine receptors (RyRs) on the SR cisternae membranes⁽¹⁶⁵⁾. The RyRs are so-called due to their affinity for the plant alkaloid ryanodine and consist of four

560 kDa monomers making the total tetrameric protein the largest yet identified at >2000 kDa⁽¹⁶⁶⁾. In cardiac muscle the arrangement of LTCCs and RyRs is in the region of 10-25 LTCCs to 100-200 RyRs^(167;168) constituting the 'couplon'⁽¹⁶⁹⁾, although some studies suggest the couplon is smaller with 10-40 RyRs⁽¹⁷⁰⁻¹⁷⁴⁾. In truth it is probably variable⁽¹⁷⁵⁾. When the LTCCs open upon the change in voltage from the AP the local $[Ca^{2+}]_i$ rises sharply (<1 ms) in the dyadic cleft to 10-20 μM free Ca^{2+} ⁽¹⁵⁹⁾. The exact quantity of Ca^{2+} influx is dependent on many factors, species being the main one. In the rabbit it has been shown Ca^{2+} entry *via* I_{Ca} through the LTCC during the AP is approximately 12 μM , which may even be as low as 6 μM due to Ca^{2+} inactivation of the LTCC⁽¹⁷⁶⁾. Other studies suggest a value of 21 μM for rabbit and 14 μM for rat using voltage clamp⁽¹⁷⁷⁾. The quantity of total Ca^{2+} required for myofilament activation for a normal ventricular twitch has been calculated as approximately 60-70 μM under steady state conditions⁽¹⁷⁸⁾. Taking into account the Ca^{2+} buffering of the cytosol of assumed to be 100:1 (bound:free Ca^{2+}) this would be an increase to 600 nM from 150 nM free Ca^{2+} ⁽¹⁴⁸⁾. Therefore, an influx of 14-21 μM total Ca^{2+} (140-210 nM free Ca^{2+}) would be insufficient to produce a contraction of normal magnitude (~40% of maximum⁽¹⁷⁹⁾) of the cardiomyocyte due to the small quantity, buffering and diffusion of Ca^{2+} ⁽¹⁸⁰⁾ (Figure 1.16). Indeed, a total $[Ca^{2+}]_i$ of 20 μM would give a contraction force of ~2% of maximum (Figure 1.16).

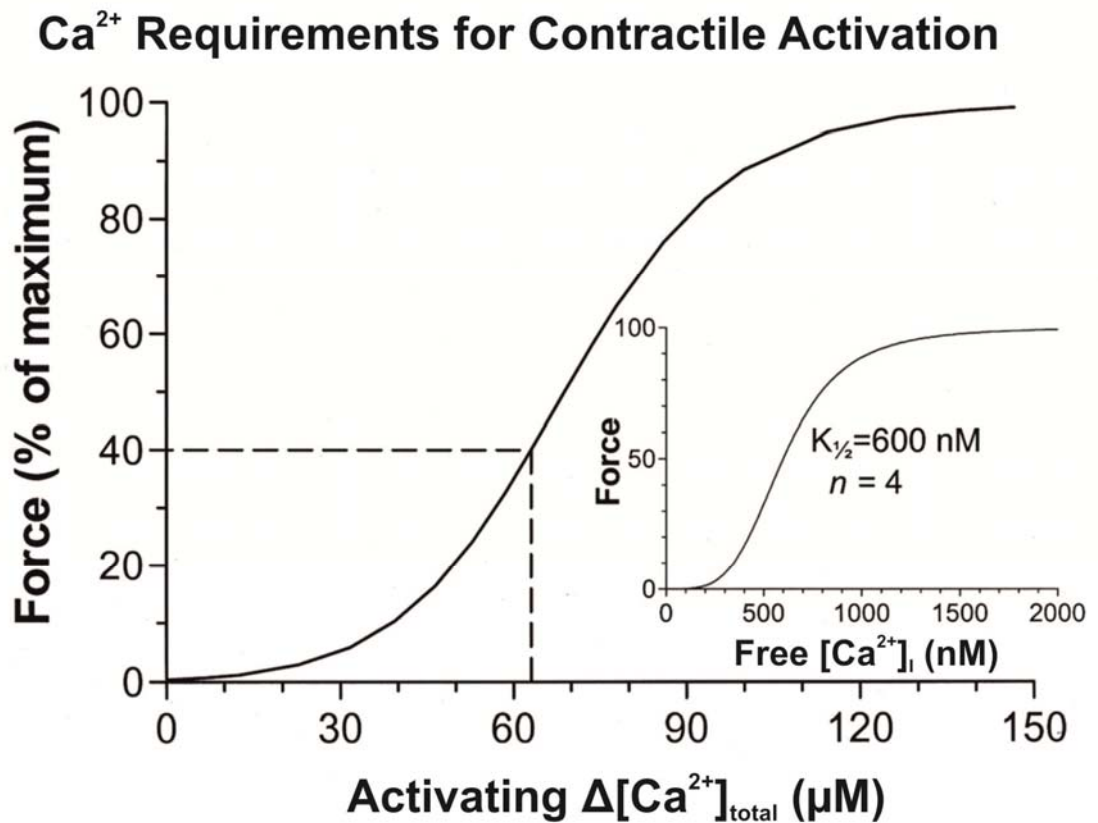


Figure 1.16: Ca²⁺ requirements for contractile activation.

Ca²⁺ requirements for contractile activation based on diastolic [Ca²⁺]_i = 150 nM and total cytosolic buffering = $244/(1+673/[Ca^{2+}]_i)-28$. This includes TnC, myosin, SERCA, calmodulin, ATP, creatine phosphate and sarcolemmal sites. (Inset) Force is shown as a function of free [Ca²⁺]_i. Force = $100/(1+1^n)$. Taken from Bers (2000) with permission⁽¹⁷⁹⁾.

1.4.1.2 Ca²⁺ Induced Ca²⁺ Release from the SR

During the 1970s and 1980s Fabiato demonstrated in experiments where the sarcolemma was carefully removed from canine Purkinje cells that the additional Ca²⁺ required came from the SR⁽¹⁸⁰⁻¹⁸⁴⁾. Removal of the sarcolemma and T-tubules allows the [Ca²⁺]_i to equilibrate with [Ca²⁺] of the solution the cell is bathed in. By altering the [Ca²⁺] of the bathing solutions it was possible to identify that application of increasing amounts of trigger Ca²⁺ resulted in a greater release of Ca²⁺ from the SR. A solution with [Ca²⁺] of 100 nM allowed accumulation of Ca²⁺ in the SR. Changing the solution [Ca²⁺] to 250 nM for 30 ms induced a release of Ca²⁺ from the SR of 1.7 μM and contraction of the cardiomyocyte. Interestingly, when [Ca²⁺] increased to 10 μM and applied for 150 ms the peak SR Ca²⁺ release was reduced to 1.2 μM and a smaller contraction⁽¹⁸⁴⁾. This suggests that high [Ca²⁺] inactivates SR Ca²⁺ release i.e. there is a peak activating concentration before a decline beyond that

concentration producing a bell curve of activation when tension is plotted against $[Ca^{2+}]$. In addition to a concentration effect, there was also a time-dependent effect. Fabiato (1985) tested different trigger Ca^{2+} activation times of 1, 5, 10, 20 and 50 ms with increasing $[Ca^{2+}]$. It was found that the longer trigger times resulted in reduced tension i.e. reducing the peak of the bell-shaped curve⁽¹⁸⁴⁾. Thus, this work by Fabiato suggests that a small Ca^{2+} influx of ~250 nM induces Ca^{2+} release from the SR amplifying the original trigger Ca^{2+} such that contraction occur. Moreover, an increase in the trigger $[Ca^{2+}]$ leads to an increase in the $[Ca^{2+}]$ amplification and subsequent contraction of the cardiomyocyte i.e. it is of a graded nature. However, beyond the optimal $[Ca^{2+}]$ ~10 μ M there is an inactivating effect producing the characteristic bell curve. Interestingly, one of the main hallmarks of ECC is the E_m dependent bell-shaped curve for I_{Ca} , change in $[Ca^{2+}]_i$ and contraction performed in intact cardiomyocytes^(148;185-189). The fact that there is such a close relationship with the change in E_m and I_{Ca} , contraction and $\Delta[Ca^{2+}]_i$ (Figure 1.17) suggests that I_{Ca} , contraction and $\Delta[Ca^{2+}]_i$ are themselves closely associated. It has been demonstrated that a change in I_{Ca} leads to the change in $[Ca^{2+}]_i$, which then leads to the change in contraction. This explains the observation of 40% contraction despite a Ca^{2+} influx that would only normally produce a 2% of maximum contraction, and that when extracellular Ca^{2+} is manipulated there is a change in amplification. Therefore the LTCC trigger activates the release of the SR Ca^{2+} store which supports a theory of Ca^{2+} induced Ca^{2+} release (CICR) in the heart.

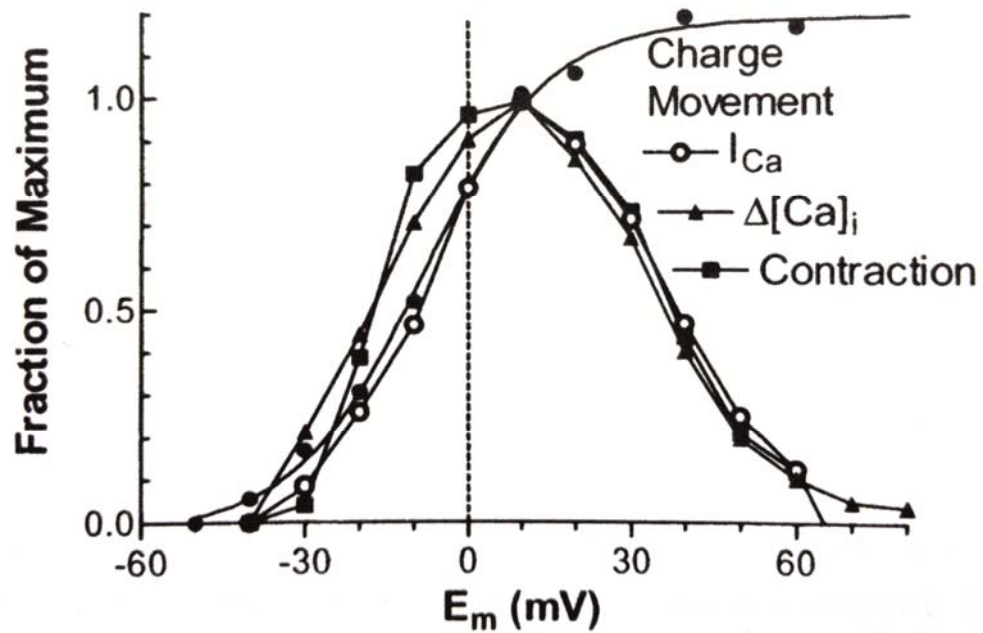


Figure 1.17: Voltage dependence of I_{Ca} , Ca^{2+} transient amplitude, contraction and charge movement in isolated guinea-pig ventricular cardiomyocytes.

I_{Ca} and Ca^{2+} transient amplitude data from Beuckelmann & Wier (1988)⁽¹⁸⁵⁾, charge movement from Hadley & Lederer (1991)⁽¹⁹⁰⁾ and contraction from Bers (2001)⁽¹⁴⁸⁾. All data were normalised to their respective maxima. Figure from Bers (2001)⁽¹⁴⁸⁾.

Thus, the relatively small rapid Ca^{2+} influx through the LTCC is enough to activate the RyRs releasing Ca^{2+} from the SR⁽¹⁵⁹⁾ (CICR). If Ca^{2+} activates the RyR, what prevents a positive feedback loop? The LTCC follows the E_m dependent bell-shaped curve as mentioned (Figure 1.17) demonstrating that higher I_{Ca} from the LTCC does not result in a runaway release of SR Ca^{2+} . Fabiato (1985) proposed that the RyR had two binding sites with different affinities and association constants⁽¹⁸⁴⁾. The initial trigger Ca^{2+} would bind with lower affinity but rapid onset resulting in SR Ca^{2+} release. The second inhibitory site would have a higher affinity for Ca^{2+} but a slower onset thereby inactivating the RyR a short time after influx, potentially explaining the reduced contraction at longer stimulation times⁽¹⁸⁴⁾. This was shown not to be the case when intact cardiomyocytes were studied, in fact contraction increased at higher $[Ca^{2+}]$ in experiments using flash photolysis of caged Ca^{2+} ⁽¹⁹¹⁾. Cannell *et al.* (1987) found that if cardiomyocytes were rapidly repolarised during the rising phase of the Ca^{2+} transient the peak was reduced⁽¹⁸⁷⁾. If there is a second inhibitory binding site on the RyR then in order to reconcile the findings of Cannell *et al.* the quantity of Ca^{2+} influx through the LTCC in the short time taken to deactivate the LTCCs must be increased for RyR inactivation to occur. However, they

calculated that the repolarisation of -24 mV to -54 mV would only increase Ca^{2+} influx by 20% according to the increased electrochemical gradient⁽¹⁵⁹⁾. A potential of -54 mV is the same potential at which the fast Na^+ channels inactivate marking the end of the effective refractory period therefore making the cardiomyocyte vulnerable to an early after depolarisation (covered in more detail in section 1.6.2.2) potentially leading to an arrhythmia⁽¹⁹²⁾. So if Fabiato's suggestion that there was sufficient influx during the repolarisation to inactivate CICR⁽¹⁸⁴⁾ was correct then Ca^{2+} could not be released and arrhythmic contractions could not occur. However, Cannell *et al.* observed that Ca^{2+} influx due to the electrochemical gradient upon repolarisation was not sufficient to explain the reduction in Ca^{2+} transient peak they observed⁽¹⁸⁷⁾ so another theory of inactivation is likely.

1.4.1.3 Local Control of CICR

1.4.1.3.1 Historical Models

Traditionally researchers had perceived the Ca^{2+} in the cardiomyocyte to be in a 'common pool' i.e. the SR is recharged by and releases into the same space. Unfortunately, a common pool model of CICR cannot amplify trigger Ca^{2+} and still be able to prevent positive feedback. This is because experimental evidence shows that when the cardiomyocyte is repolarised during the release phase⁽¹⁵⁹⁾ thereby inactivating the LTCC trigger, the Ca^{2+} transient peak is reduced. If a common pool model were true then the Ca^{2+} released would be expected to continue the release process, i.e. the process would be autonomous but this is not the case. Therefore, to attempt to establish a mathematical model of CICR, Stern (1992) looked at the ultrastructure of the cardiomyocyte and compared it to that of skeletal muscle⁽¹⁶⁵⁾. Due to the fact that the LTCC and RyR were in direct apposition in skeletal muscle⁽¹⁹³⁾ Stern considered local control theories⁽¹⁹⁴⁾. The first type was a synaptic type model where one LTCC is apposed with one RyR. In a synapse model the control could occur either; by random inactivation of the RyR and the local Ca^{2+} diffuses away; or by Ca^{2+} dependent inactivation of RyR and the local Ca^{2+} diffuses away. However, while this model permits the amplification of Ca^{2+} , it requires high conductance of the RyR for $[\text{Ca}^{2+}]_i$ to rise sufficiently to induce contraction⁽¹⁹⁴⁾. The second model Stern tried was one where one LTCC could activate several RyRs, the 'cluster-

bomb model'. This is a model where one LTCC can recruit a cluster of RyRs allowing for a graded response with amplification of the initial trigger Ca^{2+} .

1.4.1.3.2 Experimental Evidence

Experimental evidence for a localised SR Ca^{2+} release came from Cheng *et al.* (1993) in the form of local spontaneous Ca^{2+} release events of 200 nM amplitude, 2 μm diameter and 25 ms half-time decay termed 'Ca²⁺ sparks'⁽¹⁹⁵⁾. Ca^{2+} sparks occur randomly at a low frequency of $\sim 100.\text{s}^{-1}$ independent of Ca^{2+} influx at rest but several thousand can be synchronised by I_{Ca} through the LTCC which summates in time and space to form the stimulated Ca^{2+} transient⁽¹⁴⁸⁾. Due to the randomness of RyR opening at rest the process is best thought of in terms of stochastic probabilities. For example, at 10 μM [Ca^{2+}] within the dyadic cleft there is less than one free Ca^{2+} ion available (0.04) with 15 membrane-bound to activate a RyR within a 15 nm radius (dimension of the cleft)⁽¹⁴⁸⁾. In these terms the RyR activation is described in terms of open probability (P_o). It was initially proposed that a Ca^{2+} spark was the Ca^{2+} release event of a single RyR as the individual Ca^{2+} flux of a Ca^{2+} spark was calculated as $2 \times 10^{-17} \text{ mol}.\text{s}^{-1}$ (4 pA)⁽¹⁹⁶⁾, but appears to actually be from a cluster of 6-20 RyRs which would support the cluster-bomb model⁽¹⁴⁸⁾.

1.4.1.3.3 How Does Local Control Work?

Local control of Ca^{2+} sparks comes from the theory that Ca^{2+} release from a cluster of RyRs or 'couplon' is effectively an all-or-none phenomenon⁽¹⁹⁴⁾ so the release *within* a cluster can be regenerative. However, the physical distance between clusters and the requirement for high local [Ca^{2+}] to stimulate a cluster prevents them from activating one another as the released Ca^{2+} from neighbouring clusters will have diffused away. Therefore the Ca^{2+} release is limited to local regions of the cardiomyocyte and does not normally propagate i.e. the spatial and temporal characteristics of stochastic RyR opening prevent the general propagating regeneration of a common pool model. The gradation of response that was observed by Cannell *et al.* (1987)⁽¹⁸⁷⁾ can be explained by increases in Ca^{2+} influx recruiting more clusters of RyRs than by altering the amount of Ca^{2+} released from a cluster. That way, as mentioned above, the Ca^{2+} sparks from each cluster summate synchronously brought about by depolarisation of the sarcolemma during an AP.

1.4.1.3.4 Amplification of Ca^{2+}

The amplification of Ca^{2+} to 200-400 μM which can diffuse to the myofilaments⁽¹⁵⁹⁾ is a function of the fractional SR Ca^{2+} release which is dependent on both trigger Ca^{2+} and the SR Ca^{2+} content⁽¹⁹⁷⁻¹⁹⁹⁾. During a normal cardiomyocyte contraction the fractional release of the SR is 43 and 55% of its Ca^{2+} in rabbit and rat respectively^(197;198). This fractional release changes in response to altered trigger Ca^{2+} reflecting the graded nature of CICR⁽¹⁹⁸⁾. Interestingly, when the SR Ca^{2+} is altered and reduced to ~50% of normal the fractional release becomes effectively nil⁽¹⁹⁹⁾ i.e. I_{Ca} cannot trigger CICR. This could be due to an altered Ca^{2+} sensitivity of the RyR within the SR serving to prevent further depletion and allow refilling of the SR⁽¹⁴⁸⁾. This may indeed be a mechanism of terminating normal SR Ca^{2+} release to prevent a positive feedback loop. When SR Ca^{2+} content is increased the fractional release elicited is increased sharply suggesting a Ca^{2+} sensitising effect of the RyR within the SR. This may explain increased spontaneous release of Ca^{2+} in the case of SR Ca^{2+} overload (discussed in section 1.6).

1.4.1.3.5 Prevention of Positive Feedback

How does local control prevent positive feedback? There are 3 possibilities; i) local depletion of the SR Ca^{2+} , ii) inactivation of the RyR and iii) stochastic attrition^(194;200;201). Stochastic attrition means that if the LTCC and the RyRs of the associated couplon happen to be closed (channels have a finite probability of closing at any given time) at the same moment, then local $[\text{Ca}^{2+}]_i$ would fall to levels such that Ca^{2+} release from the SR is stopped. In a synapse model this would be quite likely, but for a cluster-bomb model would be harder to achieve as both the LTCC and all the RyRs of the cluster would have to be closed at a given time. SR Ca^{2+} depletion as a mechanism by which positive feedback is prevented can be tested with ryanodine or caffeine. These drugs act to induce Ca^{2+} release from the SR. When Cheng *et al.* (1993) and Satoh *et al.* (1997) performed these experiments, they found that there were long-lasting local elevations in $[\text{Ca}^{2+}]_i$ which did not decline over time^(195;202). If SR Ca^{2+} depletion was the mechanism then on the time-scale of a Ca^{2+} spark (~25 ms) one would expect a decrease in $[\text{Ca}^{2+}]_i$ to prevent regeneration of Ca^{2+} release, but the work of Cheng and Satoh shows $[\text{Ca}^{2+}]_i$ elevations lasting >200 ms^(195;202). This was confirmed by Sham *et al.* (1998) who found that early LTCC openings

produced events called Ca^{2+} spikes but that prolonged openings of the LTCC could not reactivate SR Ca^{2+} release⁽²⁰⁰⁾. These results argue against SR Ca^{2+} depletion as the prolonged LTCC opening should have elicited a response as the SR was not prevented from refilling. The results also argue against stochastic attrition as there is a finite probability of channel opening as well as closing so prolonged LTCC opening should have elicited a response if this were the case. Therefore some form of inactivation is more likely. Fabiato (1985) proposed that positive feedback of CICR was prevented by a second inactivating Ca^{2+} binding site on the RyR⁽¹⁸⁴⁾ i.e. Ca^{2+} dependent activation. However this was shown not to be the case with intact cardiomyocytes⁽¹⁹¹⁾. The work of Sham *et al.* (1998) with Ca^{2+} spikes demonstrated a use-dependent inactivation due to the failure of prolonged LTCC openings to induce SR Ca^{2+} release. These experiments used a high concentration of EGTA (4 mM) to produce the Ca^{2+} spikes. The problems that could arise are; i) additional Ca^{2+} buffering may decrease the ability of RyR to trigger neighbouring RyRs, ii) reduce local $[\text{Ca}^{2+}]_i$ around RyRs, which may either reduce local activation or limit inactivation, and iii) cytosolic Ca^{2+} buffering may decrease SERCA uptake of Ca^{2+} leading to SR Ca^{2+} depletion⁽¹⁴⁸⁾. There is probably a combination of factors affecting termination of SR Ca^{2+} release. Wang *et al.* (2001) showed a coupling fidelity between SR Ca^{2+} depletion and RyR inactivation of 0.71 at first trigger but dropping to 0.30 following a second stimulation at the same site⁽²⁰³⁾. This suggests a use-dependent inactivation.

1.4.1.3.6 A Likely Model?

Each of the above proposed models have evidence against them. Sobie *et al.* (2002) devised another theory supported by experimental data⁽²⁰⁴⁾. Anatomical observations suggest that RyR clusters are arranged in arrays with touching vertices with an accessory protein located at each vertex called FK-506 binding protein (FKBP)^(205;206). Therefore Sobie *et al.* (2002) proposed the 'sticky cluster' model where FKBP and RyR are coupled allowing for simultaneous openings/closings of RyRs within clusters⁽²⁰⁷⁾. In this model the coupling can be defined by a co-operativity factor with a maximum of 1 and <1 being reduced coupling that prolongs the duration of Ca^{2+} sparks i.e. lower co-operativity results in less efficient termination of Ca^{2+} sparks. Increases in local and SR $[\text{Ca}^{2+}]$ does not affect duration but the frequency of Ca^{2+} sparks (in a non-linear fashion).

These observations are seen with a RyR cluster size of 50⁽²⁰⁴⁾. In this model inactivation or adaptation of the RyRs is not required with the coupling of FKBP although the model does not specifically rule it out. Stochastic attrition, however, is intrinsic to this model and together with SR Ca²⁺ regulation of RyR and co-operativity with FKBP provides a model that stands up to the experimental data.

1.4.1.4 Activation of the Myofilaments

Once the RyRs have been activated and $[Ca^{2+}]_i$ rises Ca²⁺ can bind to troponin C (TnC), part of the thin filament regulatory complex (Figure 1.18). After Ca²⁺ binding TnC binds more strongly to troponin I (TnI) which pulls TnI from its actin binding site. The troponin/tropomyosin complex rolls deeper into the groove of the actin filament revealing the myosin binding domains of the actin filament. The myosin heads then attach forming a cross-bridge utilising the myosin ATPase to convert the chemical energy held within adenosine triphosphate (ATP) into mechanical energy. At rest, myosin is complexed with ATP or in a rapidly equilibrated state with adenosine diphosphate (ADP) and the inorganic phosphate (P_i) so ATP is technically hydrolysed but the energy has not been utilised yet^(208;209). As $[Ca^{2+}]_i$ rises the myosin-ADP-P_i complex interacts with actin as the troponin/tropomyosin complex rolls from the binding site releasing the P_i rapidly utilising the energy. The actin-myosin complex further pushes the troponin/tropomyosin complex into the actin groove which facilitates myosin binding at neighbouring TnC sites. The actin-myosin complex passes through two more energy state with ADP bound encompassing the 'power stroke' or myosin head rotation. Actin affinity increases through these steps until ADP dissociates. Under normal $[ATP]_i$ the actin-myosin complex binds ATP readily inducing dissociation of actin from myosin. The cycle continues until $[Ca^{2+}]_i$ declines. Without ATP the cross-bridges remain firmly attached in the state of rigor⁽¹⁴⁸⁾. The Ca²⁺-force interaction is reciprocal because cross-bridge binding and force generation enhance the affinity of Ca²⁺ binding to TnC which slows Ca²⁺ dissociation prolonging the active state.

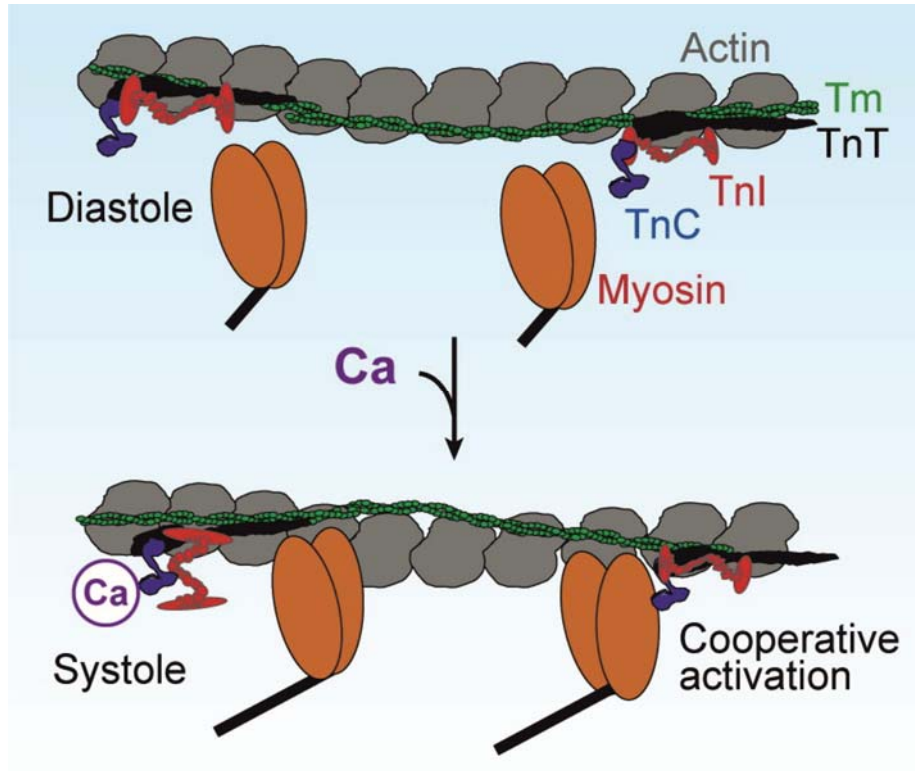


Figure 1.18: Ca^{2+} activation of the myofilaments.

Ca^{2+} binds to troponin C (TnC; blue) causing it to bind more strongly to troponin I (TnI; red). The troponin/tropomyosin complex (black/green) rolls into the actin (grey) groove revealing the binding site for myosin (orange). Binding of myosin further pushes the troponin/tropomyosin complex into the groove facilitating neighbouring myosin heads to bind (co-operative activation). Figure from Bers (2008)⁽¹⁵⁹⁾ with permission.

1.4.1.5 Inositol 1,4,5-Triphosphate Receptors

While RyRs are the primary Ca^{2+} release channel in the SR there are also inositol 1,4,5-triphosphate receptors (IP_3Rs). These are similar to RyRs in that they are large tetrameric intracellular Ca^{2+} release channels located in the SR membrane that are activated by Ca^{2+} ⁽²¹⁰⁾. However, IP_3Rs require IP_3 in addition to Ca^{2+} to be activated, therefore making them subject to the control of extracellular ligands that engage phospholipase C-activating sarcolemmal receptors such as GPCRs and tyrosine kinase⁽²¹⁰⁾. IP_3Rs are less abundant than RyRs (<1:50-100 of RyRs)⁽²¹¹⁾ but recent work shows they play a role in ECC⁽²¹²⁾. IP_3 signalling has been known about in ventricular cardiomyocytes for nearly 30 years⁽²¹³⁾ but purely as augmentation of RyR Ca^{2+} signalling⁽²¹⁴⁾. Signore *et al.* (2013) demonstrate a new mechanism that regulates ECC *via* ion channels and NCX resulting in depolarised resting membrane potential and prolongation of the AP⁽²¹²⁾. Therefore Ca^{2+} release from the IP_3R doesn't appear to affect contraction but can enhance Ca^{2+} transients *via* ion flux modulation. They found

that inhibition of RyRs had no effect on IP₃R AP modulation but intracellular Ca²⁺ buffering did⁽²¹²⁾. This suggests the existence of IP₃ signalling domains distinct from the dyadic cleft⁽²¹⁵⁾. The precedent for this is IP₃-dependent perinuclear Ca²⁺ signalling involved in excitation-transcription coupling as evidenced from imaging, immunofluorescence studies and electron microscopy⁽²¹⁶⁻²¹⁸⁾.

The relative quantities of IP₃ and IP₃R are much lower than other tissues⁽²¹⁹⁾ and in relation to RyRs in the heart⁽²²⁰⁾ such that it is unlikely to have a significant effect on [Ca²⁺]_i. Instead, it is more likely that any effect IP₃R has is local. Roderick and Knollmann (2013) suggest that Ca²⁺ released from adjacent IP₃R may “prime” the RyR for activation by LTCC Ca²⁺ influx and potentially decrease the cytosolic Ca²⁺ buffering in the vicinity of the dyad⁽²¹⁵⁾. Sigmore *et al.* (2013) also demonstrate activation of NCX the inward currents of which may explain the prolonged AP they observed⁽²¹²⁾. There was no depletion of intracellular Ca²⁺ so other channels must be affected in addition to NCX. This has potential as a source of arrhythmia generation as a previous study examining the Fas ligand causing IP₃-mediated AP prolongation and depolarised resting membrane potential resulted in an increased arrhythmia frequency⁽²²¹⁾. Arrhythmias are discussed in a later section.

1.4.2 Diastole

For the cardiomyocyte to relax again and allow the whole heart to relax and fill with blood before the next contraction, a series of events must occur to dissociate the Ca²⁺ from the myofilaments and recycle the Ca²⁺ from the cytosol back to the SR. Several mechanisms exist and there are species differences in terms of the proportion of Ca²⁺ removed from the cytosol by each mechanism. Figure 1.19 shows that during diastole Ca²⁺ is removed from the cytosol predominantly by reuptake to the SR by the sarco (endo)plasmic reticulum ATPase pump (SERCA) but also by sarcolemmal extrusion by the Na⁺/Ca²⁺ exchanger (NCX)⁽¹⁵⁸⁾. Other mechanisms of Ca²⁺ removal such as the sarcolemmal (plasma membrane) Ca²⁺ ATPase pump (PMCA) and the mitochondrial Ca²⁺ uniporter account for <25% of Ca²⁺ extrusion^(222;223). One study demonstrated that the time constant of decay (τ) for the PMCA was longer at 13.0 s in rat and 10.4 s in rabbit than either SERCA at 0.18 s and 0.29 s respectively or NCX at 1.73 s and 1.0 s so would have little effect in the normal

heart beat⁽²²⁴⁾. In the rat 92% of Ca^{2+} removal is due to SERCA and 7% due to NCX vs. 70% and 28% respectively in rabbit ventricular cardiomyocytes⁽²²⁴⁾. Human cardiomyocytes have similar Ca^{2+} handling properties to rabbits with SERCA contributing 63% and NCX contributing 37% Ca^{2+} removal in normal human cardiomyocytes⁽²²⁵⁾.

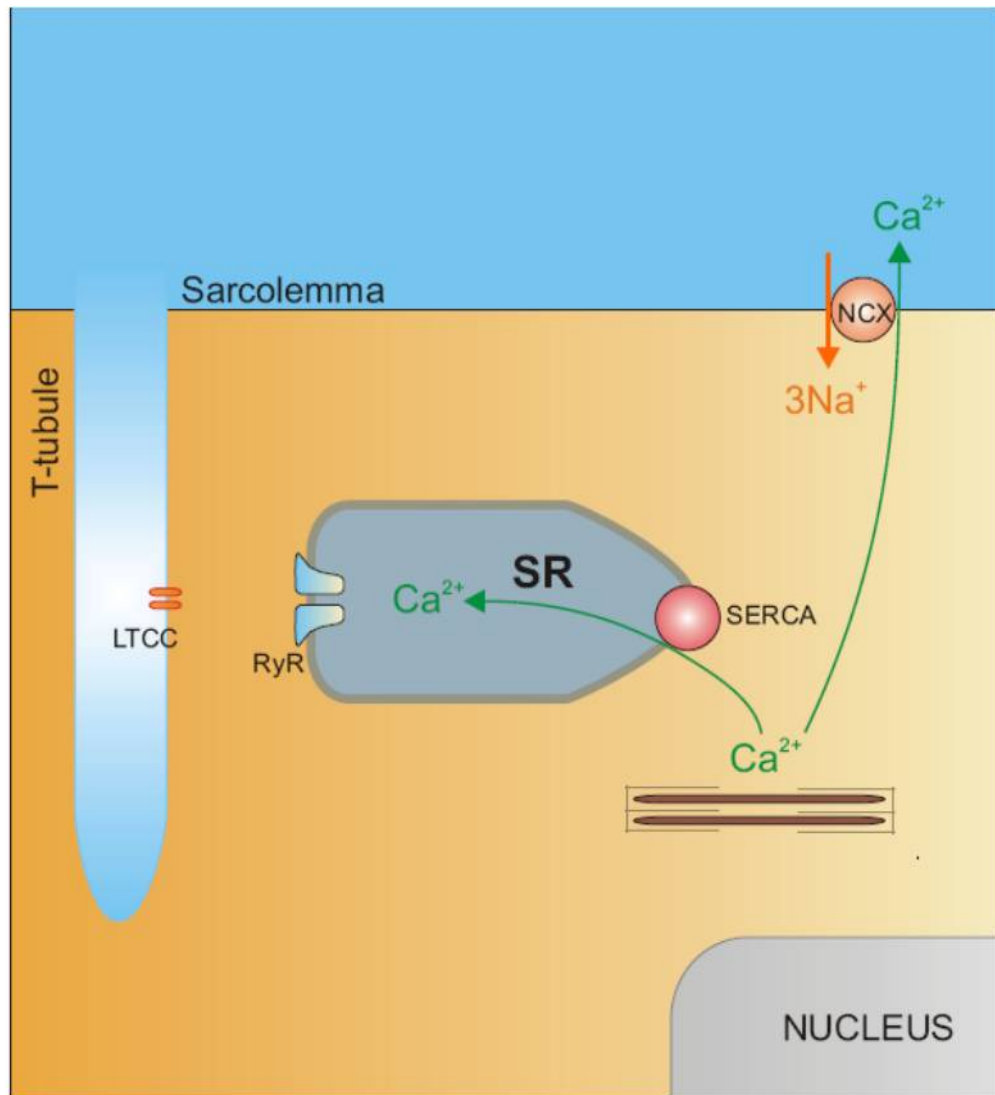


Figure 1.19: Ca^{2+} dynamics during diastole.

Ca^{2+} dissociates from the myofilaments and is removed from the cytosol *via* two main routes, sarcolemmal extrusion by the $\text{Na}^+/\text{Ca}^{2+}$ exchanger and back into the SR by the SR Ca^{2+} ATPase pump (SERCA). There is some Ca^{2+} extrusion by the plasma membrane Ca^{2+} ATPase (PMCA) and into the mitochondria but this is less than 25%.

1.4.2.1 Relaxation of the Myofilaments

The myofilaments remain active after $[\text{Ca}^{2+}]_i$ has decreased prolonging the active state of contraction i.e. a lag between decline in $[\text{Ca}^{2+}]_i$ and relaxation⁽¹⁵⁹⁾.

Bers (2008) suggests that increased Ca^{2+} affinity for TnC as a result of cross-bridge binding during contraction and slowed dissociation explains the lag between $[\text{Ca}^{2+}]_i$ and myofilament relaxation⁽¹⁵⁹⁾. Evidence in support of this is that acceleration in $[\text{Ca}^{2+}]_i$ accelerates relaxation proportionately whereas protein kinase A (PKA) dependent TnI phosphorylation (which accelerates TnC Ca^{2+} dissociation without altering $[\text{Ca}^{2+}]_i$ decline) has a much weaker lusitropic effect⁽²²⁶⁾. Altering TnC Ca^{2+} dissociation has been shown to influence relaxation⁽²²⁶⁻²²⁹⁾ therefore there is a dynamic interplay between Ca^{2+} binding, cross-bridge co-operativity and myofilament deactivation. Once the $[\text{Ca}^{2+}]_i$ has decreased the myosin remains in complex with ATP in the technically hydrolysed state (myosin-ADP- P_i) ready for the release of Ca^{2+} during the next cycle.

1.4.2.2 SR Ca^{2+} Re-uptake

The main route for Ca^{2+} to leave the cytosol is *via* re-uptake to the SR. This is achieved by the sarco (endo)plasmic reticulum Ca^{2+} ATPase pump (SERCA). SERCA is a member of the P-type ion transporting ATPases. The SERCA protein in cardiac muscle and slow twitch skeletal muscle is SERCA2a which has 4 fewer amino acids than the fast twitch skeletal muscle counterpart SERCA1a^(230;231). The general structure of SERCA consists of a cytoplasmic nucleotide binding domain where ATP binds to provide the energy for the pump action with the phosphorylation site at aspartate-351, a β strand domain and a hinge region^(232;233). There are 10 membrane spanning domains ($M_1 - M_{10}$), 5 of which have cytoplasmic helical stalks. Ca^{2+} binds with high affinity ($K_m < 1 \mu\text{M}$) to the cytoplasmic side of the pump. The Ca^{2+} is bound to M_4 - M_6 and M_8 possibly forming a channel^(234;235). The terminal phosphate of the bound ATP is transferred to aspartate-351 inducing the transition state of occlusion where Ca^{2+} cannot be released either side. The phosphorylation causes a transition from the E_1 form of the protein to E_2 which has a much lower Ca^{2+} affinity ($\sim 1 \text{ mM}$) thereby releasing the Ca^{2+} against a concentration gradient into the SR⁽¹⁴⁸⁾. In E_2 form protons are taken up and the aspartate-351 is dephosphorylated causing the protein to transition to a second occluded state. ATP binds to the nucleotide binding domain restoring the protein to the E_1 state releasing the protons ready to accept Ca^{2+} for the next cycle (Figure 1.20). It has been calculated that the likely range of SERCA concentration is 15-75 μM depending on species with rats having up 100 μM and rabbits about 19 μM ⁽²³⁶⁾. With an

estimated turnover of $10\text{-}15 \text{ ions.pump}^{-1} \cdot \text{s}^{-1}$ in dog and guinea-pig^(237;238) and ~4 fold lower affinity for Ca^{2+} than SERCA1a⁽²³⁷⁾ each pump would only have to cycle once to remove $50 \mu\text{M Ca}^{2+}$ from the cytosol⁽¹⁴⁸⁾.

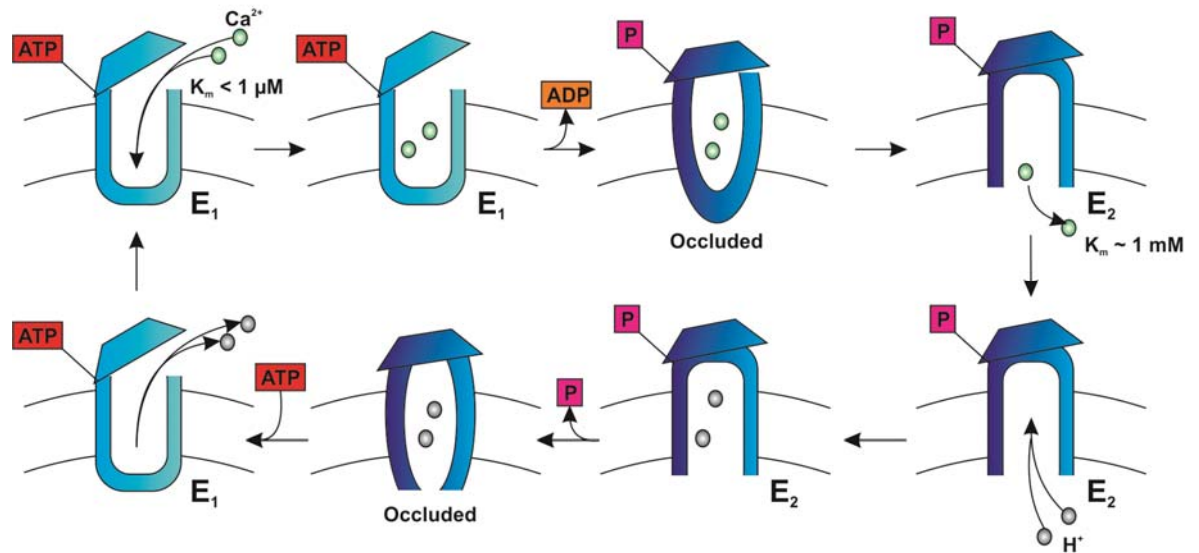


Figure 1.20: SERCA Ca^{2+} transport.

Starting from top left, two Ca^{2+} ions bind with high affinity ($< 1 \mu\text{M}$). Bound ATP is used to phosphorylate aspartate-351 altering the protein conformation from E_1 state so that the Ca^{2+} ions are occluded. The protein undergoes further conformational change to E_2 and releases the Ca^{2+} ions due to the reduced affinity ($\sim 1 \text{ mM}$). Protons are carried to reverse the conformational change from E_2 to E_1 .

1.4.2.3 SERCA Regulation

In contrast with skeletal muscle, cardiac SERCA is regulated by the protein phospholamban (PLB)⁽²³⁹⁾. PLB exists as a homopentamer (22 kDa; from five 6080 Da monomers). Each monomer consists of a hydrophilic cytosolic domain and hydrophobic transmembrane α -helix⁽²⁴⁰⁾. PLB is an endogenous inhibitor of SERCA acting to decrease Ca^{2+} transport and ATPase activity by reducing the affinity of SERCA for Ca^{2+} ^(241;242). This essentially shifts the Ca^{2+} re-uptake curve to the right. PLB can be phosphorylated at either/both of two residues; serine-16 by protein kinase A (PKA)^(239;240;243) and/or at threonine-17 by Ca^{2+} /Calmodulin Kinase II (CaMKII)^(244;245). This changes the conformation of PLB causing it to dissociate from SERCA which restores the higher Ca^{2+} affinity thereby increasing Ca^{2+} uptake to the SR (Figure 1.21).

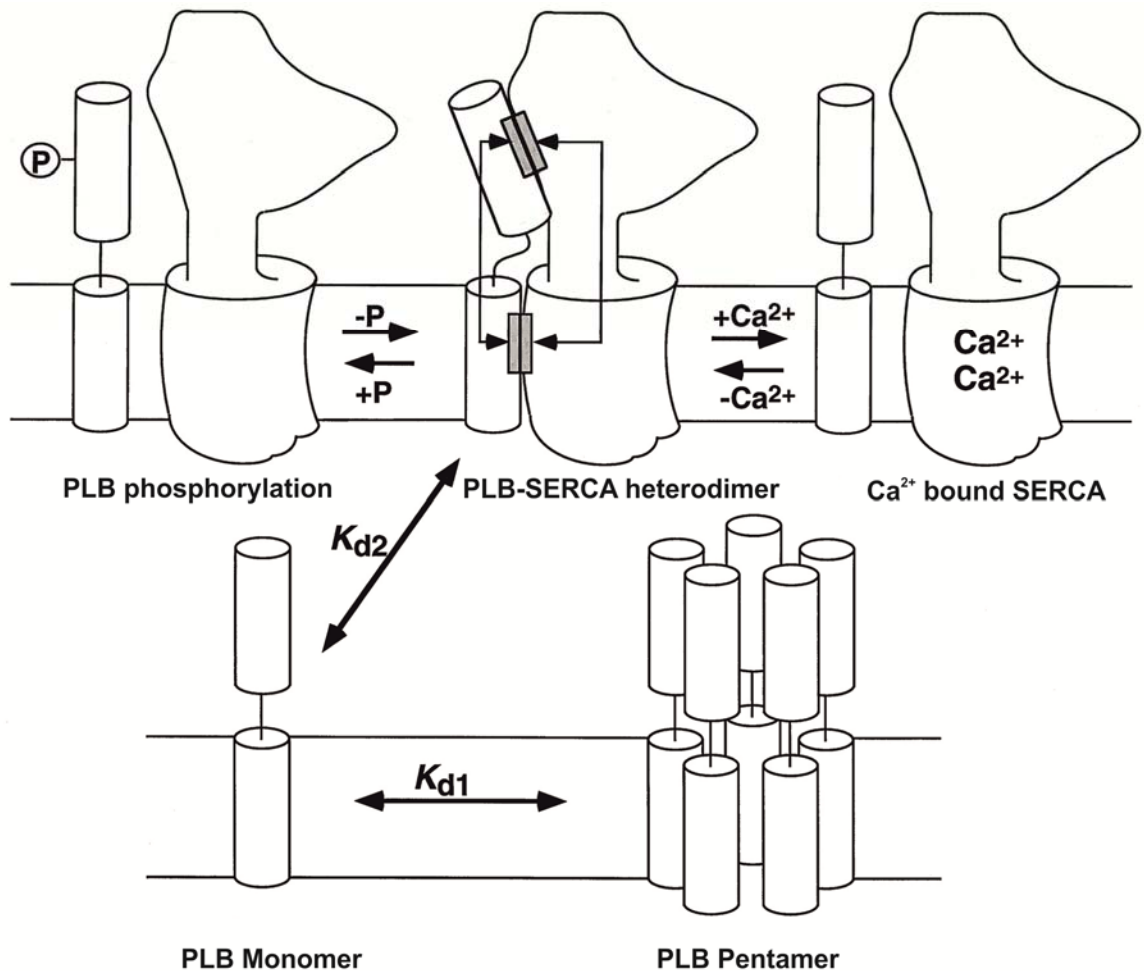


Figure 1.21: Schematic of PLB-SERCA Interaction.

PLB can exist as the monomer or the pentamer with a dissociation constant K_{d1} . Monomeric PLB binds to SERCA with a dissociation constant K_{d2} . Heterdimeric PLB-SERCA inhibits the ATPase but phosphorylation of PLB or Ca^{2+} binding to the pump can remove the inhibition. Figure from Kimura *et al.* (1997)⁽²⁴⁶⁾ with permission.

1.4.2.4 Sarcolemmal Extrusion of Ca^{2+} by $\text{Na}^+/\text{Ca}^{2+}$ Exchange

After SR re-uptake the next main contributor to reduce $[\text{Ca}^{2+}]_i$ during diastole is the $\text{Na}^+/\text{Ca}^{2+}$ exchanger (NCX). NCX is a ~110 kDa 938 amino acid protein with 9 transmembrane domains and a 550 amino acid cytoplasmic loop between the 5th and 6th transmembrane domains^(247;248). The cytoplasmic loop does not appear to be necessary for Na^+ or Ca^{2+} transport⁽²⁴⁹⁾ but does appear to be involved in allosteric regulation by Ca^{2+} ^(250;251). The NCX exchanges 3 Na^+ for 1 Ca^{2+} resulting in an electrogenic current ($I_{\text{Na/Ca}}$) which can act in either direction and contributes to the cardiac AP (Figure 1.11 & Figure 1.12). The direction NCX acts depends on E_m following a driving force equal to $E_m - E_{\text{Na/Ca}}$ (where $E_{\text{Na/Ca}} = 3E_{\text{Na}} - 2E_{\text{Ca}}$ with E_{Na} and E_{Ca} being the respective equilibrium potentials)⁽²⁵²⁾. Extrusion of Ca^{2+} is referred to as forward mode and removes the same $[\text{Ca}^{2+}]$ that entered

the cardiomyocyte *via* the LTCC during systole in order to maintain balance⁽²⁵³⁾. Extrusion of Ca^{2+} occurs as a single Ca^{2+} ion binds to the E_1 state NCX on the cytoplasmic side. This induces a conformational change through which NCX changes to the E_2 state facing outward. The Ca^{2+} is released and three extracellular Na^+ ions can bind the E_2 NCX. This induces a conformational change back to E_1 releasing the Na^+ inside the cardiomyocyte cytoplasm^{Hilgemann, 1991 757 /id} (Figure 1.22).

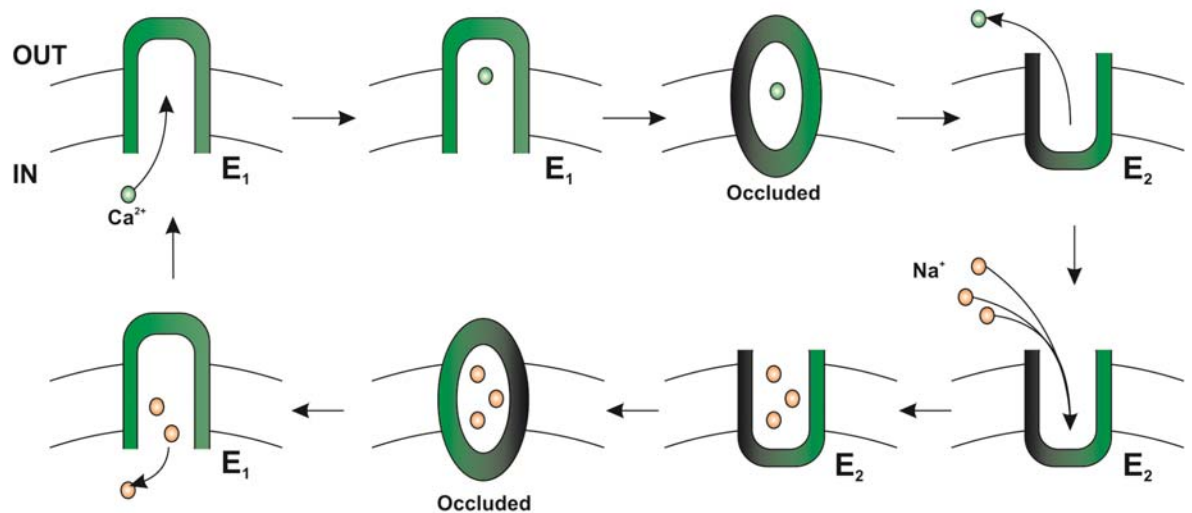


Figure 1.22: NCX Ca^{2+} transport in forward mode.

Starting from top left, a high $[\text{Ca}^{2+}]_i$ results in one Ca^{2+} ion binding to NCX causing a conformational change to the occluded form and then further change to the E_2 conformation facing the exterior of the cardiomyocyte. The Ca^{2+} is released and 3 Na^+ ions bind before a conformational change to an occluded state followed by return to E_1 occurs. The Na^+ ions are released and Ca^{2+} can bind again. Figure drawn from description by Hilgeman *et al.* (1991)^{Hilgemann, 1991 757 /id}.

Reverse mode NCX will bring Ca^{2+} into the cytoplasm and is governed by high $[\text{Na}^+]_i$ shifting E_m to more positive values than the equilibrium potential⁽²⁵²⁾. This will occur normally during depolarisation of the AP but only for a short time (<1 ms) before Ca^{2+} influx through the LTCC activates CICR and $[\text{Ca}^{2+}]_i$ rises switching NCX back to forward mode⁽¹⁵⁹⁾. There are species differences in $[\text{Na}^+]_i$ which determines the extent of Ca^{2+} extrusion by NCX. Rats for example have a higher resting $[\text{Na}^+]_i$ so Na^+ influx with concomitant Ca^{2+} extrusion by NCX has less drive meaning SERCA competes more effectively to reduced $[\text{Ca}^{2+}]_i$ thereby loading the SR at rest. This can be readily seen in resting rat cardiomyocytes as increased spontaneous contractile activity as the SR Ca^{2+} is higher which increases the sensitivity and P_o of the RyR⁽¹⁹⁹⁾. In the rabbit and human $[\text{Na}^+]_i$ is lower such

that the Ca^{2+} extrusion has a greater drive due to a higher differential concentration thereby increasing Ca^{2+} extrusion. SERCA competes relatively less effectively so the SR Ca^{2+} will have a tendency to decrease at rest⁽²⁵²⁾.

1.4.2.5 Other Ca^{2+} Removal Mechanisms

There are two other sources of Ca^{2+} removal from the cytosol; the sarcolemmal (plasma membrane) Ca^{2+} ATPase (PMCA) and the mitochondrial Ca^{2+} uniporter. The PMCA is a P-type ATPase like SERCA so it utilises the energy from ATP to transport ions. The PMCA can be stimulated by PKA and calmodulin^(255;256) enhancing both V_{\max} and K_m . However, during normal Ca^{2+} transients the transport rate is $<1\mu\text{M}\cdot\text{s}^{-1}$ so would take about 60 s to produce relaxation by itself⁽²⁵⁷⁾. When compared with the LTCC ($300\mu\text{M}\cdot\text{s}^{-1}$), RyR ($1000\mu\text{M}\cdot\text{s}^{-1}$), SERCA ($200\mu\text{M}\cdot\text{s}^{-1}$) and NCX ($30\mu\text{M}\cdot\text{s}^{-1}$) the transport of PMCA seems to be less important⁽¹⁴⁸⁾. Its purpose is more likely to be a longer term Ca^{2+} balance.

Mitochondrial transport in terms of ECC is also of limited importance as experiments by Bassani *et al.* (1992) demonstrated that inhibition of SERCA and NCX resulting in relaxation occurring over tens of seconds⁽²⁵⁷⁾. However Ca^{2+} fluxes may still be important in terms of mitochondrial function.

1.5 β -Adrenergic Stimulation

During situations of physiological or pathological stress the body responds with increased sympathetic tone leading to release of catecholamines such as adrenaline and noradrenaline. These ligands bind the adrenergic receptors including β_1 receptors in the heart. The β receptors are large 7 transmembrane proteins with a ligand binding domain on the extracellular side and the cytoplasmic C-terminal attached to GTP-binding protein (G-protein) (Figure 1.23A). Activation of the receptor results in dissociation of the α subunit which stimulates adenylyl cyclase (AC) to produce cyclic AMP (cAMP). Cyclic AMP activates PKA (and CaMKII potentially through PKA⁽²⁵⁸⁾) which phosphorylates; i) troponin I in the myofilaments acting to decrease sensitivity thereby improving lusitropy during diastole, ii) LTCC⁽¹⁵³⁾ increasing I_{Ca} , iii) PLB by PKA at serine-16^(239;240;243) (and by CaMKII at threonine-17^(240;244;245)) decreasing SERCA

inhibition, iv) RyR increasing P_o ⁽²⁵⁹⁾ (Figure 1.23A). These changes all serve to increase the inotropy and chronotropy of the heart⁽¹⁴⁸⁾.

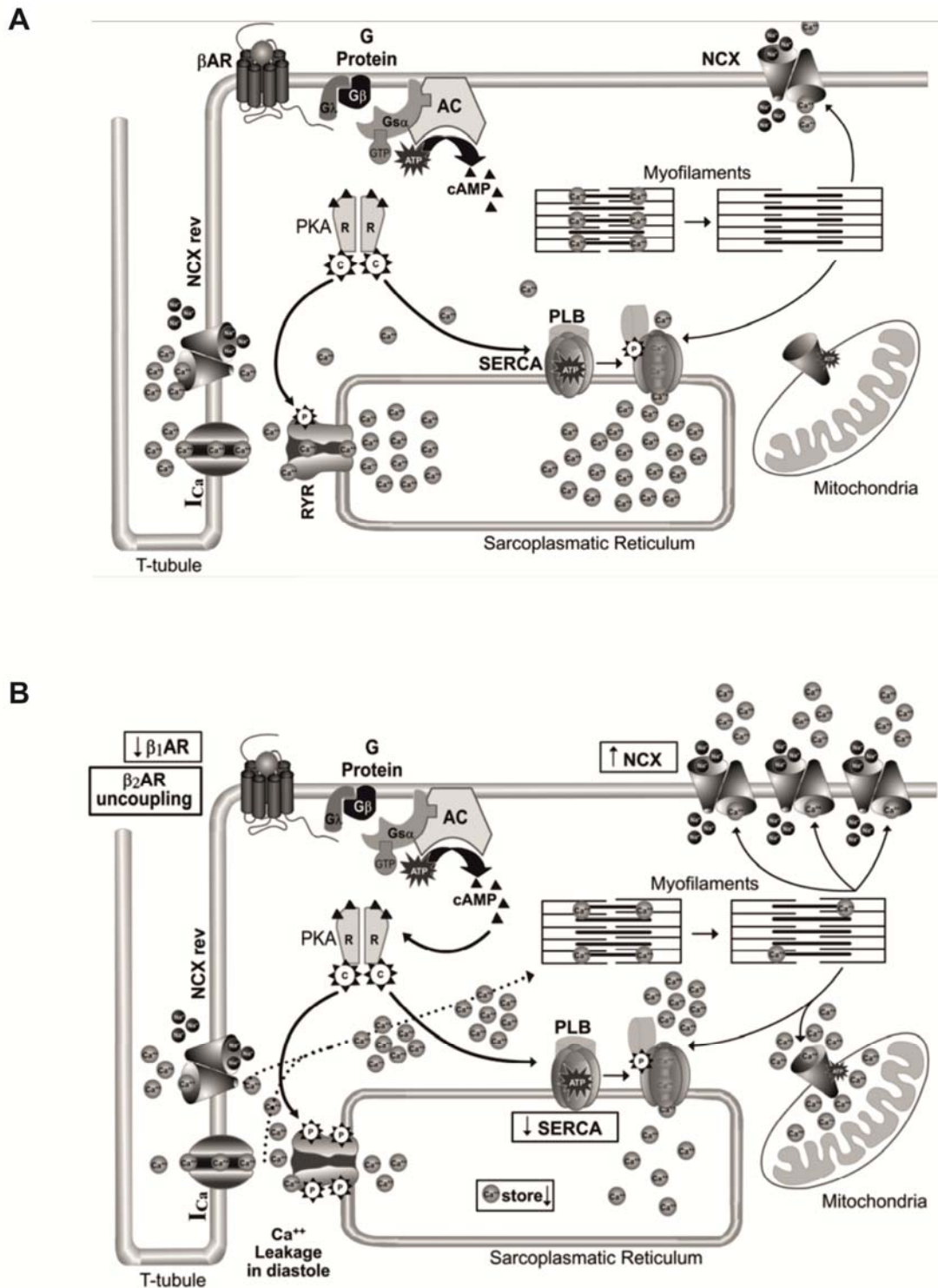


Figure 1.23: β -adrenergic signalling in the cardiomyocyte.

(A) Non-failing myocardium – β stimulation activates PKA which phosphorylates PLB disinhibiting SERCA, RyR increasing P_o , LTCC increasing Ca^{2+} influx and desensitises the myofilaments facilitating increased lusitropy. (B) Failing myocardium – proposed sequence of events from prolonged β -adrenergic exposure, PKA hyperphosphorylates RyR increasing P_o such that Ca^{2+} leaks at rest spontaneously, SERCA activity is downregulated and NCX is upregulated depleting the SR. Figure from Brum *et al.* (2006)⁽²⁶⁰⁾ with permission.

1.6 Abnormal Ca^{2+} Dynamics and Arrhythmias

Diseases of the heart can affect Ca^{2+} dynamics *via* alteration of RyRs, associated proteins, spatial organisation of couplons, RyR Ca^{2+} sensitivity, SR Ca^{2+} content and Ca^{2+} leak⁽²²²⁾. In the normal situation CICR occurs as Ca^{2+} influx through the LTCC triggers Ca^{2+} release from the RyR as described above. The Ca^{2+} release from an individual couplon or Ca^{2+} release unit is termed a Ca^{2+} spark⁽¹⁹⁵⁾ which will occur simultaneously across all couplons within the cardiomyocyte leading to a synchronous rise in $[\text{Ca}^{2+}]_i$ and contraction of the cell. Under certain circumstances, SR-mediated spontaneous Ca^{2+} release without a LTCC trigger can occur. In this case, the SR-mediated Ca^{2+} release is not synchronised by an AP throughout the T-tubules and results in an asynchronous propagating rise in $[\text{Ca}^{2+}]_i$ and wave of contraction. This event is called a Ca^{2+} wave⁽²⁶¹⁾.

1.6.1 Ca^{2+} Waves

Some types of arrhythmias can be traced back to abnormalities of Ca^{2+} handling, specifically Ca^{2+} waves when the SR is overloaded with Ca^{2+} ^(262;263). The Ca^{2+} waves occur when spontaneous Ca^{2+} sparks leak from the SR at a sufficient quantity ($\sim 100 \text{ s}^{-1}$) to trigger neighbouring couplons⁽²⁶¹⁾. Spontaneous Ca^{2+} release from the SR can be thought of in terms of a “threshold theory”⁽²⁶⁴⁾. When the SR $[\text{Ca}^{2+}]$ reaches threshold spontaneous Ca^{2+} release occurs, either from increasing the P_o of the RyR⁽²⁶⁵⁾ or the magnitude of the Ca^{2+} sparks⁽¹⁹⁵⁾. The normal SR threshold can be reached sooner by either increasing Ca^{2+} influx or decreasing Ca^{2+} efflux which will also elevate $[\text{Ca}^{2+}]_i$ thereby increasing the drive for NCX. The influx of Na^+ being electrogenic can trigger a delayed after depolarisation (DAD) which, if large enough, can trigger an AP. The SR Ca^{2+} release threshold depends on the properties of the RyR. If the P_o is increased, then the threshold is effectively lowered as a smaller $[\text{Ca}^{2+}]$ will trigger a release of Ca^{2+} . Experimentally the P_o can be increased (and threshold reduced) by caffeine⁽²⁶⁶⁾ whereas tetracaine has the opposite effect (reducing P_o and increasing the threshold)⁽²⁶⁷⁾. As would be expected of a Ca^{2+} stimulated receptor, RyR P_o is increased by higher SR and intracellular $[\text{Ca}^{2+}]$ ^(268;269). Stimulation with a β -adrenergic agonist can elevate Ca^{2+} influx *via* PKA-mediated phosphorylation of the LTCC⁽¹⁵³⁾ which will lead to an increased SR Ca^{2+} content. Likewise, the SR content can be increased by decreasing NCX action by raising

$[Na^+]_i$ through inhibition of the Na^+/K^+ ATPase with cardiac glycosides⁽²⁷⁰⁾. Alteration of RyR properties can occur pathologically altering its Ca^{2+} sensitivity. For example, in the disease catecholamine polymorphic ventricular tachycardia (CPVT) there is a mutation in the RyR^(271;272) which increases P_o in response to PKA-mediated phosphorylation beyond the normal level⁽²⁷³⁾. CPVT can also occur from mutations in the calsequestrin gene (*CASQ2*)⁽²⁷⁴⁾ and a triadin mutation has been reported⁽²⁷⁵⁾. In the case of heart failure, there are reports of hyperphosphorylation of the RyR resulting in dissociation of FKBP12.6⁽²⁷⁶⁾. FKBP12.6 acts as a diastolic inhibitor of RyR reducing P_o and aberrant Ca^{2+} release i.e. stabilising the closed state of the channel⁽²⁷⁶⁾. However, in heart failure this hypothesis remains controversial as phosphorylation of the RyR in different models of heart failure is inconsistent⁽²⁷⁷⁻²⁸⁰⁾. SERCA may also play a role in the generation of Ca^{2+} waves. The obvious effect is increased SERCA activity brought about by phosphorylation of PLB from β -adrenergic stimulation^(239;240;243) and disinhibition leads to a greater quantity of Ca^{2+} being pumped into the SR⁽¹⁹²⁾. However, SERCA can also have an opposite effect by decreasing Ca^{2+} wave propagation^(281;282) as the Ca^{2+} must diffuse through the cytoplasm from release site to release site past network SR containing SERCA i.e. SERCA is uptaking the released Ca^{2+} before it reaches the next release site⁽¹⁹²⁾.

1.6.2 Progression to Arrhythmias

1.6.2.1 Delayed After Depolarisations

Spontaneous Ca^{2+} release can lead to the generation of an “aftercontraction” or escape beat. At the single cell level, for an arrhythmic contraction to occur there is the generation of a transient inward current⁽²⁸³⁾ which can lead to a second depolarisation of the cardiomyocyte occurring after the primary SA nodal-derived AP. This is called a delayed afterdepolarisation (DAD). This has been shown to correlate with SR Ca^{2+} overload under voltage-clamp conditions⁽²⁸⁴⁾. The inward current has been shown to be initiated by the presence of Ca^{2+} at the inner surface of the sarcolemma from Ca^{2+} release from SR overload^(270;285). An electrogenic Ca^{2+} triggered sarcolemmal ion transporter is the NCX and the transient inward current has been attributed to inward NCX current⁽²⁸⁶⁾. The inward current, if large enough can reach threshold and depolarise the cell to trigger an AP⁽²⁸⁷⁾. However, the whole heart is a syncytium

of electrically coupled cells *via* connexin-43 gap-junctions⁽¹⁵⁴⁾. Any inward current occurring in one cell would be diluted across the coupled cells therefore many cells would have to exhibit a DAD simultaneously in order for an ectopic beat to occur⁽¹⁹²⁾. Winslow *et al.* (1993) used an atrial model comprising an array of 512 x 512 cardiomyocytes which suggested as many as 1,000 would be needed for an ectopic beat⁽²⁸⁸⁾.

1.6.2.2 Early After Depolarisations

Ca²⁺ waves can also be implicated in other kinds of arrhythmogenic disturbances such as spatially discordant alternans (SDA), repolarisation changes and early after depolarisations (EADs)⁽²⁸⁹⁾. EADs can occur when AP duration is prolonged which allows the L-type Ca²⁺ current to recover during the plateau phase of the AP⁽²⁸⁶⁾. This enables a second upstroke to occur. Unlike DADs which are mediated through the NCX, EADs are likely to be mediated through the L-type channels as E_m has not sufficiently repolarised to allow Na⁺ channels to have recovered from inactivation. EADs are thought to be involved in arrhythmias with prolongation of the electrocardiographic QT interval, although this is difficult to test as it would require AP recording in intact hearts⁽²⁸⁶⁾. Yet studies have shown that EADs appear to be synchronous events and not wave phenomena as seen in DADs which appear to show spatially heterogeneous Ca²⁺ increases^(290;291).

1.6.2.3 Treatment Strategies

There are three ways to target arrhythmias from Ca²⁺ waves; i) abolish the Ca²⁺ waves, ii) prevent Ca²⁺ waves producing a DAD (or EAD), iii) stop the DAD producing an ectopic beat. Preventing ectopic beats from DADs has been attempted with the local anaesthetics encainide and flecainide that reduce the excitability of the sarcolemma. Unfortunately they were shown to have dangerous adverse effects including sudden death⁽²⁹²⁾. Preventing Ca²⁺ waves from producing DADs would require inhibition of NCX to prevent the electrogenic influx of Na⁺ but this could have unwanted effects in terms of Ca²⁺ handling and may end up causing more Ca²⁺ waves as SERCA will no longer have competition and could overload the SR with Ca²⁺⁽²⁹³⁾. With regard to abolishing Ca²⁺ waves there are two approaches; prevent the SR Ca²⁺ overload that produces the

waves, or prevent the waves occurring despite Ca^{2+} overload. Preventing SR Ca^{2+} overload can be achieved by reducing the $[\text{Na}^+]_i$ thus increasing NCX mediated Ca^{2+} efflux. Local anaesthetics such as lidocaine and mexiletine inhibit the tetrodotoxin sensitive Na^+ channel thereby decreasing $[\text{Na}^+]_i$ resulting in increased Ca^{2+} efflux activity by NCX⁽²⁹⁴⁾. This must be carefully balanced so as not to cause a DAD *via* increased NCX activity. Prevention of Ca^{2+} waves without altering SR Ca^{2+} overload which would be best achieved by targeting the RyR and reducing P_o effectively increasing the SR Ca^{2+} release threshold but without altering systolic Ca^{2+} release⁽¹⁹²⁾. The RyR is regulated by FKBP12.6 during diastole preventing Ca^{2+} leak. The drug JTV519 (K201) has been suggested to increase FKBP12.6 binding decreasing the RyR P_o and has been shown to decrease occurrence of ventricular arrhythmias⁽²⁷³⁾. However, other studies propose no effect on FKBP12.6 binding from use of JTV519, although Ca^{2+} wave frequency is reduced^(295;296). The local anaesthetic tetracaine has also been shown to reduce RyR P_o ⁽²⁹⁷⁾ and increase the SR Ca^{2+} release threshold⁽²⁶⁷⁾. It was shown to abolish Ca^{2+} waves in cardiomyocytes subjected to Ca^{2+} overload by excessive β -adrenergic stimulation⁽²⁹⁸⁾. Unfortunately tetracaine would be an inappropriate drug as it has antagonistic effects at Na^+ channels required for APs; however a compound with more target specificity may be an attractive option.

1.6.3 Ca^{2+} Handling in Heart Failure

Heart failure (HF) is a disease state with weakening of myocardial contractility ultimately resulting in deterioration of ventricular pump function. This can occur following a severe myocardial insult such as a myocardial infarction (MI) where large areas of the myocardium have a reduced blood supply due to narrowing or blockage of the coronary arteries resulting in ischaemia. The remaining viable tissue can be taxed beyond its means and begin to fail. The characteristic cardiomyocyte features of HF are reduced systolic Ca^{2+} transient amplitude and prolonged Ca^{2+} transient duration⁽²⁹⁹⁻³⁰²⁾ with a concomitant reduction in the SR Ca^{2+} content⁽³⁰³⁻³⁰⁶⁾. The reduction in SR Ca^{2+} is thought to be due to an increase in diastolic Ca^{2+} leak from the SR from the RyR⁽²⁹⁹⁾ but could equally be due to reduced SERCA activity or protein levels and increased NCX activity. Reduced SERCA activity thereby reducing Ca^{2+} re-uptake to the SR during diastole could occur from reduction in SERCA expression as described by

Mercadier *et al.* (1990) in human heart failure⁽³⁰⁷⁾ or by reduced activity due to increased inhibition by PLB⁽³⁰⁸⁾. In human heart failure it has been shown that there is decreased phosphorylation of PLB at the PKA phosphorylated serine-16 residue⁽³⁰⁹⁾ and that the same is true in a rat model of heart failure⁽³¹⁰⁾. Current thinking is that CaMKII plays a role in heart failure through altered phosphorylation of PLB at the threonine-17 residue phosphorylated by CaMKII⁽³¹¹⁾. Increased NCX activity is thought to play a role in heart failure⁽³¹²⁻³¹⁵⁾, acting as increased competition for SERCA thereby reducing SR Ca²⁺ content, however these changes are inconsistent⁽³⁰²⁾. Another potential reduction in Ca²⁺ release is a reduced trigger Ca²⁺ from the LTCC. Indeed, it has been found that LTCC number has been reduced in HF⁽³¹⁶⁾. However, another study shows that the activity of LTCCs increases⁽³¹⁷⁾ which reflects an increase in β -adrenergic-mediated phosphorylation of LTCCs⁽³¹⁸⁾. What seems to be widely accepted though is diastolic Ca²⁺ leak from the SR⁽³¹⁹⁻³²³⁾, but the mechanism by which the leak occurs remains open to debate^(276;277;324). There is some evidence to suggest that hyperphosphorylation of the RyR at the CaMKII site Ser2815 can result in an increase in diastolic Ca²⁺ leak^(280;319), while the others propose PKA-mediated hyperphosphorylation of the RyR resulting in dissociation of the regulatory protein FKBP12.6^(276;324). Figure 1.23B shows the proposed changes present in heart failure. Many of the changes are a result of a chronic β -adrenergic stimulation leading to a refractory state where further stimulation has no effect therefore patients will be unable to adapt to an increase in cardiac workload⁽³²⁵⁾.

1.6.4 Ischaemia/Reperfusion Injury

Coronary heart disease (CHD) is the leading cause of death worldwide with an estimated 7 million deaths annually⁽³²⁶⁾. The disease is a narrowing and eventual blockage of the coronary arteries that supply the myocardium with blood. The result of blockage is myocardial infarction (MI) creating a region of ischaemia distal to the obstruction. Currently the most effective strategy for reducing the size of the infarct and improving clinical outcome is early reperfusion with use of thrombolytic therapy or percutaneous coronary intervention (PCI)⁽³²⁷⁾. PCI is a surgical procedure where a balloon is inserted into the blocked/narrowed coronary artery *via* a remote vessel, often a femoral or radial artery, and inflated to open the lumen of the affected coronary artery and restore blood flow to the ischaemic myocardium. Unfortunately the process of restoring blood

flow can itself be damaging - termed myocardial reperfusion injury. The injury results in death of cardiomyocytes that were viable immediately prior to reperfusion⁽³²⁸⁾. Myocardial reperfusion injury consists of four types of dysfunction. The first is myocardial stunning, a persistent mechanical dysfunction despite no irreversible damage and restoration of normal coronary flow⁽³²⁹⁾. This phenomenon is usually reversible days to weeks after the initial insult. The second type is the no-flow phenomenon where there is microvascular damage preventing restoration of blood flow to the affected region⁽³³⁰⁾. The third type is reperfusion arrhythmia brought about by Ca^{2+} overload and modulation of the Ca^{2+} handling proteins such as LTCC, RyR, SERCA and NCX⁽³³¹⁻³³⁷⁾ as discussed in section 1.6.1. The fourth type of cardiac dysfunction is termed lethal reperfusion injury⁽³²⁷⁾. There are multiple contributing factors; oxygen, Ca^{2+} and pH paradoxes and inflammation. Oxygen paradox is where reperfusion of the ischaemic tissue results in oxidative stress and release of reactive oxygen species (ROS) and myocardial enzymes⁽³³⁸⁾ including cathepsins^(339;340). Ca^{2+} paradox occurs when intracellular Ca^{2+} rises secondary to sarcolemmal damage and ROS effects inhibiting SERCA⁽³⁴¹⁻³⁴⁴⁾ and increasing P_o of the RyR^(341;345-347). The increase in Ca^{2+} can overload the cardiomyocyte leading to a state of hypercontracture and can overload the mitochondria leading to opening of the mitochondrial permeability transition pore (MPTP)⁽³²⁸⁾ which causes cell death by uncoupling of oxidative phosphorylation and ATP production. The pH paradox happens when rapid reperfusion washes out the lactic acid from anaerobic respiration leading to activation of the Na^+/H^+ exchanger and $\text{Na}^+/\text{HCO}_3^-$ symporter overwhelming the cell's pH buffering capacity⁽³⁴⁸⁾, which can depress force of contraction, raise diastolic $[\text{Ca}^{2+}]_i$ ⁽¹⁴⁸⁾. Finally inflammation; the infarct zone attracts neutrophils during the first 24 hours causing vascular plugging, release of degradative enzymes such as cysteine proteases and ROS⁽³⁴⁹⁾ (Figure 1.24).

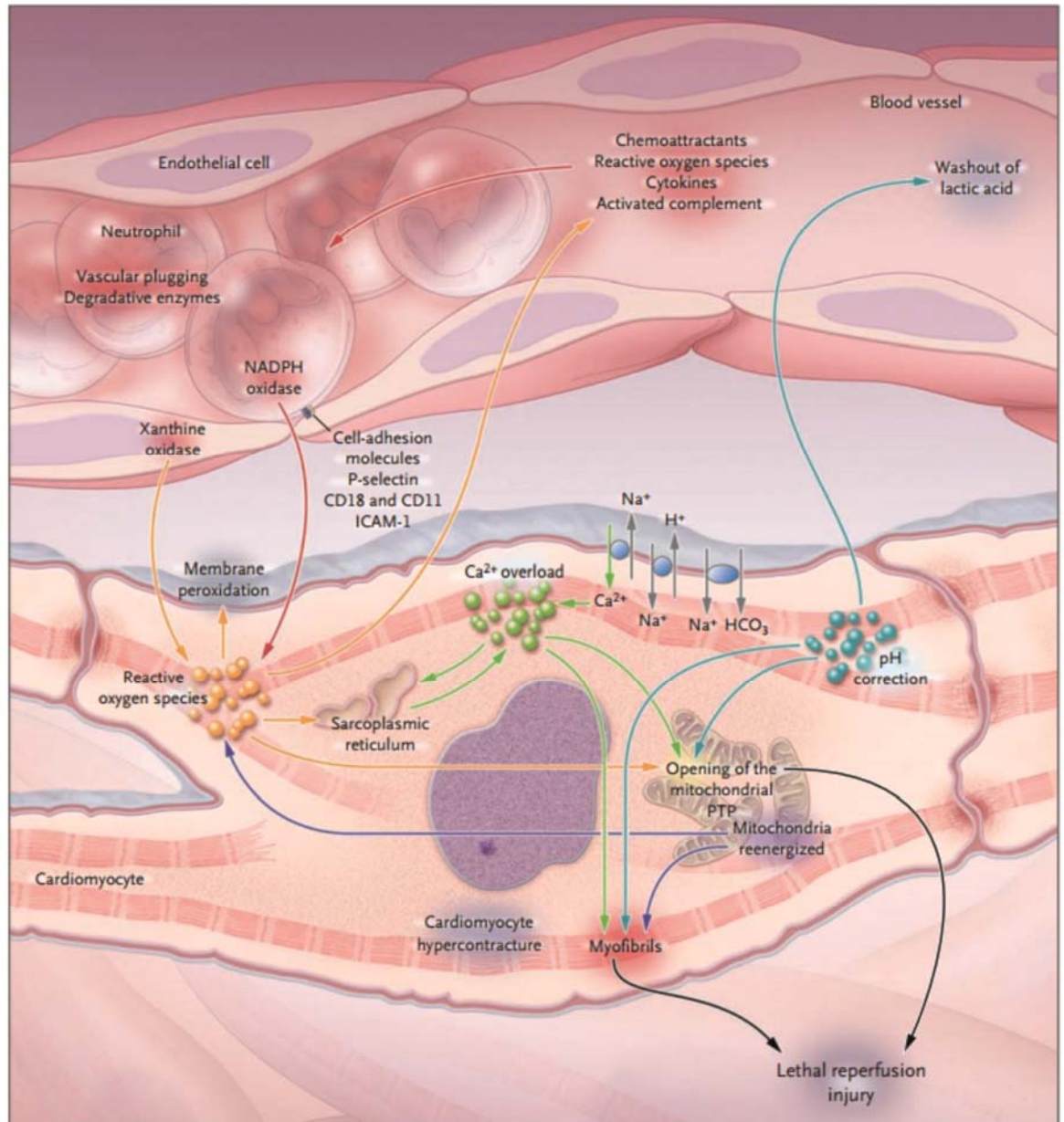


Figure 1.24: Mediators of Reperfusion Injury

During ischaemia several biochemical and metabolic processes contribute to injury. Mitochondrial re-energisation (purple), generation of ROS (orange), [Ca²⁺]_i overload (green), rapid restoration of pH (blue) and inflammation (red) all interact to mediate cardiomyocyte death through the opening of the MPTP causing hypercontracture of the cardiomyocyte. Reproduced with permission from Yellon and Hausenloy (2007)⁽³²⁷⁾, copyright Massachusetts Medical Society.

1.6.4.1 Treatment Strategies

Previous attempts at targeting individual mediators of lethal reperfusion injury have produced inconsistent results that have not translated to clinical studies, which have been extensively reviewed in Yellon and Hausenloy (2007)⁽³²⁷⁾. The current thinking is to target multiple mediators to achieve a synergistic effect. For example, ischaemic post-conditioning targets several mediators and has been shown to reduce myocardial injury in a clinical study of patients with acute

MI undergoing PCI⁽³⁵⁰⁾. Ischaemic post-conditioning was identified by Zhao *et al.* (2003) who reduced infarct size from 47% to 11% after a 45 min period of ischaemia in dogs. This was achieved by inducing three 30 s cycles of ischaemia during reperfusion⁽³⁵¹⁾. Post-conditioning acts to reduce oxidative stress, Ca²⁺ overload, improve endothelial cell function, reduce cardiomyocyte apoptosis, reduce neutrophil accumulation⁽³⁵²⁾ as well as delaying the restoration of normal pH⁽³⁵³⁾. In addition, post-conditioning also activates the reperfusion injury salvage kinase (RISK) pathway⁽³⁵⁴⁾ and inhibits MPTP opening⁽³⁵⁵⁾. Preconditioning is a similar phenomenon whereby infarct size can be reduced by initiating transient periods of ischaemia before the sustained ischaemic event and appears to act in a similar way as post-conditioning⁽³⁵⁶⁾. Several studies have tested post-ischaemic conditioning and reduced infarct size by up to 36% with improved coronary blood flow^(350;357;358). The disadvantage of post-ischaemic conditioning is that it requires surgical intervention and so is only available to patients with acute MI undergoing PCI. Therefore, pharmacologically targeting the mediators recruited by post-conditioning or indeed others that activate the RISK pathway or inhibit MPTP opening would be attractive targets. Hausenloy and Yellon have shown that agents that activate phosphatidylinositol-3-OH kinase (PI3K)-Akt and p42/p44 extracellular signal-regulated kinases (Erk 1/2) have reduced infarct sizes by up to 50%^(354;356). Other strategies examined have been atrial natriuretic peptide before PCI which reduced infarct size by 15% and improved ejection fraction by 5% but had no effect on mortality⁽³⁵⁹⁾, glucagon-like peptide 1 which reduced infarct size by up to 45%⁽³⁶⁰⁾, erythropoietin which reduced infarct size by 42%⁽³⁶¹⁾ and atorvastatin which reduced infarct size by 48%⁽³⁶²⁾. Inhibition of the MPTP has been investigated and shown that with cyclosporine or sangliferrin A (MPTP inhibitors) that infarct sizes can be reduced by 50%⁽³⁶³⁾. The role of degradative enzymes such as the cysteine proteases were investigated in the 1980s by Bolli and colleagues which showed that the cysteine proteases could play a role in acute MI but that general proteolysis was not the method by which they acted based on the technique they used⁽³⁶⁴⁾. However they acknowledge that their technique of measuring tyrosine release is not specific enough to detect selective proteolysis of particular proteins⁽³⁶⁴⁾. They did however identify proteases that could have a role in acute MI through specific inhibition with leupeptin, pepstatin and antipain, specifically cathepsins A, B, D, L and H. A second study by the same group examined infarct size after ischaemia with

protease inhibition but found no significant change⁽³⁶⁵⁾. However, recent evidence has emerged that suggest proteases and their inhibition do have a significant role in ischaemia/reperfusion injury in the brain following stroke^(366;367).

1.6.5 Endogenous Cathepsins

The maintenance of a healthy organism requires controlled biosynthesis, maturation, function and terminal breakdown of proteins. Proteolytic enzymes contribute to these processes by cleaving peptide bonds resulting in the target protein's destruction, maturation or modulation of its biological activities⁽³⁶⁸⁾. These proteolytic enzymes are broadly categorised as matrix metalloproteinases (MMPs) and cathepsins, derived from the Greek word *kathépsin* meaning to digest or boil down first identified in the 1920s⁽³⁶⁹⁾. The cathepsins can be classified according to substrate specificity; serine cathepsins (A and G), aspartic cathepsins (D and E) and cysteine cathepsins (B, C, F, H, L, K, O, S, W, V and X)⁽³⁷⁰⁾, which are the primary focus of this thesis. The cathepsins were shown to be localised within acidic intracellular organelles such as lysosomes and endosomes where their primary function was to break down unwanted proteins⁽³⁷¹⁻³⁷⁴⁾.

1.6.5.1 Cathepsins in the Whole Body

Recent studies reveal a much wider role for cathepsins in health such as antigen presentation in the immune system⁽³⁷⁵⁾, collagen turnover in bone and cartilage^(376;377) and neuropeptide and hormone processing^(378;379). A list of currently known cysteine cathepsins and their physiological functions is presented in Table 1.2 from Brix *et al.* (2008)⁽³⁸⁰⁾. Recent work has also shown a wider range of active locations and pH for cathepsins such as secretory vesicles^(381;382), the cytosol⁽³⁸³⁻³⁸⁵⁾, and the nucleus^(386;387) each of which are shown in Table 1.2.

Table 1.2: Clan C1A cysteine proteases.

Name	Tissue Expression	Function	pH
Cathepsin B	Ubiquitous	Lysosomal, extracellular; proteolytic processing of amyloid precursor protein, tumour invasion and metastasis	pH 4-6 (optimal), pH 7 (stable)
Cathepsin C	Ubiquitous	Lysosomal; activates granulocyte serine proteases, factor XIII neuraminidases	pH 6 (optimal), pH 4-7.5 (stable)
Cathepsin F	Heart, skeletal muscle, brain, testis, ovary	Lysosomal; role in tumour invasion and metastasis	pH 5.2-6.8 (optimal), pH 4.5-7.2 (stable)
Cathepsin H	Brain, kidney, liver; inflamed tonsil	Lysosomal; invariant chain (li) degradation	pH 6.8 (optimal), pH 5-8 (stable)
Cathepsin K	Predominantly in bone (osteoclasts); present in most epithelial tissues	Lysosomal, extracellular; osteoclastic bone resorption; fibrinogen and ECM degradation	pH 6 (optimal), pH 4-8 (stable)
Cathepsin L	Ubiquitous	Lysosomal, extracellular, nuclear (truncated); antigen presentation, li degradation, cell cycle regulation	pH 6 (optimal), pH 4-7 (stable)
Cathepsin S	Alveolar macrophages, spleen, testis, epithelial cells; CD4+ T-cells	Lysosomal, extracellular; li degradation, arterogenesis, antigen presentation, angiogenesis, elastolytic activity	pH 6 (optimal), pH 4.5-8 (stable)
Cathepsin V (L2)	Predominantly in thymus, testis; present in brain, corneal epithelium, skin	Lysosomal; antigen presentation, li degradation	pH 5.7 (optimal), pH 4-7.2 (stable)
Cathepsin W	Spleen, natural killer and cytotoxic T-cells	Immune response, regulation of T-cell cytotoxic activity	Not reported
Cathepsin X	Widely expressed; ubiquitous in primary tumours	Lysosomal; non-proteolytic in cell adhesion	Not reported

Moreover, the cysteine cathepsins have been shown to have roles in various disease processes such as cancer⁽³⁸⁸⁾, obesity⁽³⁸⁹⁻³⁹¹⁾, rheumatoid arthritis^(392;393) as well as cardiovascular diseases such as atherosclerosis⁽³⁹⁴⁻³⁹⁹⁾ and cardiomyopathy⁽⁴⁰⁰⁻⁴⁰²⁾ demonstrated in both animal models and human cases. For example, in cancer, cathepsins B, F, H, K, L, V, S and X have been shown to be overexpressed in many carcinomata and frequently associated with a poor prognosis⁽⁴⁰³⁻⁴⁰⁸⁾. In the case of obesity and type II diabetes, deletions of cathepsins K or L have been shown to limit obesity, and cathepsin S has been shown to be increased in both clinical cases of type II diabetes and in diabetes-prone mice^(391;409-411). The cathepsins B, L, K and S are reported to be involved in rheumatoid arthritis and osteoarthritis as levels of these cathepsins are increased within the synovial fluid of patients with these conditions⁽³⁶⁸⁾.

1.6.5.2 Cathepsins and the Cardiovascular System

As well as cancer and metabolic diseases such as diabetes, cysteine cathepsins also play a role in cardiovascular disease. For example, cathepsins B, L and S have been shown to be increased in atherosclerotic lesions of mice⁽⁴¹²⁾. Moreover, cathepsins K and S were found to be overexpressed in human atherosclerotic lesions⁽³⁹⁸⁾, and more recently, cathepsin L protein expression has also been shown to be increased in atherosclerotic lesions with a concomitant increase in circulating serum levels⁽⁴¹³⁾. Cathepsins also play a role in restenosis and neointima formation following PCI⁽⁴¹⁴⁾. Cathepsins contribute to extracellular matrix (ECM) remodelling as part of their protease activity⁽⁴¹⁴⁾, which suggests a possible role in remodelling diseases such as restenosis and neointima formation. In a rabbit model of balloon injury (a method of PCI where inflation of a balloon inserted into the coronary vessel *via* the femoral artery restores the lumen of the occluded artery), cathepsin S mRNA and protein expression were increased⁽⁴¹⁵⁾. A similar study in rats utilising a carotid balloon injury showed increased mRNA and protein expression of both cathepsins S and K⁽⁴¹⁶⁾. By their ECM remodelling activity, cathepsins also play a role in aneurysm formation. When human patients with abdominal aortic aneurysm were assessed it was found that the lesion showed increased protein expression of cathepsins K and S with a concomitant decrease in the natural cathepsin inhibitor, cystatin C⁽⁴¹⁷⁾. Moreover, further studies have demonstrated increased proteolytic activity of cathepsins B and L in the wall of the aneurysm and associated

thrombus⁽⁴¹⁸⁻⁴²⁰⁾. In the same study by Liu J *et al.* (2006) that examined serum cathepsin-L (CatL) levels in patients with atherosclerosis, raised serum levels of CatL were also found in patients with aneurysm⁽⁴¹³⁾.

1.6.5.3 Cathepsins in the Heart

Within the heart, cysteine cathepsins are expressed in all cell types (Figure 1.25). The upshot of this is that cysteine cathepsins have multiple roles in cardiac disease. A study by Cheng *et al.* (2006) showed that cathepsins B, S and K mRNA and protein expression were increased in hypertrophic and failing myocardium in the Dahl salt-sensitive rat model of hypertension⁽⁴²¹⁾. Moreover, when immunohistochemistry for cathepsins K and S was performed on the myocardium from the same rats, there was increased staining in cardiomyocytes, intra-coronary smooth muscle cells and macrophages compared to normal control myocardium⁽⁴²¹⁾. When the hypertensive rats were treated with the broad spectrum cysteine protease inhibitor E-64 (trans-epoxysuccinyl-L-leucylamido-(4-guanido) butane) or a CatS specific inhibitor, elastinolytic activity in the myocardium was blunted^(421;422). Cysteine cathepsins also play a role in cardiomyopathy. Further studies by Cheng *et al.* (2012) have observed increased mRNA expression of cathepsins B, L, S and/or K in both dilated and hypertrophic cardiomyopathy in human disease⁽⁴²³⁾.

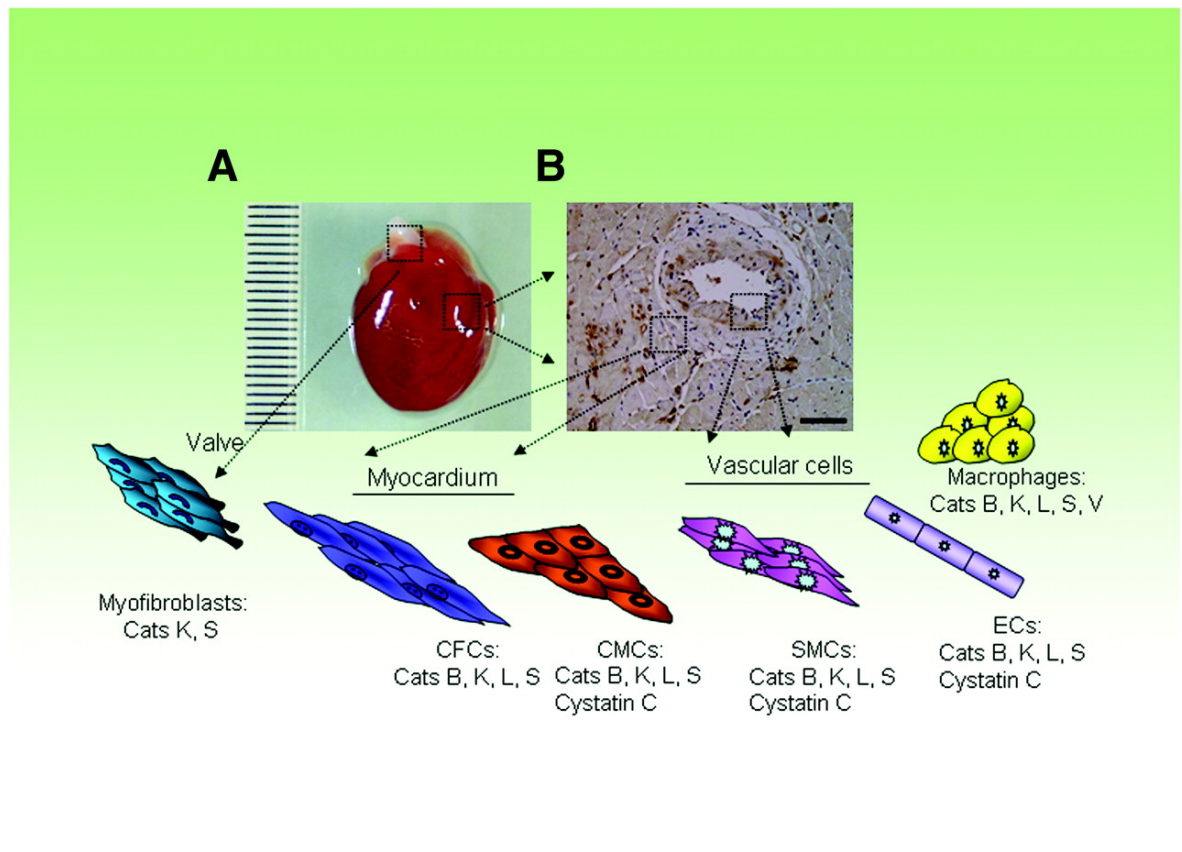


Figure 1.25: The cathepsin cysteine proteases expressed in cardiovascular cells. (A) Macroscopy of whole heart. (B) Microscopy of the myocardium, scale bar = 50 µm. Cats = cathepsins; CFC = cardiac myofibroblast; CMC = cardiomyocyte; SMC = smooth muscle cell; and EC = endothelial cell. Figure from Cheng *et al.* (2012) with permission⁽⁴²³⁾.

Although other cathepsins have been studied in cardiovascular disease such as B, K and S⁽⁴²³⁾, CatL is gaining interest. CatL is a ubiquitously expressed homeostatic enzyme involved in many disease processes⁽³⁶⁸⁾. Within the heart it is known that a basal level appears to be necessary, as a CatL knockout mouse model shows a dilated cardiomyopathy phenotype⁽⁴⁰²⁾. It also seems to play a role in cardiovascular disease involved in remodelling post-infarction⁽⁴²⁴⁾ and atherosclerosis⁽⁴¹³⁾ and appears to be increased in the serum of individuals with coronary heart disease^(425;426). However, the consequences of raised serum levels remain unclear as do the potential mechanisms of action. What has been shown, in the case of coronary artery disease, is a positive correlation of serum CatL levels and severity of disease⁽⁴²⁵⁾. Specifically, there were three findings; i) patients with unstable angina pectoris had higher serum CatL levels than those with stable angina pectoris, ii) of patients with acute coronary artery disease, those with acute MI had higher CatL serum levels than those with unstable angina pectoris, iii) patients with previous chronic MI had the highest serum CatL of all⁽⁴²⁵⁾. Furthermore, there is a strong correlation between percentage of stenosis of the left anterior descending coronary and serum CatL levels in

individual patients⁽⁴¹³⁾. A recent study by Liu *et al.* (2013) investigated the role of CatB in myocardial infarction⁽⁴²⁷⁾. In that study rats were subjected to left anterior descending coronary artery ligation followed by intraperitoneal administration of the CatB specific inhibitor CA074Me at a dose of 10 mg.kg.day⁻¹ or equivalent volume of vehicle for 4 weeks. They found the treated rats demonstrated smaller decreases in cardiac function, decreased cardiomyocyte hypertrophy and decreased fibrosis⁽⁴²⁷⁾. In addition, the serine cathepsin CatA and the aspartic cathepsin CatD have also been shown to be released and have increased proteolytic activity in hearts that have undergone ischaemia/reperfusion both experimentally and clinically^(368;428-431).

1.6.5.4 Cathepsin-L

Among the cysteine cathepsins, the most extensively described in health and disease is CatL⁽⁴²³⁾. As with the other cathepsins (Table 1.2), CatL is normally located within the lysosome with an optimal activity at pH 5.5-6.0⁽³⁷²⁾ but is active at neutral pH⁽³⁸⁰⁾. It has been demonstrated that in transgenic CatL knock-out mice that there is accumulation of material within enlarged lysosomes with ventricular dilatation and impaired cardiac contraction^(401;402). Therefore, these data suggest that a basal level of CatL is essential for maintenance of normal cardiac structure and function. Recent work has shown that cathepsins, including CatL, can be released/secreted into the extracellular space and have proteolytic activity resulting in ECM remodelling⁽³⁶⁸⁾. Moreover, as discussed above, serum levels of CatL have been shown to be increased with coronary heart disease^(413;425;426). Yet, despite this evidence, the consequences of raised serum levels of CatL remain unknown. A study by Sun *et al.* (2011) induced MI utilising a permanent coronary artery ligation technique in CatL deficient transgenic mice⁽⁴²⁴⁾. Induction of MI in the complete absence of CatL in all cell types increased infarct size at day 14 post-MI. Sun *et al.* (2011) suggested that this was caused by a reduced level of blood/bone marrow derived cell mobilisation to the site of injury to aid cardiac repair (due to their reduced ability to remodel the ECM to enable mobilisation)⁽⁴²⁴⁾. They also suggested that absence of CatL led to a reduced level of myofibroblasts and circulating fibroblasts, which would normally limit infarct dilatation⁽⁴²⁴⁾. In another study by the same group, Sun *et al.* (2013) also demonstrated that in CatL deficient mice that had undergone aortic banding, to increase afterload thereby inducing

left ventricular hypertrophy, had significantly worse systolic and diastolic function as well as reduced survival⁽⁴³²⁾. They suggested that CatL lysosomal protein degradation and activation of autophagy ameliorated the hypertrophic response to the aortic banding⁽⁴³²⁾. It is important to recognise that in both these studies transgenic mice with a complete CatL deficiency from conception were used. A deficiency from conception in all cell types will result in complex compensatory biochemical changes and alterations in cellular structure (specifically lysosomal structure), and is highly likely to lead to different responses to induction of MI or aortic banding. The recognition of potential compensatory effects becomes apparent when considering reducing the effects of CatL as a potential treatment for disease. When the effect of pharmacologically inhibiting CatL in other body systems as opposed to transgenic knock-out has been investigated, the inhibitors cause only a partial and temporary deficiency and may therefore result in a different response⁽⁴³³⁾. Overall, these observations suggest that whilst a complete CatL deficiency is deleterious to cardiac function, excess CatL may also be harmful, especially given the correlation of serum CatL levels and severity of disease in patients with coronary heart disease.

1.7 Overall Aims

The overall aims of this thesis are to:

1. Identify whether trypanosomes can have a direct effect on Ca^{2+} handling in ventricular cardiomyocytes *via* a secreted/excreted factor.
2. Identify the potential mechanism by which the trypanosomes can exert their effects and whether it is the same mechanism involved in Ca^{2+} signalling within HBMECs.
3. Characterise the Ca^{2+} handling disturbances in isolated ventricular cardiomyocytes.
4. Develop an *in vivo* model with which the cardiac phenotype of a trypanosome infection can be investigated.

5. Investigate the parallels/differences between the Ca^{2+} handling effects of trypanosome derived cathepsin-L and mammalian derived cathepsin-L.

2 CHAPTER 2 – General Methods

2.1 Trypanosome Culture and Supernatant Preparation

2.1.1 Axenic Culture of *Trypanosoma brucei brucei*

Cultures of *Trypanosoma brucei brucei* strain Lister 427 were maintained axenically in logarithmic growth phase from cryo-preserved stabilates (section 2.1.2) in a modified version of HMI-9 media which is widely used to culture mammalian bloodstream form trypanosomes^(434;435). The composition of the modified HMI-9 media was: IMDM (Iscove's Modified Dulbecco's Medium with Glutamax (Life Technologies)) supplemented with; BBCPT (0.05 mM bathocuprinone disulphonic acid, 1.5 mM L-cysteine, 2 mM sodium pyruvate, 0.16 mM thymidine, 0.2 mM β -mercaptoethanol), 1 mM hypoxanthine, 1.4 mM glucose, 0.125 mM adenosine, 0.125 mM guanosine, 30 $\mu\text{g}\cdot\text{mL}^{-1}$ kanamycin, 10 $\text{u}\cdot\text{mL}^{-1}$ penicillin, 10 $\text{u}\cdot\text{mL}^{-1}$ streptomycin and 1 $\text{mg}\cdot\text{mL}^{-1}$ methyl cellulose. Parasites were cultured in the modified HMI-9 supplemented with 20% v/v Serum Plus®, (a serum supplement containing Foetal Bovine Serum (SAFC Biosciences)) in a humid incubator at 37 °C, 5% CO₂ (in air). Trypanosome cultures were maintained in 25 cm² vented top tissue culture flasks to ensure adequate diffusion of CO₂ into the media for appropriate pH buffering at ~pH 7.4 due to 36 mM sodium bicarbonate (NaHCO₃) and 25 mM HEPES within the IMDM (Invitrogen). Phenol red within the media enabled visualisation of correct pH balance of the cultures. Counting of parasites was done in quadruplicate using an improved Neubauer Haemocytometer (Figure 2.1) and new trypanosome cultures in modified HMI-9 were seeded and maintained to achieve a concentration of 5.0×10^5 parasites. mL^{-1} for experimentation. Parasite cultures typically achieved a doubling time of 8 hr. For example, if a 10 mL culture of 5.0×10^5 parasites. mL^{-1} was required in 48 hr and the doubling time was 8 hr (determined from up to once daily haemocytometer counts), then the number of doubling times in 48 hr will be 6 (48 hr/8 hr). From a desired concentration of 5.0×10^5 parasites. mL^{-1} this would be a seeding concentration of 7.8×10^3 parasites. mL^{-1} ($(5.0 \times 10^5)/2^6$). If the concentration of parasites in the seeding culture is 5.0×10^5 parasites. mL^{-1} then the volume of seeding culture required to achieve 5.0×10^5 parasites. mL^{-1} in 48 hr would be $15.6 \mu\text{L}\cdot\text{mL}^{-1}$ ($7.8 \times 10^3/5.0 \times 10^5$). Therefore, for a 10 mL culture 156 μL of seeding culture would need to be added to 10 mL modified HMI-9. The fresh trypanosome culture will then act as the seeding culture for the next fresh culture in 48 hr etc. Cultures were

maintained in this fashion for up to 4 weeks or until the culture failed to grow/parasites died.

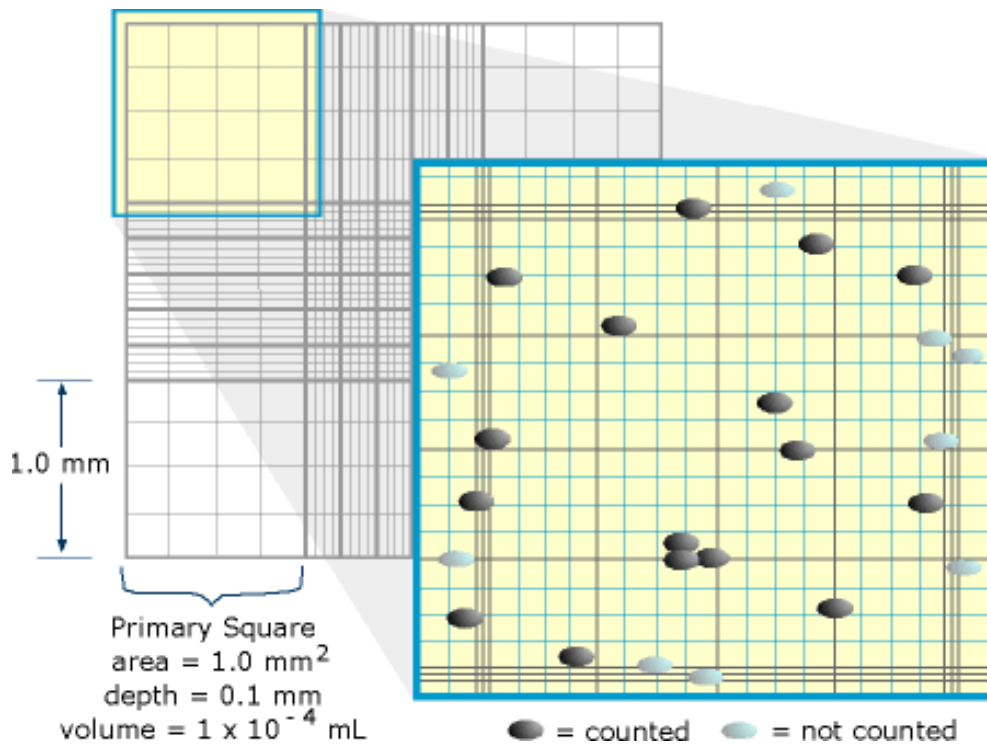


Figure 2.1: Counting trypanosomes with a Neubauer Improved Haemocytometer. Cartoon representation of the haemocytometer grid viewed through a standard light microscope. Trypanosomes were counted in each primary square to make the quadruplicate count. Cells crossing left-hand and upper borders were counted (black dots), cells crossing right-hand and bottom borders were not (light grey dots). (Figure from open source).

2.1.2 Stabilate Preparation

A stock of parasites was preserved in cryo-storage (stabilates) for the purposes of new trypanosome cultures in case of culture contamination or overgrowth. Trypanosomes were cultured to a concentration of $\sim 5.0 \times 10^5$ parasites.mL⁻¹. Modified HMI-9 media without added antimicrobials, with 10% glycerol added as a cryo-protectant was prepared as stabilate media. Trypanosome cultures in modified HMI-9 were centrifuged at a relative centrifugal force (RCF) of 857 g for 10 min and the supernatant carefully aspirated. The remaining pellet of parasite cells was gently resuspended in stabilate media to a concentration of 5.0×10^5 parasites.mL⁻¹. The resuspended parasite culture was placed in 1 mL aliquots into cryo-tubes and labelled appropriately. The cryo-tubes were frozen slowly in an insulated container with isopropyl alcohol in an outer layer in a -80 °C freezer for 24 hr. This method prevents the formation of large ice crystals

that could disrupt and kill the cells. The frozen stabilates were then removed and stored in liquid nitrogen until required.

2.1.3 Stabilate Thawing

When a new culture of trypanosomes was required modified HMI-9 media with 40% Serum Plus® (and antimicrobials) was pre-warmed to 37 °C in the incubator. The extra Serum Plus® provides additional metabolic support for the freshly thawed trypanosomes. An aliquot of stabilate was gently warmed by hand and added by pipette to 4 mL modified HMI-9 with 40% Serum Plus® without agitation. The trypanosome culture in modified HMI-9 with 40% Serum Plus® was monitored and counted daily, and reseeded as appropriate. After 72 hrs the trypanosomes were transferred to modified HMI-9 with 20% Serum Plus®, and were maintained as described in 2.1.1.

2.1.4 Preparation of Live Trypanosomes for Experimentation

Modified HMI-9 as in section 2.1.1 (hereafter referred to as control media) containing live trypanosome cultures at a concentration of $\sim 5.0 \times 10^5$ parasites.mL⁻¹ was decanted from the tissue culture flask into an appropriately sized centrifuge tube. The pH of the cultures and control media were checked using a pH meter. The pH was maintained by the 25 mM HEPES, 36 mM NaHCO₃ within the IMDM of the modified HMI-9 and 5% CO₂ within the incubator and was measured as pH 7.40 ± 0.02 , but if >0.02 different then the pH of the control media was adjusted to match the trypanosome culture with sodium hydroxide (NaOH) or hydrochloric acid (HCl) as appropriate. The living parasites were then incubated with isolated adult rat left ventricular cardiomyocytes.

2.1.5 Preparation of Supernatant

Cultures of trypanosomes as above were counted (section 2.1.1) and carefully aspirated from the tissue culture flasks into sterile centrifuge tubes. Supernatant was prepared by centrifugation of cultured trypanosomes at 857 g for 10 min. A low RCF was used to avoid causing cell lysis and the liberation of intracellular proteins. The supernatant was carefully aspirated using a pipette filler into a fresh centrifuge tube, the remaining pellet of cells was either discarded into 3% trigene disinfectant, or used for stabilate preparation (section

2.1.2). To ensure there was no contamination with live trypanosomes, supernatant was further filtered using a 0.2 µm syringe filter (Sartorius Stedim). Control media was treated in an identical manner to the supernatant (centrifuged and filtered). The supernatants were temperature matched and pH adjusted to the control HMI-9 batch used for each experiment (section 2.1.4).

2.2 Trypanosome Infections – *In Vivo* ECG Acquisition

2.2.1 *T. b. brucei* Lister 427 Infection Model

2.2.1.1 Preparation of Trypanosomes

Trypanosoma brucei brucei Lister 427 were grown in mice to adapt them to *in vivo* conditions. This step was performed by Mrs. Anne-Marie Donachie, a technician from the Wellcome Trust Centre for Molecular Parasitology, University of Glasgow. The parasites were grown in the mice for 2-3 days with daily venepuncture to check parasitaemia levels. When parasites were detectable the mice were sacrificed and blood collected in heparin. A sample of the blood was counted with a Neubauer improved haemocytometer in triplicate (section 2.1.1). The parasites were diluted under sterile conditions to 1.0×10^5 parasites in a 200 µL volume of Carter's balanced salt solution (CBSS; 25 mM HEPES, 120 mM NaCl, 5.4 mM KCl, 0.55 mM CaCl₂, 0.4 mM MgSO₄, 5.6 mM Na₂PO₄ and 11.1 mM glucose, pH 7.4).

2.2.1.2 ECG Acquisition

Adult male Wistar rats (250-300 g) were allowed a 7 day acclimatisation period upon delivery to the biological services unit. Animals were kept at the Cardiovascular Research Unit, University of Glasgow in a dedicated room licensed under the Specified Animal Pathogens (Scotland) Order 2009 (SAPO). Rats were anaesthetised by inhalation of isoflurane gas at 4-5% delivered in 1-1.5 L.min⁻¹ oxygen in an induction box. The rats were removed from the box when there was loss of the righting reflex. The animals were maintained on isoflurane delivered *via* facemask. The gas was reduced based on assessment of the animals' vital parameters to a final plane of anaesthesia at 1-1.5% in 1 L.min⁻¹ O₂. The ECG was recorded *via* the placement of intradermal electrodes. The placement sites on the rat were caudal aspects of the left and right carpi and

the medial aspects of left and right crura. The sites were cleaned with chlorhexidine as were the electrode tips. Appropriate earthing and positioning was used to minimise signal noise. To ensure reproducibility for the same rats and between rats, all animals were positioned identically based on an outline drawn on a corkboard. Electrodes were placed in the same manner (Figure 2.2A). The ECG was recorded for 15 min with an IWX228 bioamplifier (iWorx, USA). Rats were then infected with 1.0×10^5 parasites in a 200 μ L intraperitoneal injection, control rats were injected with 200 μ L CBSS. The ECG was recorded for a further 15 min following the injection before rats were recovered.

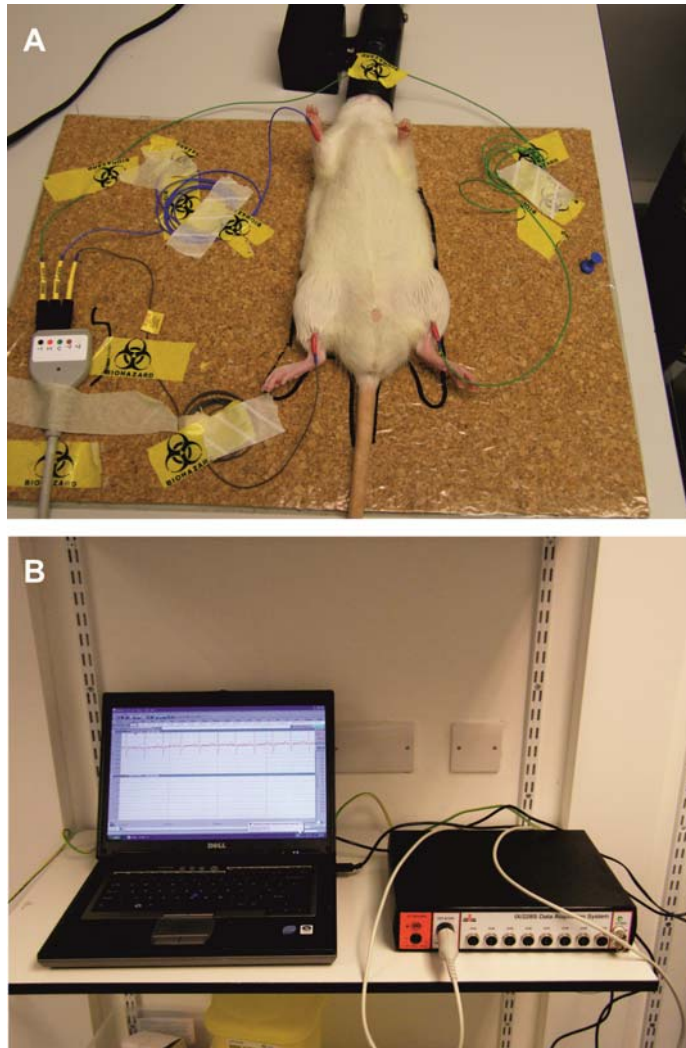


Figure 2.2: Photographs of the infected rat ECG acquisition.

(A) Rat anaesthetised and in position within the “black outline” drawn on the corkboard. ECG leads are placed in a lead II format (blue lead negative, green lead positive, grey lead earth/ground). Leads are taped down to minimise noise. The corkboard is coated in clear plastic to facilitate easy cleaning. (B) Computer and ECG acquisition equipment. An earthing lead connects the device to ground via a plumbed basin.

2.2.1.3 Health Monitoring and Parasitaemia Checks

Infection with *T. brucei* Lister 427 can cause anaemia, weight loss and immunosuppression. Eventually the parasitaemia becomes fulminant, which is fatal if allowed to persist. Parasitaemia was measured daily. A drop of blood was obtained by a small puncture of the lateral tail vein. The blood was expressed on to a glass slide and viewed with a 40x objective lens on a standard light microscope. The slide was examined and the number of parasites counted and compared to the description of Herbert and Lumsden (1976)⁽⁴³⁶⁾ (Figure 2.3).

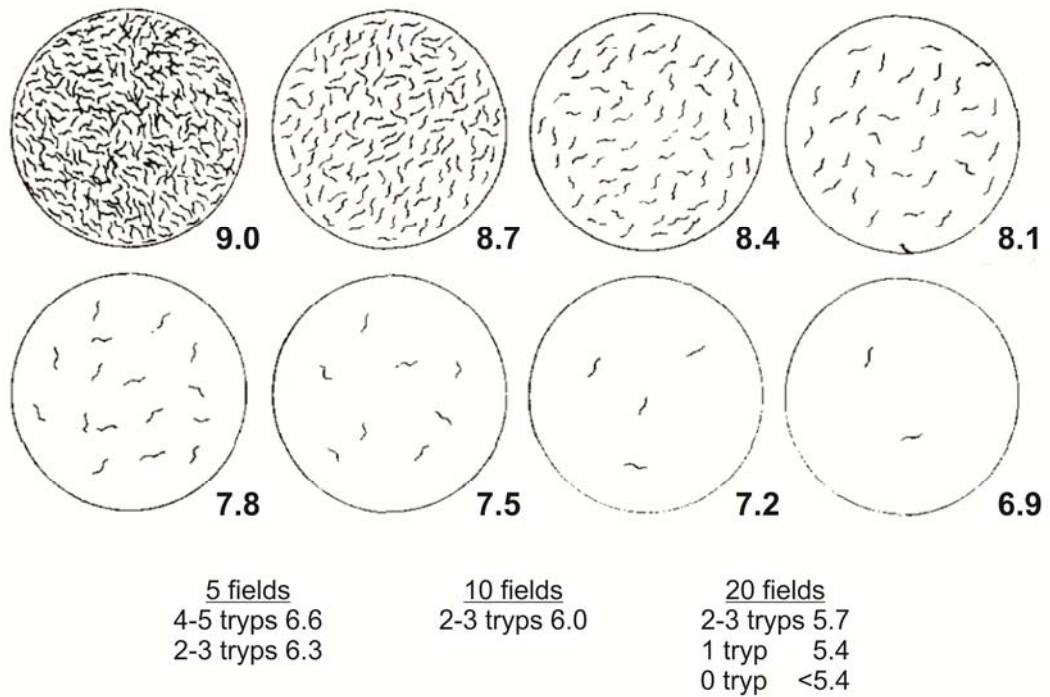


Figure 2.3: Chart and tables for estimating trypanosome parasitaemia.

Circles are the view down a 40x objective lens at blood films at different quantities of parasite. The numbers are the anti-log of the parasitaemia .mL^{-1} . For fewer parasites a greater quantity of fields must be analysed – numbers are given in the tables. Fewer than $1 \times 10^{5.4}$ parasites. mL^{-1} are not detectable from blood films. (Figure from Herbert and Lumsden (1976)⁽⁴³⁶⁾).

In addition, general clinical parameters were checked - adverse effects were recognised as lassitude persisting beyond 72 hours, or weight loss equal or greater than 25%, extreme pallor, hypothermia, sunken eyes, hunched posture, and staring coat, or where the parasitaemia exceeds 5.0×10^8 parasites. mL^{-1} for more than 2 consecutive days. In these cases animals were withdrawn from the study and humanely euthanized.

2.2.1.4 Terminal Data

Infected and control animals were anaesthetised again after 4 days and the ECGs were repeated. Animals were sacrificed and the lungs, liver and spleen weighed. The hearts were removed and Langendorff perfused (section 2.5). The pseudo-ECG was recorded for a 15 min steady state period followed by the addition of 100 nM ISO and the ECG recorded for 15 min. The concentration of ISO was increased 10 x every 15 min to 100 μM .

2.2.1.5 Data Analysis

ECG data were collected using the IWX228 bioamplifier and LabScribe 2 software (iWorx) at a sampling rate of 2,000 Hz. The ECG from the last min of each 15 min period was averaged using the advanced ECG analysis module of the programme and exported to Origin6.1 (OriginLab) for QT interval measurement (section 2.5.4.1). The entire traces were assessed for arrhythmic events according to the Lambeth Conventions⁽⁴³⁷⁾ (section 2.5.4.2).

2.2.2 *T. b. brucei* TREU 927 Infection Model

2.2.2.1 Trypanosome Preparation

A limitation of *T. brucei* Lister 427 is that it follows a logarithmic growth curve *in vivo* until the death of the infected host, therefore, the *T. brucei brucei* TREU 927 strain was used. The 927 parasites were prepared as described for 427 (section 2.2.1.1) by Anne-Marie Donachie. Blood taken from infected mice was examined and the parasites counted with a haemocytometer.

2.2.2.2 Telemetry Probe Implantation

One of the main limitations of the 427 infection model with 15 min ECG recordings is that isolated arrhythmic events may be missed. To counteract this problem, continuous ECG recordings were made using a CA-F40 biopotential telemetry implant (Data Sciences International).

2.2.2.3 Animals

Male Wistar rats aged 8-10 weeks were acquired from a licensed commercial breeder in the UK (Harlan Laboratories, UK). Animals were housed in pairs for a minimum of 7 days before use to allow an acclimatisation period. Thereafter animals were housed individually in order for the telemetry receiver plates to receive only one signal. Animals were housed in isolated accommodation under the SAPO licence as required for animals with trypanosome infections. They were given free access to water and food pellets.

2.2.2.4 Theatre Preparation

Telemetry probes were implanted under a surgical procedure (Figure 2.4). The animals were intended to be recovered from the procedure so operations were performed under aseptic conditions as much as practicable. The surgical area was prepared with the appropriate equipment required for the procedure (Figure 2.4(i)). The telemetry probe can be re-used between animals. The leads of the probe were sealed with sutures to prevent solutions from tracking up the electrode wires into the transmitter. The device was soaked in enzyme (Tergazyme®, Alconox, Inc. USA) to degrade biological material adhering to the device and leads for ≥ 5 h. The device was rinsed in water and then soaked in a cold sterilising solution consisting of peracetic acid (0.9-1.1%), hydrogen peroxide ($<1.0\%$) and acetic acid (4.9-5.5%) (Actril®, Minntech BV, Netherlands) for ≥ 5 h. The device was rinsed with sterile saline and stored in sterile saline sufficient to completely cover the device for up to 24 hours if to be implanted (Figure 2.4(i)). Devices not required for implantation were stored dry and sterilised when required. The surgical area was disinfected with chlorhexidine gluconate spray (Ecolab, UK) and covered with a sterilised drape. A heating pad to keep animals warm was covered in another sterile drape. Surgical instruments were autoclaved at $134\text{ }^{\circ}\text{C}$ prior to surgery and decontaminated between procedures (if more than one was performed) using a hot-bead steriliser (Germinator 500, SouthPointe Surgical Supply, USA). Animals were placed in a warming box immediately after regaining consciousness to provide a warm environment to recover in (Figure 2.4(ii)). Oxygen and anaesthetic agent were checked and filled as necessary.

2.2.2.5 Anaesthesia and Preparation of Animals

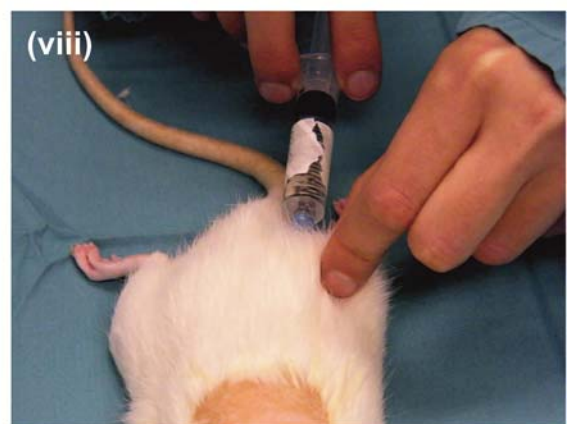
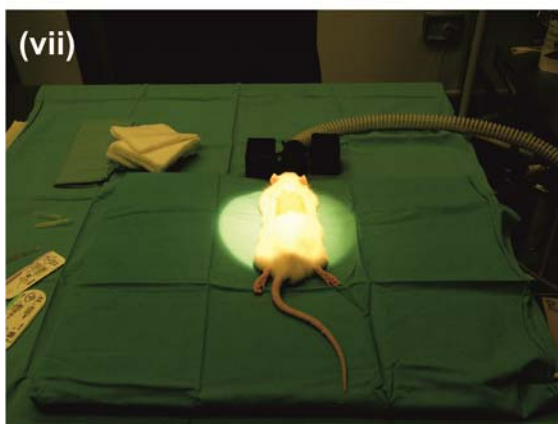
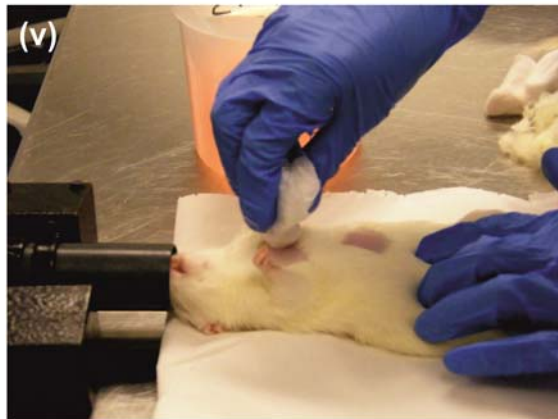
Rats were collected and weighed. Animals were anaesthetised using an inhalational vs. injectable agent for the greater control and least cardio-respiratory depressive effects of anaesthetic agents⁽⁴³⁸⁾. The inhalational anaesthetic used was isoflurane (Isoflo, Abbot Laboratories, USA) delivered in 100% O_2 . Animals were anaesthetised by placing them in a pre-filled induction box as shown in Figure 2.4(iii). Once there was a demonstrable loss of righting reflex animals were moved to facemask on 4% isoflurane at $1.5\text{ L}\cdot\text{min}^{-1}$. Fur was clipped with electric clippers over the thoracic region of the dorsum (Figure

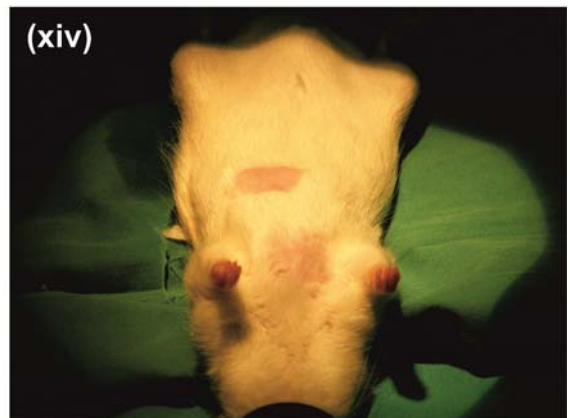
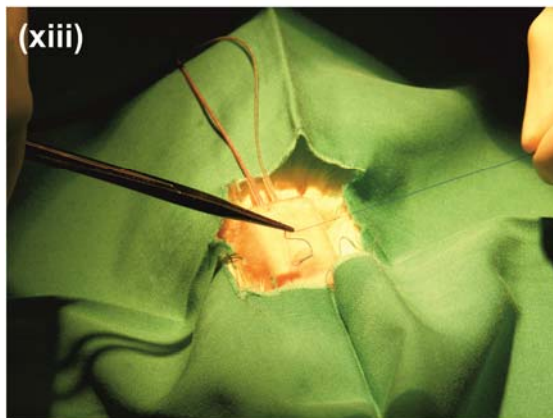
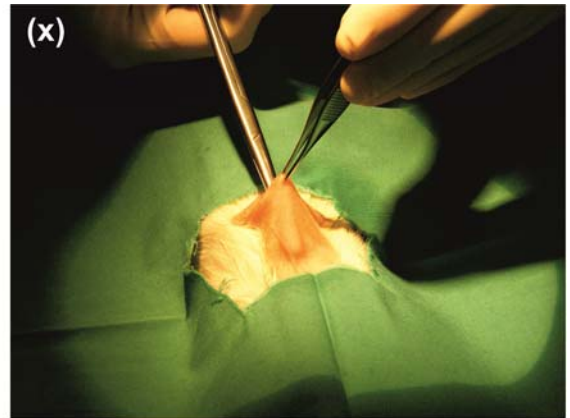
2.4(iv)) and on the ventrum over the right pectoral and xyphoid (Figure 2.4(v)). The clipped areas of skin were cleaned with warmed 10% surgical skin disinfectant (Hibiscrub, Ecolab Ltd) and gauze swabs (Figure 2.4(v-vi)). The animal was moved to the surgical table and positioned in ventral recumbency (Figure 2.4(vii)) on the heated pad to maintain the animal's temperature. Peri-operative analgesia of 5 mg.kg⁻¹ carprofen (Rimadyl, Pfizer Animal Health) was administered with 5 mL of 0.9% sterile saline subcutaneously (Figure 2.4(viii)) to maintain fluid balance under anaesthesia.

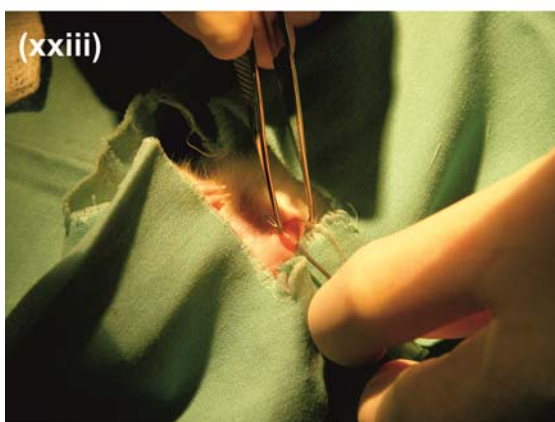
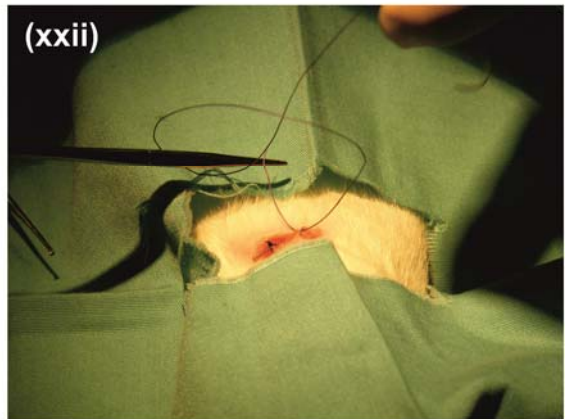
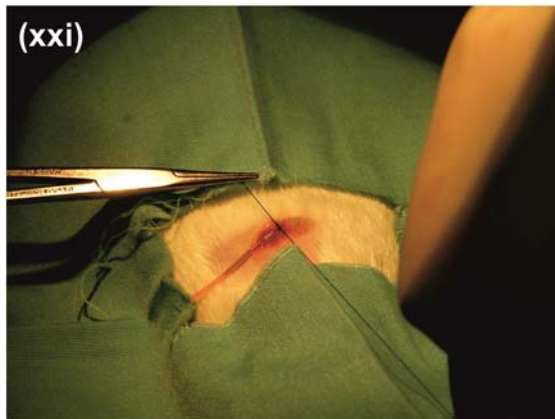
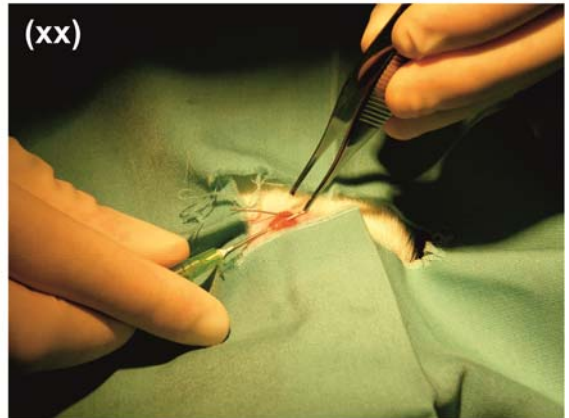
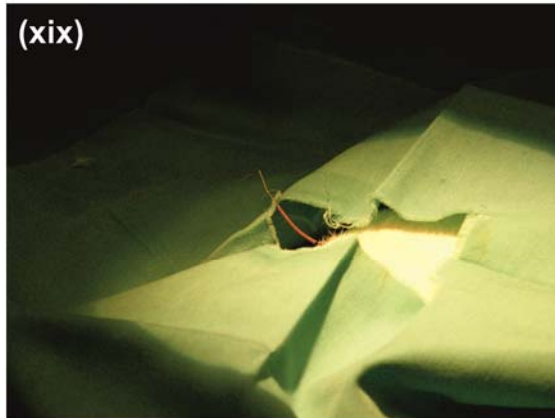
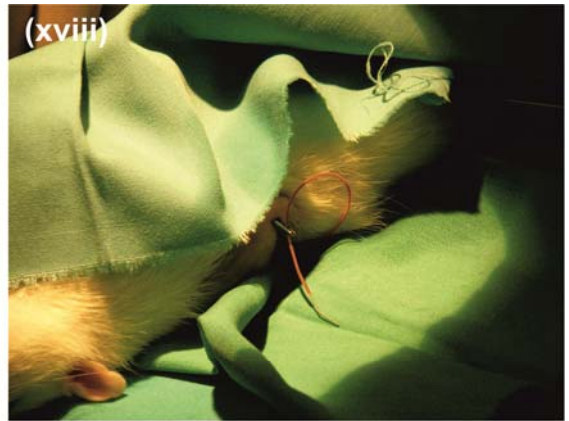
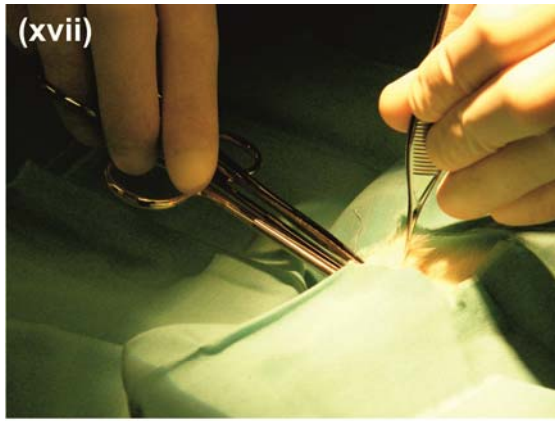
2.2.2.6 Surgical Procedure

The animal was placed in ventral recumbency and maintained with isoflurane and 100% O₂ *via* facemask throughout the procedure. Depth of anaesthesia was monitored by measuring the respiratory rate and testing the pedal pain withdrawal reflex and the isoflurane % altered accordingly from initial induction at 4.0-4.5% to a stable surgical plane of anaesthesia of 1.5-2.0%. A sterile drape with cut window was draped over the animal. A 25 mm horizontal incision was made with a scalpel blade toward the caudal edge of the clipped area of skin, mid thoracic region (Figure 2.4(ix)). This allowed the telemetry probe to be inserted over the back without impeding the animal's normal behaviour once recovered. The subcutaneous fascia was bluntly dissected with scissors (Figure 2.4(x)) to create a pocket large enough to accommodate the probe. The probe was orientated with anchor points dorsal and leads caudal (Figure 2.4(xi)) and then inserted into the pocket (Figure 2.4(xii)). The probe was anchored with 1.5 metric nylon suture (W319, Johnson & Johnson) through the skin and anchor points on the probe (Figure 2.4(xiii)). A saline soaked sterile swab was placed over the surgical site and the animal was rotated carefully into dorsal recumbency to expose the ventral sites (Figure 2.4 (xiv)). Starting with the xyphoid site a 10 mm incision was made with a scalpel blade and subcutaneous fascia bluntly dissected (Figure 2.4(xv)). A tract was dissected carefully subcutaneously around the thorax with scissors toward the right of the animal to allow the positive lead marked red by the manufacturer of the probe to be passed (Figure 2.4(xvi)). A haemostat was carefully passed through the tract and the scissors removed (Figure 2.4(xvii)). The appropriate biopotential lead was grasped with the tip of the haemostat and pulled through to the xyphoid (Figure 2.4(xviii-xix)). A length of the silicone sheath of the biopotential lead

was carefully removed to expose a length of the wire. Figure 2.4(xix) shows the lead pulled through and exposed wire after removal of a length of the red silicone. Using a 21-gauge needle a small tract was created through the underlying muscle for the exposed wire to pass through (Figure 2.4(xx)). The exposed wire is in direct contact with the muscle so will return an electrical signal to the transmitter. The removed silicone insulation was replaced over the exposed end not in the muscle to insulate against interference and noise and sutured into place with 1.5 metric nylon (Figure 2.4(xxi)). An additional suture was placed proximal to the wire insertion for further anchoring. The ventral skin incision was closed with 1.5 metric polyglactan 910 (Vicryl, W9386, Johnson & Johnson, UK) in a simple continuous pattern (Figure 2.4(xxii)). The procedure was repeated passing to the left of the animal for the negative electrode over the right pectoral to prevent the leads crossing over one another and potentially introducing noise to the signal (Figure 2.4(xxiii-xxiv)). The animal was returned to ventral recumbency. The leads were coiled and tucked into the pocket with the probe and positioned to minimise discomfort to the animal (Figure 2.4(xxv)). The skin was closed in a simple continuous pattern with 1.5 metric polyglactan 910. The gaseous anaesthesia was reduced to 0% during closing and the animal allowed to recover on 100% O₂ followed by room air until pedal withdrawal and palpebral reflexes had returned. The animal was then placed in the warm box to come round to full consciousness (Figure 2.4(xxvii)). Rats were monitored daily for signs of discomfort and wound healing and cleanliness. No follow-up analgesia was necessary as rats were comfortable and displaying normal behaviour (Figure 2.4(xxviii)).







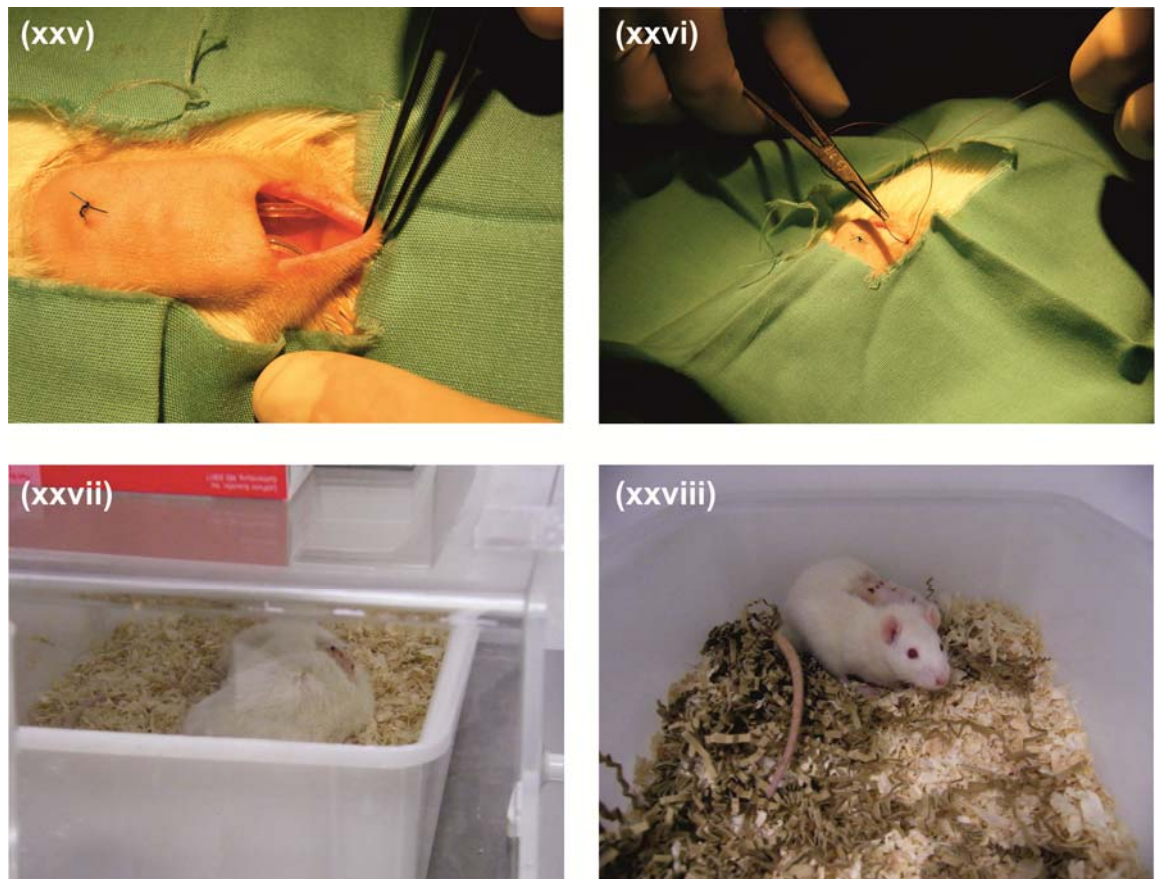


Figure 2.4: Photographs of the steps of the telemetry probe implantation procedure.

2.2.2.7 Trypanosome Infection

Rats were allowed to recover from surgery for 7 days and then were infected as described for the 427 model (section 2.2.1.2). Infection was with 1.0×10^5 *T. brucei* TREU 927 in 200 μ L CBSS *via* intraperitoneal injection. Control rats were injected with the same volume of CBSS. Rats were monitored as described above (section 2.2.1.3).

2.2.2.8 Data Acquisition and Analysis

Cages with implanted rats were placed onto receiver pads. The implanted probes were activated magnetically. Telemetry signals were relayed *via* a data exchange matrix to the computer loaded with the acquisition software Dataquest™ OpenART v4.2 (Data Sciences International). Raw ECG data was collected continuously at 2,000 Hz sampling frequency for 2 weeks and saved daily. Files were exported to Ponemah v4.8 (Data Sciences International) for analysis. The probes have a battery life of 6 months when in continuous use.

ECGs were recorded continuously for the duration of the model. ECGs were assessed for arrhythmia frequency and QT intervals as described later (section 0).

2.3 Ventricular Cardiomyocyte Isolation

2.3.1 Isolation of Adult Rat Left Ventricular Cardiomyocytes

Adult male Wistar rats (250-300 g) were humanely euthanized in accordance with Schedule 1 of the UK Animal (Scientific Procedures) Act 1986, Directive 2010/63/EU of the European Parliament and the ethical review panel of the University of Glasgow. Rats were first concussed followed by immediate cervical dislocation. Complete severance of the spinal cord was confirmed by manual palpation. The rat was placed in dorsal recumbency and the heart removed by thoracotomy (Figure 2.5A) into ice-cold isolation buffer. The heart was gently squeezed to express blood from the ventricles and placed in a second beaker of isolation buffer. The isolation buffer used was a modified isolation Krebs-Henseleit (MIKH) solution. The composition of MIKH was as follows (in mM): NaCl (120), KCl (5.4), HEPES (20), NaH₂PO₄ (0.52), MgCl₂·6H₂O (3.5), Taurine (20), Creatine (10), Glucose (11.1), pH was adjusted to 7.4 at 37 °C with NaOH. The inclusion of taurine has been suggested to protect the isolated cells from Ca²⁺ overload during Ca²⁺ paradox^(439;440). The washed heart was finely dissected to remove extraneous tissue and clear the area around the aorta. The heart was cannulated *via* the aorta in retrograde Langendorff perfusion as shown in Figure 2.5B and C. It is important that the cannula stops short of the aortic valve so that the perfusion pressure closes the aortic valve and pushes the perfusion solution into the coronary vessels (Figure 2.6). The aorta was tied to the cannula with a 1.5 metric nylon suture (Pearsall's Ltd) using a surgeon's knot (defined as 2 throws, 1 turn and 1 throw before tying) to ensure a tight locking knot. Successful cannulation was confirmed by the perfusate leaving the heart becoming transiently sanguineous and the coronary vessels becoming clear. Hearts were perfused at a rate of 7 mL·min⁻¹ with MIKH for a period of 5 min to ensure complete clearing of blood from the myocardium and coronary circulation.

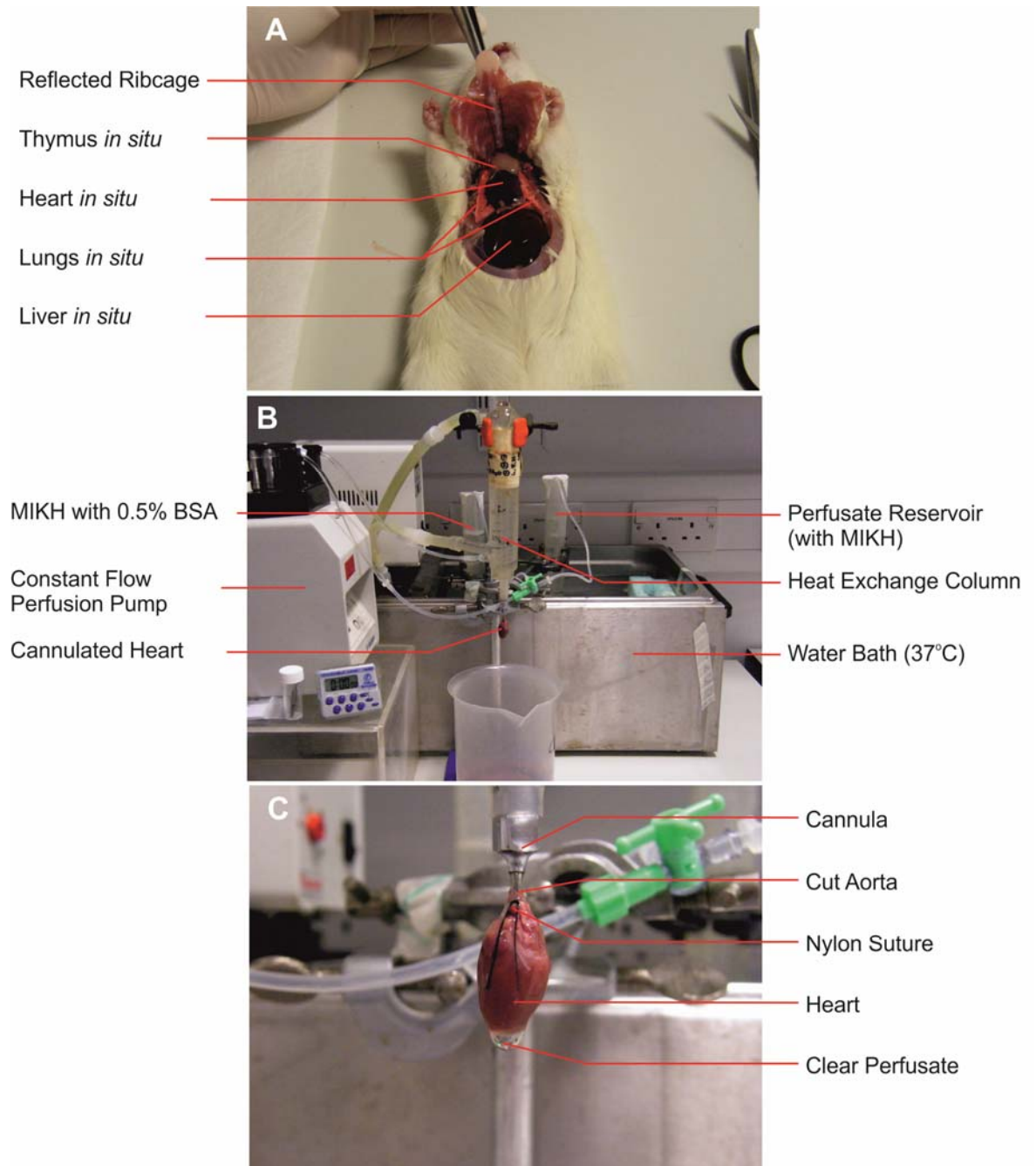


Figure 2.5: Photographs of rat heart removal and cannulation.

(A) Thoracotomy of the rat with ribcage reflected to show thoracic and proximal abdominal organs *in situ*. (B) Langendorff isolation set up with cannulated heart. The heart is perfused in retrograde Langendorff perfusion with MIKH warmed to 37 °C in the water bath and by the heat exchange column. Perfusion is maintained by constant flow perfusion pump calibrated to deliver 7 mL.min⁻¹. MIKH containing 0.5% BSA is in a separate reservoir with a 3-way tap to switch between solutions. (C) Close-up of cannulated heart tied in place with clear perfusate indicating successful perfusion of the coronary vessels.

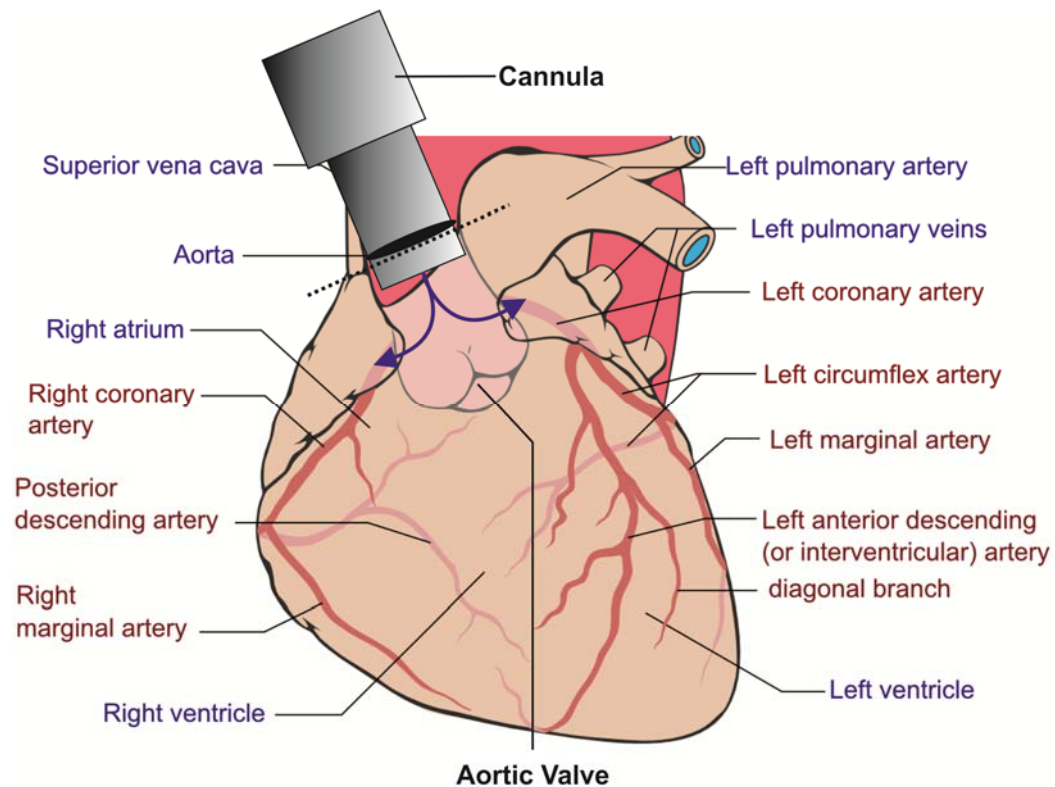


Figure 2.6: Langendorff perfusion of the heart.

The aorta is transected between the heart base and aortic arch to leave a straight cut (dashed line). The cannula is inserted through the aortic opening, marked as the black ellipse, but care taken not to push through the aortic valve (labelled). When perfusion solution is pumped through the cannula the perfusion pressure closes the aortic valve as the afterload would during diastole *in vivo*. The perfusion pressure therefore pushes the solution into the coronary vasculature, indicated by the blue arrows, to supplement the excised heart with the Krebs-Henseleit solution.

Following the clearance of blood hearts were perfused with MIKH with $0.83 \text{ mg}\cdot\text{mL}^{-1}$ collagenase I (Worthington Biochemical Corporation) and $0.1 \text{ mg}\cdot\text{mL}^{-1}$ protease XIV (Sigma-Aldrich) at the same flow rate for 8-12 min depending on particular enzyme requirements to get the best quality and yield of cardiomyocytes. Optimisation experiments were performed as detailed below when a new batch of enzyme was purchased. The collagenase is activated by the protease and digests the extracellular matrix of the heart to liberate individual cells. After perfusion with enzyme the hearts were perfused for 6.5 min with MIKH containing 0.5% bovine serum albumin (BSA). The BSA provides substrate and stops continued digestion of the tissue. Any minor leakiness of cardiomyocyte membranes can also be sealed by the BSA⁽⁴⁴¹⁾ and prevent influx of extracellular Ca^{2+} that can cause a hypercontractile state in the cardiomyocyte. The ventricles were cut from the cannula and the right ventricle separated and discarded. The left ventricular free wall and the interventricular septum were cut into strips and gently mixed to yield a single cell suspension in

MIKH containing 0.5% BSA. The Ca^{2+} in solution ($[\text{Ca}^{2+}]_o$) was raised in this suspension *via* stepwise increments of 100 μM until 1.0 mM was reached to guard against Ca^{2+} paradox⁽⁴³⁹⁾. Ca^{2+} paradox occurs when Ca^{2+} is removed, such as in the case of enzymatic digestion, and monovalent cations such as Na^+ enter the cardiomyocyte down the electrochemical gradient⁽⁴³⁹⁾. If $[\text{Ca}^{2+}]_o$ is returned to physiological concentration (1.8 mM) immediately, then Ca^{2+} can enter the cell suddenly down its concentration gradient and kill the cell. By restoring $[\text{Ca}^{2+}]$ gradually, the ion concentrations are able to equilibrate without killing the cell⁽⁴³⁹⁾. Cells were viewed on the light microscope for yield, quality and viability. Cell morphology appropriate for experimentation was the torpedo-like rod shape, striations and clear sarcolemma (membrane). Ball shaped cells were hypercontracted cells following an influx of Ca^{2+} through a damaged sarcolemma⁽⁴⁴²⁾ (Figure 2.7). This protocol is an amalgam of multiple techniques described in the literature, reviewed in Louch *et al.* (2011), that have been found to be optimal for this set-up⁽⁴⁴³⁾. The protocol was fully characterised for each enzyme batch used.

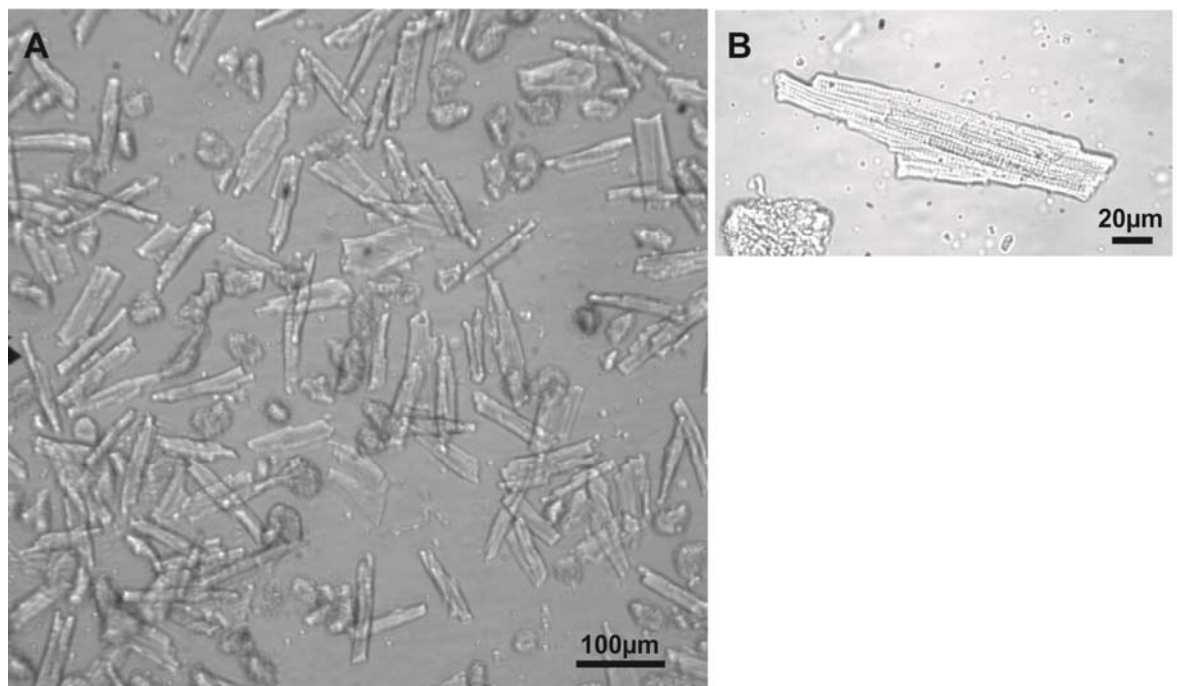


Figure 2.7: Photomicrographs of isolated cardiomyocytes.

(A) View of isolated rat left ventricular cardiomyocytes with 10x objective lens. Rod shaped cells are viable contractile cells. Ball shaped cells are hypercontracted cardiomyocytes following influx of extracellular Ca^{2+} . These cells are not viable. (B) View of single cardiomyocyte with 40x objective lens showing striations, intact sarcolemma and straight ends. Lower left of same image shows a hypercontracted cardiomyocyte.

Isolated cells were assessed for total yield, percentage of viable rod shaped cells (Figure 2.7) and percentage of cells exhibiting spontaneous contractile activity. Viability counts were performed at 0 and 1.0 mM Ca^{2+} and again in the 1.0 mM Ca^{2+} after 2 hr. When a new batch of enzyme was purchased, similar experiments were performed to ensure optimisation and consistency of the percentage rods achieved between batches.

2.3.2 Isolation of Adult Rabbit Left Ventricular Cardiomyocytes

Isolation of rabbit cardiomyocytes was performed by Mrs. Aileen Rankin, a technician in Prof. Godfrey Smith's lab; a similar protocol to adult rat cardiomyocyte isolation. Adult New Zealand White rabbits (2-2.5 kg) were given an intravenous injection of 500 U heparin and an overdose of sodium pentobarbitone ($100 \text{ mg} \cdot \text{kg}^{-1}$). Hearts were rapidly excised as described for the rat and cannulated in retrograde Langendorff perfusion *via* the aorta. The cannulated hearts were perfused with 150 mL of MIKH of the same composition as in 2.3.1 at a rate of $25 \text{ mL} \cdot \text{min}^{-1}$ ($37 \text{ }^\circ\text{C}$) to rinse away blood and reduce probability of clot formation. The MIKH was supplemented with $1.4 \text{ mg} \cdot \text{mL}^{-1}$ collagenase I and $0.1 \text{ mg} \cdot \text{mL}^{-1}$ protease XIV and perfused for ≈ 7 min. Hearts were then perfused with MIKH containing 0.1% BSA for ≈ 6 min to provide substrate for superfluous enzyme and seal up cardiomyocyte membranes to prevent hypercontraction and cell death. Hearts were cut down and the atria removed. The experiments presented in this thesis used cardiomyocytes from the left ventricle. The left ventricles were cut into strips and mixed in 20 mL 0.1% BSA MIKH with 0.125 mM CaCl_2 in a culture flask for 30-60 min. The cells were allowed to settle and the supernatant removed. The cells were then resuspended in 0.1% BSA MIKH with 0.25 mM CaCl_2 and the process repeated. This was done again for 0.5 and 1.0 mM CaCl_2 . The gradual increase in $[\text{Ca}^{2+}]$ was performed to protect the cells from Ca^{2+} paradox⁽⁴³⁹⁾ (section 2.3.1).

2.4 Cardiomyocyte Spontaneous Contractile Activity Measurements

Isolated rat left ventricular cardiomyocytes (section 2.3.1) were incubated at room temperature for 30 min with live trypanosome culture at a concentration of $\sim 5.0 \times 10^5 \text{ parasites} \cdot \text{mL}^{-1}$ or control media (i.e. modified HMI-9 prepared the

same way but without parasites) in a ratio of 1:3; cells ($\sim 1.0 \times 10^5$ cardiomyocytes in 1 mL MIKH at 1.0 mM Ca^{2+}) : culture/media (3 mL). The ratio of 1:3 was calculated to achieve a physiological $[\text{Ca}^{2+}]_o$ based upon the $[\text{Ca}^{2+}]$ of the IMDM of the media (section 2.1.1) reported by the manufacturer as 1.97 mM. Following incubation the cardiomyocytes were loaded onto a glass cover slip in a tissue bath (Cell Microcontrols) and viewed on an inverting light microscope (Nikon) with a 10x 0.25 Numerical Aperture (NA) lens. A quantity of 10-15 rod shaped cardiomyocytes per field over 10 fields was viewed for 1 min per field and the number of cells exhibiting at least one spontaneous contractile event recorded.

A further cohort of cardiomyocytes were incubated at room temperature for 30 min in control media or trypanosome culture supernatant prepared as previously described (section 2.1.5). The filter size of 0.2 μm meant parasite secretory/excretory products would remain in the media. The ratios were 1:3 as with live trypanosomes above. Cardiomyocyte spontaneous contractions were recorded and expressed a percentage of total cells as above.

2.5 Langendorff Perfusion of *ex vivo* Whole Rat Hearts

2.5.1 Principles of Langendorff Perfusion

As described above (section 2.3.1), the principle of Langendorff perfusion is to supply an excised heart with its oxygenation and nutrient requirements. This is achieved *via* cannulation of the aorta taking care not to advance beyond the aortic valve (Figure 2.6). The mock extracellular solution containing oxygen and glucose is then perfused down the aorta against the closed valve thus forced by the pressure of the column of fluid in the aorta and perfusion apparatus into the coronary vessels to supply the myocardium. The mock extracellular solution is removed *via* coronary veins to the right atrium. The chambers of the heart remain essentially “dry”. This technique was devised by Oscar Langendorff in 1895⁽⁴⁴⁴⁾. Langendorff perfusion offers many advantages: simplicity of preparation, low cost, reproducibility and isolation from other physiological systems and exocrine control such as sympathetic tone⁽⁴⁴⁵⁾. It must also be considered the potential limitations; heart function is deteriorating with time (5-10% deterioration of contractile and chronotropic function per hour)^(445;446).

2.5.1.1 Constant Flow vs. Constant Perfusion Pressure

There are two modes of perfusion used for the Langendorff technique. Langendorff himself used a constant perfusion pressure system with a sealed pressurised chamber with manometer⁽⁴⁴⁴⁾. The simplest way of maintaining a constant perfusion pressure is with a set height of a column of fluid such as positioning of the reservoir a known height above the preparation thus using gravity to maintain the pressure. The disadvantage of using gravity fed perfusion pressure is the volume of fluid required. To reduce the fluid required there are negative feedback pressure control loop peristaltic pump systems available⁽⁴⁴⁷⁾. Constant pressure systems are useful when reliance of coronary tone auto-regulation is required and if a regional ischaemia is performed, i.e. ligation of part of the vascular bed where constant flow would result in increased pressure in the remaining vasculature⁽⁴⁴⁵⁾. Constant flow systems simply rely upon a peristaltic pump to deliver the perfusate and are useful if for studying function when no vascular interventions such as regional coronary occlusions are required that with constant flow can increase the pressure and alter potentially damage tissue causing artefactual changes. For this thesis, the constant flow system was used as no vascular interventions were required because only the ECG was measured.

2.5.1.2 Measuring Physiological Parameters

2.5.1.2.1 Electrocardiogram

The Langendorff technique lends itself well for measurement of the electrocardiogram (ECG) due to excellent access to the epicardium. Electrodes can be placed in a tissue bath surrounding the heart to measure the ECG with placement of the negative electrode adjacent to the right atrium and the positive electrode adjacent to the left ventricular free wall. Data acquired can be used to measure common ECG parameters such as PR interval, QRS duration and QT interval as well as identifying occurrence of arrhythmic events.

2.5.1.3 Potential Problems

To limit preparation failure and ensure high quality, repeatable data it is important to consider the potential problems that can arise and minimise them.

2.5.1.3.1 Temperature

Maintenance of a physiological temperature throughout the experiment is important. Variations in temperature can affect myocardial contractility and heart rate in the steady state^(446;448;449). Temperature can also have effects of myocardial viability following ischaemia/reperfusion models where lower temperatures can have a cardioprotective effect⁽⁴⁵⁰⁻⁴⁵⁴⁾. The heart has a large surface-to-volume ratio making radiant heat loss a large problem. This can be minimised by: warming the perfusate to physiological temperatures, use of a heat exchange column to minimise radiation of heat from the perfusate before it enters the heart, submersion of the cannulated heart in an organ bath or exposure to a radiant heat source. In the case of an ischaemia/reperfusion model where perfusion is interrupted partially (regional ischaemia) or totally (global ischaemia) then non-perfusion sources of heat must be considered.

2.5.1.3.2 Perfusion Flow Rate

The perfusion flow and pressure must be maintained throughout the experiment. Restrictions in flow can occur in diameter changes of the tubing from one region of the system to another, potential blockages in the coronary vessels (air emboli or thrombi) or experimental interventions. Therefore it is important to measure the coronary flow from the heart. The simplest way to achieve this is to collect the coronary effluent for a fixed period of time and measure the quantity of fluid collected.

2.5.1.3.3 Maintenance of equipment

One of the most common reasons for preparation failure is microbial contamination of the perfusion system⁽⁴⁴⁵⁾. This can be minimised by the design of the system limiting the number of connectors and avoiding side branches where stagnant fluid can collect. The apparatus must be thoroughly cleaned before and after use with heated (>80 °C) double-distilled water to ensure adequate removal of bacterial substrates such as glucose. Periodic (2 weekly) deep cleaning with Decon 90, ethanol or 10% HCl can be employed. In our system a second heat exchange coil can be used while the other is being deep cleaned. Plastic tubing is periodically replaced as necessary particularly in the case of use of trypanosome supernatant and media where the media is ideal for bacterial growth.

2.5.2 System Design and Implementation

The system used in our laboratory consists of two reservoirs containing perfusion solution, which are kept at 37 °C in a water bath (Figure 2.8). A three-way stop-cock allows switching between the reservoirs so that a drug may be added to one and a control reservoir remains. A peristaltic pump set to a constant flow rate (dependent on experimental requirements) delivers perfusion solution *via* a heat exchange column and bubble trap to the cannulated heart. Although care is taken to avoid any air in the system, the bubble trap serves as a secondary measure to ensure no air enters the heart potentially causing an air embolus and damage to the myocardium. The heart is cannulated to a 3 mm outer diameter cannula (Harvard Apparatus) *via* the aorta. Care is taken to ensure the cannula does not pass the aortic valve. A small incision is made in the right ventricular outflow tract to allow free drainage of coronary effluent and prevent development of back-pressure. The heart is submerged into a heat-jacketed organ bath to maintain temperature of the preparation.

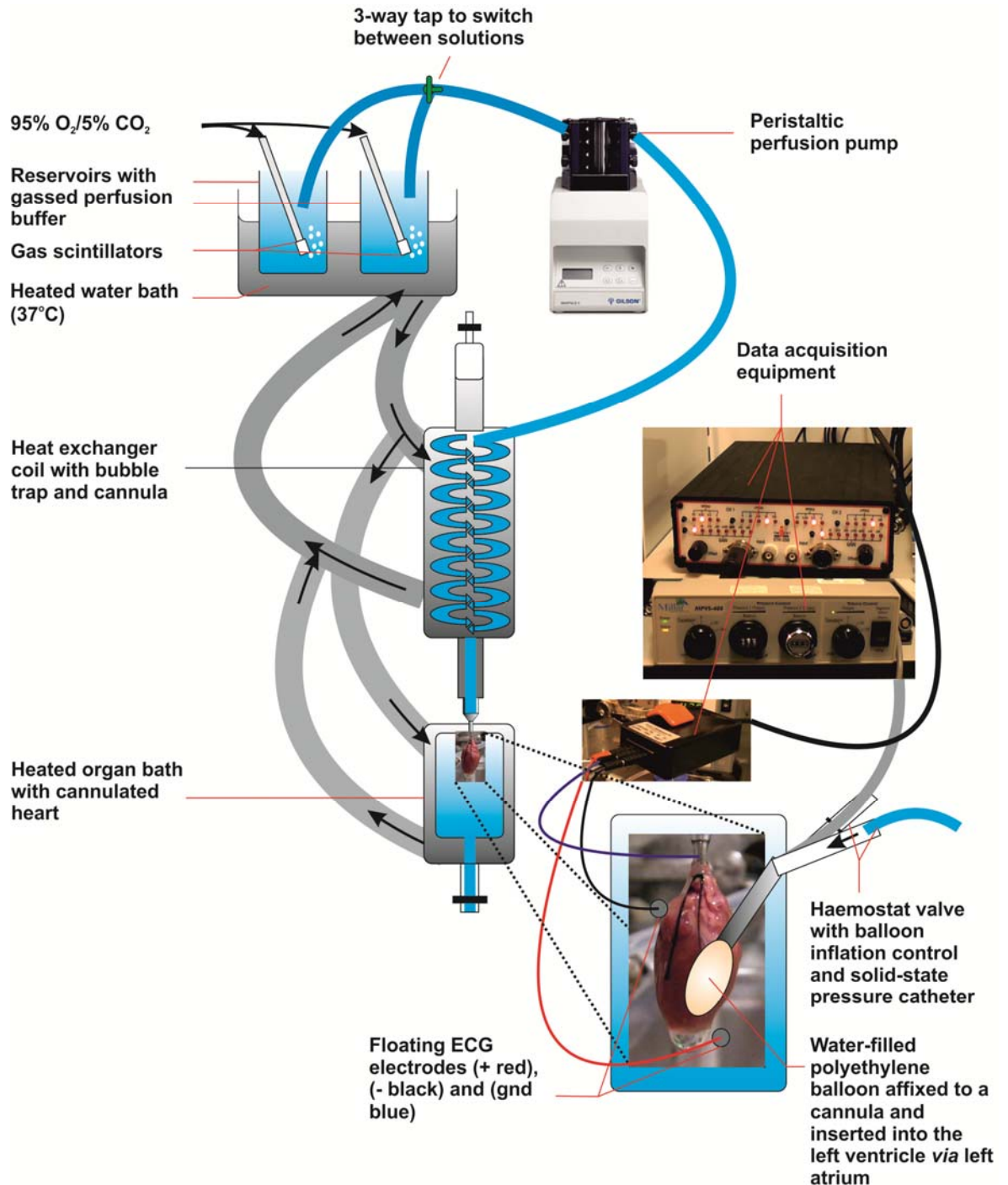


Figure 2.8: Langendorff system.

The heart is cannulated *via* the aorta and perfused. To maintain temperature the perfusion solution reservoir is kept in a water bath set to 37 °C and the supply to the heart passed through a heat exchange column. The heart is submerged in a heated organ bath. Perfusion solution is delivered *via* a peristaltic perfusion pump set to a constant flow rate. Two reservoirs with a tap to switch enable specific quantities of drug or different solutions to be perfused during an experimental protocol. The figure shows a magnified portion with the heart. ECG electrodes can be suspended in the organ bath in close proximity with the heart top record the ECG. A water-filled polyethylene balloon can be affixed to a cannula and inserted into the left ventricle *via* the left atrium if required. A haemostat valve would enable a solid-state catheter to be inserted without introduction of air and simultaneous fine control of balloon inflation, but was not conducted for this study.

2.5.3 Exclusion Criteria

Inclusion and exclusion criteria are useful when considering consistency and reproducibility. Keeping to a short as time as possible from animal sacrifice to cannulation is important to minimise myocardial damage or preconditioning^(455;456). In the rat a time of <3 min is acceptable⁽⁴⁵⁵⁾. High flow rates in a constant pressure system (or low perfusion pressures) are indicative of damage to the aorta or damage to the aortic valve. If flow rates are low or perfusion pressures high this can be an indicator of an obstruction; either obstruction of the coronary ostia by inappropriate cannulation or an embolus of air or particulate matter. Highly arrhythmic hearts could be inadequately perfused. It is good practice to set exclusion criteria during a steady state period. The table below shows exclusion criteria for commonly used mammals⁽⁴⁴⁵⁾ those of the rat were adopted for this thesis:

Table 2.1: Exclusion criteria for Langendorff perfusion of mice, rats and rabbits

Parameter	Mouse	Rat	Rabbit
Time to perfusion (min)	>4	>3	>3
Arrhythmia Duration (min)	>3	>3	>3
Heart rate (beats per min)	<320 or >620	<70 or >400	<150 or >190

2.5.4 Data Analysis

2.5.4.1 Electrocardiography

The ECG (or pseudo-ECG since this is no longer a living animal) can be measured by placement of electrodes in close approximation with the epicardium over the right atrium and left ventricle. The resulting change in voltage or ECG (section 1.3.4 for details on the ECG) was recorded with an iWorks/CBS systems bioamplifier. ECG parameters that can be measured are: PR interval, QRS duration and QT intervals (Figure 2.9). Parameters were measured manually as recommended by the AHA/ACCF/HRS recommendations for standardisation and interpretation of the electrocardiogram⁽⁴⁵⁷⁾. QT length, determined by the end of the T wave at the isoelectric point or by intersection of the tangent of the

steepest part of the T wave with the isoelectric point⁽⁴⁵⁷⁾, was measured. The QT interval was also measured at 90% repolarisation⁽⁴⁵⁸⁾ (QT₉₀) and at 50% repolarisation⁽⁴⁵⁹⁾ (QT₅₀), so as to have a clearly defined end point. QT intervals were corrected for heart rate using the Framingham method⁽⁴⁶⁰⁾:

$$QT_c = QT + 0.154 \times (1 - RR)$$

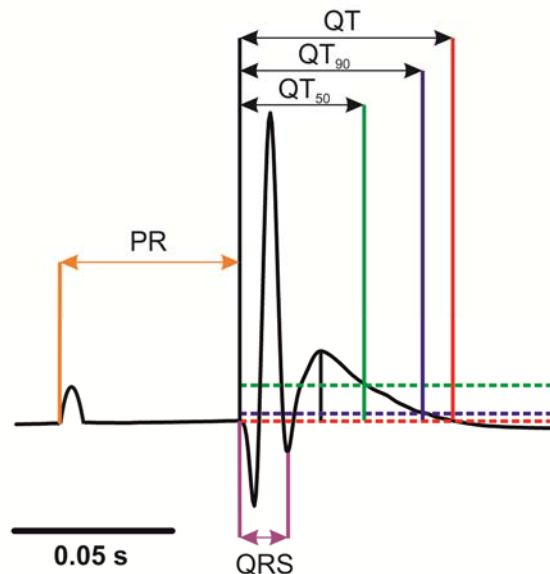


Figure 2.9: Measurable ECG parameters.

Example rat ECG with the parameters of PR interval, QRS duration and QT intervals highlighted. For this thesis the QT₉₀ and QT₅₀ were also measured by taking the 90% and 50% repolarisation points of the T wave respectively to reproducibly determine an end point of T.

2.5.4.2 Arrhythmia Classifications

To maintain consistency and enable comparison with available literature arrhythmias were classified according to the Lambeth Conventions⁽⁴³⁷⁾. Specifically, ventricular premature complexes (VPCs) were defined as discrete and identifiable premature QRS complexes (premature in relation to the P wave). Bigeminy, defined as alternating P-QRS, VPC, is classed as a distinct variant of VPC. Runs of 2-3 VPCs were defined as salvos, >4 as ventricular tachycardia (VT). Ventricular fibrillation (VF) was defined as a signal from which individual QRS complexes cannot be distinguished and a rate cannot be measured. Occurrence of VPCs as defined was counted and expressed as the number of events per min. The VPC is premature in relation to the P wave and has an identifiable QRS shape although wider (Figure 2.10).

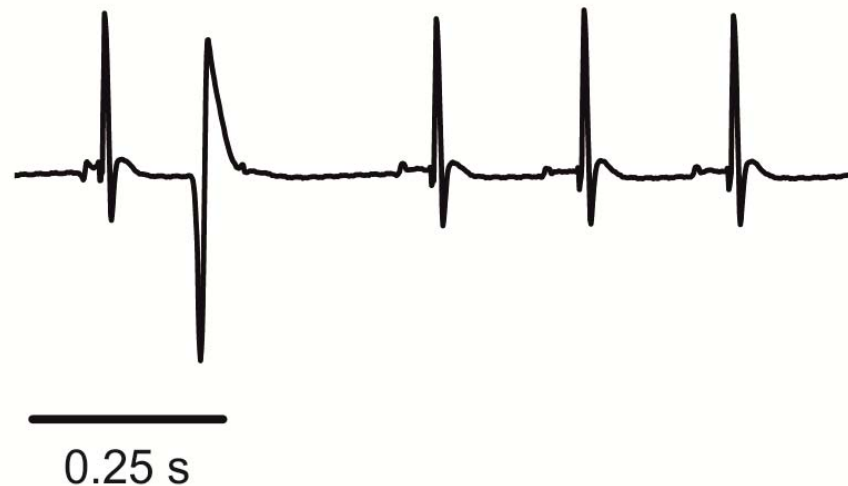


Figure 2.10: ECG recording of a rat heart with VPC.

Example recording from a rat heart in Langendorff perfusion. The trace shows an example of a premature complex in relation to the P wave. The complex resembles a QRS but is wide and bizarre.

2.6 Measuring Intracellular Calcium

2.6.1 Ca^{2+} Fluorophores for LASER-Scanning Confocal Microscopy

In order to measure intracellular Ca^{2+} dynamics with LASER-Scanning Confocal Microscopy (LSCM), a suitable probe is required. The conventional method is to use a Ca^{2+} sensitive fluorescent indicator or fluorophore⁽⁴⁶¹⁾, an excitable molecule with an affinity for the molecule or ion of interest; Ca^{2+} in the case of the work presented in this thesis. Numerous fluorophores have been developed⁽⁴⁶²⁾. They have different Ca^{2+} affinities and excitation/emission spectra such as the non-ratiometric rhod and fluo dyes⁽⁴⁶²⁾ and the ratiometric indo and fura dyes⁽⁴⁶³⁾. The principle of fluorescence imaging is that the fluorescent molecule is loaded into cells and bind to the molecule/ion of interest. The fluorophore contains electrons that are excitable at a specific energy or wavelength. The cells are then subjected to electromagnetic radiation at that excitation wavelength. High energy photons at the excitation wavelength (energy) of the fluorophore are absorbed and elevate the electrons from their ground state to a higher energy level. After a time in the order of the nanosecond range⁽⁴⁶⁴⁾ the electrons fall to their original ground state after

internal conversion releasing photons of lower energy or wavelength than the original photon (Figure 2.11).

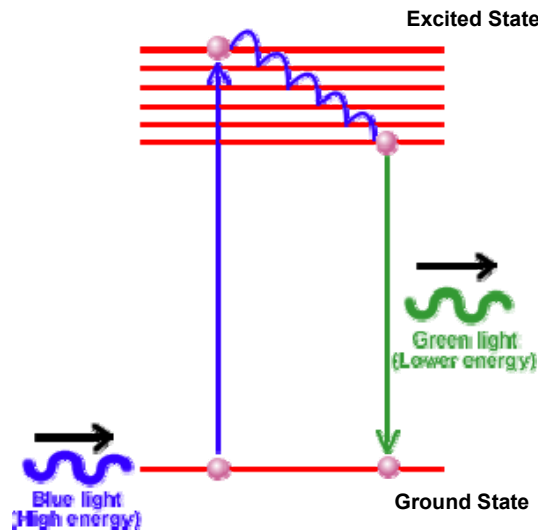


Figure 2.11: Schematic of fluorescence

High energy photons excite electrons of the fluorophore from the ground state to the higher energy excited state. Internal conversion de-excites the electrons without emitting radiation, this takes $\approx 10^{-14} - 10^{-10}$ s before the electron returns to its ground state by emission of another photon, this time at a lower energy. Imaging techniques can be used to excite fluorophores at one wavelength and collect emission light at a longer wavelength.

For LSCM (section 2.7), a fluorophore excitable at an operational wavelength is needed. The LSCM has an argon-LASER that operates in the blue region of the electromagnetic spectrum, specifically an optimum wavelength of 488 nm⁽⁴⁶⁵⁾. Ca^{2+} sensitive fluorophores have been developed that excite at this wavelength such as fluo-3⁽⁴⁶²⁾.

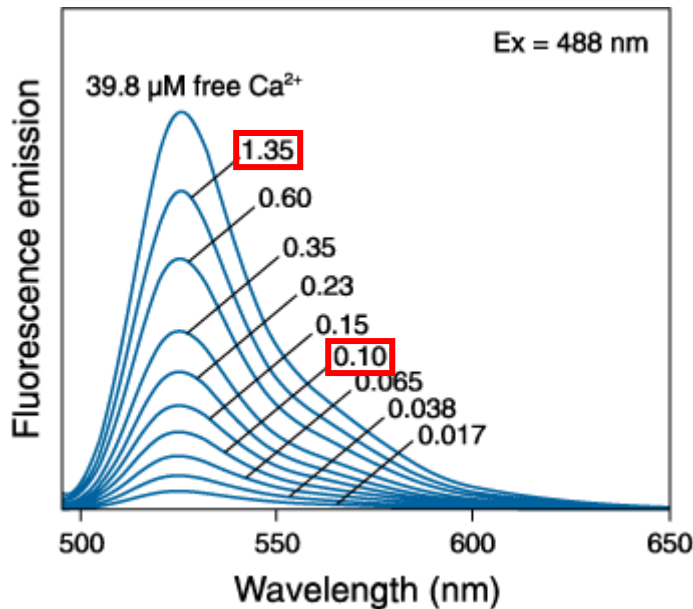


Figure 2.12: Emission spectrum for fluo-3

Emission spectra for different global intracellular concentrations of Ca^{2+} ($[\text{Ca}^{2+}]_i$). Concentrations marked in red are expected values for systolic and diastolic $[\text{Ca}^{2+}]_i$ ⁽⁴⁶⁶⁾ making fluo-3 a good choice for intracellular Ca^{2+} imaging. (Figure from Invitrogen)

Fluo-3 makes an ideal choice at normal global intracellular concentrations of Ca^{2+} ($[\text{Ca}^{2+}]_i$) as $\sim 1.0\mu\text{M}$, the expected $[\text{Ca}^{2+}]_i$ during systole⁽⁴⁶⁶⁾, and 100 nM , the expected $[\text{Ca}^{2+}]_i$ for diastole⁽⁴⁶⁶⁾. Both fluorescence levels for systolic and diastolic $[\text{Ca}^{2+}]_i$ are represented and a sufficient distance apart to give good resolution (Figure 2.12). The optimal sensitivity of the fluorophore is most reliable at $[\text{Ca}^{2+}]$ closest to the dissociation constant (K_d)⁽⁴⁶⁷⁾ which has been reported as $558 \pm 14\text{ nM}$ in the case of fluo-3 in cardiomyocytes⁽⁴⁶⁸⁾. Lower affinity indicators can be used for higher expected $[\text{Ca}^{2+}]_i$ without saturation⁽⁴⁶¹⁾.

2.6.2 Loading Cardiomyocytes with Fluorophore

It is necessary for the fluorophore to be able to enter the cell to measure $[\text{Ca}^{2+}]_i$. This can be achieved by methods such as microinjection, diffusion from patch-clamp pipettes and ester loading⁽⁴⁶⁹⁾. Most fluorophores are cell impermeable so they can be modified with acetoxymethyl esters (AM) which results in an uncharged molecule which is cell permeable^(470;471). Once the AM fluorophore is within the cell, esterases cleave the AM moiety and the impermeable indicator remains inside the cell.

2.6.3 Disadvantages of Ca²⁺ Sensitive Fluorophores

2.6.3.1 Ca²⁺ Buffering

When using fluorophores it is important to consider disadvantages. Since Ca²⁺ sensitive fluorophores function by binding Ca²⁺, high concentrations of the fluorophores can alter the Ca²⁺ buffering of the cell⁽⁴⁷²⁾. For experiments presented in this thesis the manufacturer's recommended concentration of 5 μM of fluo-3 was used which should not significantly affect buffering for these experiments⁽⁴⁷³⁾.

2.6.3.2 Cytotoxicity

Other disadvantages to be aware of are that some fluorophores can be cytotoxic resulting in inhibition of proliferation in some cell types⁽⁴⁶⁹⁾. However, the cardiomyocytes used in the studies presented here were not used for any other purpose following imaging.

2.6.3.3 Photobleaching

Excessive illumination of the fluorophores can lead to bleaching and production of Ca²⁺ insensitive forms of the fluorophores⁽⁴⁷⁴⁾. It is therefore important to reduce illumination to a level that limits photobleaching but maintains an adequate signal to noise ratio. Signals from non-ratiometric dyes are more sensitive to the artefact of photobleaching than signals from ratiometric dyes, as a ratio of two wavelengths can control for bleaching⁽⁴⁶⁹⁾. However, ratiometric indicators can have the problem that photobleaching of the two excitation or emission wavelength maxima can occur at different rates⁽⁴⁷⁴⁾. For the LSCM experiments presented in this thesis the LASER power output was kept to 15%. For both LSCM and epifluorescence experiments the protocol length was kept as short as possible and freshly loaded cells used frequently to limit any photobleaching artefact.

2.6.3.4 Compartmentalisation

A particular problem of the fluorophores, especially AM loaded indicators, is compartmentalisation. The indicators when bound to AM ester can not only easily cross the plasma membrane of cells but also cross organelle membranes

within the cell. The indicator will be present at different concentrations within the organelles compared to cytosol⁽⁴⁶⁹⁾. There are many differences between cell type, loading conditions and type of indicator. To try to limit compartmentalisation for these experiments loading temperature was kept at room temperature⁽⁴⁷⁵⁾ and loading time was kept to 10 min.

2.6.3.5 Dye leakage

Over time the fluorophores can leak from the cells into the extracellular medium. The leakage can be suppressed by low/room temperature⁽⁴⁷⁶⁻⁴⁷⁸⁾ so the indicators were loaded at room temperature and LSCM experiments performed at room temperature.

2.6.3.6 Differential Pathlength and Dye Loading

Non-ratiometric indicators in particular are subject to the effect of differential pathlength and dye loading. Differences in cellular morphology can cause heterogeneity in dye loading. Emitted photons from different regions of the cell have different “paths” to the detector and therefore have different levels of quenching (Figure 2.13). This can lead to apparent differences in $[Ca^{2+}]_i$, which are artefacts. The simplest way to correct for this phenomenon is to ratio the raw fluorescence signal (F) with the baseline (F_0)⁽⁴⁷⁹⁾. This method will only work if the cell does not change position. In the case of contracting cardiomyocytes this is difficult, since the ends of the cell move. To limit this, in the analysis for F/ F_0 ratio was calculated from a 20 pixel band adjacent to Ca^{2+} wave initiation point with the cell⁽²⁹⁶⁾. Alternatively, a ratiometric indicator can be used, which controls for movement and differential dye loads. In the case of Fura dyes, there are two excitation wavelength maxima from which the ratio between the two is calculated. Any changes of pathlength or dye loading happen to the dye and so both wavelengths will be affected equally so the ratio will not change. Unfortunately there are no available ratiometric indicators with an appropriate excitation/emission spectrum for use with an argon LASER for LASER-scanning confocal microscopy.

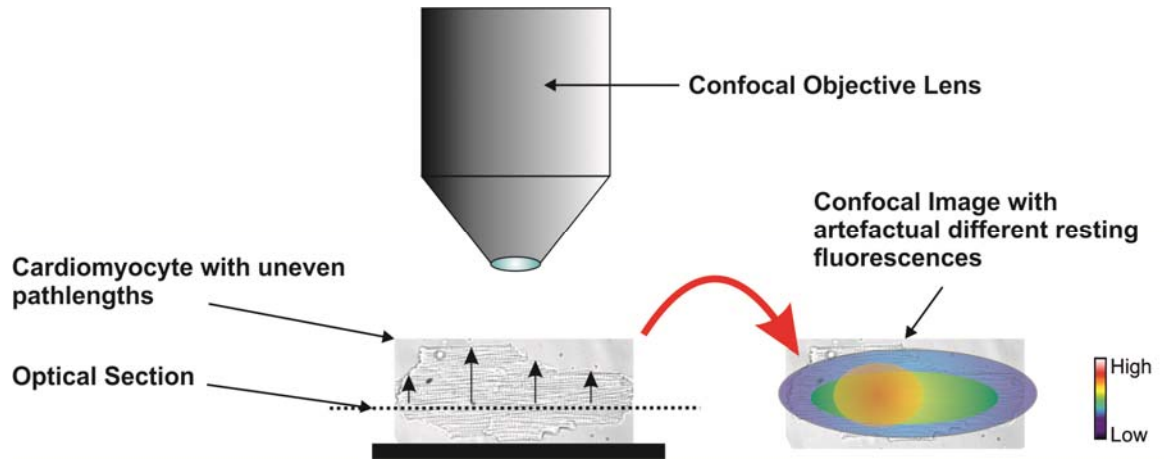


Figure 2.13: Diagram of differences in resting fluorescence signals due to different path lengths. Differences in cell morphology can lead to alterations of fluorescence quenching from photons following different pathlengths. This can lead to artefacts in $[Ca^{2+}]_i$ assessment if the ratio of F/F_0 is not taken.

2.6.4 Ratiometric Ca^{2+} Fluorophores for Epifluorescence Microscopy

To measure the stimulated Ca^{2+} transient Fura-2 and Fura-4 were used. In contrast with Fluo-3, the Fura dyes are ratiometric. Ratiometric dyes can either have two excitation (Fura) or two emission wavelength maxima (Indo)⁽⁴⁶³⁾. The major advantage of using a ratiometric dye is that differential pathlength (Figure 2.13) and differences in dye loading are corrected for. In the case of Fura dyes there are two peaks of excitation at 340 nm and 380 nm for Ca^{2+} bound and unbound, respectively, and emission at 510nm (Figure 2.14 Figure 2.15). When Ca^{2+} is released from the sarcoplasmic reticulum (SR) during systole $[Ca^{2+}]_i$ it binds to fluorophore in the cytosol and is excited by 340 nm light. During diastole, when Ca^{2+} is taken back up into the SR, the $[Ca^{2+}]_i$ drops below the K_d and Ca^{2+} dissociates from the dye. The unbound dye is excited by 380 nm light so the 340 nm signal reduces and the 380 nm signal increases. When the ratio of 340/380 nm is calculated the transient rises and falls with the release and reuptake of Ca^{2+} . As with the Fluo dyes there are different Fura dyes with different affinities. For greater resolution at lower $[Ca^{2+}]_i$, such as diastolic $[Ca^{2+}]_i$, or low amplitude Ca^{2+} waves a higher affinity dye is more useful, such as Fura-2 with a K_d of 181 ± 52 nM⁽⁴⁸⁰⁾. For higher $[Ca^{2+}]_i$ a lower affinity dye such as Fura-4F with a K_d of 1.16 ± 0.016 μ M is more useful⁽⁴⁸⁰⁾.

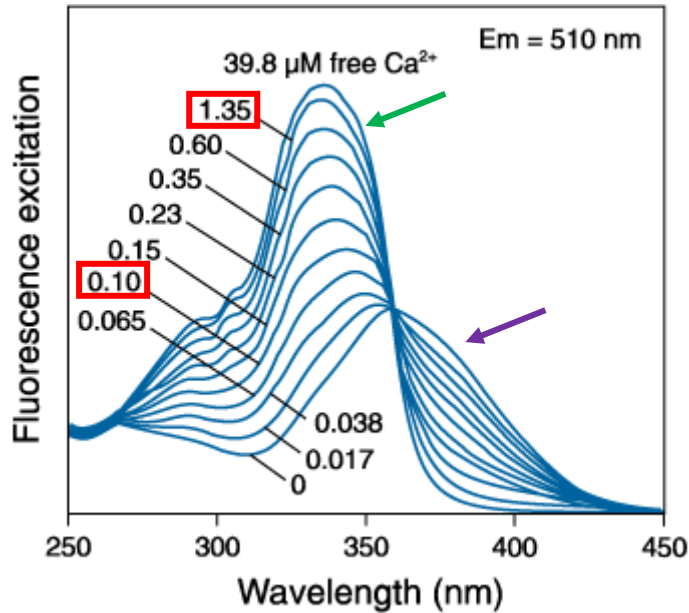


Figure 2.14: Emission spectrum for Fura-2.

Emission spectra for different global intracellular concentrations of Ca^{2+} ($[\text{Ca}^{2+}]_i$). In contrast with Fluo-3 the spectrum has two excitation peaks for Ca^{2+} bound dye (green arrow) and unbound dye (purple arrow). Concentrations marked in red are expected values for systolic and diastolic $[\text{Ca}^{2+}]_i^{(466)}$ making fura-2 a good choice for intracellular Ca^{2+} imaging closer to diastolic or minimum $[\text{Ca}^{2+}]_i$. (Figure from Invitrogen).

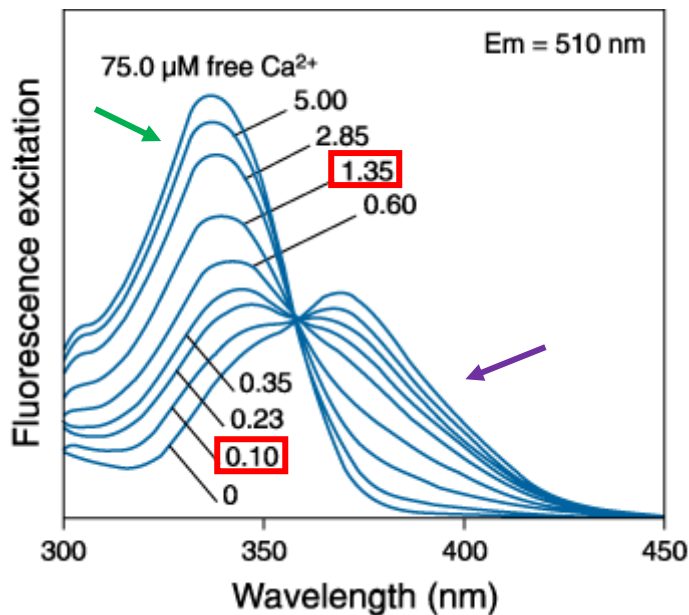


Figure 2.15: Emission spectrum for Fura-4F.

Emission spectra for different global intracellular concentrations of Ca^{2+} ($[\text{Ca}^{2+}]_i$). The two excitation peaks for Ca^{2+} bound dye (green arrow) and unbound dye (purple arrow) are shown. Concentrations marked in red are expected values for systolic and diastolic $[\text{Ca}^{2+}]_i^{(466)}$ making fura-4F a good choice for intracellular Ca^{2+} imaging closer to systolic or peak $[\text{Ca}^{2+}]_i$. (Figure from Invitrogen).

2.7 Imaging Ca^{2+} with LASER-Scanning Confocal Microscopy

2.7.1 Principles of Image Collection

Adult rat left ventricular cardiomyocytes were loaded with Fluo-3AM, excitable at 488 nm. Once excited the emitted photons are >515 nm. The confocal microscope has an Argon LASER with peak radiation intensity at 488 nm⁽⁴⁶⁵⁾. The LASER light at the excitation wavelength is passed through a series of dichromatic mirrors, which reflect wavelengths shorter than the determined wavelength and allow longer wavelength light through. The excitation LASER light is reflected through scanning mirrors that continually rotate through the x and y dimensions in an arc. This allows the user to set the scan dimensions and scan the whole specimen or specific regions. The directed excitation light is focussed onto the specimen through the objective lens of the microscope (Figure 2.16A). Emitted light from the excited fluorophore within the specimen is collected through the objective lens and de-scanned by the rotating scan mirror i.e. allowing the emitted light to return on the excitation path to the dichromatic mirrors. The light then passes through the dichromatic mirrors as it is now a lower energy and longer wavelength and hits the photo detector, in this case a photo multiplier tube (PMT). A pinhole allows only light from the in-focus focal plane of the specimen; all other focal plane light is blocked (Figure 2.16B). As out of focus emission light is rejected, only fluorescence from the focal plane is detected so the interfering fluorescence from the rest of the cell is eliminated. This allows for a much better estimation of fluorescence, thus $[\text{Ca}^{2+}]_i$, in the area of interest.

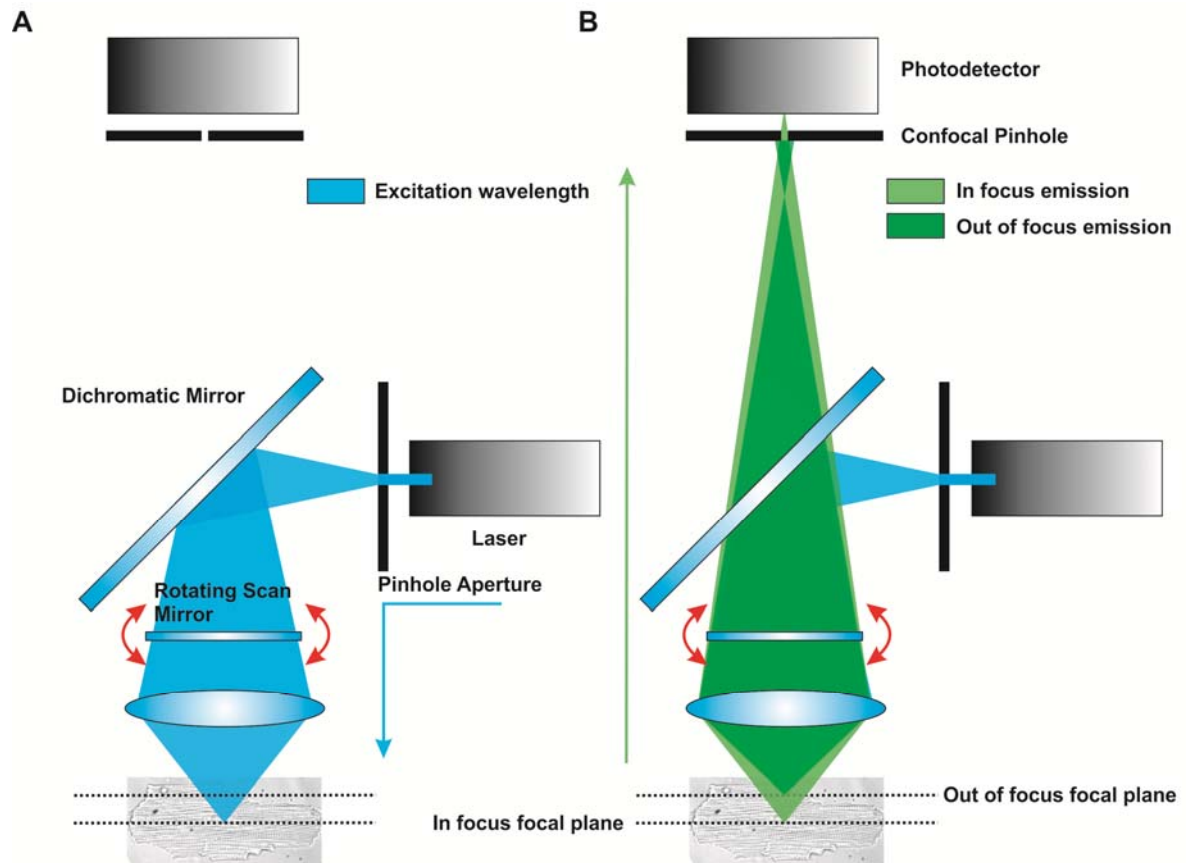


Figure 2.16: Principles of LASER-scanning confocal microscopy

(A) Excitation of fluorophore within the cell. The LASER emits light at the excitation wavelength (488 nm) passed through a series of dichromic mirrors (one shown for simplicity). The scanning mirror directs the beam through x and y axes to scan the specimen. (B) The dichromic mirrors reflect wavelengths shorter than the determined wavelength and allow longer wavelengths through. Emitted light at a longer wavelength (>515 nm from Fluo-3) passes through the dichromic mirror. A pinhole at the photo detector allows only light from the plane of focus through to the detector to give a more accurate estimation of dye fluorescence without interference from other focal depths.

2.7.2 Spatial and Temporal Resolution

Since the image is generated by scanning a LASER across the specimen point by point it takes a period of time, so the whole cell is never imaged at any one time. This presents a problem when trying to capture relatively short-lived events such as spontaneous releases of Ca^{2+} . Conventional images generated are 512×512 pixel arrays. The typical speed of scan is 500 lines per second so a 512^2 array takes approximately 1s to acquire. This time can be reduced by reducing the area scanned or bi-directional scanning. The spatial resolution is less straight forward due to the effects of diffraction. Due to the diffraction of light a point source of light cannot be imaged as a single intense point, instead it has an intense peak with peaks and troughs of intensity rippling outward, called the Airy disc. The resolution of the image can be determined from the wavelength of the light and the numerical aperture (NA) of the lens. A lens with

higher NA has greater light capturing efficiency⁽⁴⁸¹⁾ and is defined by half the angle of the collection cone (θ) and the refractive index of the immersion medium (n) to give: $NA = n\sin\theta$. The x-y resolution can then be calculated using the Rayleigh/Abbe formula⁽⁴⁸²⁾:

$$r = 0.61\lambda/NA$$

where r is the radius of the Airy disc between intensity peak and first zero. Images for this thesis were collected using a Zeiss LSM 510 with a 63x 1.2 NA water immersion lens. Therefore we can calculate the size of the Airy disc and x-y resolution at 515 nm as 0.52 μm . In the z dimension or axial resolution the formula is⁽⁴⁸²⁾:

$$r = 2\lambda/n\sin^2\theta$$

using the same λ and NA we get a z resolution of 0.72 μm . The pinhole aperture was set to 1.0 Airy unit to improve axial resolution. This ensures that only the first order maxima of the diffraction pattern are accepted into the photo detector. If the pinhole aperture were set to >1.0 Airy unit then second order or greater maxima of the diffraction pattern would be allowed through leading to loss of resolution. The trade-off by reducing the light permitted through is a loss of image brightness.

2.7.3 Image Acquisition

The depth of scan for confocal imaging systems at visible wavelengths is up to 40 μm , beyond this spherical aberration is a problem i.e. the image becomes distorted by the surface geometry of the lens⁽⁴⁸³⁾. This is suitable for isolated ventricular cardiomyocytes having a typical depth of ~ 20 μm . Ca^{2+} waves can occur at frequencies greater than the scan time and so be missed or only partially resolved if LSCM scanning speed is 1 frame. s^{-1} . Therefore Ca^{2+} wave imaging in this thesis was performed using a different technique. The scan area was reduced to a single line which the LASER scans back and forth. This technique is referred to as line-scanning. Each scan progresses across the region of interest selected by the user to give length across the cell in the x dimension. Each pass of the LASER adds a line of pixels in the y dimension to give time

producing a “waterfall” image. Each pixel in the images produced equates to 0.27 μm in x and 3.07 ms in y. The scanning LASER line was orientated parallel with the long axis of the cell (Figure 2.17A) and placed approximately equidistant between the outer edge of the cell and the nucleus/nuclei to ensure the nuclear area was not included in the scan line and alter the fluorescence signal⁽²⁹⁶⁾.

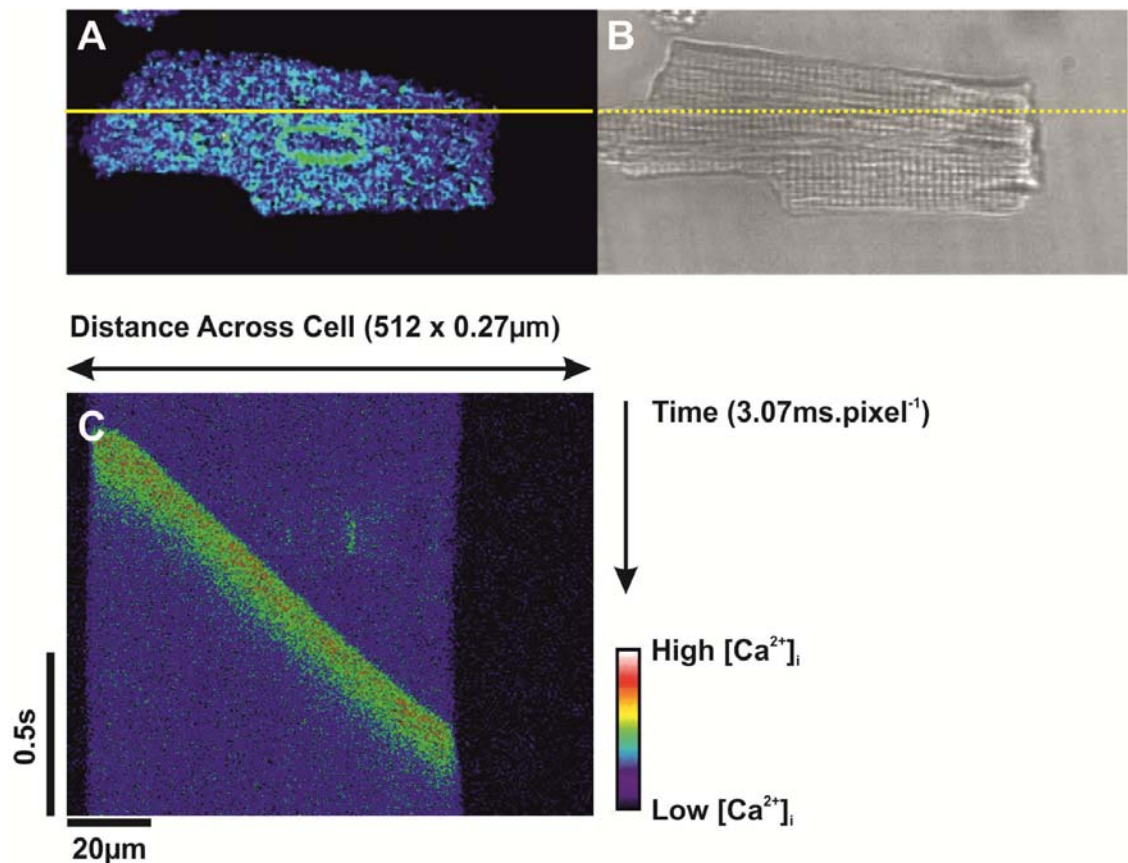


Figure 2.17: Line-scan confocal imaging.

(A) Isolated cardiomyocyte loaded with Fluo-3 dye. The yellow line indicates the scan dimension selected by the user. Care is taken to ensure the nucleus (green ellipse) is not included in the scan line. (B) The same cell imaged in standard light transmission mode with the scan line denoted by the dotted line. Note that the nucleus is not clearly visible. (C) Section of a waterfall image showing a Ca^{2+} wave in progress with distance across the cell in the x dimension and time in the y dimension. The cell is typically scanned for 1min which equates to 30,000 scans.

2.7.4 Image Analysis

Images were acquired using the Zeiss LSM 510 imaging system and software. Waterfall images were exported to ImageJ (National Institutes of Health, USA) and converted to greyscale TIFF files. These files were de-compressed in Paint Shop Pro 5 (Corel) where wave velocity was calculated by measuring the difference in pixel co-ordinates between initiation point and end point of each

wave and calculating the wave propagation gradient. Uncompressed TIFF files were processed in a programme written by Dr. Francis Burton (Nbands) that measures the mean fluorescence output from a 20 pixel band defined by the user. This output file was imported into the graph analysis software Origin6.1 (OriginLab). The baseline fluorescence F_0 was measured from each trace and applied to the raw data to give the F/F_0 . Data are expressed as the ratio of F/F_0 .

2.8 Imaging Ca^{2+} with Ratiometric Epifluorescence Imaging

2.8.1 Principles of Epifluorescence Microscopy

Essentially the technique is very similar to LSCM. The Ca^{2+} fluorophores used in these experiments was ratiometric, i.e. difference wavelengths of excitation depending on whether the dye Ca^{2+} bound or not (section 2.6.4). For the experiments in this thesis Fura-2 and Fura-4F were used. Both have excitation wavelengths of 340 nm and 380 nm (Ca^{2+} bound and unbound) so the confocal LASER source is not appropriate. Therefore the fluorophore was excited with a mercury vapour arc lamp with a spinning wheel monochromator (Cairn Research). Within the unit a diffraction grating splits the white light into its constituent wavelengths. A spinning disc of excitation filters switches rapidly between the two excitation wavelengths alternating between 340 nm and 380 nm at a rate of 250 Hz. A dichromatic mirror reflects the excitation light through the objective to illuminate and excite the fluorophore epifluorescently in the specimen on the microscope stage. The emitted light at a longer wavelength of 510 nm is allowed to pass through the dichromatic mirror to be detected by the PMT (Figure 2.18).

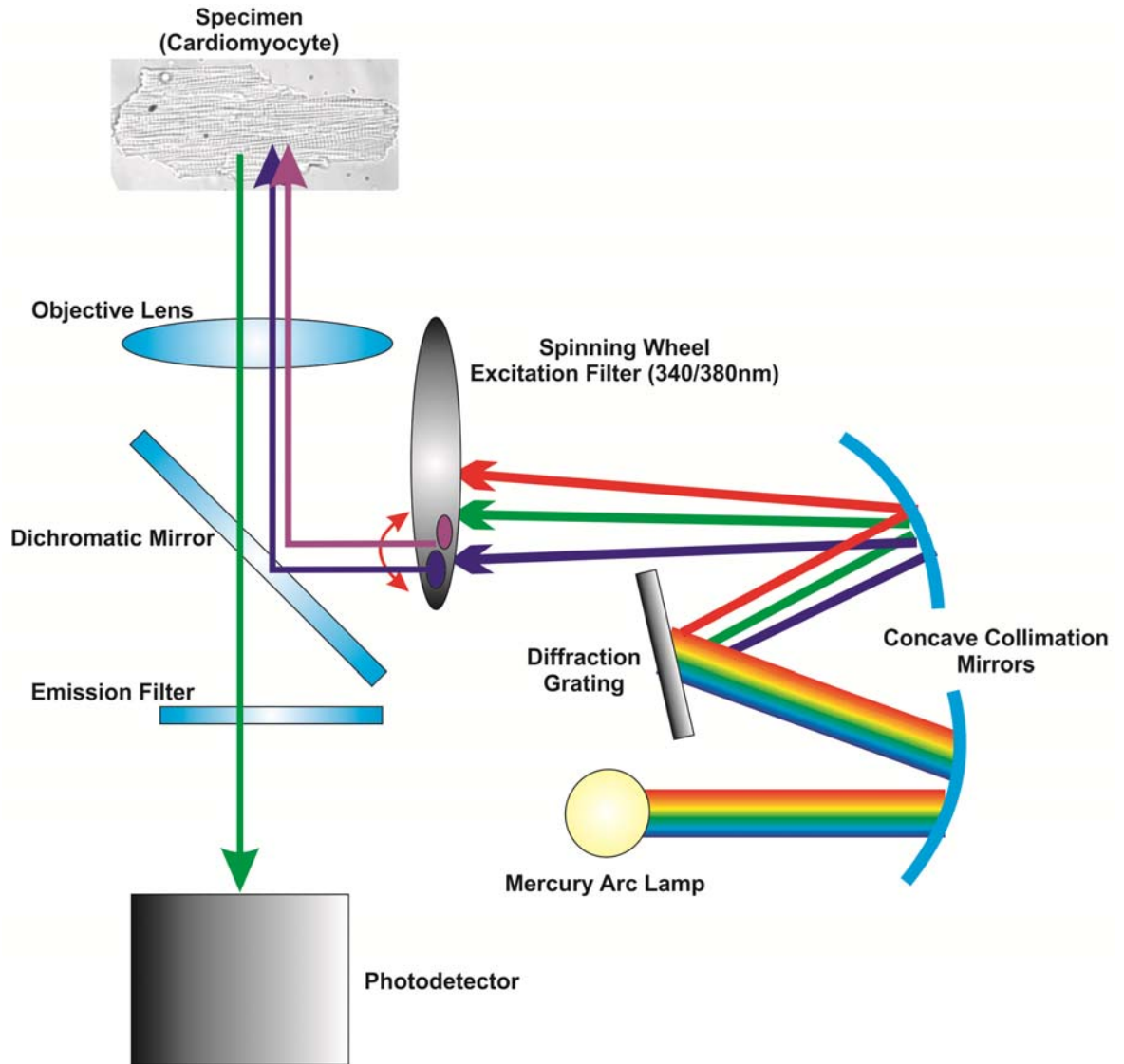


Figure 2.18: Epifluorescence imaging.

Multispectral light is emitted by the mercury vapour arc lamp. Collimating mirrors reflect the light onto a diffraction grating which splits the light into its component wavelengths. These are then collimated and pass through an excitation wavelength filter. The user can define the wavelengths with many filters in the monochromator unit. For excitation of Fura dyes excitation wavelengths of 340 nm and 380 nm (ultraviolet – shown in blue and purple) were required. A spinning wheel enables rapid switching between the two wavelengths. The dichromatic mirrors (one shown for simplicity) reflect light of wavelengths shorter than the user selected wavelength through the objective lens of the microscope to illuminate the specimen epifluorescently and excite the fluorophore. Emitted light (at 510 nm) (shown in green) is collected by the objective lens and passes through the dichromatic mirrors which allow light of longer wavelengths than selected through to the PMT photo detector.

In contrast with LSCM light from the whole specimen is collected from different focal planes rather than a single point. In these experiments we are interested in the global change in $[Ca^{2+}]_i$ so the resolution of a single scanning point is not necessary.

2.8.2 Data Acquisition and Analysis

Isolated cardiomyocytes were loaded with 5 μM Fura-2AM or Fura-4F-AM for 10min. The cells were then diluted with test solution (see individual chapter methods for details) and incubated for 30 min. This step allowed de-esterification of the fluorophore as well as incubating the cells with test solution. Cardiomyocytes were then loaded into a tissue bath (Cell Microcontrols) and superfused with test solutions at 37 °C by gravity fed perfusion pen with active pump outflow. Cells were field stimulated with 2.0 ms duration voltage pulses delivered through parallel platinum wires (stimulation voltage set to 1.5 times the threshold). The stimulation simulates the action potential that depolarizes the sarcolemma leading to the Ca^{2+} release and reuptake cycle (section 1.4). When the Fura dye is excited (section 2.6.4), the output signal is detected sequentially for each excitation wavelength by the PMT. The output signal is sent to an oscilloscope for visualisation of the signals and an analogue to digital converter (Axon Instruments). The signal is sampled at 5000 Hz to generate a trace for each excitation wavelength using Clampex 10.3 (Axon) and the ratio 340/380 calculated online. The ratio trace is the change in fluorescence corrected for movement artefact, differential dye-loading and differential pathlengths (section 2.6.4.). From the ratio trace it is possible to calculate $[\text{Ca}^{2+}]_i$ using the following⁽⁴⁶³⁾:

$$[\text{Ca}^{2+}] = K_d \times B(R - R_{\text{Min}}) / (R_{\text{Max}} - R)$$

K_d is the dissociation constant of the dye. B is the relative change in fluorescence between zero and saturating $[\text{Ca}^{2+}]$ at 380 nm. R is the ratio signal. R_{Min} is the minimum ratio before stimulation, which was reduced by 10% to account for the higher diastolic $[\text{Ca}^{2+}]_i$ in rat cardiomyocytes. R_{Max} is the saturation fluorescence achieved by killing the cell with a sharp micropipette at the end of the protocol to release Ca^{2+} bound dye to give maximum signal. R_{Min} and R_{Max} were determined for each cell. B was measured by Dr. Chris Loughrey when the system was set-up and calibrated. For Fura-2 $K_d B = 1.2 \times 10^{-6}$ and for Fura-4F $K_d B = 2.8 \times 10^{-6}$.

Data were plotted in Origin6.1 (OriginLab) and converted to $[\text{Ca}^{2+}]$, which is the Ca^{2+} transient. Average transients were calculated using macros written by Prof.

Godfrey Smith, University of Glasgow. Differentiation plots and exponential decay functions were calculated using the software's own functions.

2.9 Dissection of *T. brucei* Mechanism

2.9.1 Specific Protease Inhibitors

T. brucei secretes a cathepsin-L-like cysteine protease that induces Ca^{2+} signalling in the endothelial cells of a blood brain barrier model⁽⁶⁹⁾. Given the importance of Ca^{2+} signalling in excitation-contraction coupling of the heart it was prudent to test if a cysteine protease could be affecting Ca^{2+} in cardiomyocytes. The cysteine protease activity of *T. brucei* consists of two cysteine proteases TbCatL and TbCatB⁽¹¹²⁾ so specific protease inhibitors for TbCatL and TbCatB were tested. K11777 (N-methyl-piperazine-Phe-homoPhe-vinylsulfone-phenyl) has been developed and used against the cathepsin-L-like cysteine protease of the related parasite *T. cruzi*^(484;485) and TbCatL⁽⁶⁹⁾. Figure 2.19 shows the chemical structure and irreversible binding of K11777 to the active site of TbCatL. By blocking the active site of TbCatL, it is unable to act as a protease and cleave proteins. The reported IC_{50} of K11777 is $0.06 \mu\text{M}$ ⁽⁴⁸⁴⁾ so K11777 was added in excess at a concentration of $10 \mu\text{M}$ to control media and supernatant and spontaneous contractile events in cardiomyocytes measured as described above (section 2.4).

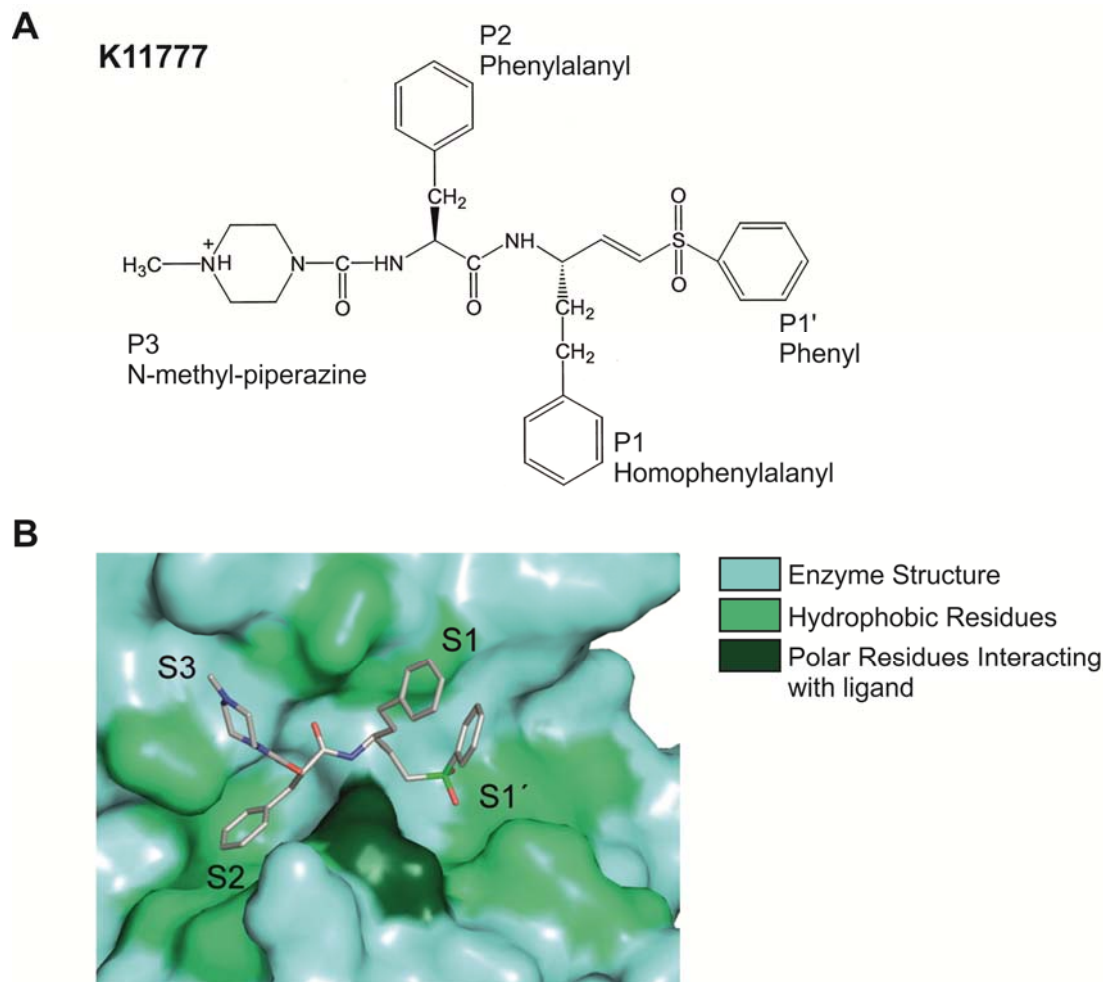


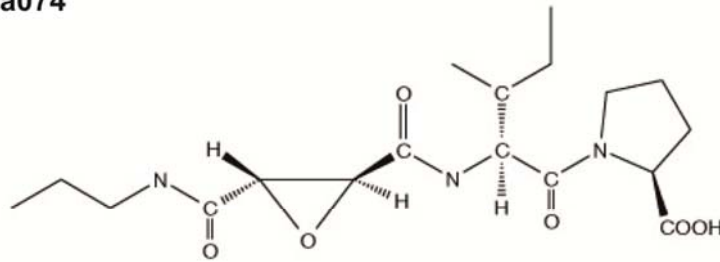
Figure 2.19: Structure and binding of K11777.

(A) Structural representation of K11777 shows the interacting domains, P1, P1', P2 and P3. (B) Representation of K11777 in the active site of TbCatL. The hydrophobic regions in light green are pockets for the interacting domains of K11777 appropriately labelled. The dark green area shows where the polar residues of TbCatL interact with the ligand forming a non-polar C-C bond. (Figure adapted from Kerr *et al.* (2009)⁽⁴⁸⁵⁾).

CA074 (L-3-trans-(propylcarbonyl)oxirane-2-carbonyl)-L-isoleucyl-L-proline) has been used to inhibit TbCatB^(69;486). Figure 2.20 shows the chemical structure and irreversible binding to the active site of TbCatB blocking its protease action. CA074 has an IC_{50} of 2.24 nM⁽⁴⁸⁷⁾, and was added to control media and supernatant at a concentration of 10 μ M and a population assay performed as described above (section 2.4).

A

Ca074



B

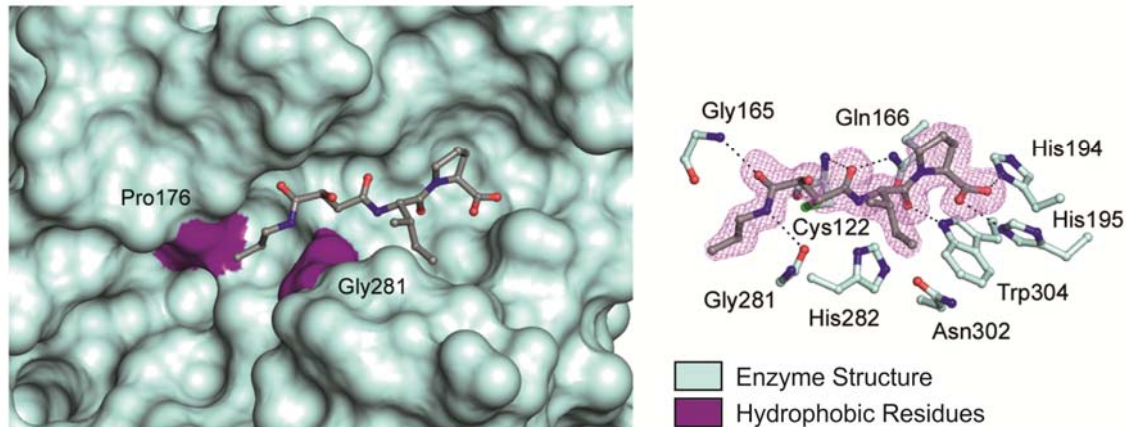


Figure 2.20: Structure and binding of CA074.

(A) Structural representation of CA074. (B) (left) Representation of CA074 in the active site of TbCatB. The hydrophobic regions in purple are pockets for the interacting domains of CA074. (B) (right) CA074 interactions with residues in the active site of CA074. (Figure adapted from Kerr *et al.* (2010)⁽⁴⁸⁶⁾).

2.9.2 Recombinant *T. brucei* Cathepsin-L

2.9.2.1 Manufacture of *T. brucei* Cathepsin-L

Recombinant TbCatL was kindly donated by Dr. Ana-Paula C. A. Lima of Instituto de Biofísica Carlos Chagas Filho, Universidade Federal do Rio de Janeiro and Prof. James H. McKerrow, University of California San Francisco Medical School. Recombinant TbCatL was stored at -80 °C and activated with the reducing agent dithiothreitol (DTT) (concentration determined by enzyme activity assay described below) prior to each use.

2.9.2.2 Recombinant TbCatL Activity Assays

The activity of the recombinant TbCatL can be measured by the cleavage of a fluorogenic substrate and subsequent measurement of the fluorescence on a spectrophotometer. The fluorogenic peptidyl substrate benzyloxycarbonyl-

phenylalanyl-arginine-7-amido-4-methyl-coumarin (Z-FR-AMC) has been used to test activity in TbCatL and shown to be effective with 120 M substrate converted by 1 M TbCatL min^{-1} with a peak activity at pH 5.0⁽¹²⁹⁾. The substrate Z-leucine-arginine-AMC (Z-LR-AMC) was also effective at converting 130 M min^{-1} at pH 6.0⁽¹²⁹⁾. TbCatL recognises the phenylalanyl-arginine residue of the substrate and cleaves the fluorogenic AMC moiety. In a spectrophotometer (Wallac Envision) reaction wells in a black background light-absorbent 96 well plate (Corning) are exposed to light at the excitation wavelength of 360 nm (Figure 2.21). Light at the emission wavelength of 480 nm is detected by a photo multiplier tube and recorded as arbitrary units of fluorescence (section 2.6.1 for details on fluorescence).

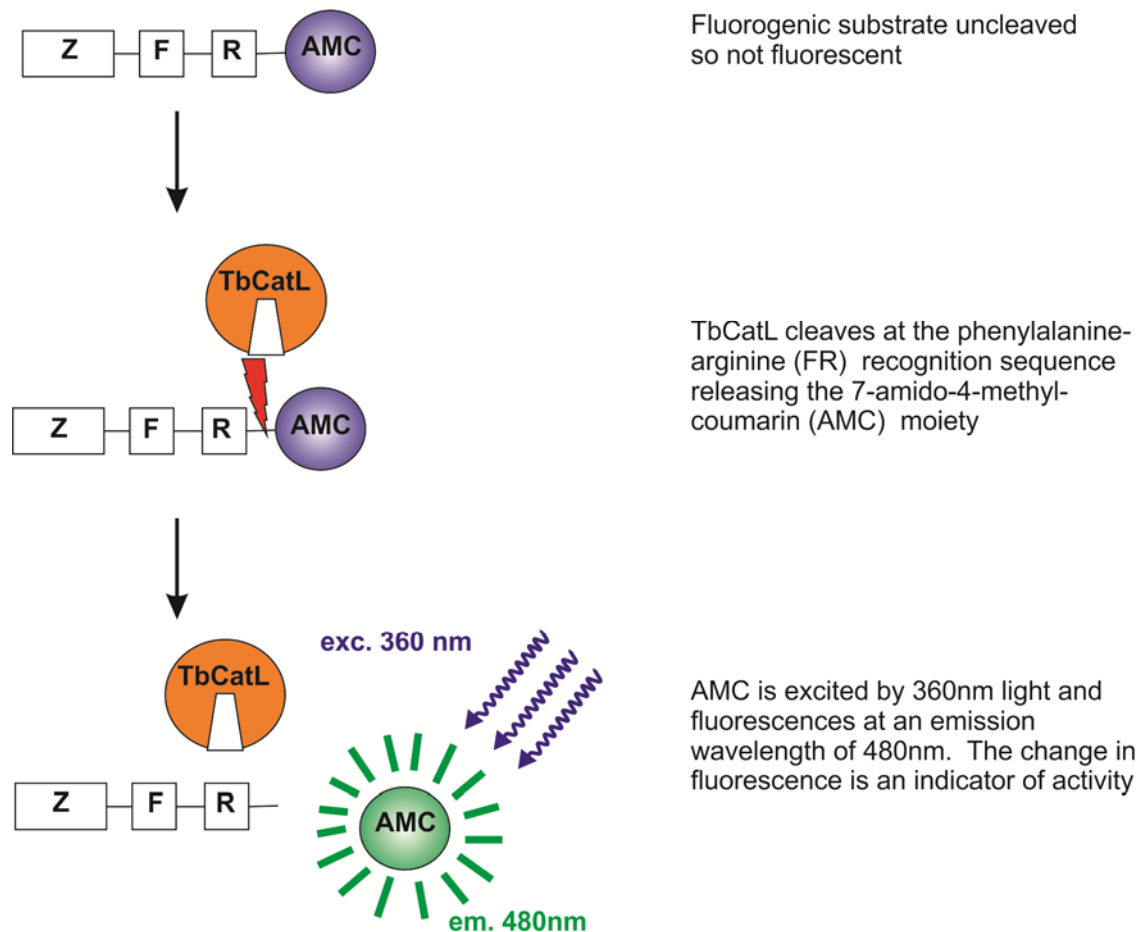


Figure 2.21: Schematic of a fluorogenic activity assay. Z-FR-AMC substrate is not fluorescent until cleaved. TbCatL recognises the phenylalanyl-arginine (FR) residues and cleaves the fluorescent 7-amido-4-methyl-coumarin (AMC) moiety. Excitation light at 360 nm excites the AMC which emits at 480 nm. The change in fluorescence from baseline is an indicator of enzyme activity.

Using a similar method to that described in Caffrey *et al.* (2001)⁽¹²⁹⁾, recombinant TbCatL was diluted to $0.1 \mu\text{g} \cdot \text{mL}^{-1}$ in assay buffer (0.1 M NaOAc pH

5.5 plus DTT at 0.1, 0.5, 1.0 and 2.0 mM). Enzyme in assay buffer or assay buffer without enzyme as a blank control (100 μL) was added to 20 μM fluorogenic substrate in the 100 μL of assay buffer in triplicate in a 96 well black plate, and measured in a spectrophotometer at 37 °C at excitation and emission frequencies of 360 and 480 nm for 30 min. The relative fluorescence of the blank control with the appropriate concentration of DTT was subtracted and plotted as arbitrary relative fluorescence units (Figure 2.22A(i)). The mean activity curves were differentiated to give the peak rate of conversion. DTT at 1.0 and 2.0 mM showed the maximal activity of the enzyme; (218 vs. 2278 vs. 5040 vs. 6548 vs. 6560 $\text{units}\cdot\text{s}^{-1}$; 0 vs. 0.1 vs. 0.5 vs. 1.0 vs. 2.0 mM DTT; Figure 2.22A(ii)).

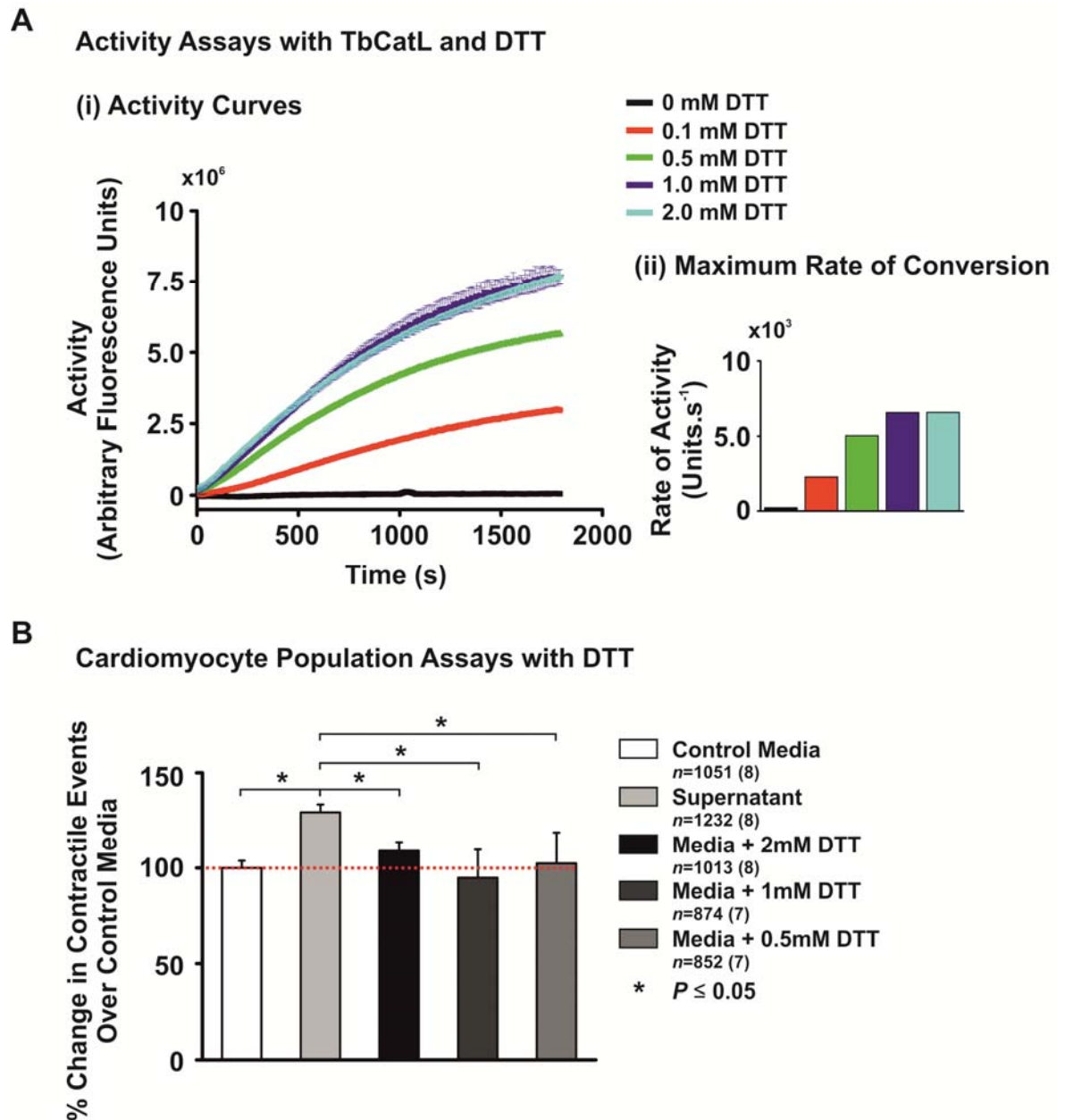


Figure 2.22: Activity assays and cardiomyocyte population assay to test activating quantity of DTT for TbCatL.

(A) (i) Activity assay with $0.1 \mu\text{g.mL}^{-1}$ TbCatL in 0.1 M NaOAc and $20 \mu\text{M}$ fluorogenic substrate Z-FR-AMC at $0, 0.1, 0.5, 1.0$ and 2.0 mM DTT . Data are plotted as mean \pm SEM curves ($n=3$) of arbitrary relative fluorescence units. (ii) Maximum rate of conversion of substrate by $0.1 \mu\text{g.mL}^{-1}$ TbCatL as fluorescence units. s^{-1} by differentiation of the curves in (i). (B) Population assay of adult rat left ventricular cardiomyocytes in media with different concentrations of DTT. Data are expressed as mean \pm SEM. n = number of cells from (isolations). Statistics were performed by multiple linear regression analysis and $P \leq 0.05$ considered significant.

2.9.2.3 Assessment of DTT Effects on Cardiomyocyte Spontaneous Contractile Events

A cohort of cardiomyocyte population assays was performed with different concentrations of DTT to test that concentrations of DTT necessary for recombinant CatL activation did not have a significant effect on spontaneous

Ca²⁺ release. Briefly, cardiomyocytes were prepared as above (section 2.3.1) and incubated with control media (section 2.1.1) with 0.5, 1.0 and 2.0 mM DTT. Cells were loaded into a tissue bath and viewed through a 10x objective lens and 10 fields of ~10 rod-shaped cardiomyocytes were viewed for 1 min per field. The numbers of cells showing spontaneous contractile events per min were recorded and expressed as percentage change over media control. Trypanosome culture supernatant was tested alongside as a positive control for differential contractility when compared to DTT. Supernatant showed a significant increase over control as expected (Chapter 3) (100 ± 4.1 vs. $129.3 \pm 4.1\%$; control ($n = 1051$ cells from 8 hearts) vs. Supernatant ($n = 1232$ cells from 8 hearts; $P < 0.05$). DTT had no significant effect compared to control; (109.0 ± 4.7 , vs. 94.9 ± 14.8 vs. $102.4 \pm 16.3\%$, 2 mM DTT ($n = 1013$ cells from 8 hearts) vs. 1 mM DTT ($n = 874$ cells from 7 hearts) vs. 0.5 mM DTT ($n = 852$ cells from 7 hearts); $P > 0.05$ when compared to control media; Figure 2.22B). When compared to supernatant there was still a significant difference ($P = 0.05$). Therefore an activating concentration of 2.0 mM DTT results in maximal recombinant TbCatL activation without having a significant effect on the cardiomyocytes.

2.9.2.4 Recombinant TbCatL in Cardiomyocyte Spontaneous Contractile Event Measurements

Recombinant TbCatL was prepared by adding at a dilution factor of 1:50 (volume of 8 μ L) to 300 μ L control media (as described in section 2.1), 100 μ L of cardiomyocytes in MIKH and 4 μ L of 0.1 M DTT giving a final concentration of 2 mM DTT. The 1:50 dilution of TbCatL gave a final concentration of 2 nM TbCatL as used in Caffrey *et al.* (2001)⁽¹²⁹⁾. The solution was incubated at room temperature for a period of 30 min to allow the DTT to activate the TbCatL and for the cardiomyocytes to be exposed to the active TbCatL, as with the supernatant and control media experiments described above (section 2.4). The percentage of cardiomyocytes exhibiting at least one spontaneous contractile event min^{-1} was measured.

2.9.3 RNA Interference of *T. brucei* Cathepsin-L

2.9.3.1 RNA Interference

RNA interference (RNAi) was performed in *Trypanosoma brucei brucei* 2T1 (a cell line derived from bloodstream form Lister 427)⁽⁴⁸⁸⁾. The trypanosomes were transfected with the plasmid pTL107 (an extrachromosomal circular piece of DNA from which genes of interest may be expressed), which was derived from the commercial plasmid pGL2084, a Gateway® (Invitrogen) modified version of the plasmid pRPa^{isl(489)}. The pTL107 plasmid contains a tetracycline inducible stem-loop RNAi cassette and target region of the gene of interest, *TbCatL*. The target region of the *TbCatL* gene contained in pTL107 corresponded to nucleotides 409-986 of the open reading frame, with the following oligonucleotides used to generate the *TbCatL* gene construct; forward 5'-GGG GAC AAG TTT GTA CAA AAA AGC AGG CTG CAG TGA CCC CAG TGA AGG A-3' and reverse 5'-GGG GAC CAC TTT GTA CAA GAA AGC TGG GTA GAC ATT GGT TTG TGC CCT T-3'. Trypanosomes containing this construct were kindly manufactured and provided for use in this study by Nathaniel Jones, University of Glasgow. The trypanosomes containing the plasmid were selectively maintained in culture with modified HMI-9 by addition of 2.5 µg.mL⁻¹ hygromycin and 0.5 µg.mL⁻¹ phleomycin as the RNAi plasmid had resistance genes to these antimicrobials so that successful transfectants can be selectively maintained. Addition of 1.0 µg.mL⁻¹ tetracycline induced the transcription of the RNAi cassette providing a dsRNA stem in the stem-loop construct homologous to *TbCatL*. RNAi induction was performed in two independent biological duplicates. Using two independent clones controlled for replication of phenotype upon RNAi induction over two independent transfection events i.e. the phenotype observed was not a random effect of the transfection, but due to inducible interference of *TbCatL*.

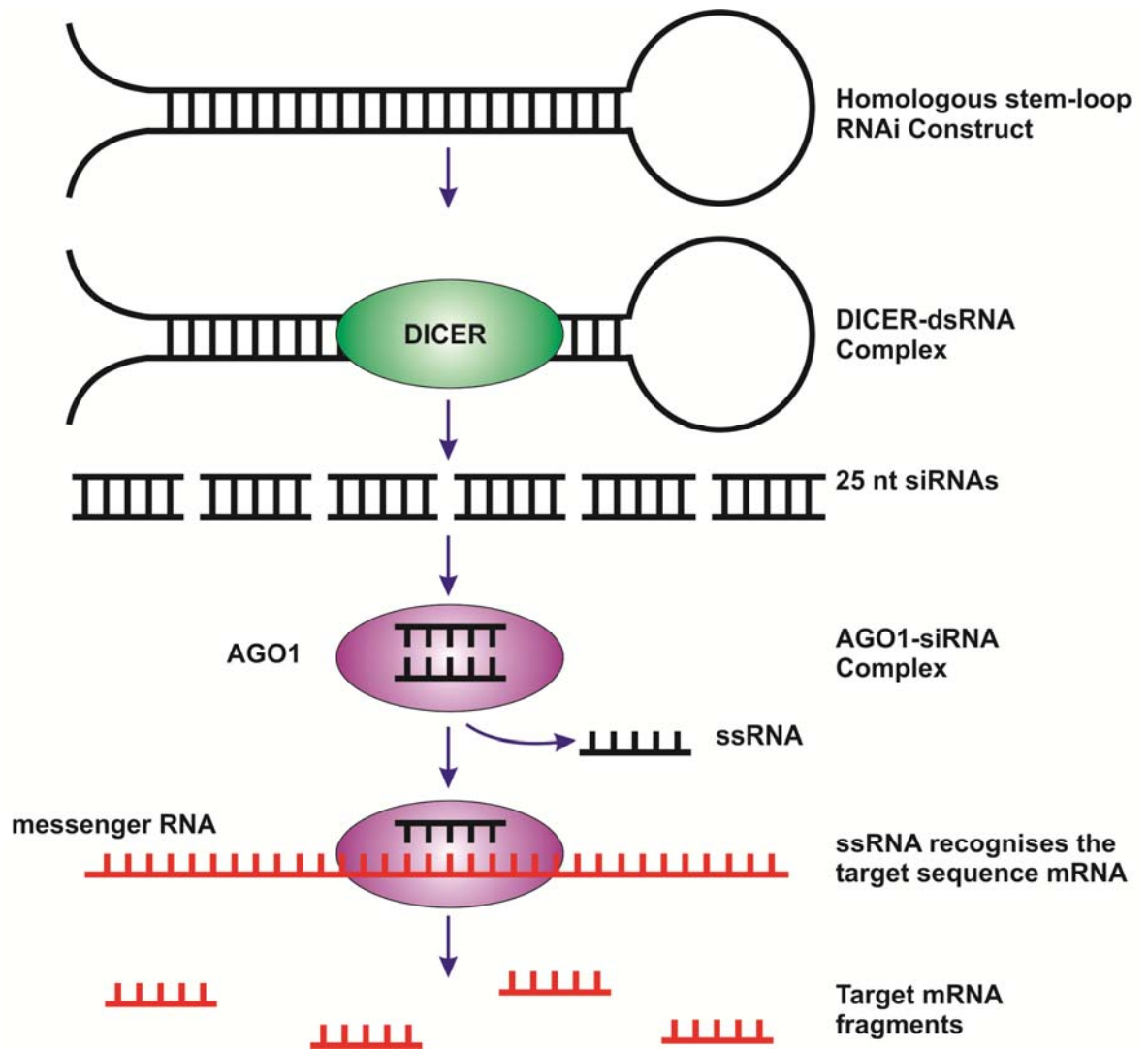


Figure 2.23: The RNAi pathway in Trypanosomatids

The mechanism by which dsRNA (or dsRNA in the stem of stem-loop constructs) is recognised and cleaved into 25 nucleotide segments is governed by the RNase III-related enzyme Dicer. The small interfering RNA (siRNA) fragments are unwound to form single-stranded RNAs (ssRNA) by RNase-H-containing protein that belongs to the argonaute (AGO1) family or Slicer. The ssRNAs display sequences recognised by the messenger RNA (mRNA) transcribed from the gene of interest which are then specifically targeted and degraded before translation. (Redrawn from Balana-Fouce and Reguera⁽⁴⁹⁰⁾).

The parasite's inherent RNAi system recognises the double-stranded RNA (dsRNA) *via* the recently characterised RNase III-related enzyme Dicer⁽⁴⁹¹⁾, which then degrades dsRNA into small interfering RNAs (siRNA) 25 nucleotides in length. A second enzyme belonging to the argonaute (AGO) family ('slicer') recognises and binds the siRNA, unwinds it to form single-stranded RNA (ssRNA), which then binds to homologous sequences in the messenger RNA of the gene of interest, *TbCatL* in this case. The *TbCatL* mRNA is then degraded by the trypanosomes' inherent degradation mechanisms (Figure 2.23)⁽⁴⁹⁰⁾.

2.9.3.2 Growth Curves

The RNAi specificity and degree of TbCatL knockdown was tested in the two independent biological duplicates. RNAi was induced with $1 \mu\text{g}\cdot\text{mL}^{-1}$ tetracycline and growth curves performed on induced vs. uninduced cultures in triplicate for the two biological duplicates. Cultures for growth curves were initiated with 1.0×10^5 parasites. mL^{-1} in modified HMI-9 with the addition of hygromycin and phleomycin as above. The cultures were counted in triplicate with an improved Neubauer haemocytometer (section 2.1.1) at 24, 48 and 72 hr time points post-induction. The cultures were reseeded every 24 hrs as a 1:10 dilution into fresh modified HMI-9 media with added antimicrobials to ensure a sufficient quantity of parasites to count accurately without overgrowth of the culture. It has been shown that TbCatL is essential for growth of the parasite⁽⁴⁹²⁾ so successful induction of RNAi should manifest as a negative growth phenotype.

2.9.3.3 Real time Quantitative PCR to Confirm Inhibition of TbCatL Expression

During RNA interference the mRNA for the gene of interest becomes degraded (Figure 2.23). In order to test the efficiency of the RNAi it is possible to indirectly measure the amount of mRNA by using the quantitative Real-Time Polymerase Chain Reaction (qRT-PCR). RNA cannot serve as a template for PCR as the technique only works on double stranded DNA. Therefore, the mRNA must be converted to double-stranded complementary DNA (cDNA) by a method called reverse transcription. The qRT-PCR is then performed on the cDNA.

2.9.3.3.1 RNA Extraction

The process of RNA extraction is complicated by the presence of ribonuclease enzymes (RNases) which are ubiquitous in the environment on skin of the user and often the laboratory bench and can rapidly degrade a sample. To minimise the risk of degradation the work area was cleaned with 70% ethanol and use of RNaseZap™ (Ambion), which destroys environmental RNases. Gloves and equipment (e.g. pipettes) were treated with RNaseZap. Tubes and pipette tips certified as RNase/DNase free were used throughout the extraction protocol. RNA was extracted from parallel cultures (section 2.9.3.2) grown to 5.0×10^5 parasites. mL^{-1} in 10 mL culture (5.0×10^6 parasites) using the RNeasy® (QIAGEN) kit. Parasites were pelleted by centrifugation at 1,500 g for 10 min. The cells

were lysed with a buffer containing guanidine-isothiocyanate and β -mercaptoethanol, which disrupts the cell membranes releasing the cellular contents into the lysate and inactivates RNases that could degrade the RNA. The lysate was homogenised by passing $\geq 5\times$ through a 23-gauge needle. One volume of 70% ethanol was added to the lysate and mixed by pipetting. The ethanol provides the appropriate conditions for RNA binding in the next step. The ethanol/lysate mixture was added 700 μL at a time to a spin-column with an RNA binding silica membrane and centrifuged for 15 s at $\geq 8,000$ g. The column was retained and the flow-through discarded. The column was then washed with proprietary buffers (RWT and RPE) designed to support RNA binding and wash out contaminants such as intracellular proteins. A final centrifugation step dried the column removing any remaining ethanol. The dry column was then placed in a sterile RNase free collection tube and 30 μL RNase free water added to the column and centrifuged for 1 min at 8,000 g. The water neutralises the pH and reduces the RNA-binding affinity to the membrane thus eluting the RNA⁽⁴⁹³⁾. RNA quantity was measured by absorbance of 220-320 nm wavelength light in a microvolume spectrophotometer (Nanodrop ND-1000, Thermo Scientific). The relationship of concentration of nucleic acid and absorbance is linear (Beer-Lambert Law), which therefore enables a readout on-screen of the RNA concentration in the sample as $\text{ng}\cdot\mu\text{L}^{-1}$.

2.9.3.3.2 Synthesis of cDNA

For qRT-PCR the RNA must be transcribed to its complementary DNA (cDNA). This is initiated by an oligonucleotide primer of poly-thymine (oligo-dT primers) that binds to the polyadenylated tail of the mRNA. The primers then direct the reverse transcriptase (RT) to synthesise a single strand of cDNA using dNTPs (adenine (A), thymine (T), cytosine (C) and guanine (G)). This forms an mRNA/DNA hybrid. To make the cDNA double-stranded the mRNA is degraded which is achieved by RNase H. The remaining single-stranded DNA forms a hairpin loop due to hydrophobic interactions and serves as the primer for the second complementary strand by a DNA-dependent DNA polymerase (Figure 2.24).

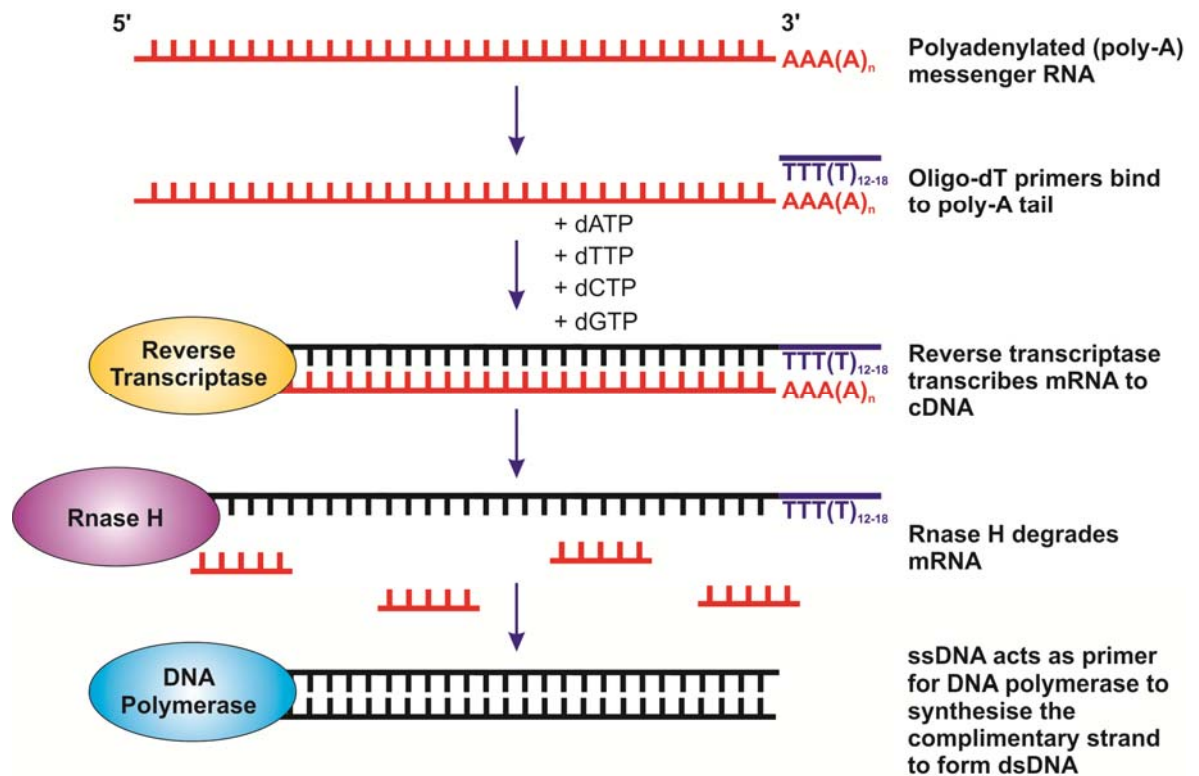


Figure 2.24: Synthesis of cDNA by reverse transcription.

Oligo-dT primers recognise and bind to poly-adenylated tail of mRNA. Reverse transcriptase transcribes the mRNA into complimentary strand of DNA. RNase H degrades the mRNA and the remaining ssDNA acts as primer for DNA polymerase to synthesise the remaining strand to produce dsDNA complimentary to the original mRNA in the sample.

For preparation of cDNA, approximately 1.0 µg of total RNA was treated with DNaseI (TURBO DNase (Ambion)) to remove any contaminating genomic DNA. Samples were incubated in a reaction volume of 25 µL (containing 2.5 µL of 10x enzyme buffer and 1 µL DNase) for 25 min at 37 °C. Following the incubation, 2.5 µL of a DNase inhibitor was added to stop the reaction.

Reverse transcription was carried out using the Omniscript RT kit (Qiagen) with 5.0 µM of each oligo dT primer (QIAGEN). The kit contains the reverse transcriptase (RT), dNTPs and an enzyme buffer containing Mg²⁺ for optimal enzyme activity. The Omniscript RT kit performs three functions: i) RNA-dependent reverse transcription to form the first cDNA strand from the mRNA, ii) RNase H activity to degrade the mRNA and iii) DNA dependent polymerase to synthesise dsDNA from the ssDNA. An additional RNase inhibitor (RNase-Out (Invitrogen)) was added to protect samples (Table 2.2), which according to the manufacturer does not affect the RNase H capability of the Omniscript RT. A parallel reaction was carried out without RT to confirm successful cDNA

synthesis and rule-out genomic DNA contamination. This process creates cDNA for all mRNA in the sample.

To measure the gene of interest PCR must be performed.

Table 2.2: Reverse Transcription Reaction Components

Component	Volume (per reaction)	Final Concentration
10x RT Buffer	5.0 μL	1x
dNTP mix (5 mM each)	5.0 μL	0.5 mM per dNTP
Oligo-dT primer (10 mM)	5.0 μL	1 μM
RNaseOut (10 units. μL^{-1})	2.5 μL	25 units
Reverse Transcriptase	2.5 μL	10 units
RNase free H ₂ O	Variable*	To final volume of 50 μL
RNA (1 μg)	Variable*	1 μg
TOTAL	50 μL	

* Variable depending on concentration of RNA in sample. Final volume made up with RNase free H₂O.

2.9.3.3.3 Quantitative RT-PCR

The Polymerase Chain Reaction (PCR) works by taking a small quantity of target DNA and amplifying it to detectable quantities. The amplification is a three step process: first by denaturing the dsDNA through heating (~90-98 °C) to break the DNA into separate strands. Secondly, short DNA sequences (primers), designed by the user, complementary to flanking regions of the gene of interest then anneal to the single strands when the temperature is reduced to 50-65 °C. Thirdly, the samples are heated to 72-80 °C to allow the DNA polymerase to synthesise complementary strands from added nucleotide bases (adenine, thymine, cytosine and guanine (dNTPs) directed by the primers. The process is repeated 30-40 times, each step doubling the quantity of DNA for the gene of interest (Figure 2.25). The requirements for a PCR reaction are:

Table 2.3: Components and functions of a PCR reaction.

Component	Function
Buffer	Maintains reaction mix at appropriate pH and provides Mg^{2+} for polymerase activity.
Deoxynucleotide Triphosphates (dNTPs)	Provide energy and nucleotides for the synthesis of DNA. Quantities are balanced to reduce mismatch errors.
Specific Primers	Short DNA sequences (20-30 nucleotides) that bind to complementary DNA sequences flanking the gene of interest and provide an initiation point for the polymerase to act
Polymerase	Heat stable enzyme that adds the complementary dNTP to the DNA template (A binds with T vv. C binds with G vv.)
Template dsDNA	Sample to be amplified

When setting up the PCR heat cycler several stages must be programmed:

1. **Initiation:** The reaction is heated to 90-98 °C and held for up to 10 min. This step is required for full denaturation of the DNA.
2. **Denaturation:** The reaction is heated to 90-98 °C for up to 1 min to disrupt the hydrogen bonds between the complementary bases of the two DNA strands to separate them.
3. **Annealing:** The reaction is cooled to 50-65 °C for up to 1 min to allow the primers to bind to their complementary sequences on the ssDNA template. The DNA polymerase then binds to the primer-template hybrid.
4. **Elongation:** The reaction is heated to 72-80 °C (for time determined by the length of sequence to be amplified). The polymerase synthesises a new strand by adding dNTPs to the template strand in the 5'-3' direction of the new strand (3'-5' of the template)
5. **Cycle Repeats:** Steps 2-4 are repeated 30-40 times to amplify the DNA product

6. **Final Elongation:** A final longer elongation step of up to 15min may be added to ensure any remaining ssDNA is completely extended.
7. **Final Hold:** If further analysis is to be performed on the sample they can be held on the cycler plate at 4 °C.

Over the course of the 30-40 cycles the reaction goes through 3 phases. The first phase is the exponential phase where there are sufficient reagents to amplify all the available templates in the annealing/elongation steps. Beyond approximately cycle 15 the reaction enters the linear phase where reagents are diminishing. The final phase is the plateau phase where all reagents have been consumed and no more products can be synthesised. With conventional PCR the product is analysed at the end of the reaction so, depending on cycle number, is likely to be in the plateau phase. Real-time PCR has the advantage of measuring the increase in product over the course of the reaction using fluorophore probes so determining the point at which the plateau is reached.

For the PCR conducted in this thesis only qRT-PCR was performed. The principle of qRT-PCR is that a DNA binding fluorophore fluoresces when bound and excited in the cycler unit so that the relative quantity of DNA can be measured. There are several methods available; the SYBR green was employed in this thesis. The SYBR green fluorophore binds to the minor groove of dsDNA. As the reaction progresses more dsDNA is present so more dye is in a bound state and excitable.

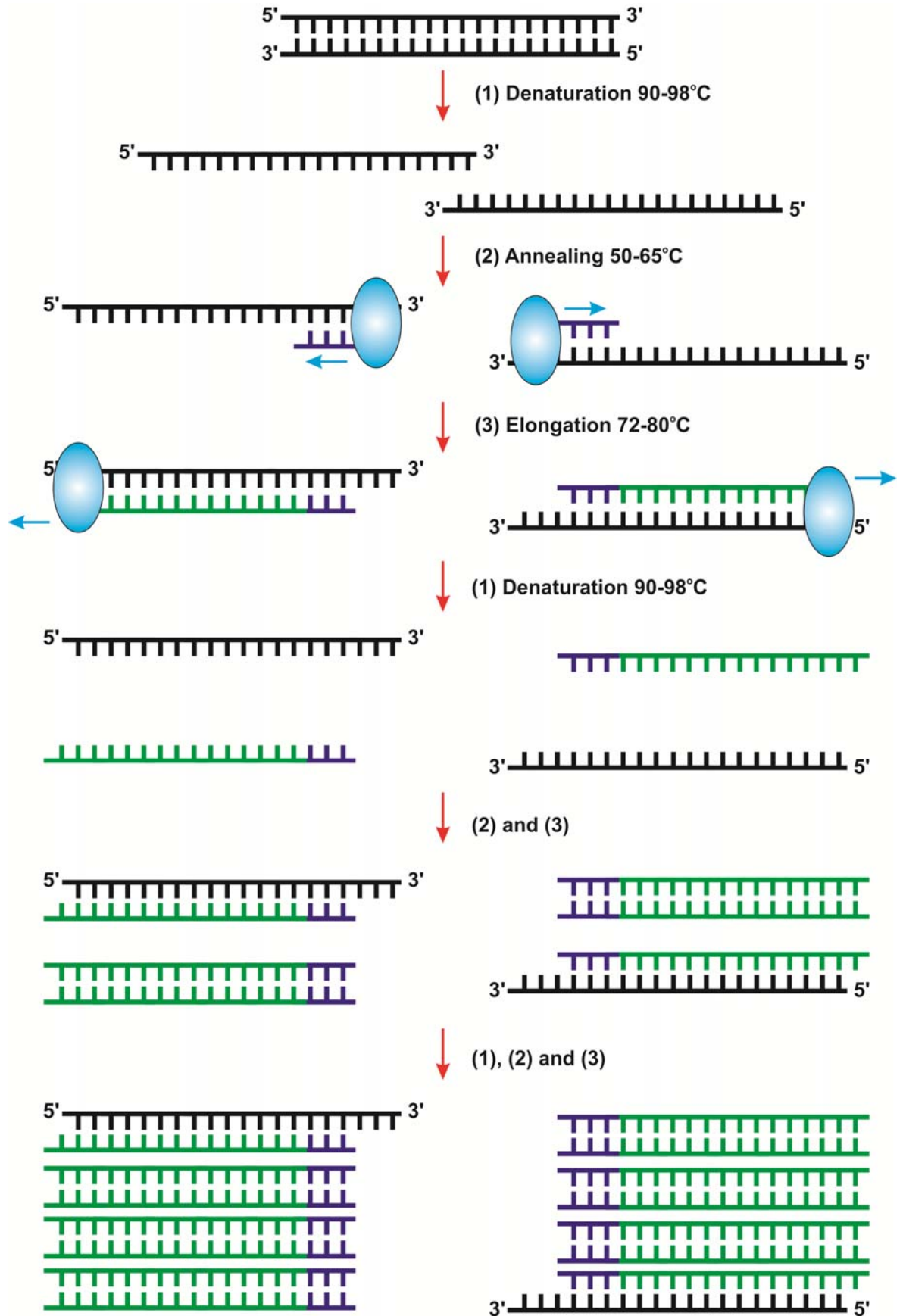


Figure 2.25: Amplification of template DNA by PCR:

Schematic of PCR showing (1) denaturation of DNA at 90-98 °C, (2) annealing at 50-65 °C and (3) elongation at 72-80 °C. Black “ladders” represent template DNA to which blue primers anneal and green synthesised DNA elongates by DNA polymerase (blue ellipses). The synthesised DNA is used as further template in the next cycle to amplify exponentially over the course of the reaction.

Samples and reagents were thawed and kept on ice. Reactions were prepared in a laminar flow hood to minimise aerosol contamination and personal protective equipment was worn to prevent user contamination of samples. Synthesised cDNA was diluted 1:5 with RNase/DNase free H₂O to increase volume and decrease pipetting error and 100ng of cDNA (2 µL) per reaction well used. The oligonucleotide primers used were designed by Dr. Liam Morrison, University of Glasgow and were: TbCatL forward 5'-TCT CGG ATA TGA CAC GTG AAG AGT-3' and reverse 5'-TCT GCG CAG CTG CAA AGT-3'. To offset individual reaction error from differing starting quantities of DNA the TbCatL product must be normalised to an endogenous control gene that is unlikely to be altered in quantity by the addition of the RNAi plasmid. This allows small differences to be detected in gene expression as any over/under expression due simply to different starting template quantities will also be evident in the endogenous control gene. Therefore, by using a stable endogenous control gene small changes in template concentration will also affect the endogenous gene by the same amount and so be removed when normalised. As a result and subtle variations in the gene of interest without any change to endogenous gene can be accepted with greater confidence. For example, if hypothetical samples A and B have different gene expressions, B is higher say, without an endogenous control it is not known whether B is truly higher, or if B had a higher starting quantity of template DNA. But if a set of primers for an endogenous control gene is used on aliquots from the same samples and that control gene is stable under the experimental manipulation, i.e. RNAi in this case won't alter its expression, then if B did have a greater starting concentration the endogenous control gene will also be increased. So if the situation arose where B was actually increased and there was a higher concentration of template then the endogenous control would be raised but by a smaller amount than B. Therefore when B was normalised sample B with endogenous primers the true change would become evident. This does not control for pipetting error because each well on the plate is unique so triplicates of each sample and primer set should be performed, i.e. samples A and B need to be run in triplicate for both target gene primers and endogenous control primers, so 6 wells for each sample, 3 with target gene primers and 3 with endogenous control primers. GPI-8 is a ubiquitously expressed transamidase that adds glycosylphosphatidylinositol (GPI) anchors to cell surface proteins⁽⁴⁹⁴⁾, and was used as the endogenous control. The primers

were: forward 5'-CGA AGC GCA TTT GGA TAG-3' and reverse 5'-ACG GCG TGA TGA CAG TGA AG-3'.

RT-PCRs were carried out in triplicate per individual sample, to control for pipetting error, on a 7500 Real-Time PCR system (Applied Biosystems), using approximately 100 ng cDNA, 1 x Power Sybr green master mix (Applied Biosystems) and 4.0 μM of the respective oligonucleotide primers, in a final reaction volume of 25 μL per well. The SYBR green mix contains the reporter fluorophore that binds to the dsDNA and reports the quantity, *AmpliTaq Gold* DNA polymerase, dNTPs and a ROX dye that is used to offset non-PCR related fluorescence. The ROX dye is a passive reference dye, i.e. it does not change fluorescence during PCR, therefore is used as a control for potential changes in fluorescence due to non-PCR factors such as instrumentation variability, well volume and pipetting error. The samples run were 3 separate cultures each of induced RNAi (1 $\mu\text{g}\cdot\text{mL}^{-1}$ tetracycline) and uninduced RNAi (no tetracycline) for both biological duplicates (STL 349 and STL 350). Each was duplicated again with GPI-8 primers as endogenous normalisation control. In parallel samples without template DNA (no template controls (NTCs)) were also run as a control for contamination. These are wells with identical components of primer and SYBR mix but no template DNA so that if any signal should be detected, there is cross-contamination of target DNA in the reaction components and the final result not be accepted. The samples and master mix of primers and SYBR mix were added to a 96-well plate and covered with an adhesive optical film to minimise sample evaporation. Cycle conditions were; 10 min heat-activation of the polymerase, then 40 cycles of 95 $^{\circ}\text{C}$ for 10min and 60 $^{\circ}\text{C}$ for 1 min for denaturation and annealing/elongation.

2.9.3.3.4 Melting Curve Analysis

A melting curve analysis step was added to the protocol to test for non-specific contaminating DNA. SYBR green binds to all dsDNA in a sample, not only the target DNA. To ensure that minimal non-specific contaminating DNA is included in the fluorescence signal a melting curve step is added to the protocol. This step is performed after the final cycle where the samples are heated slowly from 60 $^{\circ}\text{C}$ up to 95 $^{\circ}\text{C}$ causing the DNA to denature while collecting fluorescence. The melting point (T_m) is the temperature at which the dsDNA denatures into

two separate strands of ssDNA. Different lengths and base compositions of DNA will have different T_m so if the sample is purely from the amplification of the target DNA with the specific primer set the melting curve analysis should have one distinct peak (Figure 2.26B). If there is contaminating DNA or excessive primer-dimer formation (primers annealing to themselves) the melting curve will have multiple peaks. For this thesis samples were checked in this way and no contamination was detected.

2.9.3.3.5 Amplification Curve Analysis

The principal of quantifying a target gene with qRT-PCR is determining the point at which the fluorescence signal reaches a detectable threshold (C_t). The level of fluorescence is directly proportional to the quantity of DNA in the sample. The cyclor machine software automatically normalises the fluorescence against the non-PCR background fluorescence detected by the reference dye which controls for sample evaporation and pipetting error. The reference dye used by the Applied Biosystems 7500 machine is ROX. The normalised fluorescence of the reporter (R_n) is not detectable for the initial cycles of the reaction as the quantity of DNA is still too low. This level of unchanging fluorescence before the DNA has reached sufficient concentration is referred to as the baseline fluorescence. The machine software automatically selects and subtracts this baseline from R_n to give the change in fluorescence ΔR_n . Once the quantity of DNA reaches sufficient levels the fluorescence is detectable and increases. The point at which this occurs, or the cycle number it occurs, is the cycle threshold (C_t) (Figure 2.26A). Although this can be manually determined by the user, for the purposes of this thesis, the C_t detection threshold was set automatically by the Applied Biosystems software. The C_t value determines the quantification of the DNA i.e. the more DNA template you begin with the earlier fluorescence becomes detectable. Therefore C_t is inversely proportional to DNA quantity.

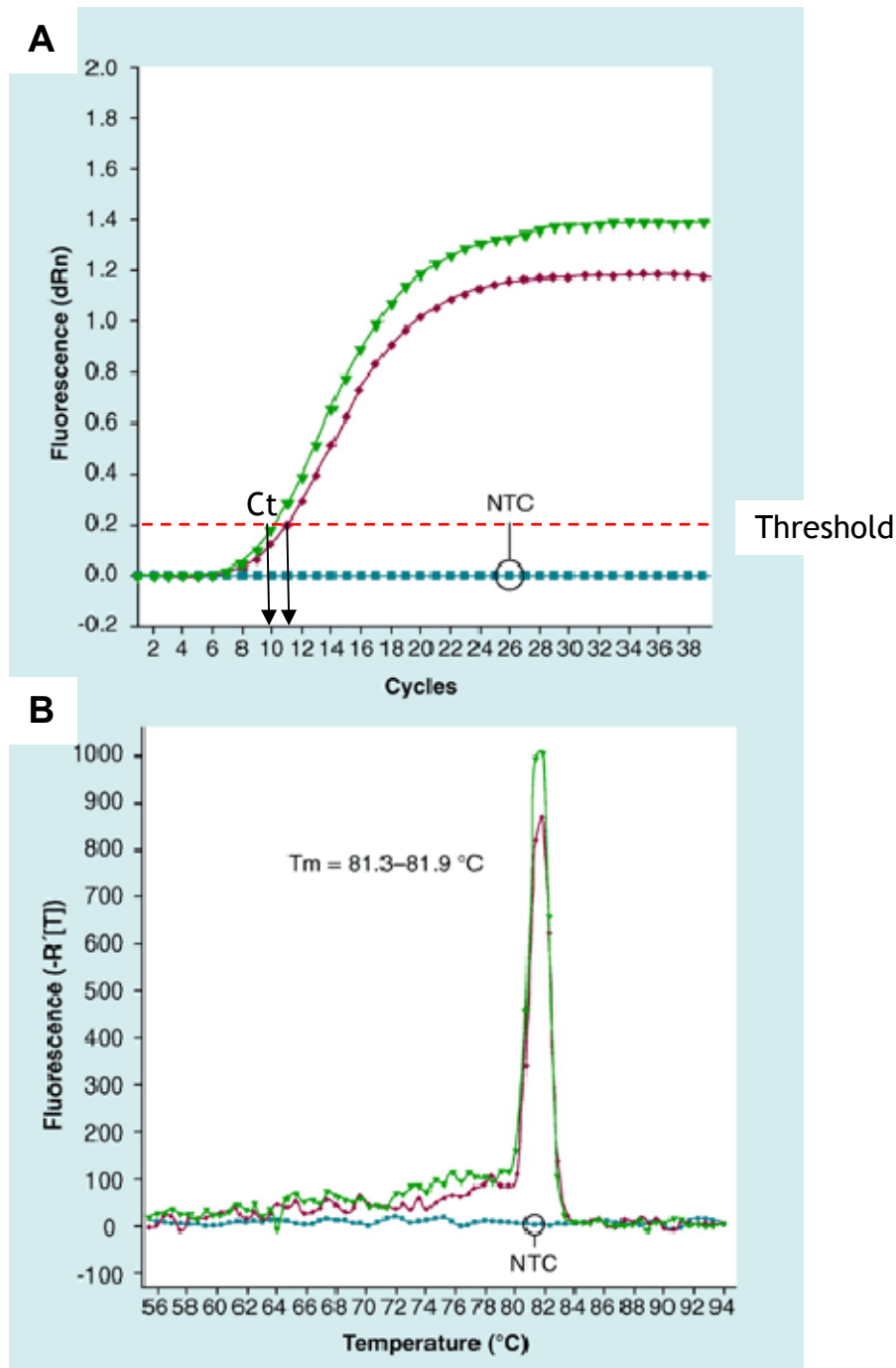


Figure 2.26: Amplification plot and melting curve examples.

(A) Amplification plot example showing two hypothetical samples and a no template control (NTC). The threshold has been set in the exponential phase of the reaction. The C_t is the cycle number at which normalised fluorescence reaches the threshold. (B) Melting curve analysis example for the same hypothetical samples. One major peak is visible so there is no contaminating DNA or primer-dimer formation. (Figure adapted from www.medscape.com).

The relative gene expression was measured for the induced RNAi cultures compared to uninduced cultures. Relative gene expression was calculated using the comparative C_t method or $2^{-\Delta\Delta C_t}$ method⁽⁴⁹⁵⁾:

$$\text{Fold change} = 2^{-\Delta\Delta C_t}$$

Where $\Delta\Delta C_t = [(C_t \text{ target gene} - C_t \text{ reference gene})_{\text{SAMPLE A}} - (C_t \text{ target gene} - C_t \text{ reference gene})_{\text{SAMPLE B}}]$. For C_t values the mean of triplicates is used. This method was appropriate since the starting cultures were from the same seeding culture.

An example calculation is shown:

		[ENDO]	<u>TbCatL</u>			
		TbCatL C_T	GPI-8 C_T	ΔC_T	$\Delta\Delta C_T$	$2^{-\Delta\Delta C_T}$ (RQ)
		18.89	21.142			
		18.825	21.883			
		18.829	21.532			
350 Uninduced	MEAN	18.85	21.52	-2.67	0.00	1.00
	SEM	0.02	0.21			

		[ENDO]	<u>TbCatL</u>			
		TbCatL C_T	GPI-8 C_T	ΔC_T	$\Delta\Delta C_T$	$2^{-\Delta\Delta C_T}$ (RQ)
		22.584	21.291			
		22.299	21.854			
		22.414	21.511			
350 Induced	MEAN	22.43	21.55	0.88	3.55	0.09
	SEM	0.08	0.16			

Figure 2.27: Sample calculations using $2^{-\Delta\Delta C_t}$ method.

Data acquired with the Applied Biosystems 7500 was imported into Excel (Microsoft). The mean C_t was calculated for the triplicates. First change in C_t (ΔC_t) was calculated and then change in C_t compared to uninduced culture ($\Delta\Delta C_t$). To get relative quantity $\Delta\Delta C_t$ was raised to the negative power.

2.10 Statistical Analysis

2.10.1 Student's Two-Sample T-Test

When only two incubation solutions were tested a two-sample Student's T-Test was the appropriate statistical test. The dependent variable was percentage of

cells exhibiting spontaneous contractile activity. Any two groups were incubated in solutions separately and are therefore independent of one another. The distribution of percentages in the two groups was checked to be normally distributed (Figure 2.28).

The null hypothesis (H_0) was that the two means were equal, the test hypothesis (H_1) was that they were not. The t statistic is determined by the difference between the means divided by the variability or standard error of the mean (SEM). If the difference in the two group means is greater than the SEM then the t statistic is large and there is evidence to reject H_0 . Standard statistical tables generate a probability or P value that H_0 is not rejected incorrectly (Type I error) or accepted incorrectly (Type II error). A P value of <0.05 has been used as acceptance criteria for H_1 in this thesis.

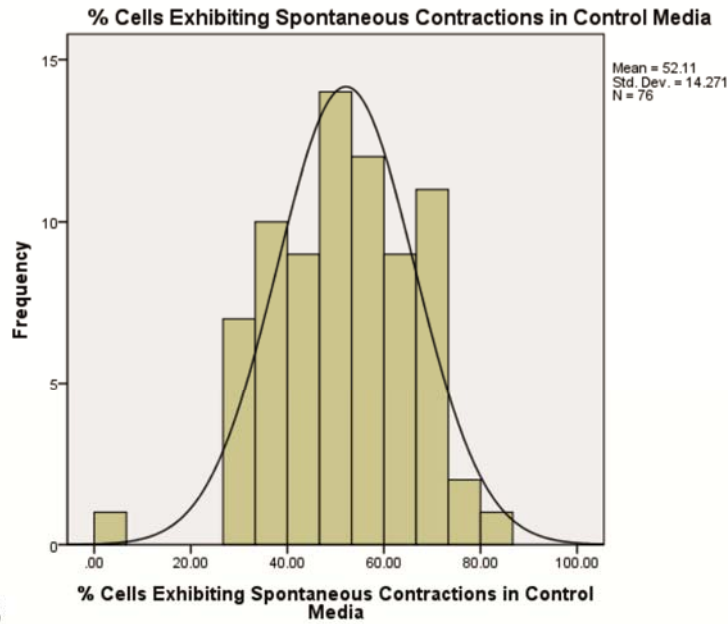
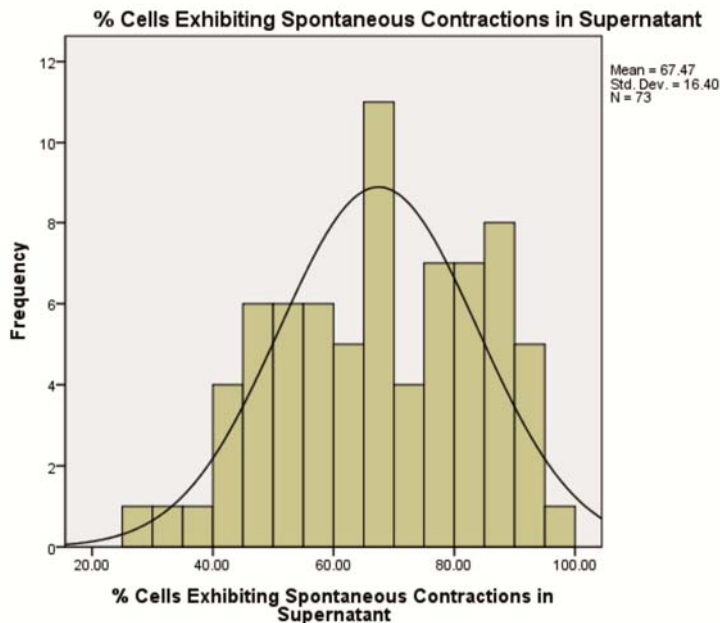
A**B**

Figure 2.28: Normality distribution plots for media and supernatant.

(A) Histogram of frequency of observations of % cells exhibiting spontaneous contractile activity with normal distribution curve in control media. (B) Histogram and normal distribution curve for cells incubated in supernatant. The data are independent, continuous and follow the assumption of normality making a two-sample Student's T-test appropriate.

2.10.2 Student's Paired T-Test

When two dependent groups are compared to one another, for example, Chapter 4 presents some data from individual cells perfused with media followed by supernatant (section 4.2.3); a paired *t*-test was used. Normality was checked for data as described in 2.10.1 and $P < 0.05$ used as acceptance of H_1 criteria.

2.10.3 ANOVA and Multiple Linear Regression

When more than two groups were compared a multiple linear regression of categorical variables was used. The dependent variable was the percentage of cells exhibiting spontaneous contractile activity within the 1 min observation period. The categorical predictors were the different solutions they were incubated in. Using an experiment discussed in section 3.3.8 as an example the solutions compared were control media vs. wild type trypanosome supernatant vs. uninduced RNAi supernatant vs. induced RNAi supernatant. The ANOVA question is normally, is the mean percentage of cells showing spontaneous contractile activity the same for all incubation solutions? The model is:

Table 2.4: Formulae for ANOVA statistical analysis

Control Media (M)	$y = \text{mean}_M + \text{error}$
WT Supernatant (S)	$y = \text{mean}_S + \text{error}$
Uninduced RNAi Supernatant (U)	$y = \text{mean}_U + \text{error}$
Induced RNAi Supernatant (I)	$y = \text{mean}_I + \text{error}$

However, the disadvantage is that this method introduces error for each comparison. A more robust method is to make the comparisons simultaneously using a multiple linear regression and minimise the sum of squared deviations i.e. the error. The categorical predictors remain the same as does the response variable, however “dummy” indicators are created and all compared to the control group, in this example control media.

Table 2.5: Formulae for dummy indicators for each incubation solution

WT Supernatant	$X_1 = 1$ for cells incubated in WT SN, 0 otherwise
Uninduced RNAi Supernatant	$X_2 = 1$ for cells incubated in media U SN, 0 otherwise
Induced RNAi Supernatant	$X_3 = 1$ for cells incubated in media I SN, 0 otherwise

The model becomes ($m = \text{mean}$):

$$y = m_M + (m_S - m_M)X_1 + (m_U - m_M)X_2 + (m_I - m_M)X_3 + \text{error}$$

$$y = \beta_0 + \beta_1X_1 + \beta_2X_2 + \beta_3X_3 + \text{error}$$

The data must be normally distributed which is checked by the plotting of residuals i.e. the difference between the observed data and the expected data. The data are normally distributed if residuals are spread evenly about the graph of expected cumulative probability vs. observed cumulative probability (Figure 2.29).

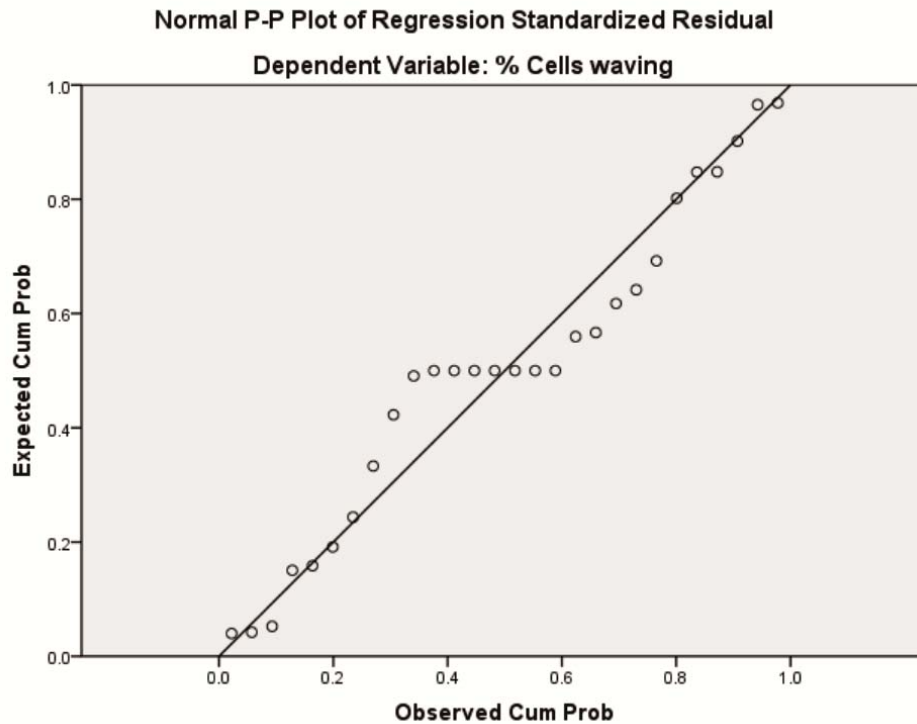


Figure 2.29: Residual plot for RNAi example data.

The plot of residuals tests the distribution of data for normality. The data lie evenly spread and close to the expected cumulative probability therefore the data are normally distributed.

Multiple linear regression analyses were performed using SPSS 19 (IBM) software. The software produces summary tables of the statistical analyses shown below for the example data. A *P* value is produced for the whole dataset acquired by ANOVA testing whether the means are different or not, which in this case is =0.001. Comparisons were made to control media referred to as “constant” in the table. The linear regression returns *P* values for each comparison showing significance for the wild-type supernatant and the uninduced RNAi supernatant, i.e. sufficient evidence to reject H_0 (means are the same) for wild-type supernatant and uninduced RNAi supernatant but not for induced RNAi supernatant (Figure 2.30).

ANOVA^b

Model		Sum of Squares	df	Mean Square	F	Sig.
1	Regression	3152.730	3	1050.910	8.031	.001 ^a
	Residual	3140.485	24	130.854		
	Total	6293.215	27			

a. Predictors: (Constant), SN349un, SN349i, SN

b. Dependent Variable: % Cells waving

Coefficients^a

Model		Unstandardized Coefficients		Standardized Coefficients	t	Sig.
		B	Std. Error	Beta		
1	(Constant)	100.000	4.324		23.129	.000
	SN	22.129	6.114	.639	3.619	.001
	SN349i	-3.036	6.114	-.088	-.497	.624
	SN349un	16.229	6.114	.469	2.654	.014

a. Dependent Variable: % Cells waving

Figure 2.30: Output tables for RNAi example data from SPSS software.

The first table is the ANOVA analysis output returning a significance value for general difference between means. Wild-type supernatant (SN), uninduced RNAi supernatant (SN349un) and induced RNAi (SN349i) are compared to control media (constant). The second table using the same nomenclature produces columns for difference in mean (B) with SEM to return a t statistic and P value.

3 CHAPTER 3 – The Effects of *Trypanosoma brucei* on Isolated Cardiomyocytes and Whole Hearts

3.1 Introduction

3.1.1 African Trypanosomiasis

Human African Trypanosomiasis (HAT or Sleeping Sickness) is a neglected disease caused by blood-borne protozoan parasites of the genus *Trypanosoma*. The parasites are transmitted to hosts by the tsetse fly (*Glossina spp.*) when it bites and takes a blood meal. There are two forms; East African, caused by *Trypanosoma brucei rhodesiense*, and West African, caused by *Trypanosoma brucei gambiense*. HAT is classically described as a chronic disease characterised by two stages^{Bucheton, 2011 385 /id}. The first being the haemolymphatic stage and the second being the meningo-encephalitic stage characterised by sleep disturbances^(45;48) giving it the colloquial name of “Sleeping Sickness”. Stage I disease with *T. b. gambiense* infection is variable with some reports describing acute progression^(43;44) while more commonly progression tends to be months to years⁽³⁸⁾. Although HAT is described as fatal if left untreated for *T. b. gambiense*⁽³⁵⁾ and *T. b. rhodesiense*⁽³⁶⁾, there are reports of untreated cases of *T. b. gambiense* being cleared from hosts or developing a long-lasting serological response without symptoms⁽³⁷⁻⁴⁰⁾. *T. brucei* infection of livestock also impacts upon human health through loss of productivity and mortality⁽⁷⁾, which has a significant impact on the economic development of sub-Saharan Africa. In humans, the West African form is by far the most common accounting for 96% of cases⁽⁴¹⁾. The World Health Organisation (WHO) have listed the reported number of human cases in Africa as 9875 in 2009, 7139 in 2010 and 6743 in 2011⁽³⁰⁾. Approximately 70 million people are thought to still be at risk in 36 sub-Saharan African countries⁽³²⁾ as well as an estimated 48 million cattle with losses of \$1-1.2 billion annually⁽⁶⁾.

3.1.2 Cardiac Involvement in HAT

The second stage of HAT typically manifests as neurological disturbances⁽⁸⁾ and, often overlooked, cardiac alterations⁽⁵¹⁾ perceived by patients as palpitations. Post mortem examination of animals⁽²⁶⁻²⁸⁾ and humans^(56;57) revealed that trypanosomes infiltrate the myocardium leading to a mononuclear inflammatory response, fibrosis and heart failure. When the electrical activity of the heart is measured using an electrocardiogram (ECG), abnormalities such as prolongation

of corrected QT (QTc), repolarisation changes and low voltage have been seen in 50% of stage I and up to 71% of stage II HAT patients⁽⁵¹⁾. Palpitations are also reported in 18% of patients compared to 5% in controls⁽⁵¹⁾. The current paradigm is that this is associated with inflammation and/or treatment.

3.1.3 Trypanosome Secreted Factor Affects Ca²⁺ Signalling in a Blood Brain Barrier Model

In a blood brain barrier (BBB) model it has been identified that a secreted factor is required for crossing the BBB, which then results in the neurological disturbances seen in clinical HAT⁽⁶⁹⁾. The study reported that the factor induced a spontaneous rise in Ca²⁺ within the endothelial cells that constitute the model. They proceeded to further characterise the factor as a cysteine protease whose effect could be abrogated with a cathepsin L specific inhibitor (K11777) but not with a cathepsin B specific inhibitor (CA074)⁽⁶⁹⁾.

3.1.4 Ca²⁺ in the Cardiomyocyte

Sarcoplasmic reticulum (SR)-mediated Ca²⁺ release, during the process of excitation-contraction coupling, leads to cardiomyocyte and whole heart contraction (systole). Cardiomyocytes relax (diastole) by lowering intracellular Ca²⁺ concentration ([Ca²⁺]_i) predominantly by SR-mediated Ca²⁺ uptake *via* the sarco (endo)plasmic reticulum Ca²⁺ ATPase (SERCA) pump but also sarcolemmal extrusion *via* the sodium/calcium exchanger (NCX)⁽¹⁵⁸⁾. Under certain circumstances (e.g. heart failure), SR-mediated Ca²⁺ release can also occur spontaneously in the absence of electrical excitation in the form of propagating Ca²⁺ waves⁽²⁶¹⁾. These events are linked to impaired contraction, abnormal electrical activity, ventricular premature complexes (which can cause palpitations) and the triggering of fatal arrhythmias⁽¹⁹²⁾.

If a cysteine protease secreted from African trypanosomes can induce spontaneous Ca²⁺ release within a BBB *in vitro* model it may also alter [Ca²⁺]_i dynamics in cardiomyocytes *via* induction of Ca²⁺ waves potentially leading to subsequent propagation that causes ventricular premature complexes or palpitations.

3.1.5 Aims

The literature reports the presence of trypanosomes within the myocardium of the host, which may lead to a mononuclear inflammatory cell infiltrate^(26;57;496). It has been postulated by Morrison *et al.* (1981)⁽²⁶⁾ that trypanosomes could release substances that affect the myocardium without an inflammatory component. This is in reference to a study by Galvao-Castro *et al.* (1978)⁽⁴⁹⁷⁾ where trypanosomes were found within the myocardium without an inflammatory cell infiltrate in mice, which had been sublethally irradiated to immunocompromise the host mice. It is possible therefore that African trypanosomes could lead to abnormalities in cardiomyocyte $[Ca^{2+}]_i$ dynamics independent of a systemic immune response.

The aims of this chapter are to: (i) establish if trypanosomes can have a direct effect on cardiomyocyte function independent of an immune response; (ii) identify how the trypanosomes can have that effect and whether it is the same factor identified as being necessary for BBB traversal; and (iii) determine if trypanosomes can have a direct effect on whole heart function independent of an immune response.

3.2 Methods

3.2.1 Adult Cardiomyocyte Isolation

Left ventricular cardiomyocytes were isolated from adult male Wistar rats (250-300 g) as described in section 2.3.1. Briefly, the rats were euthanized and the hearts removed and perfused *via* the aorta in Langendorff perfusion. The hearts were enzymatically digested with a collagenase and protease mix dissolved in MIKH (for composition see section 2.3.1) followed by MIKH with BSA. The $[Ca^{2+}]_o$ was then increased from 0 mM to 1.0 mM incrementally by 100 μ M every 5 min. The cardiomyocytes were then re-suspended in MIKH containing no BSA with a $[Ca^{2+}]_o$ of 1.8 mM.

3.2.2 Preparation of Trypanosomes, Media and Supernatant

Populations of *Trypanosoma brucei brucei* strain Lister 427 were maintained axenically in logarithmic growth phase in a modified version of the HMI-9 medium which is widely used to culture mammalian bloodstream form trypanosomes⁽⁴³⁴⁾. The modified HMI-9 composition is detailed in section 2.1.1. Briefly, (i) control media and (ii) supernatant were prepared identically as described in section 2.1.5. Every supernatant batch prepared was temperature matched and pH adjusted to the control media batch used for each experiment, the pH was 7.40 ± 0.02 at 37 °C.

3.2.3 Light Microscopy-Based Spontaneous Contractile Activity Measurements

Cardiomyocytes were incubated for 30 min in either supernatant or control media and then placed onto a cell bath containing the incubation solution. 10 separate fields containing approximately 10-15 cardiomyocytes were then imaged using a light microscope with a x20 objective lens and charge-coupled device (CCD) camera for 1 min per field. For each experimental test solution, individual cells were marked on screen once a single spontaneous contractile event occurred within that cell during the 1 min time period. Mean data was then collated from the 10 fields as a percentage of cells which had at least one wave within a 1 min time period. The percentage change of cardiomyocytes

exhibiting contractile events was calculated as the percentage increase over the level of contractile events in control media which was set as 100%.

3.2.4 Confocal Fluorescence-Based $[Ca^{2+}]_i$ Measurements

Intact isolated cardiomyocytes suspended in MIKH with a $[Ca^{2+}]_o$ of 1.8 mM (section 3.2.1) were loaded with a Ca^{2+} sensitive fluorophore (5.0 μ M Fluo-3AM, (Biotium Inc., Hayward, CA)) by incubation for ~10 min. The MIKH was then removed and the cells re-suspended in fresh 1.8 mM $[Ca^{2+}]_o$ mixed 1:4 with media or supernatant and incubated for 30 min. The incubation also served to ensure complete de-esterification of the fluorophore. Cardiomyocytes were allowed to settle on a coverslip, placed on a bath (Cell Microcontrols, Norfolk, VA). Cardiomyocytes were then superfused with control media or supernatant by perfusion pen fed from solution reservoirs by gravity with an active suction outflow. The cells were field stimulated with 2.0 ms duration voltage pulses delivered through parallel platinum wires (stimulation voltage set to 1.5 times the threshold) at a frequency of 1.0 Hz for a period of 45 s. Superfusion was maintained but stimulation was stopped and the cell allowed to rest for a further 45 s before rapid application of a 10 mM bolus of caffeine for 20 s to assess the SR Ca^{2+} content⁽⁴⁹⁸⁾. Confocal line-scan images of the cardiomyocytes were recorded using a LSM 510 confocal system (Zeiss). Fluo-3 was excited at 488 nm (Ar LASER) and measured >515 nm using epifluorescence optics of an inverted microscope with a 63X/1.2 NA water-immersion objective lens. Fluorescence was acquired in line-scan mode at 3.07 ms.line⁻¹ (1 line = 512 pixels); pixel dimension was 0.27 μ m. The scanning LASER line was orientated parallel with the long axis of the cell and placed approximately equidistant between the outer edge of the cell and the nucleus/nuclei to ensure the nuclear area was not included in the scan line⁽²⁹⁶⁾. Fluorescence data were expressed as a ratio of the quiescent fluorescence (F/F_0). F/F_0 measurements were calculated from a 60 s period of line scan trace adjacent to the point of event initiation in order to limit movement artefact⁽²⁹⁶⁾. The K_d of Fluo-3 is reported as 558 ± 15 nM ($n=6$) in intact cardiomyocytes⁽⁴⁶⁸⁾.

3.2.5 Field Stimulation and Fluorescence-Based $[Ca^{2+}]_i$ Measurements

Intact cardiomyocytes in MIKH with a $[Ca^{2+}]_o$ of 1.8 mM (section 3.2.1) were loaded with a ratiometric Ca^{2+} sensitive dye. Fura-4FAM (Invitrogen) has greater sensitivity at peak systolic cytosolic Ca^{2+} with a published K_d of $1.16 \pm 0.016 \mu M Ca^{2+}$ and Fura-2AM (Biotium Inc., Hayward, CA) has greater sensitivity to detect diastolic cytosolic Ca^{2+} with a published K_d of $0.18 \pm 0.05 \mu M Ca^{2+}$ ⁽⁴⁸⁰⁾. Cells in MIKH were incubated with Fura-4F-AM for 10 min to allow the dye to cross the cell membrane. Cells were then diluted 1 in 4 in control media or supernatant at room temperature for 30 min. The cardiomyocytes were allowed to settle on a coverslip, placed on a bath (Cell Microcontrols, Norfolk, VA) and superfused with control media/supernatant as described in section 3.3.4, at 37 °C. Cells were field stimulated with 2.0 ms duration voltage pulses delivered through parallel platinum wires (stimulation voltage set to 1.5 times the threshold). After superfusion with control media or supernatant, the SR Ca^{2+} content was determined by rapid application of 10 mM caffeine. Stimulation was stopped at the application of the caffeine. The fluorophore fluorescence ratio (340/380 nm excitation; $R_{340/380nm}$) was measured using a spinning wheel spectrophotometer (Cairn Research Ltd; sampling rate of 5000 Hz) through epifluorescence optics of a x40/1.3 NA oil immersion lens (Nikon) and data were analysed offline. The mean fluorophore fluorescence ratio was obtained by averaging 10 steady state transients (Origin).

3.2.6 RNA Interference of *Trypanosoma brucei* cathepsin L

3.2.6.1 Preparation of RNAi clones

Trypanosoma brucei brucei 2T1 (a bloodstream form cell line derived from the Lister 427 strain) was transfected with pGl2084; a Gateway® (Invitrogen, U.K.) modified version of the plasmid pRPa^{isl}⁽⁴⁹⁹⁾. The pRPa^{isl} plasmid has a tetracycline inducible stem-loop RNAi cassette⁽⁴⁸⁸⁾. The target region of the *Trypanosoma brucei* cathepsin-L gene (*TbCatL*) was from nucleotides 409-986 of the open reading frame, with the following oligonucleotides used to generate the construct; forward 5'-GGG GAC AAG TTT GTA CAA AAA AGC AGG CTG CAG TGA CCC CAG TGA AGG A-3' and reverse 5'-GGG GAC CAC TTT GTA CAA GAA

AGC TGG GTA GAC ATT GGT TTG TGC CCT T-3'(489). The cells containing the plasmid were selectively maintained in culture by addition of $2.5 \mu\text{g.mL}^{-1}$ hygromycin and $0.5 \mu\text{g.mL}^{-1}$ phleomycin. The transfection and generation of two independent *TbCatL* RNAi clones was carried out by Nathaniel Jones of the Wellcome Trust Centre for Molecular Parasitology.

3.2.6.2 Growth Curves to Assess Phenotype of RNAi

RNAi was induced with $1 \mu\text{g.mL}^{-1}$ tetracycline and growth curves performed on induced vs. uninduced cultures in triplicate for the two biological duplicates. Cultures for growth curves were initiated with 1.0×10^5 parasites.mL⁻¹ and were counted in triplicate with an improved Neubauer haemocytometer as described earlier (section 3.2.2) at 24, 48 and 72 h timepoints post-induction.

3.2.6.3 RT-PCR to Confirm Inhibition of *TbCatL* Expression

RNA was extracted from cultures grown in parallel using the RNeasy® kit (QIAGEN). For preparation of cDNA, approximately $1 \mu\text{g}$ of total RNA was treated with TURBO DNase (Ambion) according to the manufacturer's protocol. The reverse transcription was carried out using Omniscript RT kit (Qiagen) with $5 \mu\text{M}$ oligo dT primers. Real-Time PCRs were carried out in triplicate per individual sample on a 7500 Real-Time PCR system (Applied Biosystems), using approximately 100 ng cDNA, $1 \times$ Power SYBR green master mix (Applied Biosystems) and $4 \mu\text{M}$ of the respective oligonucleotide primers, in a final reaction volume of $25 \mu\text{L}$. The oligonucleotide primers used were: *TbCatL* forward 5'-TCT CGG ATA TGA CAC GTG AAG AGT-3' and reverse 5'-TCT GCG CAG CTG CAA AGT-3', with GPI-8 as the constitutively expressed endogenous control; forward 5'-CGA AGC GCA TTT GGA TAG-3' and reverse 5'-ACG GCG TGA TGA CAG TGA AG-3'. Specificity of knock-down was confirmed by analysis of *T. brucei* cathepsin B (*TbCatB*) gene expression on the same samples using *TbCatB* primers; forward 5'- TCC CAG CAG CTT CGA TTC C-3' and reverse 5'- GCG GAC TGA TCT GCA ATT TGT-3'. Relative gene expression was calculated using previously described methods⁽⁴⁹⁵⁾.

3.2.7 Langendorff Perfusion of *Ex Vivo* Adult Rat Hearts

Adult male Wistar rat hearts were excised and cannulated *via* the aorta and initially perfused in Tyrodes solution; 116 mM NaCl, 20 mM NaHCO₃, 0.4 mM Na₂HPO₄, 1.0 mM MgSO₄·7H₂O and 4.0 mM KCl. D-glucose was added on the same day as intended use to a final concentration of 11 mM. The solution was bubbled with 95% O₂ / 5% CO₂ for 15-20 min to oxygenate and buffer before CaCl₂ was added to a concentration of 1.8 mM. Hearts were cannulated *via* the aorta and perfused with Tyrodes at 10 mL·min⁻¹ to clean out the blood from the coronary vasculature. Hearts were then perfused for 10 min in control media to achieve a steady state, followed by either control media for time-controls or supernatant (10 min) and then washout with control media (10 min). Solutions were maintained at 37 °C gassed with 100% O₂ mixture (pH at 7.4). Constant flow was used (10 mL·min⁻¹). The *ex vivo* Langendorff perfused heart was ideal for these experiments because it enabled the translation of single cell data to the whole organ in the absence of the immune/inflammatory response that would be apparent *in vivo*. Pseudo-ECG was recorded (iworx) and the mean number of ventricular premature complexes (VPCs) was obtained from the 5 min at the end of each section of the protocol to ensure data was analysed from steady state. The ECG was also analysed for QT interval, the last 1 min of each section of steady state ECG trace was averaged using LabScribe2 (iWorx) and measured manually as recommended by the AHA/ACCF/HRS recommendations for standardisation and interpretation of the electrocardiogram⁽⁴⁵⁷⁾. QT length, determined by the end of the T wave at the isoelectric point or by intersection of the tangent of the steepest part of the T wave with the isoelectric point⁽⁴⁵⁷⁾, was measured. The QT interval was also measured at 90% repolarisation⁽⁴⁵⁸⁾ (QT₉₀) and at 50% repolarisation⁽⁴⁵⁹⁾ (QT₅₀), so as to have a clearly defined end point (Figure 3.9B), for media and supernatant. These data (*n* = 12) were normalised to time control hearts that were perfused only with media for the duration of the experiment (*n* = 6). QT intervals were corrected for heart rate using the Framingham method⁽⁴⁶⁰⁾:

$$QTc = QT + 0.154 \times (1 - RR)$$

3.2.8 Statistical Analysis

Data are expressed as mean \pm SEM. For Ca^{2+} transient amplitude and Ca^{2+} wave parameters comparisons were performed by applying the paired Student's *t*-test. ANOVA statistics were used in cases of multiple comparisons. Multiple linear regression analysis was used to compare nominal categorical data with continuous variables. Normality was assessed by plotting of residuals. Differences were considered significant when $P < 0.05$.

3.3 Results

3.3.1 Trypanosomes Increase Ca^{2+} Wave Frequency in Cardiomyocytes

To study whether bloodstream form trypanosomes could have a direct effect on cardiomyocytes independent of a systemic immune response, spontaneous contractile events were measured. Isolated cardiomyocytes were incubated for 30 min with either: modified HMI-9⁽⁴³⁴⁾ culture media containing approximately 5.0×10^5 parasites.mL⁻¹, supernatant derived from parasite culture, or control media. The incubated cells were then observed. Cardiomyocytes exhibiting spontaneous contractile events were noted and expressed as percentages of total cardiomyocytes examined. When incubated with live trypanosome culture the percentage of cells waving significantly increased to 145% of media levels ($52.11 \pm 1.64\%$ vs. $75.38 \pm 5.26\%$ cardiomyocytes exhibiting at least one spontaneous contractile event.min⁻¹; control media vs. live trypanosomes; $P < 0.001$; Figure 3.1B). To determine whether the effect on cardiomyocyte waving was potentially due to an excreted/secreted factor the populations of cardiomyocytes were incubated for 30 min with trypanosome culture supernatant. Cells incubated with supernatant showed a significant increase of 130% in the percentage of cells waving ($52.11 \pm 1.64\%$ vs. $67.47 \pm 1.92\%$ cardiomyocytes exhibiting at least one spontaneous contractile event.min⁻¹; control media vs. supernatant; $P < 0.001$; Figure 3.1B).

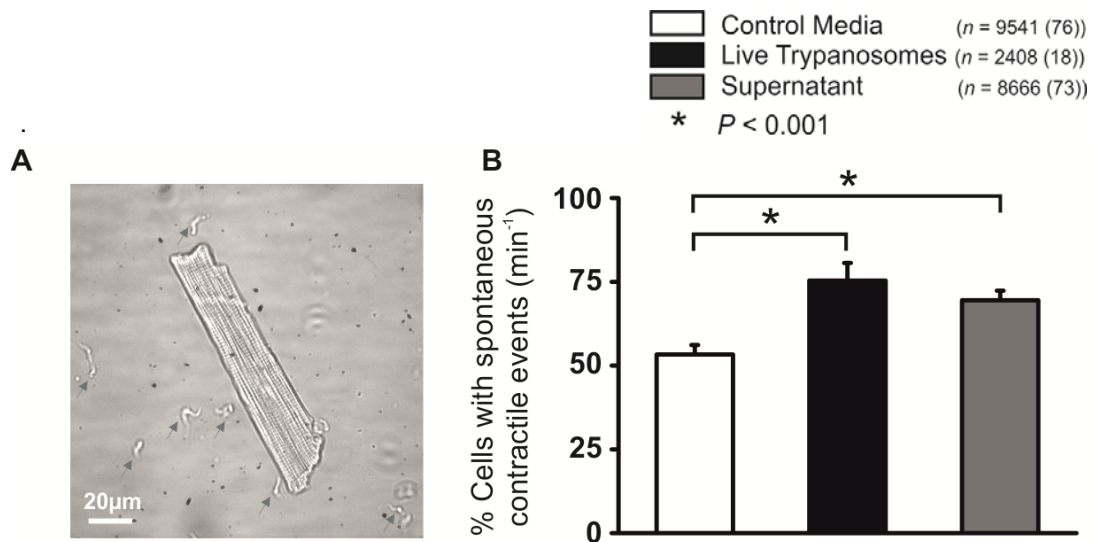


Figure 3.1: Mean percentage of cells waving.

(A) Photomicrograph of an isolated rat cardiomyocyte incubated *Trypanosoma brucei brucei* (grey arrow heads). (B) Mean % ± SEM of isolated cardiomyocytes exhibiting ≥ 1 spontaneous contractile event.min⁻¹ in media, live trypanosomes or supernatant (n = cardiomyocytes with number of hearts in parentheses). Statistical analysis was performed by ANOVA with $P < 0.05$ considered significant.

3.3.2 Contractile Event Frequency Increase Abolished by Heating

To determine if the supernatant effect was potentially due to a secreted/excreted protein (or peptide), a separate set of experiments was performed in the group by Elspeth Elliott. Cardiomyocytes were incubated in supernatant heated to >80 °C as well as control media and untreated supernatant. Data shown are percentage change of cardiomyocytes exhibiting at least one spontaneous contractile event over control media. Untreated supernatant showed the same effects as in Figure 3.1 ($100 \pm 2.68\%$ vs. $133.3 \pm 2.88\%$; control media vs. supernatant; $P < 0.001$; Figure 3.2). When supernatant was heat treated the percentage change returned to control levels ($100 \pm 2.68\%$ vs. $105.6 \pm 3.86\%$; control media vs. boiled supernatant; $P > 0.05$; Figure 3.2).

A

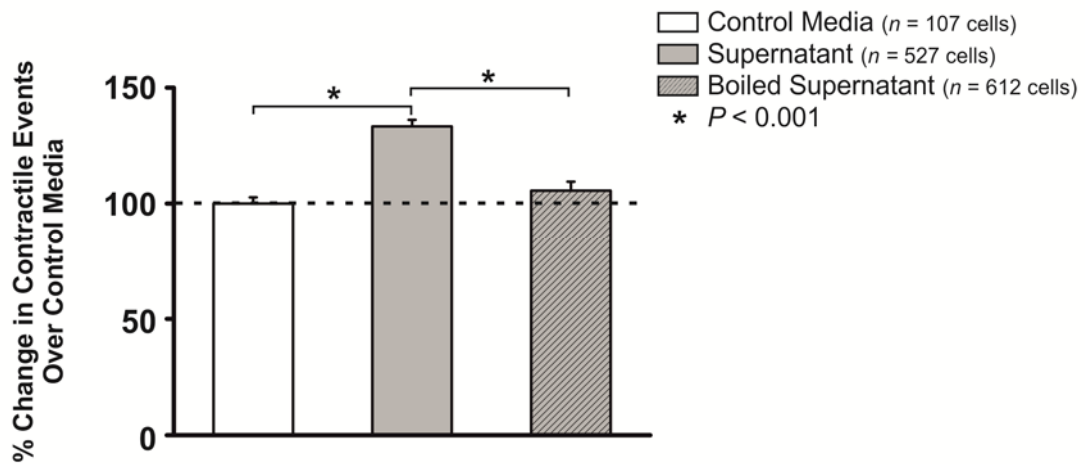


Figure 3.2: Percentage change in cells exhibiting spontaneous contractile events in heated supernatant.

Mean \pm SEM percentage change in cells showing contractile activity over control media set to 100%. Cardiomyocytes were incubated in control media ($n=107$ cells), trypanosome culture supernatant ($n=527$ cells) or supernatant that had been heated to >80 °C ($n=612$ cells) for 30 min. Populations of cells were counted for number of cells exhibiting spontaneous contractile events for 1 min. Statistical significance was determined by ANOVA and $P < 0.05$ take to be significant.

3.3.3 Ca^{2+} Wave Velocity and Frequency are Increased by Trypanosome Culture Supernatant

To characterise the intra-cardiomyocyte $[\text{Ca}^{2+}]_i$ dynamics underpinning the spontaneous contractile events (Figure 3.1), confocal imaging was performed (Figure 3.3). Cells were loaded with Fluo-3 and incubated in media or supernatant as above and then superfused with the incubation solution with field stimulation at a frequency of 1.0 Hz for 45 s followed by a post-train rest period of 45 s (Figure 3.3A). Line-scan mode was utilised to produce images of time(x) vs. distance(y) across the cardiomyocyte (Figure 3.3B(i & ii)). This revealed that the spontaneous contractile events (denoted by an inward deflection in the y-axis of the image, Figure 3.3C) were preceded by a rise of fluorescence and therefore $[\text{Ca}^{2+}]_i$, which propagated from one region of the cell to the other (Figure 3.3B (i & ii)). These events were characteristic of spontaneous SR-mediated Ca^{2+} release (Ca^{2+} waves). Ca^{2+} wave frequency in cardiomyocytes incubated with supernatant was increased to 243% of media levels (0.07 ± 0.02 vs. 0.17 ± 0.03 waves. s^{-1} ; media vs. supernatant; $P < 0.05$; (Figure 3.3B(iii))). Ca^{2+} wave velocity, calculated as Ca^{2+} wave propagation gradient (Figure 3.3C(i & ii)), was increased in supernatant to 107% of media (110.2 ± 2.2 vs. 118.4 ± 1.7 $\mu\text{m}.\text{s}^{-1}$; media vs. supernatant; $P < 0.05$; (Figure 3.3C(iii))). This data was acquired

in conjunction with Mrs. Amanda Panissidi, a veterinary undergraduate on a summer project under my supervision.

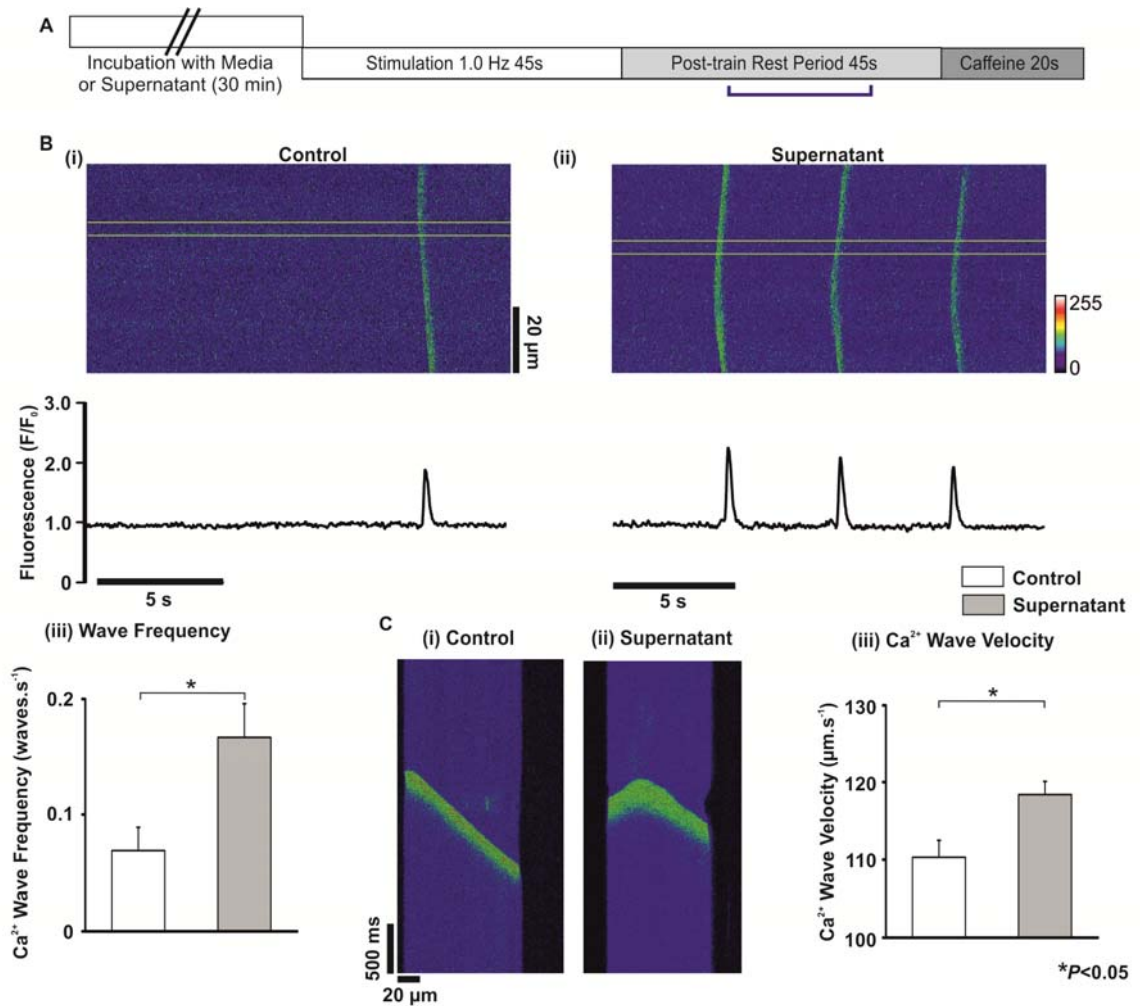


Figure 3.3: Confocal imaging of spontaneous contractile events using Fluo-3AM loaded cardiomyocytes.

Confocal analysis of Ca²⁺ waves and the caffeine-induced Ca²⁺ transients (an indication of SR Ca²⁺) content derived from administration of 10 mM caffeine. (A) Protocol used for cardiomyocytes perfused with either control media or supernatant. The blue bracket denotes the part of the protocol corresponding to images in Panel B. (B) Top panel (i & ii) shows confocal line-scan images of intracellular regions of isolated cardiomyocytes in both control media (i) and supernatant (ii). Below panel is the respective line profile trace taken from a 20 pixel region (denoted by 2 yellow lines in top image). Panel (iii) Mean ± SEM for Ca²⁺ wave frequency in control media ($n=18$) and supernatant ($n=21$). (C) Individual representative Ca²⁺ waves taken for (i) control media and (ii) supernatant with (iii) mean ± SEM Ca²⁺ wave velocity in media ($n=53$ waves from 18 cells) and supernatant ($n=158$ waves from 21 cells). Mean data were compared using a two-sample Student's T test, $P<0.05$ was taken to be significant.

3.3.4 Supernatant Increases the Rate of Stimulated Ca²⁺ Transient Decline

Experiments so far have examined diastolic Ca²⁺ release. Therefore experiments with electrically stimulated cardiomyocytes were required to examine systolic Ca²⁺ release. Cardiomyocytes were loaded with Fura-4F followed by incubation in control media or supernatant for 30 min and then superfused with the same solution and stimulated at 1.0 Hz as shown in Figure 3.4. The Ca²⁺ transient amplitude was not significantly altered, (0.91 ± 0.10 vs. 1.00 ± 0.09 μM ; control media ($n=10$) vs. supernatant ($n=14$); $P>0.05$; Figure 3.4B(iv)). The maximum rate of Ca²⁺ transient rise $d[\text{Ca}^{2+}]_i/dt_{\text{Max}}$ was not significantly altered either, (77.9 ± 7.7 vs. 76.1 ± 9.1 $\mu\text{M}\cdot\text{s}^{-1}$; control media vs. supernatant; $P>0.05$; Figure 3.4B(v)). The maximum rate of Ca²⁺ transient fall $d[\text{Ca}^{2+}]_i/dt_{\text{Min}}$ tended to be faster in supernatant, (6.6 ± 0.84 vs. 8.9 ± 0.90 $\mu\text{M}\cdot\text{s}^{-1}$; control media vs. supernatant; $P=0.086$; Figure 3.4B(vi)), although not statistically significant. However, when the rate constant of transient decay is analysed there is a significant increase; (11.3 ± 1.06 vs. 15.7 ± 1.41 s^{-1} ; control media vs. supernatant; $P<0.05$; Figure 3.4B(vii)). These data show a faster Ca²⁺ transient decline. To determine whether the increased rate of decline was due to increased SERCA activity or increased sarcolemmal efflux, a 10 mM bolus of caffeine was rapidly applied. The amplitude of the caffeine-induced Ca²⁺ transient indicates SR Ca²⁺ content as the caffeine opens the RyR releasing the Ca²⁺ stored within the SR. The decay indicates sarcolemmal extrusion, which is predominantly NCX function⁽²²⁴⁾, since the SR is effectively open so the activity of SERCA is no longer acting to remove Ca²⁺. The caffeine-induced Ca²⁺ transient amplitude was not significantly altered (1.12 ± 0.95 vs. 1.08 ± 0.95 ; control media vs. supernatant; $P>0.05$; Figure 3.4C(ii)), nor is the rate constant of decay, (1.19 ± 0.06 vs. 1.22 ± 0.07 s^{-1} ; control media vs. supernatant; $P>0.05$; Figure 3.4C(iii)).

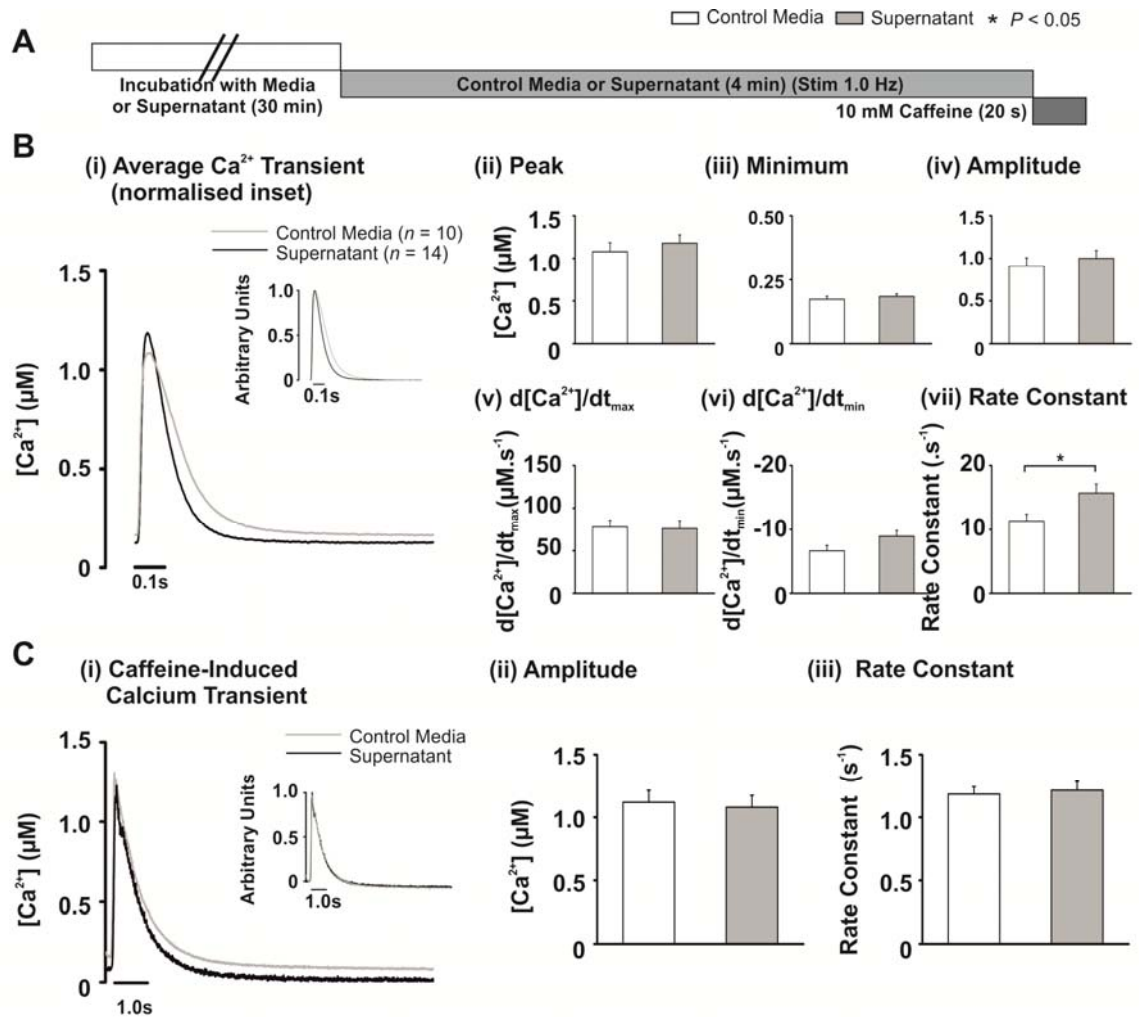


Figure 3.4: Stimulated (1.0 Hz) epifluorescent imaging of Ca^{2+} transients with Fura-4F AM (A) Protocol used in epifluorescence Ca^{2+} measurements. (B) (i) Average trace from last 12 transients in media ($n=10$; grey) or supernatant ($n=14$; black). (Inset) normalised traces overlaid. (B) Mean \pm SEM for (ii) peak $[Ca^{2+}]_i$, (iii) minimum $[Ca^{2+}]_i$, (iv) Ca^{2+} transient amplitude, (v) maximum rate of Ca^{2+} transient rise ($d[Ca^{2+}]_i/dt_{max}$), (vi) maximum rate of Ca^{2+} transient fall ($d[Ca^{2+}]_i/dt_{min}$) and (vii) rate constant of decay (s^{-1}). (C) Example traces of caffeine-induced Ca^{2+} transient in cells superfused with media ($n=10$) and supernatant ($n=14$). (i) Mean data for caffeine-induced Ca^{2+} transient amplitude and (ii) caffeine transient rate constant of decay. Statistical comparisons were made using a two-sample Student's T test, $P < 0.05$ was considered significant.

3.3.5 The Effects of Supernatant on the stimulated Ca^{2+} Transient During β -adrenergic Stimulation

3.3.5.1 Effects on the Stimulated Calcium Transient

The sympathetic nervous system and β -adrenergic signalling pathway are activated in response to both physiological and pathophysiological stresses. To examine the effects of supernatant under β -adrenergic stimulation, isoproterenol was added (ISO; 100 nM) (Figure 3.5A). Under these conditions there was no significant difference in peak $[Ca^{2+}]_i$, (1.71 ± 0.16 vs. 1.89 ± 0.11 μM ; control media ($n=13$) vs. supernatant ($n=13$); $P > 0.05$; Figure 3.5C(i)), or

amplitude, (1.52 ± 0.15 vs. 1.67 ± 0.10 μM ; control media vs. supernatant; $P > 0.05$; Figure 3.5C(iii)), of the Ca^{2+} transient. However, the diastolic or minimum $[\text{Ca}^{2+}]_i$ was significantly increased in supernatant, (195 ± 10.1 vs. 224 ± 6.5 nM; control media vs. supernatant; $P < 0.05$; Figure 3.5C(ii)). The maximum rate of Ca^{2+} transient rise was not altered by supernatant, (157 ± 17.2 vs. 150 ± 13.1 $\mu\text{M}\cdot\text{s}^{-1}$; control media vs. supernatant; $P > 0.05$, Figure 3.5C(iv)). In contrast to the cohort of cardiomyocytes perfused without the addition of ISO (Figure 3.4), there was a significant increase of 130% of control levels in maximum rate of Ca^{2+} transient fall, (16.0 ± 1.72 vs. 21.4 ± 1.98 $\mu\text{M}\cdot\text{s}^{-1}$; control media vs. supernatant; $P < 0.05$; Figure 3.5C(v)). This latter result is confirmed by the significant increase in rate constant of decay by supernatant to 126% of control levels, (16.5 ± 1.34 vs. 20.9 ± 1.31 s^{-1} ; control media vs. supernatant; $P < 0.05$; Figure 3.5C(vi)), higher than the cohort of cardiomyocytes not treated with ISO (Figure 3.4).

3.3.5.2 Effects on Spontaneous Ca^{2+} Release

Diastolic Ca^{2+} waves became apparent (Figure 3.5A and B) in supernatant. When counted, (Figure 3.5D(i)), Ca^{2+} wave frequency increases in supernatant over time. The Ca^{2+} wave frequency increased by 840% of control levels, (0.031 ± 0.013 vs. 0.26 ± 0.087 waves. s^{-1} ; control media vs. supernatant; $P < 0.05$; Figure 3.5D(ii)). The diastolic wave amplitude was also increased by supernatant to 633% of control levels, (9.44 ± 6.42 vs. 59.74 ± 20.98 nM; control vs. supernatant; $P < 0.05$; Figure 3.5D(iii)). These data are consistent with the findings in the confocal studies (Figure 3.3), which also demonstrated that supernatant increased the Ca^{2+} wave induction propensity.

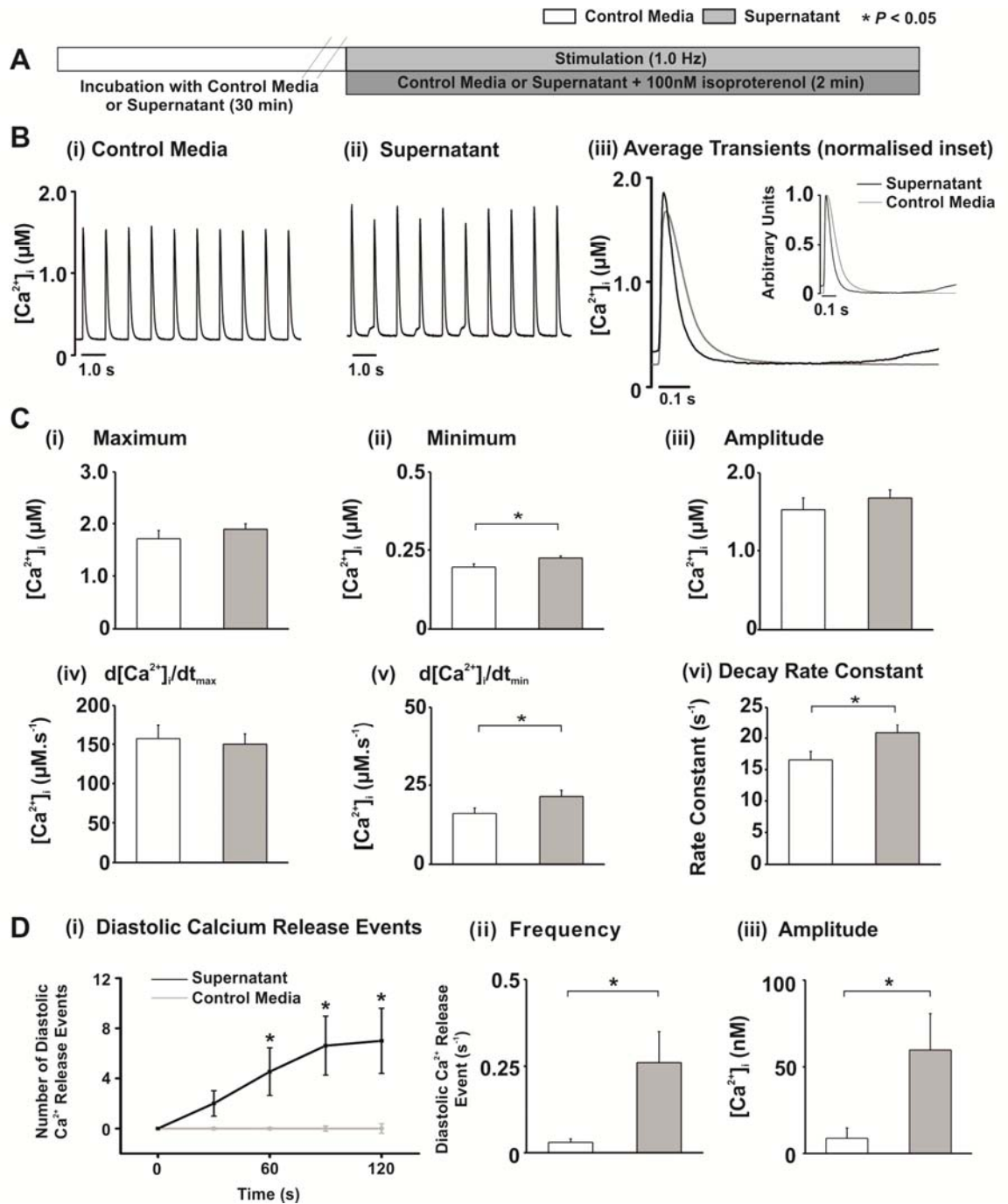


Figure 3.5: Stimulated (1.0 Hz) epifluorescent imaging of Ca^{2+} transients with 100 nM isoproterenol (ISO).

(A) Protocol with 100 nM isoproterenol. (B) Average trace from last 12 transients of representative cells superfused with media ($n=13$) or supernatant ($n=13$). (Inset) normalised traces overlaid. (C(i-vi)) Mean \pm SEM data for Ca^{2+} transient parameters. (D(i)) Number of diastolic Ca^{2+} releases during superfusion of supernatant (black) normalised to control (grey). (ii) Mean \pm SEM Ca^{2+} wave frequency (ii) Ca^{2+} wave amplitude. Statistical comparisons were performed between control and supernatant groups using a two-sample Student's T test, $P < 0.05$ was considered significant.

3.3.6 Ca²⁺ Waves are Reduced by Cathepsin-L Inhibition but not Cathepsin-B Inhibition

Nikolskaia *et al.* (2006) reported that the candidate factor allowing BBB traversal by induction of cytosolic Ca²⁺ rises in HBMECs was the cathepsin-L like cysteine protease referred to as *Trypanosoma brucei* Cathepsin-L (TbCatL)⁽⁶⁹⁾. *T. brucei* expresses two related Clan CA, Family C1 cysteine proteases; TbCatL and TbCatB^(112;500). Given these previous data, cardiomyocytes were incubated with or without the specific TbCatL inhibitor K11777⁽⁶⁹⁾ (10 µM) and spontaneous contractile events assessed within 1 min as in Figure 3.1. Supernatant increased the percentage change of contractile events to 137% of media levels (100.0 vs. 137.5 ± 5.4% cardiomyocytes with contractile events relative to control media; control media vs. supernatant; *P*<0.001; Figure 3.6A). K11777 inhibited this effect (96.8 ± 5.4 vs. 95.8 ± 2.5% cardiomyocytes with contractile events relative to control media; control media + K11777 vs. supernatant + K11777; *P*>0.05; Figure 3.6A). When repeated with CA074 (10µM; TbCatB-specific inhibitor) the percentage increase of cardiomyocytes producing contractile events was maintained (103.8 ± 4.0 vs. 127.4 ± 6.4% cardiomyocytes with contractile events relative to control media; control media + CA074 vs. supernatant + CA074; *P*<0.001; Figure 3.6A). These data suggest that the increase in spontaneous contractile events can be prevented by application of a CatL specific inhibitor (but not by a CatB specific inhibitor), and therefore could be mediated by TbCatL.

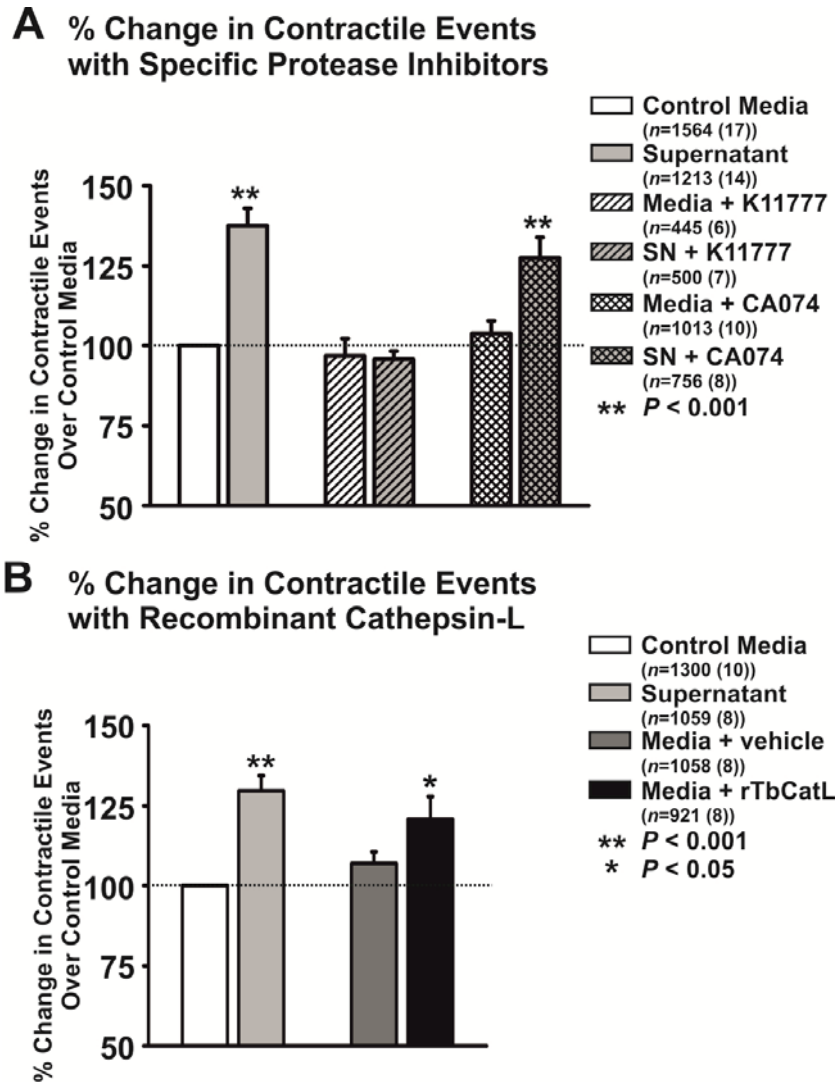


Figure 3.6: Percentage change in spontaneous contractile events with inhibitors and recombinant protein.

Mean % change \pm SEM in contractile events over media levels in isolated cardiomyocytes. (A) Specific cathepsin inhibitors. Inhibitors used were; cathepsin L inhibitor K11777 and cathepsin B inhibitor CA074. Inhibitors were added to media as controls. (B) Recombinant *T. brucei* cathepsin L. (2 nM and 2 mM dithiothreitol). The control was with appropriate vehicle. *P* values were calculated by multiple linear regression on raw data with $P < 0.05$ considered significant. *n* = number of cells from number of isolations in parentheses.

3.3.7 Recombinant TbCatL Increases Ca^{2+} Wave Frequency

When a recombinant TbCatL (rTbCatL) was added to media at a concentration of 2nM as shown to be the quantity produced by *T. brucei* by Caffrey *et al.* (2001)⁽¹²⁹⁾ the % increase of cardiomyocytes exhibiting contractile events over media was significantly greater than control vehicle (106.9 ± 3.7 vs. $120.8 \pm 7.1\%$; control media vs. rTbCatL; $P < 0.05$; Figure 3.6B). This confirms that TbCatL is having a direct effect on the cardiomyocytes.

3.3.8 Ca²⁺ Waves are Reduced by RNA Interference of TbCatL

To confirm that it is TbCatL produced by the parasites that increases Ca²⁺ waves in cardiomyocytes observed in Figure 3.1, we used two independent *T. b. brucei* clones with RNAi inducible knockdown of TbCatL⁽⁴⁸⁹⁾. Growth curves were performed on uninduced trypanosome cultures and cultures induced with tetracycline (Figure 3.7A). TbCatL is essential for survival of the parasite⁽¹²⁷⁾ so successful induction of RNAi will result in a significant growth curve reduction. In both independent clones there was a significant reduction in parasite numbers at 48 h (6.84 ± 0.07 vs. 5.78 ± 0.05 log₁₀ parasites.mL⁻¹ for clone STL349 and 6.85 ± 0.03 vs. 6.19 ± 0.11 log₁₀ parasites.mL⁻¹ for clone STL350; uninduced vs. induced; $P < 0.005$; Figure 3.7A). The reduction was even greater at 72 h (7.81 ± 0.08 vs. 5.68 ± 0.03 log₁₀ parasites.mL⁻¹ for STL349 and 7.88 ± 0.03 vs. 6.27 ± 0.13 log₁₀ parasites.mL⁻¹ for STL350; uninduced vs. induced; $P < 0.0005$; Figure 3.7A). Quantitative RT-PCR on cDNA manufactured from cultures at the 24 h time-point using both TbCatB and TbCatL primers shows that there was successful induction of RNAi and significantly reduced TbCatL (0.15 ± 0.02 for STL349 and 0.095 ± 0.005 for STL350 relative quantitation to uninduced cultures ($n=3$); $P < 0.05$; Figure 3.7B(i)) without significant reduction of TbCatB (1.92 ± 0.34 for STL349 and 1.79 ± 0.30 relative quantitation to uninduced culture ($n=3$); $P > 0.05$; Figure 3.7B(ii)).

When cardiomyocytes are incubated with the supernatant from *T. brucei* STL349 (Figure 3.7C) the percentage increase in cardiomyocytes exhibiting spontaneous contractile events in 1 min over control media when RNAi is induced was significantly reduced compared to the same clone when uninduced (97.0 ± 5.1 vs. $116.2 \pm 5.0\%$; induced vs. uninduced; $P < 0.05$; Figure 3.7C(i)). The same is true for STL350 (102.0 ± 5.7 vs. $116.5 \pm 5.6\%$; induced vs. uninduced; $P < 0.05$; Figure 3.7C(ii)). These data show that the percentage change in contractile events over media control was significantly reduced when TbCatL was selectively knocked down.

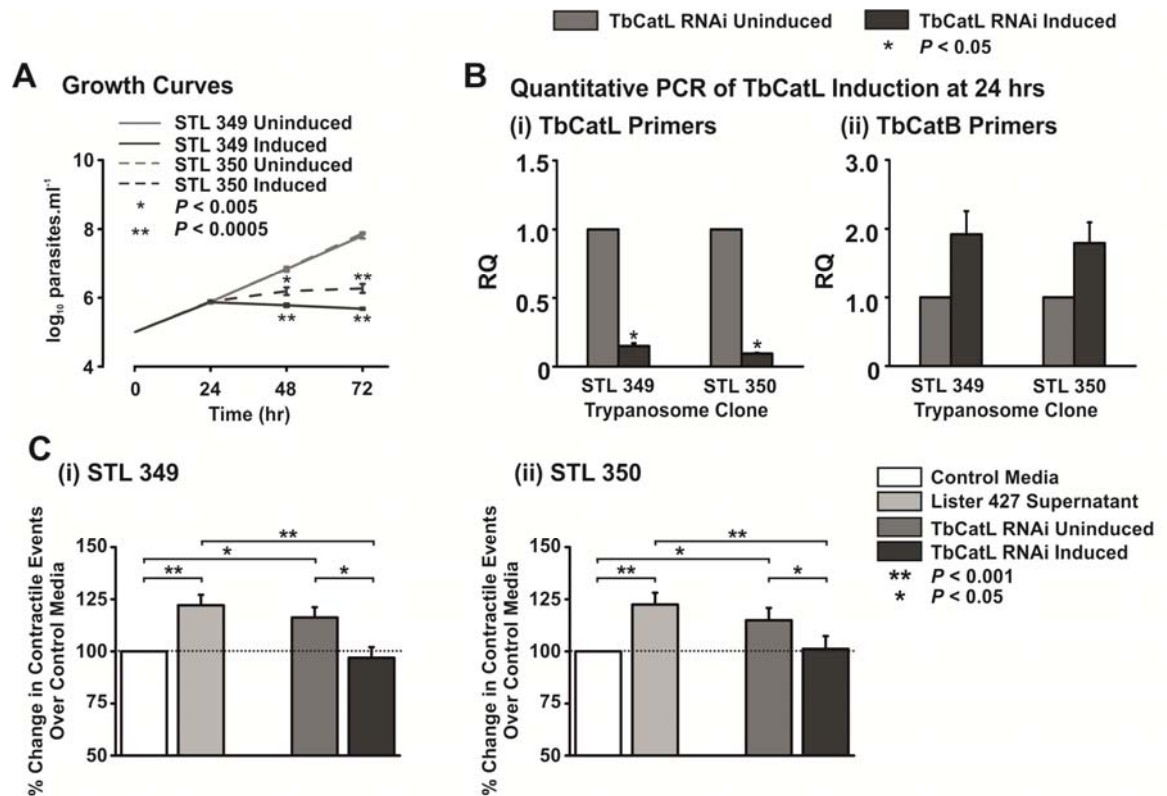


Figure 3.7: RNA interference (RNAi) of *T. brucei* cathepsin L (TbCatL). (A) Growth curves of biological duplicates (STL 349 and STL 350) with inducible TbCatL RNAi. (B) Relative gene expression for (i) TbCatL and (ii) TbCatB compared to uninduced culture in triplicate cultures for STL349 ($n=3$) and STL350 ($n=3$). (C(i)) Mean \pm SEM % change for spontaneous contractile events in cardiomyocytes for STL349. Media ($n=747(7)$), 427 supernatant ($n=817(7)$), uninduced RNAi supernatant ($n=858(7)$) and induced RNAi supernatant ($n=841(7)$). (ii) Mean \pm SEM % change for spontaneous contractile events in cardiomyocytes for STL350. Media ($n=1018(11)$), 427 supernatant ($n=1427(12)$), uninduced RNAi supernatant ($n=1597(12)$) and induced RNAi supernatant ($n=1564(12)$). n = number of cells from number of isolations in parentheses.

3.3.9 Supernatant Can Cause Arrhythmic Events in Whole Hearts

As arrhythmias have been reported in some patients with HAT⁽⁵¹⁾ experiments were performed with *ex vivo* Langendorff perfused whole rat hearts. By removing the heart from the animal the immune/inflammatory response is no longer a factor and the direct effects of trypanosome culture supernatant on the heart can be observed. The pseudo-ECG was recorded with pellet electrodes within an organ bath. Hearts were perfused for 10 min in media to achieve a steady state followed by 10 min with either media for time controls or culture supernatant and then another 10 min of washout with media (Figure 3.8A). The pseudo-ECG was examined for arrhythmic events as determined by the Lambeth Conventions⁽⁴³⁷⁾, and described in section 2.5.4.2, during the last 5 min of each section of the protocol. Example ECGs are shown in Figure 3.8B for (i) control and (ii) supernatant with ventricular premature complex (VPC). When the

arrhythmia frequency for each individual heart is plotted, all of the hearts that show an increase in arrhythmia frequency during the 2nd 10 min are in the supernatant perfusion group. During washout 83% of the hearts show a reduction in arrhythmia frequency (Figure 3.8C). The mean is shown by the grey broken line with error bars representing SEM. There was no significant difference in mean \pm SEM of the arrhythmia frequency between the different time periods of the protocol in the time control group ($n=6$); ($0.40 \pm 0.28 \text{ min}^{-1}$ vs. $0.33 \pm 0.19 \text{ min}^{-1}$ vs. $0.53 \pm 0.27 \text{ min}^{-1}$; 1st 10min vs. 2nd 10min vs. 3rd 10min; $P<0.05$). However, in the group of hearts perfused with supernatant during the 2nd 10min ($n=12$) there was a significant increase in arrhythmia frequency, which then reduced during the washout period ($0.60 \pm 0.26 \text{ min}^{-1}$ vs. $5.15 \pm 2.49 \text{ min}^{-1}$; $P<0.05$; vs. $1.36 \pm 0.73 \text{ min}^{-1}$; $P=0.07$). There was no significant difference between steady state and washout in the supernatant perfused group (Figure 3.8D(i)).

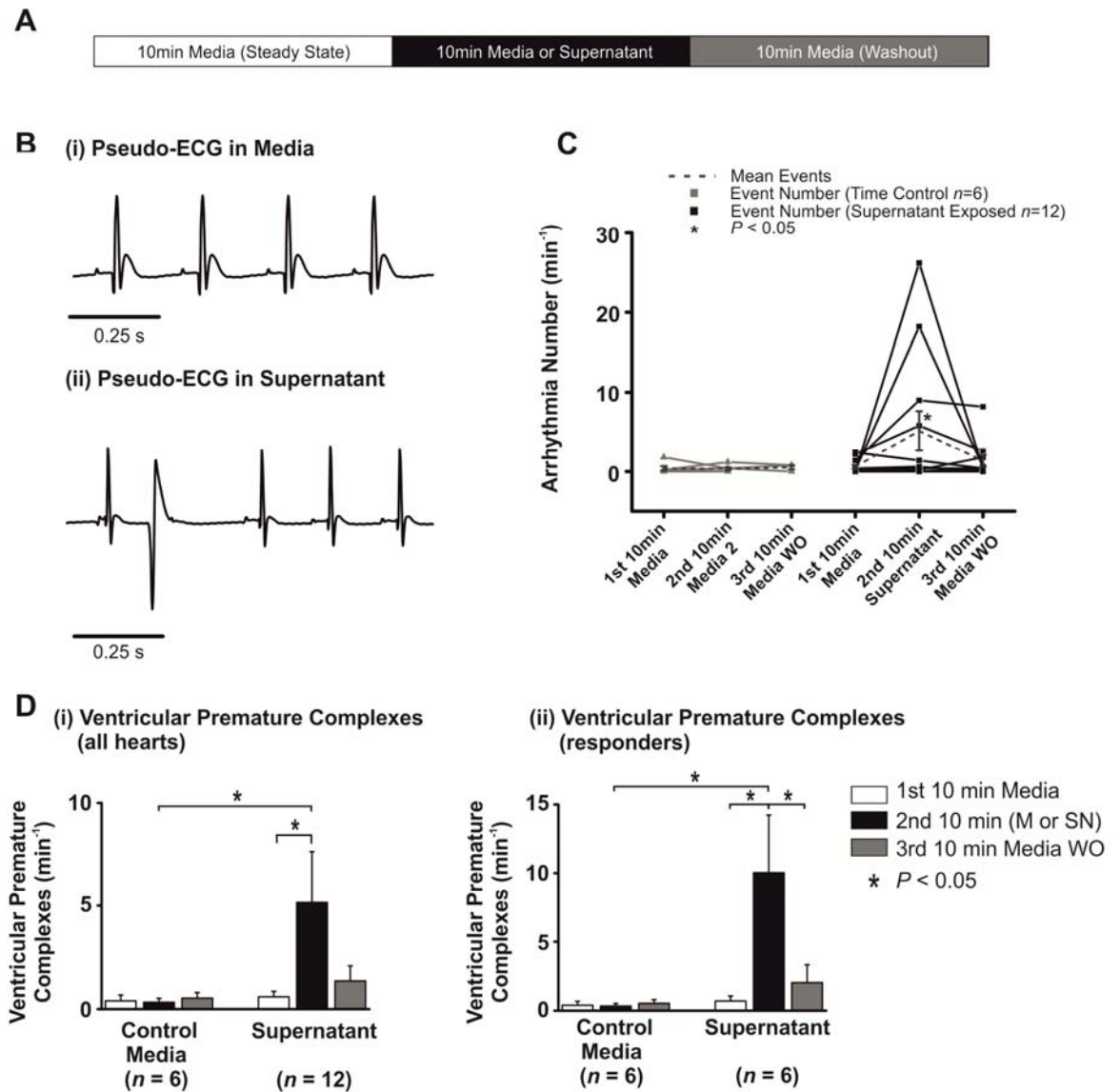


Figure 3.8 ECG data from *ex vivo* perfused rat hearts.

(A) Langendorff perfusion protocol. (B) Typical pseudo-ECG recordings (C) Number of arrhythmic events per minute in individual hearts. Time control hearts ($n=6$) (grey) on the left and supernatant exposed hearts ($n=12$) (black) on the right. The mean is shown with the dashed line, error bars indicate SEM. (D) (i) Mean \pm SEM of ventricular premature complexes per min for all time controls and supernatant perfused hearts during steady state in media (1st 10min), switch to media or supernatant (2nd 10min) and media washout (WO) (3rd 10min). (ii) Mean \pm SEM for responder hearts in media, media or supernatant, and washout with media.

3.3.10 Arrhythmic Events Occurred in a Proportion of Hearts

While the mean data of all the hearts shows an increase in arrhythmia frequency in the group of hearts perfused with supernatant, when examined further only a proportion (50%) exhibited an increase in arrhythmic events. When time controls vs. only these 'responders' are assessed (Figure 3.8D(ii)) there is no difference during the steady state period ($0.40 \pm 0.28 \text{ min}^{-1}$ vs. $0.70 \pm 0.37 \text{ min}^{-1}$; time control ($n=6$) vs. supernatant perfused responder ($n=6$); $P>0.05$). During

the second 10 min period the responders showed a significant increase in arrhythmia frequency ($0.33 \pm 0.19 \text{ min}^{-1}$ vs. $10.03 \pm 4.20 \text{ min}^{-1}$; $P < 0.05$). There was no significant difference between the washout periods (0.53 ± 0.27 vs. 2.03 ± 1.29 ; $P > 0.05$).

3.3.11 QT Interval Was Not Affected

The ECGs collected for arrhythmia analysis (Figure 3.8) were also analysed for QT interval. It has been reported in the literature that ECGs from patients with HAT have a prolongation of the QT interval⁽⁵¹⁾, which had been attributed to inflammation. Given the direct effects of supernatant on cardiomyocyte Ca^{2+} handling and arrhythmia frequency in whole hearts it was examined whether supernatant could prolong the QT interval. There was no statistical difference in the QT interval; (0.070 ± 0.005 vs. 0.074 ± 0.004 s; control media vs. supernatant; $P > 0.05$), QT_{90} (0.058 ± 0.004 vs. 0.063 ± 0.003 s; control media vs. supernatant; $P > 0.05$), or QT_{50} (0.044 ± 0.004 vs. 0.047 ± 0.004 ; control media vs. supernatant; $P > 0.05$; Figure 3.9C(i-iii)). When QT was corrected for heart rate between individuals there was no statistical difference either for QT_c (0.187 ± 0.005 vs. 0.194 ± 0.005 s; control media vs. supernatant; $P > 0.05$), QT_{90} (0.175 ± 0.003 vs. 0.177 ± 0.003 s; control media vs. supernatant; $P > 0.05$), or QT_{50} (0.161 ± 0.003 vs. 0.160 ± 0.003 ; control media vs. supernatant; $P > 0.05$; Figure 3.9D(i-iii)). There was no difference in heart rate (mean \pm SEM) between media (282 ± 17 bpm) or supernatant (278 ± 12 bpm) perfused hearts.

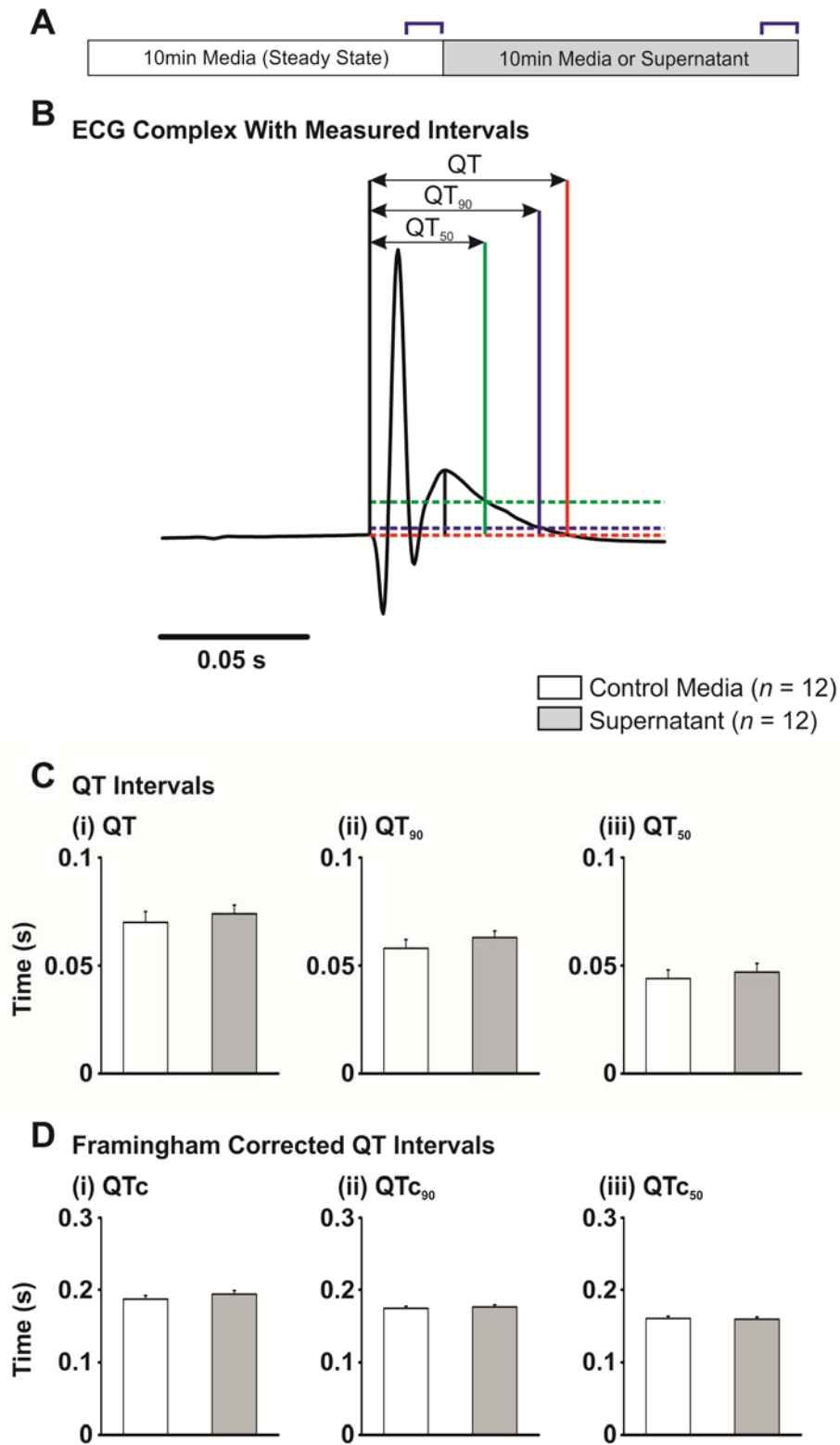


Figure 3.9: QT intervals from *ex vivo* whole rat hearts perfused with media and supernatant. (A) Protocol, blue brackets indicate period of protocol from which average ECGs were obtained. (B) Representative ECG complex showing how QT (red), QT₉₀ (blue) and QT₅₀ (green) were measured. (C) Mean \pm SEM for (i) QT, (ii) QT₉₀ and (iii) QT₅₀. (D) Mean \pm SEM for (i) QT, (ii) QT₉₀ and (iii) QT₅₀ corrected for heart rate using the Framingham method. Data were normalised to time matched controls perfused with media throughout the protocol.

3.4 Discussion

3.4.1 Trypanosomes Increase Ca^{2+} Wave Frequency in Cardiomyocytes

Classically, the clinical focus on HAT has been the neuropsychiatric disturbances. However cardiac involvement has been reported⁽⁵⁸⁾, but has usually been attributed to inflammation⁽⁵¹⁾. In fact the traditional thinking behind much of the pathology of trypanosomiasis has been that it is a result of the immune/inflammatory response to invasion of the tissues by the parasite, extensively documented in both animals⁽²⁶⁻²⁸⁾ and humans^(56;57). Therefore, inflammation was thought to be the mediator for the parasites traversing the BBB *via* disruption of the basement membrane leading to the classical CNS effects⁽⁵⁰¹⁾. However later work has shown that the parasites can cross the BBB without disruption of the tight junctional proteins between the endothelial cells⁽⁵⁰²⁾. Nikolskaia *et al.* (2006) demonstrated that *T. brucei* spp. secrete a factor that induces Ca^{2+} oscillations in human brain microvascular endothelial cells (HBMECs)⁽⁶⁹⁾. The hypothesis tested in the current study was that, like the HBMECs, trypanosomes could have an effect on cardiomyocytes without an immune/inflammatory component. The results demonstrated in the first part of this current study show that isolated adult rat left ventricular cardiomyocytes show increased spontaneous contractile activity. This can be related to altered Ca^{2+} signalling within the cardiomyocyte. Nikolskaia *et al.* (2006) postulated that the changes in $[\text{Ca}^{2+}]_i$ they observed could be due to mechanical stimulation by actively swimming parasites, which they subsequently ruled out by removing the live parasites from the culture medium, and yet continued to observe the same effect⁽⁶⁹⁾. The data presented in this thesis show the increase in spontaneous contractions was still apparent when cardiomyocytes were incubated in supernatant supporting the evidence presented in Nikolskaia *et al.* (2006)⁽⁶⁹⁾. Further results shown here (Figure 3.2) demonstrate that heat treatment of supernatant abrogates the observed effects, suggesting the responsible factor is a heat labile excreted/secreted factor. Particular care was taken in preparation of the supernatant to ensure the trypanosomes were not lysed, therefore ruling out an intracellular protein released upon parasite death.

3.4.2 Ca²⁺ Wave Velocity and Frequency are Increased by Trypanosome Culture Supernatant

Spontaneous contractions in cardiomyocytes arise from an asynchronous, spontaneous release of Ca²⁺ from the SR, termed a Ca²⁺ wave⁽²⁶¹⁾. By loading cardiomyocytes with Ca²⁺ sensitive fluorophores it was possible to image the rise and fall of cytosolic Ca²⁺ in response to incubation with the supernatant. The images obtained enabled the spontaneous Ca²⁺ waves to be further characterised to enable inferences on possible mechanisms to be drawn. As observed in the population assay (Figure 3.1), an increased frequency of Ca²⁺ waves was observed in cardiomyocytes incubated with supernatant. Increased Ca²⁺ wave frequency can occur when individual Ca²⁺ release events (Ca²⁺ sparks) trigger further release of Ca²⁺ from the SR through CICR⁽¹⁴⁸⁾. An increased Ca²⁺ wave frequency is determined by the time taken to reach SR Ca²⁺ threshold⁽¹⁹²⁾. SERCA stimulation by a direct or indirect effect of a factor in supernatant would increase the rate of accumulation of Ca²⁺ within the SR and hence decrease the time between spontaneous events^(192;503). This may have clinical repercussions as increased Ca²⁺ wave frequency is likely to increase the propensity for whole heart arrhythmias⁽¹⁹²⁾.

The velocity of Ca²⁺ wave propagation is an indicator of cluster to cluster RyR activation determined by RyR sensitivity, both dyadic and luminal, and refractoriness^(222;261;504). The results reported in this current study show a significant increase in velocity of Ca²⁺ waves present within cells incubated in supernatant. O'Neill *et al.* (2004) has shown that Ca²⁺ wave velocity was related to SERCA activity and therefore the observed increase in velocity observed in the current study may be an expected additional effect of enhanced SERCA activity⁽⁵⁰³⁾. However, it is acknowledged that the relationship between SERCA activity and Ca²⁺ wave characteristics is complex⁽⁵⁰⁵⁾.

3.4.3 Supernatant Increases the Rate of Stimulated Ca²⁺ Transient Decline

Experiments were performed on cohorts of cardiomyocytes that were incubated and superfused with media or supernatant and field stimulated at 1.0 Hz. The cells were loaded with Fura-4F and the rise and fall in cytosolic Ca²⁺ measured.

The main finding was an enhanced rate of transient decline. SERCA activity (K_{SERCA}) was estimated by measuring the rate constant of decay of the electrically stimulated Ca^{2+} transient. However, since Ca^{2+} is removed from the cytosol by reuptake into the SR by SERCA and extrusion by NCX⁽¹⁵⁸⁾, an increase in rate constant could have sarcolemmal efflux contributions. Although SERCA and NCX are not the only mechanisms involved Ca^{2+} removal during relaxation, the sarcolemmal Ca^{2+} ATPase pump and mitochondrial Ca^{2+} uptake contribute minimally, accounting for <25% of Ca^{2+} extrusion^(222;223) and occurring over a much slower time course than either SERCA or NCX⁽²²⁴⁾. In the rat 92% of Ca^{2+} removal is due to SERCA and 7% due to NCX vs. 70% and 28% respectively in rabbit left ventricular cardiomyocytes⁽²²⁴⁾. In humans, the Ca^{2+} removal contributions have been reported as 63% due to SERCA and 32% due to NCX⁽²²⁵⁾, therefore more similar to rabbit. If a high concentration caffeine bolus is rapidly applied to the cell, as well as being an indicator of $[\text{Ca}^{2+}]_{\text{SR}}$, the rate constant of decay of the caffeine-induced Ca^{2+} transient can indicate potential alterations in NCX with a much smaller component due to the other mechanisms. When the rate constant of decay of the caffeine-induced Ca^{2+} transient was measured there was no statistically significant difference. This suggests no significant alteration of extracellular extrusion, although the NCX current was not directly measured. It can be inferred that the logical explanation for an increased rate of Ca^{2+} transient decline is an increased K_{SERCA} . This can be measured as in Bode *et al.* (2011) by subtracting the rate constant of decay of the electrically stimulated Ca^{2+} transient from that of the caffeine-induced Ca^{2+} transient⁽⁵⁰⁶⁾ which gives a significant increase in K_{SERCA} of 143% (10.1 ± 1.10 vs. $14.5 \pm 1.39\text{s}^{-1}$; control vs. supernatant; $P < 0.05$). This compares well with the increase of 139% (11.3 ± 1.06 vs. $15.7 \pm 1.41\text{s}^{-1}$; $P < 0.05$) when using the rate constant of decay for the electrically stimulated transient alone. Since K_{SERCA} is increased it would be expected that there would be a concomitant increase in the caffeine-induced transient amplitude reflecting a higher $[\text{Ca}^{2+}]_{\text{SR}}$ yet this was not found. The possible mechanisms underlying these findings form the basis for the next chapter.

3.4.4 The Effects of Supernatant on the Stimulated Ca^{2+} Transient During β -adrenergic Stimulation

Cohorts of cardiomyocytes were treated as above but with the addition of 100 nM isoproterenol (ISO). β -adrenergic agonists such as ISO bind to the G-protein coupled β -adrenergic receptor which then stimulates adenylyl cyclase elevating cyclic AMP which activates protein kinase A (PKA). PKA, among other functions, phosphorylates the RyR which may increase its sensitivity and also phosphorylates the Ser16 residue on phospholamban (PLB), an inhibitory protein of SERCA⁽¹⁴⁸⁾. Another kinase also plays a role in the β -adrenergic cascade, Ca^{2+} calmodulin kinase II (CaMKII) through activation by PKA and directly from β -adrenergic stimulation⁽²⁵⁸⁾. Importantly, CaMKII also has phosphorylation sites on the RyR and Thr17 on PLB. Between stimulation pulses, diastolic release events of Ca^{2+} can be observed in cells incubated and superfused with supernatant in the presence of ISO. The rate constant of stimulated transient decline is also greater than without ISO as would be expected⁽⁵⁰⁷⁾. The fact that these effects are not present in the control media suggests the effects of the secreted factor on SR functions are enhanced by β -adrenergic stimulation.

3.4.5 Ca^{2+} Waves are Reduced by Cathepsin-L Inhibition but not Cathepsin-B Inhibition

The cysteine protease activity of trypanosomes comprise of TbCatL and TbCatB⁽⁴⁹²⁾. Nikolskaia *et al.* (2006) demonstrated that TbCatL activity was responsible for the Ca^{2+} rises in HBMECs enabling traversal of their *in vitro* BBB model. They found that the cathepsin-L specific inhibitor K11777 abrogated the parasite traversal of the model but not the cathepsin-B specific inhibitor CA074⁽⁶⁹⁾. Given the role of Ca^{2+} rises in the HBMEC model and the key role of Ca^{2+} in E-C coupling, K11777 and CA074 were applied to cohorts of cardiomyocytes that were then examined utilising spontaneous contractile activity assays (section 3.2.3). The addition of CA074 to cardiomyocytes did not alter the supernatant effect on spontaneous contractile activity of cells. When K11777 was applied to cardiomyocytes incubated in supernatant, the number of cardiomyocytes exhibiting spontaneous contractile activity was reduced to the same level observed in control media. This result supports the hypothesis that it

is the cathepsin-L-like cysteine protease TbCatL that could be causing an increase in waves.

American trypanosomiasis (aka Chagas Disease), caused by *Trypanosoma cruzi*, is characterised by significant cardiac pathology. Interestingly, a study by Barr *et al.* (1996) demonstrated a protease within the trypomastigote soluble fraction (TSF) that induces Ca^{2+} transients in canine cardiomyocytes⁽⁵⁰⁸⁾. The protease has since been shown to be an orthologous protease to TbCatL⁽⁵⁰⁹⁾. The result described by Barr *et al.* (1996) was that Ca^{2+} release was independent of an inward L-type Ca^{2+} current and due to SR Ca^{2+} release mediated by a pertussis toxin (PTx) sensitive g-protein coupled receptor⁽⁵⁰⁸⁾. The data presented in this chapter interpreted in context of the literature would suggest that TbCatL may activate a g-protein coupled receptor, causing activation of a secondary messenger, which then leads to spontaneous release of Ca^{2+} from the SR. Future work in the laboratory will aim to elucidate the sarcolemmal target for TbCatL.

3.4.6 Recombinant Cathepsin-L Increases Ca^{2+} Wave Frequency

The increase of Ca^{2+} waves has been abrogated by application of a cathepsin-L inhibitor which suggests an association of TbCatL and increased spontaneous Ca^{2+} release. To support this finding a cohort of spontaneous contractile activity assays was performed with recombinant TbCatL. These experiments showed the expected response of increased numbers of cells exhibiting Ca^{2+} waves. This suggests that it is TbCatL that is having a direct effect on spontaneous contractile activity of cardiomyocytes.

3.4.7 Ca^{2+} Waves are Reduced by RNA Interference of TbCatL

The use of recombinant TbCatL shows a gain of function effect, but to prove that TbCatL is definitively the responsible factor experiments were performed to show a loss of function phenotype. TbCatL is essential for parasite survival⁽⁴⁹²⁾ meaning that a complete gene knockout is not possible, so an inducible RNA interference (RNAi) approach was employed. Two independent clones of *T. b. brucei* were transfected with an inducible RNAi construct of the *Trypanosoma brucei* cathepsin-L (*TbCatL*) gene. Growth curves were performed to test efficacy of the RNAi which showed the expected defect in growth associated

with knockdown of an essential gene⁽⁴⁹²⁾. Quantitative PCR confirmed successful knockdown of *TbCatL* with additional PCR using *TbCatB* specific primers to ensure specificity of knockdown. When cardiomyocytes were incubated with supernatant from the induced cultures the number of cardiomyocytes exhibiting Ca^{2+} waves was reduced to the levels observed on control media. To confirm it wasn't a result of the transfection process on the trypanosomes, cardiomyocytes were also incubated in supernatant from uninduced cultures, which showed the same increase in Ca^{2+} waves as wild-type *T. b. brucei*.

These results demonstrate by three independent methods that *TbCatL* is increasing the number of cardiomyocytes that exhibit Ca^{2+} waves. These experiments were all performed in isolated cardiomyocytes, thereby removing the immune/inflammatory response. These data demonstrate for the first time a direct effect by secreted *TbCatL* on the Ca^{2+} dynamics of cardiomyocytes independent of an immune/inflammatory response. These findings also have implications in terms of treatment. Current HAT drugs are difficult to administer in the field and cause severe toxic side effects in 5-10% of cases with an average case fatality rate of 50%⁽⁵¹⁰⁾. Inhibitors of cysteine proteases are currently being tested as novel trypanocides⁽⁴⁹²⁾ but may also have a beneficial effect not only in limiting BBB traversal but potentially also cardiac dysfunction.

3.4.8 Supernatant Can Cause Arrhythmic Events in Whole Hearts

The literature reports ECG abnormalities and patient descriptions of arrhythmic disturbances or palpitations^(45;51-54) in cases of HAT. Most notably are ventricular premature complexes (VPCs) and a prolonged QT interval. To explain the clinical ECG findings in light of the evidence presented in this study the role of Ca^{2+} waves in arrhythmic heart disease has been considered. Ca^{2+} waves have been implicated in a number of arrhythmias such as delayed after depolarisations (DADs) and early after depolarisations (EADs)⁽²²²⁾.

The data in this chapter shows a significant increase in ventricular arrhythmias, specifically VPCs, in *ex vivo* intact hearts. These hearts are removed from an immune/inflammatory component so this is a direct effect from the trypanosome supernatant. Given the increase in Ca^{2+} waves observed, the faster decline of stimulated transient and the known relationship of Ca^{2+} release and

subsequent efflux by NCX⁽¹⁹²⁾ it is reasonable to suggest that the increase in Ca²⁺ waves within ventricular cardiomyocytes is linked to an increased frequency of DADs brought about by the electrogenic potential of NCX. The result is very similar to the response to β -adrenergic stimulation. In the presence of increased β -adrenergic stimulation there is increased phosphorylation of phospholamban, which reduces the inhibition on SERCA. The reduced inhibition of SERCA allows more Ca²⁺ to be taken up into the SR during diastole. Since sarcolemmal extrusion (*via* NCX) and SR reuptake (*via* SERCA) are the main Ca²⁺ removal mechanisms, they compete for the same diastolic pool of Ca²⁺ so there is less time for NCX to extrude Ca²⁺ in the presence of enhanced SERCA activity. Increased β -adrenergic stimulation also increases Ca²⁺ influx *via* stimulation of the L-type Ca²⁺ channel, which will raise diastolic [Ca²⁺]_i thereby increasing the diastolic pool of Ca²⁺ from which SERCA draws resulting in Ca²⁺ overload of the SR. SR Ca²⁺ overload would in turn, result in more diastolic Ca²⁺ waves resulting in a greater need for Ca²⁺ extrusion by NCX leading to more influx of Na⁺ increasing the likelihood of action potential threshold being reached. The action potentials rather than the Ca²⁺ waves could then propagate from cell to cell through gap junctions⁽¹⁵⁴⁾ potentially setting up an arrhythmogenic focus within the ventricular myocardium leading to the VPCs observed in this study and in the field⁽⁵¹⁾.

Ca²⁺ waves can also be linked to EADs⁽²⁸⁹⁾ and EADs are associated with prolonged QT intervals⁽²⁸⁶⁾ which have been found in HAT patients⁽⁵¹⁾. However, there was no statistically significant difference in QT intervals of hearts perfused with control media vs. supernatant (Figure 3.9) or when corrected for heart rate using the Framingham method. These findings suggest that the observed QT alterations clinically⁽⁵¹⁾ are less likely to be an acute effect but a more longer term effect which was attributed by Blum *et al.* (2007) to be a result of associated myocarditis⁽⁵¹⁾. QT is prolonged in myocarditis because the infiltration of inflammatory cells disrupts the myocardial tissue and can alter the electrical conductivity of the heart leading to alterations of depolarisation and repolarisation^(27;57). It is possible that *in vivo* there may be a synergistic effect on the myocardium of the direct effects of TbCatL with inflammation.

When patients with Chagasic cardiomyopathy were examined, a prolonged QT interval was found⁽⁵¹¹⁾. When investigated utilising mouse models of *T. cruzi*

infection, a similar prolongation of QT was also found, which correlated with the histopathological findings of infiltrating lymphocytes and macrophages⁽⁵¹²⁾. This could be the case for HAT but *in vivo* infection models would be required; these are presented and discussed in Chapter 5.

3.4.9 Arrhythmic Events Occurred in a Proportion of Hearts

Since Ca^{2+} waves have a low probability (<0.13) of propagating cell to cell⁽¹⁵⁴⁾ and DAD amplitude is diminished over a greater number of cells⁽¹⁹²⁾, multiple adjoining cells would be required to initiate an ectopic beat. In an atrial mathematical model it was identified that 1000 cells would be required in a grid of 512 x 512 to initiate an ectopic beat⁽²⁸⁸⁾. The data in this chapter suggests that TbCatL can induce Ca^{2+} waves in $67.47\% \pm 1.92$ of cells, therefore a proportion of hearts may be expected not to exhibit arrhythmias as a sufficient number of adjacent cells would not be waving. Only a proportion of hearts perfused with supernatant showed increased numbers of VPCs whereas none of the controls did. This evidence is supported by clinical field data that shows only a proportion of individuals show ECG abnormalities (71%) and palpitations (18%)⁽⁵¹⁾.

3.5 Conclusions

The data presented in this chapter demonstrates for the first time that *T. b. brucei* can cause direct effects on isolated rat left ventricular cardiomyocytes and *ex vivo* intact whole rat hearts independent of an immune/inflammatory response. How the trypanosomes have this effect is through the action of a cathepsin-L like cysteine protease, TbCatL. A possible mechanism of action is that TbCatL acts in a similar way to β -adrenergic stimulation by altering the sensitivity of the RyR to Ca^{2+} , and increasing Ca^{2+} reuptake into the SR by increased SERCA activity. However, this still needs to be investigated further and is discussed in Chapter 4.

4 CHAPTER 4 – Investigating the Mechanisms of Arrhythmogenic Sarcoplasmic Reticulum-Mediated Ca²⁺ Release Caused by *Trypanosoma brucei*

4.1 Introduction

4.1.1 Trypanosomes and Intracellular Ca^{2+}

The classical major effects of second stage Human African Trypanosomiasis (HAT) are the neuropsychiatric disturbances that give the disease its colloquial name of “Sleeping Sickness”. This occurs when the parasites cross the blood brain barrier (BBB)⁽⁶⁸⁾. Grab *et al.* (2004) showed that blood stream form trypanosomes induced oscillatory changes in $[\text{Ca}^{2+}]_i$ within endothelial cells of the an *in vitro* blood brain barrier model which enabled the parasites to cross the endothelial monolayer paracellularly⁽⁶⁷⁾. Nikolskaia *et al.* (2006) subsequently demonstrated that the oscillatory changes in $[\text{Ca}^{2+}]_i$ were caused by a cathepsin-L-like cysteine protease (TbCatL)⁽⁶⁹⁾. Grab *et al.* (2009) later postulated the membrane target leading to the oscillatory changes in $[\text{Ca}^{2+}]_i$ to be the g-protein coupled receptor (GPCR) protease activated receptor 2 (PAR-2)⁽⁶⁶⁾. Interestingly, the related parasite *Trypanosoma cruzi*, the cause of American trypanosomiasis (Chagas Disease) which has notable cardiac pathology⁽⁵¹³⁾, also produces a protease that induces $[\text{Ca}^{2+}]_i$ fluctuations in range of mammalian cells⁽⁵¹⁴⁾ and cardiomyocytes⁽⁵⁰⁸⁾. These changes in $[\text{Ca}^{2+}]_i$ are associated with host cell invasion as inhibition of Ca^{2+} transients in host cells prevents invasion^(515;516). The changes in $[\text{Ca}^{2+}]_i$ induced by *T. cruzi* were shown to be sensitive to inhibition of the pertussis toxin sensitive GPCR⁽⁵⁰⁸⁾. This suggests a putative role for Ca^{2+} in the host cell invasion for *T. cruzi*. With regard to *T. b. brucei* it is clear that it can also induce changes in $[\text{Ca}^{2+}]_i$ in host cells such as endothelial cells *in vitro*. The novel data presented in the preceding chapter demonstrates that *Trypanosoma brucei brucei* also has an effect on spontaneous Ca^{2+} release in cardiomyocytes.

4.1.2 African Trypanosomes and $[\text{Ca}^{2+}]_i$ in the Heart

As discussed in the preceding chapter recent studies have identified clinical manifestations of cardiac pathology such as palpitations and prolonged QTc intervals⁽⁵¹⁾ in patients with HAT. In post-mortem examinations of infected humans^(56;57) and experimentally infected animals⁽²⁶⁻²⁸⁾ there has been significant cardiac pathology with the presence of trypanosomes in the myocardium with or without inflammatory cell infiltrates^(26;497). The results presented in the

preceding chapter demonstrate that trypanosome supernatant increases spontaneous Ca^{2+} release and may also increase ventricular arrhythmia frequency in *ex vivo* rat hearts. This would suggest that the observed cardiac clinical signs in HAT may be related to altered intracellular Ca^{2+} handling induced by TbCatL. The mechanisms at the level of the SR underlying the increase in propensity for spontaneous Ca^{2+} release in cardiomyocytes induced by *T. brucei* remain unknown and are the focus of this chapter.

4.1.3 Mechanisms to Explore

The conclusion that TbCatL causes abnormal SR-mediated Ca^{2+} release as a result of stimulation of SERCA needs to be substantiated. Firstly, the only evidence for this conclusion is an accelerated decline of the Ca^{2+} transient in supernatant perfused cardiomyocytes. If increased spontaneous Ca^{2+} release was a result of increased SERCA activity, the SR Ca^{2+} content may be expected to be higher. Therefore, paired experiments with the same cardiomyocyte being perfused with media followed by supernatant were performed to improve the accuracy and reliability of the epifluorescence SR Ca^{2+} content experiments. Secondly, whether cathepsin-L can lead to altered $[\text{Ca}^{2+}]_i$ independent of SR Ca^{2+} release and uptake is unknown. Therefore experiments assessing the diastolic $[\text{Ca}^{2+}]_i$ with SR ATPase and RyR inhibitors were conducted. Thirdly, alteration of the Ca^{2+} transient decline could be associated with altered myofilament Ca^{2+} responsiveness^(148;517), therefore cardiomyocyte length measurements were performed in parallel with the epifluorescence Ca^{2+} measurements to assess myofilament Ca^{2+} sensitivity. Fourthly, evidence on how the extracellular cathepsin-L targets intracellular SERCA is an important question to try to answer. The dual increase of spontaneous Ca^{2+} release in the form of Ca^{2+} waves and increased SERCA activity suggest that Protein Kinase A (PKA) and/or Ca^{2+} /calmodulin Kinase II (CaMKII) may be possible targets⁽¹⁴⁸⁾. Therefore the spontaneous contractile event experiments were performed with PKA and CaMKII specific inhibitors.

4.1.4 Aims of the Chapter

It is clear that trypanosome supernatant can have a direct affect on cardiomyocyte Ca^{2+} dynamics but the host cell SR-related mechanisms remain

unclear. The primary aim of this chapter is to explore the potential SR-related mechanisms by which TbCatL could be eliciting its effects on Ca^{2+} handling and whether CaMKII and/or PKA are potential mediators of the observed effects on SR function.

4.2 Methods

4.2.1 Adult Rat Cardiomyocyte Isolation

Adult rat left ventricular cardiomyocytes were isolated from male Wistar rats as described in section 2.3.1. Briefly, hearts were removed and enzymatically digested with collagenase to break down the connective tissue. Isolated cardiomyocytes were prepared as described in in section 2.3.1. The cardiomyocytes were suspended in MIKH containing no BSA with a $[Ca^{2+}]_o$ of 1.8 mM.

4.2.2 Preparation of Control Media and Supernatant

Control media and supernatant were prepared as described in section 2.1.5. These solutions were then loaded into a gravity fed perfusion system for delivery to isolated cardiomyocytes *via* a perfusion pen at 37 °C.

4.2.3 Normal Extracellular Ca^{2+} Epifluorescence Measurements

The isolated cardiomyocytes in 1.8 mM Ca^{2+} MIKH from above were loaded with 5 μ M of the ratiometric Ca^{2+} fluorophore Fura-4F-AM (Invitrogen) by incubation for 10 min at room temperature. The cardiomyocytes were resuspended in 1.8 mM Ca^{2+} MIKH and incubated for 30 min at room temperature for de-esterification. Cardiomyocytes were loaded into a tissue bath (Cell Microcontrols) and allowed to settle onto a coverslip. Cardiomyocytes were superfused with normally prepared control media or supernatant at 37 °C by gravity fed perfusion pen with active pump outflow. Cardiomyocytes were field stimulated (1.0 Hz, 2.0 ms duration, stimulation voltage set to 1.5 x threshold) and perfused firstly with control media (60 s) followed by supernatant (60 s). Caffeine (10 mM, 20 s; without field stimulation) was applied before the protocol, after perfusion with media and after supernatant. The three caffeine boluses and two solution changes were all performed in the same isolated cardiomyocyte thus enabling accurate paired assessment of SR Ca^{2+} content between media and supernatant. Parallel experiments were performed with media for both 60 s periods as time-controls. The results obtained with supernatant were normalised to these time-controls. The Fura-4F fluorescence ratio (340/380 nm excitation; $R_{340/380nm}$) was

measured with a spinning wheel spectrophotometer (Cairn Research Ltd) at a sampling rate of 5,000 Hz. $[Ca^{2+}]_i$ was calculated from $R_{340/380nm}$ as described in General Methods. Mean Ca^{2+} transients were calculated by averaging 12 steady state transients using Origin (OriginLab).

4.2.4 Low Extracellular Ca^{2+} Epifluorescence Measurements

Cardiomyocytes were prepared as described above, but $[Ca^{2+}]_o$ was increased only to 0.5 mM. The intact cardiomyocytes were then resuspended in MIKH with 0.5 mM Ca^{2+} and loaded with 5 μ M Fura-4F-AM for 10 min. Cells were de-esterified in 0.5 mM Ca^{2+} MIKH for 30 min before being allowed to settle on a cover slip within a tissue bath as described above (section 4.2.4). Superfusate solutions of control media and supernatant were made with $[Ca^{2+}]_o$ of 0.5 mM by diluting 1 in 4 with 0 mM Ca^{2+} MIKH. A test experiment assessing the percentage change in cell exhibiting spontaneous contractile events as performed in Chapter 3 was conducted to examine whether a 1 in 4 diluted supernatant still showed an increase in cells exhibiting spontaneous contractile events compared to 1 in 4 diluted media. Cells incubated in 1 in 4 diluted supernatant with 0.5 mM $[Ca^{2+}]_o$ showed a significant increase in contractile events of 300%; ($10.33 \pm 5.23\%$ vs. $31.05 \pm 6.16\%$ cardiomyocytes exhibiting at least one spontaneous contractile event.min⁻¹; control media vs. supernatant; $P < 0.05$; Figure 4.1). This was comparable with the increase in supernatant observed at 1.8 mM $[Ca^{2+}]_o$; ($52.11 \pm 1.64\%$ vs. $67.47 \pm 1.92\%$ cardiomyocytes exhibiting at least one spontaneous contractile event.min⁻¹; control media vs. supernatant; $P < 0.001$; Figure 3.1). Therefore low $[Ca^{2+}]_o$ were performed with a 1 in 4 diluted control media or supernatant.

A

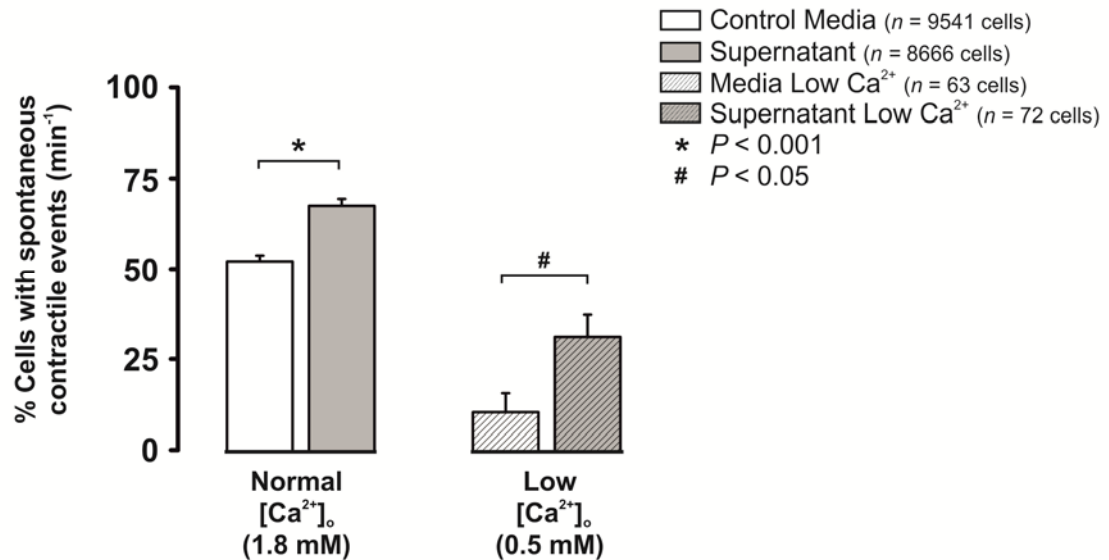


Figure 4.1: Spontaneous contractile events in low and normal [Ca²⁺]_o. Mean % ± SEM of isolated rat left ventricular cardiomyocytes exhibiting ≥1 spontaneous contractile event.min⁻¹ in media and supernatant at 1.8 mM [Ca²⁺]_o and 0.5 mM [Ca²⁺]_o. *n* = number of cardiomyocytes.

Cardiomyocytes were superfused with the 1 in 4 diluted control media or supernatant at 37 °C with field stimulation as above (section 4.2.3) using the same protocol of media (60 s) followed by supernatant (60 s) with three caffeine boluses; before protocol, after media and after supernatant. Results were normalised to time-controls.

4.2.5 First Post-Caffeine Ca²⁺ Transient Analysis

As an indicator of Ca²⁺ influx *via* the L-type Ca²⁺ channel (LTCC), the amplitude of the first Ca²⁺ transient following the application of caffeine (10 mM) was measured. The SR is essentially empty of Ca²⁺ following the application of caffeine so the [Ca²⁺]_i will predominately come from what enters through the sarcolemma *via* the LTCC⁽⁵¹⁸⁾.

4.2.6 Fractional Shortening Measurements

In parallel with normal 1.8 mM [Ca²⁺]_o epifluorescence measurements cell length was also measured. Edge detection software (Ionoptix) was used to measure the change in length of field stimulated (1.0 Hz) isolated cardiomyocytes. The change in length was plotted as a ratio over the diastolic cell length immediately before stimulation (L/L₀). Fractional shortening was calculated as the

percentage reduction from L_0 . To assess changes in myofilament Ca^{2+} sensitivity cell length was plotted against $[\text{Ca}^{2+}]_i$ during diastole.

4.2.7 Epifluorescence Measurements of Diastolic $[\text{Ca}^{2+}]_i$ During SR Inhibition

Fura-2-AM loaded cardiomyocytes were incubated with 1.0 μM thapsigargin (Merckmillipore) and 1.0 μM ryanodine (Merckmillipore) for 30 min to inhibit SR function. The cardiomyocytes were then superfused with control media for 1 min followed by perfusion with supernatant (or media for time-controls) for 4 min in the continued presence of 1.0 μM thapsigargin and ryanodine. Changes in diastolic $[\text{Ca}^{2+}]_i$ were assessed using the spinning wheel spectrophotometer as above (section 4.2.3).

4.2.8 Spontaneous Contractile Event Measurement in Isolated Cardiomyocytes With H-89 and AIP

Isolated cardiomyocytes were incubated at a dilution of 1 in 4 with control media or supernatant (cells in MKH:control media/supernatant) for 30 min with or without the PKA inhibitor H-89 (N-[2-(p-bromocinnamylamino)ethyl]-5-isoquinolinesulphonamide) (Sigma-Aldrich) at a concentration of 10 μM ^(153;519). For experiments with the CaMKII inhibitor AIP (autocamtide-2 related inhibitory peptide) (Merckmillipore) cardiomyocytes were plated in 35mm petri dishes (Corning) at a density of 25-50 cells. cm^{-2} for 60 min⁽³²⁰⁾. To improve AIP loading a myristoylated form was used that has greater cell permeability.

Cardiomyocytes were viewed under a light microscope and charged-couple device (CCD) camera at 20 x magnification enabling observation of ≥ 10 cardiomyocytes per field of view. Individual cardiomyocytes exhibiting at least one spontaneous contractile event within 1 min were noted and expressed as the percentage of the total examined cardiomyocyte number. This process was repeated over 10 fields and mean data reported.

4.2.9 Epifluorescence Measurements with CaMKII Inhibition

Epifluorescence measurements at physiological (1.8 mM) $[\text{Ca}^{2+}]_o$ in field stimulated (1.0 Hz) cardiomyocytes with Fura-4F were performed with the CaMKII inhibitor AIP. Diastolic $[\text{Ca}^{2+}]_i$ measurements in unstimulated

cardiomyocytes with Fura-2AM were also conducted with AIP. Cells were prepared by incubating in petri dishes with AIP for 60 min as above (section 4.2.8). The protocols applied in sections 4.2.3 and 4.2.7 were performed in separate cohorts of cells and analysed as described.

4.2.10 Statistical Analysis

Data are expressed as mean \pm SEM. Paired experiments were normalised to time-controls performed in parallel. Statistical comparisons were made by a paired Student's T-test on the raw data. Two-sample Student's T-tests were performed on percentage changes over controls. A significance level of $P < 0.05$ was considered significant.

4.3 Results

4.3.1 Supernatant Increased the Decay Rate Constant of the Stimulated Ca^{2+} Transient

The experiments conducted in Chapter 3 were with two separate groups of cardiomyocytes at 1.8 mM $[\text{Ca}^{2+}]_o$ incubated for 30 min. The data presented in that chapter demonstrated an increase in the decay rate constant but no statistically significant difference in the amplitude of the caffeine-induced Ca^{2+} transient (albeit with a tendency towards being lower in supernatant; Figure 3.4). Although using a 30 min incubation period ensured that the supernatant had sufficient time to act, it was not possible to perform paired experiments which reduced the sensitivity of the experiments; in particular the peak of the caffeine-induced Ca^{2+} transient. It also prevented ascertaining whether the supernatant could have acute effects. In order to address these issues, paired experiments without prior incubation were performed. Cardiomyocytes were perfused for 60 s with media followed by 60 s with supernatant (or media for time-controls) (Figure 4.2A). Results in supernatant were normalised to the time-controls.

4.3.1.1 Physiological $[\text{Ca}^{2+}]_o$ (1.8 mM)

Mean data \pm SEM was obtained from average Ca^{2+} transients from the last 12 Ca^{2+} transients in media and supernatant (Figure 4.2B). The maximum $[\text{Ca}^{2+}]_i$ was not significantly altered by supernatant; (662.4 ± 56.0 vs. 657.5 ± 55.6 nM; control media vs. supernatant; $P > 0.05$; Figure 4.2C(i)), nor was the minimum $[\text{Ca}^{2+}]_i$ significantly altered; (160.6 ± 5.3 vs. 165.7 ± 5.5 nM; control media vs. supernatant; $P > 0.05$; Figure 4.2C(i)). Therefore, the stimulated Ca^{2+} transient amplitude was also not significantly altered by supernatant; (501.8 ± 56.6 vs. 490.1 ± 55.3 nM; control media vs. supernatant; $P > 0.05$; Figure 4.2C(i)). This data supports the Ca^{2+} transient findings with incubated cardiomyocytes. With the incubated cardiomyocyte data there was a parallel increase in the decay rate constant of 110.4% of control; (12.2 ± 1.2 vs. 13.4 ± 1.4 s^{-1} ; control media vs. supernatant; $P < 0.05$; Figure 4.2C(ii)).

4.3.1.2 Low $[Ca^{2+}]_o$ (0.5 mM)

The same experiments were also performed with control media and supernatant diluted 1 in 4 with 0 mM $[Ca^{2+}]_o$ MIKH to lower the $[Ca^{2+}]_o$ to 0.5 mM (Figure 4.2A). These experiments were performed to ensure that the SR Ca^{2+} content had not reached saturation. Reduction of $[Ca^{2+}]_o$ reduced the Ca^{2+} transient amplitude to 45.9% of that in 1.8 mM $[Ca^{2+}]_o$. Similar to 1.8 mM $[Ca^{2+}]_o$ the Ca^{2+} transient peak was not affected by supernatant; (388.5 ± 23.6 vs. 395.6 ± 24.8 nM; control media vs. supernatant; $P > 0.05$; Figure 4.2C(i)), nor was the Ca^{2+} transient minimum; (158.4 ± 5.3 vs. 154.3 ± 5.2 nM; control media vs. supernatant; $P > 0.05$; Figure 4.2C(i)). Therefore the Ca^{2+} transient amplitude was also unaffected by supernatant; (230.1 ± 23.5 vs. 242.0 ± 24.8 nM; control media vs. supernatant; $P > 0.05$, Figure 4.2C(i)). However, like the 1.8 mM $[Ca^{2+}]_o$, the decay rate constant was significantly increased by supernatant to 112% of control; (8.5 ± 0.4 vs. 9.5 ± 0.4 s⁻¹; control media vs. supernatant; $P < 0.05$; Figure 4.2C(ii)).

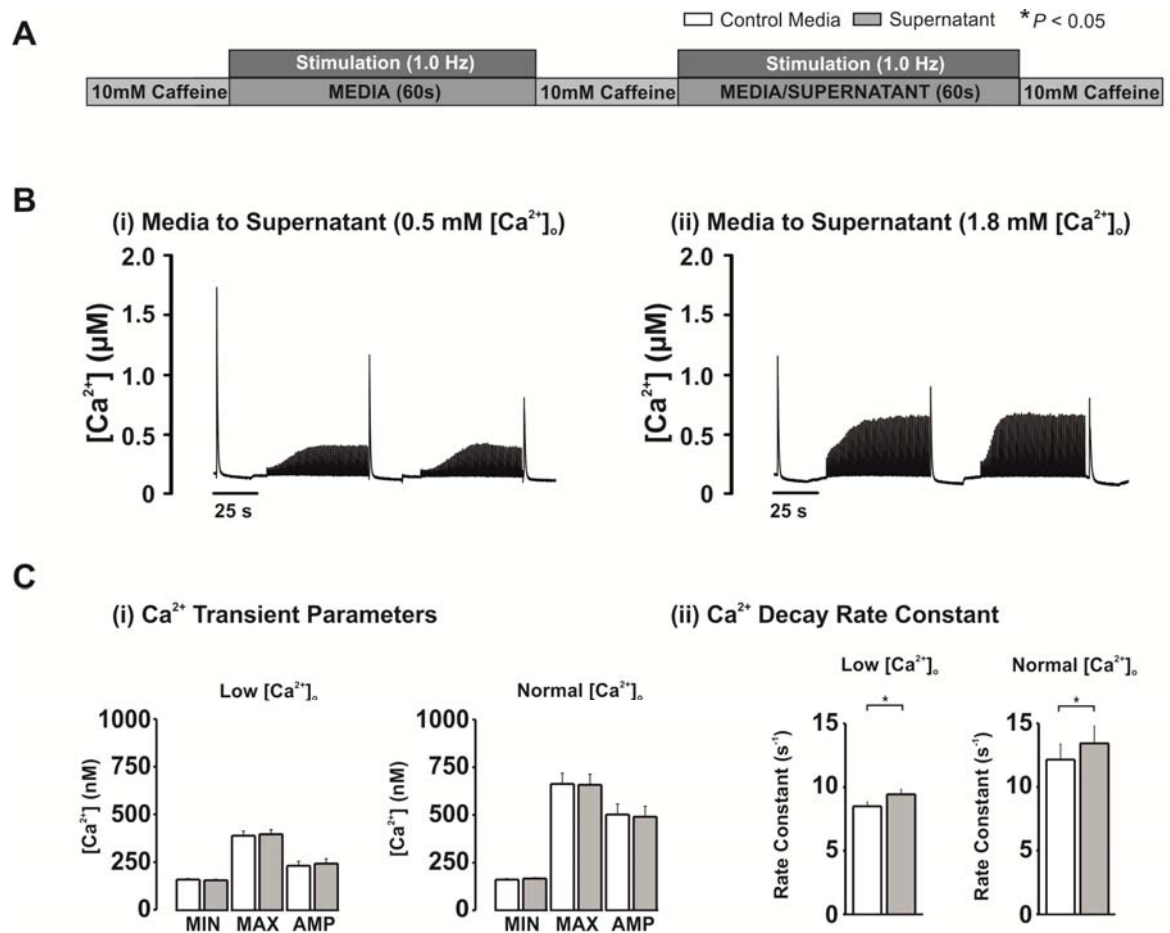


Figure 4.2: Stimulated Ca²⁺ transients at low and physiological extracellular Ca²⁺. (A) Protocol used in epifluorescence Ca²⁺ measurements. (B) Whole protocol traces at (i) low 0.5 mM [Ca²⁺]_o and (ii) normal 1.8 mM [Ca²⁺]_o. (C(i)) Mean ± SEM for average of last 12 transients for stimulated Ca²⁺ transient parameters (maximum, minimum and amplitude) normalised to time controls for low 0.5 mM [Ca²⁺]_o (*n* = 8) and normal 1.8 mM [Ca²⁺]_o (*n* = 12); for control media in the first minute (white) and supernatant in the second minute (grey). (ii) Mean ± SEM for average of last 12 transients decay rate constant for both low and normal [Ca²⁺]_o.

4.3.2 Supernatant Reduces the SR Ca²⁺ Content

SR Ca²⁺ content has a significant influence on Ca²⁺ transient characteristics. To determine the SR Ca²⁺ content the amplitude of Ca²⁺ transient induced by rapid application of 10 mM caffeine (20 s) was measured after perfusion of the cardiomyocytes with media and then supernatant in the same cell (Figure 4.3A). The paired nature of the protocol enabled more accurate determination of small changes in SR Ca²⁺ content between media and supernatant.

4.3.2.1 Physiological [Ca²⁺]_o (1.8 mM)

The caffeine-induced Ca²⁺ transient was measured in media and supernatant and normalised to time-control experiments performed in parallel. Supernatant had no significant effect on the minimum [Ca²⁺]_i (152.9 ± 5.4 vs. 170.2 ± 6.1 nM;

control media vs. supernatant; $P>0.05$; Figure 4.3B(i)). However, supernatant significantly reduced the caffeine-induced Ca^{2+} peak (913.9 ± 44.4 vs. 865.8 ± 42.0 nM; control media vs. supernatant; $P<0.05$; Figure 4.3B(i)), resulting in a significantly reduced amplitude of 91.7% of the amplitude in control media (760.9 ± 42.9 vs. 698.3 ± 39.4 nM; control media vs. supernatant; $P<0.05$; Figure 4.3B(i)). The decay rate constant of the caffeine-induced Ca^{2+} transient is an indicator of sarcolemmal extrusion of Ca^{2+} as the SR cannot re-accumulate Ca^{2+} in the continued presence of caffeine. Supernatant did not significantly alter the decay rate constant; (1.68 ± 0.08 vs. 1.45 ± 0.07 ; control media vs. supernatant; $P<0.05$) (Figure 4.3B(ii)).

4.3.2.2 Low $[\text{Ca}^{2+}]_o$ (0.5 mM)

As with the stimulated Ca^{2+} transient experiments, caffeine was applied at low $[\text{Ca}^{2+}]_o$. Similarly with the normal $[\text{Ca}^{2+}]_o$ supernatant did not significantly alter the minimum $[\text{Ca}^{2+}]_i$; (155.5 ± 5.5 vs. 150.3 ± 5.3 nM; control media vs. supernatant; $P>0.05$; Figure 4.3B(i)). However, supernatant did decrease the peak of the caffeine-induced Ca^{2+} transient to 82.7% of control (1114 ± 51.5 vs. 921.0 ± 42.6 nM; control media vs. supernatant; $P<0.05$; Figure 4.3B(i)) and the amplitude to 80.3% of control (958.7 ± 52.2 vs. 769.4 ± 41.9 nM; control media vs. supernatant; $P<0.05$; Figure 4.3B(i)). Supernatant did not significantly affect the rate constant of decay; (1.95 ± 0.13 vs. 1.78 ± 0.12 s⁻¹; control media vs. supernatant; $P>0.05$, Figure 4.3B(ii)).

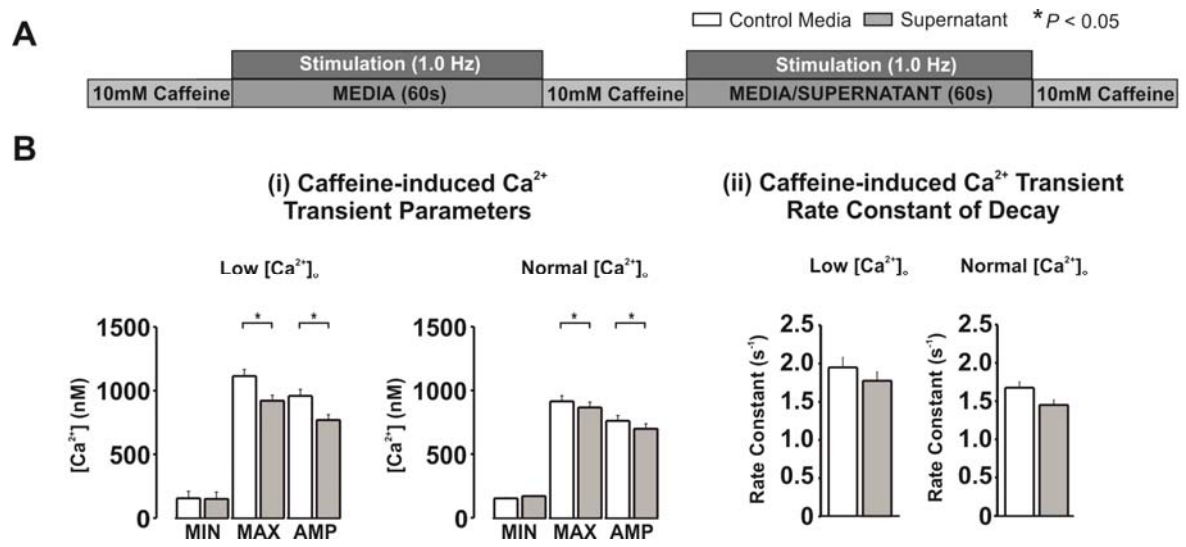


Figure 4.3: Caffeine-induced Ca^{2+} transient parameters at low and normal extracellular Ca^{2+} . (A) Protocol used in epifluorescence Ca^{2+} measurements. (B) Mean \pm SEM for caffeine-induced Ca^{2+} transient parameters (maximum, minimum and amplitude) normalised to time controls for low 0.5 mM $[\text{Ca}^{2+}]_o$ ($n = 8$) and normal 1.8 mM $[\text{Ca}^{2+}]_o$ ($n = 12$); for control media in the first minute (white) and supernatant in the second minute (grey). (ii) Mean \pm SEM for caffeine-induced Ca^{2+} transient decay rate constant for both low and normal $[\text{Ca}^{2+}]_o$.

4.3.3 Myofilament Ca^{2+} Sensitivity

An altered stimulated Ca^{2+} transient decline could be caused by altered Ca^{2+} sensitivity of the myofilaments. Therefore to examine whether supernatant could increase the Ca^{2+} transient rate of decline *via* altered Ca^{2+} sensitivity of the myofilaments, experiments were performed to measure cardiomyocyte shortening in parallel with $[\text{Ca}^{2+}]_i$ measurements following the same protocol as used to generate the data in Figure 4.2 & Figure 4.3 (Figure 4.4A). There was no significant difference in the fractional shortening percentage (7.77 ± 1.11 vs. $7.10 \pm 1.01\%$; control media vs. supernatant; $P > 0.05$; Figure 4.4C(i)). There was also no significant difference in the rates of change of cell shortening during contraction (223.0 ± 41.6 vs. $240.1 \pm 44.8 \mu\text{m}\cdot\text{s}^{-1}$; control media vs. supernatant; $P > 0.05$; Figure 4.4C(ii)), or lengthening during relaxation (179.5 ± 39.8 vs. $164.5 \pm 36.5 \mu\text{m}\cdot\text{s}^{-1}$; control media vs. supernatant; $P > 0.05$; Figure 4.4C(iii)). At the end of diastole the rates of change of $[\text{Ca}^{2+}]_i$ are minimal, therefore the minimal $[\text{Ca}^{2+}]_i$ and end-diastolic cell length can be used to assess the myofilament Ca^{2+} sensitivity in the intact cell⁽⁵²⁰⁾. There was no statistically significant difference between end-diastolic $[\text{Ca}^{2+}]_i$ (160.6 ± 5.3 vs. 165.7 ± 5.5 nM; control media vs. supernatant; $P > 0.05$) or end-diastolic cell length (117.8 ± 3.2 vs. $118.7 \pm 3.2 \mu\text{m}$; control media vs. supernatant; $P > 0.05$; Figure 4.4D).

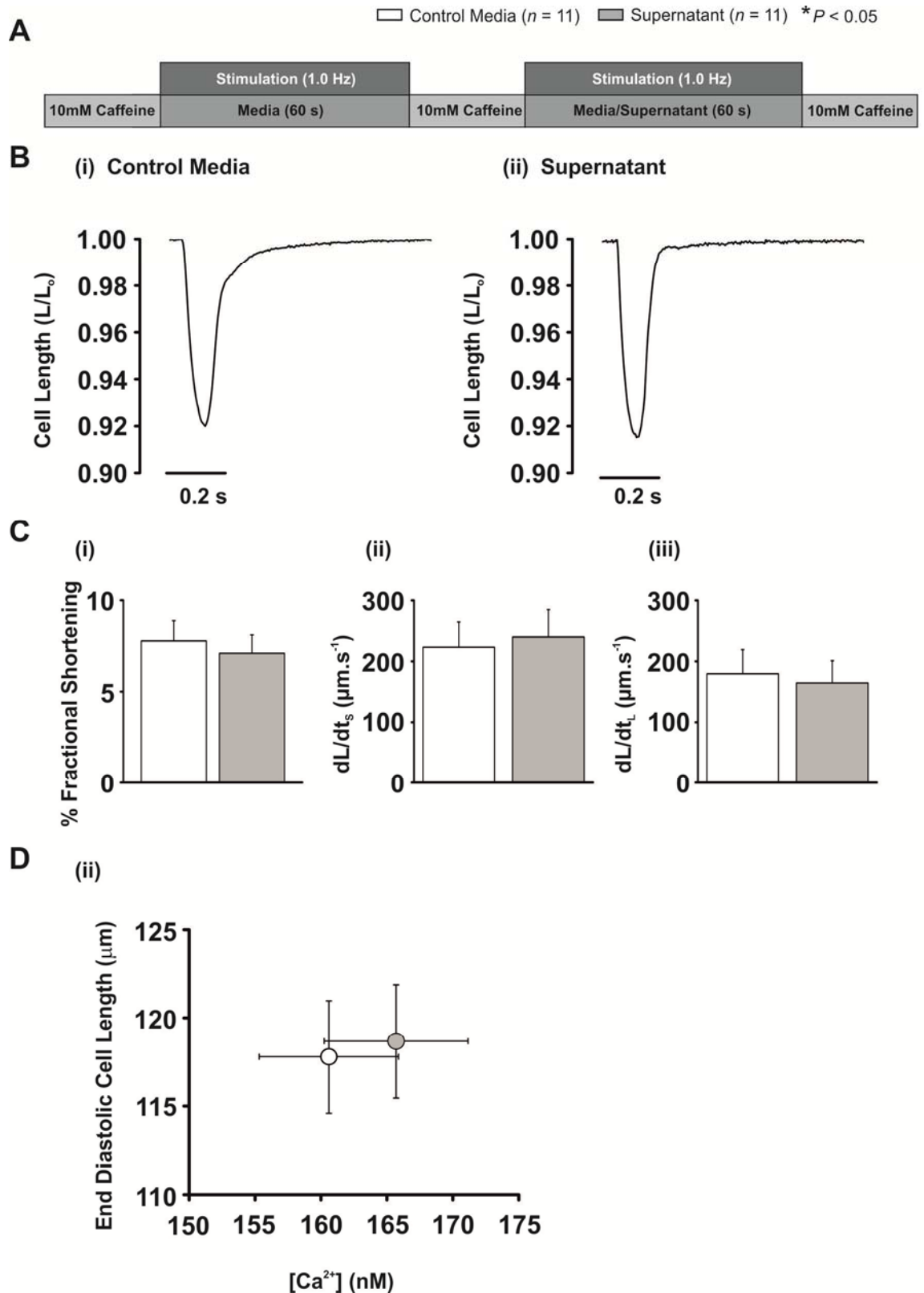


Figure 4.4: Fractional shortening of cardiomyocytes.

(A) Protocol used in parallel shortening and epifluorescence Ca^{2+} measurements. (B) Example shortening traces for (i) control media and (ii) supernatant as ratios of resting cell length (L/L_0). (C(i-iii)) mean \pm SEM of fractional shortening % of resting cell length, rate of change of shortening (dL/dt_s) and rate of change of lengthening (dL/dt_l) for media (white) and supernatant (grey) ($n = 11$). (D) Plot of mean \pm SEM of end-diastolic $[\text{Ca}^{2+}]_i$ (x axis) and end-diastolic cell length (y axis). Fluorescence ratios were 0.512 and 0.528 for media and supernatant respectively ($P > 0.05$).

4.3.4 Supernatant Increases Diastolic $[Ca^{2+}]_i$ via a Non-SR Dependent Route

In Chapter 3 experiments were conducted with the addition of a β -adrenergic agonist (100 nM isoproterenol) to examine the effects under stress. In these experiments the minimum $[Ca^{2+}]_i$ was significantly increased to 115% of control levels (Figure 3.5). In order to assess whether supernatant could alter diastolic $[Ca^{2+}]_i$ in the absence of SR-mediated Ca^{2+} release or uptake, the higher affinity Ca^{2+} fluorophore Fura-2-AM was utilised in cardiomyocytes where SR function was inhibited by the application of both thapsigargin and ryanodine (Figure 4.5). In the absence of SR-mediated Ca^{2+} release, supernatant led to a persistent significant elevation of diastolic $[Ca^{2+}]_i$ over the 4 min period compared to media (Figure 4.5).

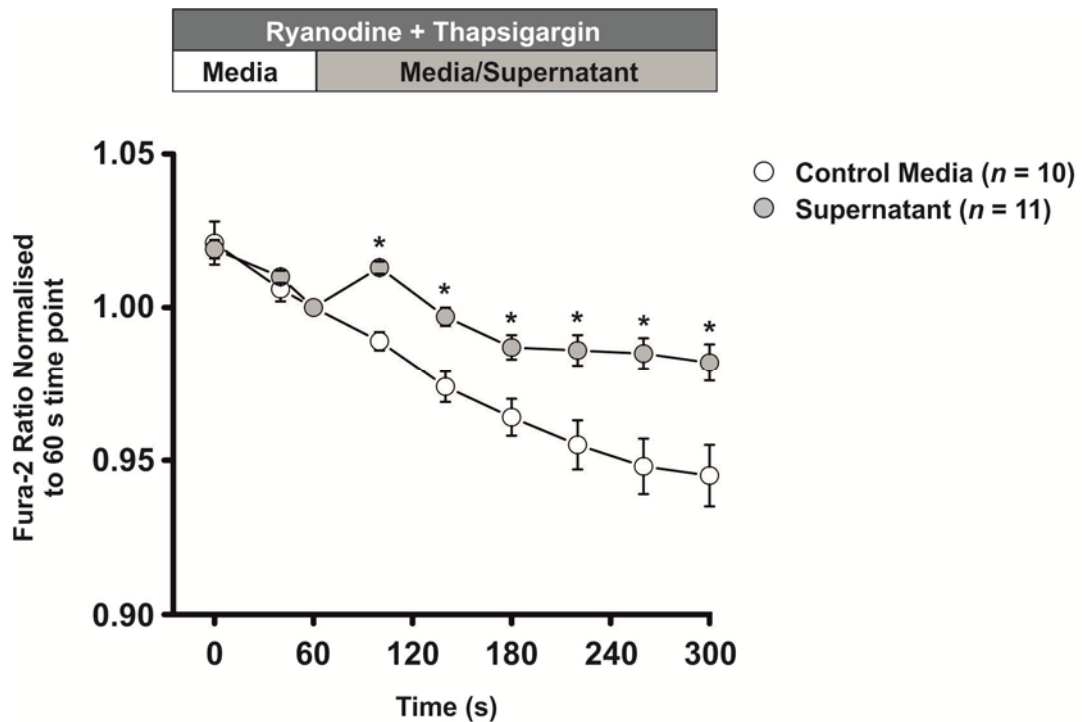


Figure 4.5: Diastolic $[Ca^{2+}]_i$ measurements with an inhibited SR. Fura-2-AM ratio during SR inhibition with thapsigargin and ryanodine in media (open; $n = 10$) and supernatant (grey; $n = 11$). Data are normalised to the 60 s time-point.

4.3.5 Supernatant Does Not Likely Alter the L-Type Ca^{2+} Channel

One possible explanation for elevation of diastolic $[Ca^{2+}]_i$ could be increased Ca^{2+} influx through the LTCC. An index of Ca^{2+} influx through the LTCC is the amplitude of the first stimulated Ca^{2+} transient after application of high

concentration caffeine. Therefore, using the protocol used to generate the data in Figure 4.2 & Figure 4.3, the amplitude of the first stimulated Ca^{2+} transient following the application of 10 mM caffeine was measured in 0.5 mM $[\text{Ca}^{2+}]_o$ and 1.8 mM $[\text{Ca}^{2+}]_o$ (Figure 4.6). Supernatant did not significantly alter the first post-caffeine Ca^{2+} transient amplitude in 0.5 mM $[\text{Ca}^{2+}]_o$ (71.3 ± 6.8 vs. 75.3 ± 7.1 nM; control media vs. supernatant; $P > 0.05$; Figure 4.6B(i)) or in 1.8 mM $[\text{Ca}^{2+}]_o$ (154.4 ± 10.3 vs. 161.5 ± 10.8 nM; control media vs. supernatant; $P > 0.05$; Figure 4.6B(ii)).

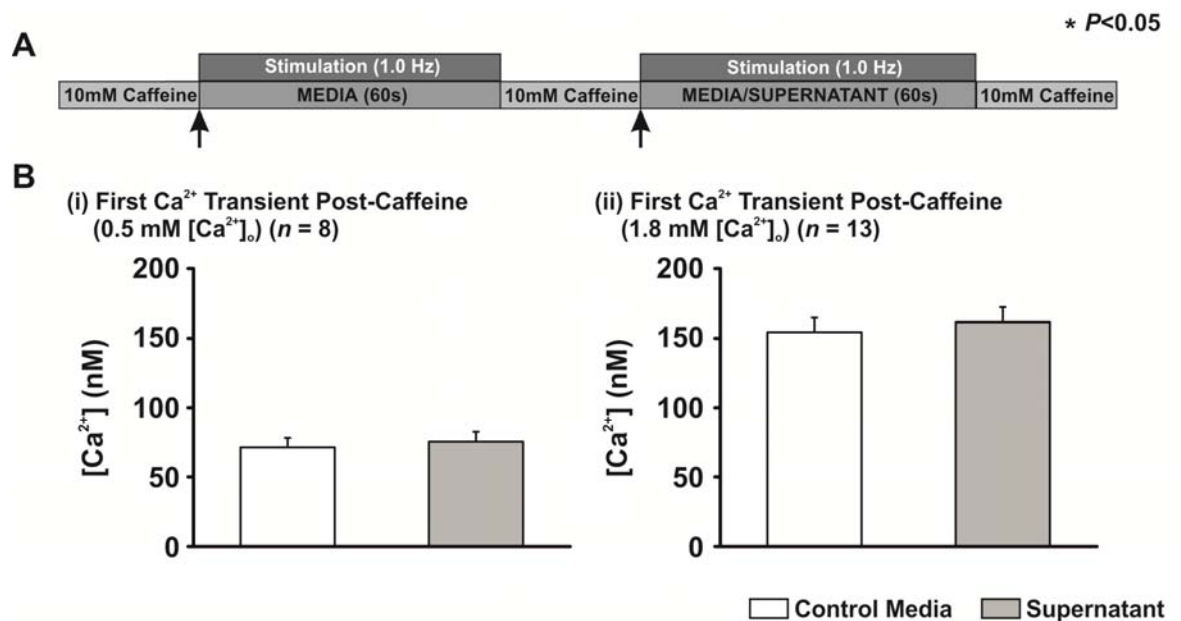


Figure 4.6: First post-caffeine Ca^{2+} amplitude at low and normal extracellular Ca^{2+} . (A) Protocol for epifluorescence Ca^{2+} measurements, arrows indicate point of the protocol Ca^{2+} transient amplitudes were measured. (B) Mean \pm SEM for first post-caffeine Ca^{2+} transient amplitude for media (open) and supernatant (grey) for (i) 0.5 mM $[\text{Ca}^{2+}]_o$ ($n = 8$) and (ii) 1.8 mM $[\text{Ca}^{2+}]_o$ ($n = 13$).

4.3.6 Supernatant Alteration of SR Function is CaMKII Dependent

To examine whether CaMKII or PKA are involved in the action of supernatant on SR function, inhibitors of these kinases were utilised in cohorts of cardiomyocytes incubated in control media or supernatant as described in Chapter 3 (section 3.2.3). The number of cells exhibiting spontaneous contractions per min was noted. The expected increase in spontaneous contractile events in supernatant was abolished in the presence of the CaMKII inhibitor AIP to 104% of media + AIP levels ($P > 0.05$; Figure 4.7A(i)). When the PKA inhibitor H-89 was used the increase in spontaneous contractile events with supernatant was increased as expected to 129% of media + H-89 ($P < 0.05$; Figure

4.7A(ii)). These experiments were performed in conjunction with Ms. Charlotte Rossor, a Masters student who was under my supervision at the time and presented in her thesis.

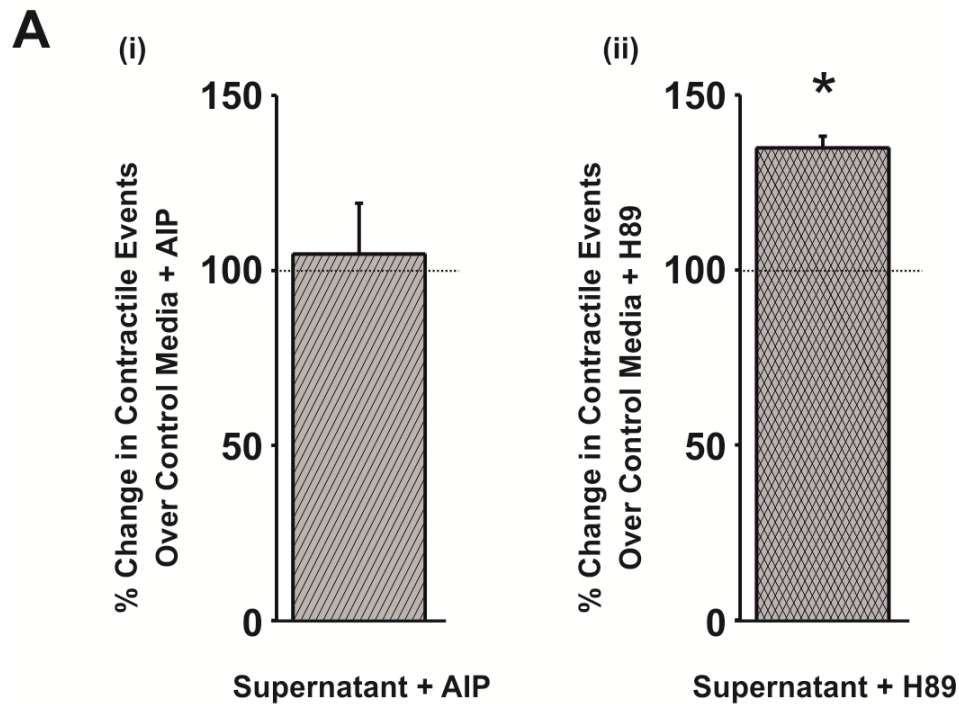


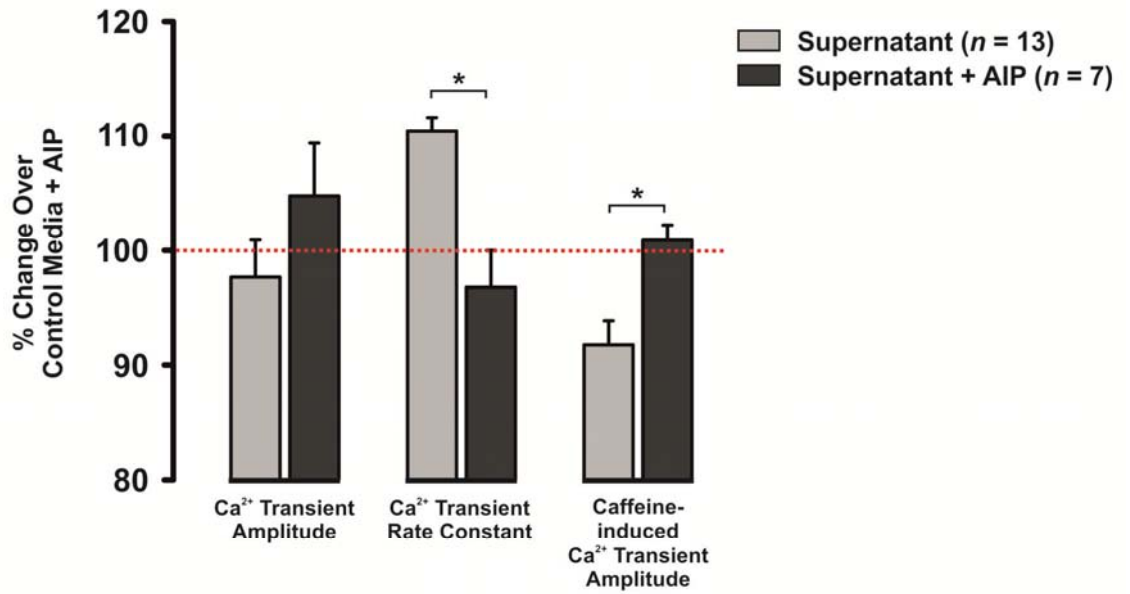
Figure 4.7: Percentage change in spontaneous contractile events with AIP or H89. Mean \pm SEM percentage change in cardiomyocytes with spontaneous contractile events with (i) supernatant + AIP ($n = 307$) vs. media + AIP ($n = 121$) and (ii) supernatant + H-89 ($n = 377$) vs. media + H-89 ($n = 305$).

4.3.7 Supernatant Effects on Ca^{2+} Handling with CaMKII Inhibition

Since the increase in spontaneous contractile events expected in supernatant was abolished by CaMKII inhibition but not PKA inhibition, further epifluorescence Ca^{2+} measurements were made with the addition of AIP. A separate cohort of cardiomyocytes were incubated with 10 μM AIP for 60 min before being loaded into a tissue bath and superfused with media for 1 min followed by supernatant for 1 min with 1.8 mM $[\text{Ca}^{2+}]_o$. Parallel time-control experiments were also performed in which cardiomyocytes were perfused with control media during the second 1 min to which the control media/supernatant traces were normalised to control for any alterations in the stimulated Ca^{2+} transients due to time. When the cardiomyocytes were perfused with supernatant and AIP, there was no significant difference in the Ca^{2+} transient amplitude percentage change (97.7 ± 3.2 vs. $104.8 \pm 4.6\%$; supernatant vs. supernatant + AIP; $P > 0.05$; Figure 4.8A). With AIP the significant increase in Ca^{2+}

transient decay rate percentage change was reduced to control levels (110.4 ± 1.2 vs. $96.8 \pm 3.2\%$; supernatant vs. supernatant + AIP; $P < 0.05$; Figure 4.8A). The significant reduction in SR Ca^{2+} content present with supernatant was abolished by addition of AIP (91.8 ± 2.1 vs. $100.1 \pm 1.3\%$; supernatant vs. supernatant + AIP; $P < 0.05$; Figure 4.8A). Experiments utilising thapsigargin and ryanodine to inhibit SR function were performed using the same protocol as that used to generate the data in Figure 4.5. In contrast with the data shown so far for AIP, there was no change in result. Supernatant + AIP showed the same significant elevation in diastolic $[\text{Ca}^{2+}]_i$ (Figure 4.8B) as supernatant (Figure 4.5).

A



B

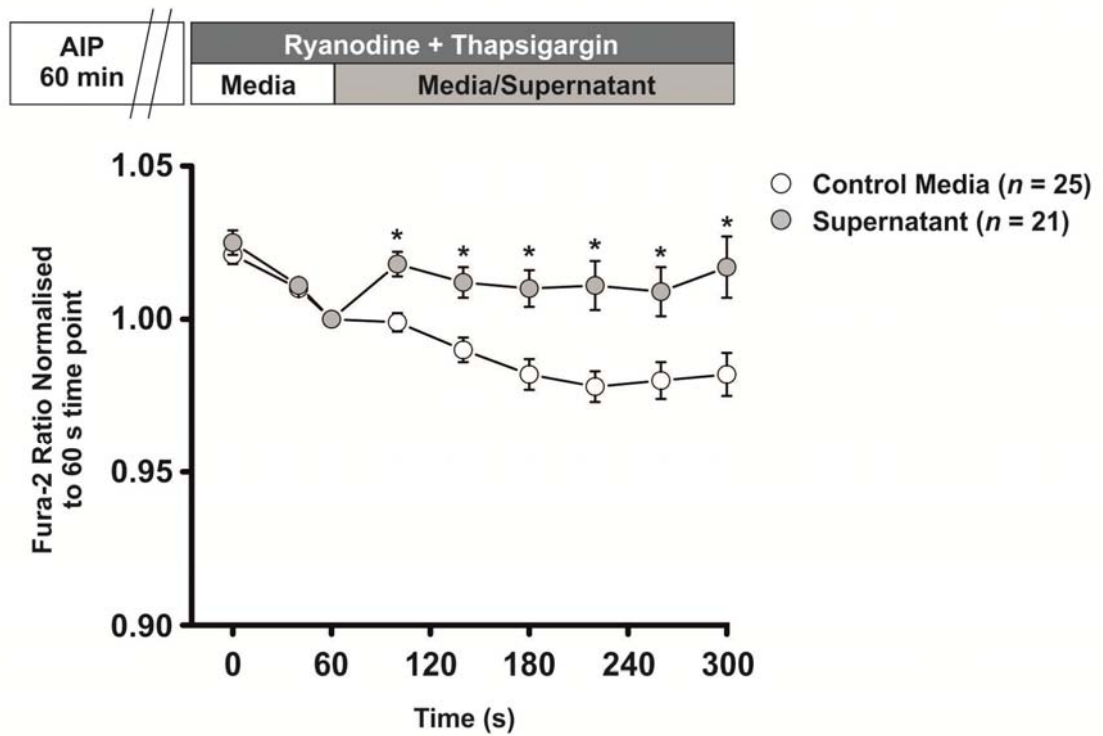


Figure 4.8: Supernatant effects on Ca²⁺ parameters with AIP.

(A) Mean \pm SEM % change in supernatant \pm AIP over control media for stimulated Ca²⁺ transient amplitude, Ca²⁺ transient decay rate constant and SR Ca²⁺ content. (B) Diastolic [Ca²⁺]_i measurements with inhibited SR in cardiomyocytes pre-incubated with 10 μ M AIP for 60 min.

4.4 Discussion

4.4.1 Supernatant Effects on SR Function

4.4.1.1 SERCA Activity is Increased by Supernatant

In Chapter 3 the data presented showed an increase in the decay rate constant (Figure 3.4) in the cohort of cardiomyocytes perfused with supernatant. This was attributed to a potential increase in SERCA activity (K_{SERCA}) which led to an increase in spontaneous Ca^{2+} release from the SR. However this was difficult to reconcile without a significant change in the SR Ca^{2+} content. Therefore paired experiments were conducted where the same cardiomyocyte was perfused with media followed by supernatant and normalised to time-controls perfused with media. This enabled more accurate assessment of Ca^{2+} transient parameters and SR Ca^{2+} content. The paired experiments supported the findings in Chapter 3 with a significantly increased stimulated Ca^{2+} transient decay rate constant of 110.4% of control in 1.8 mM $[Ca^{2+}]_o$, and again in 0.5 mM $[Ca^{2+}]_o$ of 111.1% (Figure 4.2). As discussed in Chapter 3 a faster rate of stimulated Ca^{2+} transient decline is either explained by faster SR reuptake by SERCA, or faster sarcolemmal extrusion predominantly by NCX⁽¹⁵⁸⁾. Although other Ca^{2+} extrusion mechanisms such as the PMCA and mitochondria do contribute, it is <25% of total Ca^{2+} extrusion^(222;223) over almost ten times longer than extrusion by NCX⁽²²⁴⁾. To rule out faster sarcolemmal extrusion a rapidly applied bolus of high concentration caffeine can be used to open the RyR and empty the SR of Ca^{2+} . The decay rate constant of the caffeine-induced Ca^{2+} transient will consist of sarcolemmal Ca^{2+} efflux without any SR contribution in the continued presence of caffeine, which can be measured. No statistically significant difference in caffeine-induced Ca^{2+} transient decay rate was found therefore NCX involvement is unlikely. In addition the caffeine-induced Ca^{2+} transient decay rate constant (sarcolemmal efflux but no SR reuptake) can be subtracted from the stimulated Ca^{2+} transient decay rate constant (sarcolemmal efflux and SR reuptake) to give the SR reuptake or K_{SERCA} ⁽⁵⁰⁶⁾. When this is performed the K_{SERCA} percentage change is $114.3 \pm 2.2\%$ of media control at 1.8 mM $[Ca^{2+}]_o$ which compares well with the $110.4 \pm 1.2\%$ observed when using the rate decay constant of the electrically induced transient alone (Figure 4.2C(v)). The same is true for 0.5 mM $[Ca^{2+}]_o$, the subtracted decay rate constant % change is $117.3 \pm 2.3\%$ over control media

which compares well with $111.1 \pm 2.2\%$ over media control when using the rate decay constant of the electrically induced transient alone (Figure 4.2D(v)). Therefore we can conclude that K_{SERCA} is significantly increased by 10-15% at 1.8 mM $[\text{Ca}^{2+}]_o$ and 11-17% in 0.5 mM $[\text{Ca}^{2+}]_o$.

4.4.1.2 SR Ca^{2+} Content is Reduced by Supernatant

Chapter 3 demonstrated an increase in Ca^{2+} frequency which has been attributed to increased SERCA stimulation, leading to increased SR Ca^{2+} accumulation rate and subsequent decreased time between spontaneous Ca^{2+} release events^(192;503), which was observed (Figure 4.2). There was also an increase in Ca^{2+} wave velocity, which has been shown to be related to increased SERCA activity⁽⁵⁰³⁾. However, if this were the only effect supernatant had we would expect an increase in the SR Ca^{2+} content from the greater Ca^{2+} accumulation rate. This was not observed in the data presented in Chapter 3. When the more sensitive paired experiments were conducted, what was observed was in fact a significant reduction of the SR Ca^{2+} content of 91.7% at 1.8 mM $[\text{Ca}^{2+}]_o$, and 80.3% in 0.5 mM $[\text{Ca}^{2+}]_o$, by measurement of the caffeine-induced Ca^{2+} transient amplitude. Therefore, the hypothesis is that the supernatant, in addition to the SERCA effects, may also enhance SR-mediated Ca^{2+} leak. This may explain an increase in SERCA activity with concomitant decrease in SR Ca^{2+} content. Indeed, it has been identified in by Antoons *et al.* (2006) in the muscle-LIM-protein (MLP) knock-out mouse that SERCA activity can be increased without an increase in SR Ca^{2+} content⁽⁵²¹⁾. The same study found that the inhibitory peptide of SERCA, phospholamban (PLB) has increased levels of phosphorylation at both the serine-16 and threonine-17 residues which would enhance SERCA activity⁽⁵²¹⁾. Antoons *et al.* hypothesised that in order for SR Ca^{2+} content to be unaffected yet SERCA activity to be increased, there could be a concomitant increase in diastolic Ca^{2+} leak from the RyR potentially mediated by increased phosphorylation⁽⁵²¹⁾. They measured phosphorylation at the PKA phosphorylation site serine-2809 identified by Rodriguez *et al.* (2003)⁽⁵²²⁾ but found only a modest increase attributable to increased total RyR therefore hypothesised that CaMKII could be phosphorylating the serine-2815 residue^(523;524) and may therefore be the mediator⁽⁵²¹⁾. If there is a similar mechanism involved with supernatant then there could be dual effects on SERCA perhaps *via* PLB and on the RyR phosphorylation altering the open probability (P_o). If the RyR P_o is increased then the threshold SR Ca^{2+} content

would be reduced increasing the frequency of Ca^{2+} waves⁽¹⁹²⁾. Specifically, a reduced SR Ca^{2+} release threshold would mean that less Ca^{2+} in the SR could trigger a spontaneous Ca^{2+} release. Therefore spontaneous Ca^{2+} release or Ca^{2+} waves would increase in frequency due to the lower SR Ca^{2+} release threshold. In heart failure it has been reported that there is an increased Ca^{2+} leak from the RyR caused by hyperphosphorylation of the RyR leading to dissociation of the regulatory protein FKBP12.6⁽²⁷⁶⁾. However, this hypothesis is controversial as phosphorylation of the RyR in different models of heart failure is inconsistent^(276-279;525). There is evidence to suggest increased diastolic Ca^{2+} leak from the RyR due to phosphorylation by PKA^(276;324), CaMKII^(277;311) or no phosphorylation⁽²⁷⁹⁾. The fact that AIP can abolish the increase in Ca^{2+} waves but that H-89 does not, suggests the effect observed in the current study may be CaMKII mediated phosphorylation, however to confirm this phosphorylation status of the RyR would need to be examined. The increased leak can have the result of a reduced SR Ca^{2+} content and the increased P_o can increase Ca^{2+} wave frequency leading to arrhythmias^(273;322;526) and can also occur with increased SERCA activity⁽⁵²¹⁾. This would not necessarily result in a reduced stimulated Ca^{2+} transient amplitude⁽⁵²⁷⁾, which supports the results of the current study. In the presence of β -adrenergic stimulation there can be an increase in RyR leak and sustained increase in Ca^{2+} waves^(192;320), which supports the data presented in Chapter 3 and appears to be modulated by CaMKII but not PKA⁽³²⁰⁾.

4.4.2 Supernatant Does Not Alter Myofilament Ca^{2+} Sensitivity

One explanation for an increased K_{SERCA} is altered myofilament Ca^{2+} sensitivity⁽⁵¹⁷⁾. During the normal contractile cycle Ca^{2+} is released from the SR into the cytosol and binds to troponin C (TnC) of the myofilaments facilitating the hydrolysis of ATP by the myosin ATPase to provide the energy for formation of the cross-bridges and the power stroke of the contraction. In order for the myofilaments to relax during diastole when $[\text{Ca}^{2+}]_i$ reduces the myosin ATPase must provide more ATP to break the cross-bridges⁽¹⁴⁸⁾. Under normal circumstances, Ca^{2+} released from the SR binds to TnC⁽⁵²⁸⁾. Therefore a decrease in myofilament Ca^{2+} sensitivity would reduce the Ca^{2+} buffering capacity of the myofilaments and therefore increase the diastolic $[\text{Ca}^{2+}]_i$ ⁽¹⁴⁸⁾. Decreases in Ca^{2+} buffering would be predicted to increase the available free Ca^{2+} for the stimulated Ca^{2+} transient as the myofilaments would have a reduced binding

capacity⁽⁵¹⁷⁾. This would result in an increased peak $[Ca^{2+}]_i$ and an increased rate of Ca^{2+} transient decay^(529;530), which has been shown experimentally with exogenous Ca^{2+} buffers⁽⁵³¹⁾. Alteration of myofilament Ca^{2+} sensitivity is therefore a potential mechanism of the increased K_{SERCA} observed in the current study. With decreased Ca^{2+} sensitivity of the myofilaments a greater $[Ca^{2+}]_i$ would be required to induce the same force of contraction or change in cardiomyocyte length⁽¹⁴⁸⁾. Cardiomyocyte length was measured in parallel with Ca^{2+} epifluorescence measurements by edge detection software (Ionoptix) in field stimulated cells. The change in length relative to diastolic cardiomyocyte length was calculated and the percentage change in length or fractional shortening calculated for media and supernatant normalised to time-controls. There was no statistically significant difference, suggesting that supernatant did not alter the fraction that cardiomyocytes contract during normal stimulation. At end-diastole the rate of change of $[Ca^{2+}]_i$ are minimal, thus these values can be used to assess myofilaments Ca^{2+} sensitivity in the intact cell. No significant alteration in myofilaments Ca^{2+} responsiveness is induced by the supernatant as shown in Figure 4.4C suggesting therefore that its contribution to the decline of the Ca^{2+} transient observed is not significant. The supernatant is therefore likely to be having an effect on SERCA independent of myofilament Ca^{2+} sensitivity.

4.4.3 Effects of Supernatant on Diastolic $[Ca^{2+}]_i$

Isolated cardiomyocyte experiments where SR-mediated Ca^{2+} release and uptake was inhibited (Figure 4.5) revealed that supernatant elevated $[Ca^{2+}]_i$ compared with control media. These experiments do not discriminate between reduced Ca^{2+} efflux and enhanced Ca^{2+} influx. However an increased diastolic $[Ca^{2+}]_i$ may favour spontaneous Ca^{2+} release from the SR in the form of Ca^{2+} sparks and waves⁽¹⁹⁵⁾ *via* an increased K_{SERCA} ⁽⁵⁰⁷⁾. One potential mechanism for this increase in diastolic $[Ca^{2+}]_i$ is reduced Ca^{2+} efflux *via* reduced NCX activity, the main efflux pathway. This does not appear to be the case in cardiomyocytes exposed to supernatant as the decay rate constant of the caffeine-induced Ca^{2+} was not significantly altered (Figure 4.3). Alternatively, the increase in diastolic $[Ca^{2+}]_i$ could be a result of increased influx through the LTCC as the inward Ca^{2+} current serves to trigger Ca^{2+} release from the SR but also to load the cardiomyocyte with Ca^{2+} to balance the sarcolemmal efflux⁽¹⁸²⁾. Under normal circumstances the P_o of the LTCC during diastole is low ($\approx 10^{-5}$) at resting membrane potential (-

80 mV)⁽⁵³²⁾. Choi *et al.* (2000) measured Ca^{2+} influx and efflux in quiescent rat ventricular cardiomyocytes and found a small component of influx sensitive to nifedipine, a LTCC blocker⁽⁵³³⁾. They used a holding potential of -40 mV (more positive than resting) but identified that $0.8 \mu\text{M}\cdot\text{l}^{-1}\cdot\text{s}^{-1}$ Ca^{2+} flux sensitive to nifedipine. As a result, they calculated the P_o at resting potential of 0.006. They identified that much of the Ca^{2+} influx in quiescent cardiomyocytes was Ni^{2+} sensitive, a blocker of NCX, and therefore potentially due to NCX activity in reverse mode⁽⁵³³⁾. Ni^{2+} though lacks specificity so other Ca^{2+} influx mechanisms could not be ruled out⁽⁵³³⁾. The data in the current study suggests no alteration of the NCX due to no significant differences in caffeine-induced Ca^{2+} transient decay. Schröder *et al.* identified that β -adrenergic stimulation either β_1 or β_2 could increase the P_o of the LTCC such that it was activated in physiological Tyrodes solution at resting membrane potential⁽⁵³⁴⁾. Thus P_o can be altered in the presence of a β -adrenergic agonist to increase the current through the LTCC^(532;535;536). Therefore supernatant could alter the LTCC P_o increasing the Ca^{2+} influx during diastole leading to a higher diastolic $[\text{Ca}^{2+}]_i$. To examine whether the LTCC current could be altered usually requires electrophysiological measurements of the LTCC current. However, LTCC modulation can be assessed indirectly if the amplitude of first Ca^{2+} transient following a bolus of high concentration caffeine (10 mM) is measured. The principle is that the caffeine increases the P_o of the RyR to 1 thereby effectively emptying the SR so it will no longer contribute to Ca^{2+} release. When field stimulation is applied, the change in $[\text{Ca}^{2+}]_i$ will primarily be due to Ca^{2+} influx through the LTCC⁽⁵³⁷⁾. Eisner *et al.* (2000) applied 10 mM caffeine immediately prior to a stimulation protocol that effectively emptied the SR of Ca^{2+} and measured the Ca^{2+} transients while simultaneously measuring the current across the LTCC. The amplitude of the first Ca^{2+} transient post caffeine was significantly less than the last Ca^{2+} transient but the current across the LTCC was not changed. This suggests that the difference in Ca^{2+} transient amplitude is due to the initial SR emptying and subsequent refilling with Ca^{2+} ⁽⁵³⁷⁾. Therefore the amplitude of the first post caffeine Ca^{2+} transient was used as an indicator of Ca^{2+} influx through the LTCC. The amplitude of the first post-caffeine Ca^{2+} transient was not altered with perfusion of supernatant compared to control media suggesting that the LTCC is not altered (Figure 4.6). Under some conditions, in some species, there may be Ca^{2+} entry *via* reverse NCX activity⁽⁵⁰⁷⁾, although the data presented in the

current study suggests no alteration of NCX activity in the presence of supernatant. There is some evidence to support another method of Ca^{2+} influx independent of the LTCC and NCX reversal but the mechanism remains unclear⁽⁵³⁸⁾.

4.4.4 Increase in Spontaneous Ca^{2+} Release Caused by Supernatant is Prevented by CaMKII Inhibition

The supernatant effects on K_{SERCA} and SR Ca^{2+} content coupled with increased spontaneous Ca^{2+} release support a hypothesis consistent with a potential β -adrenergic stimulation phenotype. β -adrenergic stimulation has the effects of; i) increased RyR phosphorylation increasing P_o ^(276;539) and SR Ca^{2+} leak^(299;323), ii) increased LTCC current⁽¹⁵³⁾ via PKA mediated phosphorylation, iii) increased K_{SERCA} via phosphorylation of the SERCA inhibitory molecule phospholamban (PLB) decreasing SERCA inhibition via PKA activity^(239;240;243) and CaMKII activity^(240;244;245), and finally, iv) altered myofilament Ca^{2+} sensitivity⁽¹⁴⁸⁾.

Although the data in the present study did not identify alterations in myofilament Ca^{2+} sensitivity or a detectable increase in LTCC current, the potential effects on SERCA and RyR suggest there may be a role for PKA and/or CaMKII therefore both PKA and CaMKII were investigated further. A cohort of isolated cardiomyocytes was incubated in control media and supernatant as discussed in Chapter 3 (section 3.2.3) with the PKA inhibitor H89. The percentage change in number of cardiomyocytes exhibiting at least one spontaneous contractile event in 1 min over media control was calculated. A separate cohort was treated with the CaMKII inhibitor AIP. H89 did not change the increase in spontaneous contractile events observed in supernatant suggesting that the increased spontaneous Ca^{2+} release caused by supernatant was not PKA mediated. However, when cardiomyocytes were treated with AIP the increase in contractile events in supernatant was abolished, suggesting the effect may be CaMKII mediated. In a study by Kholhaas *et al.* (2006) enhanced SR Ca^{2+} leak caused by overexpression of CaMKII was prevented by AIP without significantly altering the Ca^{2+} transient amplitude⁽³²¹⁾.

4.4.5 CaMKII Inhibition Prevents Supernatant Effects on SR Function

4.4.5.1 SERCA Activity Increase in Supernatant Prevented by AIP

Given the result of CaMKII inhibition on spontaneous contractile events the Ca^{2+} epifluorescence experiments were repeated with AIP at normal $[\text{Ca}^{2+}]_i$. There was no change in the peak and $[\text{Ca}^{2+}]_i$ amplitude of the stimulated Ca^{2+} transient when AIP was added to the supernatant. In the presence of AIP the increase in decay rate constant caused by supernatant was reduced from 110.4% to 104.8% of control media. These data support a hypothesis of CaMKII mediated enhanced SERCA activity. Indeed, it has been shown by Picht *et al.* (2007) that SR-localised AIP can inhibit a CaMKII-mediated enhancement of SERCA-mediated Ca^{2+} uptake and inhibit CaMKII-mediated phosphorylation of the RyR reducing diastolic Ca^{2+} leak⁽⁵⁴⁰⁾. Since AIP reduces both SR-mediated spontaneous Ca^{2+} release and K_{SERCA} to the levels of control media in the data presented in this chapter, the potential mechanism by which supernatant acts is *via* enhanced CaMKII activity.

4.4.5.2 SR Ca^{2+} Content Reduction in Supernatant Prevented by AIP

The reduced caffeine-induced Ca^{2+} transient amplitude in supernatant was also prevented by AIP. SR Ca^{2+} in supernatant with AIP was at 100.1% compared to 91.7% in control media. When considered with the concomitant reduction in spontaneous Ca^{2+} release without Ca^{2+} transient amplitude alteration a hypothesis of reduced CaMKII mediated SR Ca^{2+} leak due to inhibition with AIP seems likely and is supported by Kholhaas *et al.* (2006)⁽³²¹⁾. In the SR-AIP transgenic mouse of Picht *et al.* (2007) there was a significant reduction in diastolic Ca^{2+} leak from the SR measured as tetracaine-induced shifts in cytosolic Ca^{2+} ⁽⁵⁴⁰⁾. Tetracaine-induced shifts work by blocking the RyR thereby preventing Ca^{2+} leak. When applied in a Na^+ and Ca^{2+} free solution the SR Ca^{2+} content rises and cytosolic Ca^{2+} declines directly proportionally to the leak⁽³²³⁾.

4.4.6 CaMKII Inhibition Does Not Reduce Diastolic $[\text{Ca}^{2+}]_i$

Interestingly, when the experiments with SR inhibition by thapsigargin and ryanodine were repeated, the increase in diastolic $[\text{Ca}^{2+}]_i$ in supernatant was not

AIP-sensitive. The experiments performed in the current study do not differentiate between reduced Ca^{2+} efflux or enhanced Ca^{2+} influx, but increased diastolic $[\text{Ca}^{2+}]_i$ may favour the production of abnormal SR Ca^{2+} release *via* CaMKII activation⁽⁵⁴¹⁾. One potential mechanism for increased diastolic $[\text{Ca}^{2+}]_i$ is reduced NCX activity, the main sarcolemmal extrusion process. However, the data in the current study suggests no effect on NCX function. Alternatively supernatant may have enhanced Ca^{2+} influx but this is unlikely to be due to the LTCC as no difference in first post caffeine Ca^{2+} transient was apparent and is unlikely in quiescent cells⁽⁵³³⁾. Therefore supernatant may increase diastolic $[\text{Ca}^{2+}]_i$ by another means such as those seen in human brain microvascular endothelial cells (HBMECs)⁽⁶⁹⁾, an effect potentially mediated by TbCatL action on a G-protein coupled receptor (GPCR)-mediated pathway⁽⁶⁶⁾. Further investigation in the direction of GPCR targets may reveal a potential sarcolemmal target for TbCatL.

4.4.7 Proposed Mechanism

Figure 4.9 summarises the proposed mechanism for the SR Ca^{2+} handling effects observed with trypanosome supernatant. CaMKII inhibition has the effect of abolishing the changes in Ca^{2+} transient decay and SR Ca^{2+} content that supernatant elicits. The fact that the increase in diastolic $[\text{Ca}^{2+}]_i$ is not prevented by CaMKII inhibition proposes a hypothesis that; supernatant elevates diastolic $[\text{Ca}^{2+}]_i$ (which could be substantial within sub-cellular compartments) that cause CaMKII activation⁽⁵⁴¹⁾, which then increases SR-mediated Ca^{2+} leak and uptake with a net effect being an increase in Ca^{2+} waves and a reduced SR Ca^{2+} content. These changes in basal and store-based Ca^{2+} signalling observed in cardiomyocytes parallel those seen in HBMECs exposed to live trypanosomes and their culture supernatant⁽⁶⁹⁾. The effect on HBMECs was *via* a G-protein coupled receptor (GPCR) pathway⁽⁶⁶⁾. Activation of this or a similar pathway in cardiomyocytes may underlie the supernatant effect on the heart. Further investigation may reveal this sarcolemmal target.

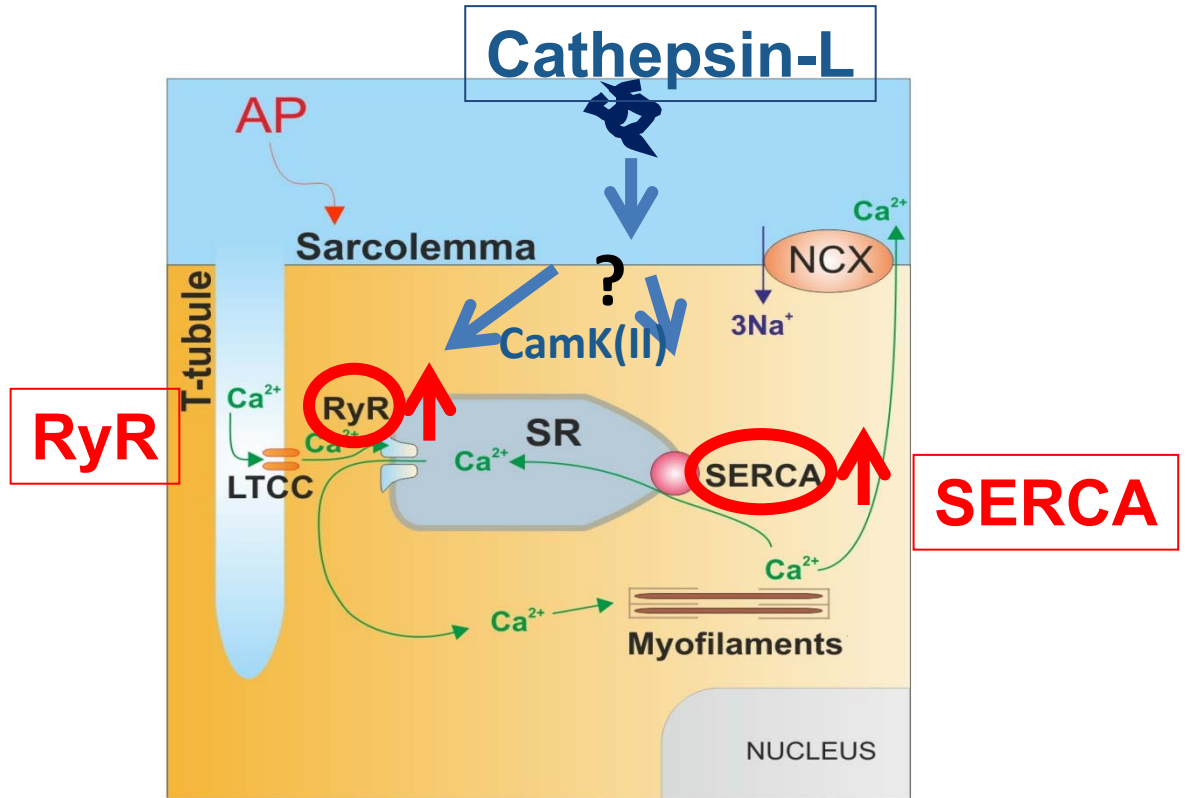


Figure 4.9: Proposed mechanism for TbCatL on Ca^{2+} handling in the ventricular cardiomyocyte

5 CHAPTER 5 – Investigating the Cardiovascular Effects of *Trypanosoma brucei* Using an *In Vivo* Infection Model in Rats

5.1 Introduction

5.1.1 Trypanosomiasis and the Heart

The classical focus of understanding trypanosomiasis has been the neurological signs, cardiovascular signs are evident both clinically⁽⁵¹⁾ and histopathologically in humans^(56;57) and experimentally infected animals⁽²⁶⁻²⁸⁾. The work in the preceding chapters demonstrates a direct effect of trypanosomes on the Ca^{2+} dynamics of cardiomyocytes facilitating the abnormal spontaneous diastolic release of Ca^{2+} that can lead to arrhythmias⁽¹⁹²⁾. This has implications not only in how HAT manifests in patients but in treatment as well. The main consideration with treatment of HAT is the stage of the disease. Stage II, once neurological signs are evident, signifies that the parasites have traversed the blood brain barrier (BBB). Therefore, treatment strategies for Stage II HAT require drugs that cross the BBB. Several of the drugs have low therapeutic margins before adverse reactions are evident⁽⁸⁾. Indeed treatment-induced cardiopathy and drug cardiotoxicity has been suspected in cases of sudden death in HAT patients^(62;542-544), although it should be noted that these reports are uncontrolled studies of fewer than 10 patients. Therefore an understanding of the cardiac involvement of African trypanosomiasis may help in; i) the development of new drugs and ii) understand and be prepared for cardiotoxicity of existing or new drugs.

There are parallels between the role of induction of Ca^{2+} fluxes by TbCatL in cardiomyocytes and in endothelial cells⁽⁶⁹⁾ which also resembles the induction of Ca^{2+} transients with *T. cruzi* causing American trypanosomiasis (Chagas disease)⁽⁵⁰⁸⁾. Therefore understanding the cardiac effects of trypanosomiasis may enable the development of drugs that are safer with regard to cardiotoxicity. Interestingly, if TbCatL is a common causative factor in alterations in Ca^{2+} dynamics in both cardiomyocytes and BBB traversal inhibition of TbCatL may also reduce BBB traversal.

5.1.2 Electrocardiographic Findings

Recent work has begun to look at some of the functional aspects of cardiac involvement in HAT. A detailed study by Blum *et al.* (2007) assessed the ECGs of patients with Stage II *T. b. gambiense* HAT and compared them to those of

healthy controls⁽⁵¹⁾. They identified a number of differences summarised in Table 5.1. Major changes were defined as low voltage and PR depression which occurred at in 71% of HAT patients⁽⁵¹⁾. They compared this to the frequency of histopathological findings on post-mortem examination of 72%^(55;56). The repolarisation changes and low voltage were identified at the end of treatment which then improved/disappeared 3 months after treatment⁽⁵¹⁾, which they attributed to treatment induced/exacerbated inflammation based on anecdotal reports^(62;542-544) of drug-induced cardiotoxicity.

Table 5.1: ECG findings in patients with HAT

	Healthy Controls		HAT Patients		P value
	n	%, mean ± SD	n	%, mean ± SD	
PQ	60	163 ± 16.07 ms	59	168 ± 26 ms	0.24
QRS	60	82 ± 10.97 ms	59	81.6 ± 8.3 ms	0.79
QTc	60	403 ± 21.01 ms	59	423 ± 3.2 ms	<0.001
Normal (no abnormal findings)	60	65%	59	22%	<0.001
Major changes	60	18%	59	71%	<0.001
Low voltage	60	7%	59	31%	<0.001
AV block I	60	3%	59	8%	0.23
PR depression	60	0%	59	8%	0.007
Repolarisation changes	60	5%	59	34%	<0.001
Precordial repolarisation changes	60	2%	59	22%	<0.001

Data from Blum *et al.* (2007)⁽⁵¹⁾ used with permission. Major changes were defined as; low voltage, AV block I, PR depression and repolarisation changes.

5.1.3 Aims of the Chapter

Cardiac signs in HAT are usually attributed to perimyocarditis^(26-28;51;56;58;61;496). However, the data in this thesis offers an alternative explanation for cardiac signs at the cellular and *ex vivo* organ level. The main aim of this chapter is to develop an animal model of trypanosome infection to enable detailed study of

electrocardiographic effects of trypanosomes *in vivo*. Ultimately, the model could be able to be used in future studies to dissect the contribution of a direct parasite induced pathology from a systemic immune response and identify potential changes in electrocardiographic profile in response to potential drug treatments. In addition, clinical infections of trypanosomiasis are often complicated by concomitant infections with other diseases. For example, Blum *et al.* (2007) found a co-infection rate of 13.3% with malaria which had the effect of further prolonging QTc from 419 ± 22 ms in confirmed cases without malaria, to 438 ± 29 ms in cases with confirmed malaria⁽⁵¹⁾. A controlled experimental infection model with ECG monitoring should avoid many of the complicating factors inherent in patient studies.

5.2 Methods

5.2.1 *T. b. brucei* Lister 427 Infections

5.2.1.1 Preparation of Trypanosomes

Trypanosoma brucei brucei Lister 427 were grown for one passage in mice to adapt them to *in vivo* conditions from being culture adapted. Lister 427 has been grown since the 1960s⁽⁵⁴⁵⁾ in media with nutrients in excess thus reducing many of the selection pressures normally found *in vivo*. Therefore, this passage is important to re-adapt the parasites to growth in the mammalian bloodstream for *in vivo* studies. This step was performed by Mrs. Anne-Marie Donachie, a technician from the Wellcome Trust Centre for Molecular Parasitology, University of Glasgow. The parasites were grown in the mice for 2-3 days with daily tail venepuncture to check parasitaemia levels. When parasites reached 1×10^7 parasites.mL⁻¹ the mice were sacrificed and blood collected in heparin to prevent coagulation. A sample of the blood was counted with a Neubauer improved haemocytometer in triplicate. The parasites were diluted under sterile conditions to 1×10^5 parasites in a 200 μ L volume of Carter's balanced salt solution (CBSS); 25 mM HEPES, 120 mM NaCl, 5.4 mM KCl, 0.55 mM CaCl₂, 0.4 mM MgSO₄, 5.6 mM Na₂PO₄ and 11.1 mM glucose, pH 7.4. The 200 μ L parasite suspension was prepared in a 1 mL syringe for injection. Matching volumes of CBSS were prepared as control injections.

5.2.1.2 ECG Acquisition

Adult male Wistar rats (250-300 g) were allowed a 7 day acclimatisation period upon delivery to the biological services unit. Animals were kept at the Cardiovascular Research Unit, University of Glasgow in a dedicated room licensed under the Specified Animal Pathogens (Scotland) Order 2009 (SAPO). Rats were anaesthetised by inhalation of isoflurane gas at 4-5% delivered in 1-1.5 L.min⁻¹ oxygen in an induction box. The rats were removed from the box when there was loss of the righting reflex. The animals were maintained on isoflurane delivered *via* facemask. The gas was reduced based on assessment of the animals' vital parameters to a final plane of anaesthesia at 1-1.5% isoflurane in 1 L.min⁻¹ O₂. The ECG was recorded *via* the placement of intradermal electrodes. The placement sites on the rat were caudal aspects of the left and right carpi

and the medial aspects of left and right crura. The sites were cleaned with chlorhexidine as were the electrode tips. Appropriate earthing and positioning was used to minimise signal noise. To ensure reproducibility for the same rats and between rats, all animals were positioned identically based on an outline drawn on a corkboard. The ECG was recorded for 15 min with an IWX228 bioamplifier (iWorx, USA). Rats were then injected *via* the intraperitoneal route with the solutions prepared above (section 5.2.1.1). The ECG was recorded for a further 15 min following the injection before rats were recovered. See General Methods for images of the procedure.

5.2.1.3 Health Monitoring and Parasitaemia Checks

Infection with *T. brucei* Lister 427 can cause anaemia, weight loss and immunosuppression. In some cases the parasitaemia can become fulminant, which can be fatal if allowed to persist. The general health of the animals was monitored daily to ensure that welfare was not compromised by the parasite infection. Animals were assessed for lassitude persisting beyond 72 hours, weight loss $\geq 25\%$, mucous membrane pallor, hunched posture and staring coat. In addition, parasitaemia levels were measured daily. A drop of blood was obtained by a small puncture of the lateral tail vein. The drop of blood expressed was smeared to a glass slide and viewed with a 40x objective lens on a standard light microscope. The slide was examined and the number of parasites counted and compared to the description of Herbert and Lumsden (1976)⁽⁴³⁶⁾ and described in further detail in section 2.2.1.3. A parasitaemia level exceeding 5.0×10^8 parasites.mL⁻¹ for more than two consecutive days was set as a cut-off point for the welfare of the animals. No animal exceeded this level during the study.

5.2.1.4 End ECG and Organ Harvest

Animals were anaesthetised on the fourth day after infection and the ECG recorded for 15 min as described above (section 5.2.1.2). Following ECG acquisition the animals were sacrificed by cervical dislocation while still under anaesthesia. Heart, liver and spleen were removed, mass recorded and compared to the tibial length defined as the length from lateral femoral

epicondyle proximally to the lateral malleolus distally to control for individual size and mass.

5.2.1.5 *In Vivo* ECG Data Analysis

ECG data were collected using the IWX228 bioamplifier and LabScribe 2 software (iWorx) at a sampling rate of 2,000 Hz. The ECG from the last 1 min (to ensure a steady state) of each 15 min period was averaged using the advanced ECG analysis module of the programme and exported to Origin6.1 (OriginLab) for R-R interval and heart rate, P-R interval and QT interval measurement with correction for heart rate using the Framingham method⁽⁴⁶⁰⁾. The whole trace was manually assessed for arrhythmic events as defined by the Lambeth Conventions⁽⁴³⁷⁾. Mean \pm SEM data for the same animal from day 0 and day 4 were compared with a paired Student's T-test. Comparisons between control and infected animals were conducted with a two-sample Student's T-test. $P < 0.05$ was taken to be statistically significant.

5.2.1.6 Langendorff Perfusion of *Ex Vivo* Hearts

The hearts removed from the infected and control rats were immersed in ice-cold Tyrodes solution; 116 mM NaCl, 20 mM NaHCO₃, 0.4 mM Na₂HPO₄, 1.0 mM MgSO₄·7H₂O and 4.0 mM KCl. D-glucose was added on the same day as intended use to a final concentration of 11 mM. The solution was bubbled with 95% O₂ / 5% CO₂ for 15-20 min to oxygenate and buffer before CaCl₂ was added to a concentration of 1.8 mM. Extraneous tissue was carefully dissected away to reveal the aorta. The hearts were blotted dry and quickly weighed before cannulation to a Langendorff perfusion apparatus. The hearts were perfused with Tyrodes solution at 10 mL·min⁻¹ and immersed in a water-jacketed chamber filled with Tyrodes solution at 37 °C. Electrodes were placed in the chamber in close approximation with the right atrium for the negative electrode and the apex of the left ventricle for the positive electrode and the pseudo-ECG recorded. Hearts were perfused for a period of 15 min steady state followed by 15 min periods each with the β -adrenergic agonist isoproterenol at concentrations of 100 nM, 1 μ M, 10 μ M and 100 μ M.

5.2.1.7 Langendorff Data Analysis

ECG data were collected using the ETH-256 bioamplifier (iWorx) and LabChart 7 (ADInstruments) software at a sampling rate of 2,000 Hz. The ECG from the last 5 min of each 15 min period was averaged using the advanced ECG analysis module of the programme and the R-R interval and heart rate, P-R interval and the QT interval with correction for heart rate using the Framingham method⁽⁴⁶⁰⁾ were measured. Traces were exported to Origin6.1 (OriginLab). The entirety of the traces was manually assessed for arrhythmic events according to the Lambeth Conventions⁽⁴³⁷⁾ and recorded as the frequency min^{-1} . Mean \pm SEM data for each isoproterenol concentration were compared to steady state for the same animal by paired Student's T-test. Comparisons between control and infected were performed with a two-sample Student's T-test. $P < 0.05$ was taken to be statistically significant.

5.2.2 *T. b. brucei* TREU 927 Infections

A limitation of *T. b. brucei* Lister 427 is that it follows a logarithmic growth curve *in vivo* until the death of the infected host. This is due to the fact that Lister 427 is a 'monomorphic' strain of *T. b. brucei* i.e. it grows in culture as the long slender bloodstream form of its lifecycle but has lost the ability to differentiate to the short stumpy stage⁽⁵⁴⁶⁾. While this makes 427 a highly useful *in vitro* model organism, it does not provide a robust model of trypanosome *in vivo* infections. During infections with wild-type 'pleomorphic' trypanosomes, as parasite numbers increase there is a density-dependent trigger for a proportion of the parasites to terminally differentiate to the short stumpy lifecycle stage⁽¹¹⁾ in preparation for transmission to the insect vector⁽¹²⁾. The trigger has not been identified but is a secreted factor putatively called 'stumpy induction factor' (SIF), which increases in concentration with the increase in parasitaemia^(11;547). The differentiation signal is cAMP-mediated⁽⁵⁴⁷⁾ but due to the long-term adaptation of 427 to *in vitro* culture and lack of selection for transmission, and therefore differentiation, 427 parasites do not differentiate under this trigger. Although SIF remains unidentified much of the regulatory pathways have been examined^(548;549). Clinical infections therefore exhibit a cyclical parasitaemia that reflects the balance between parasite replication and differentiation, as well as the host immune response, such as in cases of *T. brucei gambiense*

infection⁽¹⁰⁾. A pleomorphic strain of *T. b. brucei* that results in infections that more closely resemble the clinical situation of waxing and waning parasitaemia is *T. b. brucei* TREU 927⁽⁵⁵⁰⁾.

5.2.2.1 Preparation of Trypanosomes

The 927 parasites were prepared as described for 427 (section 5.2.1.1) by Anne-Marie Donachie. Blood taken from infected mice was examined and the parasites counted with a haemocytometer.

5.2.2.2 Telemetry Probe Implantation

A major limitation of the 15 min ECGs recorded for the 427 infections is the short window of observation. If arrhythmias are occurring at a low frequency, then a 15 min ECG may not detect them. The statistical power is also reduced. In addition the animals are under anaesthesia at the time of recording introducing potential cardiovascular depressive effects as a result of the use of inhalational agents such as isoflurane^(551;552). Therefore the decision was taken to implant CA-F40 biopotential recording devices (Data Sciences International) into rats to measure the ECG continuously in conscious animals for the duration of the study (10-12 days).

Briefly, adult male Wistar rats (250-300 g) were anaesthetised using an inhalational agent for the greater control and least cardio-respiratory depressive effects of anaesthetic agents compared with injectable anaesthetics⁽⁴³⁸⁾. The inhalational anaesthetic used was isoflurane (Isoflo, Abbot Laboratories, USA) delivered in 100% O₂. Animals were anaesthetised by placing them in a pre-filled induction box and maintained on a facemask initially with 4% isoflurane at 1.5 L.min⁻¹ reducing to 1-1.5% during surgery. Fur was clipped with electric clippers over the appropriate surgical sites for probe and lead placements (section 2.2.2.6). The clipped areas of skin were cleaned with warmed 10% surgical skin disinfectant (Hibiscrub, Ecolab Ltd) and gauze swabs. The animal was moved to the surgical table and positioned in ventral recumbency on a heated pad to maintain the animal's temperature. Peri-operative analgesia of 5 mg.kg⁻¹ carprofen (Rimadyl, Pfizer Animal Health) was administered with 5 mL of 0.9% sterile saline subcutaneously to maintain fluid balance under anaesthesia. The telemetry device was implanted subcutaneously in the dorsal thoracic region.

Tracts were tunnelled under the skin from the implant site to the right pectoral and xyphoid regions ventrally where the ECG leads were affixed with 1.5 metric nylon suture (Johnson & Johnson). The surgical incisions were closed with 1.5 metric polyglactan 910 (Vicryl, Johnson & Johnson). Further details and photographs of the procedure can be found in (section 2.2.2.2). A proportion of these procedures were performed in conjunction with Ms. Charlotte Rossor, a Masters student under my supervision.

5.2.2.3 Trypanosome Infections

The animals were allowed to recover from the surgical procedure for 1 week before they were infected as described for the 427 model in section 5.2.1.1. Infection was with 1.0×10^5 *T. brucei* 927 in 200 μ L CBSS *via* intraperitoneal injection. Control rats were injected with the same volume of CBSS. Rats were monitored daily for clinical signs of infection and parasitaemia levels by superficial tail venepuncture.

5.2.2.4 Data Acquisition and Analysis

Cages with implanted rats were placed onto receiver pads. The implanted probes were activated magnetically. Telemetry signals were relayed *via* a data exchange matrix to the computer loaded with the acquisition software Dataquest™ OpenART v4.2 (Data Sciences International). Raw ECG data was collected continuously at 2,000 Hz sampling frequency for 2 weeks and saved daily. Files were exported to Ponemah v4.8 (Data Sciences International) for analysis. ECG sections of 30 min were averaged and assessed for R-R interval, heart rate, P-R intervals and QT intervals corrected for heart rate using the Framingham method. Longer ECG traces of up to 1 hour were assessed for arrhythmias using the Lambeth Conventions as described in section 5.2.1.5.

5.2.2.5 Organ Harvest and Langendorff Perfusion

As with the 427 infections, rats were euthanized by cervical dislocation at the end of the study (or before if deemed to be suffering according to the clinical signs and parasitaemia checks previously described). The mass of the heart, lungs, liver and spleen was recorded and compared to tibial length. Hearts were immersed in ice-cold Tyrodes solution before being cannulated as described in

section 5.2.1.6. The same protocol was employed as the 427 study (section 5.2.1.6).

5.3 Results

5.3.1 *In Vivo* ECG Parameters for *T. b. brucei* Lister 427 Infection

Rats were anaesthetised and their ECGs recorded for the period of 15 min (Day 0) following infection by intraperitoneal injection with 1×10^5 *T. b. brucei* Lister 427 parasites in 200 μ L CBSS. A cohort of rats were injected with 200 μ L CBSS without parasites as controls. The animals were maintained and monitored for 4 days before being anaesthetised again and a final 15 min ECG recorded for each animal (Day 4). Each ECG trace was averaged and heart rate, P-R interval and QT intervals determined from the traces. There was no significant difference in the heart rate in the control animals between days 0 and 4 (249 ± 21 vs. 248 ± 21 bpm; Day 0 vs. Day 4; $n = 18$; $P > 0.05$; Figure 5.1B(i)), nor was there a significant difference in the infected animals (238 ± 19 vs. 226 ± 19 ; Day 0 vs. Day 4; $n = 17$; $P > 0.05$; Figure 5.1B(i)). There was no significant difference in P-R interval for the control rats (46.6 ± 0.8 vs. 46.4 ± 1.2 ms; Day 0 vs. Day 4; $P > 0.05$; Figure 5.1B(ii)), nor for the infected rats (46.4 ± 0.6 vs. 45.8 ± 0.8 ms Day 0 vs. Day 4; $P > 0.05$; Figure 5.1B(ii)). The QT changes with heart rate so a correction factor is required (QTc). The correction factor used in the current study is the Framingham method. Blum *et al.* (2007) identified a prolongation of QTc from 403 ± 24 ms to 423 ± 21 ms⁽⁵¹⁾. In the current model no alteration in QT was found in the controls between days 0 and 4 (63.3 ± 1.8 vs. 65.7 ± 1.6 ms; Day 0 vs. Day 4; $P > 0.05$; Figure 5.1B(iii)), and no significant change was found in the infected rats either (69.3 ± 3.0 vs. 66.3 ± 3.2 ms; Day 0 vs. Day 4; $P > 0.05$; Figure 5.1B(iii)). There was no significant difference in QTc for control (176.6 ± 3.0 vs. 179.1 ± 2.8 ms; Day 0 vs. Day 4; $P > 0.05$; Figure 5.1B(iv)) or infected animals (181.3 ± 3.9 vs. 176.2 ± 3.9 ms; Day 0 vs. Day 4; $P > 0.05$; Figure 5.1B(iv)). The classical end-point of the T wave is the return to the isoelectric point⁽⁴⁵⁷⁾. However, the T wave tended to approach the isoelectric point asymptotically making the true end of T difficult to define. As described in Chapter 3 (section 3.2.7) and Rees *et al.* (1993) the QT₉₀ was also measured for these ECGs⁽⁴⁵⁹⁾. As with the standard QT the QT₉₀ was not significantly altered in control (52.4 ± 1.3 vs. 53.6 ± 1.4 ms; Day 0 vs. Day 4; $P > 0.05$; Figure 5.1B(v)) or infected animals

(54.3 ± 2.3 vs. 53.0 ± 2.2 ms; Day 0 vs. Day 4; $P > 0.05$; Figure 5.1B(v)). When corrected for heart rate QTc_{90} was also unaffected for control (165.7 ± 2.9 vs. 167.1 ± 2.7 ; Day 0 vs. Day 4; $P > 0.05$; Figure 5.1B(vi)) and for infected animals (166.3 ± 4.1 vs. 162.9 ± 3.4 ; Day 0 vs. Day 4; $P > 0.05$; Figure 5.1B(vi)).

5.3.1.1 Arrhythmic Events

The ECGs were analysed for the occurrence of arrhythmic events as defined by the Lambeth Conventions⁽⁴³⁷⁾. During the 15 min periods of ECG for both the start and end of the study protocol no arrhythmic events were observed.

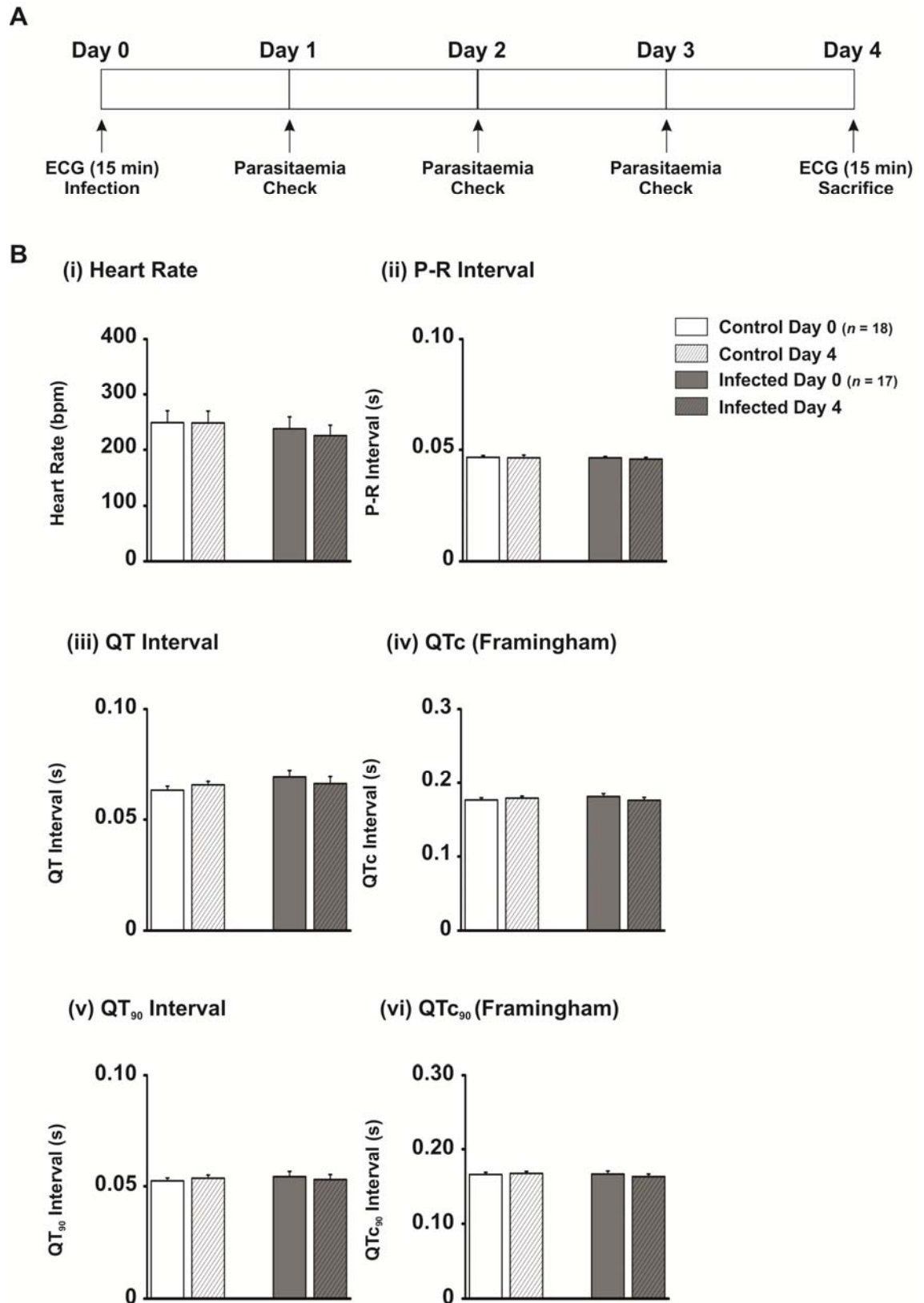


Figure 5.1: *In vivo* ECG parameters for *T. b. brucei* Lister 427 infection.

(A) Protocol used for *in vivo* *T. b. brucei* Lister 427 infection model. ECGs were recorded prior to injection with trypanosomes or control vehicle (CBSS). ECGs were recorded again on day 4 prior to sacrifice. (B(i-vi)) ECG parameters. QT was corrected for heart rate (QTc) using the Framingham method ($QTc = QT + 0.154 \times (1-RR)$). QT₉₀ was measured from the Q wave to the point on the T wave where T amplitude was 10% from the isoelectric point.

5.3.2 *Ex Vivo* Langendorff Perfused Heart Pseudo-ECG Parameters for *T. b. brucei* Lister 427 Infection

The sympathetic nervous system and β -adrenergic signalling pathway are activated in response to both physiological and pathophysiological stresses. To examine the effects of trypanosome infection under β -adrenergic stimulation under controlled conditions, a cohort of the hearts were removed from the animals and cannulated to a Langendorff perfusion system. Isoproterenol (ISO) was added at increasing doses (100 nM, 1 μ M, 10 μ M and 100 μ M) every 15 min (Figure 5.2A). The raw data for each parameter are shown in Table 5.2 and Figure 5.2.

Table 5.2: *T. b. brucei* Lister 427 *ex vivo* Langendorff raw parameters

ISO (μ M)	Heart Rate (bpm)			P-R Interval (ms)			QTc (Framingham (ms))		
	Control	Infected	<i>P</i> value	Control	Infected	<i>P</i> value	Control	Infected	<i>P</i> value
0	308 \pm 26	269 \pm 22	0.295	42.3 \pm 4.3	39.6 \pm 2.5	0.605	195.3 \pm 6.8	197.8 \pm 3.3	0.750
0.1	353 \pm 25	331 \pm 11	0.431	36.1 \pm 2.2	34.9 \pm 1.7	0.673	195.7 \pm 6.0	198.9 \pm 3.7	0.665
1.0	337 \pm 10	349 \pm 11	0.472	32.2 \pm 1.8	36.4 \pm 2.6	0.239	197.4 \pm 7.0	203.0 \pm 3.6	0.502
10.0	359 \pm 10	360 \pm 1	0.963	35.9 \pm 2.8	37.9 \pm 7.9	0.767	199.4 \pm 6.2	209.3 \pm 0.8	0.343
100.0	360 \pm 14	363 \pm 4	0.880	36.5 \pm 2.8	37.9 \pm 7.3	0.826	201.0 \pm 5.8	204.9 \pm 2.6	0.685

When normalised to the heart rate at steady state, the control hearts demonstrated a slight but not significant increase of 10-17% over steady state (1.00 \pm 0.08 vs. 1.15 \pm 0.08 vs. 1.10 \pm 0.03 vs. 1.17 \pm 0.03 vs. 1.17 \pm 0.05; steady state vs. 100 nM vs. 1 μ M vs. 10 μ M vs. 100 μ M ISO; P >0.05; Figure 5.2B(ii)). However, infected hearts demonstrated a significant increase of 23-35% over steady state (1.00 \pm 0.08 vs. 1.23 \pm 0.04 vs. 1.30 \pm 0.04 vs. 1.34 \pm 0.01 vs. 1.35 \pm 0.02; steady state vs. 100 nM vs. 1 μ M vs. 10 μ M vs. 100 μ M ISO; P <0.05; Figure 5.2B(ii)). For the P-R interval when normalised to steady state, no significant differences were observed for control (1.00 \pm 0.10 vs. 0.85 \pm 0.05 vs. 0.76 \pm 0.04 vs. 0.85 \pm 0.07 vs. 0.86 \pm 0.07; steady state vs. 100 nM vs. 1 μ M vs. 10 μ M vs. 100 μ M ISO; P >0.05; Figure 5.2C(ii)) or infected hearts (1.00 \pm 0.06 vs. 0.88 \pm 0.04 vs.

0.92 ± 0.07 vs. 0.96 ± 0.2 vs. 0.96 ± 0.2 ; steady state vs. 100 nM vs. 1 μ M vs. 10 μ M vs. 100 μ M ISO; $P > 0.05$; Figure 5.2C(ii)). Finally the QTc was assessed, which when normalised to steady state showed no significant differences for control (1.00 ± 0.03 vs. 1.00 ± 0.03 vs. 1.01 ± 0.04 vs. 1.02 ± 0.03 vs. 1.03 ± 0.03 ; steady state vs. 100 nM vs. 1 μ M vs. 10 μ M vs. 100 μ M ISO; $P > 0.05$ Figure 5.2D(ii)) or infected hearts (1.00 ± 0.02 vs. 1.01 ± 0.02 vs. 1.03 ± 0.02 vs. 1.06 ± 0.04 vs. 1.04 ± 0.01 ; steady state vs. 100 nM vs. 1 μ M vs. 10 μ M vs. 100 μ M ISO; $P > 0.05$) (Figure 5.2D(ii)).

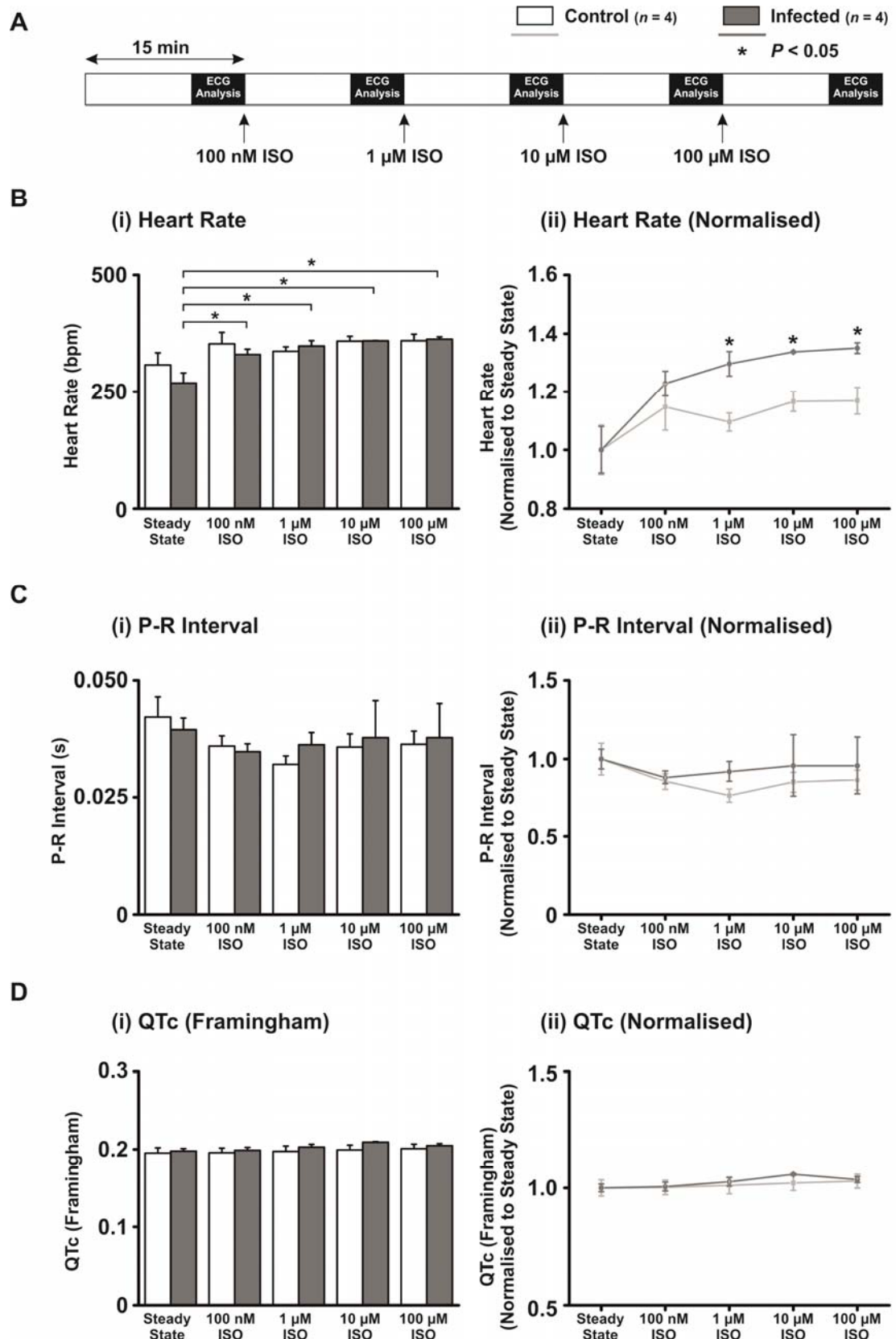


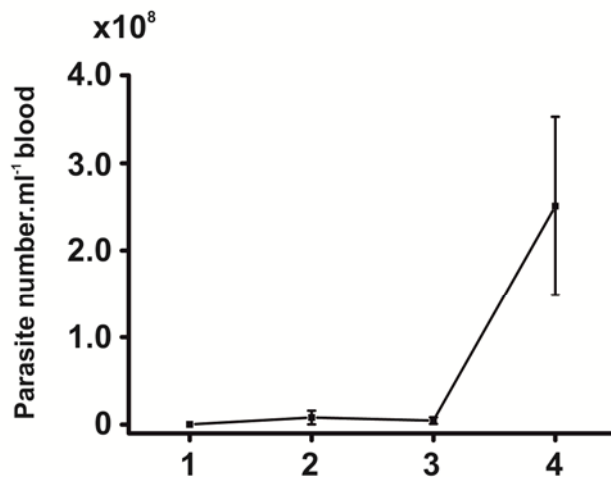
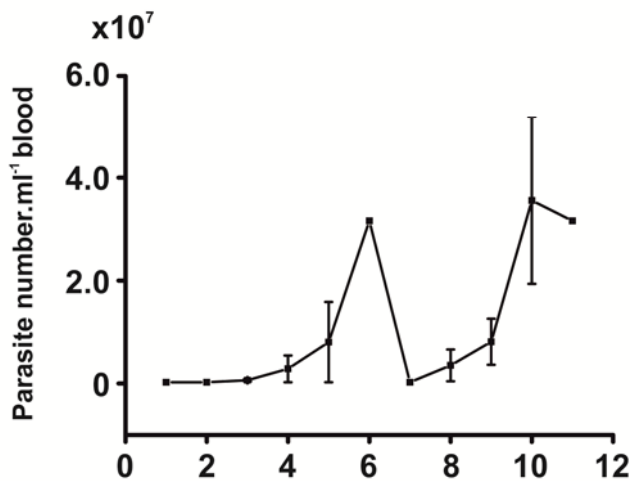
Figure 5.2: *Ex vivo* Langendorff ECG parameters for *T. b. brucei* Lister 427 infection.

(A) Protocol used in Langendorff perfusion experiments. Increasing concentrations of isoproterenol were added every 15 min and the ECG recorded throughout. (B(i)) Raw mean \pm SEM for heart rate and (ii) normalised to steady state. (C(i)) Raw mean \pm SEM for P-R interval and (ii) normalised to steady state. (D(i)) Raw mean \pm SEM for QT interval corrected for heart rate and (ii) normalised to steady state.

5.3.3 *In Vivo* ECG Parameters for *T. b. brucei* TREU 927 Infection

As discussed in section 5.2.2 a limitation of *T. brucei* Lister 427 is that it follows a logarithmic growth curve *in vivo* until the death of the infected host as it remains as the long slender bloodstream form⁽⁵⁴⁶⁾. Lister 427 has been a useful *in vitro* model of infection due to its ease of culturing (the bloodstream form of 927, for example cannot be cultured *in vitro*), but while many of its characteristics remain intact for study the loss of pleomorphism *in vivo* makes it harder to assess with infection models. Therefore, in order to develop a model that more closely resembles a clinical infection, a pleomorphic strain was used. From the Tritryp genome resource database (www.tritrypdb.org) there are 11 annotated copies of the TbCatL gene in the genomes of both 427 and 927 with no amino acid sequence differences; although trypanosomes are diploid and the consensus genome sequences are haploid so allelic differences cannot be formally ruled out⁽¹³⁹⁾. A strain of *T. b. brucei* that exhibits pleomorphism and therefore more closely resembles the clinical situation is *T. b. brucei* TREU 927⁽⁵⁵⁰⁾.

In the 427 infection model, parasite number increased exponentially over the 4 day period to a mean peak of $2.51 \times 10^8 \pm 1.02 \times 10^8$ parasites.mL⁻¹ of blood (Figure 5.3A(i)). In contrast, the parasitaemia in the 927 model follows the classical fluctuating pattern. The 927 infections showed a first peak parasitaemia of $3.16 \times 10^7 \pm 2.51 \times 10^5$ parasites.mL⁻¹ of blood on day 6 before returning toward the baseline, followed by a second peak of $3.56 \times 10^7 \pm 1.62 \times 10^7$ parasites.mL⁻¹ blood on day 10 (Figure 5.3A(ii)).

A**(i) *T.b.brucei* Lister 427 Parasitaemia Levels****(ii) *T.b.brucei* TREU 927 Parasitaemia Levels****Figure 5.3:** Parasitaemia levels for infection models.

(A(i)) Parasitaemia levels for *T. b. brucei* Lister 427 infection model. Numbers expressed as parasites.mL⁻¹ of blood x 10⁸ ($n = 21$). (A(ii)) Parasitaemia levels for *T. b. brucei* TREU 927 infection model. Numbers expressed as parasites.mL⁻¹ of blood x 10⁷ ($n = 5$).

5.3.3.1 ECG Parameters

Another limitation of the 427 study (presented in section 2.2) is the length of ECG recording. While a snapshot at the beginning and end will provide information on heart rate, P-R and QT intervals, a 15 min window may be too short to identify any arrhythmic events. To account for the snapshot limitation biopotential recording telemetry devices were implanted to record the ECG continuously for the duration of the study. The animals could also be kept conscious throughout the study as no need for anaesthesia for ECG recording was required. For heart rate there was no significant difference in the control

animals but a tendency to decrease over time (404 ± 18 vs. 348 ± 12 bpm; Day 0 vs. Day 11; $n = 5$; $P > 0.05$; Figure 5.4B(i)). However, there was a significant increase in heart rate for 927 infected animals (351 ± 22 vs. 413 ± 18 bpm; Day 0 vs. Day 11; $n = 6$; $P < 0.05$; Figure 5.4B(i)). There was no significant difference in P-R interval for control (43.2 ± 1.7 vs. 42.6 ± 1.5 ms; Day 0 vs. Day 14; $P > 0.05$; Figure 5.4B(ii)) or infected animals (41.5 ± 1.7 vs. 44.1 ± 3.2 ms; Day 0 vs. Day 14; $P > 0.05$; Figure 5.4B(ii)). The QT interval was also not significantly altered for control (51.2 ± 4.3 vs. 57.5 ± 8.0 ms; Day 0 vs. Day 14; $P > 0.05$; Figure 5.4B(iii)) or infected animals (58.1 ± 5.9 vs. 61.2 ± 7.3 ms; Day 0 vs. Day 14; $P > 0.05$; Figure 5.4B(iii)). When corrected for heart rate using the Framingham method there was no significant difference for control animals (181.9 ± 4.4 vs. 190.1 ± 11.8 ms; Day 0 vs. Day 14; $P > 0.05$; Figure 5.4B(iv)) or infected animals (185.2 ± 7.2 vs. 192.6 ± 6.9 bpm; Day 0 vs. Day 14; $P > 0.05$; Figure 5.4B(iv)).

5.3.3.2 Arrhythmic Events

When ECGs were assessed for arrhythmic events, specifically ventricular premature complexes, there was no difference in frequency for control animals (0.027 ± 0.019 vs. 0.047 ± 0.017 VPC.min⁻¹; Day 0 vs. Day 14; $P > 0.05$; Figure 5.4B(v)). However when the infected animal ECGs were assessed there was a significant increase of 539% (0.100 ± 0.034 vs. 0.539 ± 0.194 VPC.min⁻¹; Day 0 vs. Day 14; $P < 0.05$; Figure 5.4B(v)).

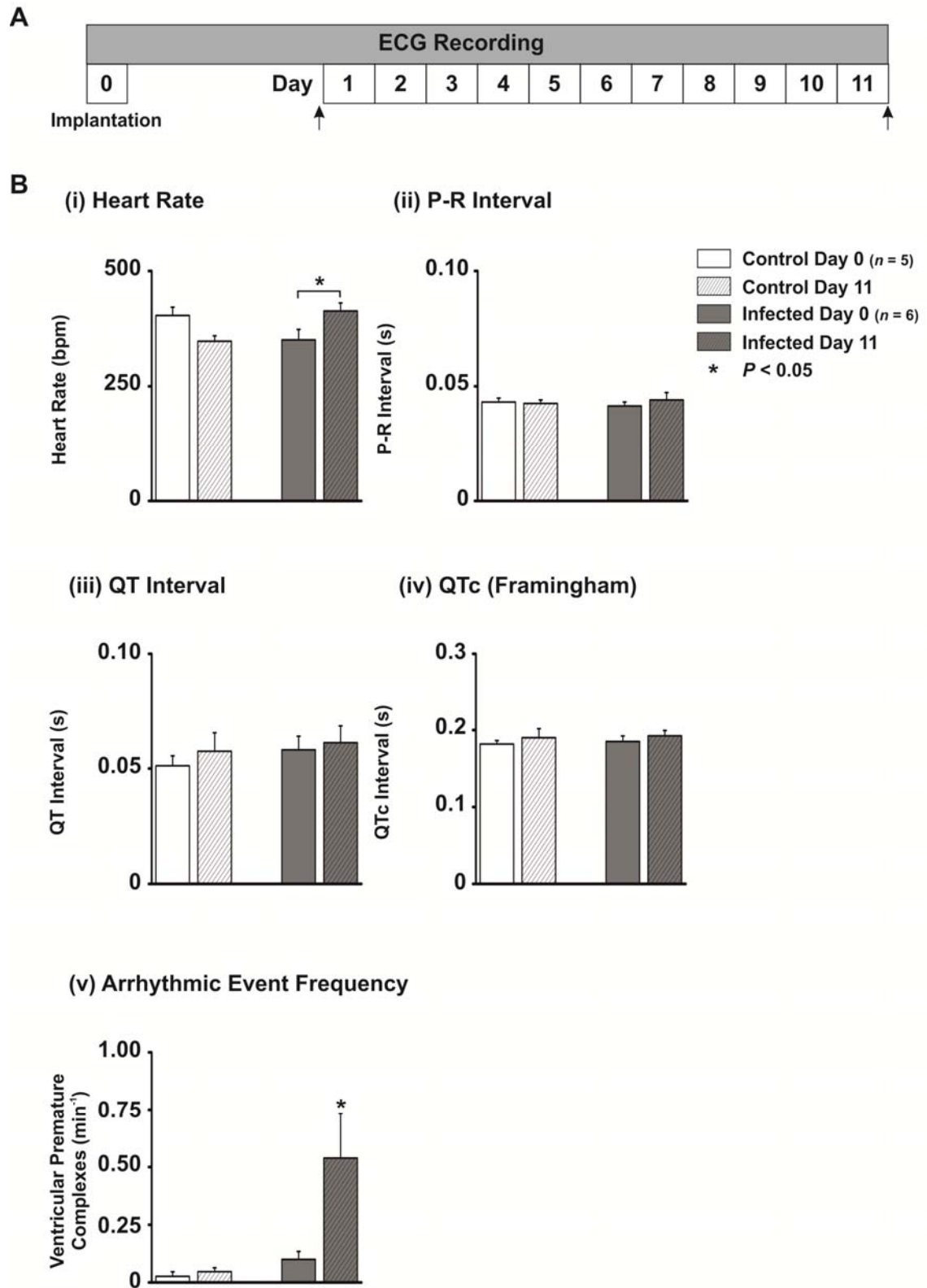


Figure 5.4: *In vivo* ECG parameters for *T. b. brucei* TREU 927 infection.

(A) Protocol used for *in vivo* *T. b. brucei* TREU 927 infection model. Biopotential telemetry devices were implanted and animals allowed to recover. ECGs were recorded continuously for the duration of the protocol. Animals were infected with 1×10^5 trypanosomes or control vehicle (CBSS) by intraperitoneal injection. (B(i-v)) ECG parameters from average traces taken prior to injection and end of the protocol. QT was corrected for heart rate (QTc) using the Framingham method ($QTc = QT + 0.154 \times (1-RR)$). Arrhythmia frequency was determined from hour long segments of trace taken prior to injection and end of the protocol.

5.3.4 *Ex Vivo* Langendorff Perfused Heart Pseudo-ECG Parameters for *T. b. brucei* TREU 927 Infection

As with the 427 infections the animals were sacrificed at the end of the protocol. The hearts were cannulated onto a Langendorff perfusion apparatus and perfused at $10 \text{ mL}\cdot\text{min}^{-1}$ with Tyrodes solution with increasing concentrations of ISO every 15 min (100 nM, 1 μM , 10 μM and 100 μM) (Figure 5.5A). The raw data for each parameter are shown in Table 5.3 and Figure 5.5.

Table 5.3: *T. b. brucei* TREU 927 *ex vivo* Langendorff raw parameters

ISO (μM)	Heart Rate (bpm)			P-R Interval (ms)			QTc (Framingham (ms))		
	Control	Infected	<i>P</i> value	Control	Infected	<i>P</i> value	Control	Infected	<i>P</i> value
0	280 \pm 16	239 \pm 11	0.073	37.4 \pm 3.2	39.1 \pm 1.7	0.665	203.3 \pm 4.9	187.8 \pm 12.0	0.265
0.1	317 \pm 4	350 \pm 31	0.321	31.1 \pm 2.2	37.1 \pm 4.3	0.245	206.3 \pm 3.2	194.2 \pm 2.2	0.015
1.0	336 \pm 18	345 \pm 23	0.780	30.0 \pm 2.0	37.5 \pm 1.9	0.028	206.5 \pm 2.8	202.8 \pm 2.8	0.451
10.0	319 \pm 5	350 \pm 14	0.073	31.1 \pm 2.3	38.3 \pm 3.5	0.118	209.1 \pm 4.3	206.8 \pm 2.4	0.655
100.0	328 \pm 20	356 \pm 19	0.334	33.2 \pm 3.4	39.5 \pm 3.9	0.252	209.5 \pm 4.4	211.9 \pm 2.8	0.657

When normalised to the heart rate at steady state, the infected hearts demonstrated a significant increase in rate over the control increase of 13-20% over steady state (1.00 \pm 0.06 vs. 1.13 \pm 0.01 vs. 1.20 \pm 0.06 vs. 1.14 \pm 0.02 vs. 1.17 \pm 0.07; steady state vs. 100 nM vs. 1 μM vs. 10 μM vs. 100 μM ISO; $P > 0.05$; Figure 5.5B(ii)) compared to an increase of 44-49% over steady state for infected hearts (1.00 \pm 0.05 vs. 1.47 \pm 0.13 vs. 1.44 \pm 0.10 vs. 1.46 \pm 0.06 vs. 1.49 \pm 0.08; steady state vs. 100 nM vs. 1 μM vs. 10 μM vs. 100 μM ISO; $P < 0.05$; Figure 5.5B(ii)). When the P-R interval was normalised to steady state, there was a significant difference between control and infected hearts. This difference was evident as a reduction in normalised P-R interval for control at 100 nM, 1 μM and 10 μM ISO of 17-20% over steady state; (1.00 \pm 0.09 vs. 0.83 \pm 0.06 vs. 0.80 \pm 0.05 vs. 0.83 \pm 0.06 vs. 0.89 \pm 0.09; steady state vs. 100 nM vs. 1 μM vs. 10 μM vs. 100 μM ISO; $P < 0.05$; Figure 5.5C(ii)). However, infected hearts did not show the same decrease (0-5% over steady state). Therefore, the P-R interval was

significantly longer relative to control hearts (1.00 ± 0.04 vs. 0.95 ± 0.11 vs. 0.96 ± 0.05 vs. 0.98 ± 0.09 vs. 1.01 ± 0.1 ; steady state vs. 100 nM vs. 1 μ M vs. 10 μ M vs. 100 μ M ISO; $P > 0.05$; Figure 5.2C(ii)). Finally the QTc normalised to steady state was assessed, which showed no significant changes for control hearts (1.00 ± 0.02 vs. 1.01 ± 0.02 vs. 1.02 ± 0.02 vs. 1.03 ± 0.02 vs. 1.03 ± 0.02 ; steady state vs. 100 nM vs. 1 μ M vs. 10 μ M vs. 100 μ M ISO; $P > 0.05$; Figure 5.5D(ii)). Infected hearts showed an increase of 3-13% over steady state in QTc but this was not statistically significant (1.00 ± 0.06 vs. 1.03 ± 0.01 vs. 1.08 ± 0.01 vs. 1.10 ± 0.01 vs. 1.13 ± 0.01 ; steady state vs. 100 nM vs. 1 μ M vs. 10 μ M vs. 100 μ M ISO; $P > 0.05$; Figure 5.2D(ii)).

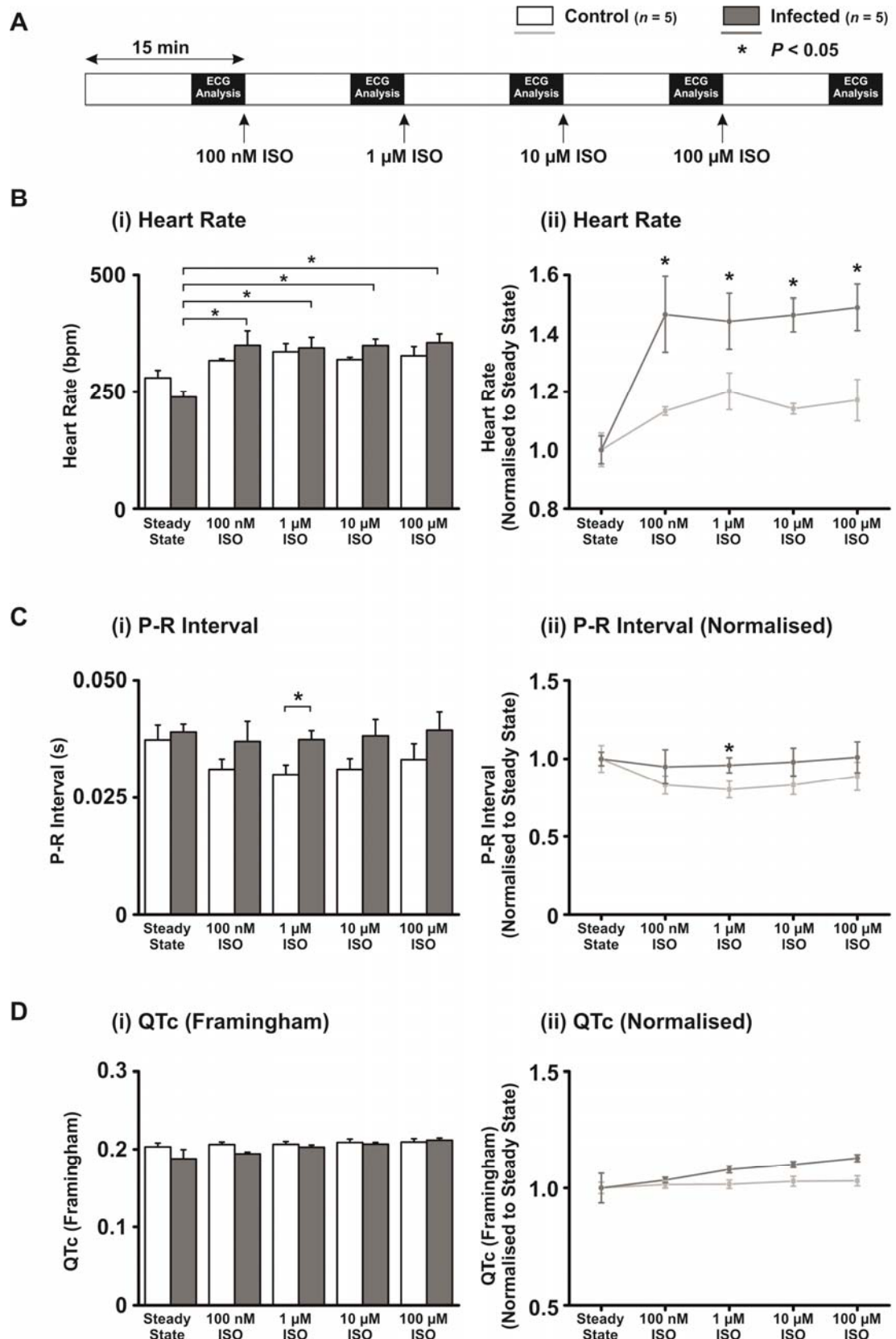


Figure 5.5: *Ex vivo* Langendorff ECG parameters for *T. b. brucei* TREU 927 infection.

(A) Protocol used in Langendorff perfusion experiments. Increasing concentrations of isoproterenol were added every 15 min and the ECG recorded throughout. (B(i)) Raw mean \pm SEM for heart rate and (ii) normalised to steady state. (C(i)) Raw mean \pm SEM for P-R interval and (ii) normalised to steady state. (D(i)) Raw mean \pm SEM for QT interval corrected for heart rate and (ii) normalised to steady state.

5.3.5 *T. b. brucei* TREU 927 Infected *Ex Vivo* Hearts Show Increased Frequency of Arrhythmias in the Presence of Isoproterenol

The pseudo-ECGs from the Langendorff perfused hearts from both models were also assessed for the frequency of VPCs during steady state, 100 nM, 1 μ M and 10 μ M ISO for both the 427 and 927 models. There was no significant increase in VPC frequency for the 427 model in control hearts (0.35 ± 0.35 vs. 0.1 ± 0.1 vs. 0.0 ± 0.0 vs. 0.0 ± 0.0 VPC.min⁻¹; steady state vs. 100 nM vs. 1 μ M vs. 10 μ M ISO; $n = 4$; $P > 0.05$; Figure 5.6B(i)) or the infected hearts (0.0 ± 0.0 vs. 0.45 ± 0.45 vs. 0.0 ± 0.0 vs. 0.0 ± 0.0 VPC.min⁻¹; steady state vs. 100 nM vs. 1 μ M vs. 10 μ M ISO; $n = 4$; $P > 0.05$; Figure 5.6B(i)). Similarly for 927 controls there was no significant increase; (0.08 ± 0.08 vs. 0.32 ± 0.23 vs. 0.28 ± 0.15 vs. 0.0 ± 0.0 VPC.min⁻¹; steady state vs. 100 nM vs. 1 μ M vs. 10 μ M ISO; $P > 0.05$; Figure 5.6B(ii)). However, infected hearts showed an increase in VPC frequency significant at 1 μ M (0.24 ± 0.16 vs. 5.24 ± 4.99 vs. 5.48 ± 1.83 ($P < 0.05$) vs. 10.4 ± 8.9 VPC.min⁻¹; steady state vs. 100 nM vs. 1 μ M vs. 10 μ M ISO; Figure 5.6B(ii)).

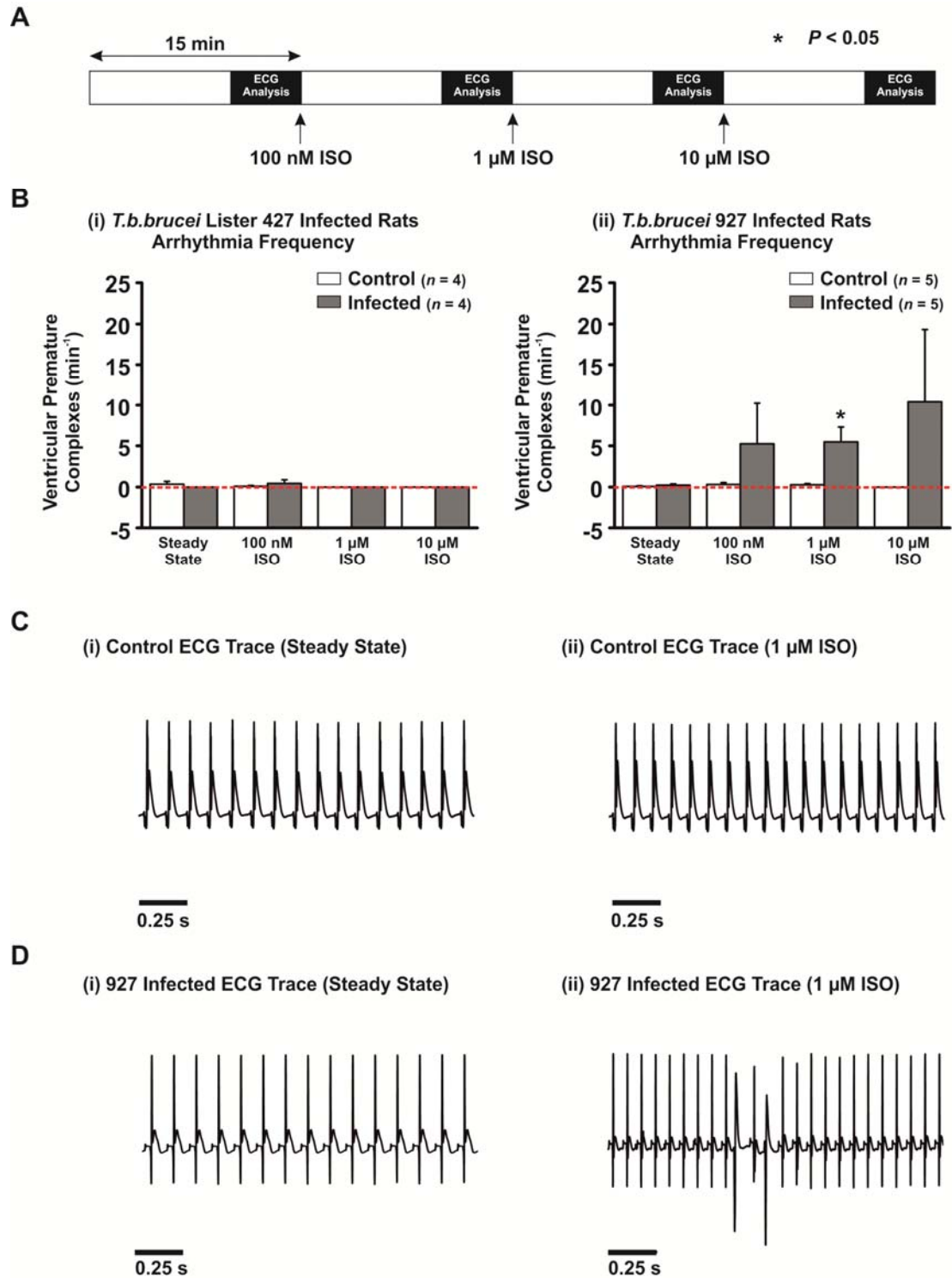


Figure 5.6: Arrhythmic events in Langendorff perfused infected and control hearts. (A) Protocol used for Langendorff perfusion experiments. Hearts were perfused at a rate of $10 \text{ mL} \cdot \text{min}^{-1}$ for 15 min steady state followed by 15 min with increasing concentrations of isoproterenol (100 nM, 1 μM , and 10 μM). (B) Mean \pm SEM for frequency of ventricular premature complexes (VPCs) for (i) *T. b. brucei* Lister 427 and (ii) *T. b. brucei* TREU 927. (C-D(i-ii)) Example pseudo-ECGs from Langendorff perfused heart from 927 infected animal and corresponding model control.

5.3.6 Organ Mass Data

5.3.6.1 *T. b. brucei* Lister 427 Infection Model

At sacrifice, on Day 4 post-infection, animals were weighed and organs removed. There was no significant difference in body mass between control and infected animals (302.7 ± 4.1 vs. 301.0 ± 3.1 g; control ($n = 24$) vs. infected ($n = 21$); $P > 0.05$; Figure 5.7A(i)). Heart mass/tibial length ratio was not significantly altered (29.3 ± 2.7 vs. 27.8 ± 4.8 mg.mm⁻¹; control vs. infected; $P > 0.05$; Figure 5.7A(ii)). Liver mass/tibial length ratio was also not significantly affected, although tended to increase (226.5 ± 5.7 vs. 246.2 ± 8.7 mg.mm⁻¹; control vs. infected; $P > 0.05$; Figure 5.7A(iii)). The lung mass/tibial length ratio was not significantly altered either (33.1 ± 2.6 vs. 31.4 ± 1.9 mg.mm⁻¹; control vs. infected; $P > 0.05$; Figure 5.7A(iv)). However, spleens were significantly increased in mass in infected animals by 199% (13.3 ± 0.4 vs. 26.5 ± 3.4 mg.mm⁻¹; control vs. infected; $P < 0.05$; Figure 5.7A(v)).

between control and infected animals although infected animals had lost some condition by the end of the study (344.0 ± 8.5 vs. 314.7 ± 15.3 g; control ($n = 5$) vs. infected ($n = 5$); $P > 0.05$; Figure 5.8A(i)). Heart mass/tibial length ratio was not significantly altered (34.1 ± 3.4 vs. 31.8 ± 5.6 mg.mm⁻¹; control vs. infected; $P > 0.05$; Figure 5.8A(ii)). Liver mass/tibial length ratio was also not significantly affected (253.3 ± 8.9 vs. 244.7 ± 17.6 mg.mm⁻¹; control vs. infected; $P > 0.05$; Figure 5.8A(iii)). Spleens were significantly increased in mass in infected animals by 292% (17.2 ± 1.6 vs. 50.2 ± 7.5 mg.mm⁻¹; control vs. infected; $P < 0.05$; Figure 5.8A(iv)).

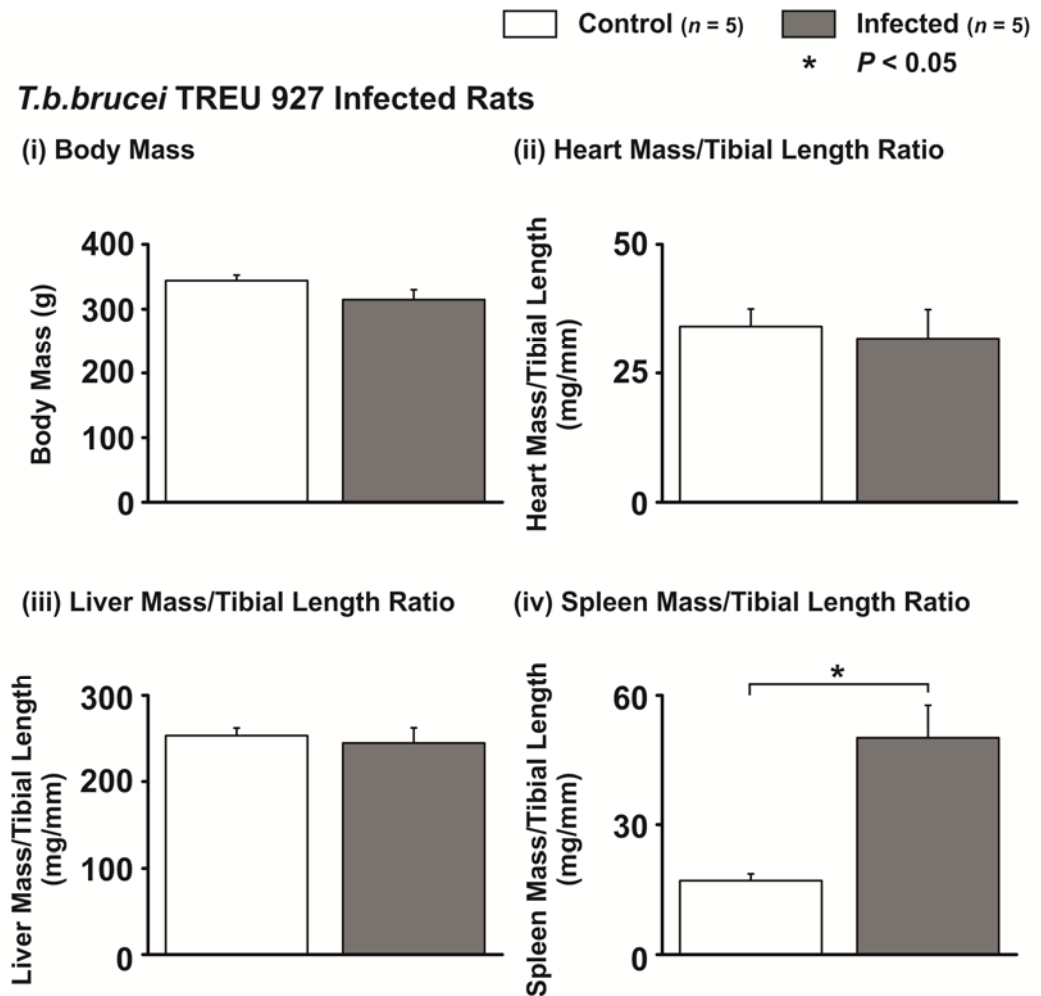
A

Figure 5.8: Organ mass data for *T. b. brucei* TREU 927 infection model.

(A(i-iv)) Mean \pm SEM for body mass and heart, liver and spleen mass to tibial length ratio for control ($n = 5$) and infected ($n = 5$).

5.4 Discussion

5.4.1 *In Vivo* ECGs for *T. b. brucei* Lister 427 Infection

Given the reported clinical cardiac-related findings in patients with HAT and the effects observed and discussed in previous chapters, an experimental infection model initially established with cultured Lister 427 trypanosomes was conducted. Adult male Wistar rats were anaesthetised and had their ECG recorded before being infected *via* an intraperitoneal injection of 1.0×10^5 parasites in 200 μL or equivalent volume of vehicle for controls. The ECGs were recorded again after 4 days. The ECGs were analysed for P-R and QTc changes and occurrence of ventricular arrhythmias that could be associated with palpitations. No significant findings were apparent between the control and infected animals, nor were there significant differences between the day 0 and day 4 ECG recordings. Blum *et al.*⁽⁵¹⁾ attributed their findings of ECG alterations in HAT patients to perimyocarditis based on the histological findings of earlier studies^(55;56;61). Therefore it is possible the lack of findings in the current model is due to the brevity of the infection and subsequent lack of time for perimyocarditis to develop⁽²⁷⁾. This is perhaps surprising given the increase in ventricular arrhythmias observed when *ex vivo* rat hearts were perfused with culture supernatant from *in vitro* Lister 427 cultures. The results presented in this thesis so far have suggested a direct effect on cardiomyocytes and indeed whole hearts independent of an immune/inflammatory response. A possible explanation could be the activity of the secreted TbCatL. Caffrey *et al.* (2001) showed that TbCatL is present in culture supernatant of *T. b. brucei*⁽¹²⁹⁾ and the preceding chapters demonstrate a role for TbCatL in altered Ca^{2+} dynamics of cardiomyocytes. With the direct application of culture supernatants to isolated cardiomyocytes or perfusion through the coronary vessels we know the TbCatL to be active and targeted to the tissue of interest. In an *in vivo* model, the picture is less distinct. The host will have many proteases (discussed in Chapter 6) and a delicate regulatory balance with endogenous inhibitors such as cystatins⁽⁵⁵³⁾. Although information on the host response to TbCatL is scarce there have been reports of host inhibitors modulating parasite protease activity in the case of *T. cruzi* infection⁽⁵⁵⁴⁾. A potential future series of experiments would be to measure the quantity of TbCatL in the host's blood by developing a TbCatL-

specific ELISA and to develop an activity assay to work on the host's blood/serum.

Four additional reasons may explain the lack of effect observed *in vivo* using Lister 427 cultures despite the occurrence of arrhythmias reported in patients with HAT and the *ex vivo* results presented in this thesis:

1. The short duration of the 427 *in vivo* model does not lead to a sufficiently large increase in the levels of TbCatL to result in a detectable level of arrhythmias in the short time frame measured (particularly given the likely role of endogenous inhibitors as discussed above).
2. The degree of extravasation of the parasite. It is known that after long-term infection (weeks) that parasites are seen infiltrating the myocardium in both humans^(56;496) and animal models^(25-28;56). However, the 427 model lasts only 4 days. Therefore the lack of effect observed with 427 infection may be due to a lack of sufficient extravasation of the parasite due to the brevity of the study. This in turn may influence the level of TbCatL directly in contact with the myocardium. Myburgh *et al.* (2013) in characterising an *in vivo* imaging system used Lister 427 as a control for vascular leakage following parietal skull thinning surgery i.e. that the 427 did not extravasate unless there was vascular damage⁽⁵⁵⁵⁾.
3. The amount of TbCatL produced by Lister 427 vs. pleomorphic strains is reduced. Caffrey *et al.* (2001) demonstrated that short-stumpy form trypanosomes produce more TbCatL than long-slender forms⁽¹²⁹⁾. Since the 427 strain does not differentiate, then the quantity of TbCatL is likely to be reduced and may account for the lack of response observed.
4. There are also limitations with the assessment of ECG parameters in the 427 *in vivo* model. The length of ECG recording time is sufficient for an assessment of ECG parameters such as QTc. However, if arrhythmic events should occur less frequently than the recording time, then the events will be missed.

5.4.2 *Ex Vivo* Langendorff Perfused Heart Pseudo-ECGs for *T. b. brucei* Lister 427 Infection

The sympathetic nervous system and β -adrenergic signalling pathway are activated in response to both physiological and pathophysiological stresses. In response to isoproterenol (ISO), cardiomyocytes and *ex vivo* hearts demonstrated enhanced Ca^{2+} handling effects (i.e. faster Ca^{2+} transient decline and more Ca^{2+} waves) in response to trypanosome supernatant (Chapter 3). However, under anaesthesia there can be inhibition of the sympathetic nervous system^(556;557). Anaesthesia may therefore be having the opposite effect, i.e. reducing the propensity for arrhythmogenic Ca^{2+} release and potential VPCs. To investigate the potential importance of the above and also explore the sensitivity of the infected hearts to ISO without a systemic autonomic influence, a cohort of hearts were removed at the end of the 4 day model and perfused on a Langendorff apparatus with increasing concentrations of ISO. There was a significant increase in the heart rate of infected hearts in response to ISO over the control hearts. In addition to the greater metabolic demand in response to infection this may indicate a greater sensitivity to β -adrenergic stimulation.

In response to β -adrenergic stimulation the slope of the pacemaker potential in atrial nodal cells is increased leading to a faster rate of depolarisation and therefore, more contractions in a given time⁽⁵⁵⁸⁾. This is achieved by activation of cAMP, which in turn will interact with ion channels to affect depolarising and repolarising currents (I_f , $I_{\text{Na}/\text{Ca}}$, $I_{\text{Ca T}}$, $I_{\text{Ca L}}$ and I_{Na} ⁽¹⁴⁸⁾). The activation of PKA by cAMP acts to phosphorylate the LTCC⁽¹⁵³⁾ (section 1.5), which increases the probability and duration of open state leading to increased force of contraction in ventricular cardiomyocytes but also increases chronotropy in SA nodal cells⁽⁵⁵⁸⁾. Furthermore, PKA phosphorylates the delayed rectifier K^+ channels, which increases the repolarising outward K^+ currents shortening the ventricular action potential (section 1.3.3) permitting more excitations. min^{-1} . The action of PKA on PLB^(239;240;243) enables faster Ca^{2+} transient decline *via* increased SERCA activity (as observed in Chapter 3) and faster SR reuptake of Ca^{2+} enhancing cardiac lusitropy enabling more contractions. min^{-1} . As well as increased β -adrenergic stimulation *via* increased sympathetic tone the hormone adrenaline acts similarly⁽⁵⁵⁸⁾. During physiological and pathophysiological stress, such as an infection, there are increased levels of circulating adrenaline and noradrenaline.

Although there was no observed increase in heart rate *in vivo*, there may be a sensitisation effect of β_1 adrenergic receptor⁽⁵⁵⁹⁾, an alteration in expression of β_1 adrenergic receptors, or altered phenotypic expression of β -adrenergic receptor polymorphisms⁽⁵⁶⁰⁾ leading to the increase in heart rate observed in response to ISO *ex vivo*. However, further work will be required to ascertain what is causing the increased responsiveness to ISO in the infected hearts. Interestingly, when the heart rate of the *ex vivo* hearts perfused with trypanosome supernatant (Chapter 3) is compared to the infected *ex vivo* hearts, there was no change over their respective controls. This suggests that any effect on heart rate is most likely not due to acute exposure to TbCatL.

Although there were no other statistically significant differences in the measured ECG parameters, there was a tendency for the control P-R interval to decrease in response to ISO as may be expected due to increased AV node conduction velocity (dromotropic effect)⁽⁵⁵⁸⁾. The P-R interval remained unchanged in the infected hearts, which, when interpreted with the slight reduction in control, could suggest some prolongation. P-R interval of >200 ms has been reported in 3.7-14% of HAT patients by other studies^(61;62), defined as 1st degree AV block. This would suggest that trypanosome infection may alter the AV node conduction velocity, which may contribute to the increase in heart rate following application of ISO, although further work measuring conduction velocity would be required to confirm this hypothesis. Blum *et al.* (2007) showed some prolongation of P-R interval suggesting 1st degree AV block but this was not significant (3% vs. 8% of subjects; control vs. infected; $P=0.23$)⁽⁵¹⁾ in comparison with their other cardiac findings, which suggests that AV node conduction is less likely to play a significant role in the cardiac pathology of HAT.

The QTc was not affected, which would support the findings of the *ex vivo* study of supernatant perfused hearts presented in Chapter 3 and a hypothesis of a direct effect on the myocardium by trypanosomes independent of an immune/inflammatory component. This is because prolongation of QTc can be attributable to an inflammatory infiltrate of the myocardium disrupting the tissue leading to altered electrical conductivity^(27;57). The QTc prolongation identified by Blum *et al.* (2007) was ascribed to an inflammatory infiltrate of the myocardium⁽⁵¹⁾. The fact that prolongation of QTc was not observed in the

current study suggests that there may not be a significant inflammatory infiltrate acting to disrupt the myocardium therefore, any effects observed may be directly mediated by the parasites.

5.4.3 *In Vivo* ECGs for *T. b. brucei* TREU 927 Infection

To more closely approximate a natural infection the strain *T. b. brucei* TREU 927 was used. These parasites do exhibit the ability to differentiate and so are pleomorphic, i.e. exist as both short stumpy and long slender forms. As a result the parasites follow the classical cyclical waxing and waning parasitaemia phenotype. Our 927 infection model was sustainable over a longer time period (up to 11 days) than the 4 day infection model of 427. Recognising the limitations of the 427 infection model as discussed above, a decision was taken to use both the longer term 927 model of infection and to use biopotential recording implants to measure the ECGs of the rats continuously. This would allow for a more complete assessment of the occurrence of ventricular arrhythmias than the 15 min “snapshot” taken in the 427 model at the commencement and termination of the study. In addition to examining the ECGs for arrhythmias, the heart rate, P-R interval and QTc were also measured on Day 0 and the end of the study. The normalised heart rate of the infected animals was significantly increased suggesting higher sympathetic tone in response to the pathophysiological stress the animals were under⁽⁵⁵⁸⁾ or indeed increased sensitivity to circulating catecholamines as discussed in section 5.3.2). The P-R interval was not significantly altered nor was QTc. Therefore, further investigation with ISO in the same hearts removed from the animals on termination and Langendorff perfused was conducted and discussed in section 5.4.5. Interestingly, with the longer period of ECG trace it was possible to identify the occurrence of ventricular arrhythmias. There was a significantly higher frequency of VPCs in the ECGs of infected animals over controls. This finding supports the data presented so far in this thesis that African trypanosomiasis can increase the propensity of arrhythmias.

5.4.4 *T. b. brucei* TREU 927 Infections Exhibit Greater Arrhythmia Frequency than Lister 427 Infections

As discussed above, 927 is a pleomorphic strain of *T. b. brucei* meaning it differentiates to the insect infective short stumpy form. The overall lower parasitaemia of 927 compared with 427 is due to a significant proportion of 927 parasites terminally differentiating in a density-dependent manner (i.e. self-regulating growth) whereas 427 will continue to divide resulting in exponential growth until the death of the host. Interestingly, Caffrey *et al.* (2001) demonstrated that short stumpy form trypanosomes produced almost 5 times the amount of cathepsin-L than long slender counterparts of the same strain⁽¹²⁹⁾. Therefore, as 927 infection is producing more stumpy form trypanosomes then it is likely that there is significantly more circulating cathepsin-L that may thus contribute to more cardiac arrhythmias. An unpublished finding (Lorna MacLean, personal communication) demonstrates that pleomorphic strains of trypanosome such as *T. b. brucei* GVR35 or *T. b. rhodesiense* IL1825 produce greater quantities of cathepsin-L in general than monomorphic 427. MacLean also measured transendothelial migration using an *in vitro* BBB model and identified that the degree of migration correlated with the quantity of cathepsin-L expression. Moreover, *T. b. rhodesiense* IL1852 expressed an increasing amount of cathepsin-L when incubated with the endothelial cells of *in vitro* BBB model depending on time of incubation from 15 min to 30 min and 60 min. At the same time-points, there was a corresponding increase in migration of parasites across the endothelial cell layer from $\sim 5.0 \times 10^4$ parasites.mL⁻¹ at 15 and 30 min and $\sim 1.8 \times 10^5$ parasites.mL⁻¹ at 60 min⁽⁵⁶¹⁾. During the same time GVR35 showed migration at 30 and 60 min of incubation with $\sim 5.0 \times 10^4$ parasites.mL⁻¹ whereas 427 showed no detectable migration during this time period⁽⁵⁶¹⁾. Therefore, this suggests that while all strains and stages of *T. brucei* spp. produce cathepsin-L⁽¹²⁹⁾ and therefore data from each is useful, the amount produced and correspondingly the transendothelial migration varies with strain and stage^(69;129;561). Furthermore, if cathepsin-L can directly affect the Ca²⁺ handling dynamics of the heart and transendothelial migration is linked, then it is reasonable to assume that the increased effect of 927 on cardiac arrhythmias over 427 could also partly be due to an increase in extravasation of parasites due to increased cathepsin-L levels and those same levels could be having a greater effect on the heart.

5.4.5 *Ex Vivo* Langendorff Perfused Heart Pseudo-ECGs for *T. b. brucei* TREU 927 Infection

As with the 427 infection model the animals were terminated at the end of the study and the hearts removed. The hearts were perfused on a Langendorff apparatus with increasing concentrations of ISO in Tyrodes and the ECG recorded. As with the 427 data, the 927 data shows a similar pattern. The normalised heart rate increases by a significantly larger margin in the infected animals over the controls. This again suggests increased sensitivity to sympathetic and β -adrenergic stimulation (section 5.4.2.). However, the intrinsic heart rate, i.e. the natural rate of the heart prior to addition of any ISO but without any neurohumoral input, was not significantly different from that of the controls. In the presence of increasing concentrations of ISO the heart rate increased to a greater degree in the infected hearts. This would suggest (as discussed with the *ex vivo* 427 infected hearts) that there could be increased sensitivity, expression or phenotype of β -adrenergic receptors. In order to investigate the hypothesis of altered β -adrenergic response exerted by TbCatL effect on intra-cardiomyocyte Ca^{2+} handling during trypanosome infection, experiments involving assessment of the β -signalling receptors/cascade would be required⁽⁵⁵⁹⁾. The data presented in the preceding chapters demonstrates TbCatL effects on Ca^{2+} handling that have similarities with increased β -adrenergic type effects, such as faster Ca^{2+} transient decay rate that could be inhibited by blocking the actions of CaMKII, posing a putative role for altered PLB phosphorylation status^(240;244;245). Diastolic Ca^{2+} leak from the RyR can also be attributable to increased β -adrenergic type effects through phosphorylation of RyR^(299;323), which could also be inhibited by CaMKII blockade. Since the single cellular effects were greater in the presence of trypanosome supernatant over control media to a greater degree with ISO, then this may suggest a potentially increased sensitivity to β -stimulation. Therefore, the similarity of the Ca^{2+} handling effects of TbCatL and β -adrenergic stimulation may result in a synergistic effect of TbCatL in the presence of ISO in the infected hearts that would not be present in the control hearts that are only exposed to ISO.

Similar to the 427 model there was reduction of P-R interval in the control hearts not mirrored by the infected hearts in response to ISO. The fact that this finding has occurred in both independent *in vivo* models improves the validity of

the observation. The P-R interval was not prolonged as there was no significant difference between controls and infected hearts during the steady state period and the value of 37.4 - 39.1 ms tallies well with reported values^(562;563). The clinical significance of this is unclear. A recent study evaluated the prognostic value of prolonged P-R interval and found no correlation with cardiac or other causes of mortality⁽⁵⁶⁴⁾ and Blum *et al.* (2007) recorded their cases of 1st degree AV block as rare and not a greater frequency than controls⁽⁵¹⁾. This suggests that changes in P-R interval are less likely to have clinical significance in HAT.

The QTc was not significantly altered. A longer term infection model that shows a perimyocarditis, as described in post-mortem studies of infected humans^(56;57) and animals⁽²⁶⁻²⁸⁾, may demonstrate the prolongation of QTc described by Blum *et al.* (2007) and isolate this finding as inflammation associated vs. a direct effect of the trypanosomes. As discussed for the 427 infection model the lack of prolongation of QTc suggests no significant immune/inflammatory infiltrate disrupting the myocardial tissue, therefore supporting a hypothesis of TbCatL mediated effects vs. inflammation.

5.4.6 *T. b. brucei* TREU 927 Infected *Ex Vivo* Hearts Show Increased Frequency of Arrhythmias

In response to the increasing concentration of ISO the frequency of VPCs increased in the 927 infected hearts compared to controls but not in the 427 infected hearts. The 927 data supports the findings presented in this thesis that infection with *T. b. brucei* has the effect of increasing VPC frequency and supports the *in vivo* results above (section 5.3.3.2). Interestingly, during *in vivo* infections without pharmacological intervention, there is an increase in VPC frequency, yet when the same hearts were removed there were no VPCs observed without the addition of ISO. This supports the hypothesis that the arrhythmias may in fact be due to a circulating factor produced during trypanosome infection. Once the hearts are removed from the direct influence of the circulation then the effect is lost. If secreted/excreted TbCatL released into the circulation has the effect of increasing cardiac arrhythmias, then removal of the heart from the circulation and TbCatL may be expected to result in fewer arrhythmias *ex vivo* compared to *in vivo*. When *ex vivo* hearts are perfused directly with trypanosome supernatant, which would contain TbCatL,

the arrhythmias can be observed. When ISO is added VPC frequency increases in the infected hearts suggesting increased sensitivity to β -adrenergic stimulation as discussed above (section 5.4.2), which increases with the increasing ISO concentration. This raises the question that the hearts may be chronically affected by the parasite infection compared with the response of healthy hearts perfused with supernatant. Studies utilising field data would be useful to dissect the potential direct effects of trypanosomes on the heart from immune/inflammatory changes. Further work would require the use of AIP, a CaMKII inhibitor, or a cathepsin-L inhibitor such as K11777, to determine if the *in vivo* effects observed are inhibited in the same way as the single cell effects. The lack of VPCs in the 427 model is difficult to reconcile but may be a result of a reduced window of observation compared to the continuous telemetry used in the 927 model. In clinical studies a reported frequency of palpitations of 18%⁽⁵¹⁾ would equate to 0.72 individual hearts in the 427 Langendorff study.

5.4.7 Organ Mass

5.4.7.1 Spleens were enlarged for both models

Splenomegaly is common finding in both experimental infections of animals⁽⁵⁶⁵⁾ and upon post-mortem examination of human infections of trypanosomiasis^(56;496). Therefore, the finding of splenomegaly in both the 427 and 927 models is consistent with the literature. Although histopathology has not been performed for the current study the literature reports that splenomegaly is due to lymphocytic infiltrates^(56;496).

5.4.7.2 Liver, lungs and heart mass were not changed

There were no significant differences in the other organ masses. This suggests that there was no significant inflammatory cell infiltrate that could alter the gross organ mass as there was with the spleen. In order to assess a lower level of inflammatory cell infiltration the organs will need to be examined histologically, which will be performed in future studies. An indicator of cardiac function is lung and liver mass. If there is left or right sided heart failure cardiac output will be reduced. As a result oedema will begin to pool in the liver for right-sided failure and in the lungs for left-sided failure. The tissue will then become oedematous and therefore have greater mass (tissue and oedema).

As no change was observed in the current study, there was no clinical manifestation of heart failure in any of the infected animals in either model.

5.4.8 A Role For Cathepsin-L In HAT

The preceding chapters have demonstrated that TbCatL from *T. b. brucei* Lister 427 can elicit effects on SERCA and the RyR mediated by CaMKII. *In vivo* the situation is more complex. It is clear from the literature that while there are no thus far identified genetic differences (allelic or gene copy number) between strain and sub-species' repertoires of cathepsin-L genes, there are clear differences in the levels of cathepsin-L expression. This seems to be dependent on the lifecycle stage of parasite, as well as sub-species and strain. It appears that the largest quantity of cathepsin-L is produced by *T. b. rhodesiense*^(69;129;561) and that the pleomorphic strains during the differentiated stumpy form phase produce more than long slender form phases or monomorphic strains locked in long slender forms^(129;561). Moreover, the larger the quantities of cathepsin-L expressed, the greater the degree of transendothelial migration there is in an *in vitro* model^(69;561). Therefore, the studies in this thesis may have underestimated the potential direct effects of trypanosomes on cardiac function, as clinically derived isolates of *T. brucei* spp. causing HAT have higher TbCatL levels than either *T. b. brucei* model used in the current study^(69;129;561). Future studies examining the *in vitro* and *in vivo* effects of a range of clinical isolates of *T. b. rhodesiense* and *T. b. gambiense*, as well as different strains of pleomorphic *T. b. brucei*, may show a more severe phenotype. Due to the inability to maintain bloodstream stages of pleomorphic strains of trypanosome in culture, only Lister 427 has been examined *in vitro* for this study. The data in this chapter demonstrates that infection with trypanosomes can result in increased ventricular arrhythmias. The result is more pronounced when a pleomorphic strain of trypanosome is used and can be related through the literature to the level of TbCatL expression. The use of ISO leads to increased heart rate and a higher frequency of VPCs *ex vivo* suggesting a sensitisation effect of TbCatL to β -adrenergic stimulation. The greater frequency of VPCs *in vivo* without ISO (in the 927 infection model) coupled with the *ex vivo* whole heart data from chapter 3 suggests the cardiac arrhythmia phenotype may be due to a secreted/excreted factor rather than an immune/inflammatory

response. Therefore, TbCatL is an attractive target for future study and development of potential therapeutic strategies to treat HAT.

6 CHAPTER 6 – The Cardiac Effects of Endogenous Extracellular Cathepsin-L

6.1 Introduction

6.1.1 Cathepsins

The cathepsins are localised within acidic intracellular organelles such as lysosomes and endosomes where their primary function is to break down unwanted proteins⁽³⁷¹⁻³⁷⁴⁾. In addition to intracellular protein turnover, cathepsins have a wider role in many homeostatic processes, and have been implicated in various diseases discussed in section 1.6.5.1. The paradigm has been that cathepsins are only active at acidic pH, but recent work has shown a wider range of active locations and more neutral pH for cathepsins such as secretory vesicles^(381;382), the cytosol⁽³⁸³⁻³⁸⁵⁾ and the nucleus^(386;387). Extracellular roles for cathepsins have been proposed specifically with regard to extracellular matrix (ECM) remodelling^(414;566;567). Under normal physiological conditions the cathepsins are primarily intracellular within lysosomes but in pathological circumstances such as inflammation and oxidative stress the cathepsins can be released to elicit degradative effects on the ECM in cancer, bone and cardiovascular tissues⁽⁵⁶⁶⁾.

6.1.2 Cathepsins in the Heart

Although other cathepsins have been studied in cardiovascular disease such as B, K and S⁽⁴²³⁾, cathepsin-L (CatL) is garnering particular attention. CatL is a ubiquitously expressed homeostatic enzyme involved in many disease processes⁽³⁶⁸⁾. Within the heart it is known that a basal level appears to be necessary, as a CatL knockout mouse model shows a dilated cardiomyopathy phenotype⁽⁴⁰²⁾. Further evidence in support of the essentiality of basal levels of CatL is that a CatL knockout mouse model of myocardial infarction (MI) had impaired healing with poorer scar formation and greater cardiac dilatation over control mice with MI⁽⁴²⁴⁾. However, in patients with cardiovascular disease there are reported increases in serum levels of CatL^(425;426). Liu J. *et al.* (2006) examined serum CatL levels in patients with atherosclerosis and demonstrated a correlation with the degree of left anterior descending coronary artery stenosis and serum CatL⁽⁴¹³⁾. Moreover, Liu Y. *et al.* (2009) identified that serum levels of CatL were significantly increased in patients correlating with severity of CHD⁽⁴²⁵⁾. They identified CatL was increased significantly from normal levels of 4

ng.mL⁻¹ in patients without CHD to 4.7 ng.mL⁻¹ in patients with stable angina pectoris, 5.5 ng.mL⁻¹ in patients with unstable angina pectoris and 6.2 ng.mL⁻¹ in patients with myocardial infarction⁽⁴²⁵⁾. However, while there is a correlation of serum CatL and severity of CHD the consequences of elevated levels of CatL remain unknown. Cathepsins A and D have previously been studied in the context of cardiac ischaemia/reperfusion injury showing increased activity^(368;428-431). For example, Linz *et al.* (2011) identified preserved ventricular wall geometry following experimental ischaemia/reperfusion (I/R) injury when CatA was inhibited⁽⁴²⁹⁾. Decker *et al.* (1997) visualised the distribution of CatD following I/R injury and identified CatD release from cardiomyocyte lysosomes⁽⁴²⁸⁾. Tiwari *et al.* (2008) identified that release of CatD during I/R injury correlated with myocardial damage with a concomitant increase in lipid peroxides and superoxide suggesting a free radical activation by CatD during I/R injury⁽⁴³⁰⁾. CatL on the other hand has been studied with regard to potential beneficial remodelling effects post-MI without reperfusion⁽⁴²⁴⁾, but despite serum increases in CHD little data exists on it with respect to a potential role in I/R injury. Inhibition of CatL and CatB has been studied in the context of neuronal ischaemia/reperfusion and shows potentially beneficial effects in the initial 24-48 hours post stroke^(366;367). For example, Anagli *et al.* (2008) identified that cathepsin B and L activity was increased in ischaemic regions of the cerebral cortex with a concomitant increase in heat shock proteins, and that inhibition of cathepsins B and L resulted in a reduced infarct size by reducing heat shock protein levels and serum albumin leakage through the blood brain barrier⁽³⁶⁶⁾. Therefore, inhibition of CatL may have similar effects in cardiac I/R injury. Another potential role could be played in reperfusion arrhythmias. It is well known that arrhythmias occur during reperfusion following an ischaemic period⁽⁵⁶⁸⁾ and is the main cause of sudden cardiac death in humans⁽⁵⁶⁹⁾. Therefore, given the relationship between arrhythmias and Ca²⁺ waves, and the role TbCatL plays on Ca²⁺ handling in cardiomyocytes (discussed in Chapters 3 and 4) it is important to investigate the effects of mammalian cathepsin-L on cardiomyocytes Ca²⁺ handling. When mammalian CatL is compared to TbCatL there is considerable homology between the pre-, pro- and central regions of the enzyme⁽¹³¹⁾. However, a 108 amino acid C-terminal extension distinguishes the TbCatL from its mammalian counterpart. This extension is thought to be involved in targeting the enzyme within cells⁽¹³¹⁾. When the substrate

specificities of mammalian CatL, and related parasite cathepsin-L-like cysteine proteases has been compared, they show essentially the same enzymatic activity⁽⁵⁷⁰⁾ but have particular amino acid residue preferences at the P₂ position of the enzyme⁽¹³¹⁾ where the S₂ region of a substrate would bind (Figure 2.19). The significance of these minor differences in amino acid residue preference with regard to effects on Ca²⁺ handling remain unexplored. Work in the lab performed by a student, Katrin Nather, and supervised by me identified that increased CatL activity could be detected in an *ex vivo* model of I/R injury compared to control hearts (Figure 6.2). Therefore the potential role of increased CatL activity in I/R injury was investigated.

6.1.3 Ischaemia/Reperfusion Injury and Heart Failure

6.1.3.1 Ischaemia/Reperfusion Injury

Coronary heart disease (CHD) is the leading cause of death worldwide with an estimated 7 million deaths annually⁽³²⁶⁾. Coronary heart disease is a narrowing and eventual blockage of the coronary arteries supplying the myocardium with blood. The result of blockage is myocardial infarction (MI) creating a region of ischaemia distal to the obstruction. The most effective strategy for reducing the size of the infarct and improving clinical outcome is early reperfusion with use of thrombolytic therapy or percutaneous coronary intervention (PCI)⁽³²⁷⁾. However the process of restoring blood flow can itself be injurious - termed myocardial reperfusion injury. The injury results in death of cardiomyocytes that were viable immediately prior to reperfusion⁽³²⁸⁾. Myocardial reperfusion injury consists of four types of dysfunction. The first is myocardial stunning, a persistent mechanical dysfunction despite no irreversible damage and restoration of normal coronary flow⁽³²⁹⁾. This phenomenon is usually reversible days to weeks after the initial insult. The second type is the no-flow phenomenon where there is microvascular damage preventing restoration of blood flow to the affected region⁽³³⁰⁾. The third type is reperfusion arrhythmia brought about by Ca²⁺ overload and modulation of the Ca²⁺ handling proteins such as LTCC, RyR, SERCA and NCX⁽³³¹⁻³³⁷⁾. The fourth type of cardiac dysfunction is termed lethal reperfusion injury⁽³²⁷⁾. Lethal reperfusion injury is thought to have several mediators. The first is the oxygen paradox where reperfusion of the ischaemic tissue results in oxidative stress and release of

reactive oxygen species (ROS) and myocardial enzymes⁽³³⁸⁾ including cathepsins^(339;340). The second is the Ca²⁺ paradox where intracellular Ca²⁺ rises secondary to sarcolemmal damage and ROS effects inhibiting SERCA⁽³⁴¹⁻³⁴⁴⁾ and increasing P_o of the RyR⁽³⁴⁴⁻³⁴⁷⁾. The increase in Ca²⁺ can overload the cardiomyocyte leading to a state of hypercontracture and can overload the mitochondria leading to opening of the mitochondrial permeability transition pore (MPTP)⁽³²⁸⁾ which causes cell death by uncoupling of oxidative phosphorylation and ATP production. The third is pH paradox where rapid reperfusion washes out the lactic acid from anaerobic respiration leading to activation of the Na⁺/H⁺ exchanger and Na⁺/HCO₃⁻ symporter overwhelming the cell's buffering capacity⁽³⁴⁸⁾. The fourth is inflammation; the infarct zone attracts neutrophils during the first 24 hours causing vascular plugging, release of degradative enzymes and ROS⁽³⁴⁹⁾. The role of cathepsins in these processes is unclear but initial studies suggest that they have degradative effects^(428-431;571). It is not understood whether they damage cell membranes or mediate their effects through activation of surface receptors.

6.1.3.2 Heart Failure

Following a severe myocardial insult such as MI the remaining viable tissue can be taxed beyond its means and begin to fail. Heart failure (HF) is a disease state with weakening of myocardial contractility, ultimately resulting in deterioration of ventricular pump function. The characteristic cardiomyocyte features of HF are reduced systolic Ca²⁺ transient amplitude and prolonged Ca²⁺ transient duration⁽²⁹⁹⁻³⁰²⁾ with a concomitant reduction in the SR Ca²⁺ content⁽³⁰³⁻³⁰⁶⁾. The specific mechanisms involved in causing the reduced SR Ca²⁺ content remain unclear and intensely debated. However, in short, SR Ca²⁺ leak through the RyR is generally accepted as an important pathophysiological mechanism^(572;573). Other less consistent findings are reductions in SERCA expression/function^(279;574-577) and/or increases in NCX function/expression^(225;303;306). These Ca²⁺ handling proteins are all targets for phosphorylation mediated by PKA and CaMKII and current thinking is that modulation of the activity of these proteins is more important than expression levels⁽³⁰²⁾. Given the apparent effects on Ca²⁺ handling proteins potentially mediated by CaMKII by TbCatL, it is possible that mammalian extracellular CatL could also directly affect cardiomyocyte Ca²⁺

handling which could offer some explanation to the pathophysiological mechanisms in ischaemic heart disease.

6.1.4 Aims of the Chapter

Our evidence suggests that extracellular TbCatL can alter intra-cardiomyocyte $[Ca^{2+}]_i$ and lead to an increase in the frequency of cardiac arrhythmias. Another disease characterised by altered Ca^{2+} handling and arrhythmias is ischaemia/reperfusion injury, which can occur during treatment by PCI following acute MI⁽³²⁷⁾. The role of mammalian extracellular cathepsin-L (CatL) on cardiomyocyte function remains unknown. This is particularly important given that CatL is increased in the serum of individuals with cardiovascular disease^(425;426).

The aims of this chapter are to establish: i) the activity of CatL at different pH levels, ii) through a preliminary study whether CatL levels are increased in the serum of human patients that have undergone reperfusion by PCI, iii) through a preliminary study what relationship there may be between severity of ischaemic heart disease and CatL serum levels in the human patients and iv) what effect CatL has on Ca^{2+} handling in cardiomyocytes. The hypothesis is that following I/R injury, CatL is released and acts on the myocardium by an as yet unidentified target to alter Ca^{2+} handling in cardiomyocytes, potentially contributing to reperfusion arrhythmias and impaired cardiac function. This hypothesis will be tested by measuring the serum CatL levels of patients by ELISA, examining data gathered at the Golden Jubilee National Hospital, Glasgow, by magnetic resonance imaging and a combination of LASER-scanning confocal microscopy and epifluorescence microscopy to dissect the Ca^{2+} handling dynamics of cardiomyocytes.

6.2 Methods

6.2.1 Fluorometric Enzyme Activity Assays

6.2.1.1 Recombinant Mouse Cathepsin-L

Recombinant mouse cathepsin-L (R&D Systems) was supplied as 20 μL of a 0.5 $\text{mg}\cdot\text{mL}^{-1}$ solution in 25 mM tris(hydroxymethyl)aminomethane (Tris) and 150 mM sodium chloride (NaCl). The enzyme was in the pro-enzyme form and so required activation according to manufacturer's instructions. Briefly, an aliquot (depending on final volume required for experimentation) of the supplied solution was diluted to 10 $\mu\text{g}\cdot\text{mL}^{-1}$ in activation buffer (25 mM sodium acetate and 5 mM dithiothreitol (DTT) at a pH of 5.0 in water) and incubated for 90 min at 37 °C. The activated enzyme was diluted to a concentration of 0.05 $\text{ng}\cdot\mu\text{L}^{-1}$ in mouse assay buffer (25 mM 2-(N-morpholino) ethanesulfonic acid (MES) and 5 mM DTT) made specifically at pH 6.0, 7.0 and 7.4.

6.2.1.2 Recombinant Human Cathepsin-L

Recombinant human cathepsin-L (R&D Systems) was supplied as 36.2 μL of a 0.279 $\text{mg}\cdot\text{mL}^{-1}$ solution of 50 mM sodium acetate and 500 mM NaCl at pH 5.0 (10 μg quantity). For activation, the enzyme was diluted to 40 $\mu\text{g}\cdot\text{mL}^{-1}$ in human assay buffer (50 mM MES and 5 mM DTT at pH 6.0 in water) at room temperature for 15 min. Activated enzyme was diluted to 0.02 $\text{ng}\cdot\mu\text{L}^{-1}$ in assay buffer (as above) at pH 6.0, 7.0 and 7.4 for the activity assay.

6.2.1.3 Recombinant Cathepsin-L Activity Assays

Activated enzyme in assay buffer was tested at the recommended pH of 6.0, at pH 7.0 and physiological pH 7.4 in triplicate. Assay buffer at the appropriate pH was used as negative control blanks. An aliquot of the fluorescent substrate Z-leu-arg-AMC (R&D systems) was diluted in human or mouse assay buffer (depending on the enzyme to be tested) to a concentration of 20 μM and protected from light. 50 μL of 20 μM substrate was added to appropriate wells in a black maxisorp 96 well plate (Nunc) followed by 50 μL negative control to the control wells. 50 μL activated enzyme was added to the test wells immediately prior to the reading time as possible, so that enzyme activity could be read immediately. The plate was read on a spectrophotometer for 30 min at an

excitation wavelength of 380 nm and emission wavelength of 460 nm corresponding with the properties of the fluorescent moiety of the substrate, 7-amino-4-methylcoumarin (AMC).

6.2.1.4 Coronary Effluent Activity Assays

Coronary effluent samples were collected from Langendorff perfused hearts into eppendorfs at a ratio of 50:50 with effluent assay buffer (50 mM sodium acetate, 2 mM ethylenediaminetetraacetic acid (EDTA) and 2 mM DTT) at pH 5.5. The samples were added last in triplicate to a 96 well plate in 50 μ L quantities to wells already containing 100 μ L effluent assay buffer and 50 μ L Z-Leu-Arg-AMC substrate and read on a spectrophotometer as above. Tyrodes solution with effluent assay buffer mixed 50:50 was used a negative control with added recombinant mouse cathepsin-L as the positive control.

6.2.1.5 Specific Inhibitor Activity Assays

Aliquots from the effluent samples with peak activity were tested again with specific cathepsin inhibitors to confirm CatL activity was present in the effluent samples. The substrate Z-Leu-Arg-AMC is cleaved by both cathepsins B and L, and so specific inhibitors of B and L were used to differentiate between these cathepsins. CA074 was used to inhibit cathepsin-B⁽⁵⁷⁸⁾ and CAA0225 was used to inhibit CatL⁽⁵⁷⁹⁾, both at concentrations of 10 μ M. Both inhibitors permanently and competitively bind the active sites of their respective targets preventing them from cleaving any substrate^(578;579). Samples were run without any inhibitor, with CatL inhibitors \pm CA074 and with CA074 only. The same set of conditions was run on the same plate with recombinant mouse CatL. Inhibitors with assay buffer only were used as blanks.

6.2.2 Cardiomyocyte Isolations

6.2.2.1 Adult Rat Left Ventricular Cardiomyocyte Isolation

Adult rat cardiomyocytes were isolated as described in section 2.3.1 and resuspended in 1.8 mM Ca^{2+} MIKH.

6.2.2.2 Adult Rabbit Left Ventricular Cardiomyocyte Isolation

Rabbit cell isolation was performed by Mrs. Aileen Rankin as described in section 2.3.2. Cells were then suspended in 1.8 mM Ca^{2+} MIKH ready for experimentation.

6.2.3 Epifluorescence Measurements of the Field Stimulated Ca^{2+} Transient

6.2.3.1 Cathepsin-L Activation

Recombinant mouse CatL was activated prior to experimentation. Two different batches were used during the course of the experiments. The first required 90 min activation at a concentration of $10 \mu\text{g}\cdot\text{mL}^{-1}$ at 37°C in activation buffer (section 6.2.1.1), the second required overnight activation at $100 \mu\text{g}\cdot\text{mL}^{-1}$ at room temperature in activation buffer according to manufacturer's recommendations (R&D Systems).

6.2.3.2 Cardiomyocyte Preparation

Intact cardiomyocytes were incubated with Ca^{2+} sensitive fluorophore ($5 \mu\text{M}$ Fura-2-AM (Biotium Inc., Hayward, CA)) for 10 min. Cells were then re-suspended in 1.8 mM Ca^{2+} MIKH with activated CatL or matching volume of activation buffer as vehicle control. Concentrations tested were 0.68 nM, 2.7 nM and 5.4 nM. Cells were incubated at room temperature for 30 min to allow enzyme to act and cells to de-esterify the Ca^{2+} sensitive dye.

6.2.3.3 Stimulated Calcium Transient Acquisition

Once the cardiomyocytes were prepared they were loaded into a tissue bath with field stimulator (Cell Microcontrols) and superfused with 1.8mM Ca^{2+} KH with CatL or vehicle *via* gravity fed perfusion pen with active outflow. Cells were field-stimulated (0.5 Hz, 2.0 ms duration, voltage set to 1.5 x threshold) for 5 min with a signal generator and stimulator (Digitimer Ltd). The fluorescence ratio (340/380 nm excitation wavelength) was measured with a spinning wheel spectrophotometer (Cairn Research UK) at a sampling rate of 5 kHz. Each cell had background light offset on the photomultiplier tube amplifier unit (Cairn Research UK). Minimum ratio (R_{\min}) was recorded prior to stimulation

and maximum ratio (R_{\max}) was measured by puncturing the cell membrane with a sharp glass micropipette manoeuvred by a micromanipulator (Scientifica).

6.2.3.4 Sarcoplasmic Reticulum Calcium Content

Sarcoplasmic reticulum (SR) Ca^{2+} content was determined by rapid application of a bolus of 10mM caffeine *via* the perfusion pen. Field-stimulation was stopped and the perfusion solution immediately changed using a c-flow pinch valve system (Cell Microcontrols).

6.2.3.5 Calcium Transient Analysis

Fluorescence ratio was converted to Ca^{2+} using the following calculation:

$$[\text{Ca}^{2+}]_i = ((\text{Ratio} - R_{\min}) / (R_{\max} - \text{Ratio})) \times (1.2 \times 10^{-6})$$

Data were analysed offline and mean $[\text{Ca}^{2+}]_i$ obtained from the average transient generated from the last 12 transients plotted using Origin (OriginLab) software.

6.2.4 Confocal Imaging of Spontaneous SR-mediated Ca^{2+} Release

6.2.4.1 Confocal Image Acquisition

Intact cardiomyocytes isolated as described in (6.2.2) were loaded with Fluo-3AM Ca^{2+} sensitive fluorophore for 10 min. Cells were resuspended and incubated in 1.8 mM Ca^{2+} MIKH with 5.4 nM activated recombinant CatL or equivalent volume of vehicle for 30 min as in section 6.2.3.2. Confocal line-scan images of cardiomyocytes were recorded using a LSM 510 confocal system (Zeiss). Fluo-3AM was excited at 488nm (Ar LASER) and measured >515 nm using epifluorescence optics of an inverted microscope with a 63 x/1.2 NA water-immersion objective lens. Fluorescence was acquired in line-scan mode at $3.07 \text{ ms.line}^{-1}$ (1 line = 512 pixels); pixel dimension was $0.27 \mu\text{m}$. The scanning LASER line was orientated parallel with the long axis of the cell and placed approximately equidistant between the outer edge of the cell and the nucleus/nuclei to ensure the nuclear area was not included in the scan line.

6.2.4.2 Confocal Image Analysis

Fluorescence data were expressed as the ratio of quiescent fluorescence (F/F_0). The fluorescence intensity profile was calculated from a 20 pixel band adjacent to the point of spontaneous event initiation. This avoids movement artefact⁽²⁹⁶⁾. Event frequency was calculated as number/time(s). The event velocity was calculated as the gradient of the wave progression across the cell expressed as $\mu\text{m}\cdot\text{s}^{-1}$. Wave decay and amplitude were calculated from the intensity profile trace.

6.2.5 Langendorff Perfusion Global Ischaemia/Reperfusion

Adult male Wistar rats (250-300 g) were euthanized in accordance with Schedule 1 of the Animal (Scientific Procedures) Act 1986 and hearts rapidly excised. Hearts were cannulated *via* the aorta in retrograde perfusion. Tyrodes solution at 1.8 mM $[\text{Ca}^{2+}]_o$ infused with 95% O_2 and 5% CO_2 was perfused through the hearts at $10 \text{ mL}\cdot\text{min}^{-1}$. The perfusion was stopped for a 30 min period of ischaemia. Control hearts (no ischaemia) were perfused continually. Perfusion was restarted and continued for 90 min. Coronary effluent was collected at 10 min and immediately prior to ischaemia, and upon reperfusion every minute for 5 min followed by every 10 min from 10 min. This technique was in conjunction with Katrin Nather, a Masters student under my supervision.

6.2.6 Enzyme-Linked Immunosorbent Assay of Human Serum

Samples of serum were obtained from patients presenting to the Golden Jubilee National Hospital (GJNH), Clydebank, Glasgow, UK with acute ST segment elevation myocardial infarction (STEMI). Samples were obtained with the patient's written consent and ethical approval from the University of Glasgow Ethical Approval Committee. An arterial blood sample was taken from an indwelling catheter inserted on clinical grounds at presentation immediately prior to percutaneous coronary intervention (PCI) (section 1.6.4) to reperfuse the heart (pre reperfusion sample). Another arterial sample was taken after intervention (immediate post reperfusion sample) as the patient was recovered. Blood samples were collected into 5 mL gel separator serum tubes and transported to the British Heart Foundation Glasgow Cardiovascular Research Centre, University of Glasgow. The samples were centrifuged at 2,400 g for 15

min to separate the serum from the cellular component. Serum was aspirated into 0.5-1.0 mL aliquots and stored at -80 °C until required. The quantity of cathepsin-L was measured by enzyme-linked immunosorbent assay (ELISA) using the manufacturer's recommended protocol (USCN Life Science Inc.) and normalised to the total protein content of the serum determined by bicinchoninic acid (BCA) assay.

6.2.7 Cardiac Magnetic Resonance Imaging

Patients were invited to return to the GJNH 6 months post primary presentation for cardiac magnetic resonance imaging (MRI) with contrast enhancement. Contrast enhancement permits visualisation of the blood flow within the tissue enabling assessment of infarct size and the area at risk. The MRI was performed by two members of GJNH clinical staff with MRI experience. Images were assessed by clinical staff at GJNH who examined; infarct size, area at risk, ejection fraction, left ventricular systolic and diastolic volume indexed to body surface area to control for variation in patient size; and the results reported for inclusion in this study. The data was sent to me for correlation with serum CatL levels measured by ELISA. Patient data was tracked by anonymous patient identification number.

6.2.8 Statistical Analysis

Data are expressed as mean \pm SEM. Statistical comparisons were made by a two-sample Student's T-test on the raw data. Multiple groups were compared with ANOVA. A significance level of $P < 0.05$ was considered significant.

6.3 Results

6.3.1 Mammalian Cathepsin-L is Active at Physiological pH

CatL is a lysosomal cysteine protease and therefore usually active at acidic pH⁽³⁶⁸⁾. The reported optimum pH for CatL is pH 5.5-6.0⁽³⁷¹⁾. However, recent findings have identified additional roles for CatL at more physiological pH such as in the cytosol⁽³⁸³⁻³⁸⁵⁾ or extracellular space⁽⁵⁸⁰⁾. To determine if extracellular CatL could act on cardiomyocytes at physiological pH enzyme activity assays were performed with recombinant mouse CatL at pH 6.0, 7.0 and 7.4. Figure 6.1 shows the activity curves (Figure 6.1A) generated when enzyme has been incubated with the fluorogenic substrate Z-LR-AMC at 37 °C and measured at excitation and emission wavelengths of 380nm and 460nm respectively on a spectrophotometer. The data show that CatL is active at all tested pH with no significant difference; ($2.88 \times 10^6 \pm 1.07 \times 10^6$ vs. $2.82 \times 10^6 \pm 1.89 \times 10^5$ vs. $2.14 \times 10^6 \pm 5.19 \times 10^6$ arbitrary fluorescence units; pH 6.0 vs. pH 7.0 vs. pH 7.4; $P > 0.05$, Figure 6.1B).

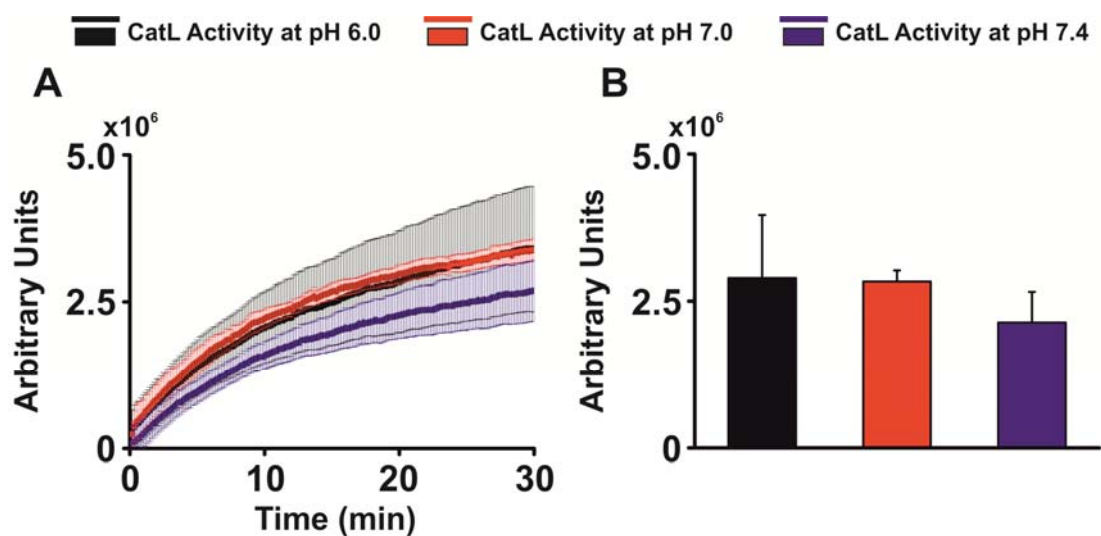


Figure 6.1: Fluorometric activity assay of recombinant mouse CatL at different pH. (A) Enzyme activity curves for recombinant mouse CatL. Activity was determined by cleavage of a fluorogenic substrate (Z-LR-AMC) measured at wavelengths of 380 nm excitation and 460 nm emission on a spectrophotometer. Neutral and physiological pH values (7.0 and 7.4) were compared to optimum pH 6.0 recommended by the manufacturer. Assay buffer without enzyme at each pH was used as a blank and subtracted from the experimental curves. Activity is present at all pH values ($n = 5$ triplicates). (B) Mean \pm SEM for enzyme activity in arbitrary units at 30 min in assay buffer at pH 6.0, 7.0 and 7.4.

6.3.2 Cathepsin-L Can be Detected in Coronary Effluent from Ischaemic Hearts

In clinical patients with ischaemic heart disease increased serum levels of CatL have been described^(425;426). Sun *et al.* (2010) found increased CatL activity in the myocardium of homogenised murine hearts following experimental induction of myocardial infarction⁽⁴²⁴⁾. However, it is not clear whether CatL is directly released by cells within the heart. Therefore, *ex vivo* Langendorff perfused rat hearts were subjected to 30 min global ischaemia with a control group of hearts perfused continuously. Coronary effluent was collected at time-points pre and post ischaemia and CatL activity measured by a fluorometric enzyme activity assay. Perfusion Tyrodes solution with fluorogenic substrate was used as a blank and subtracted from the coronary effluent data to give a relative change in fluorescence over Tyrodes and substrate alone. These experiments were performed in conjunction with Katrin Nather under my supervision. CatL activity was detected in the coronary effluents following ischaemia ($n = 3$) compared to control hearts ($n = 3$) that were perfused throughout the protocol. No activity was detected from coronary effluent samples from the period prior to ischaemia in either cohort (Figure 6.2A). Since the fluorogenic substrate is also cleavable by CatB that may be present in the effluent samples the activities of both CatB and CatL were dissected using the specific inhibitors CA074 (against CatB) and CAA0225 (against CatL) at concentrations of 10 μM . Activity was inhibited by 79% with CA074 and by 100% with CAA0225 (Figure 6.2B).

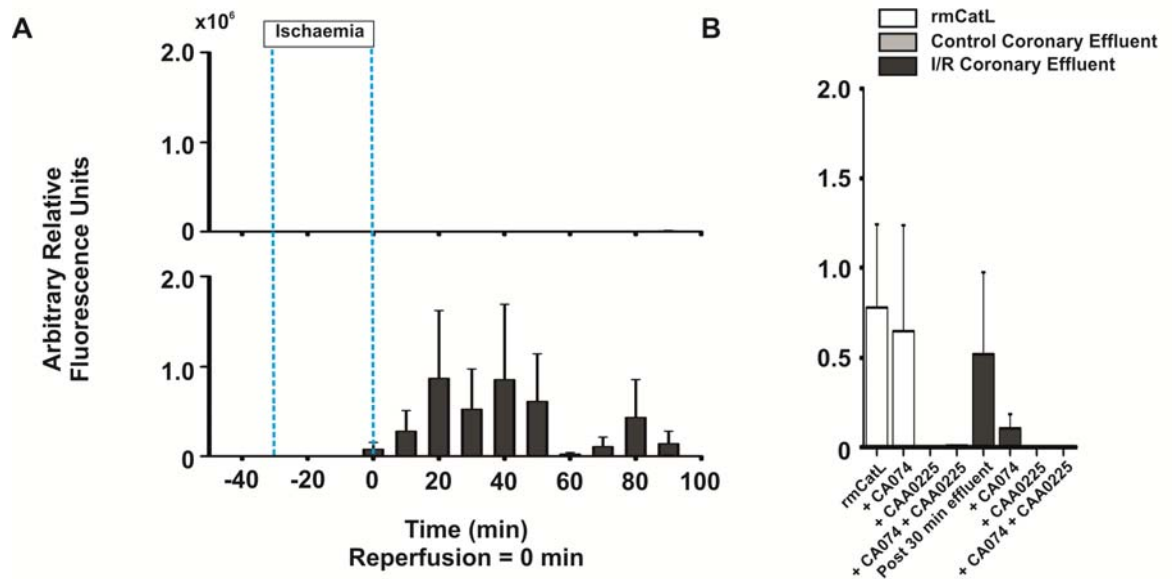


Figure 6.2: CatL activity in coronary effluent samples from ischaemia/reperfusion hearts (A) Mean \pm SEM of CatL activity in arbitrary fluorescence units as measured by fluorometric assay with Z-LR-AMC substrate for coronary effluent samples. (Top) Control ($n = 3$) hearts perfused with Tyrodes at $10 \text{ mL} \cdot \text{min}^{-1}$ and (Bottom) ischaemia/reperfusion ($n = 3$) hearts. Recombinant mouse CatL (rmCatL) at 0.68 nM was used as an assay control. (B) Mean \pm SEM of 30 min post reperfusion sample \pm CatL inhibitor CAA0225 and/or CatB inhibitor CA074. Blue lines indicate period of ischaemia. Time 0 is the first collection immediately after perfusion is restarted.

6.3.3 Cathepsin-L is Increased in Serum of Human Patients That Have Undergone Reperfusion Following Myocardial Infarction

Patients with coronary artery disease have been shown to have increased serum levels of CatL^(425;426). However, to our knowledge no-one has measured the levels of CatL following reperfusion. The data from coronary effluent samples in rat hearts suggest that there are increased levels of CatL activity following reperfusion. Therefore, as a preliminary study, serum samples were obtained from human patients that presented to the GJNH with a diagnosis of STEMI. Whole blood samples ($\sim 10 \text{ mL}$) were obtained from an indwelling (arterial) catheter inserted on clinical grounds from primary PCI by clinical staff at GJNH at the following points; pre-reperfusion by PCI and immediately post reperfusion. Thawed serum prepared as described in section 6.2.6 was measured by ELISA for CatL levels. The concentration of CatL was increased upon reperfusion (but not significantly) (4.42 ± 0.95 vs. $6.28 \pm 1.50 \text{ ng} \cdot \text{mL}^{-1}$; pre-reperfusion vs. immediately post reperfusion; ($n = 4$); $P = 0.11$ and 0.14 ; Figure 6.3A). Total serum protein levels in patients can be altered due to hydration

status and fluid therapy during the PCI procedure. Therefore total serum protein was measured by BCA assay and the quantity of CatL normalised to the total protein. There was an increase, albeit not statistically significant, in CatL in the immediately post-reperfusion serum (0.070 ± 0.012 vs. 0.110 ± 0.025 ng.mg^{-1} total protein; pre-reperfusion vs. immediately post reperfusion; $P = 0.09$ and 0.14 ; Figure 6.3B).

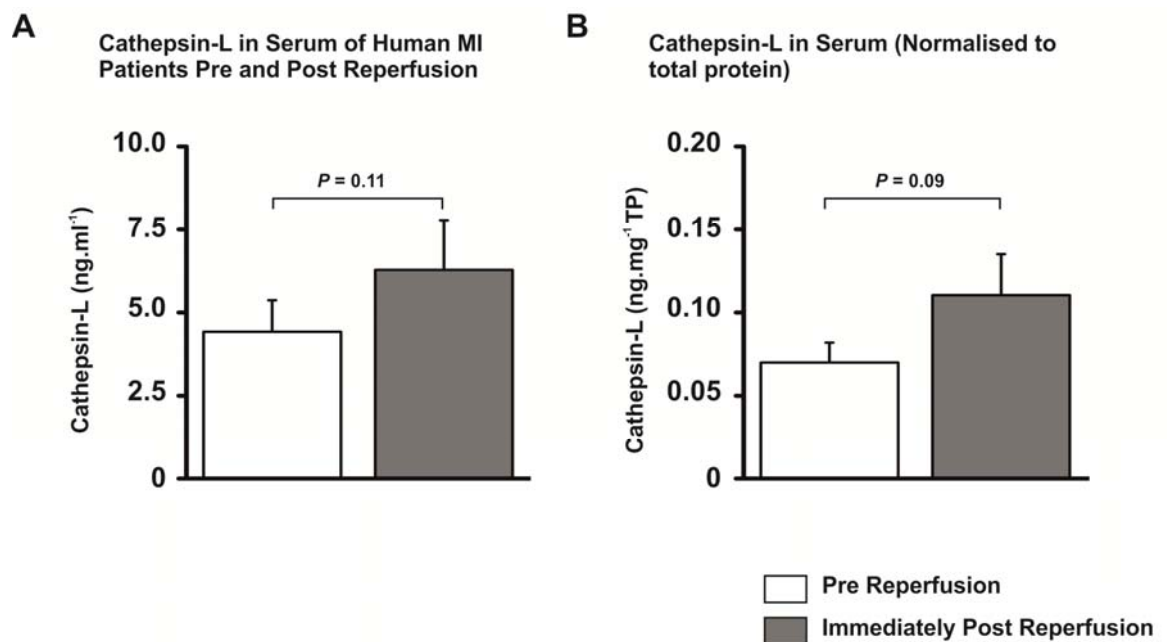


Figure 6.3: Serum concentration of CatL in human patients following myocardial infarction (A) Mean \pm SEM of serum CatL ($n = 4$) as determined by specific serum ELISA. (B) Serum CatL normalised to total protein determined by BCA protein assay.

6.3.4 Serum Cathepsin-L Levels Correlate With Severity of Cardiac Dysfunction Measured by MRI

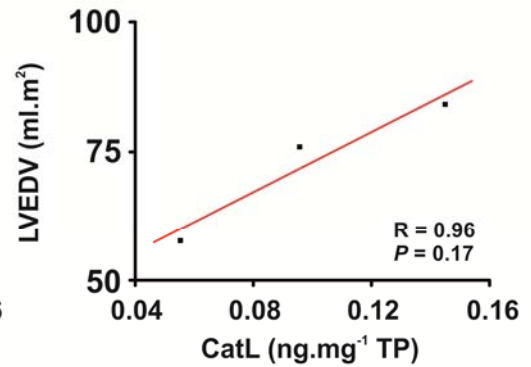
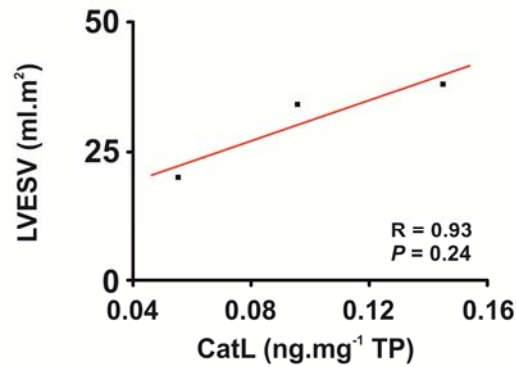
Patients that had undergone PCI for STEMI were invited back to the GJNH 6 months after initial presentation for follow-up cardiac MRI. Three of the seven patients returned. Patients were imaged by experienced clinical staff and the images were analysed by Dr. David Carrick at the GJNH, who then forwarded the data for correlation with the serum CatL levels for the same patients taken immediately post reperfusion. There was a positive correlation of left ventricular end systolic volume with serum CatL levels ($R = 0.93$; $P = 0.24$; $n = 3$; Figure 6.4A(i)). Similarly, there was a positive correlation for left ventricular end diastolic volume with serum CatL ($R = 0.96$, $P = 0.17$; Figure 6.4A(ii)). There were positive correlations for both infarct size ($R = 0.96$, $P = 0.17$; Figure 6.4A(iii)) and the area of myocardium at risk ($R = 0.98$, $P = 0.14$; Figure 6.4A(iv))

with serum CatL. The ejection fraction correlated negatively with serum CatL ($R = -0.87$, $P = 0.33$; Figure 6.4A(v)).

A

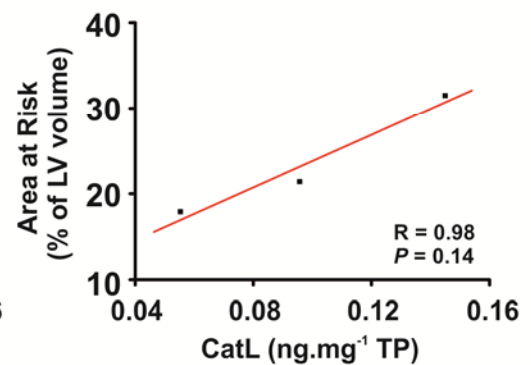
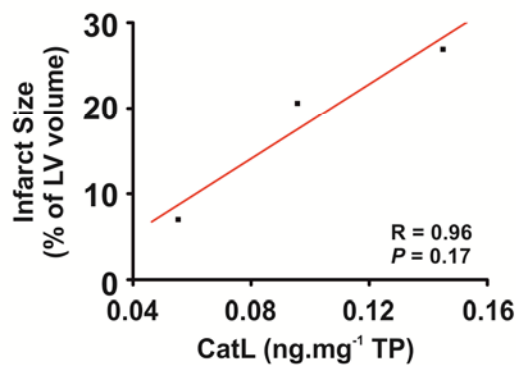
(i) Left Ventricular End Systolic Volume

(ii) Left Ventricular End Diastolic Volume



(iii) Infarct Size

(iv) Area at Risk



(v) Ejection Fraction

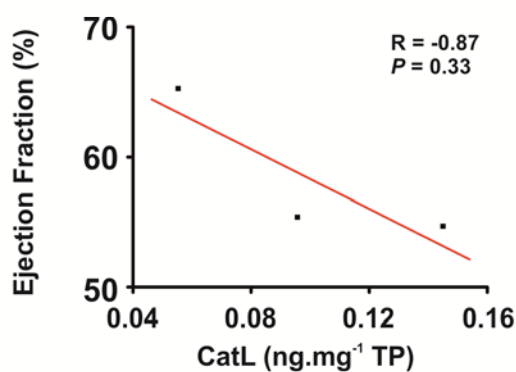


Figure 6.4: Serum CatL vs. MRI parameters.

(A(i-v)) Serum CatL level from immediately post reperfusion plotted against left ventricular end systolic volume, left ventricular end diastolic volume, infarct size, area at risk and ejection fraction. Linear best fit drawn using graphical software programme, Origin6.1 (*OriginLab*).

6.3.5 Cathepsin-L Reduces Stimulated Ca^{2+} Transient Amplitude in Rat Left Ventricular Cardiomyocytes

Increased serum levels of CatL have been shown to be associated with an increased severity of cardiac disease⁽⁴²⁵⁾. To examine whether increased levels of extracellular CatL could have a detrimental effect on cardiomyocyte Ca^{2+} handling, epifluorescent Ca^{2+} measurements were conducted with different concentrations of CatL. Concentrations tested were determined from pathological values reported in the literature^(425;426), the predicted concentrations from Figure 6.1 & Figure 6.2 and the concentration of TbCatL based on Caffrey *et al.* (2001)⁽¹²⁹⁾. Isolated rat left ventricular cardiomyocytes were incubated for 30 min with CatL (Figure 6.5A) at a concentration of 0.68 nM (1:400), 2.70 nM (1:100) and 5.40 nM (1:50) or vehicle control (Figure 6.5B(i-iv)). The peak $[\text{Ca}^{2+}]_i$ was significantly decreased to 82.9%, 62.3% and 56.3% of control respectively (552.2 ± 23.7 vs. 458.0 ± 36.8 vs. 344.3 ± 24.2 vs. 310.9 ± 29.2 nM; control vs. 0.68, vs. 2.70 vs. 5.40 nM CatL; $P < 0.05$; Figure 6.5C(ii)). The minimum $[\text{Ca}^{2+}]_i$ was not significantly altered at 0.68 or 2.70 nM CatL (67.5 ± 1.9 vs. 57.1 ± 2.5 vs. 65.5 ± 2.8 nM; control vs. 0.68, vs. 2.70 nM CatL; $P > 0.05$; Figure 6.5C(iii)). However, the minimum $[\text{Ca}^{2+}]_i$ was increased to 138.5% of control at 5.40 nM CatL (67.5 ± 1.9 vs. 93.5 ± 6.4 nM; control vs. 5.40 nM CatL; $P < 0.05$; Figure 6.5C(iii)). Ca^{2+} transient amplitude as a result of the reduced peak $[\text{Ca}^{2+}]_i$ was also significantly reduced at all concentrations of CatL to 82.7%, 57.5% and 44.8% of control respectively (484.8 ± 22.5 vs. 400.9 ± 35.5 vs. 278.8 ± 23.8 vs. 217.4 ± 26.5 nM; control vs. 0.68, vs. 2.70 vs. 5.40 nM CatL; $P < 0.05$; Figure 6.5C(iv)). In contrast with the data presented in the preceding chapters, mammalian CatL decreased the rate constant of decay to 91.3% of control at 0.68 nM, and significantly to 61.4% and 36.2% of control, 2.70 and 5.40 nM CatL respectively (12.7 ± 0.7 vs. 11.6 ± 0.8 ($P > 0.05$) vs. 7.8 ± 1.2 vs. 4.6 ± 0.4 s⁻¹; control vs. 0.68, vs. 2.70 vs. 5.40 nM CatL; $P < 0.05$; Figure 6.5C(v)). CatL activity was measured by fluorometric activity assay in the cardiomyocyte perfusate (arbitrary fluorescence units) and correlated with $[\text{Ca}^{2+}]_i$ amplitude to give an inverse linear correlation with $r^2 = -0.98 \pm 0.90$ S.D. (Figure 6.5C(vi)). Activity levels were 0.18 ± 0.02 vs. 1.42 ± 0.19 vs. $2.62 \pm 0.04 \times 10^4$ arbitrary fluorescence units normalised to no enzyme control; 0.68, vs. 2.70 vs. 5.40 nM CatL; $P < 0.05$ (Figure 6.5C(vi) inset).

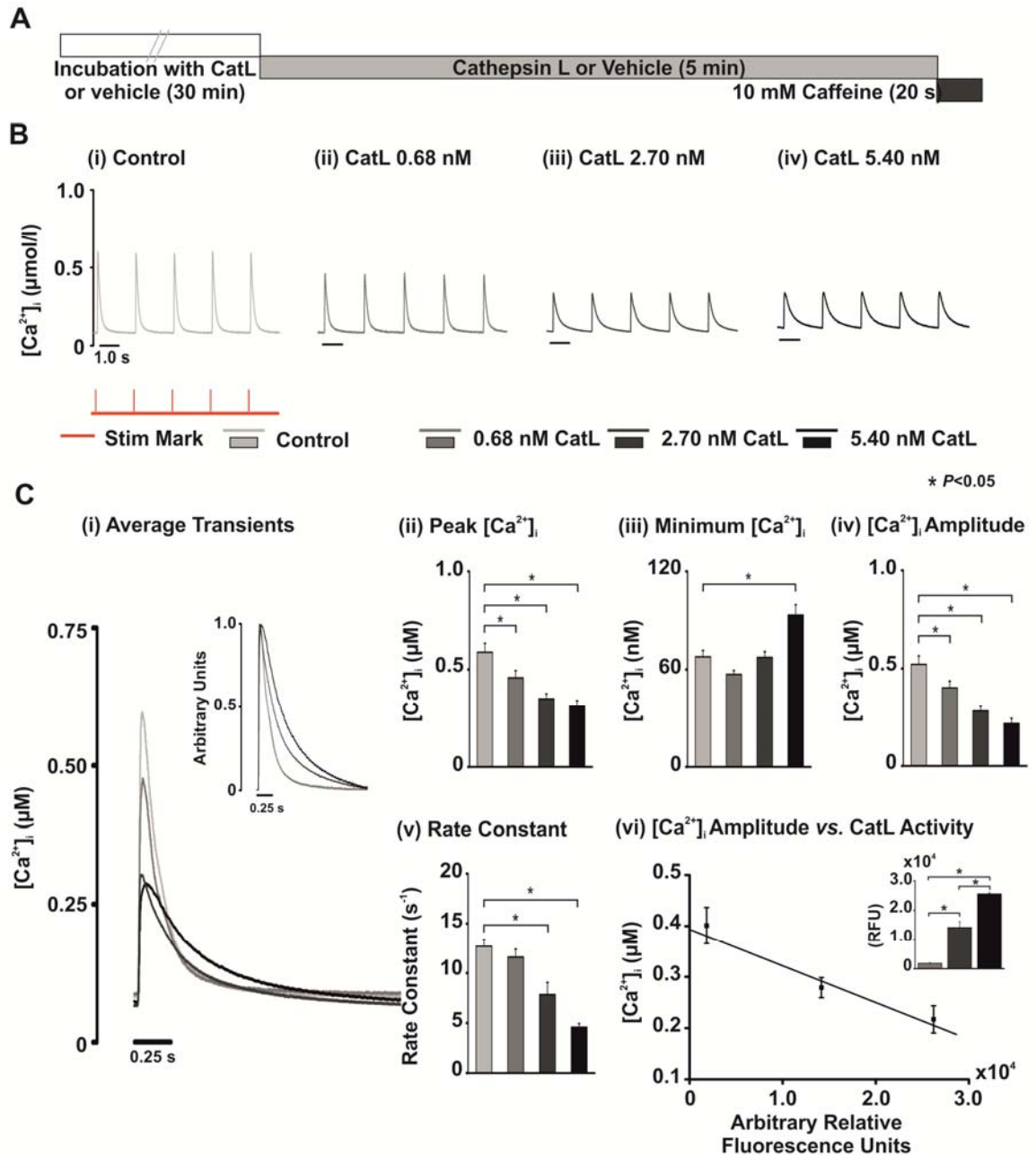


Figure 6.5: Stimulated Ca²⁺ transients at different CatL concentrations.

(A) Protocol used for epifluorescence Ca²⁺ measurements. (B) Example Ca²⁺ transient traces for (i) control, (ii) 0.68 nM CatL, (iii) 2.70 nM CatL and (iv) 5.40 nM CatL. The stimulus mark is shown in (i), the frequency was 0.5 Hz. (C(i)) Average Ca²⁺ transients for the different concentrations, (Inset) normalised average transients from (i). (ii - v) Mean ± SEM for Ca²⁺ transient parameters; control (*n* = 67), 0.68 nM CatL (*n* = 23), 2.70 nM CatL (*n* = 22) and 5.40 nM CatL (*n* = 18). (vi) Plot of the relationship between CatL activity (measured by cleavage of a fluorogenic substrate) (*n* = 3) against Ca²⁺ transient amplitude. (Inset) Activity level (RFU) for each concentration tested.

6.3.6 Cathepsin-L Reduces SR Ca²⁺ Content in Rat Left Ventricular Cardiomyocytes

Ca²⁺ transient amplitude is related to SR Ca²⁺ content therefore high concentration caffeine (10 mM; 20 s) was applied rapidly to cardiomyocytes at the end of the protocol (Figure 6.6A). The amplitude of the caffeine-induced

Ca^{2+} transient is an indicator of the SR Ca^{2+} content. The rate constant of decline is an indicator of sarcolemmal Ca^{2+} efflux. The caffeine-induced Ca^{2+} transient amplitude was significantly reduced compared to control at all concentrations of CatL (100.0 vs. 78.8 ± 5.0 vs. 81.5 ± 5.2 vs. $60.1 \pm 8.5\%$ of vehicle control; control vs. 0.68, vs. 2.70 vs. 5.40 nM CatL; $P < 0.05$; Figure 6.6C(i)). The rate constant of decay was not significantly altered at 0.68 or 2.70 nM (100.0 vs. 101.7 ± 6.0 vs. $95.0 \pm 8.9\%$ of vehicle control; control vs. 0.68, vs. 2.70 nM CatL; $P > 0.05$; Figure 6.6C(ii)), but was significantly reduced at 5.40 nM CatL; (100.0 vs. $78.9 \pm 3.9\%$; control vs. 5.40 nM CatL; $P < 0.05$; Figure 6.6C(ii)).

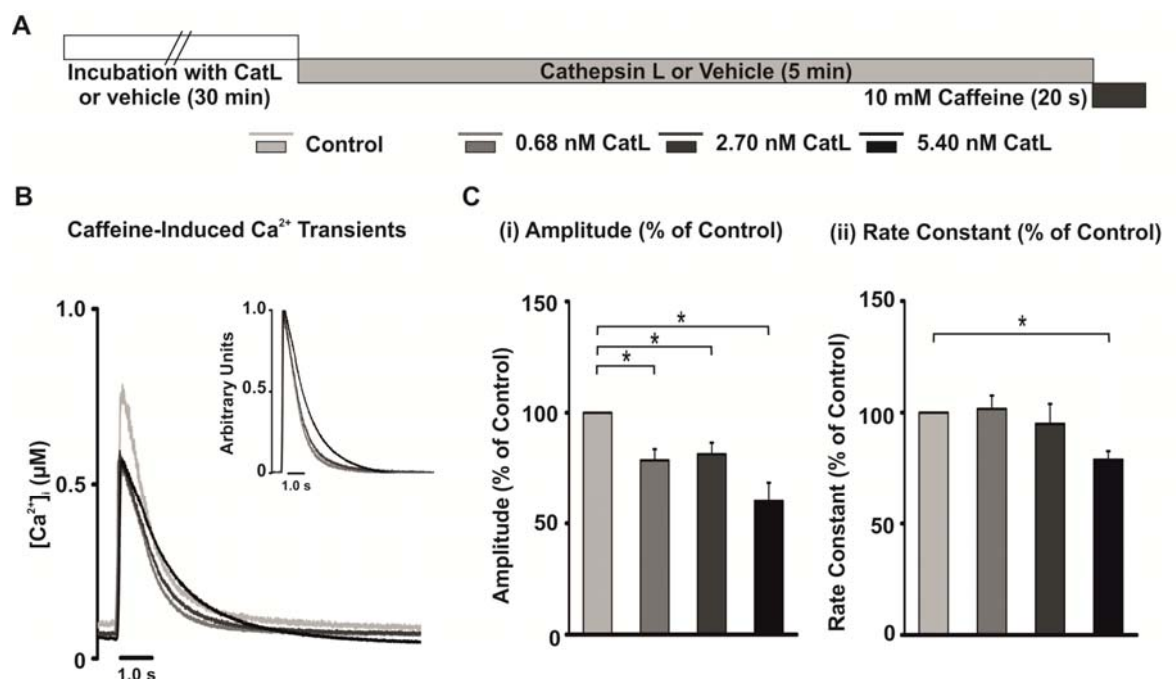


Figure 6.6: Caffeine-induced Ca^{2+} transients at different CatL concentrations.

(A) Protocol. (B) Example caffeine-induced Ca^{2+} transients. (Inset) Normalised caffeine-induced Ca^{2+} transients from (B). (C(i)) Mean \pm SEM caffeine-induced Ca^{2+} transient amplitude as % change of vehicle control (ii) Rate constant of decay as % change of vehicle control.

6.3.7 Cathepsin-L Reduces Stimulated Ca^{2+} Transient Amplitude in Rabbit Left Ventricular Cardiomyocytes

The Ca^{2+} handling dynamics of rat left ventricular cardiomyocytes are different to that of human ventricular cardiomyocytes⁽¹⁴⁸⁾ (discussed in section 1.4). In the rat Ca^{2+} transient decline is predominantly due to SERCA mediated reuptake to the SR, with reported percentage contributions of 87-92% in the rat^(223;224;581) vs. 63% in normal human ventricular cardiomyocytes and 58% in failing

cardiomyocytes⁽²²⁵⁾. The other major contributor to the Ca^{2+} transient decline during diastole is sarcolemmal efflux by NCX. In the rat this constitutes 7-9%^(223;224;581) vs. 37% in normal human cardiomyocytes and 42% in failing cardiomyocytes⁽²²⁵⁾. Therefore, to examine the SR Ca^{2+} release in an animal model with similarities to human cardiomyocyte Ca^{2+} handling the rabbit was used. The rabbit exhibits similar Ca^{2+} handling properties with SERCA reuptake contributing 70-74% of the Ca^{2+} transient decline and NCX contributing 23-28%^(257;582). Therefore epifluorescence Ca^{2+} measurements were made in rabbit left ventricular cardiomyocytes using the same protocol as for the data shown in Figure 6.5 (Figure 6.7A). The concentration of CatL used was 0.68 nM, which was identified by activity assays to be the quantity produced in Langendorff perfused hearts and is similar to that reported in patients⁽⁴²⁵⁾ (Figure 6.7B). In comparison with the rat cardiomyocytes, CatL significantly reduced the peak $[\text{Ca}^{2+}]_i$ to 65% of control (399.6 ± 52.4 vs. 260.1 ± 22.4 nM; control vs. CatL; $P < 0.05$; Figure 6.7C(ii)). Minimum $[\text{Ca}^{2+}]_i$ was not significantly altered (54.1 ± 4.6 vs. 53.3 ± 4.3 nM; control vs. CatL; $P > 0.05$; Figure 6.7C(iii)). The reduced peak $[\text{Ca}^{2+}]_i$ led to a significantly reduced $[\text{Ca}^{2+}]_i$ amplitude of 60% of control (345.5 ± 50.9 vs. 206.8 ± 2.0 nM; control vs. CatL; $P < 0.05$; Figure 6.7C(iv)). The decay rate constant was not significantly altered (7.0 ± 0.2 vs. 6.8 ± 0.3 s^{-1} ; control vs. CatL; $P < 0.05$; Figure 6.7C(v)), which is similar to the result in rat cardiomyocytes at 0.68 nM.

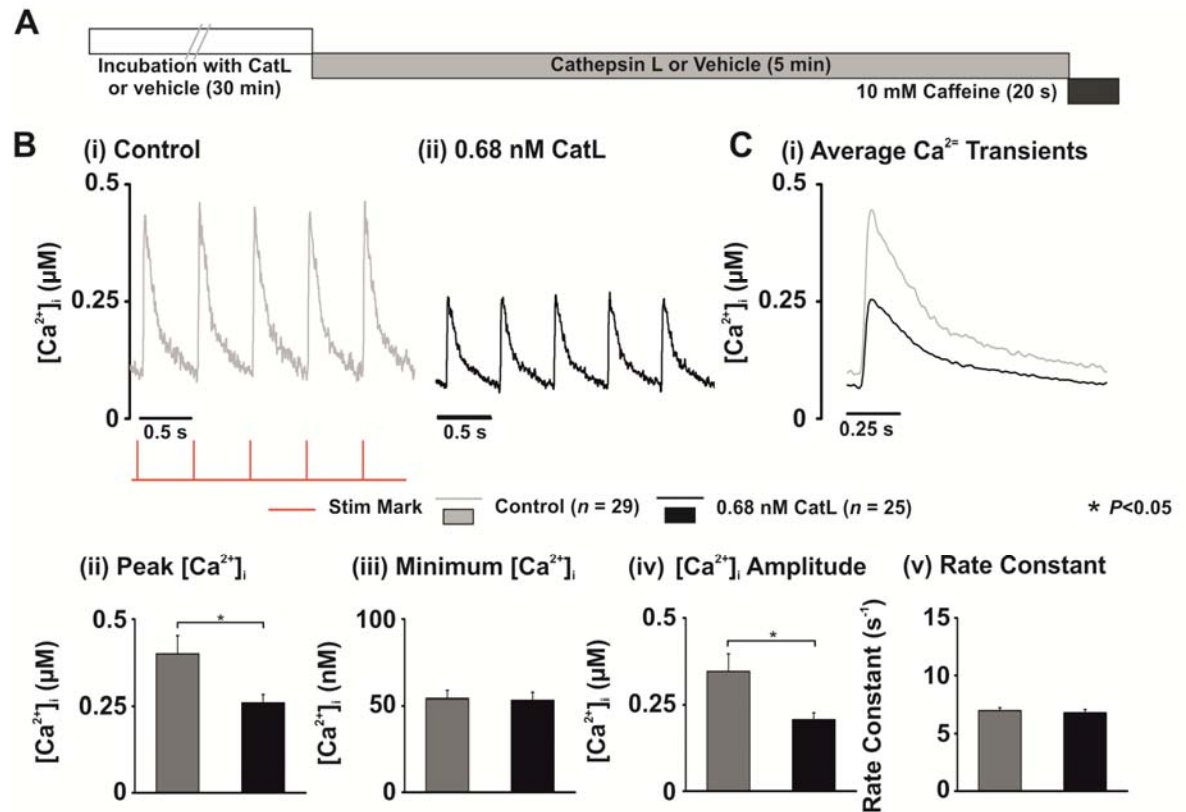


Figure 6.7: Stimulated Ca²⁺ transients with CatL in rabbit left ventricular cardiomyocytes. (A) Protocol used in epifluorescence Ca²⁺ measurements. (B) Example Ca²⁺ transient traces for (i) control and (ii) 0.68 nM CatL. The stimulus mark is shown in (i), the frequency was 2.0 Hz. (C(i)) Average Ca²⁺ transients taken from last 12 Ca²⁺ transients for media (grey) and CatL (black). (ii - v) Mean ± SEM for stimulated Ca²⁺ transient parameters for control (n = 29) and 0.68 nM CatL (n = 25).

6.3.8 Cathepsin-L Reduces SR Ca²⁺ Content in Rabbit Left Ventricular Cardiomyocytes

As with the rat cardiomyocyte experiments, the SR Ca²⁺ content was measured from the amplitude of the caffeine-induced Ca²⁺ transient at the end of the protocol (Figure 6.8A). The caffeine-induced Ca²⁺ transient amplitude was significantly reduced to 49.8% of control; (466.8 ± 121.4 vs. 232.3 ± 29.0 nM; control vs. CatL; $P < 0.05$). The rate constant of decline, an indicator of NCX function, was not significantly altered; (1.22 ± 0.11 vs. 1.25 ± 0.10 s⁻¹; control vs. CatL; $P > 0.05$) (Figure 6.8C(i-ii)).

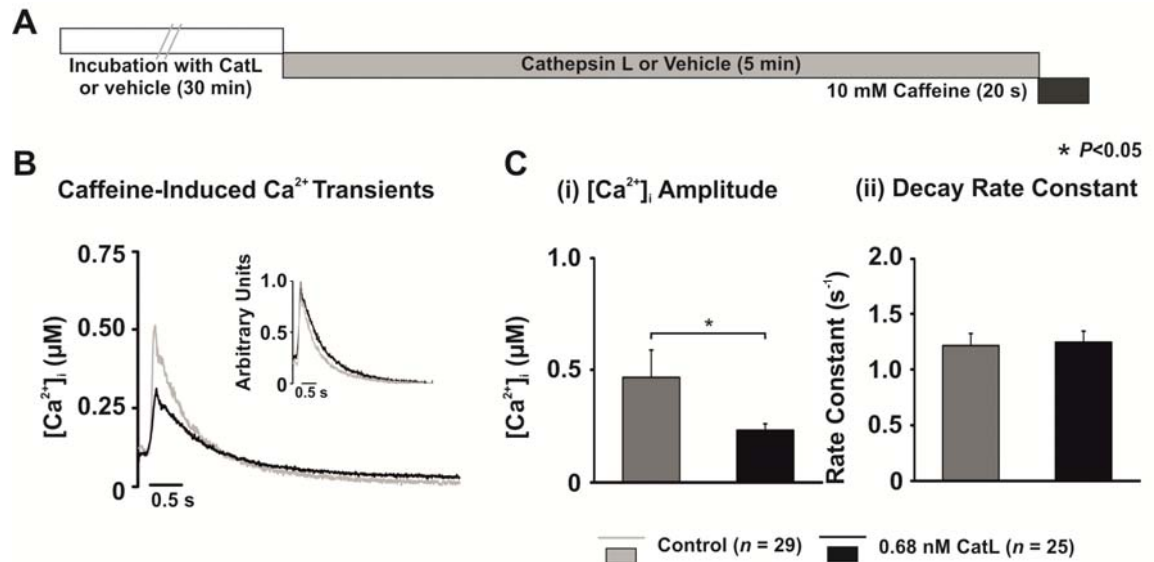


Figure 6.8: Caffeine-induced Ca^{2+} transients in rabbit cardiomyocytes with CatL. (A) Protocol used for epifluorescence Ca^{2+} measurements. (B) Example caffeine-induced Ca^{2+} transients for vehicle control (grey) and 0.68 nM CatL (black). (Inset) Normalised caffeine-induced Ca^{2+} transients from (B). (C(i – ii)) Mean \pm SEM for caffeine-induced Ca^{2+} transient amplitude and decay rate constant for control ($n = 29$) and CatL ($n = 25$).

6.3.9 Cathepsin-L Increases Ca^{2+} Wave Frequency in Resting Cardiomyocytes

Reduced SR Ca^{2+} content and reduced stimulated Ca^{2+} transient amplitude can be a result of both increased spontaneous Ca^{2+} release and altered RyR P_o lowering the Ca^{2+} release threshold of the SR⁽¹⁹²⁾. We hypothesised this may be the case with the trypanosome CatL (discussion Chapter 4). Therefore, confocal Ca^{2+} imaging experiments to examine diastolic Ca^{2+} release were performed. Recombinant CatL was used at the same concentration as the recombinant TbCatL experiments (1:50 dilution; 2.0 nM). Resting adult rat left ventricular cardiomyocytes were loaded with Fluo-3AM Ca^{2+} sensitive dye and imaged for 30 s. F/F_0 fluorescence traces were analysed for Ca^{2+} wave velocity, amplitude and decay rate constant. CatL increased the wave frequency to 136.7% of control levels (0.12 ± 0.02 vs. 0.16 ± 0.02 Ca^{2+} waves. s^{-1} ; control vs. CatL; $P < 0.05$; Figure 6.9A & B(i)). The Ca^{2+} wave velocity was not significantly altered (81.4 ± 1.9 vs. 83.3 ± 2.6 $\mu\text{m}.\text{s}^{-1}$; control vs. CatL; $P > 0.05$; Figure 6.9B(ii)) nor was Ca^{2+} wave amplitude (6.4 ± 0.6 vs. 7.2 ± 1.0 F/F_0 ; control vs. CatL; $P > 0.05$; Figure 6.9B(iii)).

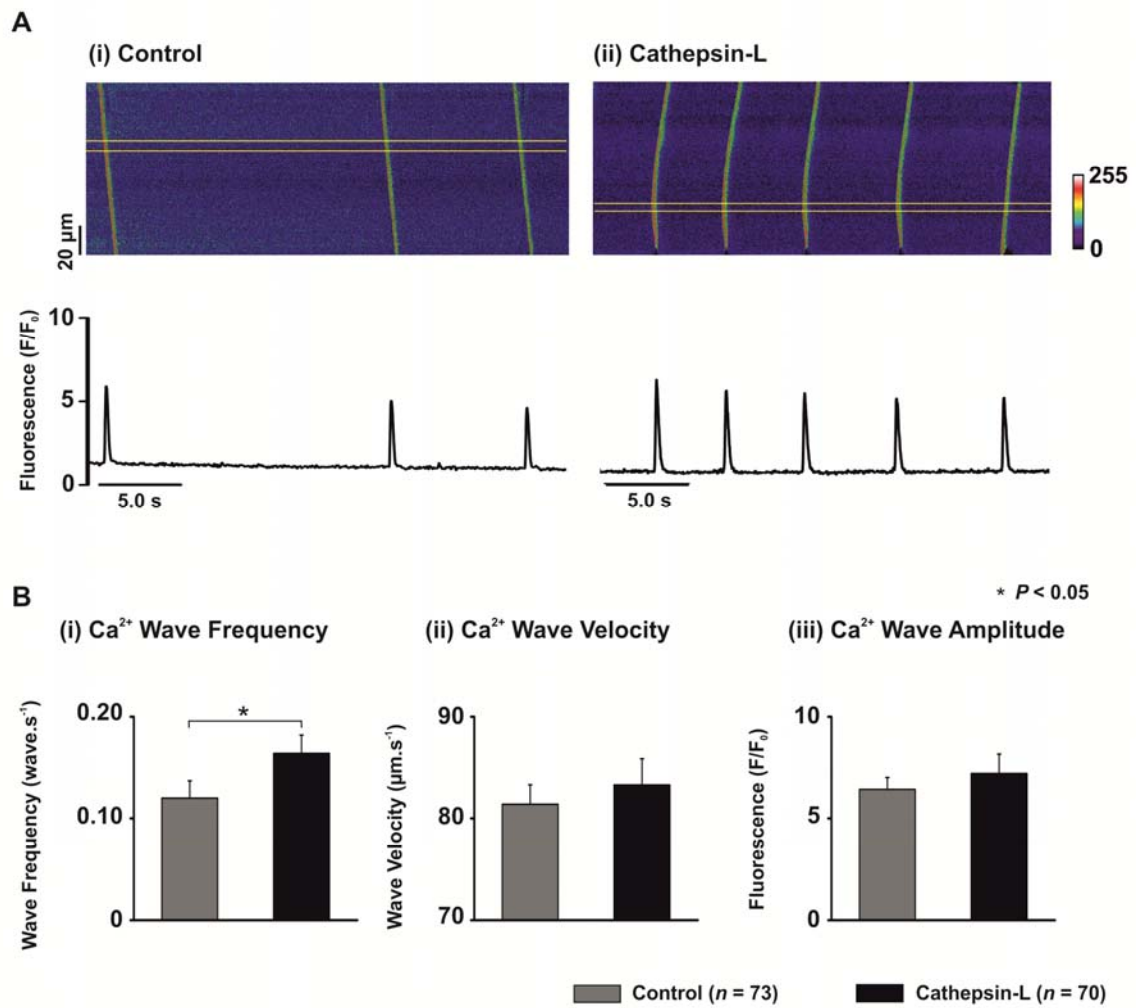


Figure 6.9: Confocal images of unstimulated cardiomyocytes.

(A) Rat left ventricular cardiomyocytes were incubated with vehicle control or 5.40 nM CatL for 30 min and then line-scans performed for 30 s. (i - ii) Representative confocal line-scan image and corresponding fluorescence trace (F/F_0) for control (i) and CatL (ii). (B(i - iii)) Ca^{2+} wave characteristics for control cardiomyocytes (grey; $n = 73$) and cardiomyocytes incubated with CatL (black; $n = 70$).

6.4 Discussion

6.4.1 Mammalian Cathepsin-L is Active at Physiological pH

Cysteine cathepsins have been shown to be localised to the acidic intracellular organelles lysosomes where they degrade unwanted proteins^(371;373;374). It has been traditionally thought that cathepsins only had limited activity at pH values other than their optimal acidic pH values^(395;567;583). However, recent work has shown that cathepsins can not only be active in other more neutral cellular compartments such as the cytosol⁽³⁸³⁻³⁸⁵⁾ and nucleus^(386;387), but are secreted into and function within extracellular spaces⁽⁴²³⁾. Indeed, extracellular cathepsin expression and activity has been identified in failing cardiac tissue^(421;422;584) and valve tissues⁽⁵⁸⁵⁻⁵⁸⁷⁾ from humans and animals. It has been proposed by Punturieri *et al.* (2000) that there is formation of a localised acidic environment in the zone of enzyme/substrate contact *via* expression of H⁺-ATPase in monocyte-derived macrophages maintaining the acidic environment⁽⁵⁸⁸⁾. However, a study by Lohmuller *et al.* (2005) used computer modelling to predict substrate cleavage specificity and conditions and found that CatL could potentially have activity at cytosolic and nuclear pH values⁽⁵⁸⁹⁾. This suggests that extracellular CatL could be active in the extracellular environment of the heart. During ischaemia the tissue becomes acidotic from the build up of lactic acid from anaerobic respiration⁽³⁴⁸⁾, which could favour extracellular CatL activity. Mature CatL has been considered as being unstable at neutral and alkaline pH with a rate constant of inactivation 17 fold faster at pH 7.4 compared with pH 7.0 at a temperature of 37 °C⁽³⁷²⁾. There is very little information in the literature regarding the activity of extracellular CatL and, therefore, to determine if mammalian CatL could be active at physiological pH, fluorometric activity assays were performed at pH 6.0, 7.0 and 7.4. Fluorometric activity assays using recombinant mouse CatL demonstrated activity not only at the optimum pH of 5.5-6.0⁽³⁷¹⁾, but at pH 7.0 and 7.4 (Figure 6.1A & B). The peak rate of activity occurred within the first 5 min but activity was present after the 30 min period of measurement at all three measured pH values.

6.4.2 Cathepsin-L is Detected in Coronary Effluent from Ischaemia/Reperfusion Hearts

CatL is ubiquitously expressed and has been shown to be expressed in cardiomyocytes^(421;422) and cardiac fibroblasts⁽⁴²¹⁾ as well as many other cell types⁽³⁸⁴⁾. It has also been shown to be secreted into the extracellular environment as a pro-enzyme to be activated by other proteases such as metalloproteinases in other body tissues, even at neutral pH⁽⁵⁹⁰⁻⁵⁹²⁾. In cases of cardiovascular disease such as myocardial infarction or coronary heart disease higher levels of circulating CatL have been identified^(413;425;426) and Sun *et al.* found increased levels of CatL activity in homogenised hearts post-MI⁽⁴²⁴⁾. However, it is not clear whether this is resulting from release of CatL from tissues associated with the heart, or derives from other organs/systemic processes. To determine if the heart could directly be releasing CatL during ischaemia/reperfusion, CatL activity was measured in the coronary effluents from *ex vivo* rat hearts. The Langendorff perfused hearts were subjected to a 30 min period of global ischaemia followed by a 90 min period of reperfusion. Activity was detected in the effluent samples which, when specifically inhibited was shown to be CatL. Utilisation of an *ex vivo* model enabled removal of any systemic contribution, therefore enabling us to determine that cells within the heart were secreting CatL and could contribute to the reported raised serum CatL levels in patients^(413;425;426). These results are supported by similar findings of raised CatB levels⁽⁵⁷¹⁾ and the serine protease CatD levels⁽⁴³⁰⁾, as well as CatL levels, in ischaemia/reperfusion injury⁽⁴³¹⁾. It remains unclear exactly how or where from the CatL is released; whether it is directly secreted during reperfusion or if it is released in response to the injury/cell damage. Several studies have examined the effects on the lysosome in response to ischaemia/reperfusion injury. The “lysosomal hypothesis”⁽⁵⁹³⁻⁵⁹⁵⁾, which suggests that I/R injury significantly reduces lysosomal integrity and also alters lysosomal distribution within cells^(339;340), leading to leakage of lysosomal enzymes into the cytoplasm and extracellular milieu causing cell necrosis and apoptosis. Other studies report a Ca²⁺ mediated redistribution and fusion of lysosomes with the plasma membranes and subsequent exocytosis of lysosomal cathepsins in skin fibroblasts⁽⁵⁹⁶⁾ and Chinese hamster ovary cells⁽⁵⁹⁷⁾ in response to injury. Ichihara *et al.* (1987) demonstrated that this same redistribution and exocytosis process of lysosomes could be inhibited in ischaemic rat hearts with the LTCC blocker

diltiazem, leading to a detectable reduction in CatD (measured in this study), and improvement in mechanical function upon reperfusion compared to untreated controls⁽⁵⁹⁸⁾. This suggests that cathepsins can be released from cells following ischaemia and have potential deleterious consequences. Therapeutic strategies that target inhibition of lysosomal enzyme release or inhibition of the enzyme activity following ischaemia could improve recovery. Therefore, the released CatL detected in the coronary effluent could potentially have an effect on cardiac function.

6.4.3 Cathepsin-L is Increased in Serum of Human Patients That Have Undergone Reperfusion Following Myocardial Infarction

ELISA has shown that CatL levels are increased in the immediately post-reperfusion samples, although not statistically significant as only a small number have been tested ($n = 4$). The quantity of CatL in these MI patients of $6.28 \pm 1.50 \text{ ng.mL}^{-1}$ (Figure 6.3A) corresponds closely to Liu *et al.* (2009) who report levels of $6.1 \pm 0.2 \text{ ng.mL}^{-1}$ for acute MI⁽⁴²⁵⁾. These data, when interpreted with the coronary effluent CatL activity, suggest that CatL could be produced/released in the affected region of the heart during ischaemia, which is then released into the circulation upon reperfusion. Studies by Stypmann *et al.* (2002) and Sun *et al.* (2010) provide evidence to support a beneficial role of CatL within the heart^(402;424). Stypmann *et al.* (2002) examined hearts of a CatL gene knockout mouse model and found that there was a dilated cardiomyopathy phenotype with interstitial fibrosis and pleomorphic nuclei⁽⁴⁰²⁾. They also identified that CatL-deficient cardiomyocytes have large fused lysosomes containing electron dense heterogeneous material when examined by electron microscopy. Sun *et al.* (2010), using the same knockout mouse strain, induced experimental MI and found greater scar dilatation, wall thinning, reduced left ventricular pressure, reduced cardiac output and increase left ventricular volume in systole and diastole compared to control wild-type mice that had undergone the same MI induction procedure⁽⁴²⁴⁾. However, CatL is important for protein turnover within cells, activation of MMPs and neovascularisation⁽⁵⁹⁹⁻⁶⁰²⁾, all of which would be inhibited in a complete CatL knockout. Therefore, it becomes difficult to determine whether the altered phenotype is a true CatL effect or whether it is due to the modulation of other mechanisms. Moreover, in

a full CatL knockout there is likely to be compensatory upregulation of other proteases, such as CatB, which may contribute to the detrimental effects rather than the lack of CatL⁽⁶⁰³⁾. If increased CatL levels were truly beneficial, then one would expect increased levels to translate to a correlated improvement of clinical signs in patients with cardiovascular disease. However, the studies that report increased CatL do not show improved recovery^(425;426). In fact Liu *et al.* show that CatL is a biomarker for severity of cardiovascular disease⁽⁴²⁵⁾. Although complete absence of CatL seems to be detrimental to cardiac function, increased levels of CatL may also be detrimental. It appears that a fine balance of CatL levels is necessary for healthy cardiac function. Further work with long-term follow-up CatL measurements correlating with MI recovery in a greater number of patients would be interesting to perform. Sun *et al.* (2011) suggested that CatL promotes fibrosis and therefore limits infarct size⁽⁴²⁴⁾. However, the long term consequences of fibrosis such as increased arrhythmogenesis, poor contraction and reduced lusitropy⁽⁶⁰⁴⁾ were not discussed. Therefore, what may be interpreted as a benefit of CatL, may actually be detrimental. Also of interest would be parallel measurements of the endogenous cathepsin inhibitor Cystatin C (CysC). Some studies have shown increases in CysC^(605;606) associated with increased risk of cardiovascular mortality, while Shi *et al.* (1999) show decreases in CysC in atherosclerosis⁽⁴¹⁷⁾. If CatL balance is of particular importance in ischaemia/reperfusion injury, then there is likely to be a contributing component from CysC, although it remains unclear what particular role it may play.

6.4.4 Cathepsin-L Effects on Ca²⁺ Handling in Rat Left Ventricular Cardiomyocytes

Epifluorescence Ca²⁺ measurements revealed a significant concentration-dependent reduction in the stimulated Ca²⁺ transient amplitude and rate constant of decay prolonging the duration of the Ca²⁺ transient. There was also a significant decrease in the amplitude of caffeine-induced Ca²⁺ transients indicating reduced SR Ca²⁺ content at all measured concentrations of CatL. At the highest concentrations of CatL (2.70 and 5.40 nM) there was a reduction in the rate decay constant of the stimulated Ca²⁺ transient. Interestingly, these changes in the stimulated Ca²⁺ transient are similar to those found in models of heart failure⁽²⁹⁹⁻³⁰²⁾, and the reduction in SR Ca²⁺ content is also recognised in

heart failure⁽³⁰³⁻³⁰⁶⁾. In heart failure it has been reported that a major factor in reduced SR Ca^{2+} is an increase in Ca^{2+} leak from the RyR⁽²⁹⁹⁾. Other potential contributors would be reduced K_{SERCA} and enhanced NCX activity⁽³⁰²⁾.

6.4.4.1 Ca^{2+} Transient Amplitude is Reduced in a Concentration Dependent Manner by CatL

Increasing concentrations of CatL showed a strong negative correlation with peak $[\text{Ca}^{2+}]_i$ and consequently $[\text{Ca}^{2+}]_i$ amplitude. Two explanations for reduced stimulated Ca^{2+} release are; i) failure of RyR activation termed defective coupling, and ii) insufficient availability of Ca^{2+} within the SR⁽³⁰²⁾. With regard to defective coupling, it has been reported that LTCC number (RyR activating channels) has been reduced in heart failure⁽³¹⁶⁾, but that LTCC activity is increased⁽³¹⁷⁾. The reported findings are consistent with an increased level of β -adrenergic stimulation and subsequent phosphorylation of the LTCC⁽³¹⁸⁾. The results with TbCatL suggested no effect on the LTCC but this has not been measured with mammalian CatL. Defective coupling could also occur if there is defective interaction between the LTCC and RyR as reported in spontaneously hypertensive rats with heart failure⁽⁶⁰⁷⁾ and rats with MI⁽⁶⁰⁸⁾ i.e. a reduced coupling gain of Ca^{2+} influx and Ca^{2+} release. With regard to insufficient availability of Ca^{2+} from the SR this was shown to be reduced in the presence of CatL and is discussed in section 6.4.4.5.

6.4.4.2 SERCA Activity is Reduced in a Concentration Dependent Manner by CatL

The decay rate constant of the stimulated Ca^{2+} transient was significantly reduced at the two higher concentrations of CatL. This shows slower diastolic Ca^{2+} removal, which could be a result of reduced reuptake to the SR by SERCA or reduced sarcolemmal efflux. The application of high concentration caffeine (10 mM; 20 s) effectively removes SERCA by opening the RyR and emptying the SR of Ca^{2+} . Therefore, to get an indication of K_{SERCA} the decay rate constant of the caffeine-induced Ca^{2+} transient (sarcolemmal efflux) can be subtracted from the decay rate constant of the stimulated Ca^{2+} transient (both SR reuptake and sarcolemmal efflux), as conducted by Bode *et al.* (2011)⁽⁵⁰⁶⁾. K_{SERCA} is reduced significantly at 2.70 and 5.40 nM CatL (95.3 ± 6.5 vs. 67.3 ± 11.9 vs. $30.7 \pm 3.3\%$ of vehicle control; 0.68 vs. 2.70 vs. 5.40 nM CatL). K_{SERCA} may be reduced in two

ways; i) reduced expression⁽³⁰⁷⁾ or ii) increased inhibition by phospholamban (PLB), either by increased quantity in relation to SERCA or altered phosphorylation⁽³⁰⁸⁾. It has been shown that a decrease in the phosphorylation at the PKA dependent site Ser16 occurs in both human⁽³⁰⁹⁾ and some animal models⁽³¹⁰⁾ of heart failure. This is thought to be a result of increased activity of the SR-associated phosphatase PP1 which dephosphorylates PLB^(310;609) *via* reduced inhibition by the inhibitor I-1^(610;611). The time course for a reduction in SERCA expression has been studied in models over the course of several weeks⁽⁶¹²⁻⁶¹⁵⁾, however, changes in SERCA protein levels can be observed in as little as 30 min⁽⁶¹⁶⁾. Therefore, in 30 min CatL exposed cells it is unclear whether there could be an alteration in the phosphorylation status of PLB (perhaps *via* altered phosphatase inhibition), a reduced level of SERCA, or a combination of both mechanisms. The current thinking is that much of the heart failure phenotype is due to altered phosphorylation status of Ca²⁺ handling proteins brought about through increased PKA activity through CaMKII activation⁽³⁰²⁾, as partial recovery of phosphorylation status results in some functional recovery^(318;617). The results presented in the preceding chapters suggest that TbCatL could be altering SR-mediated Ca²⁺ release *via* CaMKII. Therefore, the recombinant mouse CatL may be having effects on similar targets. Further work in future would be required to elucidate the mechanism responsible.

6.4.4.3 Sarcolemmal Extrusion is Reduced at Higher Concentrations of CatL

NCX function is usually thought to be increased in heart failure⁽³¹²⁻³¹⁵⁾, i.e. more Ca²⁺ extruded from the cytosol reduces the amount available for reuptake by SERCA to the SR, but these changes are not consistent⁽³⁰²⁾. In the present study Sarcolemmal extrusion was indirectly assessed by measurement of the decay rate constant of the caffeine-induced Ca²⁺ transient. At the lower concentrations of CatL NCX function was not significantly affected. However, at 5.40 nM CatL NCX function was decreased, which is in contrast to many studies showing a similar SR-mediated Ca²⁺ handling phenotype⁽³¹²⁻³¹⁵⁾. However, during ischaemia/reperfusion injury Le *et al.* (2006) has shown that the time constant of decay (τ) (the inverse of rate constant) is increased by about 40%⁽⁶¹⁶⁾, i.e. NCX function is decreased. This is more severe than the NCX effect observed in the present study, but the cardiomyocytes examined here were under normal

physiological conditions rather than following hypoxic damage. These results suggest that CatL could also have a mild effect on NCX that becomes more severe at higher concentrations in addition to the decrease in K_{SERCA} . However, further work would be required to understand this effect more fully.

6.4.4.4 Diastolic $[Ca^{2+}]_i$ is Increased by CatL

Since K_{SERCA} and NCX activity appear to be decreased in the presence of 5.40 nM CatL there should be a rise in the diastolic $[Ca^{2+}]_i$. This is indeed the case (Figure 6.5C(iii)), a finding which parallels those with TbCatL. At the lower concentrations of CatL there was still a significant decrease in K_{SERCA} but no significant change in NCX activity or diastolic $[Ca^{2+}]_i$. It is possible that there may be modulation of other Ca^{2+} extrusion mechanisms.

6.4.4.5 SR Ca^{2+} Content is Reduced by CatL

The significant reduction in caffeine-induced Ca^{2+} transient amplitude identified in the present study is a finding consistent with reduced stimulated Ca^{2+} transient amplitude⁽³⁰³⁻³⁰⁶⁾. Reduction in SR Ca^{2+} content can be a result of; i) reduced Ca^{2+} reuptake or ii) increased Ca^{2+} leak from the SR through the RyR. In the case of heart failure, SR Ca^{2+} leak is considered a major contributing factor to reduced SR Ca^{2+} content⁽³¹⁹⁻³²³⁾. However, the specific mechanisms are contentiously debated at present^(276;277;324). The present study provides evidence to support a reduced SR Ca^{2+} reuptake with the reduced K_{SERCA} but further work will be required in future to determine the exact mechanism. In conjunction with SERCA effects there could also be a concomitant leak from the RyR.

6.4.5 Cathepsin-L Effects on Ca^{2+} Handling in Rabbit Left Ventricular Cardiomyocytes

Epifluorescence Ca^{2+} measurements were repeated in rabbit left ventricular cardiomyocytes due to the differences in Ca^{2+} handling properties from rodents^(257;582). The data shown in this study suggest that CatL concentrations in the region of 0.68 nM are found in both coronary effluents from Langendorff perfused hearts that have undergone I/R injury and in the serum of patients that have had an MI and subsequent treatment, which correspond with Liu J *et al.* (2006) and Liu Y *et al.* (2009)^(413;425). Therefore, the epifluorescent Ca^{2+} imaging

experiments were performed with this concentration. The experiments were also performed at a greater stimulation frequency of 2.0 Hz representing a more physiological heart rate and hopefully give a better reflection of the potential clinical situation. Figure 6.7 shows a similarly reduced peak $[Ca^{2+}]_i$ and $[Ca^{2+}]_i$ amplitude. The rate constant of decay was not significantly altered at this concentration of CatL. When compared with the same concentration of CatL in rat cardiomyocytes there was also no statistically significant reduction, this was only seen at the higher concentrations. This suggests that K_{SERCA} modulation may only be slight in the presence of low concentration CatL vs. higher modulation at higher CatL concentrations. With the significantly reduced Ca^{2+} transient amplitude being observed, this would suggest as discussed above (section 6.4.4.1) either defective RyR coupling or reduced SR Ca^{2+} availability⁽³⁰²⁾. As with the rat cardiomyocyte experiments a bolus of high concentration caffeine was applied to the rabbit cardiomyocytes at the end of the protocol. Similarly to the results obtained with the rat model, there was a significant reduction in the caffeine-induced Ca^{2+} transient amplitude. There was no significant change in the decay rate constant which is consistent with 0.68 nM CatL in the rat cardiomyocyte data. The reduction in SR Ca^{2+} content as measured by caffeine-induced Ca^{2+} transient amplitude could explain the reduction in stimulated Ca^{2+} transient amplitude⁽³⁰³⁻³⁰⁶⁾. Without a significant change in the stimulated Ca^{2+} transient decay rate constant a significant reduction in K_{SERCA} that could explain the reduced SR Ca^{2+} content has little supporting evidence. A diastolic leak from the SR through the RyR may be a more likely explanation.

6.4.6 Cathepsin-L Increases Ca^{2+} Wave Frequency in Resting Cardiomyocytes

One measure of diastolic SR Ca^{2+} “leak” is spontaneous Ca^{2+} release in the form of Ca^{2+} waves. Rat left ventricular cardiomyocytes were loaded with Fluo-3 and imaged with a LASER-scanning confocal microscope in line-scan mode without stimulation. Since the largest effects on stimulated and caffeine-induced Ca^{2+} transient amplitude and decay were at 5.40 nM CatL, the confocal experiments were conducted with the same concentration of CatL. There was a significant increase in the Ca^{2+} wave frequency. Increased Ca^{2+} wave frequency is a manifestation of increased Ca^{2+} leak from the SR⁽¹⁹²⁾. Normally an increase in Ca^{2+} wave frequency occurs when SR Ca^{2+} content is increased as the release

threshold is reached earlier resulting in early release during diastole⁽¹⁹²⁾. However, it has been reported that in heart failure there can be hyperphosphorylation of the RyR resulting in dissociation of FKBP12.6⁽²⁷⁶⁾. FKBP12.6 may act as a diastolic inhibitor of RyR reducing P_o and aberrant Ca^{2+} release i.e. stabilising the closed state of the channel⁽²⁷⁶⁾. This hypothesis could explain a reduced SR Ca^{2+} content and subsequent reduced stimulated Ca^{2+} transient amplitude and may also lead to reperfusion arrhythmias *via* arrhythmogenic Ca^{2+} waves^(273;322;526;618;619). However, in heart failure this hypothesis remains extremely controversial as findings of RyR phosphorylation in different models of heart failure are inconsistent^(277-279;525). The situation with TbCatL, as discussed in Chapter 4, suggests a possible CaMKII-mediated effect. There is some evidence to suggest that hyperphosphorylation of the RyR at the CaMKII site Ser2815 can result in an increase in diastolic Ca^{2+} leak^(280;319). Other suggestions for a similar phenotype in the literature are that RyR activity could be enhanced by reactive oxygen species (ROS) or reactive nitrogen species (RNS)^(620;621). In the present study the phosphorylation status of the RyR was not measured, so whether there is PKA-mediated hyperphosphorylation of RyR as proposed by the Marks group^(276;324), or whether it is CaMKII-mediated hyperphosphorylation as proposed by Bers and colleagues^(277;311) or indeed, no change in phosphorylation as proposed by Valdivia's group⁽²⁷⁹⁾, cannot be determined at this time. Further work assessing the phosphorylation status of RyR may help establish by what mechanism CatL is eliciting its effects. There was no significant difference in the velocity or amplitude of the Ca^{2+} waves although both parameters tended to increase. The data presented in Figure 6.9 is from adult rat cardiomyocytes incubated with 5.40 nM CatL. Ca^{2+} waves can lead to arrhythmias *via* activation of NCX, triggering an inward electrical current through Na^+ leading to delayed afterdepolarisations (DAD)⁽¹⁹²⁾. This suggests that concentrations of CatL observed in this study and in Liu *et al.* (2009)⁽⁴²⁵⁾ could play a role in arrhythmias. Indeed, increased arrhythmia frequency upon reperfusion is a hallmark of ischaemia/reperfusion pathology⁽³³¹⁻³³⁷⁾.

In the case of reperfusion arrhythmias there is a putative role for ROS^(622;623). It has been shown that ROS can increase the P_o of the RyR^(341;345-347) and that RNS stimulated channel activity^(624;625). Interestingly ROS had an inhibitory effect on SERCA^(342-344;620), which fits the findings of the current study. The

cardiomyocytes in the present study were not subjected to ischaemic conditions. However, cathepsins can be released by ROS-mediated loss of lysosomal integrity^(339;340) and ROS can be released through cathepsin-mediated damage to mitochondrial membranes⁽⁶²⁶⁾. Therefore, one possible explanation for the increased Ca^{2+} wave frequency and decreased K_{SERCA} observed in the present study could be increased ROS production brought about by the presence of CatL. However, further experiments establishing a potential role for ROS will be required.

6.4.7 Conclusions

Little is known about the levels of CatL in patients with cardiac I/R injury. Work conducted in our laboratory has demonstrated for the first time that CatL proteolytic activity can be detected in coronary effluent samples from hearts that have undergone experimental I/R injury, but not in control hearts perfused continuously. The data presented in this thesis shows preliminary findings that serum levels of CatL are increased in human patients that have suffered MI and undergone therapeutic reperfusion and there may also be a correlation with severity of cardiovascular disease. However, this data is preliminary and will be followed up. The role that increased levels of CatL play in cardiovascular disease is not currently known. However, the work presented in the current study demonstrates that recombinant CatL has a concentration dependent effect on the SR Ca^{2+} content, the amplitude of the stimulated Ca^{2+} transient and SR-mediated Ca^{2+} release of rat cardiomyocytes. The same effects were observed in rabbit cardiomyocytes at a CatL concentration of 0.68 nM. These findings suggest that CatL may cause increased SR-mediated Ca^{2+} leak through the RyR resulting in reduced SR Ca^{2+} content leading to a reduced stimulated Ca^{2+} transient. Further work will be required to elucidate the potential sarcolemmal target for extracellular CatL and the subsequent signalling to result in the observed phenotype. Current work within our laboratory has started to examine the effects of the CatL specific inhibitor CAA0225 on cardiac function and infarct size in both *ex vivo* and *in vivo* models with promising results, therefore, making inhibition of CatL an attractive therapeutic target for ischaemic heart disease.

7 CHAPTER 7 – Conclusions

7.1 Study Rationale

The cardiac effects of American trypanosomiasis (Chagas disease) caused by *Trypanosoma cruzi* are widely known and studied in detail. However, in the case of African trypanosomiasis, for both human (human African trypanosomiasis (HAT) or 'sleeping sickness') and animal (animal African trypanosomiasis (AAT) or 'nagana') infections, cardiac involvement is often overlooked entirely due to the focus on the more overt signs of neurological disturbances (human) or anaemia and muscle wastage (animal). These clinical signs, when looked for, are electrocardiogram abnormalities such as a prolonged QT interval, repolarisation abnormalities and arrhythmias manifesting as palpitations in patients⁽⁵¹⁾, as well as reports of heart failure, ventricular dilatation and sudden cardiac death^(28;56;57). Historically, cases of human^(56;57) or experimentally infected animals⁽²⁶⁻²⁸⁾ have been examined post-mortem and evidence of perimyocarditis was identified. Thus any clinical case reports^(62;542-544) or controlled studies^(51;52) have attributed any cardiac involvement to be as a result of inflammation of the myocardium in response to parasite infiltration. However reports of cardiac signs and presence of trypanosomes within the myocardium *without* an inflammatory cell infiltrate are harder to reconcile with a hypothesis of inflammation alone^(26;497). In the case of Chagas disease, it has been found that the *T. cruzi* parasites and their culture supernatant are capable of inducing spontaneous cytosolic Ca²⁺ transients in isolated cardiomyocytes⁽⁵⁰⁸⁾ but no such study has been performed in cardiomyocytes exposed to *T. brucei spp.* and/or their culture supernatant. The most pertinent studies have been performed by Grab and colleagues (2006) assessing the ability of *T. brucei spp.* to cross the endothelial cell layer of the blood brain barrier *in vitro*⁽⁶⁹⁾. They identified that *T. b. rhodesiense* and *T. b. brucei* were able to traverse the endothelial cell layer *via* induction of Ca²⁺ fluxes within the endothelial cells facilitating alterations in the cytoskeletal components causing the cells to pull apart and fenestrate the layer^(66;67;69). They also identified that the trypanosomes induced the Ca²⁺ fluxes by secreting/excreting a cathepsin-L-like cysteine protease (TbCatL)⁽⁶⁹⁾. Therefore the rationale for this body of work was that if *T. brucei* could induce Ca²⁺ fluxes in BBB endothelial cells, and *T. cruzi* could induce Ca²⁺ fluxes or transients in cardiomyocytes, then we hypothesise that African trypanosomes could also affect intra-cardiomyocyte Ca²⁺ dynamics in the heart.

If evidence supported this hypothesis, then some of the observed cardiac clinical findings such as arrhythmias and palpitations may in fact be also attributable to a direct result of trypanosome-induced Ca^{2+} fluxes, in addition to solely the inflammatory reaction as previously thought. This would also have potential implications in terms of providing new therapeutic targets and treatments.

7.2 The Effects of *T. b. brucei* on the Heart at the Cardiomyocyte and Whole Organ Level

Although HAT is caused by *T. b. gambiense* (West African) or *T. b. rhodesiense* (East African) these subspecies are difficult to use in the lab, both due to their infectious nature to humans and also the difficulty in culturing the bloodstream form. However, the broad similarities of the animal infective subspecies *T. b. brucei* and its comparative safety and ease of culture make it an established model species of trypanosome. The most widely used strain of *T. b. brucei* used is Lister 427⁽⁴³⁴⁾. The first step in establishing the effects of *T. b. brucei* on Ca^{2+} handling in cardiomyocytes was to enzymatically isolate individual cardiomyocytes from whole hearts of rats and expose them to cultures of *T. b. brucei*. The advantage of the rat cardiomyocyte spontaneous contractile assays was the basal level of Ca^{2+} wave activity, such that any potential alteration to Ca^{2+} handling in the cardiomyocytes by trypanosomes or their supernatant could be detected without difficulty. Quantification of the result was achieved by recording the percentage of cardiomyocytes exhibiting at least one spontaneous contraction min^{-1} . The result was clearly positive and repeatable, and due to its simplicity proved a useful technique with which to test hypotheses before investigating further with more involved techniques. To establish whether the effect was from the trypanosomes themselves or a secreted/excreted factor, the culture supernatant was applied in the same manner as live cultures and the cardiomyocytes observed for spontaneous contractile events. The result was replicated and could be abolished by heating the supernatant - adding support for the secreted/excreted factor hypothesis.

The link with the spontaneous contractions and Ca^{2+} was established with Ca^{2+} sensitive fluorophores and measurements of the Ca^{2+} fluxes with LASER-scanning confocal microscopy and epifluorescence microscopy. Both these imaging techniques are well documented and used as gold standards for cardiomyocyte

Ca^{2+} studies, such that observations made can be rigorously cross-checked with published data and any conclusions be drawn robustly. This enabled determination that the contractions were mediated by spontaneous sarcoplasmic-reticulum (SR)-mediated Ca^{2+} release. The simplicity of the cardiomyocyte population assay provided a high throughput means of determining through; i) specific cathepsin inhibition, ii) gain of function effect with recombinant TbCatL and iii) loss of function effect with RNA interference that the cathepsin-L-like cysteine protease TbCatL caused the effect observed. Therefore, the same protease that is responsible for inducing Ca^{2+} fluxes in BBB endothelial cells is also responsible for SR-mediated spontaneous Ca^{2+} release in cardiomyocytes.

However, despite the strong evidence supporting an effect on cardiomyocyte Ca^{2+} dynamics, further work is required to confirm if this is single cell effect contributes to the clinical cardiac manifestations reported. Therefore, the study was expanded to incorporate analysis of whole hearts with ECG recording to measure the occurrence of potential arrhythmic events. *Ex vivo* rat hearts were perfused in Langendorff perfusion with trypanosome culture supernatant or control media and their ECGs recorded. SR-mediated spontaneous Ca^{2+} release can lead to whole heart arrhythmia through activation of the $\text{Na}^+/\text{Ca}^{2+}$ exchanger (NCX). This may cause a delayed after depolarisation (DAD) which can lead to an abnormal or ectopic heart beat if the depolarisation propagates to adjacent cells. This will be perceived as a palpitation in individuals. If the reported arrhythmias and palpitations in HAT patients could be due to the effects of TbCatL on SR-mediated spontaneous Ca^{2+} release then whole hearts exposed to supernatant may be expected to have an increased frequency of arrhythmias of ectopic origin. Indeed, in a proportion of the hearts perfused with supernatant, there were more arrhythmias observed, specifically ventricular premature complexes (VPCs). This correlates well with the published clinical data that reports only a proportion of patients exhibit palpitations. This result also supports for the first time the hypothesis of a secreted/excreted factor having a direct effect as these hearts are removed from any neurohumoral response or inflammatory processes.

7.3 The Mechanisms of SR-Mediated Ca²⁺ Release Caused by *T. b. brucei*

Following the results of Chapter 3, the aim of the Chapter 4 was to investigate the potential mechanisms behind the SR-mediated Ca²⁺ release observed. The conclusion that TbCatL causes abnormal SR-mediated Ca²⁺ release as a result of stimulation of SERCA required substantiation. First, the only evidence for this conclusion was an accelerated decline of the Ca²⁺ transient in supernatant perfused cardiomyocytes. If increased spontaneous Ca²⁺ release was a result of increased SERCA activity the SR Ca²⁺ content would be expected to be higher. Therefore, a paired protocol with the same cardiomyocyte being perfused with control media followed by supernatant lead to improvement of the accuracy and reliability of the epifluorescence experiments. Furthermore, a parallel set of paired protocol experiments using only control media were performed as time controls to which the data was normalised. Application of caffeine after each solution within the same cardiomyocyte allowed a more accurate assessment of the SR Ca²⁺ content and NCX function between control media and supernatant. This revised protocol identified that the SR Ca²⁺ content was in fact *reduced* by supernatant and not increased as would be expected with faster Ca²⁺ transient decline from SERCA stimulation. The decay of the caffeine-induced Ca²⁺ transient was not significantly altered suggesting that NCX function was not affected.

Despite the reduced SR Ca²⁺ content, the Ca²⁺ transient decline was still significantly faster and calculation of SERCA activity confirmed that SERCA stimulation is still the most likely hypothesis. However, the increased SERCA activity may not be the primary effect but a secondary response to a raised diastolic [Ca²⁺]_i. This hypothesis was tested by the inhibition of SR Ca²⁺ uptake with thapsigargin and release with ryanodine. These experiments revealed that in control media diastolic [Ca²⁺]_i reduced over the course of the protocol but that in supernatant the diastolic [Ca²⁺]_i failed to decrease, suggesting that higher [Ca²⁺]_i may contribute to the SERCA.

The contribution of myofilament Ca²⁺ sensitivity and the LTCC to changes in SERCA activity and [Ca²⁺]_i were experimentally ruled out.

The concomitant reduced SR Ca^{2+} content (despite an increased SERCA activity) and increase in Ca^{2+} wave frequency suggested that TbCatL may induce diastolic Ca^{2+} leak from the SR *via* RyR. This was probably due to an altered SR Ca^{2+} threshold or RyR sensitivity as SR Ca^{2+} content is reduced. If both SERCA and the RyR are altered by TbCatL, then the effects may be mediated by a common secondary messenger. Both RyR activity and SERCA activity *via* modified inhibition by PLB can be affected by PKA and/or CaMKII, two phosphorylating enzymes normally activated with β -adrenergic stimulation. Therefore PKA and CaMKII inhibitors were tested using the high-throughput cardiomyocyte population assay. This identified that the increase in spontaneous contractile events could be abolished by CaMKII inhibition but not PKA inhibition. With this information, the triple caffeine protocol and SR inhibition protocols were repeated with CaMKII inhibition. These experiments identified that the Ca^{2+} transient decline was no longer faster and SR Ca^{2+} content was the same for control media and supernatant; therefore, supporting the hypothesis that both RyR and SERCA activity were increased by the supernatant. Interestingly, the increase in diastolic $[\text{Ca}^{2+}]_i$ in the inhibited SR experiments was not prevented by CaMKII inhibition.

Further work in future would be to identify a sarcolemmal target for TbCatL. In the case of *T. cruzi* the cathepsin-L-like cysteine protease cruzipain targets the pertussis toxin sensitive G-protein coupled receptor⁽⁵⁰⁸⁾. For *T. brucei* spp. in the BBB endothelial cell traversal model one suggested target is another G-protein coupled receptor activated by proteases called protease-activated-receptor 2 (PAR-2)⁽⁶⁶⁾. Therefore, a similar target may be involved in the cardiac effects presented in this thesis. Preliminary work performed since completion of this work has ruled out PAR-2 in the heart, and so another target remains to be discovered. Also worth investigating further are individual channel currents. Although the current study did not show any significant effects on NCX there may be more subtle differences only identifiable by direct measurements. The NCX can reverse and be a potential source of Ca^{2+} influx possibly explaining the observed increase in diastolic $[\text{Ca}^{2+}]_i$ without an L-type component. Although often described as less important there are other Ca^{2+} handling mechanisms in the cardiomyocyte that could be further investigated such as the alternative SR

Ca²⁺ release channel the IP₃ receptor or the alternative Ca²⁺ extrusion mechanisms like the plasma-membrane Ca²⁺ ATPase (PMCA).

7.4 *In Vivo* Model of Infection and the Cardiac Effects of *T. b. brucei*

Traditionally much of the focus of research into HAT has been the neurological effects and with AAT the anaemia and muscle atrophy. Therefore *in vivo* models of infection have focused on these signs. As a result the development of a model of infection that enabled examination of the cardiac effects was required. Two strains of *T. b. brucei* were used; Lister 427 and TREU 927. Although Lister 427 proved useful for *in vitro* studies, its inability to differentiate from long-slender bloodstream form to short-stumpy form resulted in an *in vivo* model that did not last longer than 3-4 days without killing the host. As a result it was deemed that short ECGs from anaesthetised animals over the course of a 4 day infection with 427 was a model with limitations. The 927 strain was a better candidate for analysing chronic infections, as it is pleomorphic, i.e. differentiates to the short-stumpy form in a density-dependent manner, giving rise to fluctuating parasitaemias that mimic natural infections. This enabled the model to be continued for a longer period of time (up to 2 weeks). Biopotential telemetry devices were implanted to record the ECG continuously from conscious animals exhibiting normal behaviours. The result was a more realistic model and it showed a significant increase in ventricular arrhythmias. Therefore, this may be a useful model in the future testing of cardiovascular effects of potential new drugs and testing whether TbCatL inhibition can reduce the occurrence of arrhythmias. Future development of the model would be a longer term study extending to the duration of clinical infections lasting several weeks to months to estimate the relative contributions of a direct TbCatL effect and the traditional immune/inflammatory component. There is scope to combine cardiovascular monitoring with existing infection models of trypanosomiasis. Combination with new techniques such as *in vivo* imaging systems (IVIS) that use trypanosomes modified with either fluorescent proteins or reporter proteins such as luciferase enable visualisation of the course and distribution of infection including the CNS⁽⁵⁵⁵⁾. Therefore, IVIS combined with biopotential recording could help determine if there is a correlation with presence of trypanosomes or whether it is the perimyocarditis. Such a model

may also be useful to test new treatment strategies. For example, if TbCatL is responsible for both BBB traversal and cardiac arrhythmias then IVIS with ECG telemetry can test both CNS and cardiac response to TbCatL inhibition. If successful, then potentially progression of HAT to Stage II can be prevented enabling the less toxic Stage I drugs in current use to be used instead of the more toxic Stage II drugs required to cross the BBB.

7.5 The Cardiac Effects of Endogenous Extracellular Cathepsin-L

The fact that TbCatL is involved in arrhythmogenic Ca^{2+} handling in cardiomyocytes is interesting. There are many cardiovascular conditions that have abnormal Ca^{2+} dynamics at the centre of their pathophysiology such as heart failure and ischaemia/reperfusion injury. Of particular note is the role that cathepsins have in many of these conditions. In human clinical patients with coronary heart disease there is an increase in circulating levels of endogenous cathepsin-L. Since cathepsin-L can be increased in some cardiac diseases and TbCatL can elicit arrhythmogenic releases of Ca^{2+} in African trypanosomiasis the hypothesis arose as to whether the characteristic arrhythmias of ischaemia/reperfusion can be caused by raised mammalian cathepsin-L.

There is no literature available on the levels of cathepsin-L for ischaemia/reperfusion. Therefore the first step was to identify if cathepsin-L activity could be detected in the coronary effluent of *ex vivo* hearts that had undergone ischaemia/reperfusion experimentally on a Langendorff perfusion apparatus. Using an assay based on cleavage of a fluorescent substrate cathepsin-L activity was identified in effluents from hearts that had undergone the protocol but not in control hearts that were perfused throughout. In addition, a preliminary study revealed that serum samples from human patients that had suffered a myocardial infarction (MI) had elevated levels of cathepsin-L supporting the *ex vivo* heart data. The same patients also had cardiac magnetic resonance imaging on their hearts 6 months after initial presentation to assess cardiac function and infarct size. Although the numbers of patients were very low, the initial findings showed a strong correlation of post intervention cathepsin-L level and subsequent severity of signs at 6 months. Specifically

whole heart fractional shortening reduced as the cathepsin-L level increased and infarct size increased with increased cathepsin-L. These are interesting findings that warrant further investigation.

Given the effects of TbCatL on Ca^{2+} handling a similar set of experiments to Chapter 3 were performed with recombinant mouse cathepsin-L (rmCatL) on rat ventricular cardiomyocytes. LASER-scanning confocal microscopy revealed a similar increase in Ca^{2+} wave frequency with rmCatL to supernatant perfused cardiomyocytes suggesting a similar diastolic Ca^{2+} leak. Epifluorescence experiments identified a reduction in SR Ca^{2+} content but also a reduction in stimulated Ca^{2+} transient amplitude which differs from the TbCatL response. Interestingly when several different concentrations (as reported in a range of papers^(413;425;426)) of rmCatL were used there was a concentration dependent effect on the reduction of Ca^{2+} transient amplitude and SR Ca^{2+} content. The reduction was matched in rabbit ventricular cardiomyocytes, which exhibit similar Ca^{2+} handling properties to human ventricular cardiomyocytes. The observed Ca^{2+} handling phenotype resembles that of cardiomyocytes isolated from patients and animal models with heart failure. Therefore, there may be similar mechanisms involved. No mechanistic studies with mammalian cathepsin-L have been performed yet, but this work will be continued focusing on Ca^{2+} handling protein function and quantity as well as potential targets and response to specific cathepsin-L inhibition. In addition the study has since further expanded to incorporate both *ex vivo* and *in vivo* models. Initial findings are that cardiac function post ischaemia is improved in *ex vivo* hearts and *in vivo* following pre-treatment with a cathepsin-L inhibitor. This makes an attractive target for potential treatment in patients with ischaemic heart disease and following myocardial infarction that could aid in improving survivability.

7.6 Final Conclusions

The working hypothesis from Chapters 3 and 4 is that TbCatL acts on a yet to be identified sarcolemmal target which results in an elevation of intracellular Ca^{2+} . This elevation in $[\text{Ca}^{2+}]_i$ activates CaMKII which phosphorylates PLB decreasing SERCA inhibition and thereby enhancing its activity, and which also phosphorylates the RyR increasing its Ca^{2+} sensitivity and leak (Figure 7.1). This is the first time African trypanosomes have been shown to have a direct effect

on the heart independent of an immune/inflammatory response. Moreover, this pathogenic mechanism provides a platform to support future investigations that centre on inactivation of the effects of TbCatL *via* drugs that act on SR/ER-mediated Ca^{2+} signalling in order to address the neurological and cardiovascular pathology associated with HAT. Previous studies have shown that arrhythmias associated with disrupted SR function can be treated with flecainide and K201 (JTV-519)⁽⁶²⁷⁾ and this suggests a potential therapeutic approach for treatment of TbCatL induced cardiac dysfunction and other TbCatL mediated pathologies.

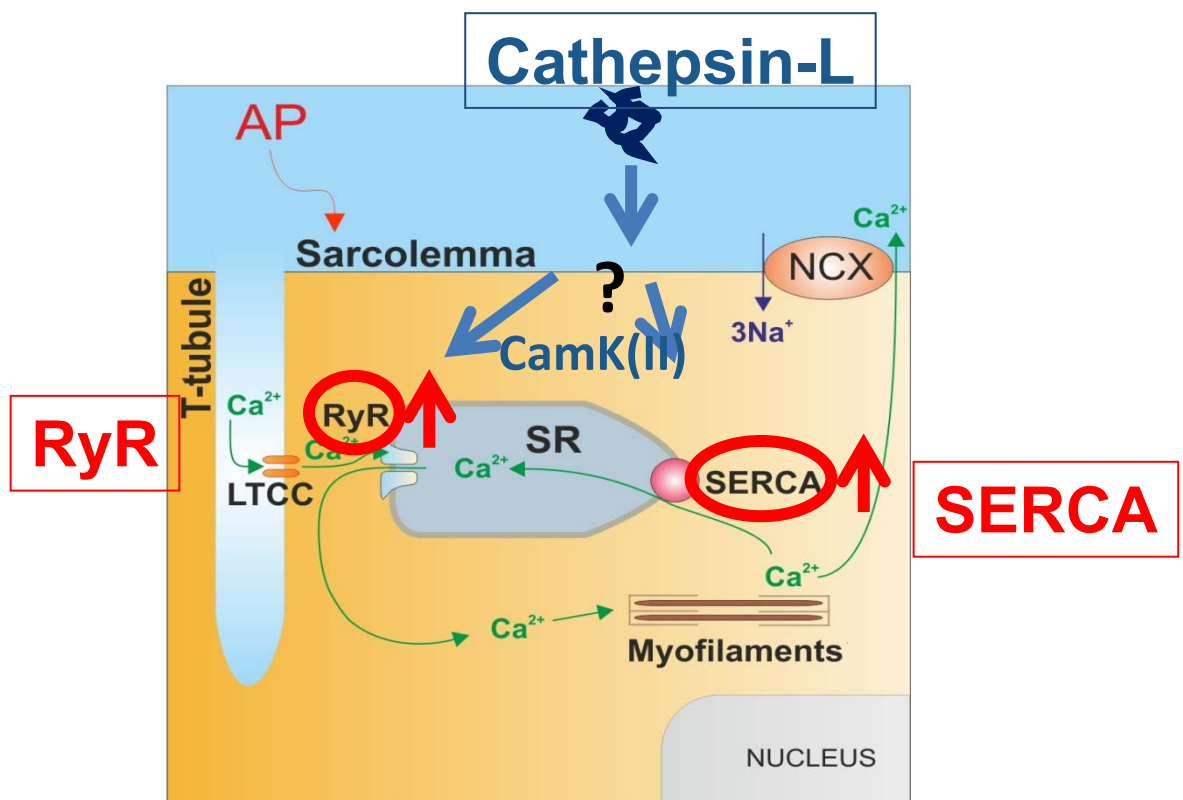


Figure 7.1: Proposed mechanism for TbCatL action on cardiomyocyte Ca^{2+} handling.

In the case of endogenous cathepsin-L the findings are very much in the preliminary stages but offers very interesting prospects for future study and development. Increased levels of cathepsin-L appear to have deleterious consequences for cardiomyocyte Ca^{2+} handling resembling the phenotype of heart failure. Hearts that have undergone experimental ischaemia/reperfusion injury and patients that have had a myocardial infarction have increased levels of cathepsin-L. Preliminary results from follow-up work show that inhibition of cathepsin-L can have a beneficial effect on cardiac function after ischaemia.

Therefore cathepsin-L and its inhibition is an attractive target for the treatment of ischaemia/reperfusion injury.

8 References

- (1) Aksoy S, Gibson WC, Lehane MJ. Interactions between tsetse and trypanosomes with implications for the control of trypanosomiasis. *Advances in Parasitology* 2003;53:1-83.
- (2) Coura JR, Vinas PA. Chagas disease: a new worldwide challenge. *Nature* 2010;465:s6-s7.
- (3) Araujo A, Jansen AM, Reinhard K, Ferreira LF. Paleoparasitology of Chagas disease: a review. *Mem Inst Oswaldo Cruz* 2009;104(Suppl 1):9-16.
- (4) Chagas C. Nova Tripanomíase humana. Estudos sobre morfologia e o ciclo evolutivo do *Schizotrypanum cruzi*, n. gen., n. sp., agente etiológico da nova entidade morbida do homem. *Mem Inst Oswaldo Cruz* 1909;1:159-218.
- (5) Lai DH, Hashimi H, Lun ZR, Ayala FJ, Lukeš J. Adaptations of *Trypanosoma brucei* to gradual loss of kinetoplast DNA: *Trypanosoma equiperdum* and *Trypanosoma evansi* are petite mutants of *T. brucei*. *Proceedings of the National Academy of Sciences* 2008 Feb 12;105(6):1999-2004.
- (6) Ilemobade AA. Tsetse and trypanosomosis in Africa : the challenges, the opportunities : vector-borne diseases : trypanosomosis. *Onderstepoort J Vet Res* 2009;76(1):35-40.
- (7) Phiri BJ, Benschop J, French NP. Systematic review of cause and factors affecting morbidity and mortality on small holder dairy farms in eastern and southern Africa. *Prev Vet Med* 2010;94:1-8.
- (8) Brun R, Blum J, Chappuis F, Burri C. Human African trypanosomiasis. *Lancet* 2010 Jan 9;375(9709):148-59.
- (9) Hendriks E, van Deursen FJ, Wilson J, Sarkar M, Timms M, Matthews KR. Life-cycle differentiation in *Trypanosoma brucei*: molecules and mutants. *Biochemical Society Transactions* 2000;28(5):531-6.
- (10) Kennedy PG. Clinical features, diagnosis, and treatment of human African trypanosomiasis (sleeping sickness). *The Lancet Neurology* 2013 Feb;12(2):186-94.
- (11) Reuner B, Vassella E, Yutzy B, Boshart M. Cell density triggers slender to stumpy differentiation of *Trypanosoma brucei* bloodstream forms in culture. *Molecular and Biochemical Parasitology* 1997;90(1):269-80.
- (12) Breidbach T, Ngazoa E, Steverding D. *Trypanosoma brucei*: *in vitro* slender-to-stumpy differentiation of culture-adapted, monomorphic bloodstream forms. *Experimental Parasitology* 2002 Aug;101(4):223-30.
- (13) David Barry J, McCulloch R. Antigenic variation in trypanosomes: Enhanced phenotypic variation in a eukaryotic parasite. *Advances in Parasitology*. Volume 49 ed. Academic Press; 2001. p. 1-70.
- (14) ILRAD 1990: Annual report of the International Laboratory for Research on Animal Diseases. 1991.
- (15) Taylor JE, Rudenko G. Switching trypanosome coats: what's in the wardrobe? *Trends in Genetics* 2006;22(11):614-20.
- (16) Marcello L, Barry JD. Analysis of the VSG gene silent archive in *Trypanosoma brucei* reveals that mosaic gene expression is prominent in antigenic variation and is favored by archive substructure. *Genome Research* 2007;17(9):1344-52.
- (17) Marcello L, Barry JD. From silent genes to noisy populations - Dialogue between the genotype and phenotypes of antigenic variation. *Journal of Eukaryotic Microbiology* 2007;54(1):14-7.

- (18) Stuart K, Brun R, Croft S, Fairlamb A, Gürtler RE, McKerrow J, et al. Kinetoplastids: Related protozoan pathogens, different diseases. *Journal of Clinical Investigation* 2008;118(4):1301-10.
- (19) Murray M, Morrison WI, Whitelaw DD. Host susceptibility to African trypanosomiasis: trypanotolerance. In: Baker and JR, editor. *Advances in Parasitology*. Volume 21 ed. Academic Press; 1982. p. 1-68.
- (20) Hajduk SL, Moore DR, Vasudevacharya J, Siqueira H, Torri AF, Tytler EM, et al. Lysis of *Trypanosoma brucei* by a toxic subspecies of human high density lipoprotein. *Journal of Biological Chemistry* 1989;264(9):5210-7.
- (21) Rifkin MR. Identification of the trypanocidal factor in normal human serum: high density lipoprotein. *Proceedings of the National Academy of Sciences of the United States of America* 1978;75(7):3450-4.
- (22) Raper J, Fung R, Ghiso J, Nussenzweig V, Tomlinson S. Characterization of a novel trypanosome lytic factor from human serum. *Infection and Immunity* 1999;67(4):1910-6.
- (23) Connor RJ. The impact of nagana. *Onderstepoort J Vet Res* 1994;61(4):379-83.
- (24) Masake RA. The pathogenesis of infection with *Trypanosoma vivax* in goats and cattle. *The Vet Record* 1980;107(24):551-7.
- (25) Morrison WI, Murray M, Whitelaw DD, Sayer PD. Pathology of infection with *Trypanosoma brucei*: disease syndromes in dogs and cattle resulting from severe tissue damage. *Contributions to microbiology and immunology* 1983;7:103-19.
- (26) Morrison WI, Murray M, Sayer PD, Preston JM. The pathogenesis of experimentally induced *Trypanosoma brucei* infection in the dog. *American Journal of Pathology* 1981;102:168-81.
- (27) Poltera AA, Hochmann A, Lambert PH. A model for cardiopathy induced by *Trypanosoma brucei brucei* in mice. A histologic and immunopathologic study. *The American Journal of Pathology* 1980;99:325-51.
- (28) Poltera AA, Sayer PD, Rudin W, Bovell D. Trypanosomal cardiac valvulitis in vervet monkeys. *Tropical Medicine and Parasitology* 1985;36:77-80.
- (29) Control and surveillance of African trypanosomiasis. Report of a WHO Expert Committee. WHO technical report series 881 World Health Organization, Geneva (1998). 1998.
- (30) Second WHO Report on Neglected Tropical Diseases. 2013.
- (31) Odiit M, Coleman PG, Liu WC, McDermott JJ, Fèvre EM, Welburn SC, et al. Quantifying the level of under-detection of *Trypanosoma brucei rhodesiense* sleeping sickness cases. *Tropical Medicine & International Health* 2005 Sep 1;10(9):840-9.
- (32) Simarro PP, Cecchi G, Franco JR, Paone M, Diarra A, Ruiz-Postigo JA, et al. Estimating and mapping the population at risk of sleeping sickness. *PLoS Negl Trop Dis* 2012 Oct 25;6(10):e1859.
- (33) WHO Global Health Observatory: Human African Trypanosomiasis. 2013.
- (34) Bucheton B, MacLeod A, Jamonneau V. Human host determinants influencing the outcome of *Trypanosoma brucei gambiense* infections. *Parasite Immunology* 2011 Aug 1;33(8):438-47.
- (35) Blum JA, Neumayr AL, Hatz CF. Human African trypanosomiasis in endemic populations and travellers. *Eur J Clin Microbiol Infect Dis* 2012;31(6):905-13.

- (36) Odiit M, Kansime F, Enyaru JC. Duration of symptoms and case fatality of sleeping sickness caused by *Trypanosoma brucei rhodesiense* in Tororo, Uganda. *East African Medical Journal* 1997;74(12):792-5.
- (37) Checchi F, Filipe JAN, Barrett MP, Chandramohan D. The natural progression of gambiense sleeping sickness: what is the evidence? *PLoS Negl Trop Dis* 2008 Dec 23;2(12):e303.
- (38) Checchi F, Filipe J, Haydon D, Chandramohan D, Chappuis F. Estimates of the duration of the early and late stage of gambiense sleeping sickness. *BMC Infectious Diseases* 2008;8(1):16.
- (39) Jammoneau V, Garcia A, Frezil JL. Clinical and biological evolution of human trypanosomiasis in Côte d'Ivoire. *Annals of Tropical Medicine and Parasitology* 2000;94(8):831-5.
- (40) Jamonneau V, Ilboudo H, Kaboré J, Kaba D, Koffi M, Solano P, et al. Untreated Human Infections by *Trypanosoma brucei gambiense* Are Not 100% Fatal. *PLoS Negl Trop Dis* 2012 Jun 12;6(6):e1691.
- (41) Simarro P, Jannin J, Cattand P. Eliminating human African trypanosomiasis: where do we stand and what comes next? *PLoS Medicine* 2008;5(2):e55.
- (42) Pickrell WO, Sudarshi D, Eligar V, Brown M, Walters RJ. Tripped up by an unusual diagnosis? *Journal of Neurology, Neurosurgery & Psychiatry* 2013 Nov 1;84(11):e2.
- (43) Garcia A, Jamonneau V, Magnus E, Laveissiere C, Lejon V, N'guessan P, et al. Follow-up of Card Agglutination Trypanosomiasis Test (CATT) positive but apparently aparasitaemic individuals in Côte d'Ivoire: evidence for a complex and heterogeneous population. *Tropical Medicine & International Health* 2000 Nov 1;5(11):786-93.
- (44) Truc P, Formenty P, Diallo PB, Komoin-Oka C, Lauginie F. Confirmation of two distinct classes of zymodemes of *Trypanosoma brucei* infecting man and wild mammals in Côte d'Ivoire: suspected difference in pathogenicity. *Annals of Tropical Medicine and Parasitology* 1997;91(8):951-6.
- (45) Blum J, Schmid C, Burri C. Clinical aspects of 2541 patients with second stage human African trypanosomiasis. *Acta Tropica* 2006 Jan;97(1):55-64.
- (46) Duggan AJ, Hutchinson MP. Sleeping sickness in Europeans: a review of 109 cases. *Journal of Tropical Medicine and Hygiene* 1966;69(6):124-31.
- (47) Stijlemans B, Guilliams M, Raes G, Beschin A, Magez S, De Baetselier P. African trypanosomiasis: From immune escape and immunopathology to immune intervention. *Veterinary Parasitology* 2007;148(1 SPEC. ISS.):3-13.
- (48) Blum J, Burri C. Treatment of late stage sleeping sickness caused by *T. b. gambiense*: a new approach to the use of an old drug. *Swiss Medical Weekly* 2002 Feb 9;132(5-6):51-6.
- (49) Buguet A, Bourdon L, Bisser S, Chapotot F, Radomski MW, Dumas M. Sleeping sickness : A major disorder of circadian rhythm. *Medecine Tropicale* 2001;61(4-5):328-39.
- (50) Kennedy PGE. Human African trypanosomiasis-neurological aspects. *Journal of Neurology* 2006;253(4):411-6.
- (51) Blum JA, Burri C, Hatz C, Kazumba L, Mangoni P, Zellweger MJ. Sleeping hearts: the role of the heart in sleeping sickness (human African trypanosomiasis). *Tropical Medicine & International Health* 2007 Dec;12(12):1422-32.
- (52) Blum JA. Ecg alterations in first and second stage human African trypanosomiasis before and after treatment. *American Journal of Tropical Medicine and Hygiene* 2008 Dec;79(6):157-8.

- (53) Blum JA, Zellweger MJ, Burri C, Hatz C. Cardiac involvement in African and American trypanosomiasis. *Lancet Infectious Diseases* 2008 Oct;8(10):631-41.
- (54) Blum JA, Schmid C, Burri C, Hatz C, Olson C, Fungula B, et al. Cardiac alterations in human African trypanosomiasis (*T.b. gambiense*) with respect to the disease stage and antiparasitic treatment. *Plos Neglected Tropical Diseases* 2009 Feb;3(2).
- (55) Collomb H, Bartoli D. The heart in human African trypanosomiasis caused by *Trypanosoma gambiense*. *Bulletin de la Societe de pathologie exotique et de ses filiales* 1967;60(2):142-56.
- (56) Adams JH, Haller L, Boa FY. Human African Trypanosomiasis (*T. b. gambiense*): a study of 16 fatal cases of sleeping sickness with some observations on acute reactive arsenical encephalopathy. *Neuropathology and Applied Neurobiology* 1986;12:81-94.
- (57) Bertrand E, Serie F, Kone I. Symptomatology generale de la trypanosomiase humaine africaine au moment du depistage. *Medecine d'Afrique Noire* 1973;20:303-14.
- (58) Bertrand E. [Cardiac involvement in human African trypanosomiasis]. *Med Trop (Mars)* 1987;47(1):91-3.
- (59) de Raadt P, Kotten JW. Myocarditis in Rhodesian trypanosomiasis. *East African Medical Journal* 1968;45(3):128-32.
- (60) Kotten JW, de Raadt P. Myocarditis in *Trypanosoma rhodesiense* infections. *Transactions of the Royal Society of tropical medicine and hygiene* 1969;63(4):485-9.
- (61) Bertrand E, Serie F, Rive J, Compaore P, Sentilhes L, Baudin L, et al. Current features of cardiac symptoms in African trypanosomiasis in humans due to *Trypanosoma gambiense* (194 cases). *Acta Cardiologica* 1974;29(5):363-81.
- (62) Fouchet M, Gateff C. Development of cardiovascular involvement in African trypanosomiasis due to *Trypanosoma gambiense*. *Medecine Tropicale* 1968;28(5):583-90.
- (63) Damian MS, Dorndorf W, Burkardt H, Singer I, Leinweber B, Schachenmayr W. Polyneuritis and myositis in African trypanosomiasis. *Deutsche Medizinische Wochenschrift* 1994;119(49):1690-3.
- (64) Tsala MP, Blackett K, Mbonifor CL, Leke R, Etoundi J. Functional and immunologic involvement in human African trypanosomiasis caused by *Trypanosoma gambiense*. *Bull Soc Pathol Exot Filiales* 1988;81(3 Pt 2):490-501.
- (65) Costello-Boerrigter LC, Boerrigter G, Redfield MM, Rodeheffer RJ, Urban LH, Mahoney DW, et al. Amino-terminal pro-B-type natriuretic peptide and B-type natriuretic peptide in the general community: Determinants and detection of left ventricular dysfunction. *Journal of the American College of Cardiology* 2006;47(2):345-53.
- (66) Grab DJ, Garcia-Garcia JC, Nikolskaia OV, Kim YV, Brown A, Pardo CA, et al. Protease activated receptor signaling is required for African trypanosome traversal of human brain microvascular endothelial cells. *Plos Neglected Tropical Diseases* 2009 Jul;3(7).
- (67) Grab DJ, Nikolskaia O, Kim YV, Lonsdale-Eccles JD, Ito S, Hara T, et al. African trypanosome interactions with an *in vitro* model of the human blood-brain barrier. *Journal of Parasitology* 2004 Oct 1;90(5):970-9.
- (68) Grab D, Kennedy P. Traversal of human and animal trypanosomes across the blood-brain barrier. *Journal of NeuroVirology* 2008;14(5):344-51.
- (69) Nikolskaia OV, de AL, Kim YV, Lonsdale-Eccles JD, Fukuma T, Scharfstein J, et al. Blood-brain barrier traversal by African trypanosomes requires calcium signaling induced by parasite cysteine protease. *J Clin Invest* 2008 May 1;118(5):1974.

- (70) Chappuis F, Loutan L, Simarro P, Lejon V, Buscher P. Options for field diagnosis of human African trypanosomiasis. *Clinical Microbiology Reviews* 2005;18(1):133-46.
- (71) Lejon V, Büscher P. Review article: Cerebrospinal fluid in human African trypanosomiasis: A key to diagnosis, therapeutic decision and post-treatment follow-up. *Tropical Medicine and International Health* 2005;10(5):395-403.
- (72) Magnus E, Vervoort T, Van Meirvenne N. A card-agglutination test with stained trypanosomes (C.A.T.T.) for the serological diagnosis of *T. b. gambiense* trypanosomiasis. *Annales de la Societe Belge de Medecine Tropicale* 1978;58(3):169-76.
- (73) Chappuis F, Pittet A, Bovier PA, Adams K, Godineau V, Hwang SY, et al. Field evaluation of the CATT/*Trypanosoma brucei gambiense* on blood-impregnated filter papers for diagnosis of human African trypanosomiasis in southern Sudan. *Tropical Medicine and International Health* 2002;7(11):942-8.
- (74) Noireau F, Force-Barge P, Cattand P. Evaluation of Testryp CATT applied to samples of dried blood for the diagnosis of sleeping sickness. *Bulletin of the World Health Organization* 1991;69(5):607-8.
- (75) Penchenier L, Grébaud P, Njokou F, Eboo Eyenga V, Büscher P. Evaluation of LATEX/*T.b.gambiense* for mass screening of *Trypanosoma brucei gambiense* sleeping sickness in Central Africa. *Acta Tropica* 2003;85(1):31-7.
- (76) Truc P, Lejon V, Magnus E, Jammoneau V, Nangouma A, Verloo D, et al. Evaluation of the micro-CATT, CATT/*Trypanosoma brucei gambiense*, and LATEX/*T.b. gambiense* methods for serodiagnosis and surveillance of human African trypanosomiasis in West and Central Africa. *Bulletin of the World Health Organization* 2002;80(11):882-6.
- (77) Noireau F, Lemesre JL, Nzoukoudi MY, Louembet MT, Gouteux JP, Frezil JL. Serodiagnosis of sleeping sickness in the Republic of the Congo: Comparison of indirect immunofluorescent antibody test and card agglutination test. *Transactions of the Royal Society of tropical medicine and hygiene* 1988;82(2):237-40.
- (78) Jammoneau V, Truc P, Garcia A, Magnus E, Büscher P. Preliminary evaluation of LATEX/*T. b. gambiense* and alternative versions of CATT/*T. b. gambiense* for the serodiagnosis of Human African Trypanosomiasis of a population at risk in Côte d'Ivoire: Considerations for mass-screening. *Acta Tropica* 2000;76(2):175-83.
- (79) Simarro PP, Louis FJ, Jannin J. Sleeping sickness, a forgotten disease: Impact in the field. *Medecine Tropicale* 2003;63(3):231-5.
- (80) Woo PT. The haematocrit centrifuge technique for the diagnosis of African trypanosomiasis. *Acta Tropica* 1970;27(4):384-6.
- (81) Mugasa CM, Adams ER, Boer KR, Dyserinck HC, Büscher P, Schallig HDHF, et al. Diagnostic accuracy of molecular amplification tests for human African trypanosomiasis – systematic review. *PLoS Negl Trop Dis* 2012 Jan 10;6(1):e1438.
- (82) Kuboki N, Inoue N, Sakurai T, Di Cello F, Grab DJ, Suzuki H, et al. Loop-mediated isothermal amplification for detection of African trypanosomes. *Journal of Clinical Microbiology* 2003;41(12):5517-24.
- (83) Njiru ZK, Mikosza AS, Armstrong T, Enyaru JC, Ndung'u JM, Thompson AR. Loop-mediated isothermal amplification (LAMP) method for rapid detection of *Trypanosoma brucei rhodesiense*. *Plos Neglected Tropical Diseases* 2008;2(1).
- (84) Njiru ZK, Mikosza ASJ, Matovu E, Enyaru JCK, Ouma JO, Kibona SN, et al. African trypanosomiasis: Sensitive and rapid detection of the sub-genus Trypanozoon by loop-mediated isothermal amplification (LAMP) of parasite DNA. *International Journal for Parasitology* 2008;38(5):589-99.

- (85) Kennedy PGE. Diagnosing central nervous system trypanosomiasis: two stage or not to stage? *Transactions of the Royal Society of tropical medicine and hygiene* 2008;102(4):306-7.
- (86) Lejon V, Reiber H, Legros D, Djé N, Magnus E, Wouters I, et al. Intrathecal immune response pattern for improved diagnosis of central nervous system involvement in trypanosomiasis. *Journal of Infectious Diseases* 2003;187(9):1475-83.
- (87) Truc P, Jammoneau V, Cuny G, Frézil JL. Use of polymerase chain reaction in human African trypanosomiasis stage determination and follow-up. *Bulletin of the World Health Organization* 1999;77(9):745-8.
- (88) Jammoneau V, Solano P, Garcia A, Lejon V, Djé N, Miezán TW, et al. Stage determination and therapeutic decision in human African trypanosomiasis: Value of polymerase chain reaction and immunoglobulin M quantification on the cerebrospinal fluid of sleeping sickness patients in Côte d'Ivoire. *Tropical Medicine and International Health* 2003;8(7):589-94.
- (89) Steverding D. A new initiative for the development of new diagnostic tests for human African trypanosomiasis. *Kinetoplastid Biology and Disease* 2006;5.
- (90) Doua F, Miezán TW, Sanon Singaro JR, Boa Yapo F, Baltz T. The efficacy of pentamidine in the treatment of early-late stage *Trypanosoma brucei gambiense* trypanosomiasis. *American Journal of Tropical Medicine and Hygiene* 1996;55(6):586-8.
- (91) Balasegaram M, Harris S, Checchi F, Hamel C, Karunakara U. Treatment outcomes and risk factors for relapse in patients with early-stage human African trypanosomiasis (HAT) in the Republic of the Congo. *Bulletin of the World Health Organization* 2006;84(10):777-82.
- (92) Lejon V, Legros D, Savignoni A, Etchegorry MG, Mbulamberi D, Büscher P. Neuro-inflammatory risk factors for treatment failure in "early second stage" sleeping sickness patients treated with Pentamidine. *Journal of Neuroimmunology* 2003;144(1-2):132-8.
- (93) Kennedy PGE. The continuing problem of human African trypanosomiasis (sleeping sickness). *Annals of Neurology* 2008;64(2):116-26.
- (94) Pepin J, Milord F. The treatment of human African trypanosomiasis. *Advances in Parasitology* 1994;33:1-47.
- (95) Barrett MP, Boykin DW, Brun R, Tidwell RR. Human African trypanosomiasis: Pharmacological re-engagement with a neglected disease. *British Journal of Pharmacology* 2007;152(8):1155-71.
- (96) Priotto G, Kasparian S, Mutombo W, Ngouama D, Ghorashian S, Arnold U, et al. Nifurtimox-eflornithine combination therapy for second-stage African *Trypanosoma brucei gambiense* trypanosomiasis: a multicentre, randomised, phase III, non-inferiority trial. *The Lancet* 2009;374(9683):56-64.
- (97) Chappuis F, Udayraj N, Stietenroth K, Meussen A, Bovier PA. Eflornithine is safer than melarsoprol for the treatment of second-stage *Trypanosoma brucei gambiense* human African trypanosomiasis. *Clinical Infectious Diseases* 2005;41(5):748-51.
- (98) Balasegaram M, Harris S, Checchi F, Ghorashian S, Hamel C, Karunakara U. Melarsoprol versus eflornithine for treating late-stage Gambian trypanosomiasis in the Republic of the Congo. *Bulletin of the World Health Organization* 2006;84(10):783-91.
- (99) Checchi F, Piola P, Ayikoru H, Thomas F, Legros D, Priotto G. Nifurtimox plus eflornithine for late-stage sleeping sickness in Uganda: A case series. *PLoS Negl Trop Dis* 2007 Nov 7;1(2):e64.
- (100) Iten M, Mett H, Evans A, Enyaru JCK, Brun R, Kaminsky R. Alterations in ornithine decarboxylase characteristics account for tolerance of *Trypanosoma brucei*

- rhodesiense* to D,L- α - difluoromethylornithine. Antimicrobial Agents and Chemotherapy 1997;41(9):1922-5.
- (101) Burri C, Brun R. Eflornithine for the treatment of human African trypanosomiasis. Parasitology Research 2003;90(SUPPL.1):S49-S52.
- (102) Abbott NJ, Ronnback L, Hansson E. Astrocyte-endothelial interactions at the blood-brain barrier. Nat Rev Neurosci 2006;7(1):41-53.
- (103) Wilhelm I, Fazakas C, Krizbai IA. *In vitro* models of the blood-brain barrier. Acta Neurobiol Exp (Wars) 2011;71(1):113-28.
- (104) Masocha W, Rottenberg ME, Kristensson K. Migration of African trypanosomes across the blood-brain barrier. Physiology and Behavior 2007;92(1-2):110-4.
- (105) Dowse TJ, Koussis K, Blackman MJ, Soldati-Favre D. Roles of proteases during invasion and egress by *Plasmodium* and *Toxoplasma*. Subcellular Biochemistry 2008;47:121-39.
- (106) Dvorak J, Mashiyama ST, Braschi S, Sajid M, Knudsen GM, Hansell E, et al. Differential use of protease families for invasion by *schistosome cercariae*. Biochimie 2008 Feb;90(2):345-58.
- (107) He C, Nora GP, Schneider EL, Kerr ID, Hansell E, Hirata K, et al. A novel *Entamoeba histolytica* cysteine proteinase, EhCP4, is key for invasive amebiasis and a therapeutic target. Journal of Biological Chemistry 2010;285(24):18516-27.
- (108) Salter JP, Lim KC, Hansell E, Hsieh I, McKerrow JH. Schistosome invasion of human skin and degradation of dermal elastin are mediated by a single serine protease. Journal of Biological Chemistry 2000;275(49):38667-73.
- (109) Bakalara N, Santarelli X, Davis C, Baltz T. Purification, cloning, and characterization of an acidic ectoprotein phosphatase differentially expressed in the infectious bloodstream form of *Trypanosoma brucei*. Journal of Biological Chemistry 2000;275(12):8863-71.
- (110) Lonsdale-Eccles JD, Grab DJ. Trypanosome hydrolases and the blood-brain barrier. Trends in Parasitology 2002 Jan 1;18(1):17-9.
- (111) Sousa K, Atouguia J, Silva M. Partial biochemical characterization of a metalloproteinase from the bloodstream forms of *Trypanosoma brucei brucei* parasites. Protein J 2010;29(4):283-9.
- (112) Abdulla MH, O'Brien T, Mackey ZB, Sajid M, Grab DJ, McKerrow JH. RNA Interference of *Trypanosoma brucei* Cathepsin B and L Affects Disease Progression in a Mouse Model. Plos Neglected Tropical Diseases 2008 Sep;2(9).
- (113) Nikolskaia OV, Lima APCD, Kim YV, Lonsdale-Eccles JD, Fukuma T, Scharfstein J, et al. Blood-brain barrier traversal by African trypanosomes requires calcium signaling induced by parasite cysteine protease. Journal of Clinical Investigation 2006 Oct;116(10):2739-47.
- (114) Nikolskaia OV, Kim YV, Kovbasnjuk O, Kim KJ, Grab DJ. Entry of *Trypanosoma brucei gambiense* into microvascular endothelial cells of the human blood-brain barrier. International Journal for Parasitology 2006 May;36(5):513-9.
- (115) Paemeleire K, de Hemptinne A, Leybaert L. Chemically, mechanically, and hyperosmolarity-induced calcium responses of rat cortical capillary endothelial cells in culture. Exp Brain Res 1999;126(4):473-81.
- (116) Murta ACM, Persechini PM, Padron TdS, de Souza W, Guimarães JA, Scharfstein J. Structural and functional identification of GP57/51 antigen of *Trypanosoma cruzi* as a cysteine proteinase. Molecular and Biochemical Parasitology 1990 Nov;43(1):27-38.

- (117) Aparicio IM, Scharfstein J, Lima AP. A new cruzipain-mediated pathway of human cell invasion by *Trypanosoma cruzi* requires trypomastigote membranes. *Infection and Immunity* 2004 Oct 1;72(10):5892-902.
- (118) Caler EV, Chakrabarti S, Fowler KT, Rao S, Andrews NW. The exocytosis-regulatory protein synaptotagmin VII mediates cell invasion by *Trypanosoma cruzi*. *The Journal of Experimental Medicine* 2001 May 7;193(9):1097-104.
- (119) Tardieux I, Webster P, Ravesloot J, Boron W, Lunn JA, Heuser JE, et al. Lysosome recruitment and fusion are early events required for trypanosome invasion of mammalian cells. *Cell* 1992 Dec 24;71(7):1117-30.
- (120) Kennedy PGE. Human African trypanosomiasis of the CNS: current issues and challenges. *J Clin Invest* 2004 Feb 15;113(4):496-504.
- (121) Kennedy PGE. Diagnostic and neuropathogenesis issues in human African trypanosomiasis. *International Journal for Parasitology* 2006 May;36(5):505-12.
- (122) Sternberg JM, Rodgers J, Bradley B, MacLean L, Murray M, Kennedy PGE. Meningoencephalitic African trypanosomiasis: Brain IL-10 and IL-6 are associated with protection from neuro-inflammatory pathology. *Journal of Neuroimmunology* 2005 Oct;167(1-2):81-9.
- (123) Masocha W, Robertson B, Rottenberg ME, Mhlanga J, Sorokin L, Kristensson K. Cerebral vessel laminins and IFN- γ define *Trypanosoma brucei brucei* penetration of the blood-brain barrier. *J Clin Invest* 2004 Sep 1;114(5):689-94.
- (124) Caffrey CR, Lima A-P, Steverding D. Cysteine peptidases of kinetoplastid parasites. 2011. p. 84-99.
- (125) Mottram JC, Helms MJ, Coombs GH, Sajid M. Clan CD cysteine peptidases of parasitic protozoa. *Trends in Parasitology* 2003 Apr;19(4):182-7.
- (126) Lonsdale-Eccles JD, Grab DJ. Lysosomal and non-lysosomal peptidyl hydrolases of the bloodstream forms of *Trypanosoma brucei brucei*. *European Journal of Biochemistry* 1987 Dec 1;169(3):467-75.
- (127) North MJ, Mottram JC, Coombs GH. Cysteine proteinases of parasitic protozoa. *Parasitology Today* 1990 Aug;6(8):270-5.
- (128) Robertson CD, North MJ, Lockwood BC, Coombs GH. Analysis of the proteinases of *Trypanosoma brucei*. *Journal of General Microbiology* 1990 May 1;136(5):921-5.
- (129) Caffrey CR, Hansell E, Lucas KD, Brinen LS, Hernandez AA, Cheng JN, et al. Active site mapping, biochemical properties and subcellular localization of rhodesain, the major cysteine protease of *Trypanosoma brucei rhodesiense*. *Molecular and Biochemical Parasitology* 2001 Nov;118(1):61-73.
- (130) Pamer EG, So M, Davis CE. Identification of a developmentally regulated cysteine protease of *Trypanosoma brucei*. *Molecular and Biochemical Parasitology* 1989 Feb;33(1):27-32.
- (131) Mottram JC, North MJ, Barry JD, Coombs GH. A cysteine proteinase cDNA from *Trypanosoma brucei* predicts an enzyme with an unusual C-terminal extension. *FEBS Letters* 1989 Dec 4;258(2):211-5.
- (132) Pamer EG, Davis CE, Eakin A, So M. Cloning and sequencing of the cysteine protease cDNA from *Trypanosoma brucei rhodesiense*. *Nucleic Acids Research* 1990 Oct 25;18(20):6141.
- (133) Campetella O, Henriksson J, Aslund L, Frasch AC, Pettersson U, Cazzulo JJ. The major cysteine proteinase (cruzipain) from *Trypanosoma cruzi* is encoded by multiple

- polymorphic tandemly organized genes located on different chromosomes. *Molecular and Biochemical Parasitology* 1992;50(2):225-34.
- (134) Fish WR, Nkhungulu ZM, Muriuki CW, Ndegwa DM, Lonsdale-Eccles JD, Steyaert J. Primary structure and partial characterization of a life-cycle-regulated cysteine protease from *trypanosoma (Nannomonas) congolense*. *Gene* 1995;161(1):125-8.
- (135) Mackey ZB, O'Brien TC, Greenbaum DC, Blank RB, McKerrow JH. A cathepsin B-like protease is required for host protein degradation in *Trypanosoma brucei*. *Journal of Biological Chemistry* 2004 Nov 12;279(46):48426-33.
- (136) Garcia MP, Nóbrega OT, Teixeira ARL, Sousa MV, Santana JM. Characterisation of a *Trypanosoma cruzi* acidic 30 kDa cysteine protease. *Molecular and Biochemical Parasitology* 1998 Mar 15;91(2):263-72.
- (137) Nóbrega OT, Santos Silva MA, Teixeira ARL, Santana JM. Cloning and sequencing of tccb, a gene encoding a *Trypanosoma cruzi* cathepsin B-like protease. *Molecular and Biochemical Parasitology* 1998 Nov 30;97(1-2):235-40.
- (138) Mendoza-Palomares C, Biteau N, Giroud C, Coustou V, Coetzer T, Authié E, et al. Molecular and biochemical characterization of a cathepsin B-like protease family unique to *Trypanosoma congolense*. *Eukaryotic Cell* 2008 Apr 1;7(4):684-97.
- (139) TriTrypDB: Kinetoplastid genomics resource. 2013.
- (140) Tazeh NN, Silverman JS, Schwartz KJ, Sevova ES, Sutterwala SS, Bangs JD. Role of AP-1 in developmentally regulated lysosomal trafficking in *Trypanosoma brucei*. *Eukaryotic Cell* 2009 Sep 1;8(9):1352-61.
- (141) Scory S, Stierhof YD, Caffrey CR, Steverding D. The cysteine proteinase inhibitor Z-Phe-Ala-CHN₂ alters cell morphology and cell division activity of *Trypanosoma brucei* bloodstream form. *Kinetoplastid Biology and Disease* 2007;6(2).
- (142) O'Brien TC, Mackey ZB, Fetter RD, Choe Y, O'Donoghue AJ, Zhou M, et al. A parasite cysteine protease is key to host protein degradation and iron acquisition. *Journal of Biological Chemistry* 2008 Oct 24;283(43):28934-43.
- (143) MBAWA ZR, GUMM ID, SHAW E, Lonsdale-Eccles JD. Characterisation of a cysteine protease from bloodstream forms of *Trypanosoma congolense*. *European Journal of Biochemistry* 1992 Feb 1;204(1):371-9.
- (144) Boulangé A, Serveau C, Brillard M, Minet C, Gauthier F, Diallo A, et al. Functional expression of the catalytic domains of two cysteine proteinases from *Trypanosoma congolense*. *International Journal for Parasitology* 2001 Nov;31(13):1435-40.
- (145) Chagas JR, Authié E, Serveau C, Lalmanach G, Juliano L, Gauthier F. A comparison of the enzymatic properties of the major cysteine proteinases from *Trypanosoma congolense* and *Trypanosoma cruzi*. *Molecular and Biochemical Parasitology* 1997 Sep;88(1-2):85-94.
- (146) Authié E. Trypanosomiasis and trypanotolerance in cattle: A role for congopain? *Parasitology Today* 1994;10(9):360-4.
- (147) Lalmanach G, Boulangé A, Serveau C, Lecaille F, Scharfstein J, Gauthier F, et al. Congopain from *Trypanosoma congolense*: drug target and vaccine candidate. *bchm* 2002;383:739.
- (148) Bers DM. Excitation-contraction coupling and cardiac contractile force. Second ed. 2001.
- (149) Katz AM. Physiology of the Heart. Lippincott-Williams & Wilkins, Philadelphia; 2001.

- (150) Pitt GS, Zühlke RD, Hudmon A, Schulman H, Reuter H, Tsien RW. Molecular basis of calmodulin tethering and Ca^{2+} -dependent inactivation of L-type Ca^{2+} channels. *Journal of Biological Chemistry* 2001 Aug 17;276(33):30794-802.
- (151) Erickson MG, Alseikhan BA, Peterson BZ, Yue DT. Preassociation of calmodulin with voltage-gated Ca^{2+} channels revealed by FRET in single living cells. *Neuron* 2001 Sep 27;31(6):973-85.
- (152) Pate P, Mochca-Morales J, Wu Y, Zhang JZ, Rodney GG, Serysheva II, et al. Determinants for calmodulin binding on voltage-dependent Ca^{2+} channels. *Journal of Biological Chemistry* 2000 Dec 15;275(50):39786-92.
- (153) Yuan W, Bers DM. Protein kinase inhibitor H-89 reverses forskolin stimulation of cardiac L-type calcium current. *American Journal of Physiology - Cell Physiology* 1995 Mar 1;268(3):C651-C659.
- (154) Lamont C, Luther PW, Balke CW, Wier WG. Intercellular Ca^{2+} waves in rat heart muscle. *The Journal of Physiology* 1998 Nov 1;512(3):669-76.
- (155) Jaimovich E, Venosa RA, Shrager P, Horowicz P. Density and distribution of tetrodotoxin receptors in normal and detubulated frog sartorius muscle. *The Journal of General Physiology* 1976 Apr 1;67(4):399-416.
- (156) Kirsch GE, Nichols RA, Nakajima S. Delayed rectification in the transverse tubules: origin of the late after-potential in frog skeletal muscle. *The Journal of General Physiology* 1977 Jul 1;70(1):1-21.
- (157) Almers W, Palade PT. Slow calcium and potassium currents across frog muscle membrane: measurements with a vaseline-gap technique. *The Journal of Physiology* 1981 Mar 1;312(1):159-76.
- (158) Bers DM. Cardiac excitation-contraction coupling. *Nature* 2002 Jan 10;415(6868):198-205.
- (159) Bers DM. Calcium Cycling and Signaling in Cardiac Myocytes. *Annu Rev Physiol* 2008 Feb 13;70(1):23-49.
- (160) Ringer S. A third contribution regarding the influence of the inorganic constituents of the blood on the ventricular contraction. *The Journal of Physiology* 1883 Aug 1;4(2-3):222-5.
- (161) Ringer S. A further contribution regarding the influence of the different constituents of the blood on the contraction of the heart. *The Journal of Physiology* 1883 Jan 1;4(1):29-42.
- (162) Ringer S. Concerning the influence exerted by each of the constituents of the blood on the contraction of the ventricle. *The Journal of Physiology* 1882 Aug 1;3(5-6):380-93.
- (163) Ringer S. Regarding the action of hydrate of soda, hydrate of ammonia, and hydrate of potash on the ventricle of the frog's heart. *The Journal of Physiology* 1882 Jan 1;3(3-4):195-202.
- (164) Hayashi T, Martone ME, Yu Z, Thor A, Doi M, Holst MJ, et al. Three-dimensional electron microscopy reveals new details of membrane systems for Ca^{2+} signaling in the heart. *Journal of Cell Science* 2009 Apr 1;122(7):1005-13.
- (165) Lai FA, Anderson K, Rousseau E, Liu QY, Meissner G. Evidence for a Ca^{2+} channel within the ryanodine receptor complex from cardiac sarcoplasmic reticulum. *Biochemical and Biophysical Research Communications* 1988 Feb 29;151(1):441-9.
- (166) Takeshima H, Nishimura S, Matsumoto T, Ishida H, Kangawa K, Minamino N, et al. Primary structure and expression from complementary DNA of skeletal muscle ryanodine receptor. *Nature* 1989;339(6224):439-45.

- (167) Bers DM, Stiffel VM. Ratio of ryanodine to dihydropyridine receptors in cardiac and skeletal muscle and implications for E-C coupling. *The American Journal of Physiology* 1993;264(6 Pt 1):C1587-C1593.
- (168) Wibo M, Bravo G, Godfraind T. Postnatal maturation of excitation-contraction coupling in rat ventricle in relation to the subcellular localization and surface density of 1,4-dihydropyridine and ryanodine receptors. *Circulation research* 1991 Mar 1;68(3):662-73.
- (169) Stern MD, Pizarro G, Ríos E. Local control model of excitation-contraction coupling in skeletal muscle. *Journal of General Physiology* 1997;110(4):415-40.
- (170) Bridge JHB, Ershler PB, Cannell MB. Properties of Ca^{2+} sparks evoked by action potentials in mouse ventricular myocytes. *Journal of Physiology* 1999;518(2):469-78.
- (171) Mejia-Alvarez R, Kettlun C, Rios E, Stern M, Fill M. Unitary Ca^{2+} current through cardiac ryanodine receptor channels under quasi-physiological ionic conditions. *Journal of General Physiology* 1999;113(2):177-86.
- (172) Lukyanenko V, Györke I, Subramanian S, Smirnov A, Wiesner TF, Györke S. Inhibition of Ca^{2+} sparks by ruthenium red in permeabilized rat ventricular myocytes. *Biophysical Journal* 2000;79(3):1273-84.
- (173) Izu LT, Mauban JRH, Balke CW, Wier WG. Large currents generate cardiac Ca^{2+} sparks. *Biophysical Journal* 2001;80(1):88-102.
- (174) Lipp P, Egger M, Niggli E. Spatial characteristics of sarcoplasmic reticulum Ca^{2+} release events triggered by L-type Ca^{2+} current and Na^{+} current in guinea-pig cardiac myocytes. *Journal of Physiology* 2002;542(2):383-93.
- (175) Inoue M, Bridge JHB. Variability in couplon size in rabbit ventricular myocytes. *Biophysical Journal* 2005 Nov;89(5):3102-10.
- (176) Puglisi JL, Yuan W, Bassani JWM, Bers DM. Ca^{2+} influx through Ca^{2+} channels in rabbit ventricular myocytes during action potential clamp : influence of temperature. *Circulation research* 1999 Sep 17;85(6):e7-e16.
- (177) Yuan W, Ginsburg KS, Bers DM. Comparison of sarcolemmal calcium channel current in rabbit and rat ventricular myocytes. *The Journal of Physiology* 1996 Jun 15;493(Pt 3):733-46.
- (178) Harrison SM, Bers DM. Influence of temperature on the calcium sensitivity of the myofilaments of skinned ventricular muscle from the rabbit. *The Journal of General Physiology* 1989 Mar 1;93(3):411-28.
- (179) Bers DM. Calcium fluxes involved in control of cardiac myocyte contraction. *Circulation research* 2000 Aug 18;87(4):275-81.
- (180) Fabiato A. Calcium-induced release of calcium from the cardiac sarcoplasmic reticulum. *The American Journal of Physiology* 1983;245(1):C1-C14.
- (181) Fabiato A, Fabiato F. Contractions induced by a calcium-triggered release of calcium from the sarcoplasmic reticulum of single skinned cardiac cells. *The Journal of Physiology* 1975 Aug 1;249(3):469-95.
- (182) Fabiato A. Simulated calcium current can both cause calcium loading in and trigger calcium release from the sarcoplasmic reticulum of a skinned canine cardiac Purkinje cell. *The Journal of General Physiology* 1985 Feb 1;85(2):291-320.
- (183) Fabiato A. Rapid ionic modifications during the aequorin-detected calcium transient in a skinned canine cardiac Purkinje cell. *The Journal of General Physiology* 1985 Feb 1;85(2):189-246.

- (184) Fabiato A. Time and calcium dependence of activation and inactivation of calcium-induced release of calcium from the sarcoplasmic reticulum of a skinned canine cardiac Purkinje cell. *The Journal of General Physiology* 1985 Feb 1;85(2):247-89.
- (185) Beuckelmann DJ, Wier WG. Mechanism of release of calcium from sarcoplasmic reticulum of guinea-pig cardiac cells. *The Journal of Physiology* 1988 Nov 1;405(1):233-55.
- (186) Callewaert G, Cleemann L, Morad M. Epinephrine enhances Ca^{2+} current-regulated Ca^{2+} release and Ca^{2+} reuptake in rat ventricular myocytes. *Proceedings of the National Academy of Sciences* 1988 Mar 1;85(6):2009-13.
- (187) Cannell MB, Berlin JR, Lederer WJ. Effect of membrane potential changes on the calcium transient in single rat cardiac muscle cells. *Science* 1987;238(4832):1419-23.
- (188) duBell WH, Houser SR. Voltage and beat dependence of Ca^{2+} transient in feline ventricular myocytes. *American Journal of Physiology - Heart and Circulatory Physiology* 1989 Sep 1;257(3):H746-H759.
- (189) London B, Krueger JW. Contraction in voltage-clamped, internally perfused single heart cells. *The Journal of General Physiology* 1986 Oct 1;88(4):475-505.
- (190) Hadley RW, Lederer WJ. Properties of L-type calcium channel gating current in isolated guinea pig ventricular myocytes. *The Journal of General Physiology* 1991 Aug 1;98(2):265-85.
- (191) Nabauer M, Morad M. Ca^{2+} -induced Ca^{2+} release as examined by photolysis of caged Ca^{2+} in single ventricular myocytes. *The American Journal of Physiology* 1990;258(1 Pt 1):C189-C193.
- (192) Venetucci LA, Trafford AW, O'Neill SC, Eisner DA. The sarcoplasmic reticulum and arrhythmogenic calcium release. *Cardiovascular Research* 2008 Jan 15;77(2):285-92.
- (193) Block BA, Imagawa T, Campbell KP, Franzini-Armstrong C. Structural evidence for direct interaction between the molecular components of the transverse tubule/sarcoplasmic reticulum junction in skeletal muscle. *The Journal of Cell Biology* 1988 Dec 1;107(6):2587-600.
- (194) Stern MD. Theory of excitation-contraction coupling in cardiac muscle. *Biophysical Journal* 1992 Aug;63(2):497-517.
- (195) Cheng H, Lederer WJ, Cannell MB. Calcium Sparks - elementary events underlying excitation-contraction coupling in heart-muscle. *Science* 1993 Oct 29;262(5134):740-4.
- (196) Fill M, Coronado R. Ryanodine receptor channel of sarcoplasmic reticulum. *Trends in Neurosciences* 1988;11(10):453-7.
- (197) Bassani JW, Bassani RA, Bers DM. Twitch-dependent SR Ca accumulation and release in rabbit ventricular myocytes. *American Journal of Physiology* 1993;265(2 Pt 1):C533-C540.
- (198) Bassani JW, Yuan W, Bers DM. Fractional SR Ca release is regulated by trigger Ca and SR Ca content in cardiac myocytes. *American Journal of Physiology - Cell Physiology* 1995 May 1;268(5):C1313-C1319.
- (199) Shannon TR, Ginsburg KS, Bers DM. Potentiation of fractional sarcoplasmic reticulum calcium release by total and free intra-sarcoplasmic reticulum calcium concentration. *Biophysical Journal* 2000 Jan;78(1):334-43.
- (200) Sham JSK, Song LS, Chen Y, Deng LH, Stern MD, Lakatta EG, et al. Termination of Ca^{2+} release by a local inactivation of ryanodine receptors in cardiac myocytes. *Proceedings of the National Academy of Sciences* 1998 Dec 8;95(25):15096-101.

- (201) Lukyanenko V, Wiesner TF, Györke S. Termination of Ca^{2+} release during Ca^{2+} sparks in rat ventricular myocytes. *The Journal of Physiology* 1998 Mar 15;507(3):667-77.
- (202) Satoh H, Blatter LA, Bers DM. Effects of $[\text{Ca}^{2+}]_i$, SR Ca^{2+} load, and rest on Ca^{2+} spark frequency in ventricular myocytes. *American Journal of Physiology - Heart and Circulatory Physiology* 1997 Feb 1;272(2):H657-H668.
- (203) Wang SQ, Song LS, Lakatta EG, Cheng H. Ca^{2+} signalling between single L-type Ca^{2+} channels and ryanodine receptors in heart cells. *Nature* 2001;410(6828):592-6.
- (204) Sobie EA, Dilly KW, dos Santos Cruz J, Lederer WJ, Jafri MS. Termination of cardiac Ca^{2+} sparks: an investigative mathematical model of calcium-induced calcium release. *Biophysical Journal* 2002;83(1):59-78.
- (205) Sharma MR, Penczek P, Grassucci R, Xin HB, Fleischer S, Wagenknecht T. Cryoelectron microscopy and image analysis of the cardiac ryanodine receptor. *Journal of Biological Chemistry* 1998 Jul 17;273(29):18429-34.
- (206) Samsó M, Wagenknecht T. Contributions of electron microscopy and single-particle techniques to the determination of the ryanodine receptor three-dimensional structure. *Journal of Structural Biology* 1998;121(2):172-80.
- (207) Marx SO, Gaburjakova J, Gaburjakova M, Henrikson C, Ondrias K, Marks AR. Coupled gating between cardiac calcium release channels (ryanodine receptors). *Circulation research* 2001 Jun 8;88(11):1151-8.
- (208) Goldman YE. Kinetics of the actomyosin ATPase in muscle fibers. *Annu Rev Physiol* 1987 Mar 1;49(1):637-54.
- (209) Brenner B. Mechanical and structural approaches to correlation of cross-bridge action in muscle with actomyosin ATPase in solution. *Annu Rev Physiol* 1987 Mar 1;49(1):655-72.
- (210) Foskett JK, White C, Cheung KH, Mak D-OD. Inositol trisphosphate receptor Ca^{2+} release channels. *Physiological Reviews* 2007 Apr 1;87(2):593-658.
- (211) Lipp P, Laine M, Tovey SC, Burrell KM, Berridge MJ, Li W, et al. Functional InsP_3 receptors that may modulate excitation-contraction coupling in the heart. *Current Biology* 2000 Aug 1;10(15):939-51.
- (212) Signore S, Sorrentino A, Ferreira-Martins J, Kannappan R, Shafaie M, Del Ben F, et al. Inositol 1, 4, 5-trisphosphate receptors and human left ventricular myocytes. *Circulation* 2013 Sep 17;128(12):1286-97.
- (213) Nosek TM, Williams MF, Zeigler ST, Godt RE. Inositol trisphosphate enhances calcium release in skinned cardiac and skeletal muscle. *American Journal of Physiology - Cell Physiology* 1986 May 1;250(5):C807-C811.
- (214) Harzheim D, Movassagh M, Foo RSY, Ritter O, Tashfeen A, Conway SJ, et al. Increased InsP_3 Rs in the junctional sarcoplasmic reticulum augment Ca^{2+} transients and arrhythmias associated with cardiac hypertrophy. *Proceedings of the National Academy of Sciences* 2009 Jul 7;106(27):11406-11.
- (215) Roderick HL, Knollmann BC. Inositol 1,4,5-trisphosphate receptors: "Exciting" players in cardiac excitation-contraction coupling? *Circulation* 2013 Sep 17;128(12):1273-5.
- (216) Wu X, Zhang T, Bossuyt J, Li X, McKinsey TA, Dedman JR, et al. Local InsP_3 -dependent perinuclear Ca^{2+} signaling in cardiac myocyte excitation-transcription coupling. *J Clin Invest* 2006 Mar 1;116(3):675-82.
- (217) Higazi DR, Fearnley CJ, Drawnel FM, Talasila A, Corps EM, Ritter O, et al. Endothelin-1-stimulated InsP_3 -Induced Ca^{2+} release is a nexus for hypertrophic signaling in cardiac myocytes. *Molecular Cell* 2009 Feb 27;33(4):472-82.

- (218) Escobar M, Cardenas C, Colavita K, Petrenko NB, Franzini-Armstrong C. Structural evidence for perinuclear calcium microdomains in cardiac myocytes. *Journal of Molecular and Cellular Cardiology* 2011 Mar;50(3):451-9.
- (219) Bezprozvanny I, Ehrlich BE. Inositol (1,4,5)-trisphosphate (InsP₃)-gated Ca channels from cerebellum: conduction properties for divalent cations and regulation by intraluminal calcium. *The Journal of General Physiology* 1994 Nov 1;104(5):821-56.
- (220) Remus TP, Zima AV, Bossuyt J, Bare DJ, Martin JL, Blatter LA, et al. Biosensors to measure inositol 1,4,5-trisphosphate concentration in living cells with spatiotemporal resolution. *Journal of Biological Chemistry* 2006 Jan 6;281(1):608-16.
- (221) Shilkrut M, Gealekman O, Rosen D, Berke G, Woodcock E, Binah O. Electrophysiologic perturbations and arrhythmogenic activity caused by activation of the Fas receptor in murine ventricular myocytes: Role of the inositol trisphosphate pathway. *Journal of cardiovascular electrophysiology* 2001 Feb 1;12(2):185-95.
- (222) Cheng H, Lederer WJ. Calcium sparks. *Physiology Reviews* 2008;88:1491-545.
- (223) Choi HS, Eisner DA. The role of sarcolemmal Ca²⁺-ATPase in the regulation of resting calcium concentration in rat ventricular myocytes. *The Journal of Physiology* 1999 Feb 15;515(1):109-18.
- (224) Bassani JW, Bassani RA, Bers DM. Relaxation in rabbit and rat cardiac cells: species-dependent differences in cellular mechanisms. *The Journal of Physiology* 1994 Apr 15;476(2):279-93.
- (225) Pieske B, Maier LS, Bers DM, Hasenfuss G. Ca²⁺ handling and sarcoplasmic reticulum Ca²⁺ content in isolated failing and nonfailing human myocardium. *Circulation research* 1999 Jul 9;85(1):38-46.
- (226) Li L, DeSantiago J, Chu G, Kranias EG, Bers DM. Phosphorylation of phospholamban and troponin I in β -adrenergic-induced acceleration of cardiac relaxation. *American Journal of Physiology Heart and Circulatory Physiology* 2000;278(3):H769-H779.
- (227) Kentish JC, McCloskey DT, Layland J, Palmer S, Leiden JM, Martin AF, et al. Phosphorylation of troponin I by protein kinase A accelerates relaxation and crossbridge cycle kinetics in mouse ventricular muscle. *Circulation research* 2001 May 25;88(10):1059-65.
- (228) Peña JR, Wolska BM. Troponin I phosphorylation plays an important role in the relaxant effect of β -adrenergic stimulation in mouse hearts. *Cardiovascular Research* 2004 Mar 1;61(4):756-63.
- (229) Pi Y, Kemnitz KR, Zhang D, Kranias EG, Walker JW. Phosphorylation of troponin I controls cardiac twitch dynamics: Evidence from phosphorylation site mutants expressed on a troponin I-null background in mice. *Circulation research* 2002 Apr 5;90(6):649-56.
- (230) Brandl CJ, deLeon S, Martin DR, MacLennan DH. Adult forms of the Ca²⁺ATPase of sarcoplasmic reticulum. Expression in developing skeletal muscle. *Journal of Biological Chemistry* 1987 Mar 15;262(8):3768-74.
- (231) Brandl CJ, Green NM, Korczak B, MacLennan DH. Two Ca²⁺ ATPase genes: Homologies and mechanistic implications of deduced amino acid sequences. *Cell* 1986 Feb 28;44(4):597-607.
- (232) MacLennan DH, Green NM. Structural biology. Pumping ions. *Nature* 2000;405(6787):633-4.
- (233) Toyoshima C, Nakasako M, Nomura H, Ogawa H. Crystal structure of the calcium pump of sarcoplasmic reticulum at 2.6 Å resolution. *Nature* 2013;405(6787):647-55.

- (234) Clarke DM, Maruyama K, Loo TW, Leberer E, Inesi G, MacLennan DH. Functional consequences of glutamate, aspartate, glutamine, and asparagine mutations in the stalk sector of the Ca^{2+} -ATPase of sarcoplasmic reticulum. *Journal of Biological Chemistry* 1989 Jul 5;264(19):11246-51.
- (235) Clarke DM, Loo TW, Inesi G, MacLennan DH. Location of high affinity Ca^{2+} -binding sites within the predicted transmembrane domain of the sarcoplasmic reticulum Ca^{2+} -ATPase. *Nature* 1989;339(6224):476-8.
- (236) Hove-Madsen L, Bers DM. Sarcoplasmic reticulum Ca^{2+} uptake and thapsigargin sensitivity in permeabilized rabbit and rat ventricular myocytes. *Circulation research* 1993 Nov 1;73(5):820-8.
- (237) Shigekawa M, Finegan JA, Katz AM. Calcium transport ATPase of canine cardiac sarcoplasmic reticulum. A comparison with that of rabbit fast skeletal muscle sarcoplasmic reticulum. *Journal of Biological Chemistry* 1976 Nov 25;251(22):6894-900.
- (238) Levitsky DO, Benevolensky DS, Levchenko TS, Smirnov VN, Chazov EI. Calcium-binding rate and capacity of cardiac sarcoplasmic reticulum. *Journal of Molecular and Cellular Cardiology* 1981 Sep;13(9):785-96.
- (239) Tada M, Kirchberger MA, Katz AM. Phosphorylation of a 22,000-dalton component of the cardiac sarcoplasmic reticulum by adenosine 3':5'-monophosphate-dependent protein kinase. *Journal of Biological Chemistry* 1975 Apr 10;250(7):2640-7.
- (240) Simmerman HK, Collins JH, Theibert JL, Wegener AD, Jones LR. Sequence analysis of phospholamban. Identification of phosphorylation sites and two major structural domains. *Journal of Biological Chemistry* 1986 Oct 5;261(28):13333-41.
- (241) Hicks MJ, Shigekawa M, Katz AM. Mechanism by which cyclic adenosine 3':5'-monophosphate-dependent protein kinase stimulates calcium transport in cardiac sarcoplasmic reticulum. *Circulation research* 1979 Mar 1;44(3):384-91.
- (242) Inui M, Chamberlain BK, Saito A, Fleischer S. The nature of the modulation of Ca^{2+} transport as studied by reconstitution of cardiac sarcoplasmic reticulum. *Journal of Biological Chemistry* 1986 Feb 5;261(4):1794-800.
- (243) Kirchberger MA, Tada M, Katz AM. Adenosine 3':5'-monophosphate-dependent protein kinase-catalyzed phosphorylation reaction and its relationship to calcium transport in cardiac sarcoplasmic reticulum. *Journal of Biological Chemistry* 1974 Oct 10;249(19):6166-73.
- (244) Bartel S, Vetter D, Schlegel WP, Wallukat G, Krause EG, Karczewski P. Phosphorylation of phospholamban at threonine-17 in the absence and presence of β -adrenergic stimulation in neonatal rat cardiomyocytes. *Journal of Molecular and Cellular Cardiology* 2000 Dec;32(12):2173-85.
- (245) Wegener AD, Simmerman HK, Lindemann JP, Jones LR. Phospholamban phosphorylation in intact ventricles. Phosphorylation of serine 16 and threonine 17 in response to beta-adrenergic stimulation. *Journal of Biological Chemistry* 1989 Jul 5;264(19):11468-74.
- (246) Kimura Y, Kurzydowski K, Tada M, MacLennan DH. Phospholamban inhibitory function is activated by depolymerization. *Journal of Biological Chemistry* 1997 Jun 13;272(24):15061-4.
- (247) Iwamoto T, Nakamura TY, Pan Y, Uehara A, Imanaga I, Shigekawa M. Unique topology of the internal repeats in the cardiac $\text{Na}^+/\text{Ca}^{2+}$ exchanger. *FEBS Letters* 1999 Mar 12;446(2-3):264-8.
- (248) Nicoll DA, Ottolia M, Lu L, Lu Y, Philipson KD. A new topological model of the cardiac sarcolemmal $\text{Na}^+/\text{Ca}^{2+}$ exchanger. *Journal of Biological Chemistry* 1999 Jan 8;274(2):910-7.

- (249) Matsuoka S, Nicoll DA, Reilly RF, Hilgemann DW, Philipson KD. Initial localization of regulatory regions of the cardiac sarcolemmal Na^+ - Ca^{2+} exchanger. *Proceedings of the National Academy of Sciences* 1993 May 1;90(9):3870-4.
- (250) Ottolia M, Nicoll DA, Philipson KD. Roles of two Ca^{2+} -binding domains in regulation of the cardiac Na^+ - Ca^{2+} exchanger. *Journal of Biological Chemistry* 2009;284(47):32735-41.
- (251) Matsuoka S, Hilgemann DW. Steady-state and dynamic properties of cardiac sodium-calcium exchange ion and voltage dependencies of the transport cycle. *Journal of General Physiology* 1992;100(6):963-1001.
- (252) Ottolia M, Torres N, Bridge JHB, Philipson KD, Goldhaber JI. Na/Ca exchange and contraction of the heart. *Journal of Molecular and Cellular Cardiology* 2013 Aug;61(0):28-33.
- (253) Bridge JH, Smolley JR, Spitzer KW. The relationship between charge movements associated with I_{Ca} and $I_{\text{Na-Ca}}$ in cardiac myocytes. *Science* 1990;248(4953):376-8.
- (254) Hilgemann DW, Collins A, Cash DP, Nagel GA. Cardiac Na^+ - Ca^{2+} exchange system in giant membrane patches. *Annals of the New York Academy of Sciences* 1991 Dec 1;639(1):126-39.
- (255) Caroni P, Carafoli E. The Ca^{2+} -pumping ATPase of heart sarcolemma. Characterization, calmodulin dependence, and partial purification. *Journal of Biological Chemistry* 1981 Apr 10;256(7):3263-70.
- (256) Caroni P, Carafoli E. Regulation of Ca^{2+} -pumping ATPase of heart sarcolemma by a phosphorylation-dephosphorylation Process. *Journal of Biological Chemistry* 1981 Sep 25;256(18):9371-3.
- (257) Bassani RA, Bassani JW, Bers DM. Mitochondrial and sarcolemmal Ca^{2+} transport reduce $[\text{Ca}^{2+}]_i$ during caffeine contractures in rabbit cardiac myocytes. *The Journal of Physiology* 1992 Jul 1;453(1):591-608.
- (258) Grimm M, Brown JH. β -Adrenergic receptor signaling in the heart: Role of CaMKII. *Journal of Molecular and Cellular Cardiology* 2010 Feb;48(2):322-30.
- (259) Valdivia HH, Kaplan JH, Ellis-Davies GCR, Lederer WJ. Rapid adaptation of cardiac ryanodine receptors: modulation by Mg^{2+} and phosphorylation. *Science* 1995;267(5206):1997-2000.
- (260) Brum PC, Rolim NPL, Bacurau AVN, Medeiros A. Neurohumoral activation in heart failure: the role of adrenergic receptors. *Anais da Academia Brasileira de Ciências* 2006;78:485-503.
- (261) Cheng H, Lederer MR, Lederer WJ, Cannell MB. Calcium sparks and $[\text{Ca}^{2+}]_{(i)}$ waves in cardiac myocytes. *American Journal of Physiology-Cell Physiology* 1996 Jan;39(1):C148-C159.
- (262) Eisner DA, Valdeolmillos M. A study of intracellular calcium oscillations in sheep cardiac Purkinje fibres measured at the single cell level. *Journal of Physiology* 1986;VOL. 372:539-56.
- (263) Wier WG, Cannell MB, Berlin JR, Marban E, Lederer WJ. Cellular and subcellular heterogeneity of $[\text{Ca}^{2+}]_{(i)}$ in single heart cells revealed by fura-2. *Science* 1987;235(4786):325-8.
- (264) Díaz ME, Trafford AW, O'Neill SC, Eisner DA. Measurement of sarcoplasmic reticulum Ca^{2+} content and sarcolemmal Ca^{2+} fluxes in isolated rat ventricular myocytes during spontaneous Ca^{2+} release. *The Journal of Physiology* 1997 May 15;501(Pt 1):3-16.

- (265) Sitsapesan R, Williams AJ. Regulation of the gating of the sheep cardiac sarcoplasmic reticulum Ca^{2+} -release channel by luminal Ca^{2+} . *The Journal of Membrane Biology* 1994;137(3):215-26.
- (266) Trafford AW, Sibbring GC, Díaz ME, Eisner DA. The effects of low concentrations of caffeine on spontaneous Ca release in isolated rat ventricular myocytes. *Cell calcium* 2000 Oct;28(4):269-76.
- (267) Overend CL, Eisner DA, O'Neill SC. The effect of tetracaine on spontaneous Ca^{2+} release and sarcoplasmic reticulum calcium content in rat ventricular myocytes. *The Journal of Physiology* 1997 Aug 1;502(Pt 3):471-9.
- (268) Sitsapesan R, Williams AJ. Regulation of current flow through ryanodine receptors by luminal Ca^{2+} . *J Membrane Biol* 1997;159(3):179-85.
- (269) Lukyanenko V, Viatchenko-Karpinski S, Smirnov A, Wiesner TF, Györke S. Dynamic regulation of sarcoplasmic reticulum Ca^{2+} content and release by luminal Ca^{2+} -sensitive leak in rat ventricular myocytes. *Biophysical Journal* 2001 Aug;81(2):785-98.
- (270) Kass RS, Lederer WJ, Tsien RW, Weingart R. Role of calcium ions in transient inward currents and aftercontractions induced by strophanthidin in cardiac Purkinje fibres. *The Journal of Physiology* 1978 Aug 1;281(1):187-208.
- (271) Priori SG, Napolitano C, Tiso N, Memmi M, Vignati G, Bloise R, et al. Mutations in the cardiac ryanodine receptor gene (hRyR2) underlie catecholaminergic polymorphic ventricular tachycardia. *Circulation* 2001 Jan 16;103(2):196-200.
- (272) Priori SG, Napolitano C, Memmi M, Colombi B, Drago F, Gasparini M, et al. Clinical and molecular characterization of patients with catecholaminergic polymorphic ventricular tachycardia. *Circulation* 2002 Jul 2;106(1):69-74.
- (273) Wehrens XHT, Lehnart SE, Huang F, Vest JA, Reiken SR, Mohler PJ, et al. FKBP12.6 deficiency and defective calcium release channel (ryanodine receptor) function linked to exercise-induced sudden cardiac death. *Cell* 2003 Jun 27;113(7):829-40.
- (274) Lahat H, Pras E, Olender T, Avidan N, Ben-Asher E, Man O, et al. A missense mutation in a highly conserved region of *CASQ2* is associated with autosomal recessive catecholamine-induced polymorphic ventricular tachycardia in bedouin families from Israel. *The American Journal of Human Genetics* 2001 Dec;69(6):1378-84.
- (275) Bhuiyan ZA, Hamdan MA, Shamsi ETA, Postma AV, Mannens MM, Wilde AA, et al. A novel early onset lethal form of catecholaminergic polymorphic ventricular tachycardia maps to chromosome 7p14-p22. *Journal of cardiovascular electrophysiology* 2007 Oct 1;18(10):1060-6.
- (276) Marx SO, Reiken S, Hisamatsu Y, Jayaraman T, Burkhoff D, Rosemblyt N, et al. PKA phosphorylation dissociates FKBP12.6 from the calcium release channel (ryanodine receptor): defective regulation in failing hearts. *Cell* 2000 May 12;101(4):365-76.
- (277) Bers DM, Eisner DA, Valdivia HH. Sarcoplasmic reticulum Ca^{2+} and heart failure: roles of diastolic leak and Ca^{2+} transport. *Circulation research* 2003 Sep 19;93(6):487-90.
- (278) George CH, Jundi H, Thomas NL, Fry DL, Lai FA. Ryanodine receptors and ventricular arrhythmias: Emerging trends in mutations, mechanisms and therapies. *Journal of Molecular and Cellular Cardiology* 2007 Jan;42(1):34-50.
- (279) Jiang MT, Lokuta AJ, Farrell EF, Wolff MR, Haworth RA, Valdivia HH. Abnormal Ca^{2+} release, but normal ryanodine receptors, in canine and human heart failure. *Circulation research* 2002 Nov 29;91(11):1015-22.
- (280) Maier LS, Bers DM. Role of Ca^{2+} /calmodulin-dependent protein kinase (CaMK) in excitation-contraction coupling in the heart. *Cardiovascular Research* 2007 Mar 1;73(4):631-40.

- (281) Davia K, Bernobich E, Ranu HK, del Monte F, Terracciano CMN, MacLeod KT, et al. SERCA2a overexpression decreases the incidence of aftercontractions in adult rabbit ventricular myocytes. *Journal of Molecular and Cellular Cardiology* 2001 May;33(5):1005-15.
- (282) del Monte F, Lebeche D, Guerrero JL, Tsuji T, Doye AA, Gwathmey JK, et al. Abrogation of ventricular arrhythmias in a model of ischemia and reperfusion by targeting myocardial calcium cycling. *Proceedings of the National Academy of Sciences of the United States of America* 2004 Apr 13;101(15):5622-7.
- (283) Berlin JR, Cannell MB, Lederer WJ. Cellular origins of the transient inward current in cardiac myocytes. Role of fluctuations and waves of elevated intracellular calcium. *Circulation research* 1989;65:115-26.
- (284) Lederer WJ, Tsien RW. Transient inward current underlying arrhythmogenic effects of cardiotonic steroids in Purkinje fibres. *The Journal of Physiology* 1976 Dec 1;263(2):73-100.
- (285) Kass RS, Tsien RW, Weingart R. Ionic basis of transient inward current induced by strophanthidin in cardiac Purkinje fibres. *The Journal of Physiology* 1978 Aug 1;281(1):209-26.
- (286) Clusin WT. Calcium and cardiac arrhythmias: DADs, EADs and alternans. *Critical Reviews in Clinical Laboratory Science* 2003;40(3):337-75.
- (287) Ferrier GR, Sounders JH, Mendez C. A cellular mechanism for the generation of ventricular arrhythmias by acetylstrophanthidin. *Circulation research* 1973 May 1;32(5):600-9.
- (288) Winslow RL, Varghese A, Noble D, Adlakha C, Hoythya A. Generation and propagation of ectopic beats induced by spatially localized Na⁺-K pump inhibition in atrial network models. *Proceedings of the Royal Society of London Series B: Biological Sciences* 1993 Oct 22;254(1339):55-61.
- (289) Xie LH, Weiss JN. Arrhythmogenic consequences of intracellular calcium waves. *American Journal of Physiology - Heart and Circulatory Physiology* 2009 Sep;297(3):H997-H1002.
- (290) Lankipalli RS, Zhu T, Guo D, Yan G-X. Mechanisms underlying arrhythmogenesis in long QT syndrome. *Journal of electrocardiology* 2005;38(4):69-73.
- (291) Schlotthauer K, Bers DM. Sarcoplasmic reticulum Ca²⁺ release causes myocyte depolarisation. Underlying mechanism and threshold for triggered action potentials. *Circulation research* 2000;87:774-80.
- (292) Preliminary Report: Effect of encainide and flecainide on mortality in a randomized trial of arrhythmia suppression after myocardial infarction. *N Engl J Med* 1989 Aug 10;321(6):406-12.
- (293) Sipido KR, Varro A, Eisner D. Sodium calcium exchange as a target for antiarrhythmic therapy. *Handbook of Experimental Pharmacology* 2006;171(159):199.
- (294) Eisner DA, Lederer WJ, Sheu SS. The role of intracellular sodium activity in the antiarrhythmic action of local anaesthetics in sheep Purkinje fibres. *The Journal of Physiology* 1983 Jul 1;340(1):239-57.
- (295) Hunt DJ, Jones PP, Wang R, Chen W, Bolstad J, Chen K, et al. K201 (JTV519) suppresses spontaneous Ca²⁺ release and [3H]ryanodine binding to RyR2 irrespective of FKBP12.6 association. *The Biochemical Journal* 2007;404(3):431-8.
- (296) Loughrey CM, Otani N, Seidler T, Craig MA, Matsuda R, Kaneko N, et al. K201 modulates excitation-contraction coupling and spontaneous Ca²⁺ release in normal

- adult rabbit ventricular cardiomyocytes. *Cardiovascular Research* 2007 Nov 1;76(2):236-46.
- (297) Xu L, Jones R, Meissner G. Effects of local anesthetics on single channel behavior of skeletal muscle calcium release channel. *The Journal of General Physiology* 1993 Feb 1;101(2):207-33.
- (298) Venetucci LA, Trafford AW, Díaz ME, O'Neill SC, Eisner DA. Reducing ryanodine receptor open probability as a means to abolish spontaneous Ca^{2+} release and increase Ca^{2+} transient amplitude in adult ventricular myocytes. *Circulation research* 2006 May 26;98(10):1299-305.
- (299) Belevych A, Kubalova Z, Terentyev D, Hamlin RL, Carnes CA, Györke S. Enhanced ryanodine receptor-mediated calcium leak determines reduced sarcoplasmic reticulum calcium content in chronic canine heart failure. *Biophysical Journal* 2007;93(11):4083-92.
- (300) Hasenfuss G, Pieske B. Calcium cycling in congestive heart failure. *Journal of Molecular and Cellular Cardiology* 2002;34(8):951-69.
- (301) Houser SR, Margulies KB. Is depressed myocyte contractility centrally involved in heart failure? *Circulation research* 2003;92(4):350-8.
- (302) Sipido KR, Eisner D. Something old, something new: Changing views on the cellular mechanisms of heart failure. *Cardiovascular Research* 2005;68(2):167-74.
- (303) Lindner M, Erdmann E, Beuckelmann DJ. Calcium content of the sarcoplasmic reticulum in isolated ventricular myocytes from patients with terminal heart failure. *Journal of Molecular and Cellular Cardiology* 1998;30(4):743-9.
- (304) Pogwizd SM, Qi M, Yuan W, Samarel AM, Bers DM. Upregulation of $\text{Na}^+/\text{Ca}^{2+}$ exchanger expression and-function in an arrhythmogenic rabbit model of heart failure. *Circulation research* 1999;85(11):1009-19.
- (305) Hobai IA, O'Rourke B. Decreased sarcoplasmic reticulum calcium content is responsible for defective excitation-contraction coupling in canine heart failure. *Circulation* 2001;103(11):1577-84.
- (306) Piacentino III V, Weber CR, Chen X, Weisser-Thomas J, Margulies KB, Bers DM, et al. Cellular basis of abnormal calcium transients of failing human ventricular myocytes. *Circulation research* 2003;92(6):651-8.
- (307) Mercadier JJ, Lompré AM, Duc P, Boheler KR, Fraysse JB, Wisnewsky C, et al. Altered sarcoplasmic reticulum Ca^{2+} -ATPase gene expression in the human ventricle during end-stage heart failure. *J Clin Invest* 1990 Jan 1;85(1):305-9.
- (308) MacLennan DH, Kranias EG. Phospholamban: a crucial regulator of cardiac contractility. *Nat Rev Mol Cell Biol* 2003;4(7):566-77.
- (309) Dash R, Frank KF, Carr AN, Moravec CS, Kranias EG. Gender influences on sarcoplasmic reticulum Ca^{2+} -handling in failing human myocardium. *Journal of Molecular and Cellular Cardiology* 2001 Jul;33(7):1345-53.
- (310) Huang B, Wang S, Qin D, Boutjdir M, El-Sherif N. Diminished basal phosphorylation level of phospholamban in the postinfarction remodeled rat ventricle: role of β -adrenergic pathway, G_i protein, phosphodiesterase, and phosphatases. *Circulation research* 1999 Oct 29;85(9):848-55.
- (311) Fischer TH, Herting J, Tirilomis T, Renner A, Neef S, Toischer K, et al. Ca^{2+} /calmodulin-dependent protein kinase II and protein kinase A differentially regulate sarcoplasmic reticulum Ca^{2+} leak in human cardiac pathology. *Circulation* 2013 Aug 27;128(9):970-81.

- (312) Pogwizd SM, Schlotthauer K, Li L, Yuan W, Bers DM. Arrhythmogenesis and contractile dysfunction in heart failure: Roles of sodium-calcium exchange, inward rectifier potassium current, and residual β -adrenergic responsiveness. *Circulation research* 2001;88(11):1159-67.
- (313) Sipido KR, Volders PGA, De Groot SHM, Verdonck F, Van De Werf F, Wellens HJJ, et al. Enhanced Ca^{2+} release and Na/Ca exchange activity in hypertrophied canine ventricular myocytes: Potential link between contractile adaptation and arrhythmogenesis. *Circulation* 2000;102(17):2137-44.
- (314) Ahmmed GU, Dong PH, Song G, Ball NA, Xu Y, Walsh RA, et al. Changes in Ca^{2+} cycling proteins underlie cardiac action potential prolongation in a pressure-overloaded guinea pig model with cardiac hypertrophy and failure. *Circulation research* 2000;86(5):558-70.
- (315) Litwin SE, Bridge JHB. Enhanced Na^+ - Ca^{2+} exchange in the infarcted heart: Implications for excitation-contraction coupling. *Circulation research* 1997;81(6):1083-93.
- (316) Tomaselli GF, Marbán E. Electrophysiological remodeling in hypertrophy and heart failure. *Cardiovascular Research* 1999 May 1;42(2):270-83.
- (317) Schröder F, Handrock R, Beuckelmann DJ, Hirt S, Hullin R, Priebe L, et al. Increased availability and open probability of single L-type calcium channels from failing compared with nonfailing human ventricle. *Circulation* 1998 Sep 8;98(10):969-76.
- (318) Chen X, Piacentino V, Furukawa S, Goldman B, Margulies KB, Houser SR. L-type Ca^{2+} channel density and regulation are altered in failing human ventricular myocytes and recover after support with mechanical assist devices. *Circulation research* 2002 Sep 20;91(6):517-24.
- (319) Ai X, Curran JW, Shannon TR, Bers DM, Pogwizd SM. Ca^{2+} /Calmodulin-Dependent Protein Kinase Modulates Cardiac Ryanodine Receptor Phosphorylation and Sarcoplasmic Reticulum Ca^{2+} Leak in Heart Failure. *Circulation research* 2005 Dec 9;97(12):1314-22.
- (320) Curran J, Hinton MJ, Ríos E, Bers DM, Shannon TR. β -Adrenergic enhancement of sarcoplasmic reticulum calcium leak in cardiac myocytes is mediated by calcium/calmodulin-dependent protein kinase. *Circulation research* 2007 Feb 16;100(3):391-8.
- (321) Kohlhaas M, Zhang T, Seidler T, Zibrova D, Dybkova N, Steen A, et al. Increased sarcoplasmic reticulum calcium leak but unaltered contractility by acute CaMKII overexpression in isolated rabbit cardiac myocytes. *Circulation research* 2006 Feb 3;98(2):235-44.
- (322) Lehnart SE, Terrenoire C, Reiken S, Wehrens XHT, Song LS, Tillman EJ, et al. Stabilization of cardiac ryanodine receptor prevents intracellular calcium leak and arrhythmias. *Proceedings of the National Academy of Sciences* 2006 May 16;103(20):7906-10.
- (323) Shannon TR, Pogwizd SM, Bers DM. Elevated sarcoplasmic reticulum Ca^{2+} leak in intact ventricular myocytes from rabbits in heart failure. *Circulation research* 2003;93(7):592-4.
- (324) Marks AR. A guide for the perplexed: towards an understanding of the molecular basis of heart failure. *Circulation* 2003 Mar 25;107(11):1456-9.
- (325) Leimbach WN, Wallin BG, Victor RG, Aylward PE, Sundlöf G, Mark AL. Direct evidence from intraneural recordings for increased central sympathetic outflow in patients with heart failure. *Circulation* 1986 May 1;73(5):913-9.
- (326) WHO: The top 10 causes of death. 2011.

- (327) Yellon DM, Hausenloy DJ. Myocardial reperfusion injury. *N Engl J Med* 2007 Sep 13;357(11):1121-35.
- (328) Piper HM, García-Dorado D, Ovize M. A fresh look at reperfusion injury. *Cardiovascular Research* 1998 May 1;38(2):291-300.
- (329) Braunwald E, Kloner RA. The stunned myocardium: prolonged, postischemic ventricular dysfunction. *Circulation* 1982 Dec 1;66(6):1146-9.
- (330) Ito H. No-reflow phenomenon and prognosis in patients with acute myocardial infarction. *Nat Clin Pract Cardiovasc Med* 2006;3(9):499-506.
- (331) Manning AS, Hearse DJ. Reperfusion-induced arrhythmias: Mechanisms and prevention. *Journal of Molecular and Cellular Cardiology* 1984;16(6):497-518.
- (332) Goldberg S, Greenspon AJ, Urban PL, Muza B, Berger B, Walinsky P, et al. Reperfusion arrhythmia: A marker of restoration of antegrade flow during intracoronary thrombolysis for acute myocardial infarction. *American Heart Journal* 1983;105(1):26-32.
- (333) Tzivoni D, Keren A, Granot H, Gottlieb S, Benhorin J, Stern S. Ventricular fibrillation caused by myocardial reperfusion in Prinzmetal's angina. *American Heart Journal* 1983;105(2):323-5.
- (334) Cevher O, Monica P, Tamas LH, Kerry S Russell, Raymond RR. Role of uncoupling protein 3 in ischemia-reperfusion injury, arrhythmias and preconditioning. *American Journal of Physiology - Heart and Circulatory Physiology* 2013 Mar 1.
- (335) Brooks WW, Conrad CH, Morgan JP. Reperfusion induced arrhythmias following ischaemia in intact rat heart: role of intracellular calcium. *Cardiovascular Research* 1995 Apr 1;29(4):536-42.
- (336) Yasutake M, Ibuki C, Hearse DJ, Avkiran M. Na^+/H^+ exchange and reperfusion arrhythmias: protection by intracoronary infusion of a novel inhibitor. *American Journal of Physiology - Heart and Circulatory Physiology* 1994 Dec 1;267(6):H2430-H2440.
- (337) Priori SG, Mantica M, Napolitano C, Schwartz PJ. Early afterdepolarizations induced in vivo by reperfusion of ischemic myocardium. A possible mechanism for reperfusion arrhythmias. *Circulation* 1990 Jun 1;81(6):1911-20.
- (338) Hearse DJ, Humphrey SM, Chain EB. Abrupt reoxygenation of the anoxic potassium-arrested perfused rat heart: A study of myocardial enzyme release. *Journal of Molecular and Cellular Cardiology* 1973 Aug;5(4):395-407.
- (339) Li W, Yuan XM. Increased expression and translocation of lysosomal cathepsins contribute to macrophage apoptosis in atherogenesis. *Annals of the New York Academy of Sciences* 2004 Dec 1;1030(1):427-33.
- (340) Rozhin J, Sameni M, Ziegler G, Sloane BF. Pericellular pH affects distribution and secretion of cathepsin B in malignant cells. *Cancer Research* 1994 Dec 15;54(24):6517-25.
- (341) Zima AV, Copello JA, Blatter LA. Effects of cytosolic NADH/NAD⁺ levels on sarcoplasmic reticulum Ca^{2+} release in permeabilized rat ventricular myocytes. *The Journal of Physiology* 2004 Mar 15;555(3):727-41.
- (342) Scherer NM, Deamer DW. Oxidative stress impairs the function of sarcoplasmic reticulum by oxidation of sulfhydryl groups in the Ca^{2+} -ATPase. *Archives of Biochemistry and Biophysics* 1986 May 1;246(2):589-601.

- (343) Morris TE, Sulakhe PV. Sarcoplasmic reticulum Ca^{2+} -pump dysfunction in rat cardiomyocytes briefly exposed to hydroxyl radicals. *Free Radical Biology and Medicine* 1997;22(1–2):37-47.
- (344) Kukreja RC, Okabe E, Schrier GM, Hess ML. Oxygen radical-mediated lipid peroxidation and inhibition of Ca^{2+} -ATPase activity of cardiac sarcoplasmic reticulum. *Archives of Biochemistry and Biophysics* 1988 Mar;261(2):447-57.
- (345) Kawakami M, Okabe E. Superoxide anion radical-triggered Ca^{2+} release from cardiac sarcoplasmic reticulum through ryanodine receptor Ca^{2+} channel. *Molecular Pharmacology* 1998 Mar 1;53(3):497-503.
- (346) Anzai K, Ogawa K, Kuniyasu A, Ozawa T, Yamamoto H, Nakayama H. Effects of hydroxyl radical and sulfhydryl reagents on the open probability of the purified cardiac ryanodine receptor channel incorporated into planar lipid bilayers. *Biochemical and Biophysical Research Communications* 1998 Aug 28;249(3):938-42.
- (347) Boraso A, Williams AJ. Modification of the gating of the cardiac sarcoplasmic reticulum Ca^{2+} -release channel by H_2O_2 and dithiothreitol. *American Journal of Physiology - Heart and Circulatory Physiology* 1994 Sep 1;267(3):H1010-H1016.
- (348) Lemasters JJ, Bond JM, Chacon E, Harper IS, Kaplan SH, Ohata H, et al. The pH paradox in ischemia-reperfusion injury to cardiac myocytes. In: Karmazyn M, editor. *Myocardial Ischemia: Mechanisms, Reperfusion, Protection*. 76 ed. Birkhauser Basel; 1996. p. 99-114.
- (349) Vinten-Johansen J. Involvement of neutrophils in the pathogenesis of lethal myocardial reperfusion injury. *Cardiovascular Research* 2004 Feb 15;61(3):481-97.
- (350) Staat P, Rioufol G, Piot C, Cottin Y, Cung TT, L'Huillier I, et al. Postconditioning the human heart. *Circulation* 2005 Oct 4;112(14):2143-8.
- (351) Zhao ZQ, Corvera JS, Halkos ME, Kerendi F, Wang NP, Guyton RA, et al. Inhibition of myocardial injury by ischemic postconditioning during reperfusion: comparison with ischemic preconditioning. *American Journal of Physiology - Heart and Circulatory Physiology* 2003 Jul 14;285(2):H579-H588.
- (352) Zhao ZQ, Vinten-Johansen J. Postconditioning: Reduction of reperfusion-induced injury. *Cardiovascular Research* 2006 May 1;70(2):200-11.
- (353) Cohen MV, Yang XM, Downey JM. The pH hypothesis of postconditioning: Staccato reperfusion reintroduces oxygen and perpetuates myocardial acidosis. *Circulation* 2007 Apr 10;115(14):1895-903.
- (354) Hausenloy DJ, Yellon DM. New directions for protecting the heart against ischaemia-reperfusion injury: targeting the Reperfusion Injury Salvage Kinase (RISK)-pathway. *Cardiovascular Research* 2004 Feb 15;61(3):448-60.
- (355) Hausenloy DJ, Yellon DM. The mitochondrial permeability transition pore: its fundamental role in mediating cell death during ischaemia and reperfusion. *Journal of Molecular and Cellular Cardiology* 2003 Apr;35(4):339-41.
- (356) Hausenloy DJ, Tsang A, Yellon DM. The reperfusion injury salvage kinase pathway: A common target for both ischemic preconditioning and postconditioning. *Trends in Cardiovascular Medicine* 2005 Feb;15(2):69-75.
- (357) Laskey WK. Brief repetitive balloon occlusions enhance reperfusion during percutaneous coronary intervention for acute myocardial infarction: A pilot study. *Cathet Cardiovasc Intervent* 2005 Jul 1;65(3):361-7.
- (358) Ma X, Zhang X, Li C, Luo M. Effect of postconditioning on coronary blood flow velocity and Endothelial function and LV recovery after myocardial infarction. *Journal of Interventional Cardiology* 2006 Oct 1;19(5):367-75.

- (359) Kitakaze M, Asakura M, Kim J, Shintani Y, Asanuma H, Hamasaki T, et al. Human atrial natriuretic peptide and nicorandil as adjuncts to reperfusion treatment for acute myocardial infarction (J-WIND): two randomised trials. *The Lancet* 1927 Oct;370(9597):1483-93.
- (360) Bose AK, Mocanu MM, Carr RD, Brand CL, Yellon DM. Glucagon-like peptide 1 can directly protect the heart against ischemia/reperfusion injury. *Diabetes* 2005 Jan 1;54(1):146-51.
- (361) Bullard AJ, Govewalla P, YELLON DM. Erythropoietin protects the myocardium against reperfusion injury in vitro and in vivo. *Basic Res Cardiol* 2005;100(5):397-403.
- (362) Bell RM, Yellon DM. Atorvastatin, administered at the onset of reperfusion, and independent of lipid lowering, protects the myocardium by up-regulating a pro-survival pathway. *Journal of the American College of Cardiology* 2003 Feb 5;41(3):508-15.
- (363) Hausenloy DJ, Duchon MR, Yellon DM. Inhibiting mitochondrial permeability transition pore opening at reperfusion protects against ischaemia-reperfusion injury. *Cardiovascular Research* 2003 Dec 1;60(3):617-25.
- (364) Bolli R, Cannon RO, Speir E, Goldstein RE, Epstein SE. Role of cellular proteinases in acute myocardial infarction. I. Proteolysis in nonischemic and ischemic rat myocardium and the effects of antipain, leupeptin, pepstatin and chymostatin administered *in vivo*. *Journal of the American College of Cardiology* 1983;2(4):671-80.
- (365) Bolli R, Cannon RO, Speir E, Goldstein RE, Epstein SE. Role of cellular proteinases in acute myocardial infarction. II. Influence of *in vivo* suppression of myocardial proteolysis by antipain, leupeptin and pepstatin on myocardial infarct size in the rat. *Journal of the American College of Cardiology* 1983;2(4):681-8.
- (366) Anagli J, Abounit K, Stemmer P, Han Y, Allred L, Weinsheimer S, et al. Effects of cathepsins B and L inhibition on postischemic protein alterations in the brain. *Biochemical and Biophysical Research Communications* 2008 Feb 1;366(1):86-91.
- (367) Kohda Y, Yamashita T, Sakuda K, Yamashita J, Ueno T, Kominami E, et al. Dynamic changes of cathepsins B and L expression in the monkey hippocampus after transient ischemia. *Biochemical and Biophysical Research Communications* 1996 Nov 12;228(2):616-22.
- (368) Reiser J, Adair B, Reinheckel T. Specialized roles for cysteine cathepsins in health and disease. *Journal of Clinical Investigation* 2010;120:3421-31.
- (369) Willstätter R, Bamann E. Erste Abhandlung über die Enzyme der Leukozyten. *Hoppe-Seyler's Z Physiol Chem* 1929;180(1-3):127-43.
- (370) Mutwil M, Øbro J, Willats WGT, Persson S. GeneCAT—novel webtools that combine BLAST and co-expression analyses. *Nucleic Acids Research* 2008 Jul 1;36(suppl 2):W320-W326.
- (371) Turk B, Turk V, Turk D. Structural and functional aspects of papain-like proteinases and their protein inhibitors. *Biological Chemistry* 1997;378(4):141-50.
- (372) Turk B, Dolenc I, Turk V, Bieth JG. Kinetics of the pH-induced inactivation of human cathepsin L. *Biochemistry* 1993;32(1):375-80.
- (373) Turk B, Turk D, Salvesen GS. Regulating cysteine protease activity: essential role of protease inhibitors as guardians and regulators. *Current Pharmaceutical Design* 2002;8(18):1623-37.
- (374) Turk B, Turk D, Turk V. Lysosomal cysteine proteases: more than scavengers. *Biochimica et Biophysica Acta (BBA) - Protein Structure and Molecular Enzymology* 2000 Mar 7;1477(1-2):98-111.

- (375) Honey K, Rudensky AY. Lysosomal cysteine proteases regulate antigen presentation. *Nat Rev Immunol* 2003;3(6):472-82.
- (376) Deal C. Potential new drug targets for osteoporosis. *Nat Clin Pract Rheum* 2009;5(1):20-7.
- (377) Stoch S, Wagner J. Cathepsin K Inhibitors: A novel target for osteoporosis therapy. *Clin Pharmacol Ther* 2008;83(1):172-6.
- (378) Friedrichs B, Tepel C, Reinheckel T, Deussing J, von Figura K, Herzog V, et al. Thyroid functions of mouse cathepsins B, K, and L. *J Clin Invest* 2003 Jun 1;111(11):1733-45.
- (379) Funkelstein L, Toneff T, Mosier C, Hwang SR, Beuschlein F, Lichtenauer UD, et al. Major role of cathepsin L for producing the peptide hormones ACTH, β -Endorphin, and α -MSH, illustrated by protease gene knockout and expression. *Journal of Biological Chemistry* 2008 Dec 19;283(51):35652-9.
- (380) Brix K, Dunkhorst A, Mayer K, Jordans S. Cysteine cathepsins: Cellular roadmap to different functions. *Biochimie* 2008 Feb;90(2):194-207.
- (381) Puri N, Roche PA. Mast cells possess distinct secretory granule subsets whose exocytosis is regulated by different SNARE isoforms. *Proceedings of the National Academy of Sciences* 2008 Feb 19;105(7):2580-5.
- (382) Wartmann T, Mayerle J, Kähne T, Sahin-Tóth M, Ruthenbürger M, Matthias R, et al. Cathepsin L inactivates human trypsinogen, whereas cathepsin L-deletion reduces the severity of pancreatitis in mice. *Gastroenterology* 2010 Feb;138(2):726-37.
- (383) Faul C, Donnely M, Merscher-Gomez S, Chang Y, Franz S, Delfgaauw J, et al. The actin cytoskeleton of kidney podocytes is a direct target of the antiproteinuric effect of cyclosporine A. *Nature Medicine* 2008;14(9):931-8.
- (384) Reiser J, Oh J, Shirato I, Asanuma K, Hug A, Mundel TM, et al. Podocyte migration during nephrotic syndrome requires a coordinated interplay between cathepsin L and α_3 Integrin. *Journal of Biological Chemistry* 2004 Aug 13;279(33):34827-32.
- (385) Sever S, Altintas MM, Nankoe SR, Iler CC, Ko D, Wei C, et al. Proteolytic processing of dynamin by cytoplasmic cathepsin L is a mechanism for proteinuric kidney disease. *J Clin Invest* 2007 Aug 1;117(8):2095-104.
- (386) Goulet B, Baruch A, Moon NS, Poirier M, Sansregret LL, Erickson A, et al. A cathepsin L isoform that is devoid of a signal peptide localizes to the nucleus in S phase and processes the CDP/Cux transcription factor. *Molecular Cell* 2004 Apr 23;14(2):207-19.
- (387) Neal IA, Madhulika S, Dianne V, Brandon C, Binu P, Jing Z, et al. Acceleration of polycystic kidney disease progression in cpk mice carrying a deletion in the homeodomain protein Cux1. *American Journal of Physiology - Renal Physiology* 2008 Dec 4;295(6):F1725-F1734.
- (388) Mohamed MM, Sloane BF. Cysteine cathepsins: multifunctional enzymes in cancer. *Nat Rev Cancer* 2006;6(10):764-75.
- (389) Taleb S, Canello R, Poitou C, Rouault C, Sellam P, Levy P, et al. Weight loss reduces adipose tissue cathepsin S and its circulating levels in morbidly obese women. *Journal of Clinical Endocrinology & Metabolism* 2006 Mar 1;91(3):1042-7.
- (390) Yang M, Zhang Y, Pan J, Sun J, Liu J, Libby P, et al. Cathepsin L activity controls adipogenesis and glucose tolerance. *Nat Cell Biol* 2007;9(8):970-7.
- (391) Yang M, Sun J, Zhang T, Liu J, Zhang J, Shi MA, et al. Deficiency and inhibition of cathepsin K reduce body weight gain and increase glucose metabolism in mice. *Arteriosclerosis, Thrombosis, and Vascular Biology* 2008 Dec 1;28(12):2202-8.

- (392) Hou WS, Li W, Keyszer G, Weber E, Levy R, Klein MJ, et al. Comparison of cathepsins K and S expression within the rheumatoid and osteoarthritic synovium. *Arthritis & Rheumatism* 2002 Mar 1;46(3):663-74.
- (393) Asagiri M, Hirai T, Kunigami T, Kamano S, Gober HJ, Okamoto K, et al. Cathepsin K-dependent toll-like receptor 9 signaling revealed in experimental arthritis. *Science* 2008 Feb 1;319(5863):624-7.
- (394) Jaffer FA, Kim DE, Quinti L, Tung CH, Aikawa E, Pande AN, et al. Optical visualization of cathepsin K activity in atherosclerosis with a novel, protease-activatable fluorescence sensor. *Circulation* 2007 May 1;115(17):2292-8.
- (395) Liu J, Sukhova GK, Sun JS, Xu WH, Libby P, Shi GP. Lysosomal cysteine proteases in atherosclerosis. *Arteriosclerosis, Thrombosis, and Vascular Biology* 2004 Aug 1;24(8):1359-66.
- (396) Öörni K, Sneck M, Brömme D, Pentikäinen MO, Lindstedt KA, Mäyränpää M, et al. Cysteine protease cathepsin F is expressed in human atherosclerotic lesions, is secreted by cultured macrophages, and modifies low density lipoprotein particles *in vitro*. *Journal of Biological Chemistry* 2004 Aug 13;279(33):34776-84.
- (397) Sasaki T, Kuzuya M, Nakamura K, Cheng XW, Hayashi T, Song H, et al. AT1 blockade attenuates atherosclerotic plaque destabilization accompanied by the suppression of cathepsin S activity in apoE-deficient mice. *Atherosclerosis* 2010 Jun;210(2):430-7.
- (398) Sukhova GK, Shi GP, Simon DI, Chapman HA, Libby P. Expression of the elastolytic cathepsins S and K in human atheroma and regulation of their production in smooth muscle cells. *J Clin Invest* 1998 Aug 1;102(3):576-83.
- (399) Sun J, Sukhova GK, Zhang J, Chen H, Sjöberg S, Libby P, et al. Cathepsin K Deficiency Reduces Elastase Perfusion-Induced Abdominal Aortic Aneurysms in Mice. *Arteriosclerosis, Thrombosis, and Vascular Biology* 2012 Jan 1;32(1):15-23.
- (400) Petermann I, Mayer C, Stypmann J, Biniossek ML, Tobin DJ, Engelen MA, et al. Lysosomal, cytoskeletal, and metabolic alterations in cardiomyopathy of cathepsin L knockout mice. *The FASEB Journal* 2006 Jun 1;20(8):1266-8.
- (401) Spira D, Stypmann J, Tobin DJ, Petermann I, Mayer C, Hagemann S, et al. Cell type-specific functions of the lysosomal protease cathepsin L in the heart. *Journal of Biological Chemistry* 2007 Dec 21;282(51):37045-52.
- (402) Stypmann J, Gläser K, Roth W, Tobin DJ, Petermann I, Matthias R, et al. Dilated cardiomyopathy in mice deficient for the lysosomal cysteine peptidase cathepsin L. *Proceedings of the National Academy of Sciences* 2002 Apr 30;99(9):6234-9.
- (403) Gocheva V, Zeng W, Ke D, Klimstra D, Reinheckel T, Peters C, et al. Distinct roles for cysteine cathepsin genes in multistage tumorigenesis. *Genes & Development* 2006 Mar 1;20(5):543-56.
- (404) Vasiljeva O, Papazoglou A, Krüger A, Brodoefel H, Korovin M, Deussing J, et al. Tumor cell-derived and macrophage-derived cathepsin B promotes progression and lung metastasis of mammary cancer. *Cancer Research* 2006 May 15;66(10):5242-50.
- (405) Gondi CS, Lakka SS, Yanamandra N, Olivero WC, Dinh DH, Gujrati M, et al. Adenovirus-mediated expression of antisense urokinase plasminogen activator receptor and antisense cathepsin B inhibits tumor growth, invasion, and angiogenesis in gliomas. *Cancer Research* 2004 Jun 15;64(12):4069-77.
- (406) Tummalapalli P, Spomar D, Gondi CS, Olivero WC, Gujrati M, Dinh DH, et al. RNAi-mediated abrogation of cathepsin B and MMP-9 gene expression in a malignant meningioma cell line leads to decreased tumor growth, invasion and angiogenesis. *International Journal of Oncology* 2007;31(5):1039-50.

- (407) Sevenich L, Schurigt U, Sachse K, Gajda M, Werner F, Müller S, et al. Synergistic antitumor effects of combined cathepsin B and cathepsin Z deficiencies on breast cancer progression and metastasis in mice. *Proceedings of the National Academy of Sciences* 2010 Feb 9;107(6):2497-502.
- (408) Gocheva V, Wang HW, Gadea BB, Shree T, Hunter KE, Garfall AL, et al. IL-4 induces cathepsin protease activity in tumor-associated macrophages to promote cancer growth and invasion. *Genes & Development* 2010 Feb 1;24(3):241-55.
- (409) Kitamoto S, Sukhova GK, Sun J, Yang M, Libby P, Love V, et al. Cathepsin L deficiency reduces diet-induced atherosclerosis in low-density lipoprotein receptor–knockout mice. *Circulation* 2007 Apr 17;115(15):2065-75.
- (410) Maehr R, Mintern JD, Herman AE, Lennon D, Mathis D, Benoist C, et al. Cathepsin L is essential for onset of autoimmune diabetes in NOD mice. *J Clin Invest* 2005 Oct 3;115(10):2934-43.
- (411) Huang X, Vaag A, Carlsson E, Hansson M, Ahrén B, Groop L. Impaired Cathepsin L Gene Expression in Skeletal Muscle Is Associated With Type 2 Diabetes. *Diabetes* 2003 Sep 1;52(9):2411-8.
- (412) Jormsjö S, Wuttge DM, Sirsjö A, Whatling C, Hamsten A, Stemme S, et al. Differential expression of cysteine and aspartic proteases during progression of atherosclerosis in apolipoprotein E-deficient mice. *The American Journal of Pathology* 2002 Sep;161(3):939-45.
- (413) Liu J, Sukhova GK, Yang JT, Sun J, Ma L, Ren A, et al. Cathepsin L expression and regulation in human abdominal aortic aneurysm, atherosclerosis, and vascular cells. *Atherosclerosis* 2006 Feb;184(2):302-11.
- (414) Lutgens SPM, Cleutjens KBJM, Daemen MJAP, Heeneman S. Cathepsin cysteine proteases in cardiovascular disease. *The FASEB Journal* 2007 Oct 1;21(12):3029-41.
- (415) Burns-Kurtis CL, Olzinski AR, Needle S, Fox JH, Capper EA, Kelly FM, et al. Cathepsin S expression is up-regulated following balloon angioplasty in the hypercholesterolemic rabbit. *Cardiovascular Research* 2004 Jun 1;62(3):610-20.
- (416) Cheng XW, Kuzuya M, Sasaki T, Arakawa K, Kanda S, Sumi D, et al. Increased expression of elastolytic cysteine proteases, cathepsins S and K, in the neointima of balloon-injured rat carotid arteries. *The American Journal of Pathology* 2004 Jan;164(1):243-51.
- (417) Shi GP, Sukhova GK, Grubb A, Ducharme A, Rhode LH, Lee RT, et al. Cystatin C deficiency in human atherosclerosis and aortic aneurysms. *J Clin Invest* 1999 Nov 1;104(9):1191-7.
- (418) Gacko M, Chyczewski L, Chrostek L. Distribution, activity and concentration of cathepsin B and cystatin C in the wall of aortic aneurysm. *Polish Journal of Pathology* 1999;50(2):83-6.
- (419) Gacko M, Glowinski S. Cathepsin D and cathepsin L activities in aortic aneurysm wall and parietal thrombus. *Clinical Chemistry and Laboratory Medicine* 1998;36(7):449-52.
- (420) Gacko M, Glowinski S. Activities of proteases in parietal thrombus of aortic aneurysm. *Clinica Chimica Acta* 1998;271(2):171-7.
- (421) Cheng XW, Obata K, Kuzuya M, Izawa H, Nakamura K, Asai E, et al. Elastolytic Cathepsin Induction/Activation System Exists in Myocardium and Is Upregulated in Hypertensive Heart Failure. *Hypertension* 2006 Nov 1;48(5):979-87.
- (422) Cheng XW, Murohara T, Kuzuya M, Izawa H, Sasaki T, Obata K, et al. Superoxide-dependent cathepsin activation is associated with hypertensive myocardial remodeling

- and represents a target for angiotensin II type 1 receptor blocker treatment. *The American Journal of Pathology* 2008 Aug;173(2):358-69.
- (423) Cheng XW, Shi GP, Kuzuya M, Sasaki T, Okumura K, Murohara T. Role for cysteine protease cathepsins in heart disease: focus on biology and mechanisms with clinical implication. *Circulation* 2012 Mar 27;125(12):1551-62.
- (424) Sun M, Chen M, Liu Y, Fukuoka M, Zhou K, Li G, et al. Cathepsin-L contributes to cardiac repair and remodelling post-infarction. *Cardiovascular Research* 2011 Feb 1;89(2):374-83.
- (425) Liu Y, Li X, Peng D, Tan Z, Liu H, Qing Y, et al. Usefulness of serum cathepsin L as an independent biomarker in patients with coronary heart disease. *The American Journal of Cardiology* 2009 Feb 15;103(4):476-81.
- (426) Zhang J, Wang P, Huang YB, Li J, Zhu J, Luo X, et al. Plasma cathepsin L and its related pro/antiangiogenic factors play useful roles in predicting rich coronary collaterals in patients with coronary heart disease. *The Journal of International Medical Research* 2010;38(4):1389-403.
- (427) Liu A, Gao X, Zhang Q, Cui L. Cathepsin B inhibition attenuates cardiac dysfunction and remodeling following myocardial infarction by inhibiting the NLRP3 pathway. *Molecular Medicine Reports* 2013;8(2):361-6.
- (428) Decker RS, Poole AR, Griffin EE, Dingle JT, Wildenthal K. Altered distribution of lysosomal cathepsin D in ischemic myocardium. *Journal of Clinical Investigation* 1997;99:911-21.
- (429) Linz W, Hubschle T, Horstick G, Wohlfahrt P, Juretschke H-P, Linz D, et al. Effect of Cathepsin A inhibition on cardiac function and remodelling in rats with heart failure induced by ischemia and long-term reperfusion. *Circulation* 2011;124:A8779.
- (430) Tiwari M, Hemalatha T, Ganesan K, Nayeem M, Murali Manohar B, Balachandran C, et al. Myocardial ischemia and reperfusion injury in rats: lysosomal hydrolases and matrix metalloproteinases mediated cellular damage. *Mol Cell Biochem* 2008;312(1-2):81-91.
- (431) Turski WA, Zaslonka J. Activity of cathepsin D and L in the heart muscle of coronary patients during coronary-aortal bypass graft operation. *Medical Science Monitor* 2000;6:853-60.
- (432) Sun M, Ouzounian M, de Couto G, Chen M, Yan R, Fukuoka M, et al. Cathepsin-L ameliorates cardiac hypertrophy through activation of the autophagy-lysosomal dependent protein processing pathways. *Journal of the American Heart Association* 2013 Apr 24;2(2).
- (433) Lankelma JM, Voorend DIM, Barwari T, Koetsveld J, Van der Spek AH, De Porto APNA, et al. Cathepsin L, target in cancer treatment? *Life Sciences* 2010 Feb 13;86(7-8):225-33.
- (434) Hirumi H, Hirumi K. Continuous cultivation of *Trypanosoma brucei* bloodstream forms in a medium containing a low concentration of serum protein without feeder cell layers. *Journal of Parasitology* 1989;75(6):985-9.
- (435) Voorheis P. Modified HMI-9 Recipe. Personal Communication 2010.
- (436) Herbert WJ, Lumsden WHR. *Trypanosoma brucei*: A rapid "matching" method for estimating the host's parasitemia. *Experimental Parasitology* 1976 Dec;40(3):427-31.
- (437) Walker MJA, Curtis MJ, Hearse DJ, Campbell RWF, Janse MJ, Yellon DM, et al. The Lambeth Conventions: guidelines for the study of arrhythmias in ischaemia, infarction, and reperfusion. *Cardiovascular Research* 1988 Jul 1;22(7):447-55.

- (438) Richardson CA, Flacknell PA. Anaesthesia and post-operative analgesia following experimental surgery in laboratory rodents: are we making progress? *Alternatives to Laboratory Animals* 2005;33(2):119-27.
- (439) Chapman RA, Rodrigo GC, Tunstall J, Yates RJ, Busselen P. Calcium paradox of the heart: a role for intracellular sodium ions. *American Journal of Physiology - Heart and Circulatory Physiology* 1984 Nov 1;247(5):H874-H879.
- (440) Takahashi K, Schaffer S, Azuma J. Taurine prevents intracellular calcium overload during calcium paradox of cultured cardiomyocytes. *Amino Acids* 1997;13:1-11.
- (441) Zhang R, Yu Z, Wang Y. Isolation of cardiomyocytes from the adult mouse heart. *Acta Physiologica Sinica* 2004;56(5):656-60.
- (442) Fabiato A, Fabiato F. Excitation-contraction coupling of isolated cardiac fibers with disrupted or closed sarcolemmas: calcium-dependent cyclic and tonic contractions. *Circulation research* 1972 Sep 1;31(3):293-307.
- (443) Louch WE, Sheehan KA, Wolska BM. Methods in cardiomyocyte isolation, culture, and gene transfer. *Journal of Molecular and Cellular Cardiology* 2011 Sep;51(3):288-98.
- (444) Langendorff O. Untersuchungen am uberlebenden saugethierherzen. *Pflugers Archive* 1895;61:291-332.
- (445) Bell RM, Mocanu MM, Yellon DM. Retrograde heart perfusion: The Langendorff technique of isolated heart perfusion. *Journal of Molecular and Cellular Cardiology* 2011 Jun;50(6):940-50.
- (446) Sutherland FJ, Hearse DJ. The isolated blood and perfusion fluid perfused heart. *Pharmacological Research* 2000 Jun;41(6):613-27.
- (447) Shattock MJ, Miller JIA, Bray DG, Waldron CB. An electronic feedback circuit to control a peristaltic pump for constant-pressure perfusion of isolated hearts or other organs. *The Journal of Physiology* 1997 Dec 1;505(P):4P.
- (448) Sutherland FJ, Shattock MJ, Baker KE, Hearse DJ. Mouse isolated perfused heart: Characteristics and cautions. *Clinical and Experimental Pharmacology and Physiology* 2003 Nov 1;30(11):867-78.
- (449) Fukunami M, Hearse D. The inotropic consequences of cooling: Studies in the isolated rat heart. *Heart Vessels* 1989;5(1):1-9.
- (450) Ferrari R, Bongrani S, Raddino R, Di Lisa F, Visioli O. Effect and action mechanism of hypothermia to preserve the ischaemic myocardium (author's transl). *Giornale italiano di cardiologia* 1980;10(11):1496-507.
- (451) Miller JAJr, Miller FS. Mechanisms of hypothermic protection against anoxia. *Advances in experimental medicine and biology* 1972;33(0):571-86.
- (452) Hale SL, Kloner RA. Myocardial hypothermia: a potential therapeutic technique for acute regional myocardial ischemia. *Journal of cardiovascular electrophysiology* 1999;10(3):405-13.
- (453) Hale SL, Kloner RA. Myocardial temperature reduction attenuates necrosis after prolonged ischemia in rabbits. *Cardiovascular Research* 1998 Dec 1;40(3):502-7.
- (454) Khaliulin I, Clarke SJ, Lin H, Parker J, Suleiman MS, Halestrap AP. Temperature preconditioning of isolated rat hearts – a potent cardioprotective mechanism involving a reduction in oxidative stress and inhibition of the mitochondrial permeability transition pore. *The Journal of Physiology* 2007 Jun 15;581(3):1147-61.

- (455) Awan MM, Taunyane C, Aitchison KA, Yellon DM, Opie LH. Normothermic transfer times up to 3 min will not precondition the isolated rat heart. *Journal of Molecular and Cellular Cardiology* 1999 Mar;31(3):503-11.
- (456) Minhaz U, Koide S, Shohtsu A, Fujishima M, Nakazawa H. Perfusion delay causes unintentional ischemic preconditioning in isolated heart preparation. *Basic Research in Cardiology* 1995;90(5):418-23.
- (457) Rautaharju PM, Surawicz B, Gettes LS. AHA/ACCF/HRS recommendations for the standardization and interpretation of the electrocardiogram: Part IV: The ST segment, T and U waves, and the QT interval: A scientific statement from the American Heart Association Electrocardiography and Arrhythmias Committee, Council on Clinical Cardiology; the American College of Cardiology Foundation; and the Heart Rhythm Society: Endorsed by the International Society for Computerized Electrocardiology. *Circulation* 2009 Mar 17;119(10):e241-e250.
- (458) Rees SA, Curtis MJ. Specific IK1 blockade: a new antiarrhythmic mechanism? Effect of RP58866 on ventricular arrhythmias in rat, rabbit, and primate. *Circulation* 1993 Jun 1;87(6):1979-89.
- (459) Rees SA, Tsuchihashi K, Hearse DJ, Curtis MJ. Combined administration of an Ik(ATP) activator and I_{to} blocker increases coronary flow independently of effects on heart rate, QT interval, and ischaemia-induced ventricular fibrillation in rats. *Journal of Cardiovascular Pharmacology* 1993;22(3).
- (460) Sagie A, Larson M, Goldberg R, Bengtson J, Levy D. An improved method for adjusting the QT interval for heart rate (the Framingham Heart Study). *Am J Cardiol* 1992;70(7):797-801.
- (461) Stricker SA, Whitaker M. Confocal laser scanning microscopy of calcium dynamics in living cells. *Microsc Res Tech* 1999 Sep 15;46(6):356-69.
- (462) Minta A, Kao JP, Tsien RY. Fluorescent indicators for cytosolic calcium based on rhodamine and fluorescein chromophores. *Journal of Biological Chemistry* 1989 May 15;264(14):8171-8.
- (463) Grynkiewicz G, Poenie M, Tsien RY. A new generation of Ca²⁺ indicators with greatly improved fluorescence properties. *Journal of Biological Chemistry* 1985 Mar 25;260(6):3440-50.
- (464) Wilms CD, Eilers J. Photo-physical properties of Ca²⁺-indicator dyes suitable for two-photon fluorescence-lifetime recordings. *Journal of Microscopy* 2007 Mar 1;225(3):209-13.
- (465) Bridges WB. Laser oscillation in singly ionised argon in the visible spectrum. *Applied Physics Letters* 1964;4(7):128-30.
- (466) Bers DM, Guo T. Calcium signaling in cardiac ventricular myocytes. *Annals of the New York Academy of Sciences* 2005 Jun 1;1047(1):86-98.
- (467) Meyer T, Wensel T, Stryer L. Kinetics of calcium channel opening by inositol 1,4,5-triphosphate. *Biochemistry* 1990;29(1):32-7.
- (468) Loughrey CM, MacEachern KE, Cooper J, Smith GL. Measurement of the dissociation constant of Fluo-3 for Ca²⁺ in isolated rabbit cardiomyocytes using Ca²⁺ wave characteristics. *Cell calcium* 2003 Jul;34(1):1-9.
- (469) Takahashi A, Camacho P, Lechleiter JD, Herman B. Measurement of intracellular calcium. *Physiological Reviews* 1999 Jan 10;79(4):1089-125.
- (470) Tsien RY. A non-disruptive technique for loading calcium buffers and indicators into cells. *Nature* 1981;290:527-8.

- (471) Tsien RY, Pozzan T, Rink TJ. Calcium homeostasis in intact lymphocytes: cytoplasmic free calcium monitored with a new, intracellularly trapped fluorescent indicator. *The Journal of Cell Biology* 1982 Aug 1;94(2):325-34.
- (472) Han JK, Fukami K, Nuccitelli R. Reducing inositol lipid hydrolysis, Ins(1,4,5)P₃ receptor availability, or Ca²⁺ gradients lengthens the duration of the cell cycle in *Xenopus laevis* blastomeres. *The Journal of Cell Biology* 1992 Jan 1;116(1):147-56.
- (473) Hofer GF, Hohenthanner K, Baumgartner W, Groschner K, Klugbauer N, Hofmann F, et al. Intracellular Ca²⁺ inactivates L-type Ca²⁺ channels with a Hill coefficient of approximately 1 and an inhibition constant of approximately 4 μM by reducing channel's open probability. *Biophysical Journal* 1997 Oct;73(4):1857-65.
- (474) Becker PL, Fay FS. Photobleaching of fura-2 and its effect on determination of calcium concentrations. *American Journal of Physiology - Cell Physiology* 1987 Oct 1;253(4):C613-C618.
- (475) Roe MW, Lemasters JJ, Herman B. Assessment of Fura-2 for measurements of cytosolic free calcium. *Cell calcium* 1990;11(2-3):63-73.
- (476) Di Virgilio F, Steinberg TH, Silverstein SC. Inhibition of Fura-2 sequestration and secretion with organic anion transport blockers. *Cell calcium* 1990 Feb;11(2):57-62.
- (477) Malgaroli A, Milani D, Meldolesi J, Pozzan T. Fura-2 measurement of cytosolic free Ca²⁺ in monolayers and suspensions of various types of animal cells. *The Journal of Cell Biology* 1987 Nov 1;105(5):2145-55.
- (478) McDonough PM, Button DC. Measurement of cytoplasmic calcium concentration in cell suspensions: correction for extracellular Fura-2 through use of Mn²⁺ and probenecid. *Cell calcium* 1989 Apr;10(3):171-80.
- (479) Cheng H, Song LS, Shirokova N, González A, Lakatta EG, Ríos E, et al. Amplitude distribution of calcium sparks in confocal images: theory and studies with an automatic detection method. *Biophysical Journal* 1999 Feb;76(2):606-17.
- (480) Wokosin DL, Loughrey CM, Smith GL. Characterization of a range of fura dyes with two-photon excitation. *Biophysical Journal* 2004 Mar;86(3):1726-38.
- (481) Piston DW. Choosing objective lenses: the importance of numerical aperture and magnification in digital optical microscopy. *The Biological Bulletin* 1998 Aug 1;195(1):1-4.
- (482) McConnel G, Amos WB, Wilson T. *Confocal Microscopy. Handbook of Comprehensive Biophysics.* 2011.
- (483) Dempster J, Wokosin D. Fluorescence imaging systems: A quick overview of the technology. *Physiology News* 2002;48:12-4.
- (484) Jacobsen W, Christians U, Benet LZ. *In vitro* evaluation of the disposition of a novel cysteine protease inhibitor. *Drug Metabolism and Disposition* 2000 Nov 1;28(11):1343-51.
- (485) Kerr ID, Lee JH, Farady CJ, Marion R, Rickert M, Sajid M, et al. Vinyl sulfones as antiparasitic agents and a structural basis for drug design. *Journal of Biological Chemistry* 2009 Sep 18;284(38):25697-703.
- (486) Kerr ID, Wu P, Marion-Tsukamaki R, Mackey ZB, Brinen LS. Crystal structures of TbCatB and rhodesain, potential chemotherapeutic targets and major cysteine proteases of *Trypanosoma brucei*. *PLoS Negl Trop Dis* 2010 Jun 8;4(6):e701.

- (487) Murata M, Miyashita S, Yokoo C, Tamai M, Hanada K, Hatayama K, et al. Novel epoxysuccinyl peptides Selective inhibitors of cathepsin B, in vitro. *FEBS Letters* 1991 Mar 25;280(2):307-10.
- (488) Alsford S, Kawahara T, Glover L, Horn D. Tagging a *T. brucei* RRNA locus improves stable transfection efficiency and circumvents inducible expression position effects. *Molecular and Biochemical Parasitology* 2005 Dec;144(2):142-8.
- (489) Jones N, Mottram J. High-throughput cloning of stem-loop RNAi constructs for *Trypanosoma brucei*. Personal Communication 2011.
- (490) Balaña-Fouce R, Reguera RM. RNA interference in *Trypanosoma brucei*: a high-throughput engine for functional genomics in trypanosomatids? *Trends in Parasitology* 2007 Aug;23(8):348-51.
- (491) Shi H, Tschudi C, Ullu E. An unusual Dicer-like1 protein fuels the RNA interference pathway in *Trypanosoma brucei*. *RNA* 2006;12(12):2063-72.
- (492) Steverding D, Sexton DW, Wang X, Gehrke SS, Wagner GK, Caffrey CR. *Trypanosoma brucei*: Chemical evidence that cathepsin L is essential for survival and a relevant drug target. *International Journal for Parasitology* 2012 May 1;42(5):481-8.
- (493) QIAgen RNeasy Mini Handbook. 2010.
- (494) Lillico S, Field MC, Blundell P, Coombs GH, Mottram JC. Essential roles for GPI-anchored proteins in African trypanosomes revealed using mutants deficient in GPI-8. *Molecular Biology of the Cell* 2003;14(3):1182-94.
- (495) Livak KJ, Schmittgen TD. Analysis of Relative Gene Expression Data Using Real-Time Quantitative PCR and the $2^{-\Delta\Delta CT}$ Method. *Methods* 2001 Dec;25(4):402-8.
- (496) Poltera AA, Owor R, Cox JN. Pathological aspects of human African trypanosomiasis (HAT) in Uganda. A post-mortem survey of fourteen cases. *Virchows Archiv A, pathological anatomy and histology* 1977;373(3):249-65.
- (497) Galvao-Castro B, Hochmann A, Lambert PH. The role of the host immune response in the development of tissue lesions associated with African trypanosomiasis in mice. *Clinical and Experimental Immunology* 1978;33(1):12-24.
- (498) Kalyanasundaram A, Viatchenko-Karpinski S, Belevych AE, Lacombe VA, Hwang HS, Knollmann BC, et al. Functional consequences of stably expressing a mutant calsequestrin (CASQ2^{D307H}) in the CASQ2 null background. *American Journal of Physiology - Heart and Circulatory Physiology* 2012 Jan 1;302(1):H253-H261.
- (499) Gateway Technology: A universal technology to clone DNA sequences for functional analysis and expression in multiple systems. 2010.
- (500) Berriman M, Ghedin E, Hertz-Fowler C, Blandin G, Renauld H, Bartholomeu DC, et al. The genome of the African trypanosome *Trypanosoma brucei*. *Science* 2005 Jul 15;309(5733):416-22.
- (501) Pentreath VW, Baugh PJ, Lavin DR. Sleeping sickness and the central nervous system. *Onderstepoort J Vet Res* 1994;61(4):369-77.
- (502) Mulenga C, Mhlanga JDM, Kristensson K, Robertson B. *Trypanosoma brucei brucei* crosses the blood-brain barrier while tight junction proteins are preserved in a rat chronic disease model. *Neuropathology and Applied Neurobiology* 2001;27(1):77-85.
- (503) O'Neill SC, Miller L, Hinch R, Eisner DA. Interplay between SERCA and sarcolemmal Ca²⁺ efflux pathways controls spontaneous release of Ca²⁺ from the sarcoplasmic reticulum in rat ventricular myocytes. *The Journal of Physiology* 2004 Aug 15;559(1):121-8.

- (504) Swietach P, Spitzer KW, Vaughan-Jones RD. Modeling calcium waves in cardiac myocytes: importance of calcium diffusion. *Frontiers in Bioscience* 2010;15:661-80.
- (505) Stokke MK, Hougen K, Sjaastad I, Louch WE, Briston SJ, Enger UH, et al. Reduced SERCA2 abundance decreases the propensity for Ca^{2+} wave development in ventricular myocytes. *Cardiovascular Research* 2010 Apr 1;86(1):63-71.
- (506) Bode EF, Briston SJ, Overend CL, O'Neill SC, Trafford AW, Eisner DA. Changes of SERCA activity have only modest effects on sarcoplasmic reticulum Ca^{2+} content in rat ventricular myocytes. *The Journal of Physiology* 2011 Oct 1;589(19):4723-9.
- (507) Eisner D, Bode E, Venetucci L, Trafford A. Calcium flux balance in the heart. *Journal of Molecular and Cellular Cardiology* 2013 May;58(0):110-7.
- (508) Barr SC, Han W, Andrews NW, Lopez JW, Ball BA, Pannabecker TL, et al. A factor from *Trypanosoma cruzi* induces repetitive cytosolic free Ca^{2+} waves in isolated primary canine cardiac myocytes. *Infection and Immunity* 1996;64(5):1770-7.
- (509) Doyle PS, Zhou YM, Hsieh I, Greenbaum DC, McKerrow JH, Engel JC. The *Trypanosoma cruzi* protease cruzain mediates immune evasion. *PLoS Pathog* 2011 Sep 1;7(9):e1002139.
- (510) Legros D, Ollivier G, Gastellu-Etchegorry M, Paquet C, Burri C, Jannin J, et al. Treatment of human African trypanosomiasis—present situation and needs for research and development. *The Lancet Infectious Diseases* 2002 Jul;2(7):437-40.
- (511) Williams-Blangero S, Magalhaes T, Rainwater E, Blangero J, Corrêa-Oliveira R, VandeBerg JL. Electrocardiographic characteristics in a population with high rates of seropositivity for *Trypanosoma cruzi* Infection. *The American Journal of Tropical Medicine and Hygiene* 2007 Sep 1;77(3):495-9.
- (512) Eickhoff CS, Lawrence CT, Sagartz JE, Bryant LA, Labovitz AJ, Gala SS, et al. ECG detection of murine Chagasic cardiomyopathy. *Journal of Parasitology* 2010 May 5;96(4):758-64.
- (513) Ribeiro AL, Nunes MP, Teixeira MM, Rocha MOC. Diagnosis and management of Chagas disease and cardiomyopathy. *Nat Rev Cardiol* 2012;9(10):57-589.
- (514) Burleigh BA, Andrews NW. A 120-kDa Alkaline Peptidase from *Trypanosoma cruzi* Is Involved in the Generation of a Novel Ca^{2+} -signaling Factor for Mammalian Cells. *Journal of Biological Chemistry* 1995 Mar 10;270(10):5172-80.
- (515) Rodríguez A, Rioult MG, Ora A, Andrews NW. A trypanosome-soluble factor induces IP_3 formation, intracellular Ca^{2+} mobilization and microfilament rearrangement in host cells. *The Journal of Cell Biology* 1995 Jun 1;129(5):1263-73.
- (516) Tardieux I, Nathanson MH, Andrews NW. Role in host cell invasion of *Trypanosoma cruzi*-induced cytosolic-free Ca^{2+} transients. *The Journal of Experimental Medicine* 1994 Mar 1;179(3):1017-22.
- (517) Huke S, Knollmann BC. Increased myofilament Ca^{2+} -sensitivity and arrhythmia susceptibility. *Journal of Molecular and Cellular Cardiology* 2010 May;48(5):824-33.
- (518) Elliott EB, McCarroll D, Hasumi H, Welsh CE, Panissidi AA, Jones NG, et al. *Trypanosoma brucei* cathepsin-L increases arrhythmogenic sarcoplasmic reticulum-mediated calcium release in rat cardiomyocytes. *Cardiovascular Research* 2013 Nov 1;100(2):325-35.
- (519) Hussain M, Drago GA, Bhogal M, Colyer J, Orchard CH. Effects of the protein kinase A inhibitor H-89 on Ca^{2+} regulation in isolated ferret ventricular myocytes. *Pflügers Arch* 1999;437(4):529-37.

- (520) Wisløff U, Loennechen JP, Falck G, Beisvag V, Currie S, Smith G, et al. Increased contractility and calcium sensitivity in cardiac myocytes isolated from endurance trained rats. *Cardiovascular Research* 2001 Jun 1;50(3):495-508.
- (521) Antoons G, Vangheluwe P, Volders PGA, Bito V, Holemans P, Ceci M, et al. Increased phospholamban phosphorylation limits the force–frequency response in the MLP^{-/-} mouse with heart failure. *Journal of Molecular and Cellular Cardiology* 2006 Mar;40(3):350-60.
- (522) Rodriguez P, Bhogal MS, Colyer J. Stoichiometric phosphorylation of cardiac ryanodine receptor on serine 2809 by calmodulin-dependent kinase II and protein kinase A. *Journal of Biological Chemistry* 2003 Oct 3;278(40):38593-600.
- (523) Currie S, Loughrey CM, Craig M-A, Smith GL. Calcium/calmodulin-dependent protein kinase II associates with the ryanodine receptor complex and regulates channel function in rabbit heart. *Biochemical Journal* 2004;377:357-66.
- (524) Wehrens XHT, Lehnart SE, Reiken SR, Marks AR. Ca²⁺/calmodulin-dependent protein kinase II phosphorylation regulates the cardiac ryanodine receptor. *Circulation research* 2004 Apr 2;94(6):e61-e70.
- (525) Liu N, Colombi B, Memmi M, Zissimopoulos S, Rizzi N, Negri S, et al. Arrhythmogenesis in catecholaminergic polymorphic ventricular tachycardia: insights from a RyR2 R4496C knock-in mouse model. *Circulation research* 2006 Aug 4;99(3):292-8.
- (526) Díaz ME, Graham HK, Trafford AW. Enhanced sarcolemmal Ca²⁺ efflux reduces sarcoplasmic reticulum Ca²⁺ content and systolic Ca²⁺ in cardiac hypertrophy. *Cardiovascular Research* 2004 Jun 1;62(3):538-47.
- (527) Trafford AW, Díaz ME, Sibbring GC, Eisner DA. Modulation of CICR has no maintained effect on systolic Ca²⁺: simultaneous measurements of sarcoplasmic reticulum and sarcolemmal Ca²⁺ fluxes in rat ventricular myocytes. *The Journal of Physiology* 2000 Jan 15;522(2):259-70.
- (528) Shannon TR, Ginsburg KS, Bers DM. Reverse mode of the sarcoplasmic reticulum calcium pump and load- dependent cytosolic calcium decline in voltage-clamped cardiac ventricular myocytes. *Biophysical Journal* 2000;78(1):322-33.
- (529) Kataoka A, Hemmer C, Chase PB. Computational simulation of hypertrophic cardiomyopathy mutations in Troponin I: Influence of increased myofilament calcium sensitivity on isometric force, ATPase and [Ca²⁺]_i. *Journal of Biomechanics* 2007;40(9):2044-52.
- (530) Miller T, Szczesna D, Housmans PR, Zhao J, De Freitas F, Gomes AV, et al. Abnormal contractile function in transgenic mice expressing a familial hypertrophic cardiomyopathy-linked troponin T (I79N) mutation. *Journal of Biological Chemistry* 2001;276(6):3743-55.
- (531) Díaz ME, Trafford AW, Eisner DA. The effects of exogenous calcium buffers on the systolic calcium transient in rat ventricular myocytes. *Biophysical Journal* 2001;80(4):1915-25.
- (532) Bean BP. Two kinds of calcium channels in canine atrial cells. Differences in kinetics, selectivity, and pharmacology. *Journal of General Physiology* 1985;86(1):1-30.
- (533) Choi HS, Trafford AW, Eisner DA. Measurement of calcium entry and exit in quiescent rat ventricular myocytes. *Eur J Physiol* 2000;440(4):600-8.
- (534) Schröder F, Herzig S. Effects of β₂-adrenergic stimulation on single-channel gating of rat cardiac L-type Ca²⁺ channels. *American Journal of Physiology Heart and Circulatory Physiology* 1999;276:H834-H843.

- (535) Reuter H. The dependence of slow inward current in Purkinje fibres on the extracellular calcium-concentration. *The Journal of Physiology* 1967 Sep 1;192(2):479-92.
- (536) Tsien RW. Calcium channels in excitable cell membranes. *Annu Rev Physiol* 1983 Oct 1;45(1):341-58.
- (537) Eisner DA, Choi HS, Díaz ME, O'Neill SC, Trafford AW. Integrative analysis of calcium cycling in cardiac muscle. *Circulation research* 2000 Dec 8;87(12):1087-94.
- (538) Kupittayanant P, Trafford AW, Díaz ME, Eisner DA. A mechanism distinct from the L-type Ca current or Na-Ca exchange contributes to Ca entry in rat ventricular myocytes. *Cell calcium* 2006;39(5):417-23.
- (539) Lokuta AJ, Rogers TB, Lederer WJ, Valdivia HH. Modulation of cardiac ryanodine receptors of swine and rabbit by a phosphorylation-dephosphorylation mechanism. *Journal of Physiology* 1995;487(3):609-22.
- (540) Picht E, DeSantiago J, Huke S, Kaetzel MA, Dedman JR, Bers DM. CaMKII inhibition targeted to the sarcoplasmic reticulum inhibits frequency-dependent acceleration of relaxation and Ca²⁺ current facilitation. *Journal of Molecular and Cellular Cardiology* 2007 Jan;42(1):196-205.
- (541) Braun AP, Schulman H. The multifunctional calcium/calmodulin-dependent protein kinase: from form to function. *Annu Rev Physiol* 1995 Oct 1;57(1):417-45.
- (542) Dupont B, Charmot G, Lapresle C. Trypanosomiasis presenting with trypanids and complicated by myopericarditis (author's translation). *La Nouvelle Presse Médicale* 1979;8:1579-81.
- (543) Robertson D, Knight R. Observations on the polyneuropathy and the disordered pyruvate metabolism by nitrofurazone in cases of sleeping sickness due to *Trypanosoma rhodesiense*. *Acta Tropica* 1964;21:239-63.
- (544) Schyns C, Janssen P. Electrocardiographic findings in sleeping sickness. *Acta Cardiologica* 1955;10:266-78.
- (545) The origin and peripateticism of the *Trypanosoma brucei* strain known as Lister 427. 2013.
- (546) Hirumi H, Hirumi K, Doyle JJ, Cross GAM. *In vitro* cloning of animal-infective bloodstream forms of *Trypanosoma brucei*. *Parasitology* 1980;80(02):371-82.
- (547) Vassella E, Reuner B, Yutzy B, Boshart M. Differentiation of African trypanosomes is controlled by a density sensing mechanism which signals cell cycle arrest via the cAMP pathway. *Journal of Cell Science* 1997 Nov 1;110(21):2661-71.
- (548) Szöör B, Dyer NA, Ruberto I, Acosta-Serrano A, Matthews KR. Independent pathways can transduce the life-cycle differentiation signal in *Trypanosoma brucei*. *PLoS Pathog* 2013 Oct 17;9(10):e1003689.
- (549) MacGregor P, Matthews KR. Identification of the regulatory elements controlling the transmission stage-specific gene expression of PAD1 in *Trypanosoma brucei*. *Nucleic Acids Research* 2012 Sep 1;40(16):7705-17.
- (550) van Deursen FJ, Shahi SK, Turner R, Hartmann C, Matthews KR, Clayton CE, et al. Characterisation of the growth and differentiation in vivo and in vitro-of bloodstream-form *Trypanosoma brucei* strain TREU 927. *Molecular and Biochemical Parasitology* 2001 Feb;112(2):163-71.
- (551) Bosnjak ZJ, Kampine JP. Effects of halothane, enflurane, and isoflurane on the SA node. *Anesthesiology* 1983;58:314-21.

- (552) Graves CL, McDermott RW, Bidwai A. Cardiovascular effects of isoflurane in surgical patients. *Anesthesiology* 1974;41(5):486-9.
- (553) Turk B, Brzin J, Kotnik M, Lenarcic B, Popovic T, Ritonja A, et al. Human cysteine proteases and their protein inhibitors stefins, cystatins and kininogens. *Biomedica biochimica acta* 1986;45(11-12):1375-84.
- (554) Scharfstein J, Lima A-P. Roles of naturally occurring protease inhibitors in the modulation of the host cell signaling and cellular invasion by *Trypanosoma cruzi*. *Subcellular Biochemistry* 2008;47:140-54.
- (555) Myburgh E, Coles JA, Ritchie R, Kennedy PGE, McLatchie AP, Rodgers J, et al. In Vivo Imaging of Trypanosome-Brain Interactions and Development of a Rapid Screening Test for Drugs against CNS Stage Trypanosomiasis. *PLoS Negl Trop Dis* 2013 Aug 22;7(8):e2384.
- (556) Galletly DC, Westernberg AM, Robinson BJ, Corfiatis T. Effect of halothane, isoflurane and fentanyl on spectral components of heart rate variability. *British Journal of Anaesthesia* 1994 Feb 1;72(2):177-80.
- (557) Picker O, Scheeren TWL, Arndt JO. Inhalation anaesthetics increase heart rate by decreasing cardiac vagal activity in dogs. *British Journal of Anaesthesia* 2001 Nov 1;87(5):748-54.
- (558) Levick JR. *An Introduction to Cardiovascular Physiology*. 3rd ed. Oxford University Press; 2000.
- (559) El-Armouche A, Jaeckel E, Boheler KR, Boknik P, Hertle B, Neumann J, et al. Ouabain treatment is associated with upregulation of phosphatase inhibitor-1 and Na⁺/Ca²⁺-exchanger and β-adrenergic sensitization in rat hearts. *Biochemical and Biophysical Research Communications* 2004 May 21;318(1):219-26.
- (560) Leineweber K, Heusch G. β1- and β2-Adrenoceptor polymorphisms and cardiovascular diseases. *British Journal of Pharmacology* 2009 Sep 1;158(1):61-9.
- (561) MacLean L. *Trypanosoma brucei* transmigration rates. Personal Communication 2013.
- (562) Beinfield WH, Lehr D. P-R interval of the rat electrocardiogram. *American Journal of Physiology -- Legacy Content* 1968 Jan 1;214(1):205-11.
- (563) Normann SJ, Priest RE, Benditt EP. Electrocardiogram in the normal rat and its alteration with experimental coronary occlusion. *Circulation research* 1961;9:282-7.
- (564) Aro AL, Anttonen O, Kerola T, Junttila MJ, Tikkanen JT, Rissanen HA, et al. Prognostic significance of prolonged PR interval in the general population. *European Heart Journal* 2013 May 14.
- (565) Morrison LJ, McLellan S, Sweeney L, Chan CN, MacLeod A, Tait A, et al. Role for parasite genetic diversity in differential host responses to *Trypanosoma brucei* infection. *Infection and Immunity* 2010 Mar 1;78(3):1096-108.
- (566) Müller A, Dhalla N. Role of various proteases in cardiac remodeling and progression of heart failure. *Heart Fail Rev* 2012;17(3):395-409.
- (567) Chapman HA, Riese RJ, Shi GP. Emerging roles for cysteine proteases in human biology. *Annu Rev Physiol* 1997 Oct 1;59(1):63-88.
- (568) Goldstein S, Landis JR, Leighton R, Ritter G, Vasu CM, Lantis A, et al. Characteristics of the resuscitated out-of-hospital cardiac arrest victim with coronary heart disease. *Circulation* 1981 Nov 1;64(5):977-84.

- (569) Wang Y, Wang Q, Zhao Y, Gong D, Wang D, Li C, et al. Protective effects of estrogen against reperfusion arrhythmias following severe myocardial ischemia in rats. *Circulation Journal* 2010;74(4):634-43.
- (570) Costa TFR, Reis FCG, Lima AP. Substrate inhibition and allosteric regulation by heparan sulfate of *Trypanosoma brucei* cathepsin L. *Biochimica et Biophysica Acta (BBA) - Proteins and Proteomics* 2012 Mar;1824(3):493-501.
- (571) Annecke T, Chappell D, Chen C, Jacob M, Welsch U, Sommerhoff CP, et al. Sevoflurane preserves the endothelial glycocalyx against ischaemia–reperfusion injury. *British Journal of Anaesthesia* 2010 Apr 1;104(4):414-21.
- (572) Dibb K, Eisner D. A small leak may sink a great ship but what does it do to the heart? *The Journal of Physiology* 2010 Dec 15;588(24):4849.
- (573) Fischer T, Maier L, Sossalla S. The ryanodine receptor leak: how a tattered receptor plunges the failing heart into crisis. *Heart Fail Rev* 2013;18(4):475-83.
- (574) Movsesian MA, Karimi M, Green K, Jones LR. Ca⁽²⁺⁾-transporting ATPase, phospholamban, and calsequestrin levels in nonfailing and failing human myocardium. *Circulation* 1994 Aug 1;90(2):653-7.
- (575) Pieske B, Kretschmann B, Meyer M, Holubarsch C, Weirich J, Posival H, et al. Alterations in intracellular calcium handling associated with the inverse force–frequency relation in human dilated cardiomyopathy. *Circulation* 1995 Sep 1;92(5):1169-78.
- (576) Schmidt U, Hajjar RJ, Helm PA, Kim CS, Doye AA, Gwathmey JK. Contribution of abnormal sarcoplasmic reticulum ATPase activity to systolic and diastolic dysfunction in human heart failure. *Journal of Molecular and Cellular Cardiology* 1998 Oct;30(10):1929-37.
- (577) Schwinger RHG, Böhm M, Schmidt U, Karczewski P, Bavendiek U, Flesch M, et al. Unchanged protein levels of SERCA II and phospholamban but reduced Ca²⁺ uptake and Ca²⁺-ATPase activity of cardiac sarcoplasmic reticulum from dilated cardiomyopathy patients compared with patients with Nonfailing Hearts. *Circulation* 1995 Dec 1;92(11):3220-8.
- (578) Yamamoto A, Kaji T, Tomoo K, Ishida T, Inoue M, Murata M, et al. Crystallization and preliminary X-ray study of the cathepsin B complexed with CA074, a selective inhibitor. *Journal of Molecular Biology* 1992 Oct 5;227(3):942-4.
- (579) Takahashi K, Ueno T, Tanida I, Minematsu-Ikeguchi N, Murata M, Kominami E. Characterization of CAA0225, a novel inhibitor specific for cathepsin L, as a probe for autophagic proteolysis. *Biological and Pharmaceutical Bulletin* 2009;32(3):475-9.
- (580) Müller AL, Hryshko LV, Dhalla NS. Extracellular and intracellular proteases in cardiac dysfunction due to ischemia–reperfusion injury. *International Journal of Cardiology* 2013;(0).
- (581) Negretti N, O'Neill SC, Eisner DA. The relative contributions of different intracellular and sarcolemmal systems to relaxation in rat ventricular myocytes. *Cardiovascular Research* 1993 Oct 1;27(10):1826-30.
- (582) Puglisi JL, Bassani RA, Bassani JW, Amin JN, Bers DM. Temperature and relative contributions of Ca transport systems in cardiac myocyte relaxation. *American Journal of Physiology* 1996;270(5):H1772-H1778.
- (583) Novinec M, Grass RN, Stark WJ, Turk V, Baici A, Lenarcic B. Interaction between human cathepsins K, L, and S and elastins: mechanism of elastinolysis and inhibition by macromolecular inhibitors. *Journal of Biological Chemistry* 2007 Mar 16;282(11):7893-902.

- (584) Cheng XW, Okumura K, Kuzuya M, Jin Z, Nagata K, Obata K, et al. Mechanism of diastolic stiffening of the failing myocardium and its prevention by angiotensin receptor and calcium channel blockers. *Journal of Cardiovascular Pharmacology* 2009;54(1):47-56.
- (585) Helske S, Syväranta S, Lindstedt KA, Lappalainen J, Öörni K, Mäyränpää MI, et al. Increased expression of elastolytic cathepsins S, K, and V and their inhibitor cystatin C in stenotic aortic valves. *Arteriosclerosis, Thrombosis, and Vascular Biology* 2006 Aug 1;26(8):1791-8.
- (586) Rabkin E, Aikawa M, Stone JR, Fukumoto Y, Libby P, Schoen FJ. Activated interstitial myofibroblasts express catabolic enzymes and mediate matrix remodeling in myxomatous heart valves. *Circulation* 2001 Nov 20;104(21):2525-32.
- (587) Kartik B, Philippe S, Hanjoong J, Ajit PY. Elevated cyclic stretch alters matrix remodeling in aortic valve cusps: implications for degenerative aortic valve disease. *American Journal of Physiology - Heart and Circulatory Physiology* 2009 Mar 2;296(3):H756-H764.
- (588) Punturieri A, Filippov S, Allen E, Caras I, Murray R, Reddy V, et al. Regulation of elastolytic cysteine proteinase activity in normal and cathepsin K-deficient human macrophages. *The Journal of Experimental Medicine* 2000 Sep 18;192(6):789-800.
- (589) Lohmüller T, Wenzler D, Hagemann S, Kiess W, Peters C, Dandekar T, et al. Toward computer-based cleavage site prediction of cysteine endopeptidases. *Biological Chemistry* 2003;384:899.
- (590) Everts V, Korper W, Hoeben KA, Jansen ID, Bromme D, Cleutjens KB, et al. Osteoclastic bone degradation and the role of different cysteine proteinases and matrix metalloproteinases: differences between calvaria and long bone. *J Bone Miner Res* 2006 Sep 1;21(9):1399-408.
- (591) Felbor U, Dreier L, Bryant RAR, Ploegh HL, Olsen BR, Mothes W. Secreted cathepsin L generates endostatin from collagen XVIII. *EMBO J* 2000;19(6):1187-94.
- (592) Maciewicz RA, Etherington DJ. A comparison of four cathepsins (B, L, N and S) with collagenolytic activity from rabbit spleen. *The Biochemistry Journal* 1988;256(2):433-40.
- (593) Decker RS, Poole AR, Crie JS, Dingle JT, Wildenthal K. Lysosomal alterations in hypoxic and reoxygenated hearts. II. Immunohistochemical and biochemical changes in cathepsin D. *American Journal of Pathology* 1980;98(2):445-56.
- (594) Decker RS, Wildenthal K. Lysosomal alterations in hypoxic and reoxygenated hearts. I. Ultrastructural and cytochemical changes. *American Journal of Pathology* 1980;98(2):425-44.
- (595) Wildenthal K. Lysosomal alterations in ischemic myocardium: Result or cause of myocellular damage? *Journal of Molecular and Cellular Cardiology* 1978 Jul;10(7):595-603.
- (596) Reddy A, Caler EV, Andrews NW. Plasma membrane repair is mediated by Ca²⁺-regulated exocytosis of lysosomes. *Cell* 2001 Jul 27;106(2):157-69.
- (597) Jaiswal JK, Andrews NW, Simon SM. Membrane proximal lysosomes are the major vesicles responsible for calcium-dependent exocytosis in nonsecretory cells. *The Journal of Cell Biology* 2002 Nov 25;159(4):625-35.
- (598) Ichihara K, Haneda T, Onodera S, Abiko Y. Inhibition of ischemia-induced subcellular redistribution of lysosomal enzymes in the perfused rat heart by the calcium entry blocker, diltiazem. *Journal of Pharmacology and Experimental Therapeutics* 1987 Sep 1;242(3):1109-13.

- (599) Riese RJ, Mitchell RN, Villadangos JA, Shi GP, Palmer JT, Karp ER, et al. Cathepsin S activity regulates antigen presentation and immunity. *J Clin Invest* 1998 Jun 1;101(11):2351-63.
- (600) Turk V, Turk B, Gun-iar G, Turk D, Kos J. Lysosomal cathepsins: structure, role in antigen processing and presentation, and cancer. *Advances in Enzyme Regulation* 2002;42(0):285-303.
- (601) Wille A, Gerber A, Heimburg A, Reisenauer A, Peters C, Saftig P, et al. Cathepsin L is involved in cathepsin D processing and regulation of apoptosis in A549 human lung epithelial cells. *bchm* 2004;385:665.
- (602) Yang Z, Cox JL. Cathepsin L increases invasion and migration of B16 melanoma. *Cancer Cell International* 2007;7(8).
- (603) Reinheckel T, Deussing J, Roth W, Peters C. Towards specific functions of lysosomal cysteine peptidases: phenotypes of mice deficient for cathepsin B or cathepsin L. *bchm* 2001;382:735.
- (604) Nguyen TP, Qu Z, Weiss JN. Cardiac fibrosis and arrhythmogenesis: The road to repair is paved with perils. *Journal of Molecular and Cellular Cardiology*(0).
- (605) Alehagen U, Dahlström U, Lindahl TL. Cystatin C and NT-proBNP, a powerful combination of biomarkers for predicting cardiovascular mortality in elderly patients with heart failure: results from a 10-year study in primary care. *European Journal of Heart Failure* 2009 Apr 1;11(4):354-60.
- (606) Patel PC, Ayers CR, Murphy SA, Peshock R, Khera A, de Lemos JA, et al. Association of cystatin C with left ventricular structure and function: the Dallas heart study. *Circulation: Heart Failure* 2009 Mar 1;2(2):98-104.
- (607) Gomez AM, Valdivia HH, Cheng H, Lederer MR, Santana LF, Cannell MB, et al. Defective excitation-contraction coupling in experimental cardiac hypertrophy and heart failure. *Science* 1997 May 2;276(5313):800-6.
- (608) Gomez AM, Guatimosim S, Dilly KW, Vassort G, Lederer WJ. Heart Failure After Myocardial Infarction: Altered Excitation-Contraction Coupling. *Circulation* 2001 Aug 7;104(6):688-93.
- (609) Neumann J, Eschenhagen T, Jones LR, Linck B, Schmitz W, Scholz H, et al. Increased expression of cardiac phosphatases in patients with end-stage heart failure. *Journal of Molecular and Cellular Cardiology* 1997 Jan;29(1):265-72.
- (610) Carr AN, Schmidt AG, Suzuki Y, del Monte F, Sato Y, Lanner C, et al. Type 1 phosphatase, a negative regulator of cardiac function. *Molecular and Cellular Biology* 2002 Jun 15;22(12):4124-35.
- (611) El-Armouche A, Rau T, Zolk O, Ditz D, Pamminger T, Zimmermann WH, et al. Evidence for protein phosphatase inhibitor-1 playing an amplifier role in β -adrenergic signaling in cardiac myocytes. *The FASEB Journal* 2003 Jan 2.
- (612) Hasenfuss G. Animal models of human cardiovascular disease, heart failure and hypertrophy. *Cardiovascular Research* 1998;39(1):60-76.
- (613) Zarain-Herzberg A, Afzal N, Elimban V, Dhalla NS. Decreased expression of cardiac sarcoplasmic reticulum Ca^{2+} -pump ATPase in Congestive Heart Failure due to myocardial infarction. *Molecular and Cellular Biochemistry* 1996;163-164:285-90.
- (614) Boluyt MO, O'Neill L, Meredith AL, Bing OHL, Brooks WW, Conrad CH, et al. Alterations in cardiac gene expression during the transition from stable hypertrophy to heart failure: Marked upregulation of genes encoding extracellular matrix components. *Circulation research* 1994;75(1):23-32.

- (615) Kiss E, Ball NA, Kranias EG, Walsh RA. Differential changes in cardiac phospholamban and sarcoplasmic reticular Ca^{2+} -ATPase protein levels: Effects on Ca^{2+} transport and mechanics in compensated pressure-overload hypertrophy and congestive heart failure. *Circulation research* 1995;77(4):759-64.
- (616) Le C, Xi-Yuan L, Jun L, Ji-Dong F, Zhao-Nian Z, Huang-Tian Y. Intermittent hypoxia protects cardiomyocytes against ischemia-reperfusion injury-induced alterations in Ca^{2+} homeostasis and contraction via the sarcoplasmic reticulum and $\text{Na}^{+}/\text{Ca}^{2+}$ exchange mechanisms. *American Journal of Physiology - Cell Physiology* 2006 Mar 10;290(4):C1221-C1229.
- (617) Reiken S, Gaburjakova M, Gaburjakova J, He Kl, Prieto A, Becker E, et al. β -Adrenergic receptor blockers restore cardiac calcium release channel (ryanodine receptor) structure and function in heart failure. *Circulation* 2001 Dec 4;104(23):2843-8.
- (618) Lakkireddy V, Bub G, Baweja P, Syed A, Boutjdir M, El-Sherif N. The kinetics of spontaneous calcium oscillations and arrhythmogenesis in the *in vivo* heart during ischemia/reperfusion. *Heart Rhythm* 2006 Jan;3(1):58-66.
- (619) Zhang Y, Huang ZJ, Dai DZ, Feng Y, Na T, Tang XY, et al. Downregulated FKBP12.6 expression and upregulated endothelin signaling contribute to elevated diastolic calcium and arrhythmogenesis in rat cardiomyopathy produced by l-thyroxin. *International Journal of Cardiology* 2008 Nov 28;130(3):463-71.
- (620) Zima AV, Blatter LA. Redox regulation of cardiac calcium channels and transporters. *Cardiovascular Research* 2006 Jul 15;71(2):310-21.
- (621) Tocchetti CG, Wang W, Froehlich JP, Huke S, Aon MA, Wilson GM, et al. Nitroxyl improves cellular heart function by directly enhancing cardiac sarcoplasmic reticulum Ca^{2+} cycling. *Circulation research* 2007 Jan 5;100(1):96-104.
- (622) Meerson FZ, Belkina LM, Sazontova TG, Saltykova VA, Arkhipenko Y. The role of lipid peroxidation in pathogenesis of arrhythmias and prevention of cardiac fibrillation with antioxidants. *Basic Research in Cardiology* 1987;82(2):123-37.
- (623) Park JL, Lucchesi BR. Mechanisms of myocardial reperfusion injury. *Ann Thorac Surg* 1999 Nov;68(5):1905-12.
- (624) Xu L, Eu JP, Meissner G, Stamler JS. Activation of the cardiac calcium release channel (ryanodine receptor) by poly-S-nitrosylation. *Science* 1998 Jan 9;279(5348):234-7.
- (625) Stoyanovsky D, Murphy T, Anno PR, Kim YM, Salama G. Nitric oxide activates skeletal and cardiac ryanodine receptors. *Cell calcium* 1997 Jan;21(1):19-29.
- (626) Repnik U, Stoka V, Turk V, Turk B. Lysosomes and lysosomal cathepsins in cell death. *Biochimica et Biophysica Acta (BBA) - Proteins and Proteomics* 2012 Jan;1824(1):22-33.
- (627) Elliott EB, Hasumi H, Otani N, Matsuda T, Matsuda R, Kaneko N, et al. K201 (JTV-519) alters the spatiotemporal properties of diastolic Ca^{2+} release and the associated diastolic contraction during β -adrenergic stimulation in rat ventricular cardiomyocytes. *Basic Res Cardiol* 2011;106(6):1009-22.